Gebhard Mathis
Editor

Chest Sonography

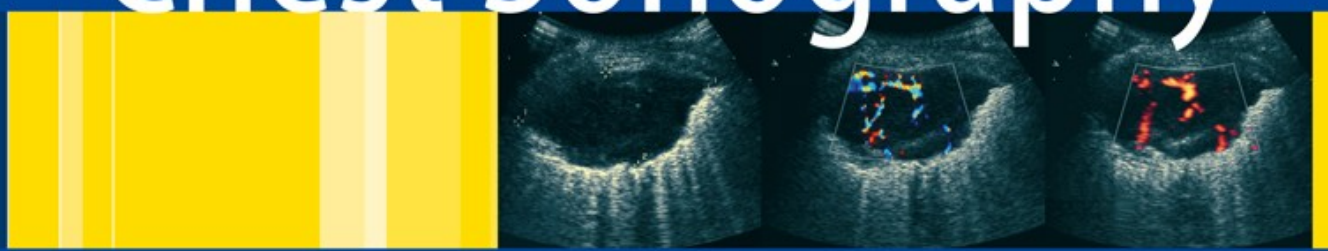

Second Edition

Springer

Gebhard Mathis (Ed.)

Chest Sonography

Gebhard Mathis (Ed.)

Chest Sonography

Second Edition

With 321 Figures and 25 Tables

Springer

Prof. Dr. Gebhard Mathis
Internistische Praxis
Bahnhofstrasse 16/2
6830 Rankweil
Austria

Library of Congress Control Number: 2007930215

ISBN 978-3-540-72427-8 Springer Berlin Heidelberg New York

Springer is a part of Springer Science+Business Media
springer.com

Editor: Dr. Ute Heilmann, Heidelberg, Germany
Desk Editor: Meike Stoeck, Heidelberg, Germany
Reproduction, typesetting and production: LE-TEX Jelonek, Schmidt & Vöckler GbR, Leipzig, Germany
Cover design: Frido Steinen-Broo, EStudio, Calamar, Spain

SPIN 12029181

Printed on acid-free paper 21/3180/YL 5 4 3 2 1 0

Preface

The scope of application of chest sonography has been significantly widened in the last few years. Portable ultrasound systems are being used to an increasing extent in preclinical sonography, at the site of trauma, in the ambulance of the emergency physician or in ambulance helicopters. In the emergency room, at the intensive care unit and in clinical routine, chest sonography has proved its worth as a strategic instrument to be used directly after the clinical investigation. It helps the investigator to decide—very rapidly—whether a traumatized patient is suffering such severe internal hemorrhage that he needs to be transported to the operating room immediately or whether there still is time for further investigations like CT. Several diagnoses such as pneumothorax, pneumonia or pulmonary embolism can be established immediately.

Numerous recent publications have significantly deepened our knowledge of chest sonography: the sonomorphology of the normal pleura has been described more accurately on cadavers and in histological sections. The sonoanatomy of the upper aperture of the thorax has been extended to include imaging of the brachial plexus, which allows more precise administration of regional anesthesia and the application of a smaller quantity of the anesthetic. Monumental studies on lymph node staging in the presence of bronchial carcinoma have been presented. Here sonography is markedly superior to CT. The high value of endoluminal accesses has been explained in greater detail and with greater precision.

The present new issue has been extended to include two subjects. Contrast sonography is currently at the threshold of being introduced for the differentiation of subpleural lung lesions—in some instances the sonomorphology of the B-mode image and color-Doppler sonography are still ambiguous. The second new section is an elucidation of clinical sonography from symptoms to diagnosis.

I am most deeply indebted to the team of authors for their creative cooperation and timely submissions. I also thank Springer-Verlag for their close collaboration and careful production of the book.

The purpose of this pictorial atlas is to help colleagues serve their patients better. It will hopefully enable clinicians to establish diagnoses rapidly at the patient's bedside with greater accuracy and efficiency, and to initiate appropriate therapeutic measures on time.

Rankweil, August 2007
Gebhard Mathis

Contents

Contributors

Jouke T. Annema
Longziekten, C3-P
Leids Universitair Medisch Centrum
Postbus 9600, 2300 RC Leiden
The Netherlands
E-mail: j.t.annema@lumc.nl

Sonja Beckh
Klinikum Nürnberg Nord
Flurstraße 17, 90340 Nuremberg
Germany
E-mail: beckh@klinikum-nuernberg.de

Wolfgang Blank
Klinikum am Steinenberg, Kreiskliniken Reutlingen
Medizinische Klinik Akademisches Lehrkrankenhaus
der Universität Tübingen
Steinenbergstraße 31, 72764 Reutlingen
Germany
E-mail: blank_w@kreiskliniken-reutlingen.de

Ralf Eberhardt
Innere Medizin/Pulmonologie
Thoraxklinik Heidelberg gGmbH
Amalienstraße 5
69126 Heidelberg
Germany
E-mail: ralf.eberhardt@thoraxklinik-heidelberg.de

Christian Görg
Zentrum für innere Medizin
Baldingerstraße, 35043 Marburg
Germany
E-mail: christian.goerg@staff.uni-marburg.de

Felix J.F. Herth
Innere Medizin/Pulmonologie
Thoraxklinik Heidelberg gGmbH
Amalienstraße 5, 69126 Heidelberg
Germany
E-mail: felix.herth@thoraxklinik-heidelberg.de

Gebhard Mathis
Internistische Praxis
Bahnhofstrasse 16/2
6830 Rankweil
Austria
E-mail: gebhard.mathis@cable.vol.at

Klaus F. Rabe
Longziekten, C3-P
Leids Universitair Medisch Centrum
Postbus 9600, 2300 RC Leiden
The Netherlands
E-mail: k.f.rabe@lumc.nl

Joachim Reuss
Medizinische Klinik
Bunsenstraße 120, 71032 Böblingen
Germany
E-mail: joachim_reuss@web.de

Andreas Schuler
Helfenstein Klinik
Eybstr. 16, 73312 Geislingen
Germany
E-mail: andreas.schuler@helfenstein-klinik.de

Maud Veseliç
Longziekten, C3-P
Leids Universitair Medisch Centrum
Postbus 9600, 2300 RC Leiden
The Netherlands

1 Indications, Technical Prerequisites and Investigation Procedure

S. Beckh

1

1.1 Indications

Sonography is a long-established supplementary imaging procedure in the diagnosis of pleural effusions. Technical advancement and ongoing scientific evidence have caused the spectrum of application for sonography in diseases of the chest to be steadily extended over the last few years (Stender et al. 1994; Broaddus and Light 1994; Müller 1997; Kinasewitz 1998; Beckh 2002; Fig. 1.1).

The sonographic image does not provide a complete overview of the chest; however, it does image a certain section of it, which, given a specific problem under investigation, provides valuable additional information to substantiate overview radiographs. Occasionally sonography is the only noninvasive diagnostic procedure that throws significant light on pathological findings (Walz and Muhr 1990; Fraser et al. 1999).

Up to 99% of the ultrasound wave is reflected in the healthy lung. Intrapulmonary processes can be detected by sonography only when they extend up to the visceral pleura or can be imaged through a sound-conducting medium such as fluid or consolidated lung tissue (Fig. 1.2).

Sonic shadow zones are caused by nearly complete absorption of the ultrasound wave in bone, especially behind the sternum, scapula and vertebral column. Limitations caused by rib shadows can at least partially be balanced by respiratory mechanics.

From a percutaneous route the immediate retrosternal and posterior portions of the mediastinum cannot be viewed. A complementary method for this location is transesophageal and transbronchial sonography, which, however, are invasive investigation procedures in terms of effort and handling. (Lam and Becker 1996; Arita et al. 1996; Silvestri et al. 1996; Becker et al. 1997; Broderick et al. 1997; Serna et al. 1998; Aabakken et al. 1999; Herth et al. 2004; Fig. 1.3).

Sonography provides diagnostic information when individual structures of the thorax are investigated:

1. Thorax wall
   (a) Benign lesions
      - Benign neoplasms (e.g., lipoma)
      - Hematoma
      - Abscess
      - Reactivated lymph nodes
      - Perichondritis, Tietze's syndrome
      - Rib fracture

   (b) Malignant lesions
      - Lymph node metastases (initial diagnosis and course of disease during treatment)
      - Invasive, growing carcinomas
      - Osteolysis

2. Pleura
   (a) Solid structures: thickening of the pleura, callus, calcification, asbestosis plaques
   (b) Space-occupying mass
      - Benign: fibrous tumor, lipoma
      - Malignant: circumscribed metastases, diffuse carcinosis, malignant pleural mesothelioma

   (c) Fluid: effusion, hematothorax, pyothorax, chylothorax
   (d) Dynamic investigation
      - Pneumothorax

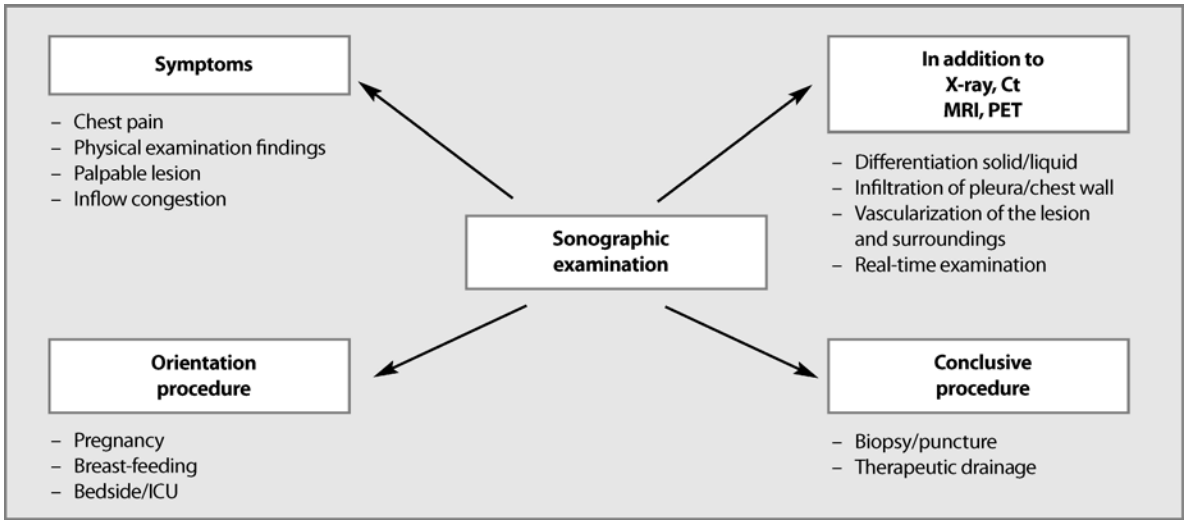

Fig. 1.1 Spectrum of application of sonography for pleural and pulmonary disease

- Distinguishing between effusion and callus formation
- Adherence of a space-occupying mass
- Invasion by a space-occupying mass
- Mobility of the diaphragm

3. Formation of peripheral foci in the lung
   (a) Benign: inflammation, abscess, embolism, atelectasis
   (b) Malignant: peripheral metastasis, peripheral carcinoma, tumor/atelectasis
4. Mediastinum, percutaneous
   (a) Space-occupying masses in the upper anterior mediastinum
   (b) Lymph nodes in the aorticopulmonary window
   (c) Thrombosis of the vena cava and its supplying branches
   (d) Imaging collateral circulation
   (e) Pericardial effusion

Further pathological alterations in the heart visualized by sonography will not be described in this book. For this subject the reader is referred to pertinent textbooks on echocardiography.

1.2 Technical Requirements in Terms of Equipment

All the apparatuses used for sonographic investigation of the abdomen and thyroid may also be used to examine the thorax. A high-resolution linear transducer of 5–10 MHz is suitable for imaging the *thorax wall* and the *parietal pleura* (Mathis 2004). More recently introduced probes of 10–13 MHz are excellent for evaluating *lymph nodes* (Gritzmann 2005), pleura and the surface of the lung.

For investigation of the *lung* a convex or sector probe of 3–5 MHz provides adequate depth of penetration.

Vector, sector or narrow convex probes are recom-

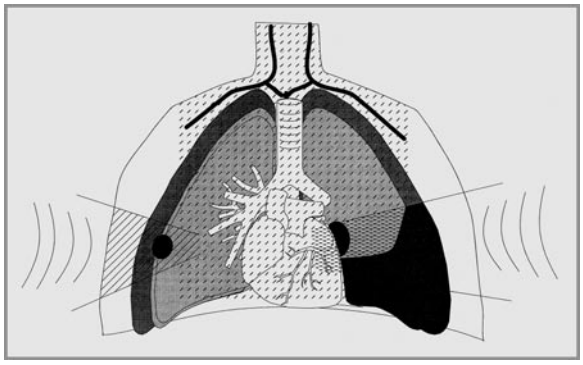

Fig. 1.2 Structures and pathological changes accessible to sonography

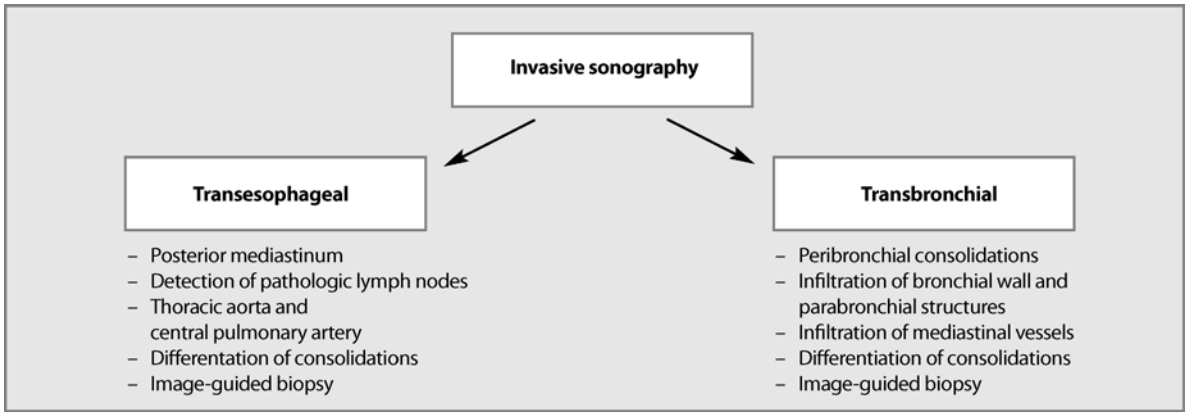

Fig. 1.3 Indications for invasive sonography

mended for the *mediastinum*. The smaller the connecting surface, the better the transducer can be placed in the jugulum or the supraclavicular fossa. The range of frequency should be 3.5–5 MHz. It should be noted that device settings commonly used for examining the heart are not suitable for the rest of the mediastinum. Contrast, image rate and gray-scale depth balance must be adjusted to image structures of the mediastinum.

Transesophageal sonography requires a special probe with a suitable connecting tube to the sonography device. Endobronchial sonography is performed with special, thin high-frequency probes (12–20 MHz) that are introduced via the working tube of the flexible bronchoscope. Currently very few manufacturers offer suitable probes along with a sonography unit.

1.3 Investigation Procedure

1.3.1 Thorax Wall, Pleura, Diaphragm, Lung

The investigation is performed as far as possible with the patient seated, during inspiration and expiration, if necessary in combination with respiratory maneuvers such as coughing or "sniffing." Raising the arms and crossing them behind the head causes intercostal spaces to be extended and facilitates access. The transducer is moved from ventral to dorsal along the longitudinal lines in the thorax (Fig. 1.4):

- Parasternal line
- Middle and lateral clavicular line
- Anterior, middle and posterior axillary line
- Lateral and medial scapular line
- Paravertebral line

Every finding should be allocated to its respective anatomic location and the latter should be specifically mentioned.

Subsequent transverse transducer movement parallel to the ribs in the intercostal space (Fig. 1.5) provides the additional information required for accurate localization of the respective finding.

The investigation of foci behind the scapula needs maximum adduction of the arms until the contralateral shoulder is encircled (Fig. 1.6). The supraclavicular access allows the investigator to view the tip of the lung and the region of the brachial plexus (Sect. 1.3.2).

From suprasternal, the anterior upper mediastinum can be viewed. From the abdomen, in subcostal section by the transhepatic route on the right side (Fig. 1.7) and to a lesser extent through the spleen on the left side, the diaphragm is examined. Additionally, the longitudinal resonance plane from the flank images both phrenicocostal recesses (Fig. 1.8)

The supine patient is examined in the same manner. The abdominal access is better for this purpose. However, viewing intercostal spaces might be more difficult, as the mobility of the shoulder girdle is usually somewhat restricted.

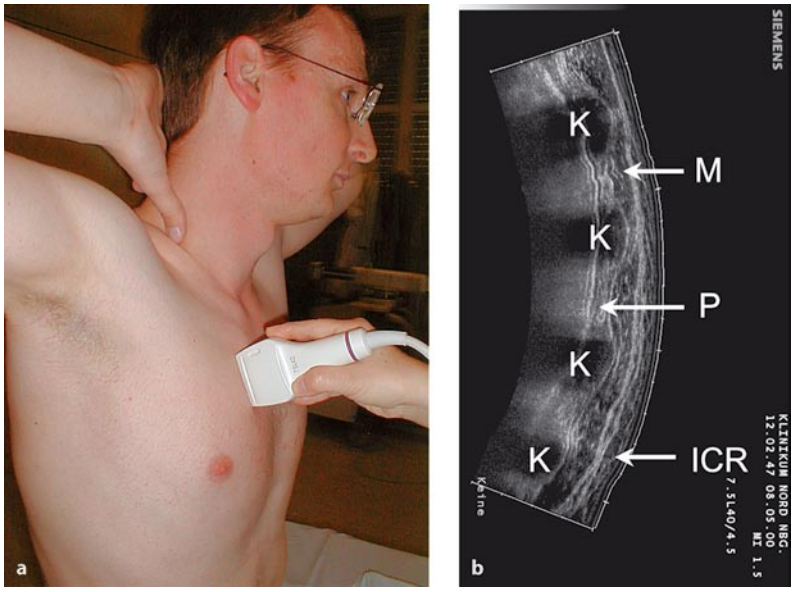

Fig. 1.4 Examination of the seated patient. **a** Linear probe placed longitudinally on the right parasternal line. **b** Corresponding sonographic longitudinal panoramic image (SieScape). *K* cartilage at the point of insertion of the rib, *ICR* intercostal space, *M* muscle, *P* line of the pleura

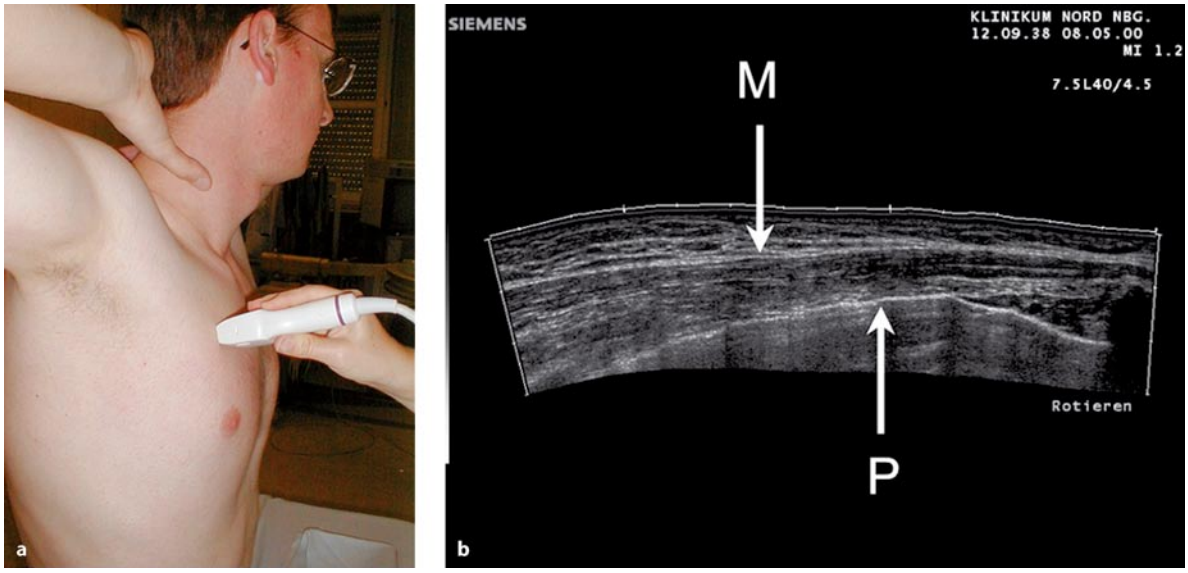

Fig. 1.5 Examination of the seated patient. **a** Linear probe placed parallel to the ribs in the third intercostal space. **b** Corresponding sonographic transverse panoramic image (SieScape). *M* muscle, *P* line of the pleura

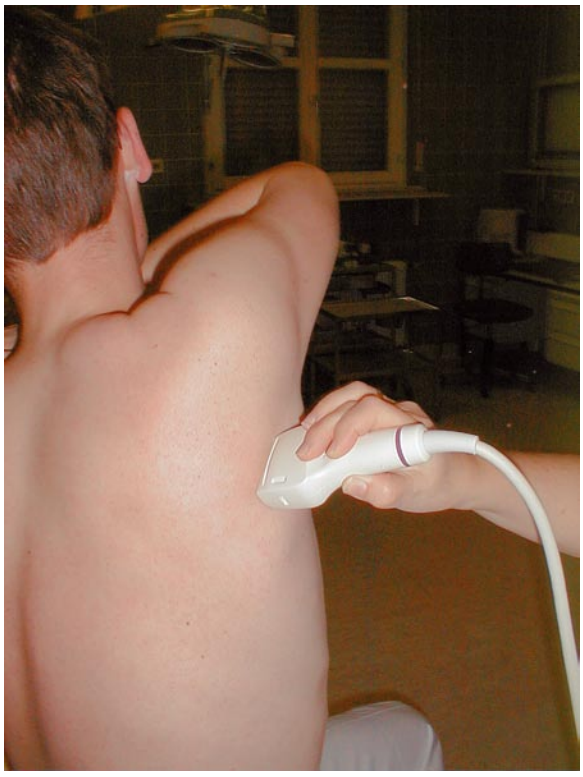

Fig. 1.6 Position of the patient when structures behind the scapula are examined

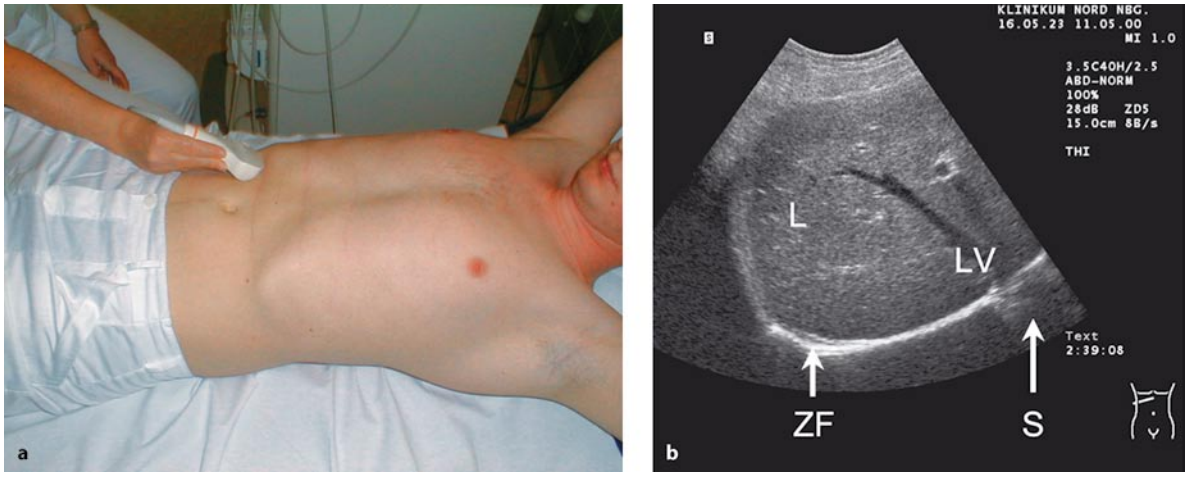

Fig. 1.7 Transhepatic examination. **a** Convex probe placed subcostally from the right. Slight tilting in cranial direction. **b** Corresponding sonographic image. *L* liver, *LV* liver vein, *ZF* diaphragm, *S* reflection of the liver above the diaphragm

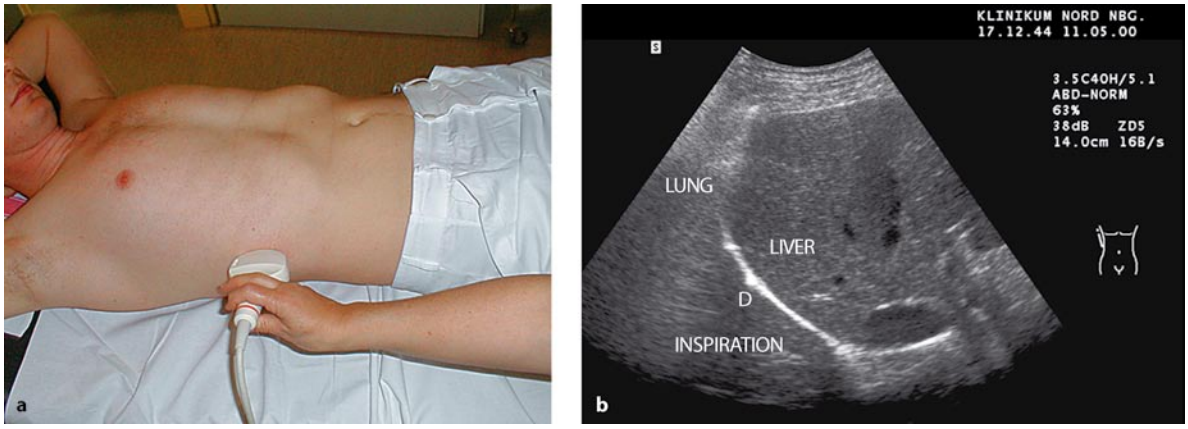

Fig. 1.8 Examination from the lateral aspect. **a** Convex probe placed longitudinally in the mid portion of the right axillary line. **b** Corresponding sonographic image. *D* diaphragm. The normal mobile lung is shifted during inspiration into the phrenicocostal recess and covers the upper margin of the liver

1.3.2 Investigation of the Supraclavicular Region

The investigation of the supraclavicular region requires special transducer movements. High-resolution probes allow the imaging of nerves. The viewing of the branches of the brachial plexus means an diagnostic enrichment in sonography of diseases of the chest. The plexus and its branches should be examined in the following cases:

- Infiltration of Pancoast's tumor
- Trauma (birth, accident)
- Punctures of the supraclavicular region
- Anesthesia of the brachial plexus

The examination starts on the lateral base of the neck (Fig. 1.9). The branches of the brachial plexus lead lateral and downward between the gap of M. scalenus anterior and medius. They reach the axilla between the first rib and the clavicula. Infraclavicular placement of the probe shows the course of the nerve along the axillary artery (Fig. 1.10).

The investigation procedure terminates with the probe placed in the axilla (Fig. 1.11)

The procedure for transesophageal and transbronchial sonography is described in the respective chapters.

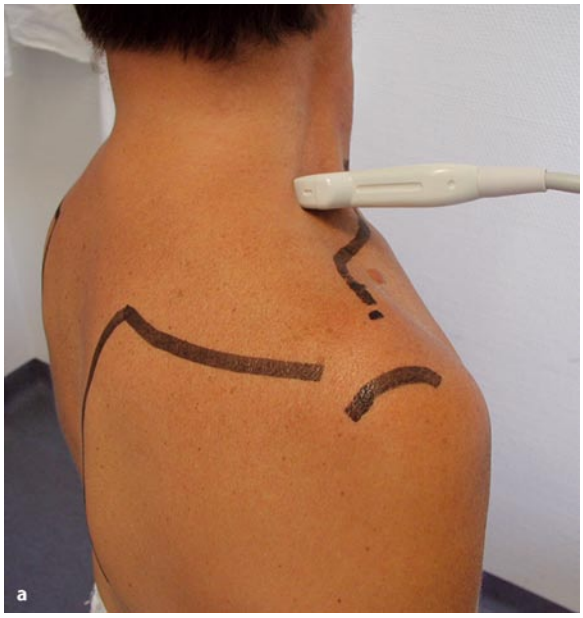

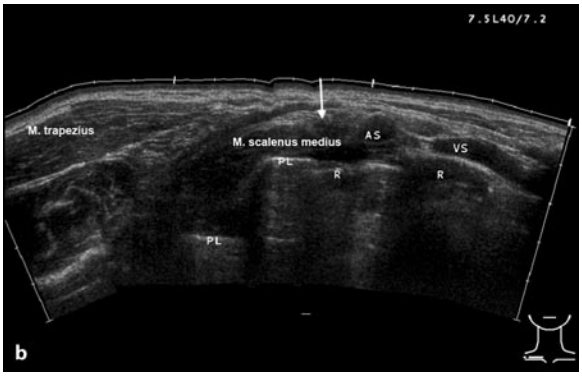

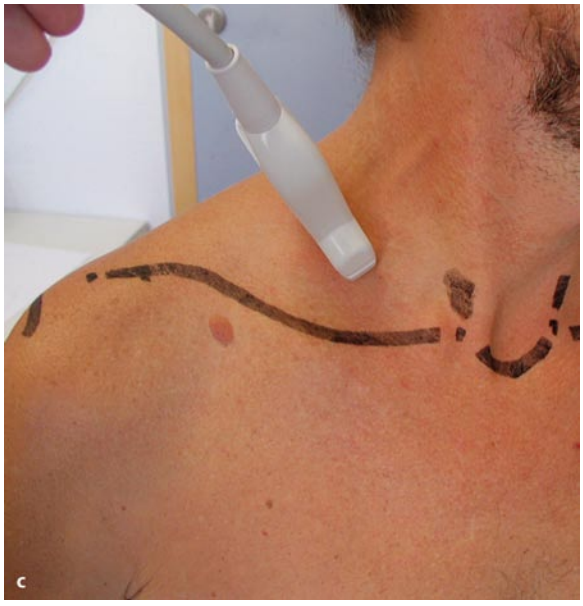

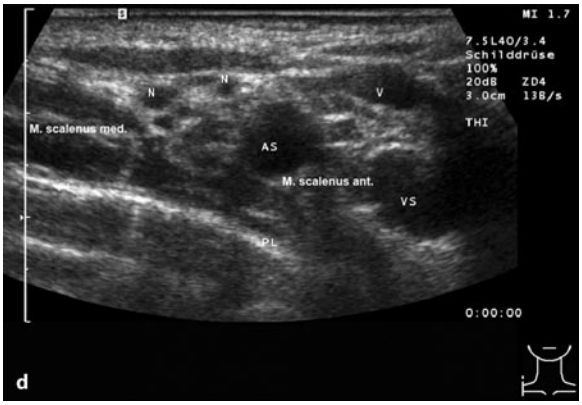

Fig. 1.9 Examination of the supraclavicular region. **a** Linear probe placed longitudinally on the lateral base of the neck **b** Corresponding sonographic panoramic image. *AS* a. subclavia, *VS* v. subclavia, *R* rib, *PL* pleura, *arrow* branch of brachial plexus. **c** Linear probe placed medium sagittal on the lateral base of the neck. **d** Corresponding sonographic image. *N* Branches of brachial plexus, *V* v. anonyma

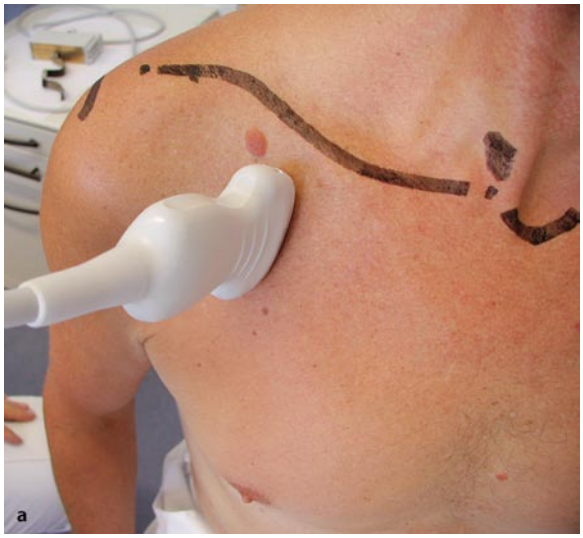

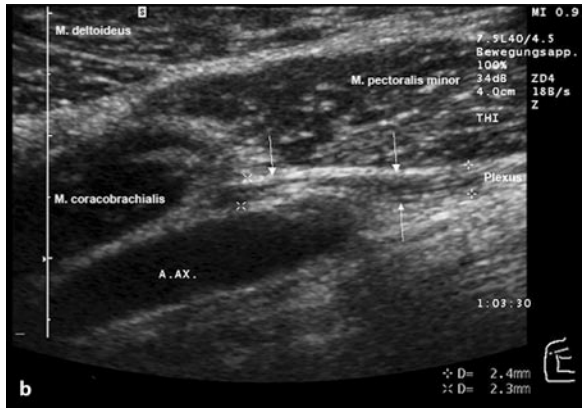

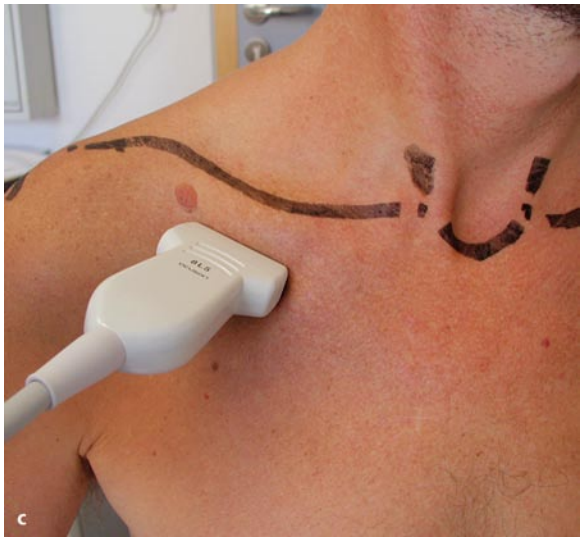

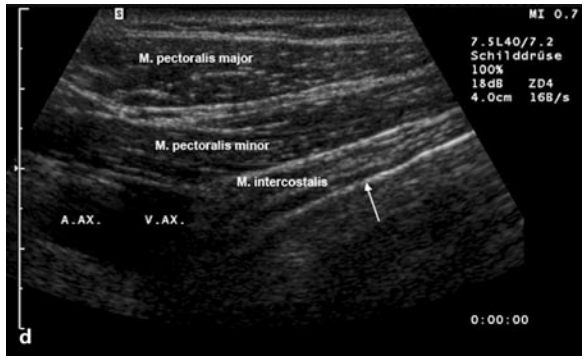

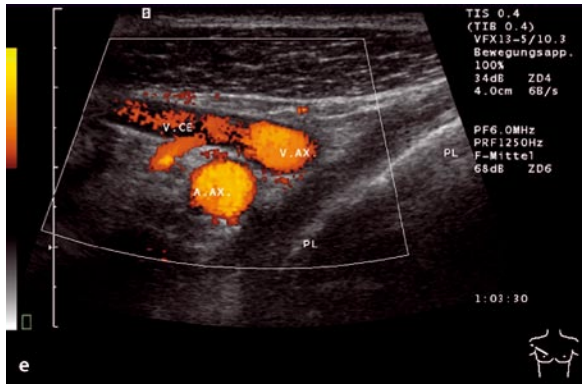

Fig. 1.10 **a** Linear probe placed oblique longitudinally in the middle clavicular line. **b** Corresponding sonographic image. *A.AX.* a. axillaris. The *arrows* and *crosses* mark the course of the plexus nerve. **c** Linear probe placed infraclavicular transverse in the middle clavicular line parallel to clavicula. **d** Corresponding sonographic image. The *arrow* points to pleural line. **e** Corresponding color image. *V.CE.* v. cephalica

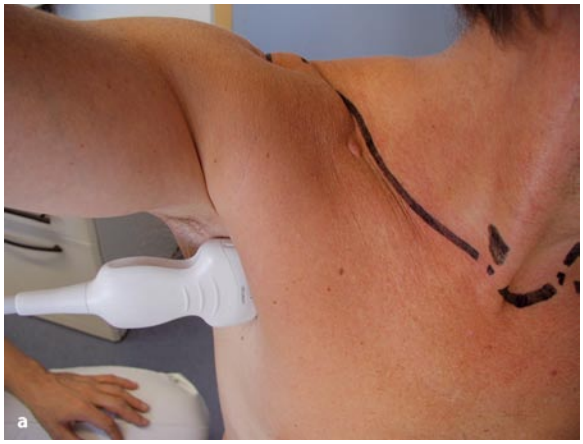

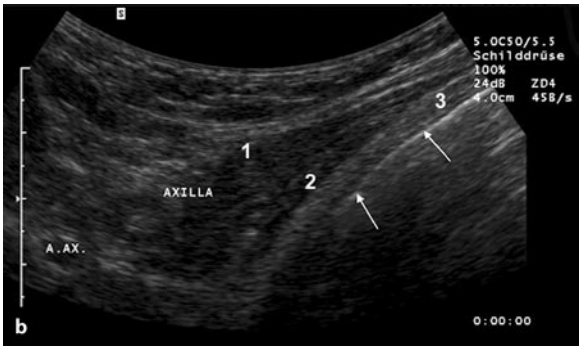

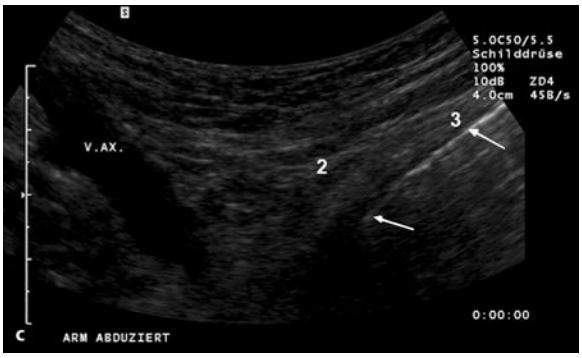

Fig. 1.11 **a** Linear probe placed longitudinally in the mid axilla. **b** Corresponding sonographic imaging, probe inclined dorsad. *1* m. serratus anterior, *2* m. intercostalis, *3* pleural line (*arrows*). **c** Corresponding sonographic image, probe inclined ventrad

1.4 Summary

The high resolution of the sonographic image and the real-time examination make a major contribution to the diagnosis of diseases of the chest. Structures of the chest wall and pleural lesions are visualized by ultrasound. Pulmonary consolidations are detected if they reach the visceral pleura, or if they are situated behind an acoustic window. The anterior and superior mediastinum is accessible percutaneously with certain positions of the probe. For thoracic sonography a linear probe (5–10 MHz) for close resolution and a convex or sector transducer (3,5–5 MHz) for access to deeper areas is recommended. The investigation of the supraclavicular region requires high-resolution transducers (5–13 MHz) for making visible the nerves of the brachial plexus.

References

Aabakken L, Silvestri GA, Hawes R et al (1999) Cost-efficacy of endoscopic ultrasonography with fine-needle aspiration vs. mediastinotomy in patients with lung cancer and suspected mediastinal adenopathy. Endoscopy 31:707711

Arita T, Matsumoto T, Kuramitsu T et al (1996) Is it possible to differentiate malignant mediastinal nodes from benign nodes by size? Reevaluation by CT, transesophageal echocardiography, and nodal specimen. Chest 110:1004–1008

Becker HD, Messerschmidt E, Schindelbeck F et al (1997) Endobronchialer Ultraschall. Pneumologie 51:620–629

Beckh S, Bölcskei PL, Lessnau KD (2002) Real-time chest ultrasonography. A comprehensive review for the pulmonologist. Chest 122:1759–1773

Broaddus VC, Light RW (1994) Disorders of the pleura: general principles and diagnostic approach. In: Murray JF, Nadel JA (eds) Textbook of respiratory medicine. Saunders, Philadelphia, pp 638–644

Broderick LS, Tarver RD, Conces DJ Jr (1997) Imaging of lung cancer: old and new. Semin Oncol 24:411–418

Fraser RS, Müller NL, Colman N, Paré PD (1999) Fraser and Paré's diagnosis of diseases of the chest. Saunders, Philadelphia, pp 299–338

Gritzmann N (2005) Sonography of the neck: current potentials and limitations. Ultraschall Med 26:185–196

Herth FJ, Becker HD, Eberhardt R (2004) Endobronchialer Ultraschall beim Bronchialkarzinom. Radiologe 44:457–464

Kinasewitz GT (1998) Disorders of the pleural space. Pleural fluid dynamics and effusions. In: Fishman AP (ed) Fishman's pulmonary diseases and disorders. McGraw-Hill, New York, pp 1396–1397

Lam S, Becker HD (1996) Future diagnostic procedures. Chest Surg Clin N Am 6: 363–380

Mathis G (2004) Thoraxsonography—part I: chest wall and pleura. Schweiz Rundschau Med Prax 93:615–621\CEnote{Please check this reference against the references in Sect. 1.2 as the year given there is 1997}

Müller W (1997) Ultraschall-Diagnostik. In: Rühle KH (ed) Pleura-Erkrankungen. Kohlhammer, Stuttgart, pp 31–44

Serna DL, Aryan HE, Chang KJ et al (1998) An early comparison between endoscopic ultrasound-guided fine-needle aspiration and mediastinoscopy for diagnosis of mediastinal malignancy. Am Surg 64:1014–1018

Silvestri GA, Hoffmann BJ, Bhutani MS et al (1996) Endoscopic ultrasound with fine-needle aspiration in the diagnosis and staging of lung cancer. Ann Thorac Surg 61:1441–1445

Stender HS, Majewski A, Schober O et al (1994) Bildgebende Verfahren in der Pneumologie. In: Ferlinz R (ed) Pneumologie in Praxis und Klinik. Thieme, Stuttgart, pp 176–178

Walz M, Muhr G (1990) Sonographische Diagnostik beim stumpfen Thoraxtrauma. Unfallchirurg 93:359–363

2 The Chest Wall

G. Mathis, W. Blank

The chest wall—with the exception of the parietal pleura behind the ribs—is well accessed by sonography because of its position immediately next to the ultrasound transducer (Sakai et al. 1990). Any suspicious findings on palpation of the chest (whether inflammatory or neoplastic) may be an indication for chest sonography. Quite often the subsequent procedure consists of sonographic control investigations and sonography-guided aspiration. Chest trauma is an excellent indication for sonography of the chest wall. Fractures of the rib and the sternum can be diagnosed with great accuracy. Concomitant conditions such as local hematoma, pleural effusion or pneumothorax can also be identified by sonography (Mathis 1997).

Indications for sonography of the chest wall:

- Pain
- Ambiguous findings on palpation
- Ambiguous X-ray findings
- Chest trauma
- Tumor staging
- Intervention
- Follow-up

Pathological sonography findings in the chest wall:

1. Soft tissue
   (a) Accumulation of fluid
      - Hematoma
      - Seroma
      - Lymphatic cyst
      - Abscess

   (b) Tumors
      - Lipoma
      - Fibroma
      - Sarcoma
      - Metastases
      - Invasion by carcinoma

   (c) Lymph nodes
      - Inflammatory lymph nodes
      - Malignant lymphoma
      - Lymph node metastases

2. Bone
   (a) Fractures
      - Ribs
      - Sternum
      - Clavicle
      - Scapula

   (b) Osteolysis—metastases
      - Bronchial carcinoma
      - Breast carcinoma
      - Prostate carcinoma
      - Multiple myeloma
      - Others

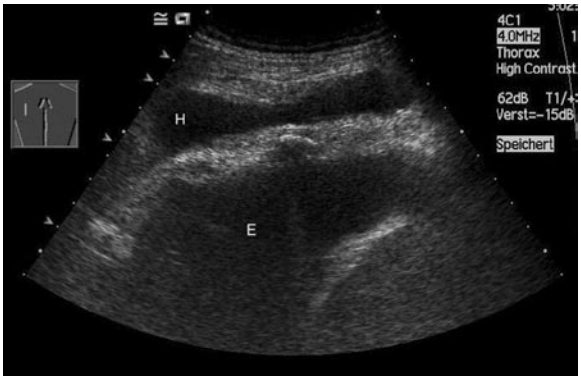

Fig. 2.1 A subcutaneous hematoma after blunt trauma *(H)*. At this site the hematoma is largely anechoic. Pleural fluid *(E)* behind the chest wall—hemothorax

2.1 Soft Tissue

2.1.1 Accumulation of Fluid

2.1.1.1 Hematoma

Depending on the erythrocyte content and the degree of organization—hence also depending on the age of the lesion—hematomas may be accompanied by various echo patterns. They are usually anechoic or hypoechoic (Fig. 2.1). Occasionally one finds fine, hazy central echoes. In rare cases there may be intermediate forms or denser echoes in the central region. Organized hematomas may have very inhomogeneous echoes.

2.1.1.2 Seroma, Lymphatic Cyst

Postoperative seromas are largely anechoic, round or bizarre in shape and have no capsule. Lymphatic cysts are similar in terms of structure, usually round or oval. The occluded lymphatic vessel can be visualized (Fig. 2.2).

2.1.1.3 Abscess

The cellular and protein content of the cavity of an abscess may result in different central structures. The content of

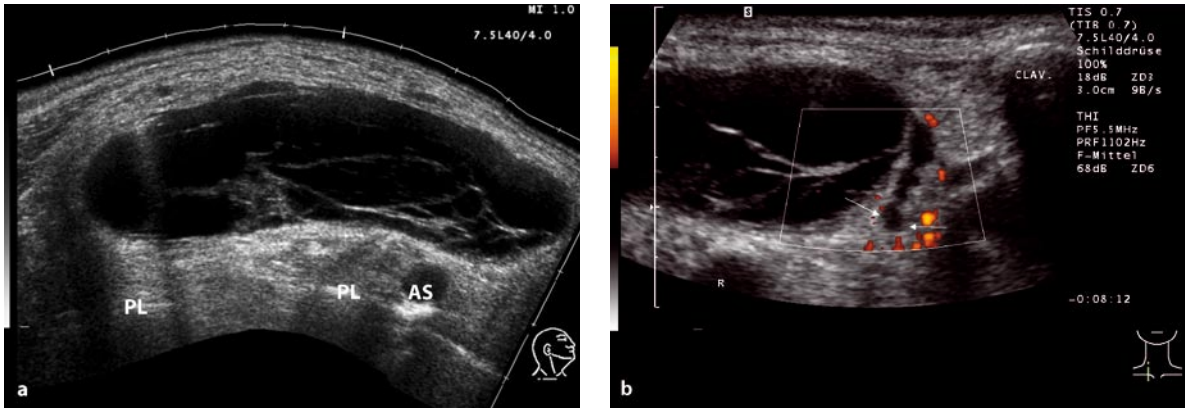

Fig. 2.2 Painful postoperative swelling in the lateral region of the neck on the left side. **a** Sonography reveals an echo-free, chambered space-occupying lesion measuring 10 cm×4 3 cm in size. **b** An occluded lymph tract (*arrows*)

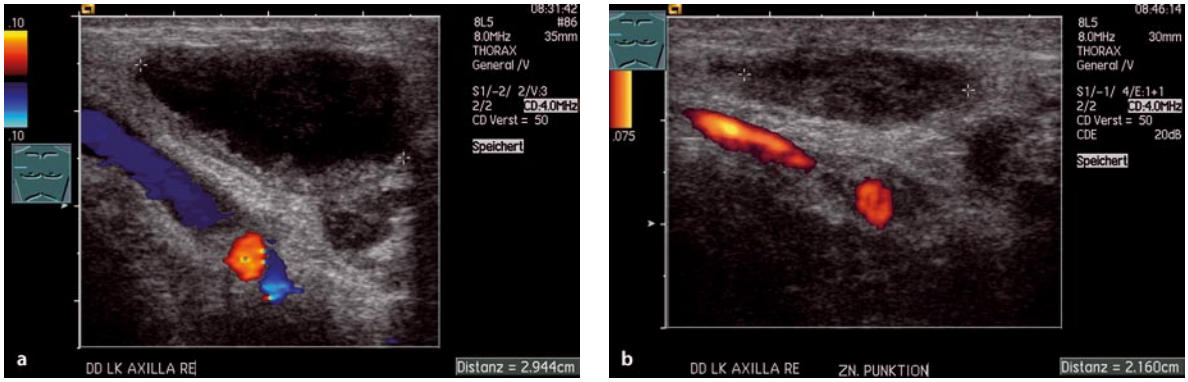

Fig. 2.3 A painful swelling in the region of the right axilla is indicative of a sweat gland abscess. **a** Sonography reveals a largely anechoic space-occupying lesion measuring 3 cm×1.5 cm in size. The moderately echogenic margin is indicative of a starting capsular formation. **b** Sonography-guided aspiration yields pus. The residual fluid is absorbed

abscesses may be similar to that of hematomas. Differentiation may be difficult because intermediate stages such as infected hematomas may be present. Capsular formations of different degrees are an important distinction criterion for abscesses. Floating internal structures may be present (Fig. 2.3).

2.1.2 Tumors

2.1.2.1 Lipoma, Fibroma

The echogenicity of lipomas and fibromas depends on their cellular fat content, their connective tissue content, and impedance differences in interstitial tissue. The sonographic texture may vary from hypoechoic to relatively echodense forms and the lesions may be poorly demar-

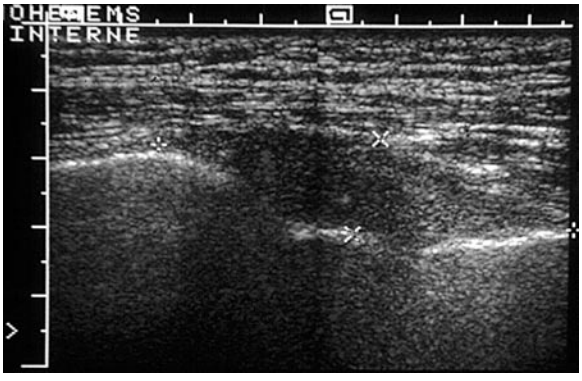

Fig. 2.4 Fibrolipoma in the parietal pleura. The reason for referring the patient was a suspected peripheral lung carcinoma on the chest X-ray. On the basis of the sonographic investigation, the tumor was attributed to pleural gliding of the chest wall and could be demarcated from the lung. The diagnosis was confirmed by sonography-guided biopsy. There has been no change in size for 10 years

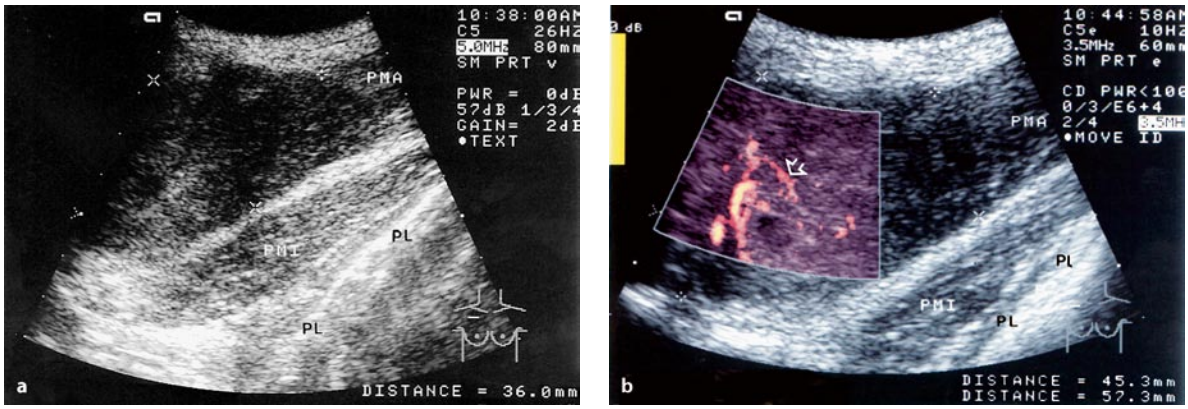

Fig. 2.5 **a** Muscle lymphoma. A 20-year-old man who experienced pain in the chest wall when exercising (bodybuilding). Clinical investigation showed hardening and swelling in the pectoral muscles on the right side. On sonography there was a hypoechoic transformation in the lateral portions of the pectoralis major muscle, which was interpreted as hemorrhage on B-mode sonography. **b.** Evidence of a markedly vascularized lesion on color-Doppler sonography; atypical vessels (corkscrew, fluctuations in diameter, "high-velocity" signals) The surgical biopsy revealed a non-Hodgkin's lymphoma in the pectoral muscle

cated from the surrounding tissue. A capsule may be present (Fig. 2.4).

2.1.2.2 Sarcomas, Soft-Tissue Metastases

Invasive growth is one of the main criteria of a malignant space-occupying lesion. The texture is usually hypoechoic and may be combined with inhomogeneous hyperechoic portions. Color-Doppler sonography may be useful for the assessment of hypoechoic structures suspected of malignancy. The type of vascularization and the course of the vessels may help to confirm a suspected malignant lesion (Fig. 2.5).

Knowledge of the vascularization pattern is also very useful when performing sonography-guided aspiration. At this favorable location close to the transducer, sonography-guided aspiration is a most useful method to obtain histological material and finally to confirm the diagnosis.

2.1.3 Lymph Nodes

Subcutaneous palpable swellings are usually caused by lymph nodes. The sonomorphology of lymph nodes is indicative of their origin and allows cautious assessment of the benign or malignant nature of the lesion when viewed in conjunction with the clinical condition. High-frequency probes yield a differentiated B-mode image. The vascularization pattern on color-Doppler sonography images provides further information about the type of lymph node (Bruneton et al. 1986; Hergan et al. 1994). The possibilities of assessing the benign or malignant nature of a lesion have been definitely improved by better resolution of the B-mode image as well as the use of various Doppler procedures to assess the pattern of vascularization (Chang et al. 1994; Tschammler et al. 1998; Table 2.1).

However, the benign or malignant nature of a lesion should be established with caution on the basis of sonomorphological criteria alone; the final assessment can only be made by histological confirmation of the diagnosis after aspiration or on the basis of disease progression. Changes in sonomorphology are of great significance in clinical practice. Thus, sonography controls may be used to confirm the diagnosis in cases of inflammatory disease and to document the success of therapy in cases of malignant lymph nodes.

2.1.3.1 Inflammatory Lymph Nodes

Inflammatory lymph nodes seldom exceed 20 mm in size. Usually they have smooth margins, are oval, triangular or longitudinal in shape (Fig. 2.6). In cases of lymphadenitis, lymph nodes are typically arranged in a pearl-like fashion along the lymph node sites. In keeping with the anatomy, one frequently finds a more or less marked echogenic central zone which is termed a hilar fat sign, representing fat and connective tissue in the center of the lymph node. This sign is seen particularly during the healing phase of inflammatory processes (Fig. 2.7). The zone that is sharply demarcated from the surrounding tissue is hypoechoic. In this region one frequently finds vessels running a regular course on Doppler ultrasound images. The hilum of the lymph node with its arteries and veins is also visualized.

Table 2.1 Sonomorphology of lymph nodes

	Inflammatory	Malignant lymphoma	Lymph node metastasis
Morphology	Oval, longitudinal	Round, oval	Round
Margin	Smooth	Smooth	Irregular
Demarcation	Sharp	Sharp	Blurred
Growth	Bead-like	Expansive, displacing	Invasive
Mobility	Good	Good, moderate	Poor
Echogenicity	Hypoechoic margin "signs of hilar fat"	Hypoechoic, cystic	Inhomogeneous echoes
Vascularization	Regular, central	Irregular	Corkscrew-like

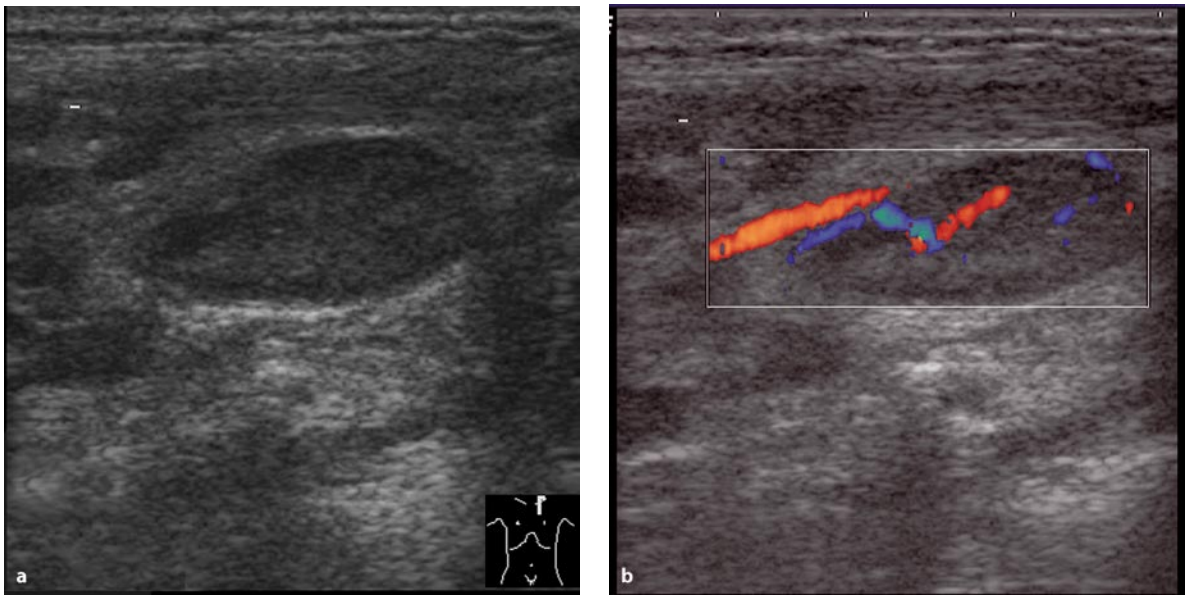

Fig. 2.6 Reactive inflammatory lymph node in the presence of listeriosis. Hypoechoic margin, regular perfusion

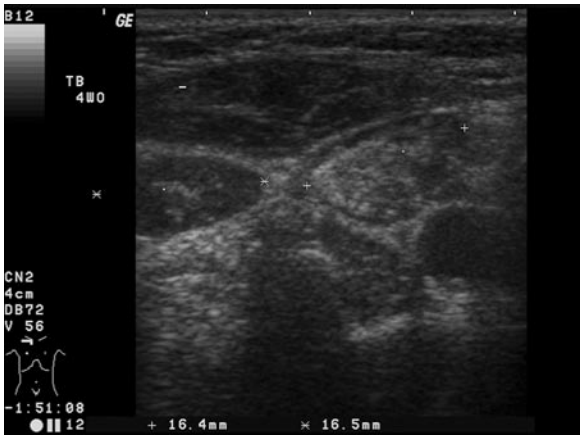

Fig. 2.7 Healing lymph node in the presence of tuberculosis. A narrow hypoechoic margin and a large echogenic center

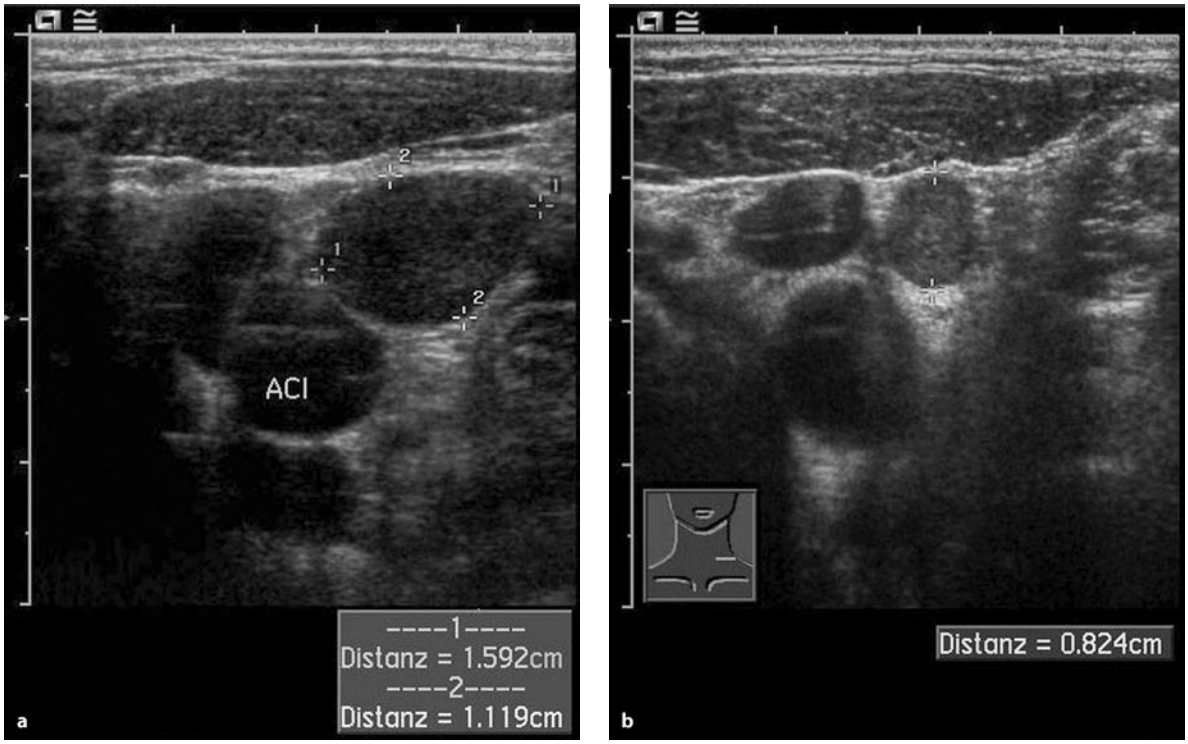

Fig. 2.8 Hodgkin's lymphoma. **a** At the time of diagnosis. **b** After three chemotherapy cycles. Reduced in size by more than 50%, then complete remission

2.1.3.2 Malignant Lymphoma

A homogeneous, hypoechoic lesion with sharp margins is characteristic of malignant lymphoma. Centrocytic and Hodgkin's lymphomas are usually nearly anechoic in terms of structure and look like cysts in such cases. Malignant lymphomas may be round, tightly oval, or very rarely triangular in shape (Figs. 2.8, 2.9). The presence of vessels on both sides (sandwich) is also indicative of a malignant lymphoma. Malignant lymphomas may be strongly vascularized, but the vascularization may be irregular in the margins.

Acutely inflammatory lymph nodes look very similar to malignant lymphoma

2.1.3.3 Lymph Node Metastases

Lymph node metastases appear inhomogeneous on the ultrasound image. Moderately hyperechoic portions are often predominant. The demarcation to the surrounding tissue is usually blurred. Aggressive growth may be manifested as invasion of muscles and vessels (Gritzmann et al. 1990; Fig. 2.10). The size of lymph nodes is an unreliable criterion. However, metastases are more often larger than the maximum size of 20 mm achieved by inflammatory lymph nodes. Morphology is an important criterion. Metastatic lymph nodes tend to be round. One occasionally finds reactive lymph nodes in the vicinity of metastatic ones.

The vascularization pattern of lymph node metastases is typical: vessels are frequently located at the margin, irregularly organized, run a chaotic course, flow in various directions, and tend to change their color (Tschammler et al. 2002).

Nonpalpable lymph nodes can also be visualized; therefore, sonography of the axilla is recommended for preoperative staging and monitoring the progress of breast carcinoma (Bruneton et al. 1984; Hergan et al. 1996; Fig. 2.11).

Currently, sonography is routinely demanded for staging a bronchial carcinoma because it is markedly superior to computed tomography in showing lymph node metastases in the supraclavicular groove (N3) and invasion of the chest wall (Suzuki et al. 1993). Nonpalpable lymph nodes are frequently discovered by this procedure (Fultz et al. 2002; van Overhagen et al. 2004). The cervical

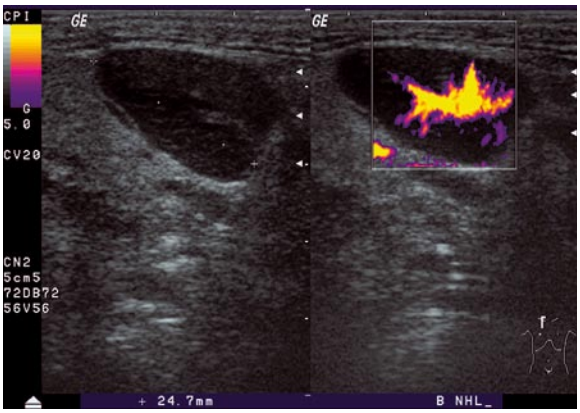

Fig. 2.9 B-cell chronic lymphocytic leukemia : hypoechoic lymph node with minimal hilar signs; strong and somewhat irregular vascularization

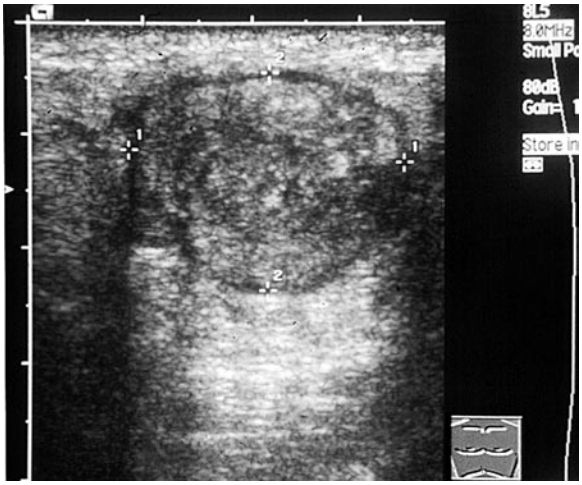

Fig. 2.10 Lymph node metastasis of an epidermoid lung carcinoma. Invasive growth into the vicinity. On palpation the mobility of the lesion was markedly reduced. The affected lymph node itself is characterized by inhomogeneous echoes, is onion-shaped in terms of structure, and invades its surroundings.

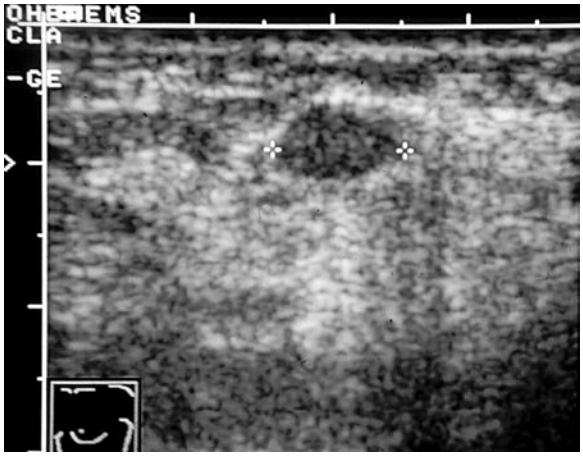

Fig 2.11 Nonpalpable axillary lymph node metastasis measuring 7 mm in size, in the presence of breast carcinoma

lymph nodes must be searched for because their presence indicates stage M1 disease.

Lymph node metastases are good parameters to monitor therapy. If the patient responds to chemotherapy or radiotherapy, reactive lymph nodes may persist (Fig. 2.12).

2.2 The Bony Chest

2.2.1 Fractures of the Ribs and the Sternum

Radiological diagnosis of the chest may prove difficult; nondislocated fractures are frequently not seen. Lesions in the ribs and the sternum can be visualized well by sonography (Fenkl et al. 1992; Dubs-Kunz 1992; Bitschnau et al. 1997; Table 2.2). The fracture gap, dislocation and bone fragments are directly visualized. Soft-tissue hematoma, fluid in the pleura and lung contusions are also seen (Wüstner et al. 2005).

The following procedure proved its worth in clinical practice: The patient points to the site of maximum pain. This area is investigated. Quite often a fracture can be diagnosed immediately at this site

If the fracture gap is larger than the lateral resolution capacity of the ultrasound device, the gap is directly accessible to ultrasound diagnosis—which is usually the case. A nondislocated fracture can also be identified indirectly by reverberation echoes—the so-called chimney phenomenon. These reverberation artifacts occur at the

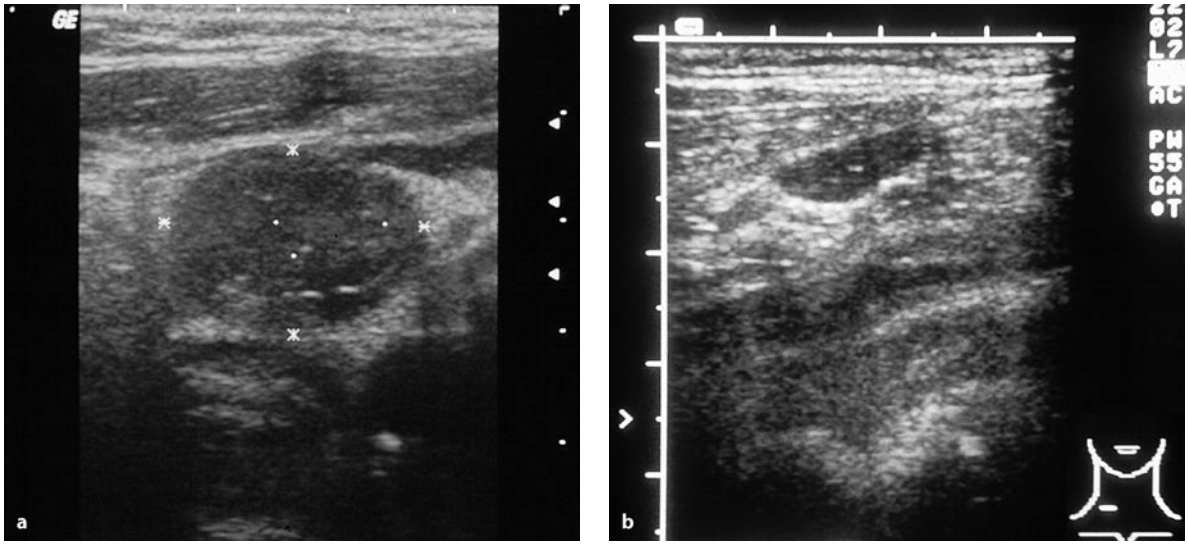

Fig. 2.12 **a** Cervical lymph node metastasis of a large-cell carcinoma of the lung. **b** After two cycles of chemotherapy this lymph node metastasis had resolved and now looks like a reactive lymph node

Table 2.2 Sonography criteria for fractures of the ribs and the sternum

Direct signs	Concomitant indirect signs
At the site of pain	Hematoma
Cortical gap	Reverberation echoes/ "chimney phenomenon"
Step in cortical bone	Pleural effusion
Dislocation	Pneumothorax
	Lung contusion lesions

margins of the fracture fragments and extend vertically in depth. In the absence of dislocation, the chimney phenomenon can be triggered by gentle pressure on the site of pain. Fractures in the rib and the sternum are characterized by the same sonomorphology. The criteria are direct evidence of a cortical gap or a cortical step (Fig. 2.13), and are indirect evidence of a local hematoma, a chimney phenomenon or an accompanying pleural effusion (Fig. 2.14).

Knowledge of the anatomy and anatomical variants is the most important requirement for assessment of the sternum. Thus, the usually discreet interruption of cortical bone in the region of synchondrosis between the corpus and the manubrium of the sternum should not be mistaken for a fracture. Besides, various possibilities of incorrect fusion of bones, which may occur in rare cases, should be taken into account (Fig. 2.15).

When monitoring the progression of disease one first finds a local hematoma as a hypoechoic/anechoic margin in the region of the fracture gap. Subsequent callus formation is marked by initial organization of the structure and thickening. The starting calcification causes fine acoustic shadows and may extend to complete ossification. Once ossification has occurred, one may find just a protrusion of the continuous, marked cortical reflex (Fig. 2.16). Healing disorders also can be easily identified by the absence of continuous ossification. Thickening starts from the third or fourth week after trauma. Complete restitution is usually achieved after a few months (Friedrich and Volkenstein 1994; Riebel and Nasir 1995).

Several studies have confirmed that chest sonography is a useful procedure in traumatology (Leitgeb et al. 1990; Mariacher Gehler and Michel 1994). As an adjunct to conventional X-rays, sonography provides significant additional information (Griffith et al. 1999). In a nonselected patient population with suspected rib fractures, sonography demonstrated twice as many fractures as did chest X-rays, including a targeted X-ray (Bitschnau et al. 1997). Sonography was particularly useful to assess the ventral region. In cases of rib fractures in conjunction with a fracture of the clavicle, however, conventional X-rays were superior.

For the patient it is very important to establish whether he/she has a chest contusion or a fracture because the two conditions have different consequences for his/her ability to work. In cases of severe chest trauma, the extent of an accompanying pleural effusion or hema-

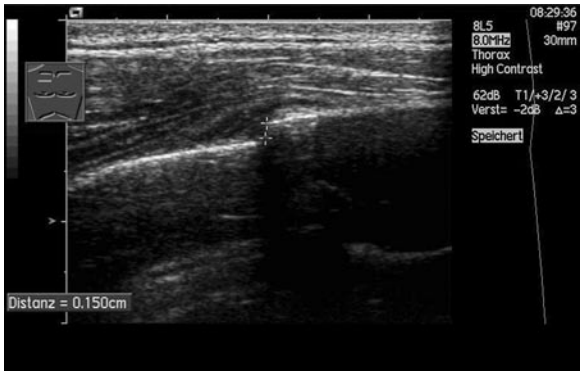

Fig. 2.13 Rib fracture with a step of 1.5 mm. This fracture could not be seen on X-rays. No accompanying hematoma above the fracture site

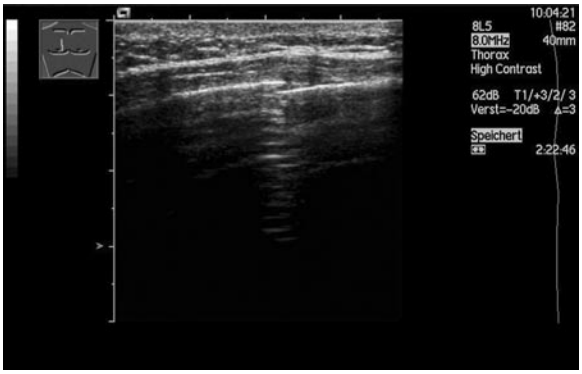

Fig. 2.14 Rib fracture with reverberation echoes, the "chimney phenomenon." In the absence of dislocation this phenomenon can be provoked by gentle pressure on the site of pain

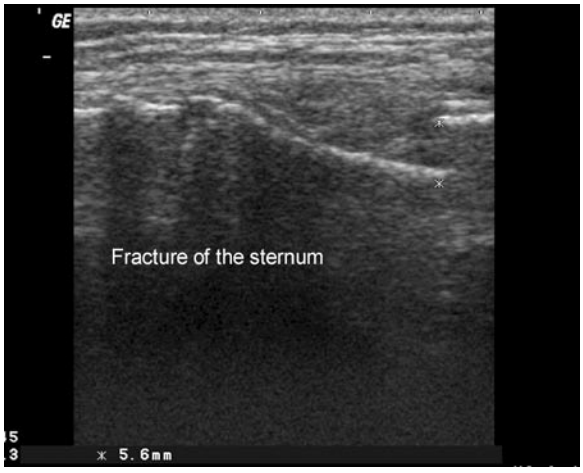

Fig. 2.15 *Right*: Fracture of the sternum after a rear-end collision (+ - +). *Left*: the uneven surface at the synchondrosis of the manubrium

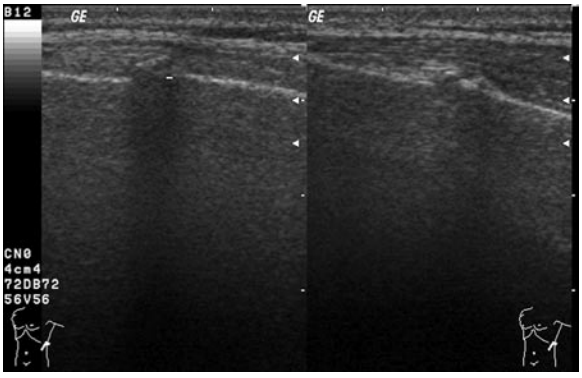

Fig. 2.16 Ten-week-old rib fracture. Recalcified uneven protrusion at the previous fracture site

toma or lung contusion (Figs. 2.17, 2.18) can be rapidly and accurately estimated by sonography. Thus, the use of sonography is very meaningful in the emergency setting (Walz and Muhr 1990; Wischofer et al. 1995; Wüstner et al. 2005).

2.2.2 Osteolysis

Osteolyses are usually metastases and are characterized by an interrupted and destroyed cortical reflex with pathological echo transmission (Fig. 2.19). Osteolytic metastases are usually seen as well-demarcated round or oval space-occupying lesions with a partly hypoechoic and a partly rough echo structure. Color-coded duplex sonography reveals corkscrew-like neoformation of vessels (Fig. 2.20).

Sonography-guided aspiration is the procedure to be used if the clinician wishes to make a histological diagnosis of the osteolysis because osteolyses are located close to the transducer head—in a very favorable location for sonographic diagnosis. During ongoing therapy, osteolyses may serve as monitoring parameters for the bony chest in the presence of diseases such as multiple myeloma (Figs. 2.21), small-cell bronchial carcinoma (Fig. 2.22), prostate carcinoma or breast carcinoma. Any increase or decrease in size and any change in the sonomorphological internal structure can be compared and documented. Recalcification under therapy is seen earlier than it is on X-rays.

A peripheral bronchial carcinoma invading the chest wall (Pancoast's tumor) is better assessed by sonography than by computed tomography; the same is true for invasion of the subclavian vessels (Szuzuki et al. 1993; Fig. 2.23).

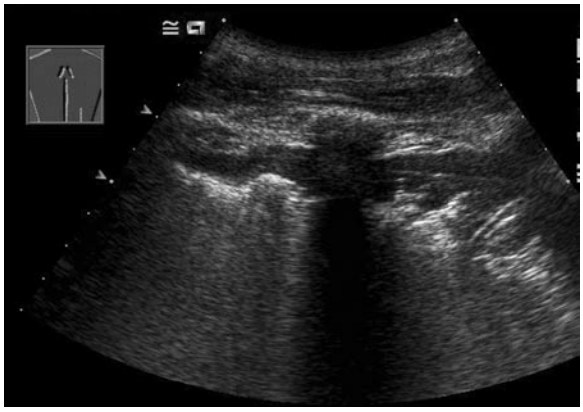

Fig. 2.17 Lung contusion: plate formed supleural lung consolidation

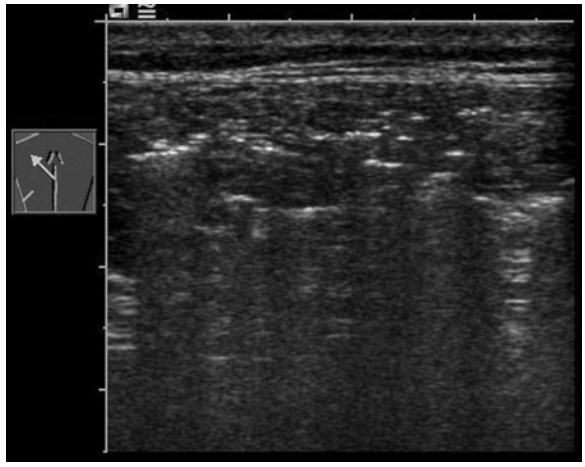

Fig. 2.18 Emphysema of the skin. Numerous subcutaneous air reflections greatly impair the image in terms of depth. The chest wall is not seen

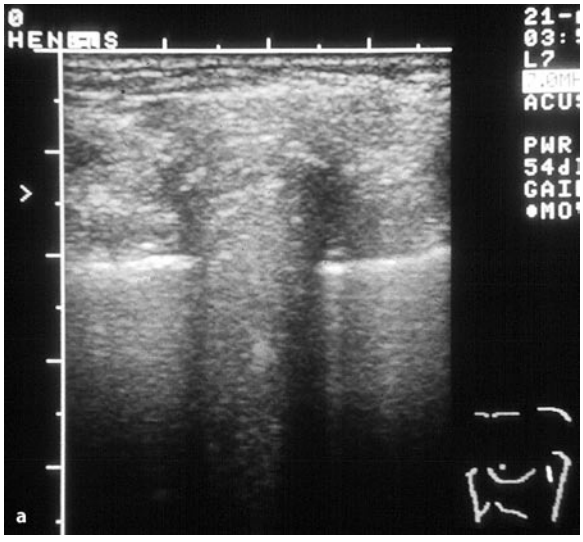

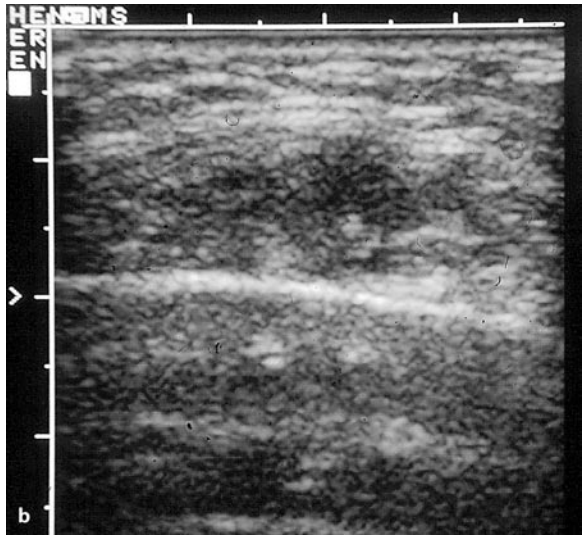

Fig. 2.19 **a** Cross section of an osteolytic rib metastasis in the presence of a pleuropulmonary adenocarcinoma. **b** Longitudinal section of the metastasis. The rib is raised, the cortical reflex largely destroyed, the echotexture of the metastasis is inhomogeneous. The pathological echo transmission also allows the pleura to be visualized

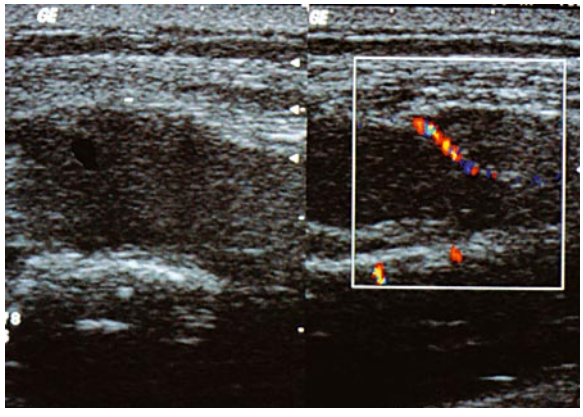

Fig. 2.20 A highly malignant non-Hodgkin's lymphoma invading the ribs, with pathological neoformation of vessels on color-Doppler sonography. The diagnosis was established by sonography-guided aspiration

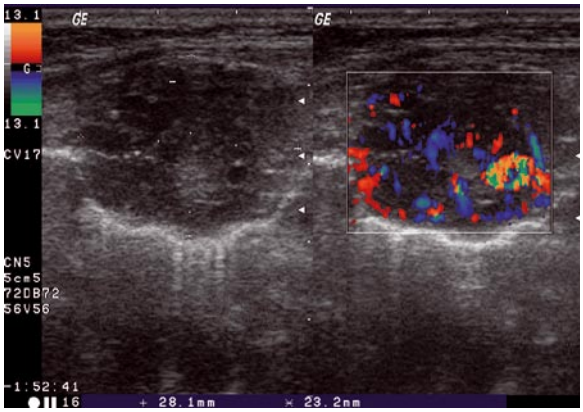

Fig. 2.21 Multiple myeloma with typically strong vascularization. The diagnosis was established by sonography-guided biopsy

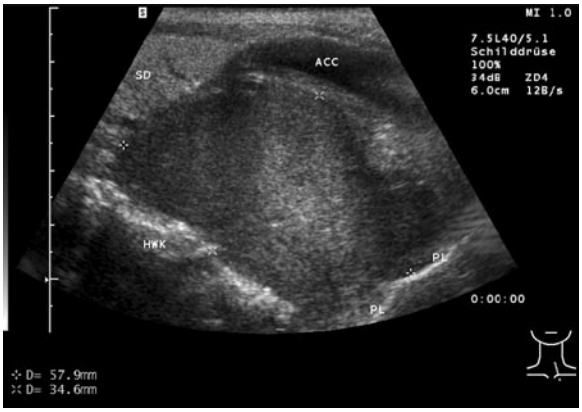

Fig. 2.22 Lung carcinoma growing into the upper aperture of the thorax. *ACC* a. carotis communis

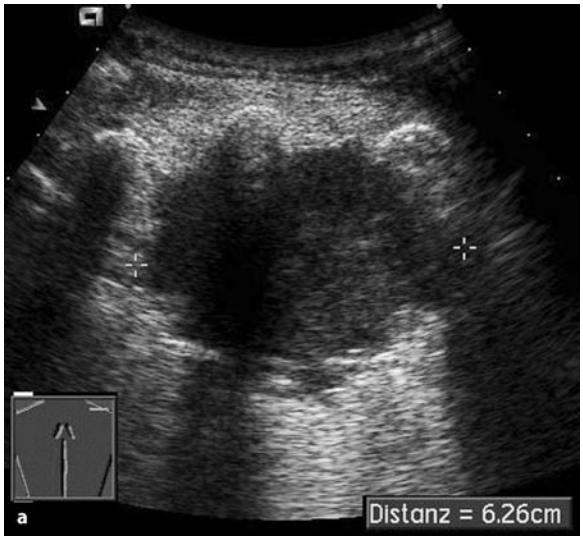

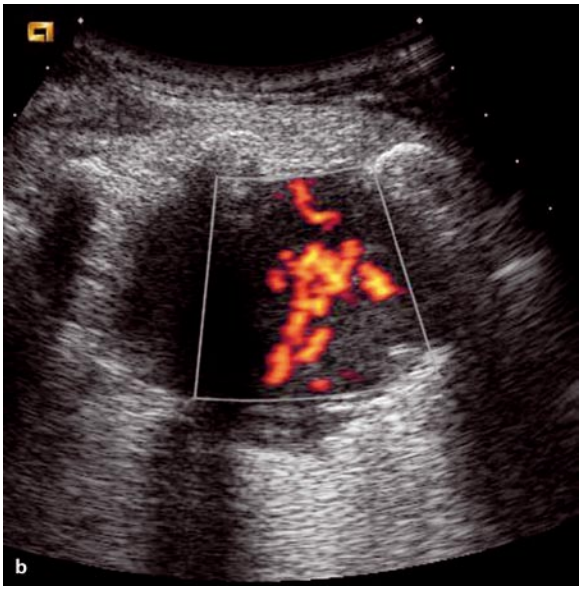

Fig. 2.23 **a** Epidermoid carcinoma at the right apex of the lung, in dorsal location, invading the chest wall. **b** Irregular vascularization pattern—vascular inferno

2.3 Summary

Visualization of lymph nodes and cautious assessment of the malignant or benign nature of a lesion is an important indication for sonography of the chest wall. All ambiguous lesions in the chest wall are well accessible to sonography-guided aspiration for histological confirmation of the diagnosis, if such confirmation is required for therapy. The risk of aspiration is very low owing to the favorable location of the lesions. Once malignancy has been proven, the progression of chest wall lesions under therapy can be monitored.

Fractures of the ribs as well as the sternum can be visualized well by sonography. Fracture diagnosis by sonography is not only much more sensitive than with conventional X-rays but also allows accompanying soft-tissue lesions, hematomas and pleural effusions to be detected rapidly and reliably.

References

Bitschnau R, Gehmacher O, Kopf A, Scheier M, Mathis G (1997) Ultraschalldiagnostik von Rippen- und Sternumfrakturen. Ultraschall Med 18:158–161

Bruneton JN, Caramella E, Aubanel D, Hery M, Ettore F, Boublil JL, Picard L (1984) Ultrasound versus clinical examination for axillary lymph node involvement in breast cancer. Ultrasound 153:297

Bruneton JN, Caramella E, Hery M, Aubanel D, Manzino JJ, Picard L (1986) Axillary lymph node metastases in breast cancer: preoperative detection with US. Radiology 158:325–326

Chang DB, Yuan A, Yu CJ, Luh KT, Kuo SH, Yang PC (1994) Differentiation of benign and malinant cervical lymph nodes with color doppler sonography. AJR Am J Roentgenol 162:965–968

Dubs-Kunz B (1992) Sonographische Diagnostik von Rippenfrakturen. In: Anderegg A, Despland P, Henner H, Otto R (eds) Ultraschalldiagnostik '91. Springer, Berlin, pp 268–273

Dubs-Kunz B (1996) Sonography of the chest wall. Eur J Ultrasound 3:103–111

Fenkl R, v Garrel T, Knappler H (1992) Diagnostik der Sternumfraktur mit Ultraschall—eine Vergleichsstudie zwischen Radiologie und Ultraschall. In: Anderegg A, Despland P, Henner H, Otto R (eds) Ultraschalldiagnostik '91 Springer, Berlin, pp 274–279

Friedrich RE, Volkenstein RJ (1994) Diagnose und Repositionskontrolle von Jochbogenfrakturen. Ultraschall Med 15:213–216

Fultz PJ, Feins RH et al (2002) Detection and diagnosis of nonpalpable supraclavicular lymph nodes in lung cancer at CT and US. Radiology 222:245–251

Griffith JF, Rainer TH, Ching AS, Law KL, Cocks RA, Metreweli C (1999) Sonography compared with radiography in revealing acute rib fracture. AJR Am J Roentgenol 173:1603–1609

Gritzmann N, Grasl MC, Helmer M, Steiner E (1990) Invasion of the carotid artery and jugular vein by lymph node metastases: detection with sonography. AJR Am J Roentgenol 154:411–414

Hergan K, Amann T, Oser W (1994) Sonopathologie der Axilla: Teil II. Ultraschall Med 15:11–19

Hergan K, Haid A, Zimmermann G, Oser W (1996) Preoperative axillary sonography in breast cancer: value of the method when done routinely. Ultraschall Med 17:14–17

Leitgeb N, Bodenteich A, Schweighofer F, Fellinger M (1990) Sonographische Frakturdiagnostik. Ultraschall Med 11:206–209

Mariacher Gehler S, Michel BA (1994) Sonography: a simple way to visualize rib fractures (letter). AJR Am J Roentgenol 163:1268

Mathis G (1997) Thoraxsonography—Part I: chest wall and pleura. Ultrasound Med Biol 23:1141–1153

Riebel T, Nasir R (1995) Sonographie geburtstraumatischer Extremitätenläsionen. Ultraschall Med 16:196–199

Sakai F, Sone S, Kiyono K et al (1990) High resolution ultrasound of the chest wall. Fortschr Röntgenstr 153:390–394

Suzuki N, Saitoh T, Kitamura S (1993) Tumor invasion of the chest wall in lung cancer: diagnosis with US. Radiology 187:39–42

Tschammler A, Ott G, Schang T, Seelbach-Goebel B, Schwager K, Hahn D (1998) Lymphadenopathy: differentiation of benign from malignant disease—color Doppler US assessment of intranodal angioarchitecture. Radiology 208:117-–123

Tschammler A, Beer M, Hahn D (2002) Differential diangosis of lymphadenopathy: power Doppler vs color Doppler sonography. Eur Radiol 12:1794–1799

van Overhagen H et al (2004) Metastases in supraclavicular lymph nodes in lung cancer: assessment with palpation, US and CT: Radiology 232:75–80

Walz M, Muhr G (1990) Sonographische Diagnostik beim stumpfen Thoraxtrauma. Unfallchirurg 93:359–363

Wischofer E, Fenkl R, Blum R (1995) Sonographischer Nachweis von Rippenfrakturen zur Sicherung der Frakturdiagnostik. Unfallchirurg 98:296–300

Wüstner A, Gehmacher O, Hämmerle S Schenkenbach C, Häfele H, Mathis G (2005) Ultraschalldiagnostik beim stumpfen Thoraxtrauma. Ultraschall Med 26:285–290

3 The Pleura

J. Reuss

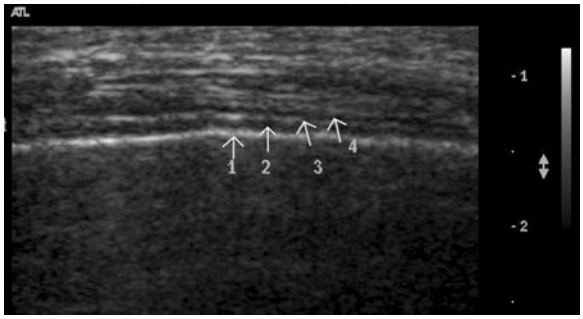

Fig. 3.1 Chest wall with normal smooth visceral pleura (*arrow 1*). On the outside, the echo-poor pleural gap (*arrow 2*) and then the echogenic (echo-rich) parietal pleura (*arrow 3*). The extra pleural fatty lamella varies in strength. The seemingly thicker visceral pleura is actually an artifact due to reflection of the air-containing lung

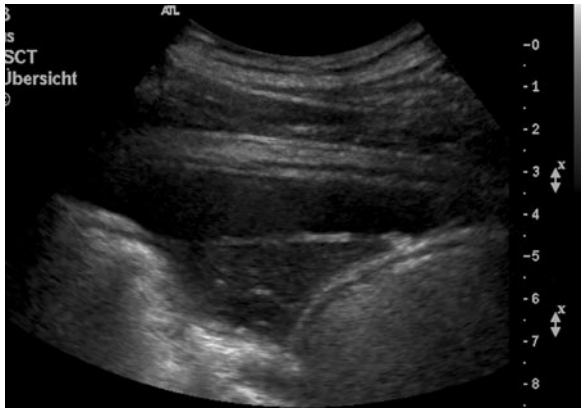

Fig. 3.2 Subpleural infiltration in a patient with a pulmonary embolism and plural effusion; hence, the visceral pleura is distinguishable from the total reflection of the air in the lung. The visceral and parietal pleurae are shown with the same strength and density

Besides the chest wall, the pleura is the thoracic structure which can be reached most easily and best depicted sonographically. With the appropriate examination method, the whole costal and diaphragmatic pleura can be visualized. The visceral pleura, which is hidden behind the ribs, can be shifted to the intercostal space by means of breathing maneuvers. From the jugular direction, the upper, forward mediastinum with its parts of the pleura can be captured. The lower, rear mediastinal and paravertebral sections of the pleura are not usually not discernible on transthoracic sonography. According to estimates based on transverse sections of the thorax using computed tomography, at least 60–70% of the pleura surface can be visualized sonographically (Reuss 1996). Most diseases of the pleura affect the costal and diaphragmatic pleural segments. The value of color duplex sonography of the pleura, however, has not been systematically evaluated, but it is helpful in differentiating tumor-like lesions and infiltrations, especially in the thoracic wall and in the lung. Color duplex sonography, spectral Doppler sonography and contrast-enhanced sonography have gained a position of importance in the differential diagnosis of space-occupying lesions at the level of the pleura. Light, efficient and portable sonography apparatuses in emergency situations and at the intensive care unit show a high concurrence rate of up to 89% with high-end devices, not only for investigations of the abdomen and the retroperitoneum but also for the pleura (Ziegler et al. 2004).

3.1 Normal Pleura

The normal pleura is only 0.2–0.4 mm thick and hence at the resolution limits of even modern ultrasound systems (Bittner et al. 1995). Due to the different acoustic impedance at the interface of the pleural sheets, a depiction is nonetheless sonographically feasible. The parietal pleura shows as a fine echogenic line, the pleural cavity as an echo-free to highly hypoechogenic parallel band (Börner et al. 1987). At this level the healthy lung is also seen to glide during breathing. The actual thickness of the pleural sheets is exaggerated in that process.

The essentially finer visceral pleura is submerged in the thick line of total reflection of the ultrasound at the air-filled lung (Fig. 3.1). As soon as the peripheral lung—due to a pathological process—is free of air, the actual visceral pleura can be marked-off as a fine echogenic line (Fig. 3.2).

In day-to-day ultrasound practice, the described line of total reflection is know as the visceral pleura. In an ultrasound-anatomy study it becomes evident that the hypoechoic layer outside the parietal pleura, which may differ to an individual degree, corresponds to the extrapleural lamella of fat (Reuß et al. 2002). With the help of high-resolution transducers, on sonographic investigation the line of the parietal pleura can, in fact, be divided into two layers. In terms of preparatory anatomy and histology the two layers are the parietal pleura and the external endothoracic fascia (Fig. 3.3).

Comet-tail artifacts are believed to result from reverberation between the visceral pleura and air in the superficial alveoles of the lung. Therefore, comet-tail artifacts also move in conjunction with the lung and in dependence of breathing. They are rarely seen in the normal pleura (Fig. 3.4). A large collection of these—also termed aurora signs in the published literature—are indicative of subpleural parenchymatous changes such as those occurring in the presence of interstitial lung disease. However,

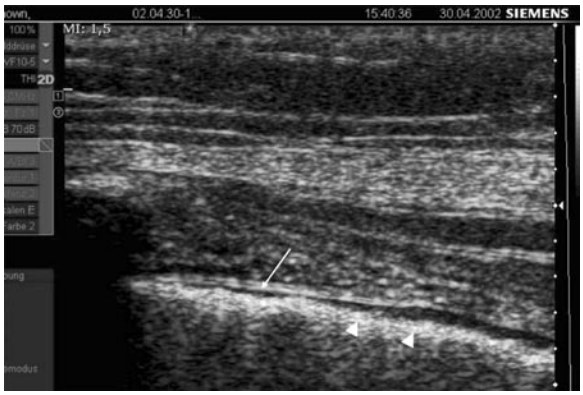

Fig. 3.3 Clearly recognizable double contour in the area of the parietal pleura (*arrow*), corresponding with the actual parietal pleura and endothoracic fascia. Note the disproportionally thick visceral pleura (*arrowheads*) due to artifact

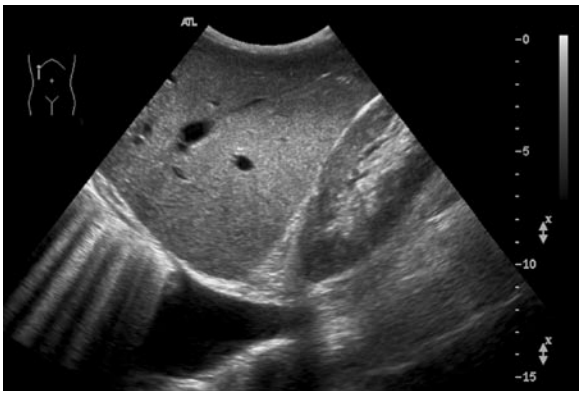

Fig. 3.4 Numerous comet-trail artifacts on the diaphragmatic pleura. Given the existing pleural effusion, the comet-trail artifacts are likely due to a partial collapse of the lung and not an expression of an interstitial parenchymal pathology of the lung

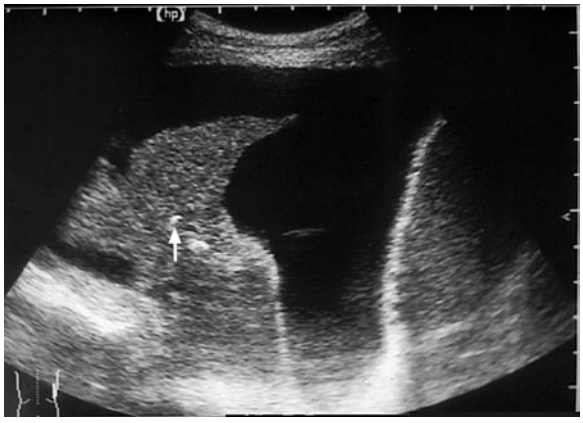

Fig. 3.5 Large, almost echo-free pleural effusion. The echoes in the depth are artifacts. Compressed lung with only a small volume of residual air in the central bronchi (*arrow*)

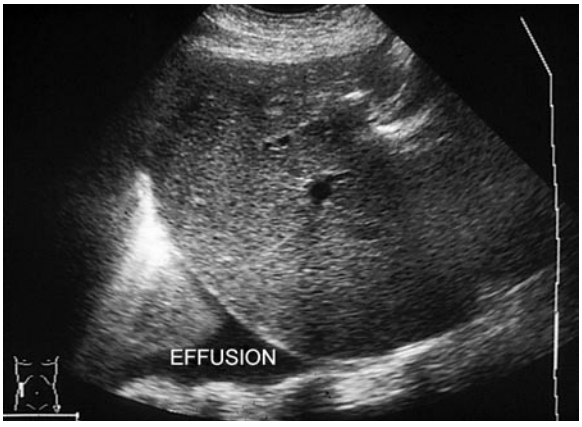

Fig. 3.6 Small dorsal pleural effusion between spine and diaphragm in a transhepatic view

the environment also appears to influence the occurrence of the aurora sign. When viewing the basal pleura by the transhepatic access through a fatty liver, this phenomenon is more rare than during investigation through a normal liver, independent of the otherwise confirmed underlying lung disease (Kohzaki et al. 2003). In cases of interstitial lung disease the visceral pleural appears markedly more irregular, partly waved or serrated, and thicker than the marking caused by artifacts.

The respiratory shift of the lung against the parietal pleura can be observed easily, even without comet-tail artifacts. The respiratory movement of the lung is greatest dorsolateral and caudal. Patients suffering from asthma or emphysema display, even under normal conditions, minimal respiratory lung movement only. The absence of respiratory shift is a diagnostic sign of inflammatory or tumorous adhesions of the pleura. Due to interposed air, no respiratory shift in the case of pneumothorax can be seen. Sonography, being a real-time application, again has a major advantage over other imaging modalities.

3.2 Pleural Effusion

Although pleural effusions could be observed very early on with B-image sonography, chest radiography is still the main method of choice for establishing the presence of or following up pleural effusions (Joyner et al. 1967). At least in order to control pleural effusions, sonography should be used as the method of choice today. In fact, sonography is now used as a diagnostic measure to clarify pleural

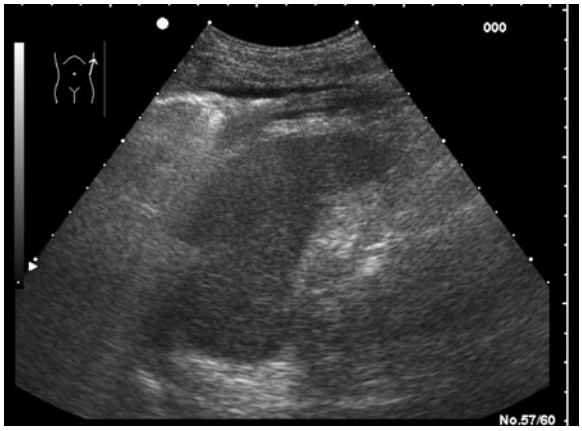

Fig. 3.7 Very small, stripe-like postoperative pleural effusion in the rib-diaphragm angle. The distortion of the area of effusion during a dynamic examination contraindicates circumscribed pleural thickening

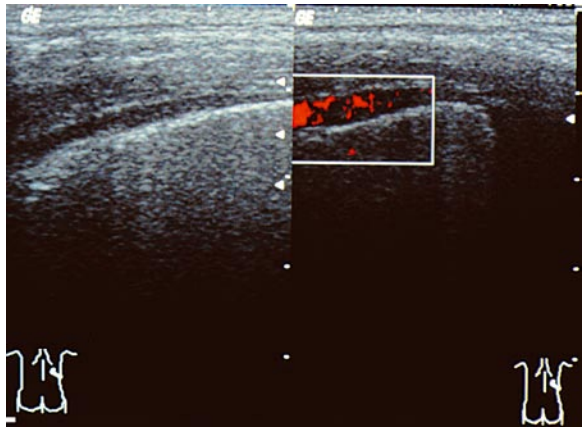

Fig. 3.8 Small effusion in the costophrenic angle. The color Doppler signals in the effusion originate from the pulse- and respiration-synchronous shifting of the fluid and characterize the not completely echo-free formation as an effusion

effusions and also is a fixed element of guidelines issued by pneumological societies (Maskell and Butland 2003).

Pleural effusions are echo-free since they are liquid formations. The pleura sharply delineates the effusions (Fig. 3.5). Large effusions can be verified easily by ultrasound, whereas smaller effusions between the chest wall and diaphragm or parallel to the pleura in the delimitation to the hypoechogenic swelling of the pleura are hard to distinguish (Fig. 3.6, Fig. 3.7).

The effusion is echo-free, displays a change of form during breathing and sometimes septa or floating echoes occur. Additionally, a color Doppler signal can be caused by the shifting of liquid in the effusion synchronous with respiration (Fig. 3.8). One study showed that 10% of false positive results could be corrected and the specificity of sonographic verification of small effusions rose from 68 to 100% due to the use of this color Doppler signal in addition to the B-mode examination (Wu et al. 1994). There are no false positive results for medium or large effusions, since atelectases, a raised diaphragm, tumors, or pleural fibrosis are sonographically unmistakable, whereas they are unclearly delineated on X-ray. The sonographic exclusion of pleural effusions is possible, with the exception of effusions captured in the interlobar space (Fig. 3.9).

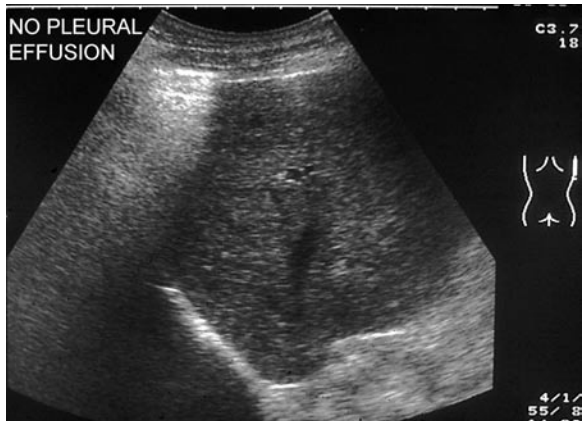

Fig. 3.9 No fluid between liver and lung, thus excluding a free-floating effusion. To exclude an effusion in the pleura altogether, the entire pleura must be examined

3.2.1 Detection Limit

On average, a minimum of 150 ml of pleural effusion is required to enable detection on standard X-ray with the patient in a standing position (Collins et al. 1972). Sonography is far more reliable at verifying pleural effusions (sensitivity 100%; specificity 99.7%) than conventional X-ray of the thorax with the patient in a standing position (sensitivity 71%; specificity 98.5%) (Goecke and Schwerk 1990). Effusions of as little as 5 ml can be identified without problem sonographically laterodorsal in the angle between the chest wall and the diaphragm with patients in either a standing or sitting position (Gryminski et al. 1976). In fact, physiological quantities of fluid in healthy individuals and the minimally increased quantity of fluid in pregnant women can be identified by sonography with the patient lying on the side and supporting himself/herself with the elbow. Thus, evidence of these infinitesimal quantities of fluid does not permit the investigator to conclude the presence of pleural disease (Kocijancic et al. 2004, 2005).

By turning the supine patient slightly sidewards, small dorsal effusions can also be identified. The examination can be carried out at the bedside and repeated anytime for follow-up purposes. Using X-ray, effusions

Table 3.1 Evidence of pleural effusions on chest X-ray in supine patients. Of 110 single examinations on 50 patients, effusions were correctly identified sonographically in every case. (From Kelbel et al. 1990)

Pleural effusion	Right	Left	Both sides
Correct evidence	Sensitivity 47% Specificity 71%	Sensitivity 55% Specificity 93%	Sensitivity 38%
Correct volumes	57%	24%	
Volume < 200 ml	Sensitivity 23%	Sensitivity 30%	
Volume > 500 ml	Sensitivity 83%	Sensitivity 73%	
Additionla atelectases	Sensitivity 7%	Sensitivity 13,5%	

Table 3.2 Formulae to estimate the volume of pleural effusions

Formula	Publication
LSF (cm^2) × U (cm) × 0,89 = E (ml)	Lorenz et al. 1988
QSF (cm^2) × H (cm) × 0,66 = E (ml)	Kelbel et al. 1990
LH (cm) × 90 = E (ml), correlation coefficient r = 0,87	Goecke und Schwerk 1990
LH (cm^2) + SH (cm) × 70 = E (ml), correlation coefficient r = 0,87	Goecke und Schwerk 1990
D (mm) × 47,6–837 = E (ml)	Eibenberger et al. 1994

D, thickness of effusion layer, supine position; *E*, effusion volume empirical factors; *H*, effusion height; *LH*, lateral height of effusion, sitting position; *LSF*, median of planes of longitudinal sections through the effusion in six positions; *QSF*, horizontal plane through the effusion; *SH*, median subpulmonary height of effusion, sitting position; *U*, circumference of the hemithorax

can be verified in only half the number of patients in a supine position. Even large effusions on both sides and leaking dorsally cannot be recognized (Table 3.1). Effusion and atelectasis cannot be distinguished from one another radiologically, often leading to an overestimation of the volume of effusion shown on X-ray (Kelbel et al. 1990). Investigations in ventilated ARDS patients show that, compared to computed tomography, an accompanying pleural effusion was identified by auscultation in 61% of cases, on chest X-ray in supine position in 47% of cases, and on ultrasound in 93% of cases (Lichtenstein et al. 2004).

3.2.2 Volume Estimation

Sonographic methods to estimate the volume of pleural effusion differ in terms of their accuracy and practicability. For practical purposes, the method published by Goecke and Schwerk (1990) is easy to perform and saves time (Table 3.2).

An estimated result differing by less than 10% of the actual volume can be achieved by multiplying the median planes of longitudinal sections in six positions from parasternal to paravertebral with the determined circumference of the hemithorax and the empirical factor of 0.89 (Lorenz et al. 1988).

Another method, which achieves a good correlation of measured data and actual volume of the effusion, is to multiply the cross plane, determined planimetrically, with the maximum height of the effusion and the empirical factor 0.66 (Fig. 3.10, Fig. 3.11; Kelbel et al. 1990).

In addition, the volume of a pleural effusion has been estimated using multiple empirical formulas including the lateral height of the effusion, the subpulmonary height of the effusion, or the thickness of the mantle of the effusion around the lungs.

An easy to perform method which is also adequate for general purposes measures the lateral height of the effusion at the chest wall. The determined value in centimeters, multiplied by the empirical factor 90 amounts to the effusion volume in milliliters (r = 0.68). Small ef-

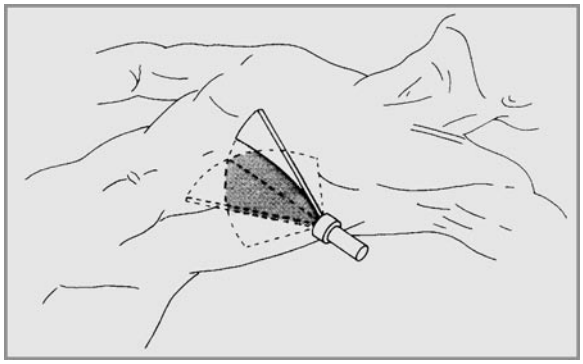

Fig. 3.10 An estimation of the volume of pleural effusions in the supine patient. (From Börner et al. 1987)

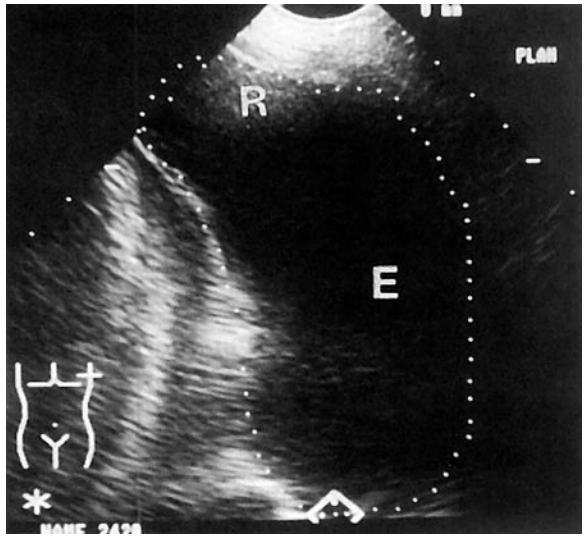

Fig. 3.11 An example of effusion planimetry. The cardiac effusion in a supine, intensive-care patient can be well estimated, followed up and documented. *E*, effusion; *N*, noise artifacts

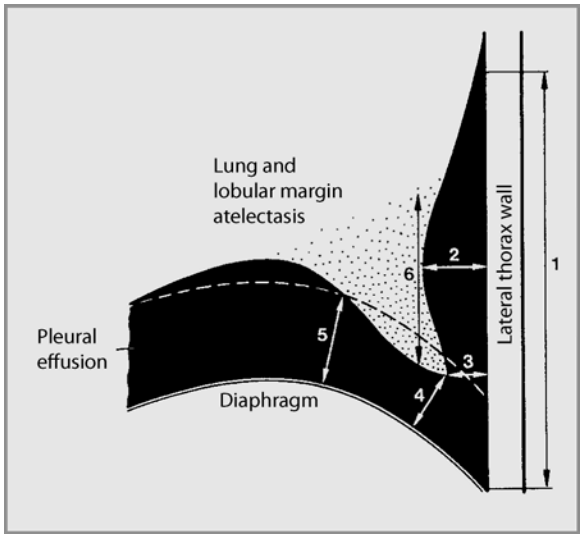

Fig. 3.12 Pleural effusion volumetry in sitting patients. Useful parameters include the maximal extent of effusion (*1*), the basal distance between lung and diaphragm (*4*), and the subpulmonary effusion height (*5*). The thickness of the lateral mantle of the effusion (*2*), the distance between the basal lung atelectasis and the chest wall (*3*), and the height of the basal atelectasis (*6*) are not suitable parameters for estimation of the volume of effusion. (From Goecke and Schwerk 1990)

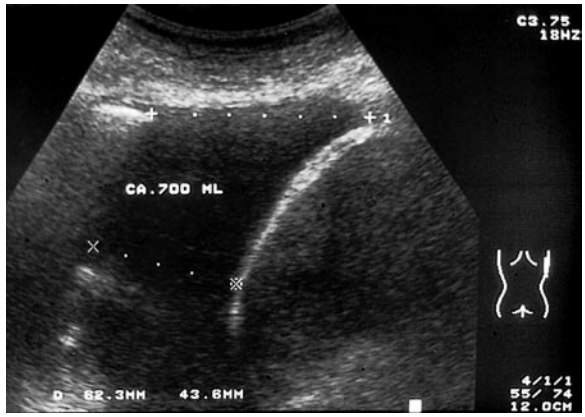

Fig. 3.13 A simple estimation of effusion volume by measuring the height of the subpulmonary effusion and the maximum height. Estimated volume 700 ml, actual volume 800 ml. (From Goecke and Schwerk 1990)

fusions will be overestimated using this approximation formula. The total of the basal lung-diaphragm distance and the lateral height of the effusion multiplied by 70 will result in more precise estimates (r = 0.87; Fig. 3.12, Fig. 3.13; Goecke and Schwerk 1990).

The estimation of the volume of a pleural effusion based on sonography is more precise than the estimation based on radiology. In a study, the radiological volume estimation—compared to the sonographic one—was correct in 57% of cases concerning the right hemithorax and correct in only 24% of cases concerning the left hemithorax (Kelbel et al. 1990). The sonographic volume estimation correlates closer with the actual punctured volume than the radiological method (r = 0.80 vs. r = 0.58, $p < 0.05$; Eibenberger et al. 1994).

In the supine patient, the sonographic measurement of the thickness of the dorsal fluid layer is closer to the actual volume, determined by thoracocenteses, than the estimated volume, based on radiologic examination. A simplified approximation is $y = 50x - 800$, where y represents the sought volume of the effusion and x the thickness of the effusion in millimeters measured at a right angle to the chest wall (original formula $y = 47.6x - 837$; Eibenberger et al. 1994). The deviation of the estimated results from the actual volume of the effusion can be considerable.

3.2.3 Type of Effusion

The type of pleural effusion is also important for diagnostic purposes. Transudates contain no components which could serve as ultrasound reflectors and are therefore echo-free. Exudates, with their high protein content and cell-containing or sanguineous effusions often appear echogenically in ultrasound images (Fig. 3.14, Fig. 3.15). Under real-time conditions, echoes float or swirl with respiration and heartbeat, making circular movements, and can hence be distinguished easily from the echoes of artifacts. These dancing echoes are especially common in cases of malignant effusions but do not appear to be pathognomonic in character (Fig. 3.16; Chian et al. 2004).

According to prospective studies, transudates are always echo-free, whereas exudates can be both echo-free and echogenic. Relatively homogeneous echogenicity is believed to be a typical sign of empyema or hemothorax. The author's personal experience has shown that an empyema as well as a hemothorax may be completely devoid of echoes. Additional findings such as septation or nodular pleural changes always indicate an exudate (Yang et al. 1992). Very rarely, transudates can be faintly echogenic. There is no explanation for this ultrasound phenomenon (Reuss 1996). Hence, if there is diagnostic interest, the pleural effusion should always be punctured. Further investigation of the effusion fluid provides valuable information for further diagnostic procedures (Maskell and Butland 2003). Particularly in cases of small effusions and critically ill persons, usonography-guided percutaneous transthoracic aspiration and if necessary thoracocentesis can be performed safely, without difficulties, and without errors in puncture, even at the patient's bedside (Yu et al. 1992). Sonography-guided puncture has also markedly increased the success rate achieved by experienced clinicians (Diacon et al. 2003).

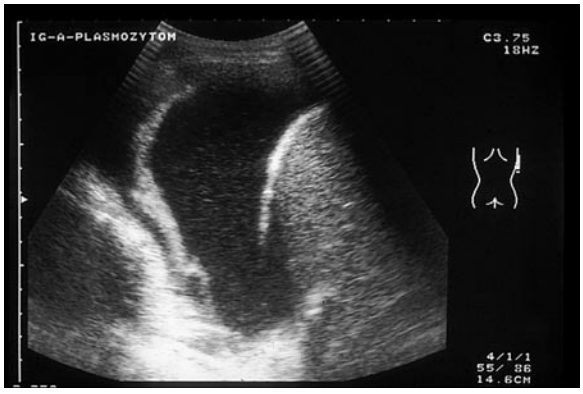

Fig. 3.14 Echogenic protein-rich effusion in a patient with an IgA plasmocytoma. In contrast to artificial echoes, these echoes are swirling pulse- and respiration-synchronous in the effusion during real-time-examination

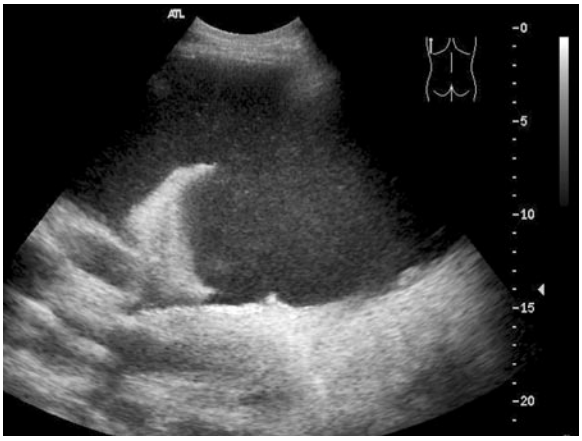

Fig. 3.15 Homogenous echogenic pleural effusion with pointed atelectasis. Lack of fever and inflammation rule out pleural empyema. Hemothorax is unlikely due to absence of trauma. Puncture shows a collection of lymph, the cause of which is a mediastinal metastatic bronchial carcinoma with destruction of the thoracic duct

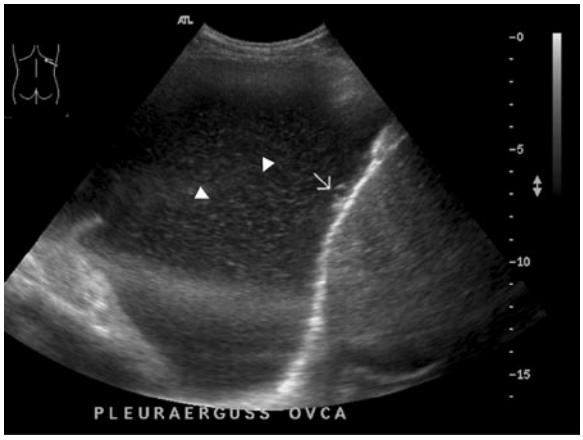

Fig. 3.16 Malignant pleural effusion in connection with metastatic ovarian cancer. Even on the static picture one can see the dynamic circular movement of the effusion echo (*arrowheads*). In depth, clear, stripe-like artifact echoes. Open (*arrow*) small pleural metastasis on the diaphragm

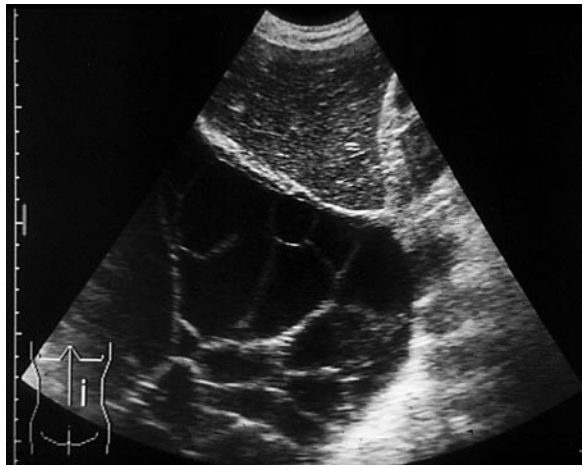

Fig. 3.17 Honeycomb-like appearance of a postinflammatory effusion. In such cases, ultrasound avoids frustrating attempts to perform thoracocentesis with the potential risk of injury

Analysis of pleural effusion:

- Appearance
- LDH
- Total protein
- Total cell count
- Cell differentiation
- Granulocytes
- Lymphocytes
- Eosinophils
- pH
- Bacteriological culture
- Cytology

In addition optionally:

- Glucose
- Amylase/lipase
- Tuberculosis culture

3.2.4 Complicated Pleural Effusion

Infected or septated and loculated pleural effusions are also described as complicated ones. Infection of a parapneumonic effusion can be proved or excluded only by puncture or aspiration. Sonography is a sensitive method to demonstrate loculated lesions or septation. Sonography can help to prevent unsuccessful thoracocentesis of a loculated effusion or even perform targeted puncture of large loculations (Fig. 3.17).

The varying echogenicity of the contents of individual chambers may be a sign of a partial empyema (Fig. 3.18).

3.2.5 Pleural Empyema

Radiological signs of round and sharp angles between effusion or empyema and the chest wall proved inadequate to distinguish between lung abscesses, adherent pleural effusions and pleural empyema (Fig. 3.19; Baber et al. 1980; Stark et al. 1983). These signs are also seen on sonography. Sonography-guided puncture provides clarity about the contents of a cavity.

Pleural empyema often look encapsulated, not free floating, and are often faintly to moderately echogenic, relatively homogeneous effusions, whereby the pleura is moderately thickened in a capsule-like fashion (Fig. 3.20). On the computer tomographic images, pleural empyemas have a thinner, more regular, smooth cavity wall compared to peripheral subpleural pulmonary abscesses (Baber et al. 1980; Layer et al. 1999). The splitting of the pleural sheets around the empyema can also be seen on sonographic images (Fig. 3.21, Fig. 3.22). The fibrinous bands and septa, which are easy to detect sonographically, are difficult to delineate on computed tomography (Fig. 3.18). Empyemas mostly display moderately distinctive infiltrations in the adjacent lung, whereas pulmonary abscesses show extended inflammatory infiltrations of the surrounding areas and a rather thick wall.

Sonography-guided transthoracic drainage of empyema with 10–14-Fr catheters, if indicated also with larger catheters, is nearly a standard procedure today. Whether fibrinolytic agents administered by the intrapleural route might resolve septations, improve the success of drainage and thus reduce surgical interventions and fatal outcomes has been discussed for a long time. A recently published study reported no advantage for streptokinase with re-

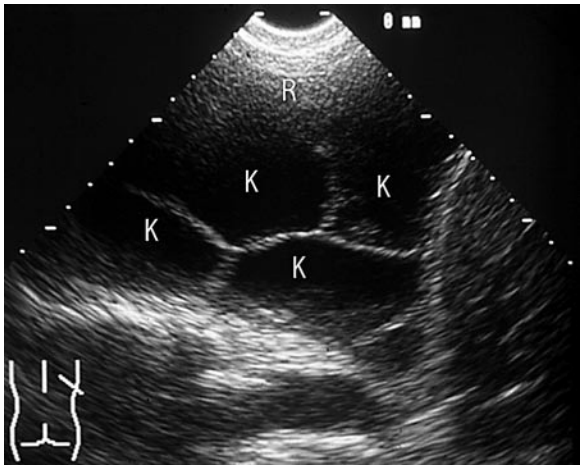

Fig. 3.18 Pleural empyema with several cavities (*K*). The aspirate from different cavities was sometimes purulent, sometimes serous. *R*, artifact

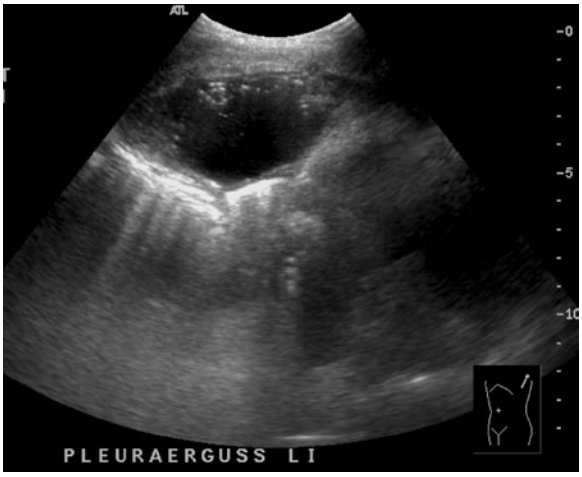

Fig. 3.19 A trapped pleural effusion detached on all sides, after previous pancreatitis. On X-ray investigation the entity is seen as a tumour close to the pleura. The effusion cannot be reliably differentiated in terms of image morphology. Therefore, targeted puncture may be required

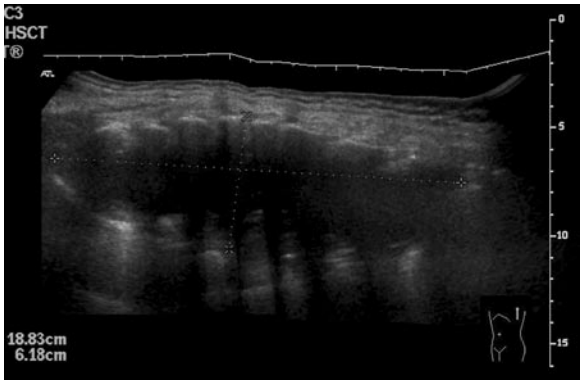

Fig. 3.20 Pleuritic empyema with an extension over many intercostal areas. Ribs and their shadows show up well. Measuring of the volume and showing all of the empyema is only sonographically possible with the "panorama" function

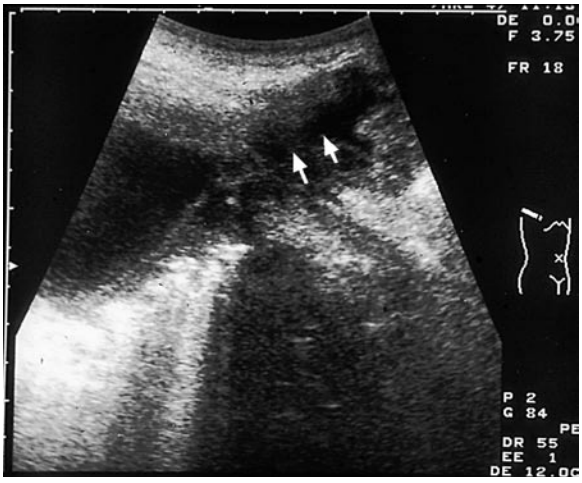

Fig. 3.21 Pleural empyema with a thick, but nevertheless smooth wall and clearly visible split pleura. The empyema drained spontaneously by a fistula through the chest wall, surrounded by extensive inflammatory infiltrations (*arrows*)

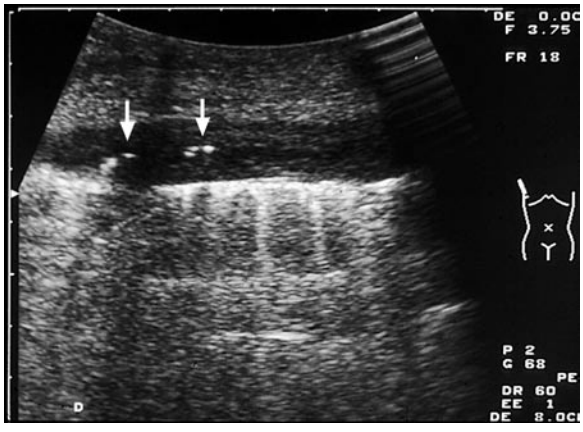

Fig. 3.22 Clearly visible regular and well delineated thickening of the parietal and visceral pleura in an already drained empyema. Small air bubbles in the completely emptied cavity (*arrows*)

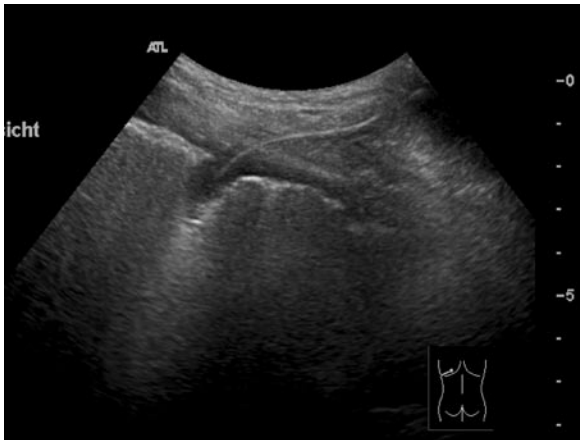

Fig. 3.23 The patient has undergone successful pleurodesis. The drain used to administer the talcum suspension is still in position. The surrounding portion of the pleura is hypoechoic and thickened. The dynamic investigation shows no gliding whatever

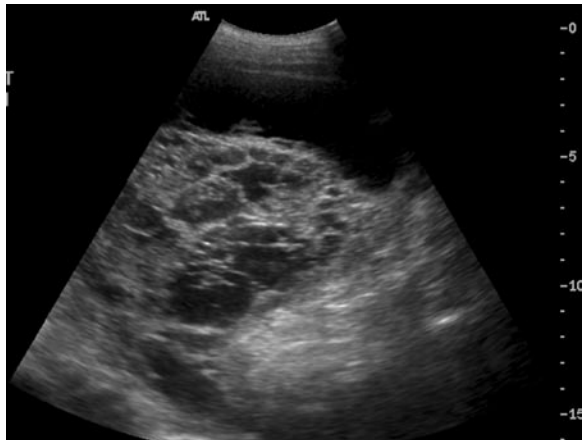

Fig. 3.24 Large fibrin clot after attempted pleural fixation in the basal (but not the lateral) direction toward the diaphragm to the chest wall. In addition to the clot, there is a larger effusion latterly; the clot itself contains small blebs of liquid

gard to the primary endpoints of the study, namely surgery or death. In fact, the majority of severe undesired effects occurred in the group given streptokinase (Maskell et al. 2005). In this study, however, cross-section imaging procedures were very rarely used to assess the empyema (Katikireddy and Dube 2005).

In terms of differential diagnosis it may prove difficult to distinguish between a peripheral lung abscess and a pleural empyema. Lung abscesses are usually marked by extensive inflammatory invasion into the environs, which, in conjunction with surrounding atelectatic portions of the lung may confirm the impression of an apparently very thick wall. The quantity of air in air-filled abscess cavities changes when the patient is re-positioned – which is a very reliable sign of the cavity being connected with the bronchus and, therefore, the presence of an abscess. After previous attempts at puncture, however, empyemas may contain artificial air. Gas-forming germs are rare in cases of pleural empyema.

Crucial for the therapy is that one does not drain through ventilated lung and that pleural shifting at the prospective site of the drainage is blocked. Through an adhered pleura, abscesses can be drained without the risk of causing a consecutive empyema.

3.2.6 Pleurodesis

In cases of malignant pleural disease with recurrent large pleural effusions and subsequent dyspnea, mainly in pleural carcinosis, pleurodesis is a great boon as a palliative measure. Best results are achieved by performing thoracoscopy with talc pleurodesis. However, this cannot be performed at all sites and in all patients. In case of catheter pleurodesis, first a drainage catheter is placed under sonographic guidance and the pleural cavity above the catheter is aspirated until it is empty. After sonography-controlled complete evacuation of the pleura, a pleurodesis agent such as a talc suspension is administered through the catheter. The success of pleurodesis can be checked later by sonography. Gliding of the pleura is completely eliminated if the pleurodesis is performed successfully (Fig. 3.23). The success of the procedure can also be confirmed after thoracoscopic pleurodesis following a spontaneous pneumothorax (Leo et al. 2005). If the pleurodesis is not entirely successful, distinction between residual effusion with septation, lung invasion or partial atelectasis of the lung is better achieved by sonography than by radiological imaging procedures (Fig. 3.24).

3.3 Solid Pleural Changes

The only visible reactions of the pleura to disease are exudation of fluid and edema. Pleural edema can appear diffuse, circumscribed, band-like, nodular, regular, irregular, hypoechogenic, or complexly structured. If the lung is still shifting with respiration, the swelling can unambiguously be associated with the parietal or visceral pleura, depending on whether the lung is still moving or not.

If the pleural sheets are adhered, the position of the former pleural cavity can often only be guessed at by means of a faintly echogenic, partly interrupted line. Swellings of the pleura occur if something is inflamed or if a primary or secondary tumorous disease exists. From

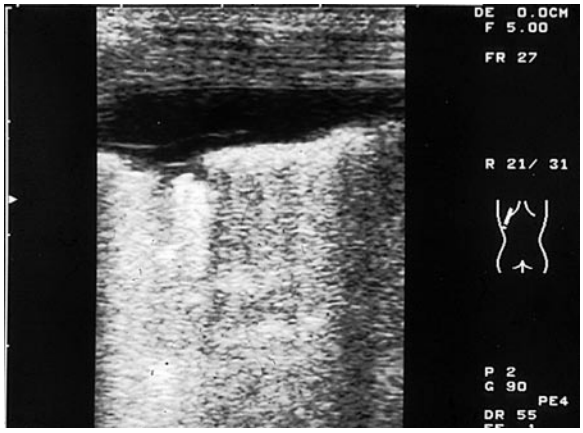

Fig. 3.26 Tuberculous pleurisy without thickening of the parietal pleura, irregular visceral pleura with tiny circumscribed nodules, subpleural pulmonary infiltrations, and fibrinous threads in the effusion. Mycobacterium tuberculosis were found in the effusion

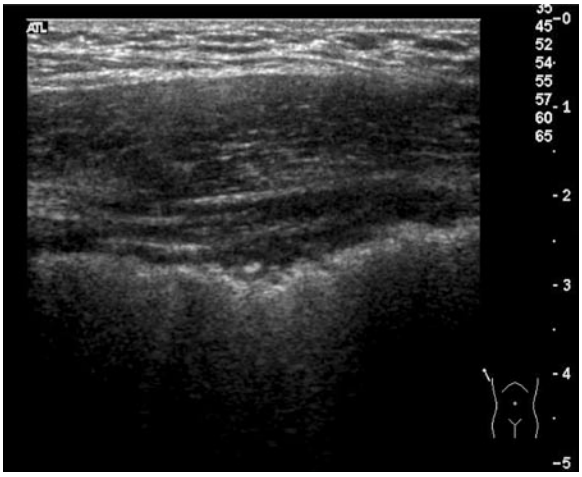

Fig. 3.25 Acute pleuritis with medium echogenic, thickened pleurae; the line of the parietal pleura is thus very irregularly edgy. This diagnosis accounts for chest tenderness

the sonographic structure and form of the pleural swelling, it is not possible to establish its etiology with certainty, even though images such as hypoechogenic nodules are typical signs for metastases (Yang et al. 1992).

3.3.1 Pleuritis

Clinically, pleuritis is difficult to diagnose and often the diagnosis can only be reached by excluding other diseases which cause thoracic pain. Angina pectoris, myocardial infarction, and pain in the bones or nerves are usually the things that spring to mind first. Chest X-rays often show a blurred or even absent contour of the diaphragm. They can also demonstrate an effusion in the pleural recesses, but on the whole these are nonspecific or completely inconspicuous (Loddenkemper 1994).

Most patients with pleuritis have sonographically conspicuous findings of the pleura (Table 3.3). The parietal pleura is generally hypoechogenically thickened, especially during the early stages of pleuritis (Fig. 3.25; Bittner et al. 1995). Thickening of the visceral pleura often involves the surface of the lung tissue, which displays small, round to wedge-shaped areas. Besides the actual swellings of the pleura, fibrinous bands as superimposed layers begin to appear in due course. These fibrinous bands can even be echogenic. They occur in the accompanying effusion as uneven or pronged dips, threads or bands, which—at a later stage of the pleuritis—divide the effusion into numerous cavities by a network of septa (Fig. 3.26, Fig. 3.27, Fig. 3.17).

Color Doppler sonography of the expected hyperemia in pleurisy has, so far, proved to be rather disappointing. Intensified vascularization could be observed in only 23.4% of cases and hence this method is limited in its application as a diagnostic signal (Gehmacher

Table 3.3 Sonographic findings in pleurisy (frequency). (From Gehmacher et al. 1997)

Rough appearance and interruption of the normally smooth pleura (89,4%)
Small subpleural consolidations of between 0,2 and 2,0 cm (63,8%)
Localized parietal and basal pleural effusions (63,8%)

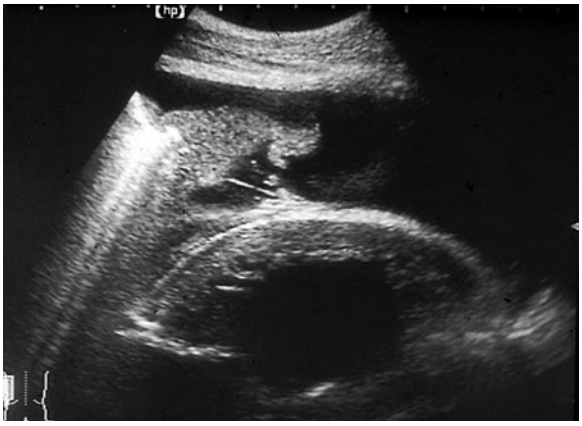

Fig. 3.27 Lung atelectasis, fixed to the pleura near the pericardium by fibrinous bands, inflammatory effusion

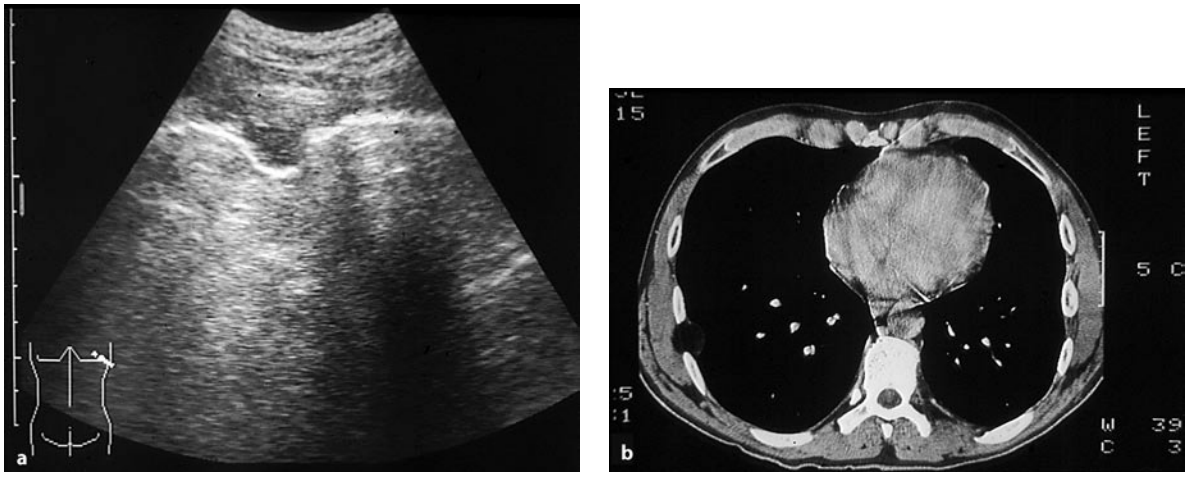

Fig. 3.28 **a** A small, round, well-delineated tumor in the parietal pleura, the lung shifted along the tumor during respiration. The tumor is isoechogenic with the chest wall musculature. On routine chest-X-ray, an indistinct opacity next to the pleura was discovered **b** On computed tomography, a well-delineated, fat-isodense tumor was seen, consistent with a pleural lipoma. No biopsy was carried out, but the tumor showed a constant size in follow-up examinations over many years

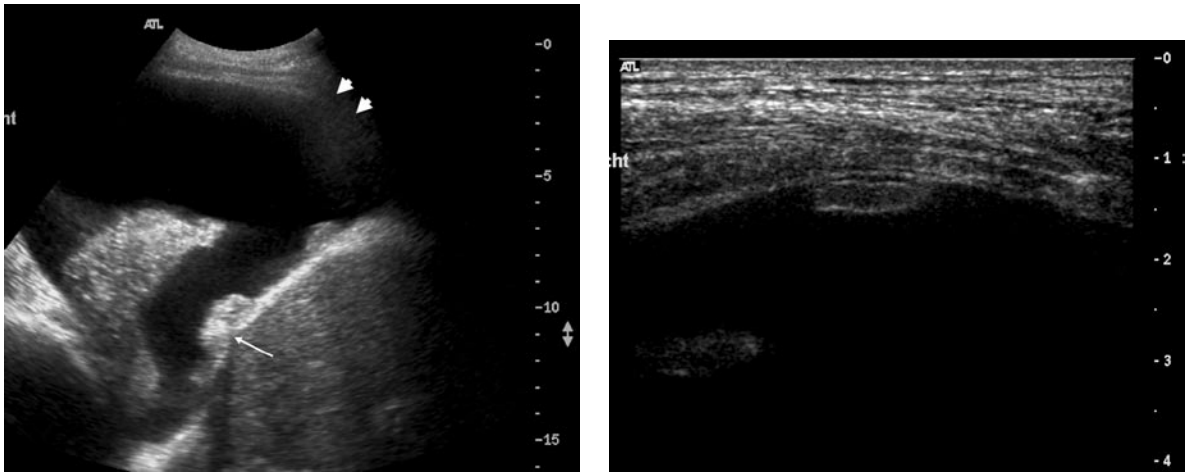

Fig. 3.29 Lentil-shaped pleural metastases on the diaphragm. The larger of the two metastases shows a belly button-like inversion of the diaphragm (*arrow*). Large pleural effusion with atelectasis of the lower lung lobe. Artifacts are due to bad coupling of the ultrasound probe (*arrowheads*)

Fig. 3.30 Metastasis of breast cancer, sitting on the otherwise unchanged parietal pleura parietalis. A surrounding large pleural effusion

et al. 1997). Contrast enhancement (e.g., Sonovue®) allows demonstration of hyperemia of the inflamed and thickened pleura (Jörg et al. 2005).

3.3.2 Benign Pleural Tumors

Benign pleural tumors such as lipomas, schwannomas, chondromas, or benign pleural mesotheliomas are very rare and usually attract attention on chest X-ray as they are mostly unclear, sharply delineated pleural lesions (Theros and Feigin 1977). They account for less than 5% of all pleural tumors (Saito et al. 1988). However, benign pleural tumors are often the reason for further diagnostic measures aimed at excluding pleural metastases or peripheral bronchogenic carcinomas. Benign pleural tumors are moderately echogenic and delineated sharply by a fine capsule. They can displace adjacent structures, but they do not display invasive, destructive growth into their surroundings (Fig. 3.28). It is not always possible to distinguish between displacement and invasion sonographically. Transpleural tumor growth with no respira-

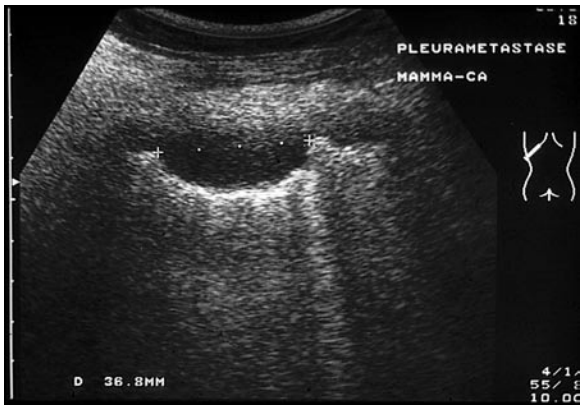

Fig. 3.31 Hemispheric hypoechogenic pleural metastasis with poorly delineated lateral processes and chest wall infiltration. Absent pleural effusion. Known breast carcinoma. In such an unusual pleural finding, a peripheral bronchial carcinoma cannot be excluded

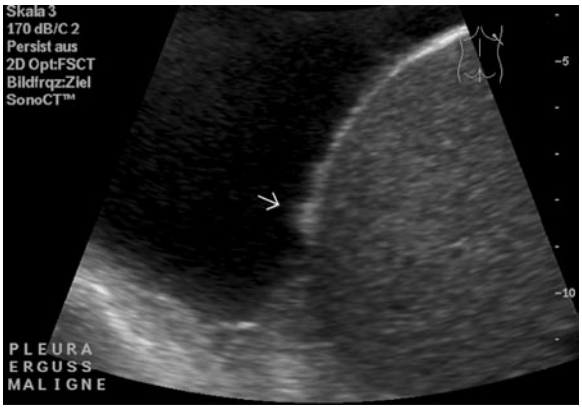

Fig. 3.32 Small metastasis on the diaphragm (*arrow*), initially only recognizable as an irregularity. In the following clinical course, growth of the metastasis and malignant pleural effusion

tory movement of the lung is an indication of malignant growth and infiltration. Small accompanying pleural effusions around the tumor or in the angle between the chest wall and diaphragm can also occur with benign tumors. Sonographic classification of the individual benign pleural tumors is not possible. Histologic classification of benign tumors, based on small fine needle biopsy specimens, or even only on a cytological specimen, is more difficult for the pathologist than to find evidence of a malignancy. Hyperechoic shadowy calcifications point to a benign process. Sonographic density measurements of the tissue as in computer tomography, e.g., to identify fat in lipomas, are not currently available, but they are being developed.

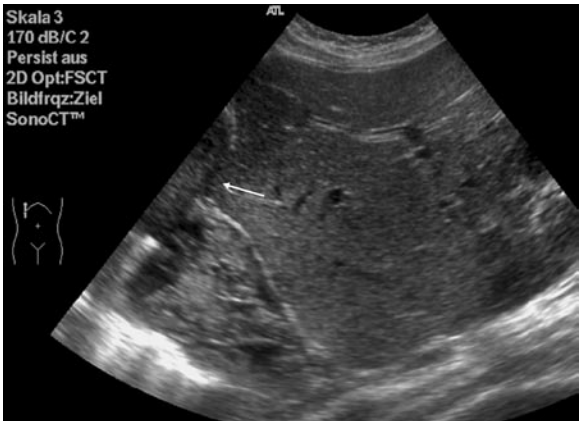

Fig. 3.33 Widespread pleural carcinoma after the initial diagnosis of endometrial cancer 2 years ago. The pleural carcinoma has infiltrated the diaphragm, changed the shape of the diaphragm, and partially destroyed it (*arrow*); the tumor has spread to the liver

3.3.3 Pleural Metastases

The development of pleural metastases usually parallels that of a pleural effusion. This "sonographic window" makes the detection and depiction of metastases easier. Most metastases are found at the costal pleura or on the diaphragm, as well as in the angle between the diaphragm and the chest wall, i.e., in transthoracically accessible areas—even without an accompanying effusion (Fig. 3.29, Fig. 3.30, Fig. 3.31).

Pleural metastases are mainly hypoechogenic to moderately echogenic. They are located mainly on the pleura and look like nodular, round-shaped to hemispherical or broad-based polypoid formations, which protrude prominently into the effusion.

Depending on the location of the metastases, they can be detected on the screen measuring from 1–2 mm (Fig. 3.32). Large metastases can invade deep into the surrounding tissue, i.e., the lung or chest wall, such that the original point of invasion is no longer visible (Fig. 3.33). Signs of infiltration include a faint, interrupted, or even absent delimitation of the metastasis from its surroundings, or a pseudopodium-like offshoot which, due to its lower echogenicity compared to the chest wall or the diaphragm, is often readily visible. Single, well delineated metastases cannot be distinguished from benign pleural tumors due to their similar sonomorphology. The existence of several similar formations is a very typical finding in pleural metastases and an all but conclusive finding, especially if a corresponding primary disease exists. Hence, confirmation with biopsy may not always be necessary. The transthoracic, sonographically guided needle biopsy contributes essentially to the further diag-

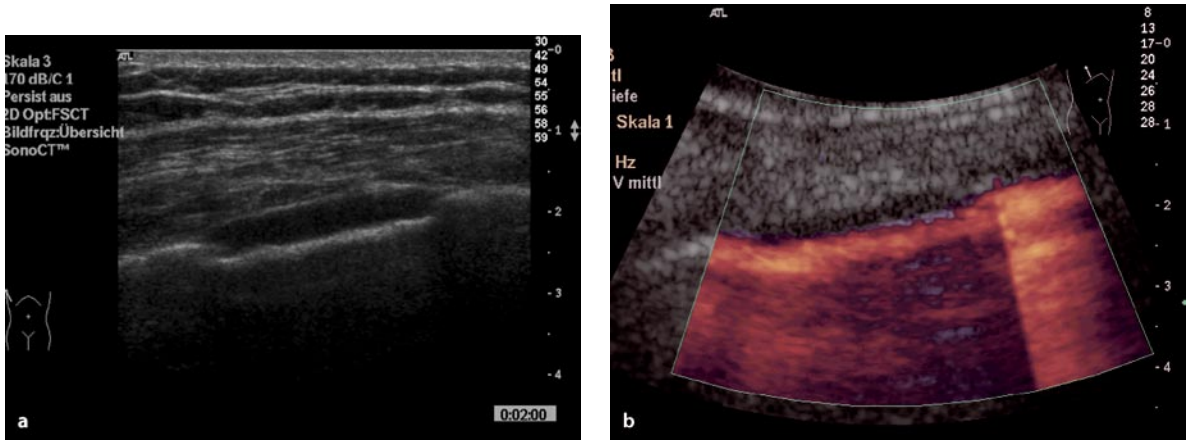

Fig. 3.34 **a** Echo-poor asbestos plaque with typical mesa-shape contour (dorsolateral right). **b** Lung and visceral pleurae move with breathing in relation to the plaque

nosis of a suspected but unknown primary tumor. Pleural metastases are found most frequently with breast cancer or bronchial carcinomas. Single metastases located in the visceral pleura can, sonomorphologically, resemble peripheral bronchial carcinomas (Fig. 3.31). Similar to peripheral bronchial carcinomas, pleural metastases can spread from one pleural sheet to the other and hence lead to concretion of the pleural sheets, accompanied by a lack of respiratory movement of the lung (Suzuki et al. 1993). Extensive or sheet-like infiltrations of the pleura in metastatic carcinomatosis with or without effusion are rarely seen. Sonomorphologically, they are hard to distinguish from the hypoechogenic inflammatory thickening on the one hand, and the tapestry-like mesothelioma on the other. Even needle biopsy can fail to resolve the problem of whether malignant and inflammatory-reactive, fibrinous or sanguineous parts lie next to each other.

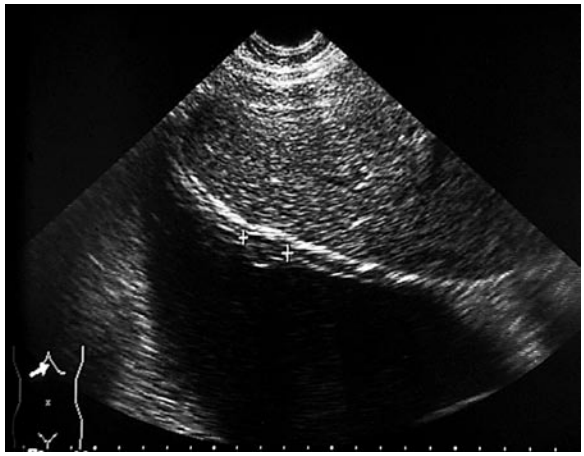

Fig. 3.35 Initial diagnosis of a pleuritic mesothelioma, covering, in a wallpaper-like fashion: almost the entire pleura of the right hemithorax, with some single knotted thicker parts (between the crosshairs, metering *crosses*, gage *crosses*). Patient had difficulty breathing for 2 days. X-ray showed a white hemithorax on the right. This condition is due to decades of work-related exposure to asbestos

3.3.4 Malignant Pleural Mesothelioma

The incidence of asbestos-induced malignant pleural mesothelioma is increasing significantly (Mowé and Tellnes 1995). The period of latency between exposure to asbestos and tumor manifestation can be more than 20 years and hence the number of diseases caused by asbestos is expected to rise within the next 10–20 years even though the use of asbestos has—to a large extent—been disallowed.

Patients with asbestos-related plaques in the pleura bear the risk of developing a pleural mesothelioma. Asbestos-related plaques are seen as calcified or non-calcified pleural thickening, typically occurring in the dorsolateral portions of the costal region of the parietal pleura. High-risk groups are examined at regular intervals by occupational healthcare specialists. Sonography, with its high local resolution, would be a useful instrument to monitor the pleural changes of these high-risk groups; however, it has not yet been evaluated in major studies. Using preferably high resolution transducers, one can depict the predominantly moderately echogenic swellings of the parietal pleura with its often smooth border and the lung shifting against these plaques during respiration. Not even small effusions should occur together with these plaques. Plaques may also appear as flat formations running out into the normal pleura (Fig. 3.34, J. Reuss, unpublished data). Approximately 10% of plaques become

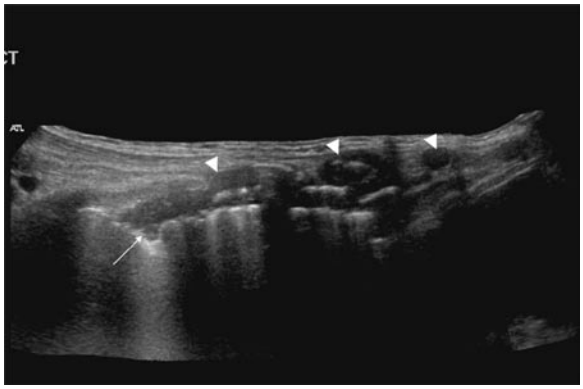

Fig. 3.36 Mesothelioma. Widespread infiltration of the thoracic wall with spread around the ribs (*arrow heads*), as well infiltration of the lung (*arrow*)

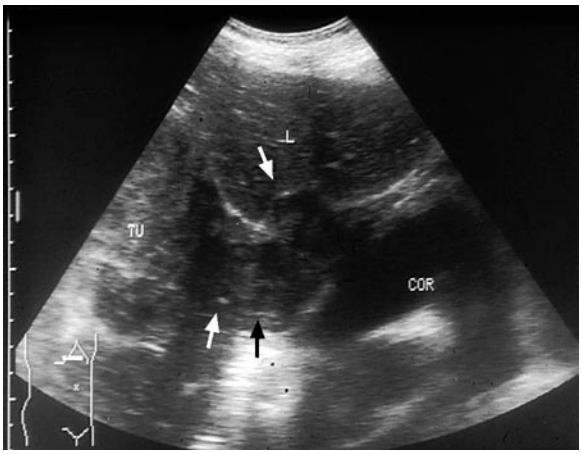

Fig. 3.37 Advanced mesothelioma with breakthrough of the diaphragm (*open arrow*) and infiltration into cardiac wall (*lower arrows*). L liver, TU tumor, Cor heart

calcified, are then highly echogenic, and cause shadows (Wernecke 2000).

Mesotheliomas have very irregular, partly angular, unclear borders. In addition to tumorlike formations, mesotheliomas can also present as extensive, tapestry-like growths with nodules (Fig. 3.35).

Using high-frequency transducers, invasions of the chest wall and the diaphragm are visualized as striped, hypoechoic ramifications at the time of diagnosis (Fig. 3.36, Geiger et al. 2003). Spread to the contralateral pleura occurs early. In a recently presented study, 28% of patients were already affected at the time of the initial diagnosis (Geiger et al. 2003). The effusions might be echogenic particularly in cases of hemorrhage. The radiographic image of a white hemithorax may also conceal a mesothelioma.

The diagnosis can be established on the basis of effusion cytology or blind pleural biopsy (Rahmel needle, Abrams needle) in no more than 30% of patients. Biopsies taken by thoracoscopy allow the diagnosis to be established in more than 90% of cases (Adams et al. 2001). Percutaneous biopsies under sonographic guidance achieve nearly the same rate of accuracy (Heilo et al. 1999). For the pathologist, a distinction between activated mesothelia and mesothelioma cells is difficult when the specimen is small.

After operative or thoracoscopic excision of biopsy specimens, 40% of patients with mesothelioma develop vaccination metastases in the chest wall. However, 0–15% also develop these after percutaneous biopsy and particularly along the drainage canals after aspiration of large effusions (Boutin and Rey 1993; Geiger et al. 2003;, Heilo et al. 1999). Therefore, short-term irradiation of the affected area in the chest wall, e.g., at a dose of 7 Gy administered three times, is recommended. Regrettably, very few patients with malignant pleural mesothelioma are suitable candidates for curative surgery (Sugarbaker et al. 1995).

Computed tomography is the standard method used to diagnose mesotheliomas. Recent preoperative studies have shown that sonographic methods are almost as good as computed tomography or magnetic resonance imaging (Layer et al. 1999). Sonographically detected chest wall infiltrations almost always proved to be true positive, and only a few false positive results occurred.

The region around the diaphragm is, owing to the transverse sections, difficult to examine using computed tomography and can only be judged correctly using reconstruction. As the section angle can be chosen, sonography can help to detect infiltrations and reduce mobility of the diaphragm. Coronary sections of magnetic resonance imaging are not advantageous in this area. Sonographically, the right diaphragm can be accessed a lot better than the left diaphragm. False negative results based on a sonographic examination concern mostly the left half of the diaphragm. The results can be improved if the proximal stomach is filled with water and a consequent examination of the left diaphragm is carried out from ventral, dorsal, and translienal. The sonographic depiction of an invasion of the pericardium is very specific as the sonographic images are moving ones (Fig. 3.37, Layer et al. 1999).

3.3.5 Transpleural Growth of Tumors

When peripheral lung tumors reach the visceral pleura and cross the pleural space, they infiltrate the parietal pleura and the chest wall. On sonography the peripheral lung tumor is usually seen as a hypoechoic mass extending up to the chest wall. Local breath-dependent

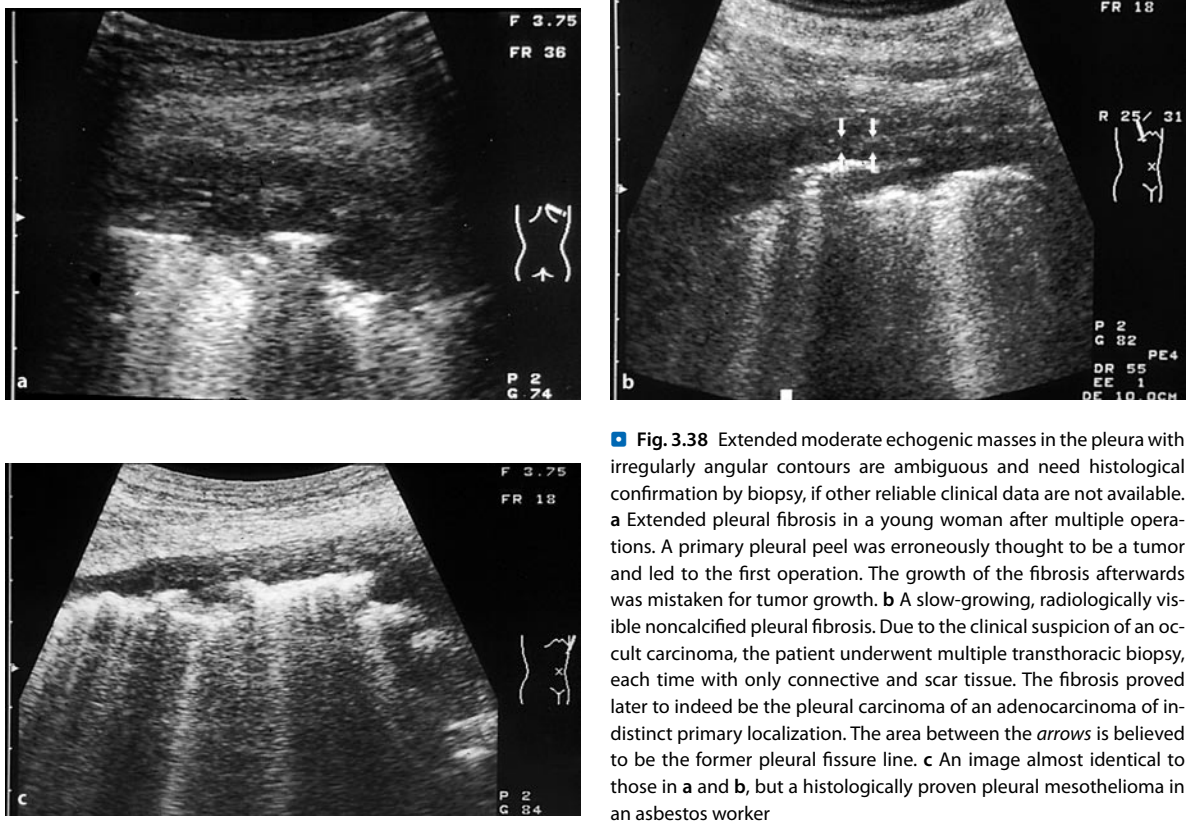

Fig. 3.38 Extended moderate echogenic masses in the pleura with irregularly angular contours are ambiguous and need histological confirmation by biopsy, if other reliable clinical data are not available. **a** Extended pleural fibrosis in a young woman after multiple operations. A primary pleural peel was erroneously thought to be a tumor and led to the first operation. The growth of the fibrosis afterwards was mistaken for tumor growth. **b** A slow-growing, radiologically visible noncalcified pleural fibrosis. Due to the clinical suspicion of an occult carcinoma, the patient underwent multiple transthoracic biopsy, each time with only connective and scar tissue. The fibrosis proved later to indeed be the pleural carcinoma of an adenocarcinoma of indistinct primary localization. The area between the *arrows* is believed to be the former pleural fissure line. **c** An image almost identical to those in **a** and **b**, but a histologically proven pleural mesothelioma in an asbestos worker

movability of the pleura, the gliding sign, is absent. For peripheral bronchial carcinoma this usually means stage IIIa disease in the presence of a local T3 tumor according to the UICC classification; it also signifies a correspondingly higher risk and poorer prognosis. In this difficult situation, any curative surgery will require a chest wall resection. For a surgeon, it is essential to establish the existence of any chest wall infiltration preoperatively. So far computed tomography has been the standard procedure for assessment of invasion. Areas between the tumor and the chest wall frequently appear on CT as tissue. Therefore, chest wall invasion tends to be overestimated. On STIR sequences in magnetic resonance tomography, the dividing layer of water can still be demarcated, as in sonography (Shiotani et al. 2000). Sonographic evidence of a preserved extrapleural lamella of fat rules out actual chest wall invasion. However, sole evidence of the absence of the gliding sign is not adequate proof of invasion; it may also be due to accompanying inflammatory changes.

In a retrospective surgically controlled study, sonography (sensitivity 100%, specificity 98%, accuracy 98%) was clearly superior to conventional computed tomography (sensitivity 68%, specificity 66%, accuracy 67%) (Suzuki et al. 1994). A prospective, surgically controlled study comparing ultrasound, computed tomography, and ultrasound guided needle biopsy showed that sonography is superior in the preoperative identification of infiltrations of the chest wall (sensitivity US 76.9%, CT 69.2%, biopsy 61.5%), while its specificity is lower (US 68.8%, CT 75.0%) (Nakano et al. 1994). A recent prospective study comparing computed tomography and sonography demonstrated the higher sensitivity of sonogrpahy in visualizing an invasive situation (Herth et al. 2003). Therefore, in cases of suspected invasion, sonography of the pleura and the chest wall is a mandatory procedure (see Fig. 4.25, Fig. 4.26).

3.3.6 Pleural Fibrosis

Large calcified old pleural peels do not usually need any examination other than standard X-ray examination for diagnosis. Noncalcified thickenings manifest themselves radiologically as streaky opacities adjacent to the chest wall or in the angle between chest wall and diaphragm. Sonographically, one can distinguish between solid and liquid formations. A newly developed fibrosis can be so

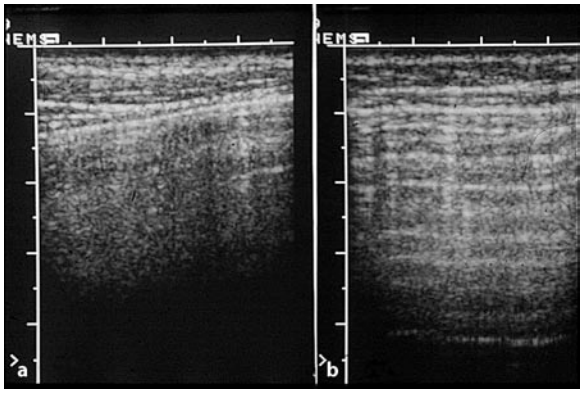

Fig. 3.39 Pneumothorax. The left healthy side (**a**) shows a respiratory shifting pleural reflex and clearly less reverberations. On the side of the pneumothorax (**b**), the reverberations are intensified and no respiratory shift is visible

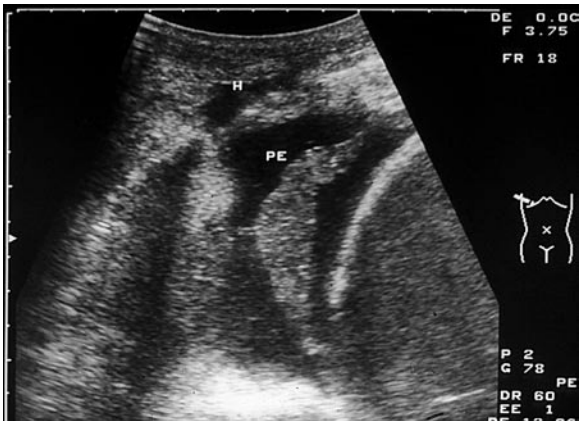

Fig. 3.40 An emergency examination in the surgical emergency unit performed on a roofer after falling from a roof. The patient had dyspnea and severe thoracic pain on the right side in the area of a visible and palpable fluctuating hematoma. Echo-free, but sanguineous pleural effusion (*PE*) and lung atelectasis. Partly ruptured chest wall with deposition of fluid in the chest wall which fluctuated during dynamic examination, corresponding to the visible and palpable hematoma (*H*)

hypoechogenic that - especially if the signal gain is not adjusted optimally - the thickening appears to be echo-free and hence is often misinterpreted as an effusion. Pleural peels with adhered pleural sheets do not show respiratory movement of the lung, which an effusion would still show. The "color-Doppler sign" of narrow effusions of the mantle has already been described (Fig. 3.6).

Even an old fibrosis of many decades standing can be very hypoechogenic, even though fibroses tend to increase their echogenicity with increasing age. Calcifications are shadow-producing deposits in the pleural fibrosis. Differentiating between calcification and the adjacent air-filled lung is difficult; absent reverberations, however, are an indication of calcification. There are no reliable sonomorphologic criteria to differentiate pleural fibrosis, pleural carcinoma, and mesothelioma (Fig. 3.38). With a color Doppler, cyst-like inclusions, which sometimes exist within the thickening, can be distinguished from thick vessels within the thickening.

3.4 Pneumothorax

Reverberation artifacts behind air in the pleura are a lot coarser and more regular than those at the outer surface of the lung (Fig. 3.39). A major criterion of pneumothorax, however, is absent respiratory movement of the lung, which can usually be well observed during a dynamic examination. Asthmatics and patients with distinct emphysema, however, can have low lung shift during respiration even under normal conditions. The pleural gap seen as a hypoechoic line between the blades of the pleura is absent in cases of pneumothorax. In the presence of a partial pneumothorax with incomplete collapse of the lung, the area of transition between the breath-dependent, moving lung and the air column in the pleura, apparently seen on sonography, is visualized as the so-called lung point (Lichtenstein et al. 2000).

Diagnostic signs of pneumothorax:

- Absence of the gliding sign
- Rough repetitive echoes
- No visualization of the pleural gap
- No comet-tail artifacts
- "lung point"

In cases of seropneumothorax additionally:

- Movable level of air and water
- Hyperechogenic reflectors (air bubbles) in the effusion

Due to total reflection of the ultrasound wave at the time of its entry into the layer of air in the pleura, usually no conclusions can be drawn about the thickness of the layer of air and the residual size of the lung. A small apical pneumothorax is seen on ultrasonography only in the upper field of the lung when the supraclavicular groove is used as the access pathway. In cases of a non-adherent

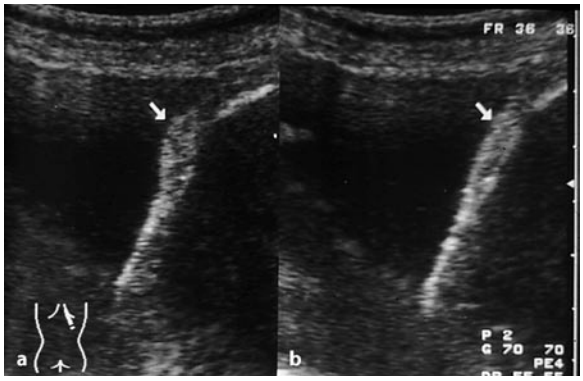

Fig. 3.41 Ultrasound image of the diaphragm with a pleural effusion, the transition from the muscular part to the thinner membranous part of the diaphragm in the dome is clearly demonstrable. During inspiration, the muscular part (**a**, *arrow*) shortens and thickens and relaxes during expiration (**b**, *arrow*)

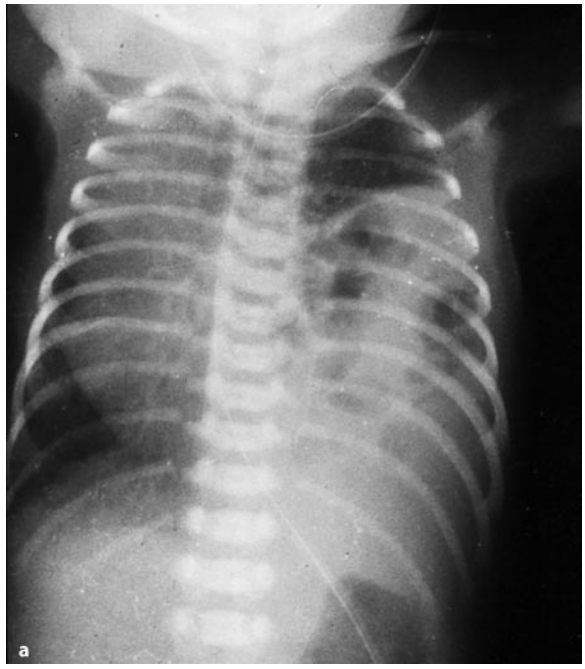

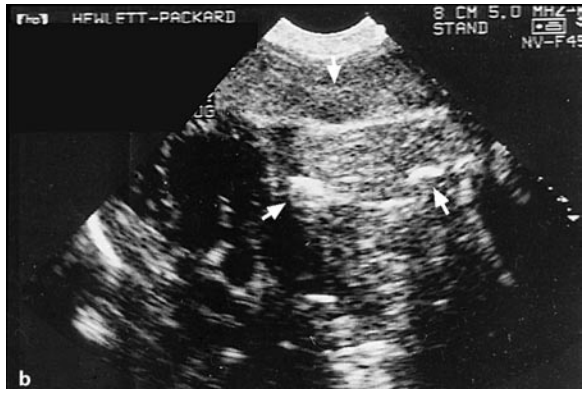

Fig. 3.42 **a** In the chest-X-ray of a newborn, air-containing intestinal organs in the left hemithorax are shown as a sign of a congenital diaphragmatic hernia on the left side. **b** Typical sonogram of the same newborn with a congenital diaphragmatic hernia on the left side with the stomach beneath the well distinguishable heart (*arrows*). Subxiphoidal cross section. (Images kindly provided by M. Teufel, Böblingen District Hospital, Germany)

pleura, the phenomenon of apparently missing motion of the lung during respiration—with the patient positioned appropriately on his/her side—can only be observed through lateral portions of the lung. This is indicative of the presence of a small pneumothorax that does not require drainage. If the patient develops a pneumothorax under puncture, once the ultrasound wave enters the air the investigator is unable to view any targets of puncture beyond the parietal pleura. On the other hand, a pneumothorax can be excluded with sufficient certainty by the use of ultrasound—for instance after puncture.

Recent studies have demonstrated the high sensitivity of sonography (85–100%) for the diagnosis of pneumothorax (Herth et al. 2003; Reissig and Kroegel 2005). By showing the so-called lung point, a small pneumothorax that evades detection by a chest X-ray in supine position can be seen in the ventilated patient at the intensive care unit (Lichtenstein and Menu 1995).

3.5 Thorax Trauma

Following thorax injury, a pleural effusion is the symptom which can be best identified sonographically. Fresh, sanguineous effusions are often not, or not yet, echogenic (Fig. 3.40). Exact documentation of the volume of the effusion is important for later follow-up. Other injuries of the chest wall and contusions of the lung are discussed in corresponding chapters of this book. After a thorax trauma, one should always check the pericardium to exclude a traumatic pericardial effusion as a matter of routine.

3.6 The Diaphragm

Specific sonographic-scientific publications concerning the diaphragm are rare to date, even though the diaphragm is depicted automatically during abdominal or thoracic sonography, and hence can be assessed both morphologically and functionally.

Anatomically, the diaphragm is symmetric and consists of a pars membranacea which lies more in the dome, as well as of muscular parts which are located towards

the ribs, spinal column, and sternum. From these muscular parts, the dorsally inserting diaphragmatic crura next to the lumbar spine can be distinguished. Between these crura run the aorta and the inferior vena cava.

Sonographically, the pars membranacea is easy to distinguish from the pars muscularis due to its location in the dome of the diaphragm and its lower thickness. The layer of muscles can be recognized as a hypoechogenic plate, whereas - in the dome -the diaphragm appears as a fine echogenic line in the section image. The muscle plate of the diaphragm shortens and thickens during inspiration (Fig. 3.41). A distinct swelling of the diaphragmatic musculature can be observed now and again in patients with chronic obstructive diseases of the lung.

The diaphragmatic crura can be best depicted in longitudinal sections viewed laterally, on the left side through the retroperitoneum, and appear as moderately echogenic, elongated thread-like structures next to the spinal column. In a cross section of the epigastric region, the diaphragmatic crura can be found next to the aorta and the inferior caval vein, directly above the origin of the celiac trunk coming out of the aorta. The extension of the diaphragmatic crura lateral of the trunk to caudal can differ individually.

Diaphragmatic hernia can be depicted sonographically, but not without difficulty. Therefore, when treating an adult, sonography is not the primary imaging method if there is a clinical suspicion. Hernias in infants and newborn babies can be detected by evidence of abdominal organs, e.g., stomach, intestines, liver, or spleen in the thorax (Fig. 3.42).

Sonography is not a useful method for diagnosing the quite frequent axial hiatal hernias at the gastroesophageal junction. They can be distinguished endoscopically and the rugae of the stomach in the hernia can be depicted.

Ruptures of the diaphragm after a serious blunt abdominal trauma can also be recognized by a displacement of abdominal organs. In individual cases, the outline of the ruptures and the ensuing hiatus can be depicted during emergency sonographic examination of the abdomen (Fig. 3.43). One should not be misled by an apparent diaphragmatic hiatus originating at an artifact corresponding to the outline shadow. The change in location of this hiatus with the changing position of the transducer is typical of this artifact.

In many cases, a—mostly sanguineous—pleural effusion resulting from an injury exists, which improves visibility into the thorax and makes the examination of the diaphragm easier. If the patient is seriously injured, an additional computed tomography is unavoidable in order to detect further thoracic or retroperitoneal injuries, which could not be depicted satisfactorily, if at all, sonographically.

Primary tumors of the diaphragm are very rare and are seldom diagnosed in the early stages of the disease; at best, they are an incidental finding (Fig. 3.44). Metastases in the diaphragm are also very rare; they can be the cause of unexplained pain due to an infiltration of the adjacent nervous tissue (Fig. 3.45). In several cases, mainly in the context of metastatic breast cancer, the metastases could only be depicted using sonography, while in some cases they could be established on biopsy (J. Reuss, unpublished data). Typical of metastases in the diaphragm is inclusion in the structure of the diaphragm. Metastases of the pleura and peritoneum are both positioned on the surface of the diaphragm. Large pleural metastases can grow deep into the diaphragm; they can even break through it, similar to pleural mesothelioma (Fig. 3.33).

The sonographic real-time examination is the most suitable method for a functional examination of the diaphragm. A normal, equilateral up and down of the diaphragm in harmony with respiration can be observed. Mobility can be documented either elegantly by means of „time-motion“ or, with the transducer in constant position, the diaphragm is seen on the ultrasound image during inspiration and expiration. Short video clips are optimal as documentation of diaphragmatic dysfunction. Paralysis of the diaphragm instantly attracts attention due to the absence of or paradoxical diaphragmatic movement. Pediatricians can document diaphragmatic paralysis following birth trauma without the need of X-ray examinations (Fig. 3.46). Pleural thickening close to the ribs causes immobility of the lateral diaphragm because of adhesion of the diaphragmatic angle. However, one still observes some residual mobility, which at least excludes the presence of complete phrenic paralysis. Old adhesions of the pleura may be seen as very discrete and narrow entities. Thus, the dynamic investigation that demonstrates “hanging” is very essential. Sonography is very important in the process of clarifying a radiologically established, one-sided diaphragmatic eventration. Invasive thoracic or abdominal lesions with subsequent diaphragmatic eventration and absent respiratory movement are usually obvious due to their considerable extent. Apart from intra- and extraorganic tumors, excessive organ enlargement such as, e.g., a fatty liver or splenic enlargement due to, for example, a myeloproliferative disease can be causes for a diaphragmatic eventration. A subpulmonary effusion is frequently misinterpreted on chest X-ray as a double-sided diaphragmatic eventration. This can be easily recognized and further diagnosed sonographically. Other causes of a one-sided diaphragmatic eventration include subphrenic abscess or subphrenic encapsulated ascites, which can be depicted sonographically. The sonographic examination is unambiguous in these cases and hence no further imaging procedures are necessary.

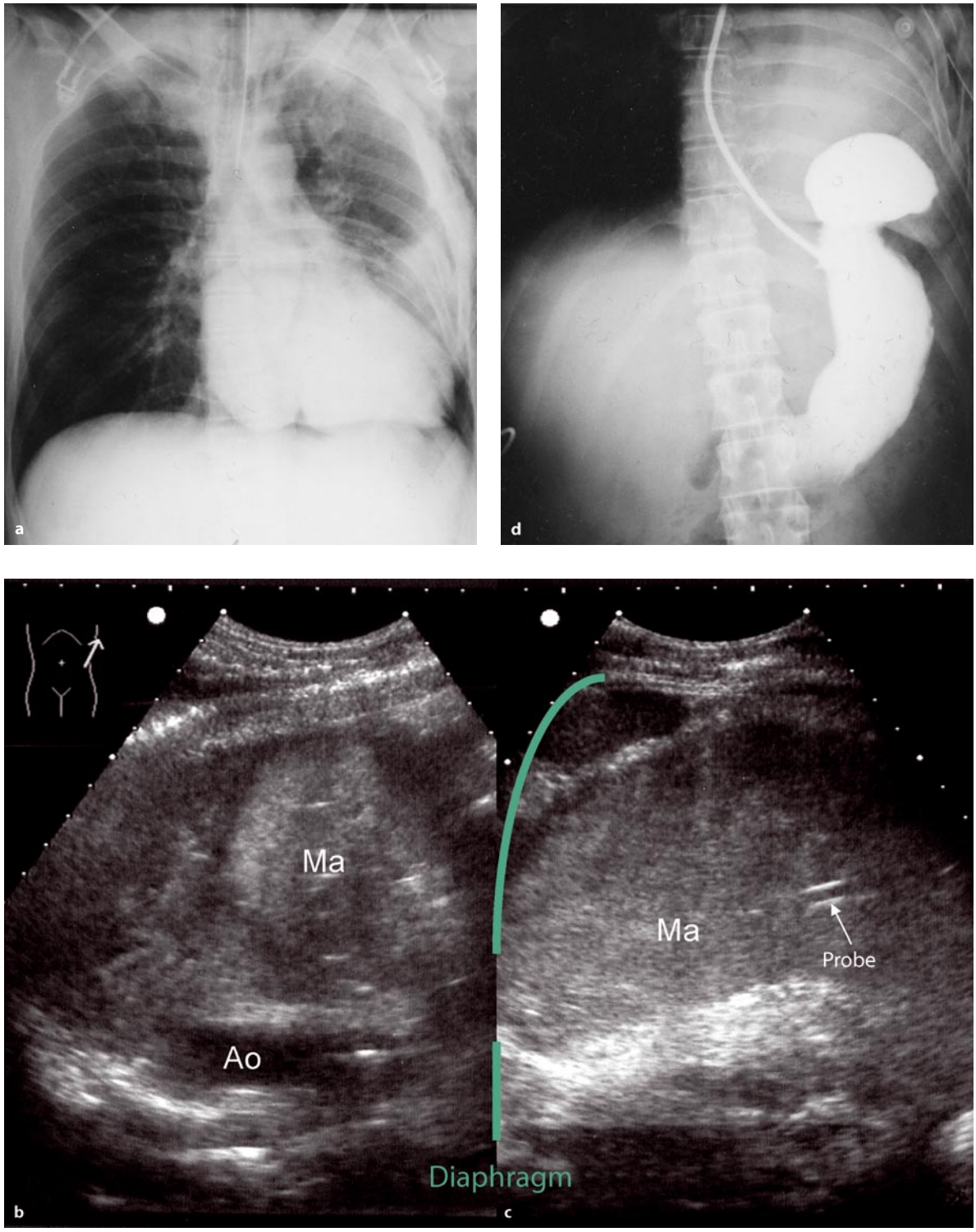

Fig. 3.43 Male patient after a fall from a third-floor balcony. The patient suffered an immediate hemothorax; there was insufficient oxygenation during artificial/mechanical ventilation. **a** A laterobasal left-sided shading appeared on the chest x-ray, and necessitated and emergency ultrasound because of suspected residual hemothorax. **b** The chest has an odd, round structure, filled with echogenic liquid. **c** Below the diaphragm are parts of the stomach clearly evidenced by the stomach probe. The stomach can be traced during dynamic exam through the diaphragm into the thorax (photomontage). **d** The diagnosis was confirmed after filling the stomach with contrast medium through the probe. (The CT scan upon arrival of the patient showed the thoracic part of the stomach, but it was misinterpreted)

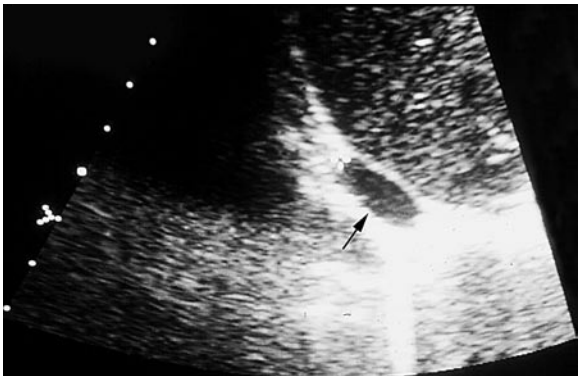

Fig. 3.44 Rare finding of a diaphragmatic lipoma. This was an incidental finding. The smoothly delineated tumor (*arrow*) presented similarly on computed tomography and showed fat density

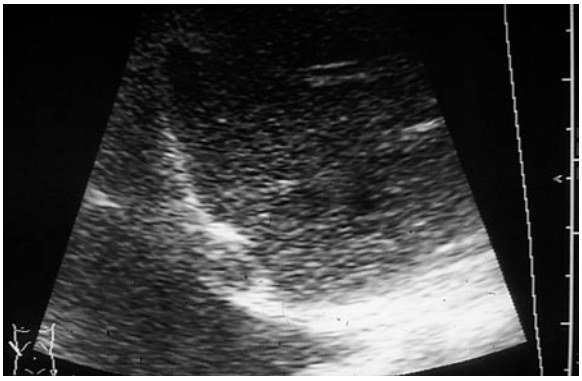

Fig. 3.45 Sonomorphologically similar finding to that in Fig. 3.30 in a patient with known bronchial carcinoma without any known metastasis up to that day. The finding was detected during a routine abdominal sonography. The finding was not comprehensible on computed tomography. An ultrasound-guided biopsy confirmed the clinical suspicion of metastasis of the known bronchogenic carcinoma

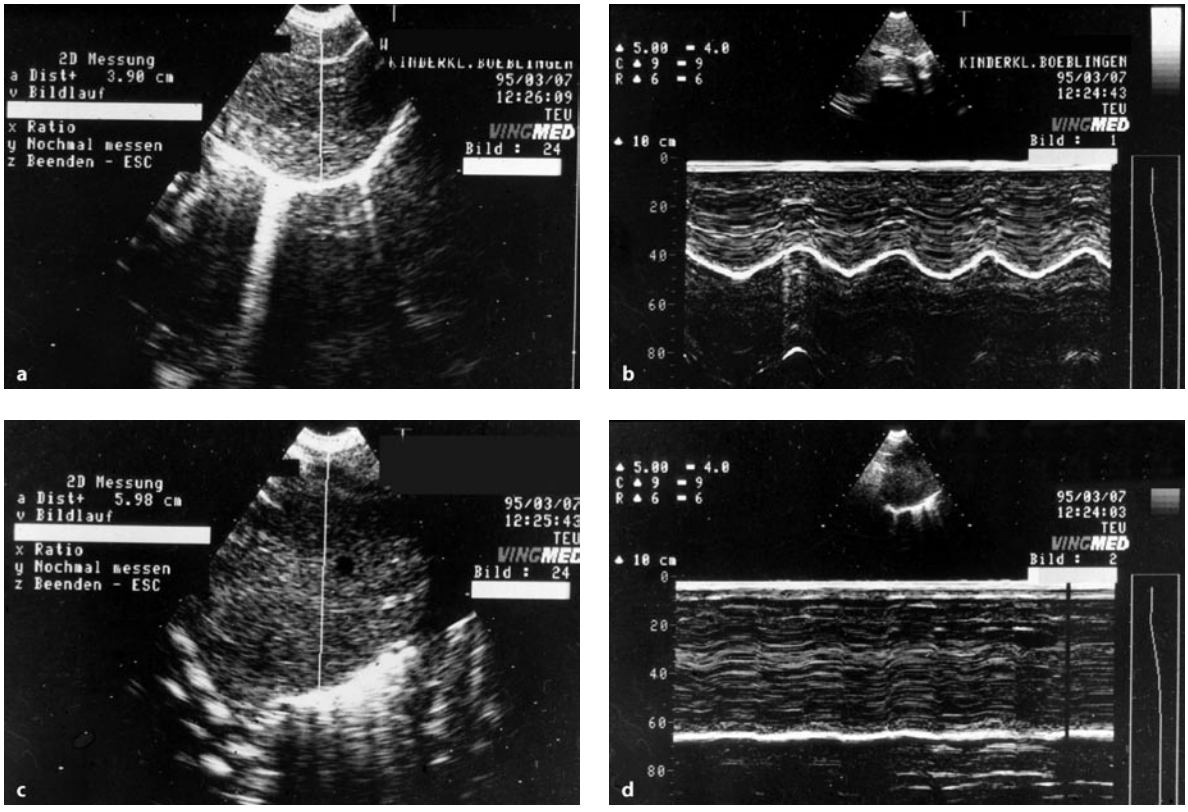

Fig. 3.46 Traumatic paralysis of the diaphragm was suspected in a newborn infant. This suspicion was confirmed by a dynamic ultrasound examination on the right side. The finding was documented with a time-motion recording. **a,b** Healthy left side with definite rhythmic movements of the diaphragm, corresponding to the sinus curve-like line in the time-motion-recording. **c,d** Injured right side with the motionless diaphragm, corresponding to the almost straight line in the time-motion recording. (Images kindly provided by M. Teufel, Böblingen District Hospital, Germany)

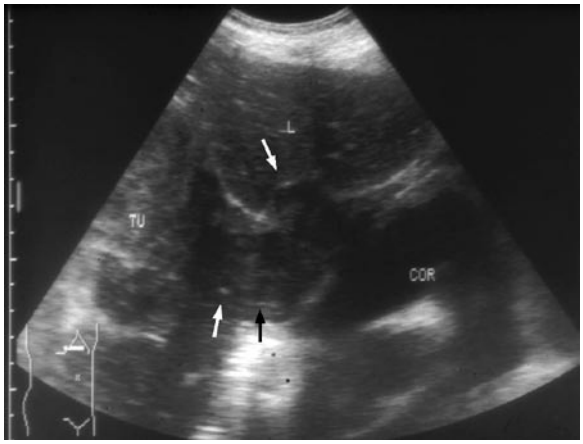

Fig. 3.47 Advanced pleural mesothelioma with penetration of the diaphragm and infiltration of the cardiac wall. *L*, liver; *TU*, tumor; *COR*, heart

The diaphragmatic humps often observed on routine chest X-ray can also be imaged excellently on abdominal sonography. Rugae of the diaphragm which lead to crenation of the liver and less often of the spleen sometimes mimic focal lesions in these organs. An "unfortunate" transverse section through such a diaphragmatic fissure might feign the existence of a target-like tumor. The relation becomes clear if longitudinal and transverse sections are taken. The doubling of the diaphragm can then also be depicted unambiguously (Fig. 3.47).

3.7 Summary

Despite the physical limitations of ultrasound, approximately 70% of the pleural surface can be accessed by sonography, especially from the costal and diaphragmatic aspects.

The normal parietal pleura can be visualized and delineated from circumscribed as well as diffuse pathological thickening. The normal visceral pleura is hidden by the total reflection at the surface of the aerated lung.

Sonographic evidence of a pleural effusion can be obtained from a diameter of 5 ml upwards. Ultrasound is much more sensitive than chest X-ray, especially with the patient in supine position; false-positive findings are not encountered. A more accurate estimation of the quantity of effusion can be made. Exudates are echogenic in one third of cases. Pleural thickening, nodular changes in the pleura, septa, and the formation of cavities occur only in cases of pleural exudates, whereas transudates are always anechoic.

Pleural metastases are characteristically hypoechoic and nodular-polypoid. Conclusions with regard to the primary tumor can be made only on the basis of histology. Pleural mesotheliomas can be delineated almost as clearly on sonography as on computed tomography, and the specificity of the former may be greater. Sonomorphological differentiation between mesothelioma, carcinosis and thickening may be difficult. A pneumothorax is clearly seen on ultrasonography. Morphological and, in particular, functional diagnosis of the diaphragm by means of sonography is both reliable and convincing.

References

Adams RF, Gray W, Davies RJ, Gleeson FV (2001) Percutaneous image-guided cutting needle biopsy of the pleura in the diagnosis of malignant mesothelioma. Chest 120: 1798-1802

Baber CE, Hedlund LW, Oddson TA, Putman CE (1980) Differentiating empyemas and peripheral pulmonary abscess. Radiology 135:755–758

Bittner RC, Schnoy N, Schönfeld N et al. (1995) Hochauflösende Magnetresonanztomographie (HR-MRT) von Pleura und Thoraxwand: Normalbefund und pathologische Veränderungen. Fortschr Röntgenstr 162:296–303

Börner N, Kelbel C, Lorenz J, Weilemann LS, Meyer J (1987) Sonographische Volumetrie und Drainage von Pleuraergüssen. Ultraschall Klein Prax 2:148–152

Boutin C, Rey F (1993) Thoracoscopy in pleural malignant mesothelioma: A prospective study of 188 consecutive patients. I. Diagnosis. Cancer 72: 389-393

Chian CF, WL Su, LH Soh et al. (2004) Echogenic swirling pattern as a predictor of malignant pleural effusions in patients with malignancies. Chest 126: 129-134

Collins JD, Burwell D, Furmanski S, Lorber P, Steckel RJ (1972) Minimal detectable pleural effusions. Radiology 105:51–53

Eibenberger KL, Dock WI, Ammann ME, Dorffner R, Hörmann MF, Grabenwöger F (1994) Quantification of pleural effusion: Sonography versus radiography. Radiology 191:681–684

Geiger D, Düll T, von Pawel J et al. (2003) Thoraxwandinfiltration und Stichkanalinvasion beim malignen Pleuramesotheliom. Ultraschall in Med 24: 34 abstract

Gehmacher 0, Kopf A, Scheier M, Bitschnau R, Wertgen T, Mathis G (1997) Ist eine Pleuritis sonographisch darstellbar? Ultraschall in Med 18:214–219

Goecke W, Schwerk WB (1990) Die Real-Time-Sonographie in der Diagnostik von Pleuraergüssen. In: Gebhardt J, Hackelöer B-J, v. Klinggräff G, Seitz K, ed., Ultraschalldiagnostik 89. Springer, Berlin Heidelberg New York, Tokio

Görg C, Bert T, Görg K (2005) Contrast-enhanced sonography for differential diagnosis of pleurisy and focal pleural lesions of unknown cause. Chest 128:3894-9

Gryminski J, Krakówka P, Lypacewicz G (1976) The diagnosis of pleural effusion by ultrasonic and radiologic techniques. Chest 70:33–37

Heilo A, Stenwig AE, Solheim P (1999) Malignant pleural mesothelioma: US-guided histologic core-needle biopsy. Radiology 211: 657-659

Herth F, Schmitteckert H, Schulz M, Becker H (2003) Diagnostik des Pneumothorax mittels transthorakalem Ultraschall—eine prospektive Untersuchung. Ultraschall in Med 24 (Suppl 1):S30, abstract

Herth F, Schulz M, Schmitteckert H, Becker H (2003) Vergleich transthorakaler Ultraschall (TTUS) mit Computertomographie (CT) zur Beurteilung der Tumorinvasion in die Brustwand beim Bronchialkarzinom. Ultraschall in Med 24 (Suppl 1): S33, abstract

Joyner CR Jr, Herman RJ, Reid JM (1967) Reflected ultrasound in the detection and localization of pleural effusion. JAMA 200/5: (129–132) 399–402

Katikireddy CK, Dube DS (2005) A Trial of intrapleural streptokinase. NEJM 352: 2243

Kelbel C, Börner N, Schadmand S, Swars H, Weilemann LS (1990) Diagnostik von Pleuraergüssen bei intensivpflichtigen Patienten: Sonographie und Radiologie im Vergleich. In: Gebhardt J, Hackelöer BJ, v. Klinggräff G, Seitz K (ed), Ultraschalldiagnostik '89, Springer, Berlin, Heidelberg, New York, Tokio

Kocijancic I, Kocijancic K, Cufer T (2004) Imaging of pleural fluid in healthy individuals. Clin Radiol 59: 826-829

Kocijancic I, Pusenjak S, Kocijancic K, Vidmar G (2005) Sonographic detection of physiologic pleural fluid in normal pregnant women. J Clin Ultrasound 33: 63-66

Kohzaki S, Tsurusaki K, Uetani M et al. (2003) The aurora sign: an ultrasonographic sign suggesting parenchymal lung disease, Br J Radiol 76: 437-443

Layer G, Schmitteckert H, Steudel A, Tuengerthal S, Schirren J, van Kaick G, Schild HH (1999) MRT, CT und Sonographie in der präoperativen Beurteilung der Primärtumorausdehnung beim malignen Pleuramesotheliom. Fortschr Röntgenstr 170:365–370

Leo F, Dellamonica J, Venissac N et al. (2005) Can chest ultrasonography assess pleurodesis after VATS for spontaneous pneumothorax? Eur J Cardiothorac Surg 28: 47-49

Lichtenstein D, Goldstein I, Mourgeon E et al. (2004) Comparative diagnostic performances of auscultation, chest radiography, and lung ultrasonography in acute respiratory distress syndrome. Anesthesiology 100: 1-2

Lichtenstein DA, Menu Y (1995) A bedside ultrasound sign ruling out pneumothorax in the critically ill: lung sliding. Chest 108: 345-348

Lichtenstein D, Meziere G, Bidermann P, Gepner A (2000) The „lung point": an ultrasound sign specific to pneumothorax. Intensive Care Med 26: 1434-1440

Loddenkemper R (1994) Pleuraerkrankungen. In: Ferlinz R, ed.: Pneumologie in Praxis und Klinik. Thieme, Stuttgart, New York, S 712–717

Lorenz J, Börner N, Nikolaus HP (1988) Sonographische Volumetrie von Pleuraergüssen. Ultraschall 9:212–215

Maskell NA, Butland RJA (2003) BTS guidelines for the investigation of a unilateral pleural effusion in adults. Thorax 58: ii8

Maskell NA, Davies CWH, Nunn AJ et al. (2005) U.K. controlled trial of intrapleural streptokinase for pleural infection (MIST1). NEJM 352: 865-874

Mowé G, Tellnes G (1995) Malignant pleural mesothelioma in Norway 1960 -1992. Tidsskr Nor Laegeforen 115:706–709

Nakano N, Yasumitsu T, Kotake Y, Morino H, Ikezoe J (1994) Preoperativ histologic diagnosis of chest wall invasion by lung cancer using ultrasonically guided biopsy. J Thoracic Cardiovasc Surg 107:891-895

Reissig A, Kroegel C (2005) Accuracy of transthoracic sonography in excluding postinterventional pneumothorax and hydropneumothorax. Comparison to chest radiography. Eur J Radiol 53: 463-470

Reuss J (1996) Sonographic imaging of the pleura: nearly 30 years experience. Europ J Ultrasound 3:125–139

Reuß J, Blank W, Drews U et al. (2002) Sonographisch-anatomischer Vergleich des Aufbaus der inneren Thoraxwand zwischen Interkostalmuskulatur und Pleuraspalt. Ultraschall in Med 23 (Suppl–1): S70, abstract

Ruffie P, Feld R, Minkin S, et al. (1989) Diffuse malignant mesothelioma of the in Ontario and Quebec: A retrospective study of 332 patients. J Clin Oncol 7:1157–1186

Sahn SA (1988) The pleura. Am Rev Respir Dis 138:184–234

Saito T, Kobayashi H, Kitamura S (1988) Ultrasonic approach to diagnosing chest wall tumors. Chest 94:1271–1275

Stark DD, Federle MP, Goodman PC, Podrsky AE, Webb WR (1983) Differentiating lung abscess and empyema: radiography and computed tomography. AJR 141:163–167

Sugarbaker DJ, Jaklitsch MT, Liptay MJ (1995) Mesothelioma and radical multimodality therapy: who benefits? Chest 107:345—350

Shiotani S, Sugimura K, Sugihara M et al. (2000) Detection of minute pleural fluid in the pleural retracted space associated with peripheral lung cancer: evaluation with MR imaging. Radiat Med 18: 21-27

Sugarbaker DJ, Jaklitsch MT, Liptay MJ (1995) Mesothelioma and radical multimodality therapy: who benefits? Chest 107:345–350

Suzuki N, Saitoh T, Kitamura S (1993) Tumor invasion of the chest wall in lung cancer: diagnosis with US. Radiology 187:39–42

Wernecke K (2000) Ultrasound study of the pleura. Eur Radiol 10: 1515-1523

Wu RG, Yuan A, Liauw YS, Chang DB, Yu CJ, Wu HD, Kuo SH, Luh KT, Yang PC (1994) Image comparison of real-time gray-scale ultrasound and color Doppler ultrasound for use in diagnosis of minimal pleural effusion. Am J Respir Crit care Med 150:510–514

Yang PC, Luh KT, Chang DB, Wu HD, Yu CJ, Kuo SH (1992) Value of sonography in determining the nature of pleural effusion: analysis of 320 cases. AJR 159:29–33

Yu CJ, Yang PC, Chang DB, Luh KT (1992) Diagnostic and therapeutic use of chest sonography: value in critically ill patients. AJR 159:695–701

Ziegler CM, Seitz K, Leicht-Biener U, Mauch M (2004) Detection of therapeutically relevant diagnoses made by sonography of the upper abdomen: portable versus high-end-sonographic units—a prospective study. Ultraschall Med 25:428-432

4 Subpleural Lung Consolidations

4.1 Inflammatory Consolidations in the Lung

G. Mathis

4.1.1 Pneumonia

4.1.1.1 Pathophysiological Prerequisites

In cases of lobular and segmental pneumonia, large amounts of air are displaced from the lung as a result of extensive fibrinous exudation. Affected lobes or segments are depleted of air and sink in water. The phase of engorgement and hepatization, i.e., the first week of the disease, offers good conditions for pathological echo transmission. In this phase, pneumonia is imaged well on the sonogram. In the phase of lysis, the inflamed portion of the lung is ventilated to an increasing extent. Air reflexes superimpose deeper infiltrations. The image on sonography at this time may underestimate the actual extent of disease.

Focal pneumonias and interstitial pneumonias barely extend up to the pleura and are therefore poorly accessible to sonographic imaging. However, bronchial pneumonias are often accompanied by involvement of the pleura and are therefore partly visualized by sonography.

4.1.1.2 Sonomorphology of Pneumonia

A number of sonomorphological criteria are characteristic of, but not specific for, pneumonic infiltrations. They are of varying intensity in the course of disease.

Sonomorphology of pneumonia:

- Similar to the liver in the early stage
- Lentil-shaped air trappings
- Bronchoaerogram
- Fluid bronchogram (poststenotic)
- Blurred and serrated margins
- Reverberation echoes at the margin
- Hypoechoic to anechoic in the presence of abscess (microabscesses!)

4.1.1.3 Phase of Engorgement

In the initial phase of disease, i.e., in the phase of engorgement, the pneumonic lesion is hypoechoic, relatively homogeneous and hepatoid in form. Its configuration is bizarre. It is rarely explicitly segmental like the pulmonary infarction or rounded like carcinomas and metastases. Its margins are irregular, serrated and somewhat blurred (Figs. 4.1, 4.2).

4.1.1.4 Fluid Alveologram

In a densely subpleural location one finds a broad and highly hypoechoic strip of varying extent and intensity (superficial fluid alveologram). Whether echogenic air bubbles are also visible or are seen again in subpleural location depends on the extent and the stage of disease (Targhetta et al. 1992; Fig. 4.1b).

4.1.1.5 Bronchoaerogram

A marked bronchoaerogram (bronchopneumogram, air bronchogram) with treelike ramifications is seen in 87% of cases. The intensive reflexes of the bronchial tree run between consolidated portions of the parenchyma. In all stages of the disease the bronchoaerogram is more pronounced than in cases of pulmonary embolism. Quite often one finds a small number of, and in most cases numerous, lenticular internal echoes just a few millimeters in size (Fig. 4.1b). These echoes indicate the presence of air in the small bronchi. In other words, this is a partial image of a bronchoaerogram. These internal echoes can be partly explained by congested secretion of highly diverse impedance (Weinberg et al. 1986; Anzböck et al 1990; Mathis et al. 1992; Gehmacher et al. 1995). The bronchoaerogram visualized by sonography cannot be equated with that seen on a radiograph. Viral pneumonias are often less ventilated and/or reveal less pronounced bronchoaerograms (Fig. 4.3).

4.1.1.6 Fluid Bronchogram

The fluid bronchogram is a further sonographic criterion of pneumonia. It is marked by anechoic tubular structures along the bronchial tree. The bronchial wall is echogenic and the fluid in the segmental bronchi is hypoechoic. The reflexes around the bronchi are wider than those along vessel walls. Given good resolution, the bronchial walls are ribbed and the vessel walls are smooth; therefore, tubular structures can be easily classified on B-mode images (Fig. 4.4). In the case of doubt, color-coded duplex sonography helps to distinguish between vessels and bronchi (Fig. 4.5). The fluid bronchogram is seen in approximately 20% of patients with pneumonia and develops in the early phase of the disease as a result of

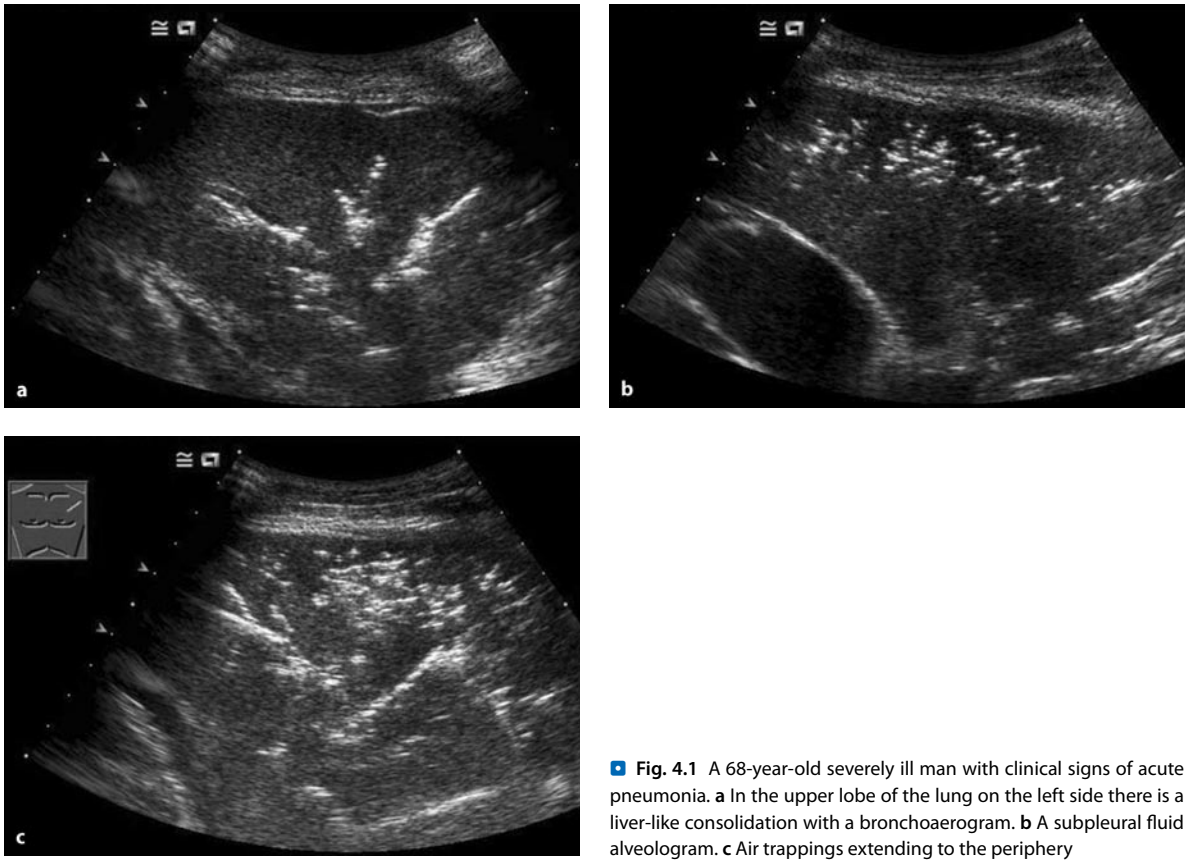

Fig. 4.1 A 68-year-old severely ill man with clinical signs of acute pneumonia. **a** In the upper lobe of the lung on the left side there is a liver-like consolidation with a bronchoaerogram. **b** A subpleural fluid alveologram. **c** Air trappings extending to the periphery

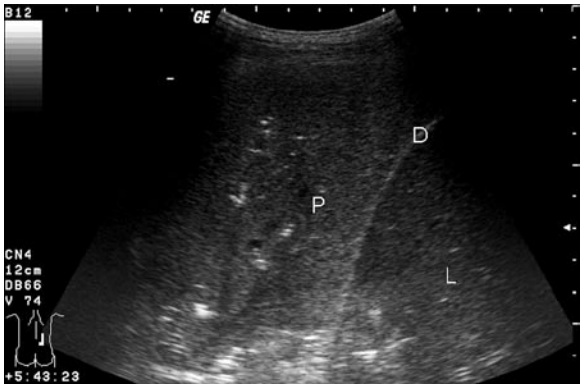

Fig. 4.2 Oblique section of lobar pneumonia in the right lower lobe. The pneumonic infiltrate (*P*) is similar to the liver in terms of echotexture (*L*). *D* diaphragm

bronchial secretion or owing to bronchial obstruction. A persistent fluid bronchogram always raises suspicion of poststenotic pneumonia and is an indication for bronchoscopic investigation (Fig. 4.6). A tumor may be found or ruled out; the obstructive secretory embolus is aspirated and material obtained for bacteriological investigation (Yang et al. 1992; Targhetta et al. 1992).

4.1.1.7 Poststenotic Pneumonia

Poststenotic pneumonias that develop in the periphery or the margin of carcinomas are better delineated from the tumor by means of sonography than by X-ray investigation. Poststenotic pneumonia is typically characterized by a fluid bronchogram (Fig. 4.6d). For investigation of this condition as well, dynamic sonotomography is com-

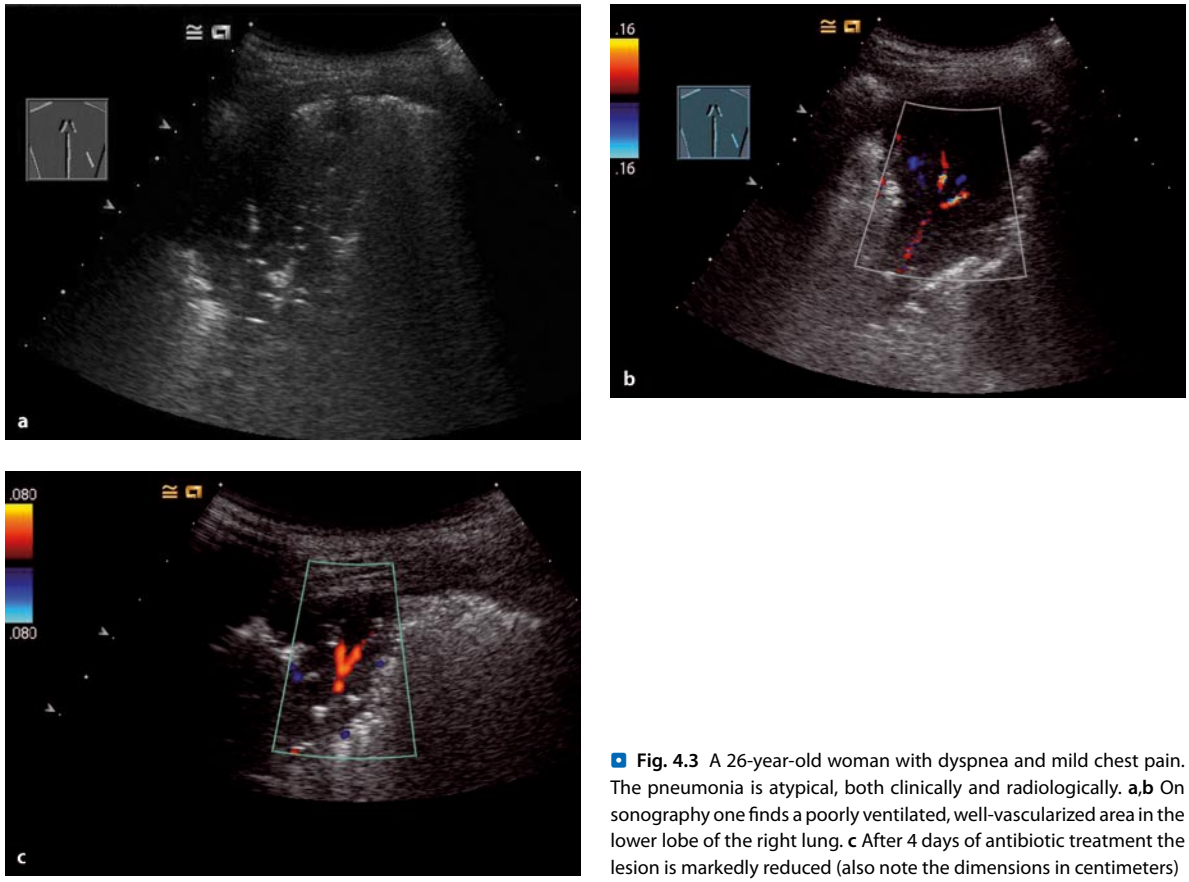

Fig. 4.3 A 26-year-old woman with dyspnea and mild chest pain. The pneumonia is atypical, both clinically and radiologically. **a**,**b** On sonography one finds a poorly ventilated, well-vascularized area in the lower lobe of the right lung. **c** After 4 days of antibiotic treatment the lesion is markedly reduced (also note the dimensions in centimeters)

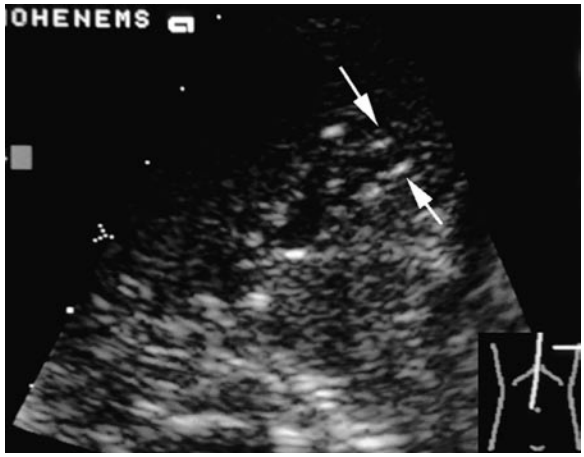

Fig. 4.4 Fluid bronchogram in the presence of poststenotic pneumonia. The bronchus can be distinguished by its wider reflexes than the reflexes seen in vessels. The bronchus varies in terms of wall thickness and is marked by a ribbed pattern

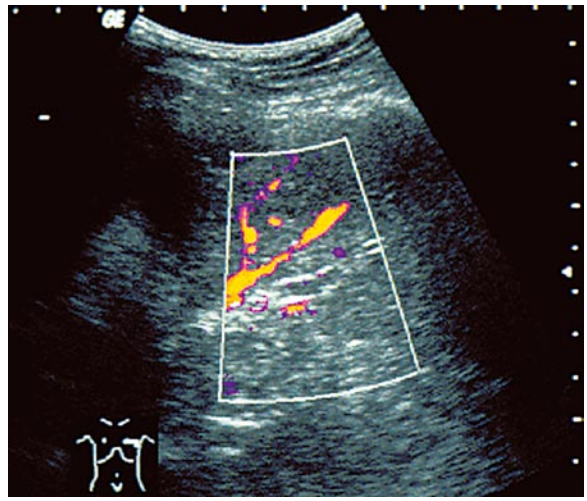

Fig. 4.5 Poststenotic pneumonia in the upper lobe on the left side. The vessels can be demarcated even better on color-coded duplex sonography. The reflex of the bronchus is interrupted and is also wider

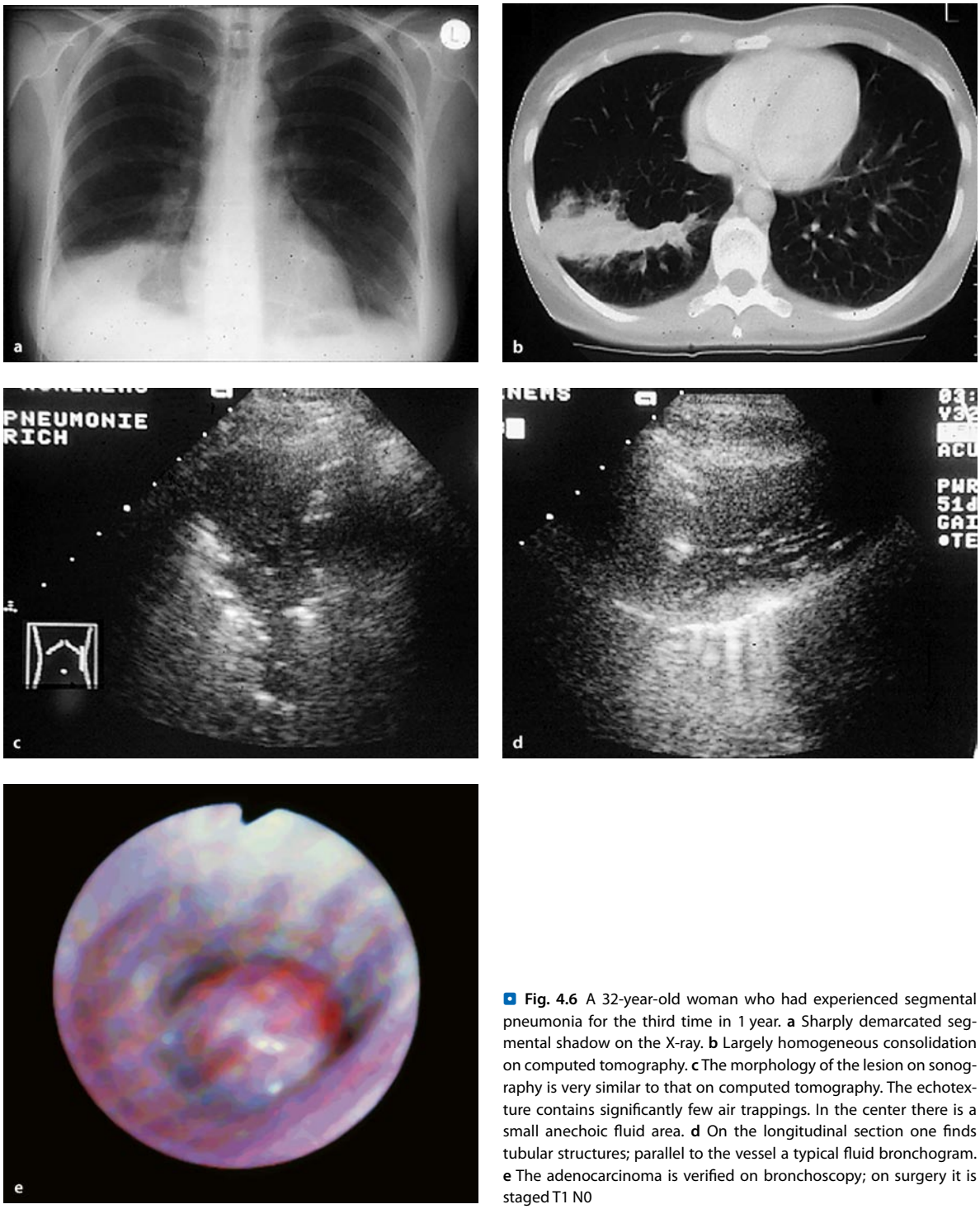

Fig. 4.6 A 32-year-old woman who had experienced segmental pneumonia for the third time in 1 year. **a** Sharply demarcated segmental shadow on the X-ray. **b** Largely homogeneous consolidation on computed tomography. **c** The morphology of the lesion on sonography is very similar to that on computed tomography. The echotexture contains significantly few air trappings. In the center there is a small anechoic fluid area. **d** On the longitudinal section one finds tubular structures; parallel to the vessel a typical fluid bronchogram. **e** The adenocarcinoma is verified on bronchoscopy; on surgery it is staged T1 N0

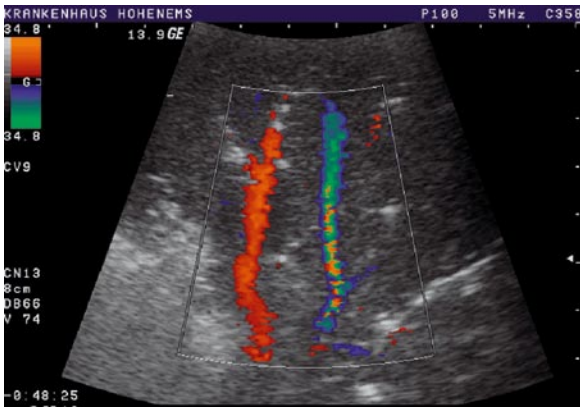

Fig. 4.7 On color-coded duplex sonography pneumonia is seen as an accentuated, regular pattern of circulation

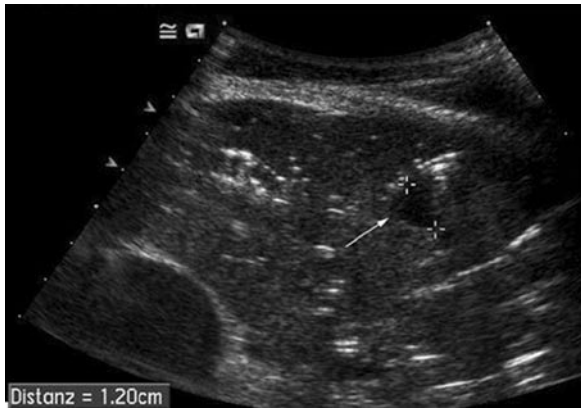

Fig. 4.8 Microabscess on the fourth day of a lobar pneumonia in the upper lobe of the left lung, which could not be seen on X-ray. This abscess healed on its own.

parable with computed tomography. Monitoring the effectiveness of therapy is important in this setting—is the pneumonia subsiding or is the tumor increasing in size (Braun et al. 1990; Yang et al. 1990)?

4.1.1.8 Circulation

On color-coded duplex sonography pneumonia has a typical appearance: circulation is uniformly increased, ramified, and the vessels run a normal course. In fact, circulation is increased in the entire infiltrate up to beneath the pleura (Fig. 4.7). This is interesting when pneumonia needs to be differentiated from pulmonary infarctions that have poor or no blood flow, or even from tumors with an irregular circulation pattern. Carcinomas are strongly vascularized in their margins. Owing to neovascularization, vessels in the margins of carcinomas are characterized by a typical corkscrew pattern (Gehmacher et al. 1995; Mathis 1997).

4.1.1.9 Abscess Formation

Bacterial pneumonias tend to develop colliquations and form abscesses. This is the case in approximately 6% of patients with lobar pneumonia (this figure refers to radiographic investigations). Sonography more commonly reveals *microabscess* (Yang et al. 1991, 1992; Mathis 1997).

The *sonomorphology of pulmonary abscess* is highly characteristic: round or oval and largely anechoic lesions (Fig. 4.8). Depending on whether a capsule is formed, the margin is smooth, echodense and white (Fig. 4.9). Blurred internal echoes are indicative of high cell content or viscous pus rich in protein. In cases of abscesses due to gas-forming pathogens, highly echogenic small air trappings move actively within the fluid in concordance with the respiratory rhythm. Septa are seen as echodense, fluttering threads. Artificial noise caused by the impedance difference between infiltrated parenchyma and abscess fluid is occasionally observed close to the transducer head; however, this should not be mistaken for internal echoes. Genuine internal echoes are always present in the depth of the image as well. In the early stage, small abscesses are seen as pathological collections of fluid and are found in an irregular anatomical location in the consolidated, liver-like infiltrate. Smooth margins and the echogenic capsule are absent. Microabscesses cannot be easily distinguished from vessels on color-Doppler imaging.

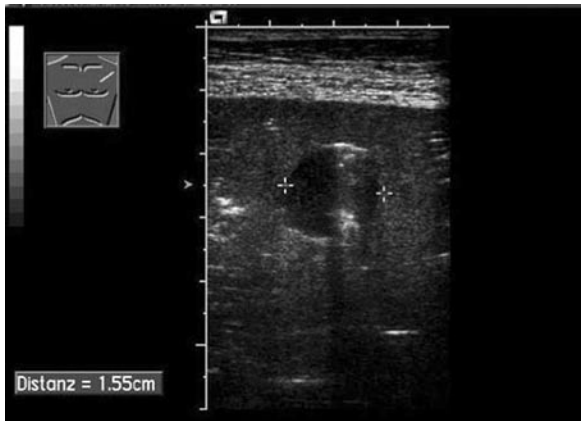

Fig. 4.9 Colliquated abscesses with persistent fever. Sonography-guided aspiration showed a surprisingly large number of tubercle bacilli

Considering the scarce quantity of material for bacteriological investigation obtained from the sputum or from bronchial lavage, it is useful to taken *a specimen for the detection of pathogens* by means of sonography-guided aspiration (Fig. 4.9). When the puncture is performed with an ordinary injection needle, a thorough sonographic preinvestigation should be performed, if necessary under sonographic visual guidance, to ensure that air-filled lungs and vessels are avoided. The cause of pulmonary infections can be determined by this method in 80% of cases (Yang et al. 1992; Chen et al. 1993; Lee et al. 1993; Liaw et al. 1994; Mathis 1997).

Lung abscess drainage may be performed under sonographic or computed tomography visual monitoring. The selection of the instrument depends on the size of the lesion and the consistency of the contents of the abscess. Microabscesses measuring up to 2 cm in size can be punctured and emptied by ordinary aspiration. Large abscesses with thick viscous pus require large suction and lavage drains; several types of such drains are commercially available. The position of the catheter is controlled by sonography. The catheter is seen as a two-layered reflex (Fig. 9.20). The risk of a pneumothorax is minimized when one passes through the chest wall obliquely, in a regular fashion, and enters the lung at the site where the abscess is closest to the pleura. The risk of a dreaded bronchopleural fistula is minimized when the correct approach is used, i.e., when one only traverses the homogeneous infiltrate and avoids ventilated areas (Yang et al. 1990; van Sonnenberg et al. 1991; Blank 1994; Mathis et al. 1999).

4.1.1.10 Healing Phase

When pneumonia is in the phase of healing, the infiltrated lung tissue is ventilated to an increasing extent. Such air gives rise to reflection and reverberation artifacts. The pneumonia recedes on the sonography image and usually appears smaller than on the chest radiograph (Figs. 4.10, 4.11).

The primary diagnosis of pneumonia is always based on the clinical appearance and the chest radiograph, as the extent of infiltration may be underestimated on sonography. The latter is useful to monitor the course of disease, especially in pregnant women and children (Schirg and Larbig 1999).

Indications for sonography in the presence of pneumonia:

- Pleural/basal shadow
- Visualization of abscesses
- Isolation of pathogens
- Abscess drainage
- Controls

4.1.2 Tuberculosis

Lung tuberculosis is characterized by several features on the radiograph, and even more so on chest sonography. The value of sonography in general has not been adequately researched. However, in certain settings its value is beyond dispute. It provides better detection of pathogens by sonography-guided aspiration or even biopsy and thus facilitates the visualization of subpleural colliquations and concomitant pleural fluid (Yuan et al. 1993; Kopf et al. 1994; Mathis 1997; Figs. 4.12–4.14).

Tuberculotic lung lesions may be seen on sonography as rounded or irregular structures of relatively homogeneous texture. Depending on the size of the lesion, these infiltrates may also be accompanied by air trappings as in pneumonia. Nodular dissemination, as in miliary tuberculosis, is visualized as multiple subpleural nodes measuring a few millimeters in size (Fig. 4.15).

Sonomorphology of lung tuberculosis:

- Narrow pleural effusions
- Thickened and fragmented visceral pleural reflexes
- A few or numerous hypoechoic lesions in subpleural location
- Pneumonic lesions
- Formation of cavities

Colliquations can be imaged well, but air in cavities might be a disturbing factor and might limit visualization. Even very small quantities of the specific pleural effusion are seen. Pleural thickening may also be revealed. A patient's response to tuberculostatic therapy can be monitored well with sonography, especially in cases of pleural and subpleural tuberculosis lesions.

An old tuberculoma may raise suspicion of carcinoma on sonography as it does on radiographs, but rarely has "crow's feet" (Fig. 4.16). Subpleural tuberculotic scars may be relatively echodense and star-shaped; in the presence of calcifications they might cause acoustic shadows.

The *value of sonography* in pulmonary tuberculosis lies in the detection of small pleural effusions that escape detection on X-ray investigation. Such effusions can be aspirated under sonographic guidance in order to confirm the diagnosis. Diagnostic aspiration is also useful in cases of subpleural nodules. When therapy is monitored, subpleural lesions can be better followed on so-

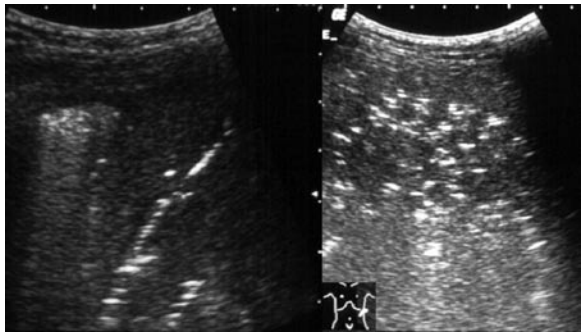

Fig. 4.10 Engorgement phase of clinically typical pneumococcal pneumonia on the *left*. *Right*: Healing and reventilation after 5 days. Typical healing phase of bacterial pneumonia under treatment. The lesion is receding, the air trappings are increasing, and a large number of reverberation artifacts are seen

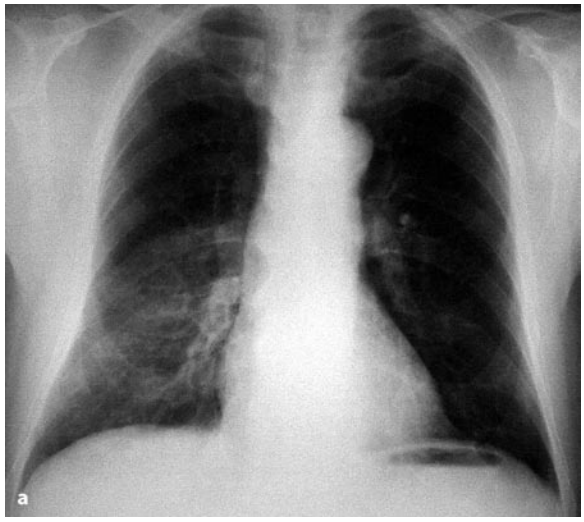

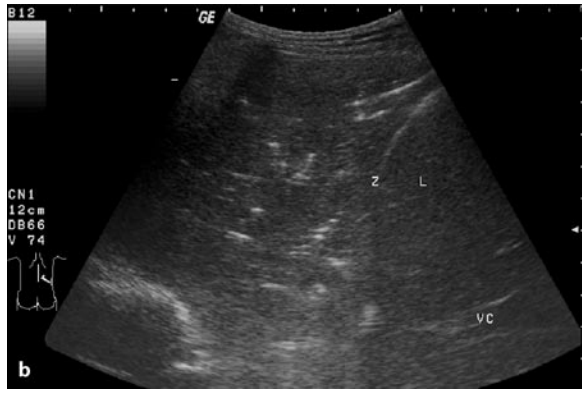

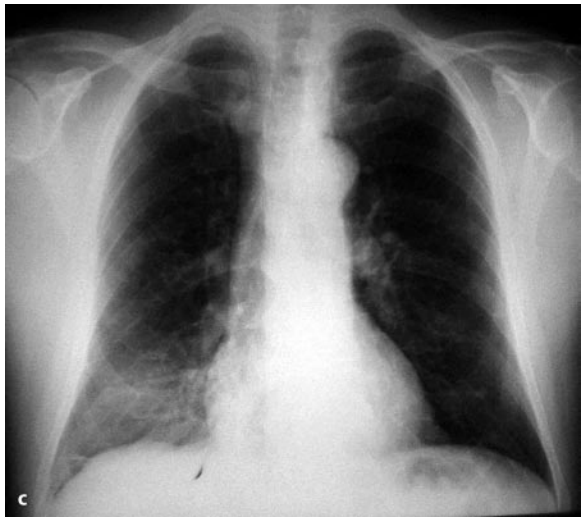

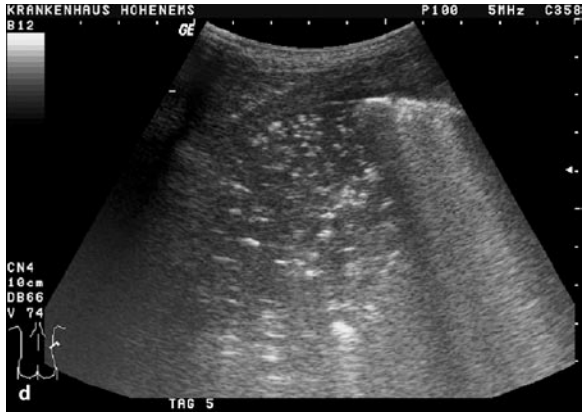

Fig. 4.11 A 72-year-old man with clinically severe pneumonia. **a** Typical appearance on X-ray. **b** On sonography the echotexture is similar to that of the liver, with a pronounced bronchoaerogram. *Z* diaphragm, *L* liver, *VC* vena cava. After 1 week of antibiotic therapy the patient is afebrile and has recovered to the extent that he can be discharged. **c** On the X-ray there still is a marked residual infiltrate. **d** Sonography only shows a receding infiltration

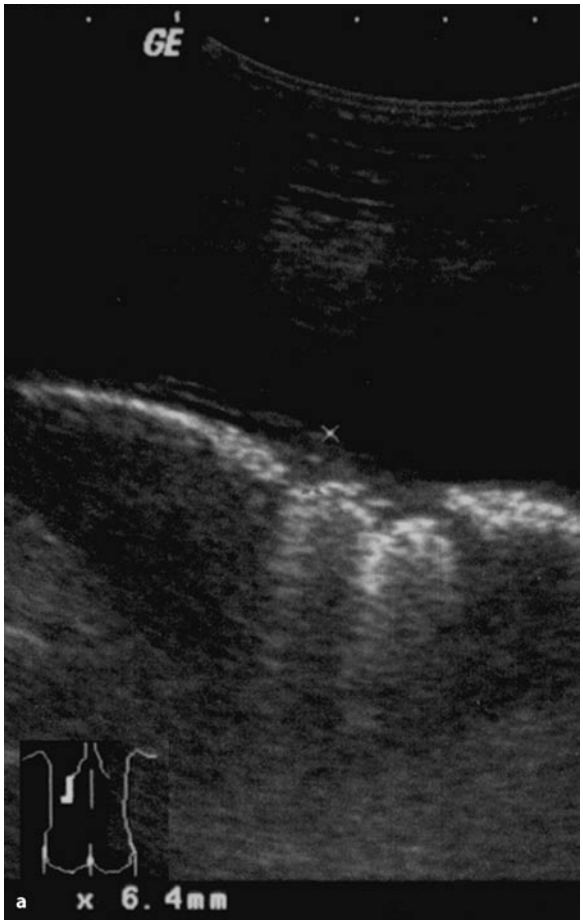

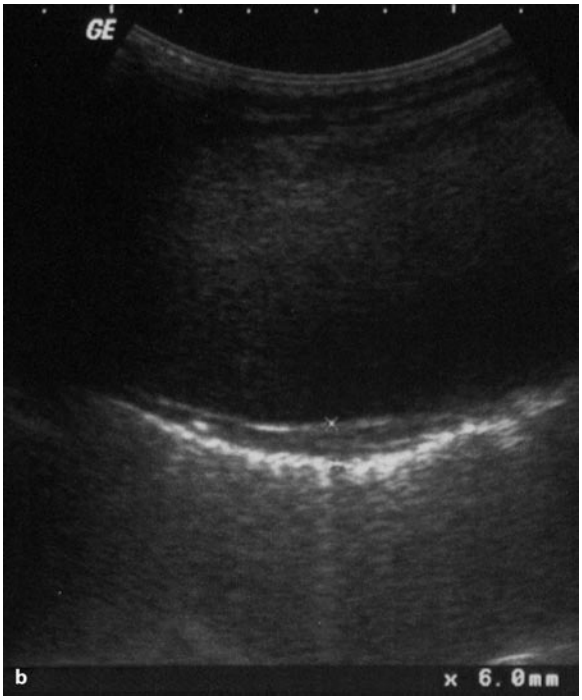

Fig. 4.12 a,b Persistent pleural effusion in a 32-year-old woman. Note the nodular and large thickening below the visceral pleura, seen through the 15-mm-wide pleural effusion. The diagnosis of tuberculosis was confirmed by sonography-guided biopsy

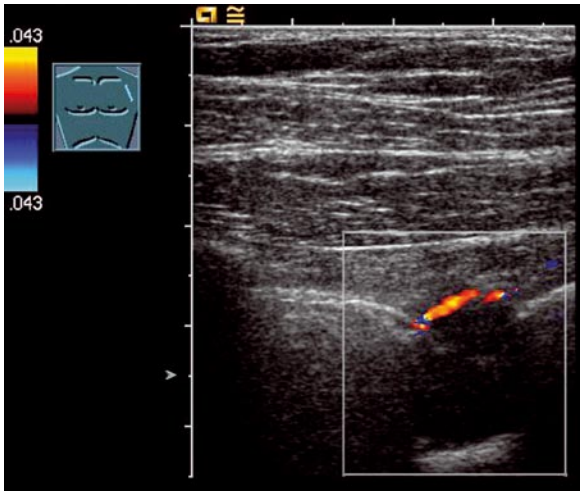

Fig. 4.13 Peripheral lung lesion on a routine X-ray of a young woman. On sonography one finds a hypoechoic, poorly vascularized lesion. Biopsy indicated tuberculosis

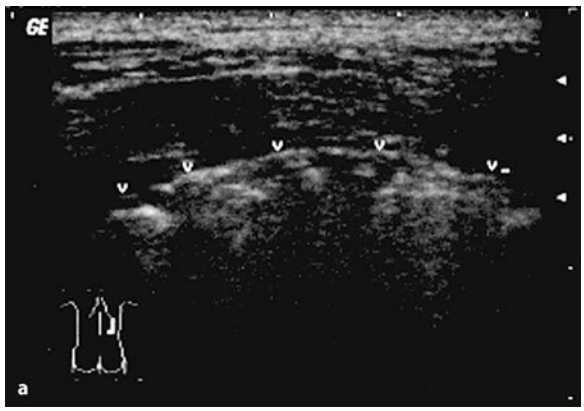

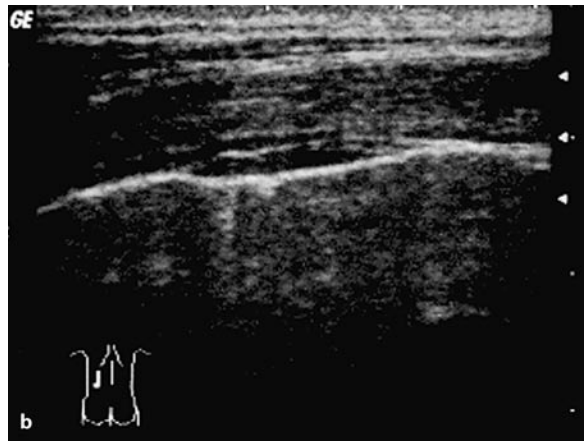

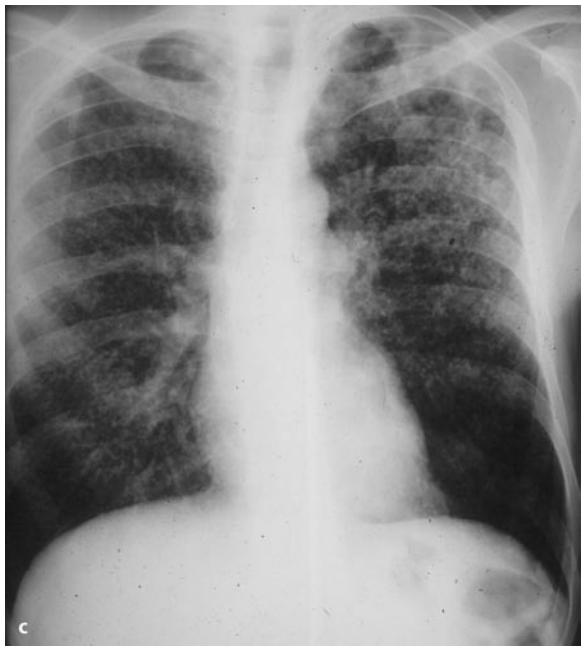

Fig. 4.14 Miliary tuberculosis. **a** Fragmented pleura (*arrowheads*) with numerous subpleural nodes measuring 2–3 mm in size. **b** Focal pleural effusion measuring 2 mm in width, which obviously was not seen on the chest X-ray **c** Chest X-ray showing miliary tuberculosis

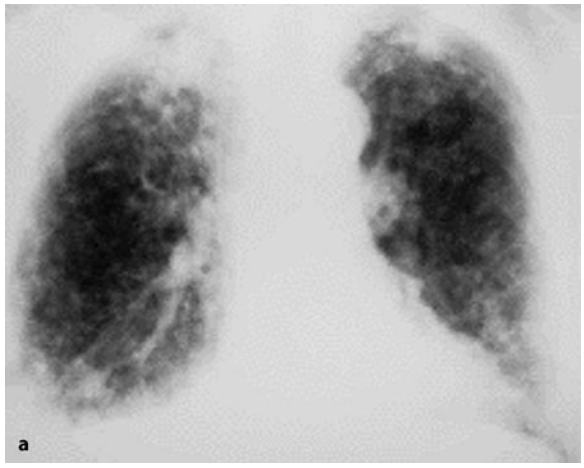

Fig. 4.15 A 50-year-old man, alcoholic and cachectic, admitted because of fever, dyspnea, cough and respiratory pain. **a** The X-ray showed speckled lesions in all fields of the lung, primarily indicative of miliary tuberculosis. Differential diagnosis, alveolar cell carcinoma. **b–e** *see next page*

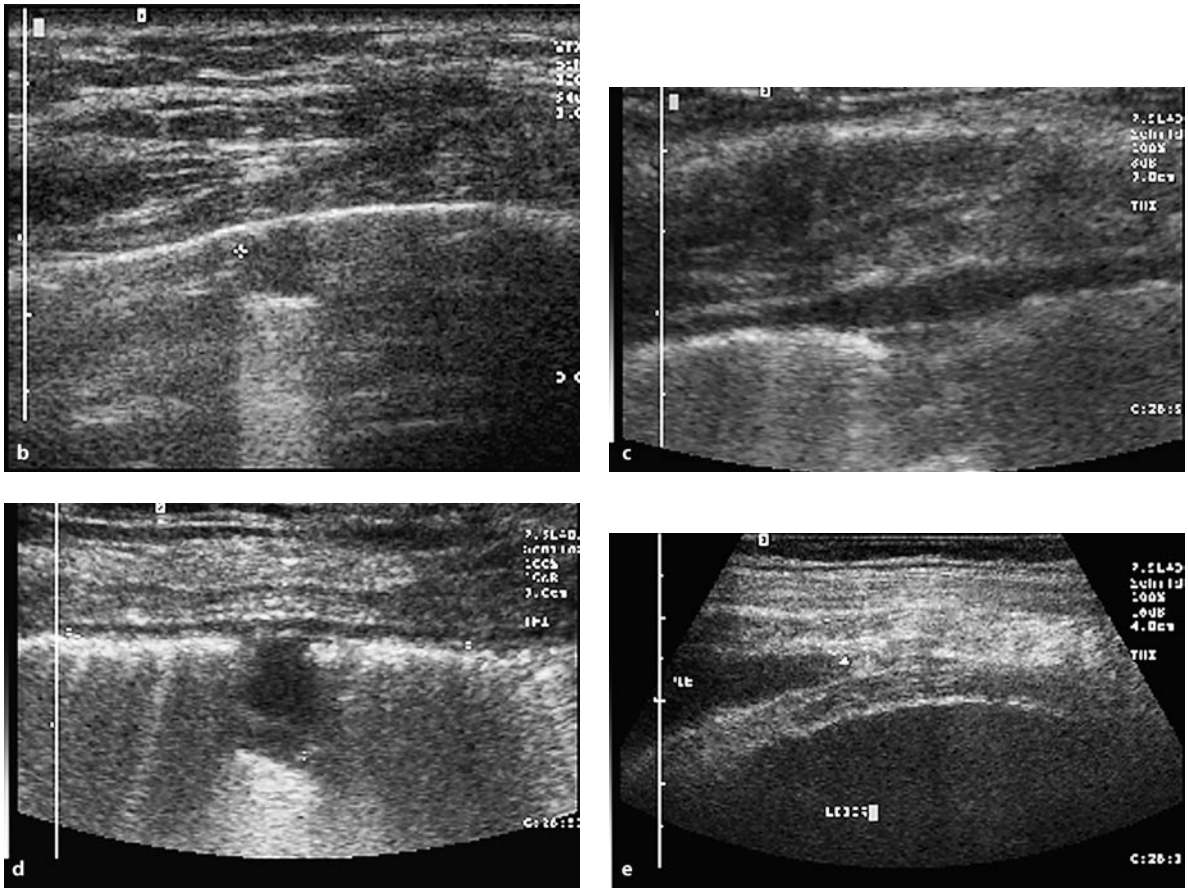

Fig. 4.15 *(continued)* **b** Sonography shows multiple hypoechoic lesions, movable on breathing, in subpleural location. **c** An accompanying pleural effusion can be assigned to the peripheral lesions in the lung. **d** A subpleural hypoechoic density is visualized. The lesion measuring 8.5 mm in size is rather liquid in character. **e** The tiny miliary foci (2–3 mm in size) on the parietal pleura can be visualized in the marginal sinus as an accompanying pleural effusion (*arrow*). The diagnosis of miliary tuberculosis was confirmed by sonography-guided aspiration of the liquid lesion

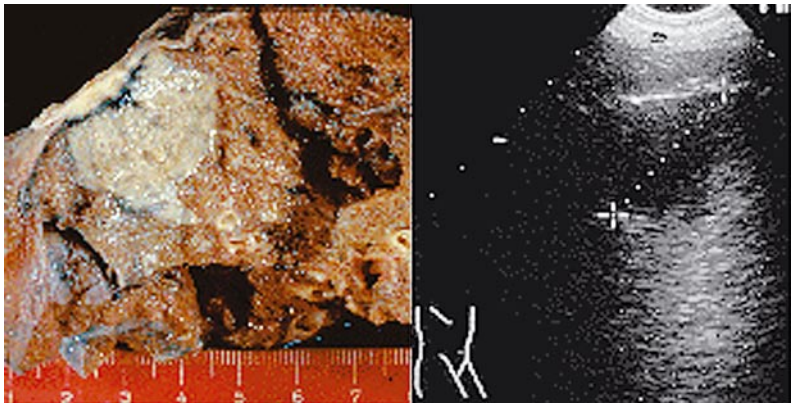

Fig. 4.16 An 81-year-old man whose X-ray raised suspicion of a peripheral lung carcinoma. On sonography the round lesion is clearly seen. Sonography-guided aspiration revealed "no malignant cells." The band of the visceral pleura is remarkably well preserved. The autopsy showed an old and scarred tuberculoma

nography than on radiographs. X-ray controls need not be performed. However, sonographic imaging of cavities is limited when air is present in the cavity. Chest radiographs and computed tomography are indispensable in this setting.

In cases of rarer infectious lung consolidations such as aspergillosis or echinococcus, typical lesions can be visualized and significant additional information (in addition to the information available from radiographs) obtained (Fig. 4.17).

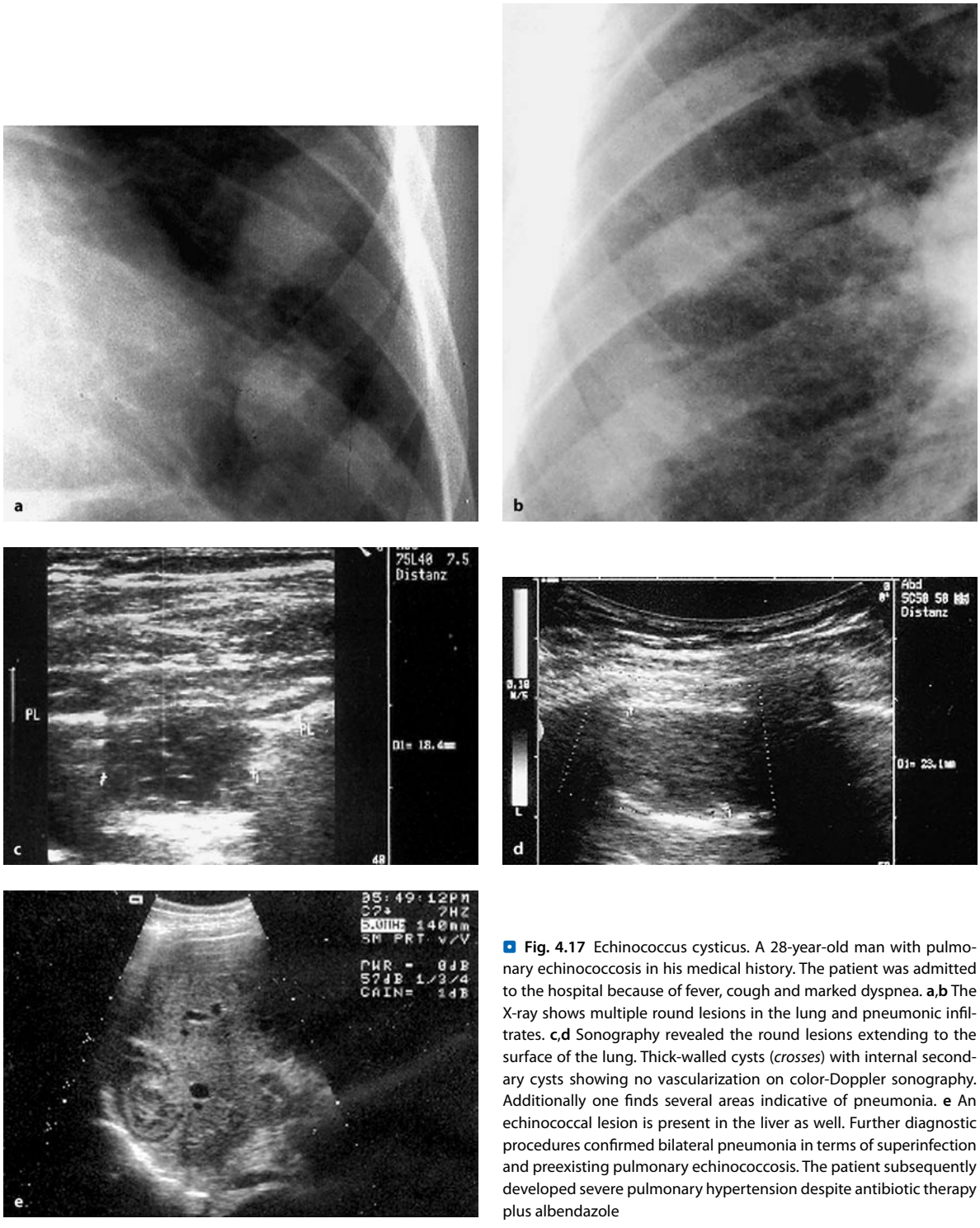

Fig. 4.17 Echinococcus cysticus. A 28-year-old man with pulmonary echinococcosis in his medical history. The patient was admitted to the hospital because of fever, cough and marked dyspnea. **a**,**b** The X-ray shows multiple round lesions in the lung and pneumonic infiltrates. **c**,**d** Sonography revealed the round lesions extending to the surface of the lung. Thick-walled cysts (*crosses*) with internal secondary cysts showing no vascularization on color-Doppler sonography. Additionally one finds several areas indicative of pneumonia. **e** An echinococcal lesion is present in the liver as well. Further diagnostic procedures confirmed bilateral pneumonia in terms of superinfection and preexisting pulmonary echinococcosis. The patient subsequently developed severe pulmonary hypertension despite antibiotic therapy plus albendazole

4.1.3 Interstitial Lung Disease

Technically sonography is entirely unsuitable to diagnose diseases of the lung framework. However, it was shown that such diseases are frequently accompanied by *involvement of the pleura* and the latter is significantly better visualized by sonography than by other imaging procedures:

- Minimal pleural effusions
- Fragmented pleura with several comet-tail artifacts
- Subpleural consolidations (Figs. 4.18, 4.19)

The value of the method lies in the detection of a grave condition and in steering the diagnostician's attention towards a specific target.

Therapy controls are highly efficient in cases of minimal pleural effusions and subpleural infiltrations; no method is superior to sonography in this regard (Wohlgenannt et al. 2000; Reißig and Kroegel 2003).

4.1.4 Summary

Pneumonic lung infiltrations are characterized by typical changes in terms of sonomorphology (bronchoaerograms, colliquations, parapneumonic effusions). Pneumonias may be first discovered at the bedside. The extent of infiltration may be underestimated owing to artifacts on sonography. Reventilation is well correlated with clinical progression.

The value of chest sonography in pneumonia lies in the assessment of accompanying pleural fluid, timely detection of abscess formation, sonography-guided collection of pathogens, and controls particularly in pregnant women and children.

In cases of tuberculosis and diseases of the frame of the lung, sonography is the optimum method to visualize small pleural effusions and subpleural consolidations; therefore, it is indispensable to control the progress of the disease.

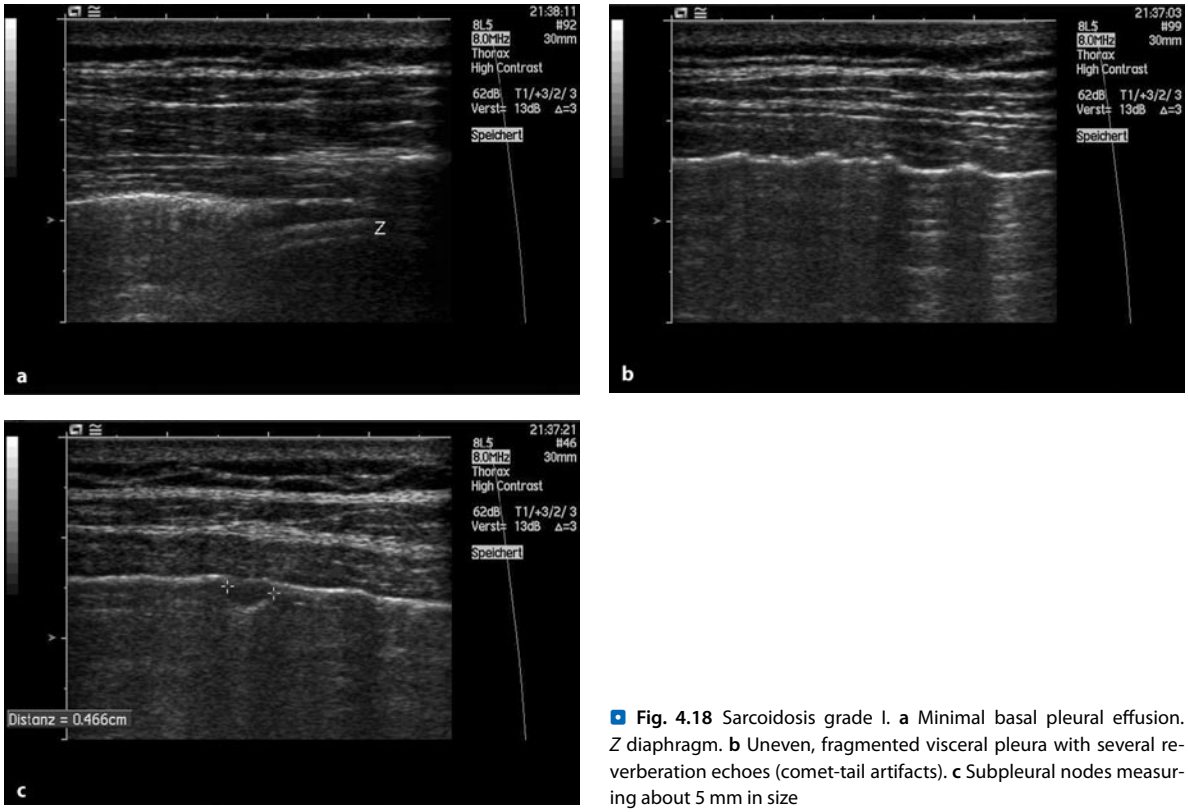

Fig. 4.18 Sarcoidosis grade I. **a** Minimal basal pleural effusion. *Z* diaphragm. **b** Uneven, fragmented visceral pleura with several reverberation echoes (comet-tail artifacts). **c** Subpleural nodes measuring about 5 mm in size

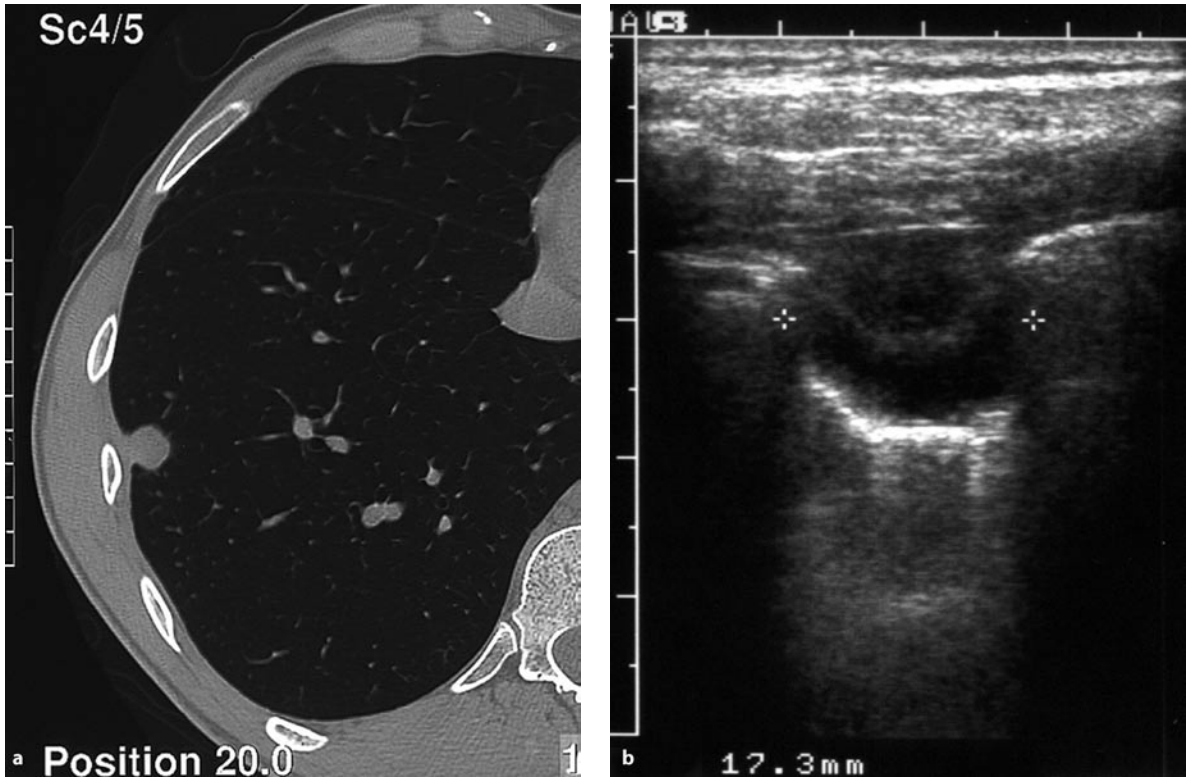

Fig. 4.19 **a** The patient was referred for identification of the primary lesion in the presence of a "metastatic lung." **b** Sonography-guided biopsy of the subpleural lesion indicated a rheumatic nodule

References

Anzböck W, Braun U, Stellamor K (1990) Pulmonale und pleurale Raumforderungen in der Sonographie. In: Gebhardt J, Hackelöer BJ, von Klingräff G, Seitz K (eds) Ultraschalldiagnostik '89. Springer, Berlin, pp 394–396

Blank W (1994) Sonographisch gesteuerte Punktionen und Drainagen. In: Braun B, Günther R, Schwerk WB (eds) Ultraschalldiagnostik Lehrbuch und Atlas, vol III-11.1. ecomed, Landsberg/Lech, pp 15–22

Braun U, Anzböck W, Stellamor K (1990) Das sonographische Erscheinungsbild der Pneumonie. In: Gebhardt J, Hackelöer BJ, von Klingräff G, Seitz K (eds) Ultraschalldiagnostik '89. Springer, Berlin, pp 392–393

Chen CH, Kuo ML, Shih JF, Chang TP, Perng RP (1993) Etiologic diagnosis of pulmonary infection by ulrasonically guided percutaneous lung aspiration. Chung Hua Taiwan 51:5

Gehmacher O, Mathis G, Kopf A, Scheier M (1995) Ultrasound imaging of pneumonia. Ultrasound Med Biol 21:1119–1122

Kopf A, Metzler J, Mathis G (1994) Sonographie bei Lungentuberkulose. Bildgebung 61(S2):12

Lee LN, Yang PC, Kuo SH, Luh KT, Chang DB, Yu CJ (1993) Diagnosis of pulmonary cryptococcosis by ultrasound guided perdutaneous aspiration. Thorax 48:75–78

Liaw YS, Yang PC et al (1994) The bacteriology of obstructive pneumonitis. Am J Respir Crit Care Med 149:1648–1653

Mathis G (1997) Thoraxsonography—part II: peripheral pulmonary consolidation. Ultrasound Med Biol 23:1141–1153

Mathis G, Metzler J, Fußenegger D, Feurstein M, Sutterlütti G (1992) Ultraschallbefunde bei Pneumonie. Ultraschall Klin Prax 7:45–49

Mathis G, Bitschnau R, Gehmacher O, Dirschmid K (1999) Ultraschallgeführte transthorakale Punktion. Ultraschall Med 20:226–235

Reissig A, Kroegel C (2003) Transthoracic sonography of diffuse parenchymal lung disease: the role of comet tail artefacts. J Ultrasound Med 22:173–180

Schirg E, Larbig M (1999) Wert des Ultraschalls bei der Diagnostik kindlicher Pneumonien. Ultraschall Med 20:34

Targhetta R, Chavagneux R, Bourgeois JM, Dauzat M, Balmes P, Pourcelot L (1992) Sonographic approach to diagnosing pulmonary consolidation. J Ultrasound Med 11:667–672

van Sonnenberg E, Agostino H, Casola G, Wittich GR, Varney RR, Harker C (1991) Lung abscess: CT-guided drainage. Radiology 178:347–351

Weinberg B, Diaboumakis EE, Kass EG, Seife B, Zvi ZB (1986) The air bronchogram: sonographic demonstration. AJR Am J Roentgenol 147:593-–595

Wohlgenannt S, Gehmacher O, Mathis G (2001) Thoraxsonographische Veränderungen bei interstitiellen Lungenerkrankungen. Ultraschall Med 22:27–31

Yang PC, Lee YC, Wu HD, Luh KT (1990) Lung tumors associated with obstructive pneumonitis: US studies. Radiology 174:593–595

Yang PC, Luh KT, Lee YC (1991) Lung abscesses: ultrasonography and ultrasound-guided transthoracic aspiration. Radiology 180:171–175

Yang PC, Luh KT, Chang DB, Yu CJ, Kuo SH, Wu HD (1992) Ultrasonographic evaluation of pulmonary consolidation. Am Rev Resp Dis 146:757–762

Yuan A, Yang PC, Chang DB et al (1993) Ultrasound guided aspiration biopsy for pulmonary tuberculosis with unusual radiographic appearances. Thorax 48:167–170

4.2 Neoplastic Consolidations in the Lung: Primary Lung Tumors and Metastases

S. Beckh

In diagnostic imaging of malignant lung lesions, sonography is a valuable adjunct to sectional images obtained by radiological procedures (Müller 1997; Fraser et al. 1999; Detterbeck et al. 2003). Owing to its high resolution, the sonography image yields very important additional information. For instance, vessels can be imaged without contrast medium (Yang 1996; Hsu et al 1998; Görg and Bert 2004; Chap. 7).

Lung consolidations are seen on sonography only when no aerated tissue hinders the echo transmission. For staging of the disease and planning treatment in cases of malignant lung disease, procedures that provide sectional images such as computed tomography or magnetic resonance tomography are absolutely essential in order to obtain an overview of the entire chest (van Kaick and Bahner 1998; Tuengerthal 2003; Knopp et al. 1998; Schönberg 2003). As a rule the sonographic investigation is performed when the findings of various radiographic procedures are known. Given specific symptoms, however, a targeted symptom-oriented investigation is also meaningful (Chap. 10).

In the diagnosis of lung carcinoma, the specific questions to be answered by the sonographic investigation are the following:

- Criteria to determine the benign or malignant nature of the disease
- Imaging guidance for biopsy
- Contribution to staging (Table 4.1)
- Whether surgery and resection can be performed
- Controls to monitor therapy
- Visualizing vascular complications (inflow congestion, thrombosis)

Pulmonary malignancies may have a highly variable *echotexture*. They are usually hypoechoic, moderately echodense or very inhomogeneously structured; more rarely they are nearly anechoic (Mathis 1997; Mathis et al. 1999; Table 4.2). However, the echotexture alone does not allow the investigator to draw conclusions about the malignant or benign nature of the disease (Figs. 4.20, 4.21).

Table 4.1 Structures visualized by sonography in tumor, node, metastasis (*TNM*) staging

TNM status	Structures visualized by sonography
T1	Tumor <3 cm, extending to the periphery of the lung (Fig. 4.20)
T2	Tumor >3 cm, invading the visceral pleura, partial atelectasis (Figs. 4.22, 4.31a)
T3	Tumor invading the chest wall, diaphragm, parietal pericardium; complete atelectasis (Figs. 4.25, 4.27d, e)
T4	Tumor invading the mediastinum, heart, large vessels; malignant pleural effusion (Fig. 4.28)
N1	Ipsilateral peribronchial lymph node on endobronchial sonography (Chap. 6)
N2	Ipsilateral mediastinal and/or subcarinal lymph node on transesophageal sonography (Sect. 5.2)
N3	Supraclavicular lymph node (Fig. 4.30a)
M1	Metastases in the abdomen and the soft tissues (Fig. 4.30b)

Adapted from Thomas et al. (2002)

Table 4.2 Sonomorphology of lung carcinomas

Morphology	Echotexture	Vessels	Complex structures
Sharp margins	Inhomogeneous	Displacement of vessels	Residual ventilated areas
Rounded	Hypoechoic	Destruction of vessels	Accompanying pneumonia at the margin
Polypoid	Rarely echogenic	Interruption of vessels	Solid space-occupying lesion/pneumonia
Ramifications	Rarely anechoic	Neovascularization	Bacterial/fungal colonization
Serrated margin	Necrotic areas	–	Bizarre pattern in large necroses

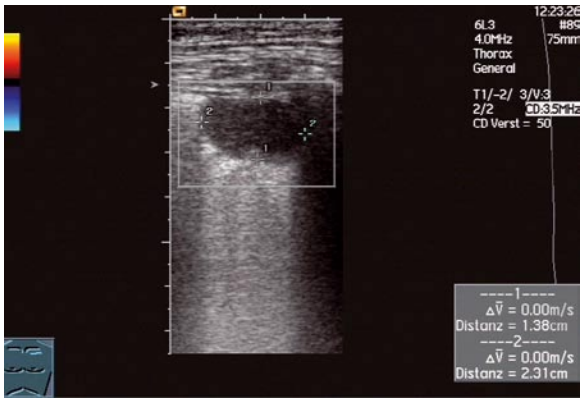

Fig. 4.20 A small hypoechoic lesion in a 78-year-old man: an incidental finding in the upper lobe of the left lung, in infraclavicular location. Sonography-guided biopsy indicated squamous cell carcinoma

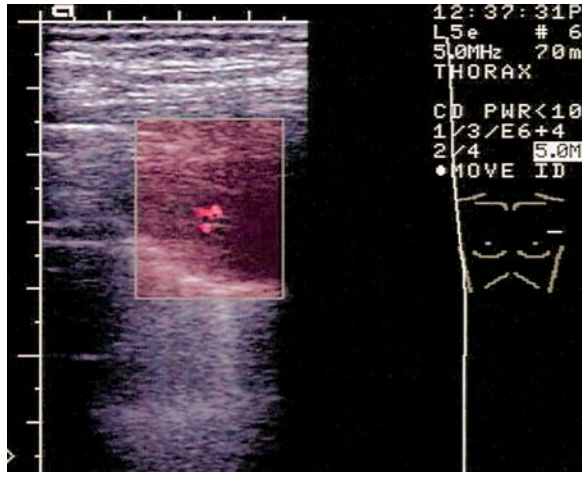

Fig. 4.21 A 40-year-old man with recurrent eosinophilic pleural effusion. X-rays showed a peripheral lesion in the upper lobe of the left lung. On sonography in the anterior axillary line in the second intercostal region there is a hypoechoic peripheral pulmonary lesion with central vessels and rather sharp margins. Removal of the lesion by thoracoscopy led to the diagnosis of hyalinosis and callus. The source of the pleural effusions is still not clear

In contrast to acute inflammatory infiltrations, the sonomorphology of malignant lesions does not change during a short course of disease. Chronic carnifying pneumonia and peripheral callused cicatricial lesions are problematic in terms of differential diagnosis; it may be difficult to differentiate these entities from malignant disease (Mathis 1997).

Decisive criteria to grade the malignant or benign nature of a pulmonary lesion are the following:

- *Contours* of the lung surface
- *Margins* to ventilated lung tissue
- *Invasion* of adjacent structures (chest wall, diaphragm, pericardium)
- *Destruction* of normal tissue architecture
- *Displacement* of regular vessels
- *Neovascularization*
- *Differentiation between a central space-occupying lesion and a poststenotic invasion/atelectasis*

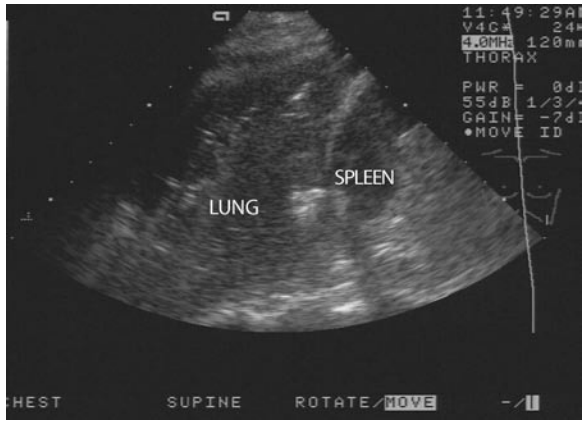

Fig. 4.22 Small-cell lung carcinoma invading the lower lobe of the left lung (diagnosed by bronchoscopic biopsy), irregular lung surface, narrow pleural effusion

4.2.1 Contours of the Lung Surface

The *contours* of the lung surface are very well delineated from the surrounding pleural fluid. Figure 4.22 shows the uneven surface of the lower lobe of the left lung, invaded by a small-cell lung carcinoma.

A benign inflammatory infiltration would never lead to such irregular deformation of the lung surface.

4.2.2 Delineation of Margins from Ventilated Lung Tissue

Malignant lesions are often very *sharply demarcated* from lung tissue (Fig. 4.23). Occasionally, however, one finds *fringed or finger-shaped ramifications* into the normally ventilated parenchyma—a sign of invasive growth (Fig. 4.24).

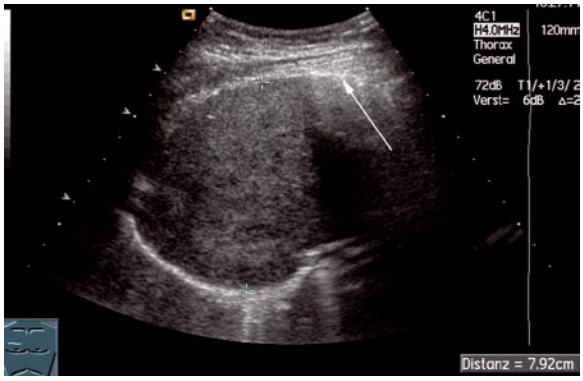

Fig. 4.23 Large hypoechoic space-occupying lesion in the upper lobe of the right lung, sharply demarcated from ventilated lung tissue. In medial location (*arrow*) one finds an unremarkable echogenic pleural line. Sonography-guided biopsy indicated poorly differentiated neuroendocrine carcinoma G4

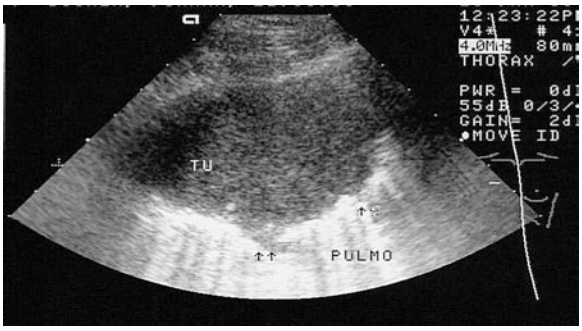

Fig. 4.24 Hypoechoic space-occupying lesion in the upper lobe of the right lung with fringed branches into the ventilated lung tissue (*arrows*). Histological investigation of the resected upper lobe yielded a mixed-cell lung carcinoma (squamous cell or large-cell carcinoma)

In contrast to inflammatory lesions, such solid malignant formations in marginal zones are not ventilated and therefore are more sharply demarcated from the surrounding tissue.

4.2.3 Invasion of Adjacent Structures—Chest Wall, Diaphragm and Pericardium

Practically at first glance, a malignancy *invading* adjacent structures is indicative of the aggressive nature of the tumor (Suzuki et al. 1993). In the case of a Pancoast's tumor, a space-occupying lesion penetrating the dome of the pleura is clearly visualized (Fig. 4.25).

Malignant invasion of the chest wall frequently causes local pain. Targeted investigation of the region with the transducer will help to diagnose the condition early (Fig. 4.26).

Invasion into adjacent structures of the chest wall is a very reliable sign of malignant growth. In terms of differential diagnosis only one disease is likely to be present here, namely, actinomycosis or nocardiosis (Corrin 1999; Fig. 4.27a–c).

The inflammation frequently spreads into the chest wall. The regular cardinal anatomic structures of the lung, however, are well preserved within the pneumonic infiltration of tissue. In conjunction with clinical symptoms and bacteriological investigation, they permit the investigator to make the correct diagnosis.

The diaphragm on the right side of the chest is usually fully visible, with the liver serving as the sonic window. On the left side, tumors lying medial to the spleen are only seen if there is an effusion or when the tumor itself serves as the sonic window. In the latter case the insertion at the diaphragm may be seen as in Fig. 4.27d.

For staging of the disease and planning therapy, among other factors the relation between the tumor and the pericardium is important. Owing to the excellent resolution and the possibility of dynamic investigation, tumor invasion of the parietal pericardium can be clearly visualized (Fig. 4.27e).

4.2.4 Destruction of the Normal Tissue Architecture and Displacement of Regular Vessels

Malignant invasion *destroys* the normal texture of tissue. Bronchial branches may be displaced or fully destroyed (Fig. 4.28).

The original normal vessels are either displaced (Figs. 4.25, 4.29a) or disappear altogether (Fig. 4.28).

In some cases, vessels of the tumor itself are found particularly in the margin (Fig. 4.29b). Such vessels are convoluted and marked by changes in diameter (Yuan et al. 1994; Mathis 1997; Hsu et al. 1996, 1998).

4.2.5 Additional Investigations to Assess the Possibility of Resection

For further planning of treatment in terms of *whether the entity can be operated on and resected*, a detailed dynamic investigation has to be performed (Beckh and Bölcskei 2003). In order to decide between video-assisted thoracoscopy (VATS) and thoracotomy it is important to know

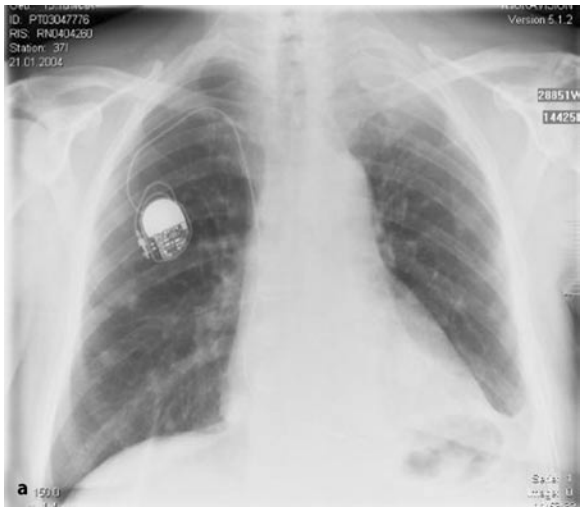

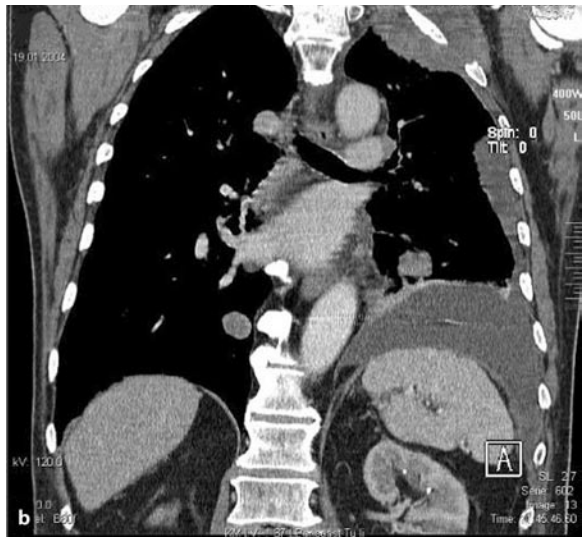

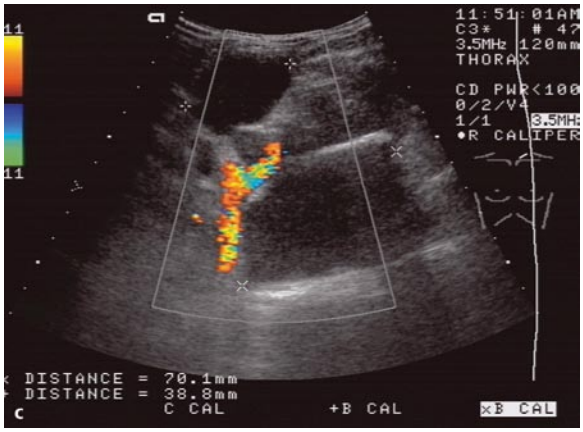

Fig. 4.25 **a** A 72-year-old man with pain in the left chest for several months; initially interpreted as angina pectoris. On the overview X-ray a shadow was noted on the left side in apical location. **b** On the coronary computed tomography section there was a space-occupying lesion on the left side in apical location, surrounding the first rib and penetrating the soft tissue. **c** Corresponding sonographic image: large hypoechoic tumor formation penetrating the dome of the pleura and invading the supraclavicular soft tissue. The subclavian artery is slightly compressed and displaced medially by the tumor. Sonography-guided biopsy indicated moderately differentiated adenocarcinoma developing within scar and connective tissue

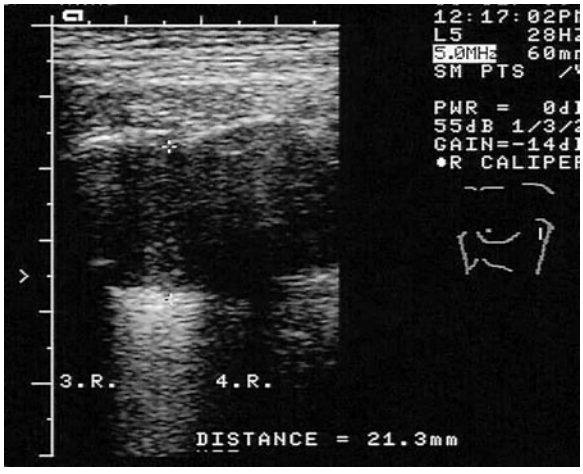

Fig. 4.26 This woman slipped on a staircase 6 months ago and has been experiencing renewed pain in the left chest for 4 weeks. Computed tomography shows a suspected hematoma. On sonography there is a space-occupying lesion invading the muscles of the chest wall and causing obvious destruction of the third and fourth rib laterally. Sonography-guided biopsy indicated poorly differentiated adenocarcinoma

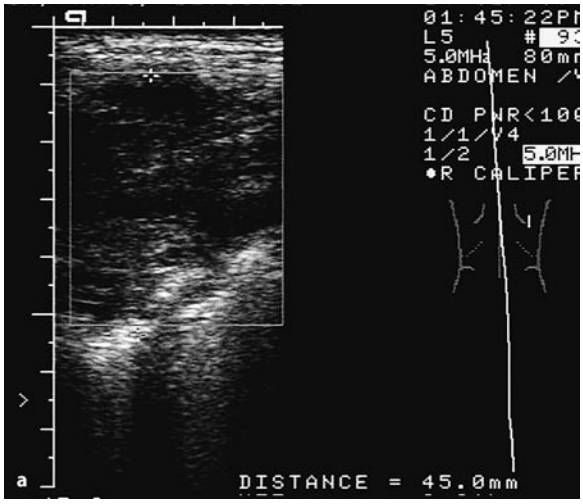

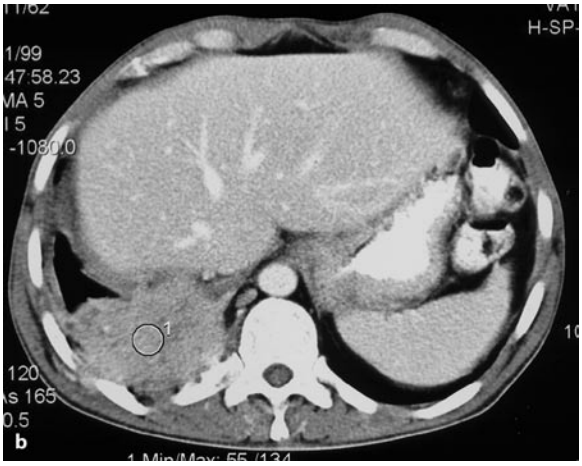

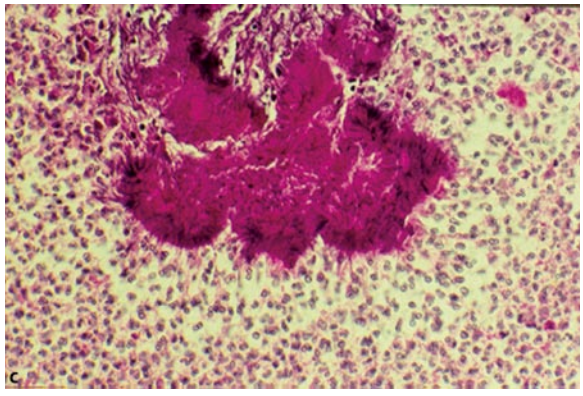

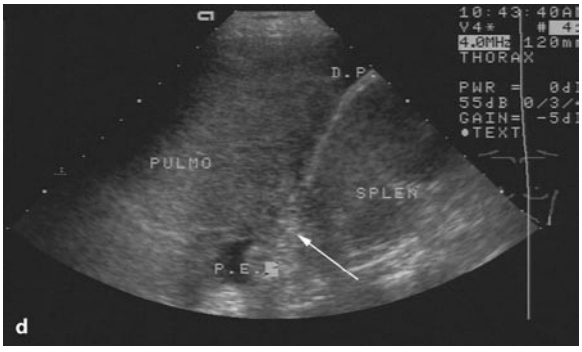

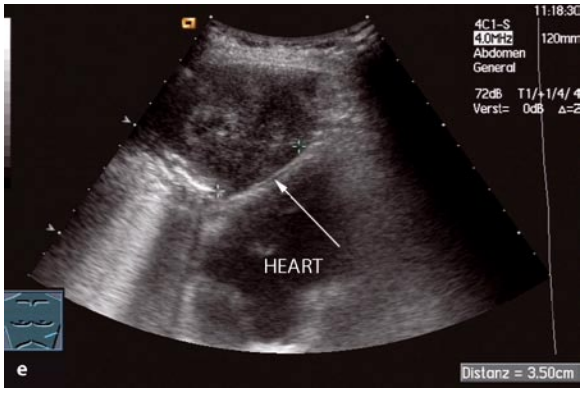

Fig. 4.27 **a** This 37-year-old man was severely ill: high fever and dyspnea. On sonography the lesion was clearly found to be crossing margins. Regular branches of the bronchial tree and vessels were well preserved; therefore, a malignancy was considered very unlikely despite the large size of the lesion. **b** Corresponding computed tomography image with the invasion which is continuing from the right lower lobe into the chest wall. **c** The biopsy specimen obtained from surgery shows evidence of actinomyces. Under high-dose penicillin therapy the invasion resolved within 10 weeks and a narrow basal callus formation remained. (Histological specimen provided by Peter Wünsch, Institute of Pathology, Klinikum Nürnberg, Nuremberg.) **d** Large tumor below the left lower lobe, inserting into the diaphragm (*arrow*). Histology of the sonographic biopsy and the operation specimen indicated benign fibrous tumor of the pleura. **e** Tumor in the lingula, invading about 3.5 cm of the parietal pericardium (*arrow*). Sonographic biopsy indicated poorly differentiated adenocarcinoma

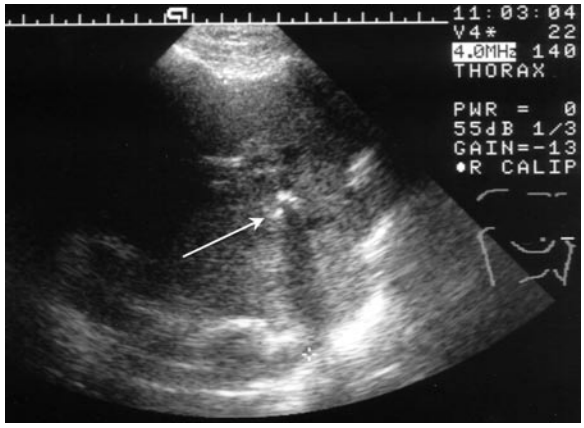

Fig. 4.28 A 50-year-old man with retrosternal pain that initially raised suspicion of coronary heart disease. Sonography showed a large tumor in the upper lobe in left parasternal location, penetrating the mediastinum and fully destroying the bronchial branches. In the tumor there is a calcification accompanied by obliteration of echoes in the dorsal aspect (*arrow*). Sonographic biopsy indicated poorly differentiated adenocarcinoma with tumor cell complexes in lymphatic recesses

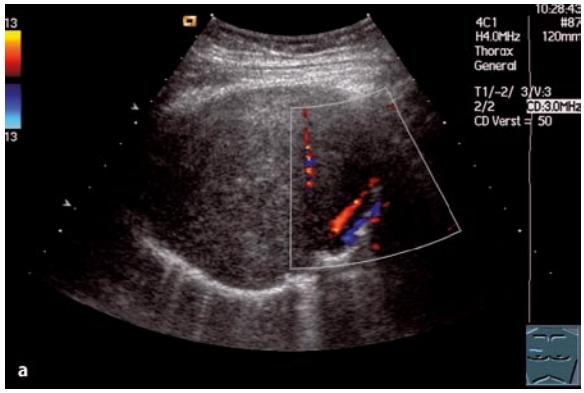

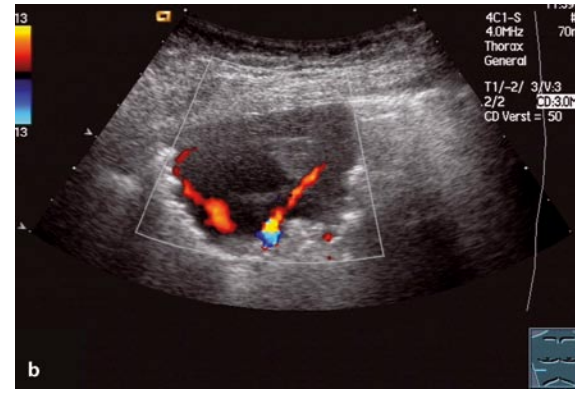

Fig. 4.29 **a** Large tumor in the upper lobe of the right lung, displacing the artery and vein of the upper lobe in medial direction. Sonographic biopsy indicated poorly differentiated neuroendocrine carcinoma. **b** Tumor in the lateral middle lobe with central necrosis; in the marginal areas there are strong, convoluted vessels of changing diameter

whether the pathological entity is widely fixed to the parietal pleura or is freely movable in conjunction with the lung (Landreneau et al. 1998). However, adherence alone does not permit the investigator to decide whether the lesion is malignant or benign.

In the course of tumor staging, sonography is more suitable than computed tomography to demonstrate metastases in supraclavicular lymph node regions (Fultz 2002; Fig. 4.30a)

The basic diagnostic procedures must include sonography of the abdomen in order to identify metastases (Fig. 4.30b).

4.2.5.1 Tumor-Related Complications in Mediastinal Vessels

In case of mediastinal tumor spread, the vena cava and its supplying vessels must be examined in order to identify compression syndromes or thrombosis (Ko et al. 1994; Fig. 4.30c).

4.2.5.2 Differentiation of a Central Space-Occupying Lesion from an Atelectasis

Atelectatic lung tissue is a suitable sonic window to the tumor that occludes the branch of the bronchus. Quite often sonography (Fig. 4.31a) allows better differentiation of the tumor from nonventilated lung tissue than computed tomography (Fig. 4.31b).

In the presence of additional pleural effusion the contours of the tumor-bearing atelectatic portion of the lung are rendered (Fig. 4.31c).

4.2.6 Heterogeneous Structural Pattern

The assessment of malignant lesions might be rendered difficult by their highly *heterogeneous structural pattern* (Pan et al. 1993; Table 4.2.).

Tumor consolidations may still contain residually ventilated bronchial branches (Fig. 4.27e) or *colliquations* and/or *necrotic zones* (Figs. 4.29b, 4.32)

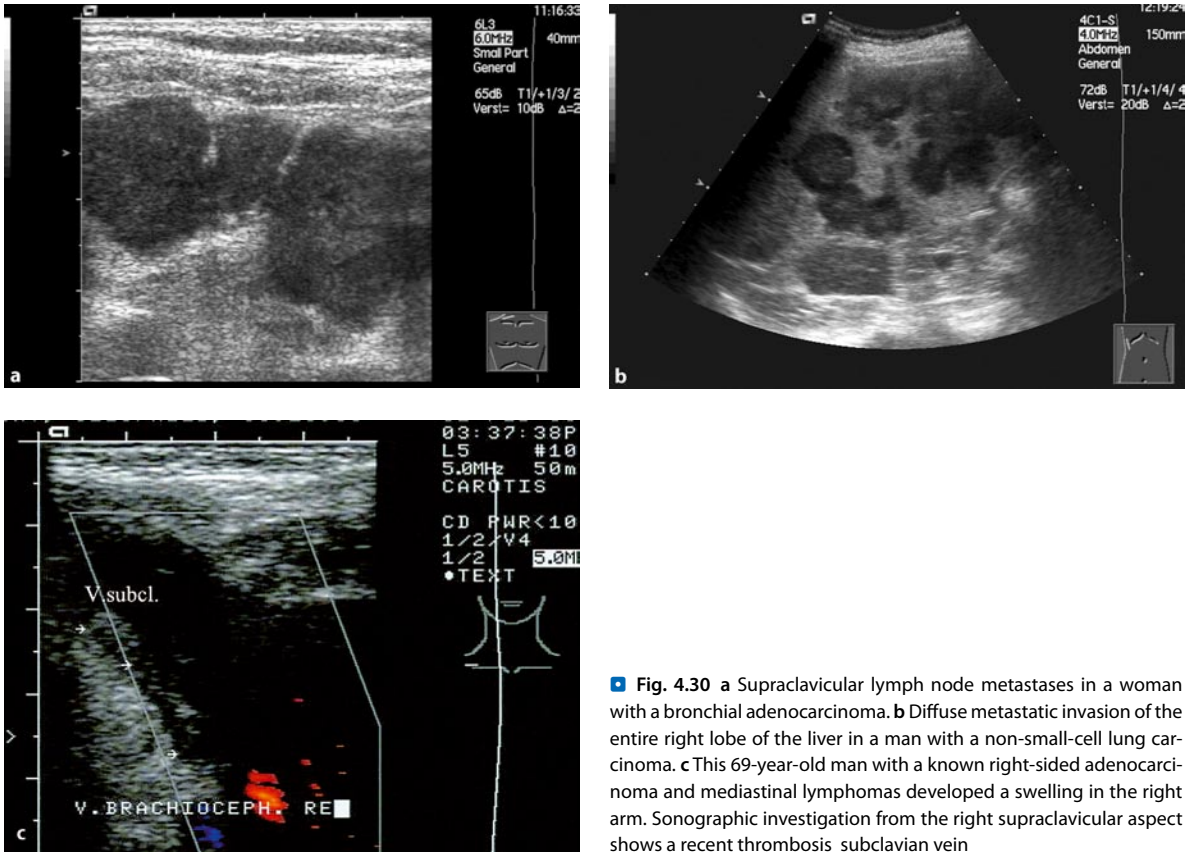

Fig. 4.30 **a** Supraclavicular lymph node metastases in a woman with a bronchial adenocarcinoma. **b** Diffuse metastatic invasion of the entire right lobe of the liver in a man with a non-small-cell lung carcinoma. **c** This 69-year-old man with a known right-sided adenocarcinoma and mediastinal lymphomas developed a swelling in the right arm. Sonographic investigation from the right supraclavicular aspect shows a recent thrombosis subclavian vein

Lung tissue adjacent to a tumor might be affected by inflammation (Fig. 4.32) or contain calcifications (Fig. 4.28).

In a diseased portion of the lung, solid portions of the tumor might exist along with complex inflammatory infiltrations (Fig. 4.33).

Sonographic assessment of bronchoalveolar carcinoma is highly problematic. On the one hand, multiple peripheral consolidations with variable air content might mimic multifocal pneumonia (Görg et al. 2002; Fig. 4.34). On the other hand, one may only find an uncharacteristic uneven lung surface (Fig. 4.35).

In all cases of ambiguous pulmonary lesions, sonography may serve as an important aid in decision-making. It helps the investigator to decide about the subsequent diagnostic procedure—either immediately in terms of a sonography-assisted biopsy (Mathis et al. 1999; Beckh et al. 2002), or as a complementary imaging method to select the appropriate surgical procedure.

4.2.7 Pulmonary Metastases

Pulmonary metastases are documented on sonography when they reach the margin of the lung. Owing to poor visibility in this region, sonography is not a suitable screening method. Metastases have no small air trappings and are usually homogeneously hypoechoic; occasionally they have branches extending into tissue (Mathis et al. 1999). Pathological vessels are predominantly found at the margin (Fig. 4.36, Table 4.3).

4.2.8 Summary

Sonography does not permit the investigator to make a distinction between metastases and peripheral carcinoma. The interpretation must take the patient's medical history and survey radiographs into account. In terms of differential diagnosis, the formation of lesions in the parietal pleura must be excluded by dynamic investigation. Even benign pulmonary lesions, e.g., hamartoma or heman-

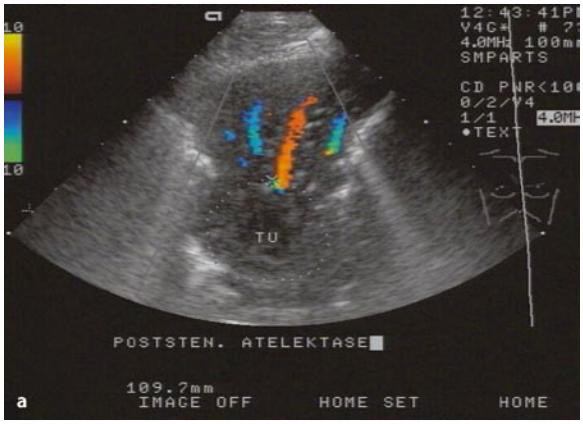

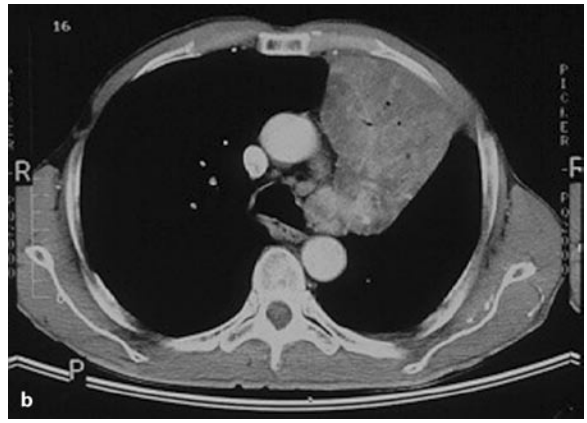

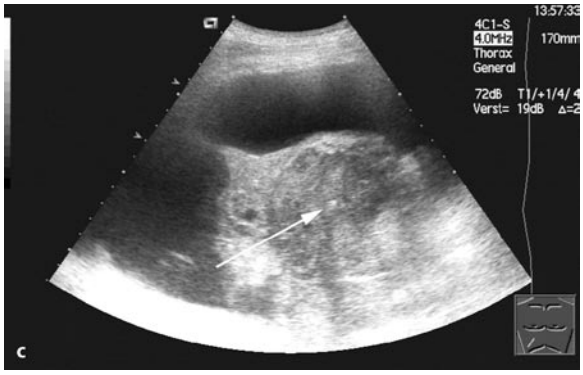

Fig. 4.31 **a** Central tumor in the left upper lobe (*broken line*); behind it there is atelectatic lung tissue with a regular vascular architecture. **b** Computed tomography image of the tumor and the atelectasis in the upper lobe. **c** Large tumor (*arrow*) in the right lower lobe; in the marginal area there is atelectatic lung tissue surrounded by a pleural effusion. Sonographic biopsy of the tumor indicated small-cell carcinoma

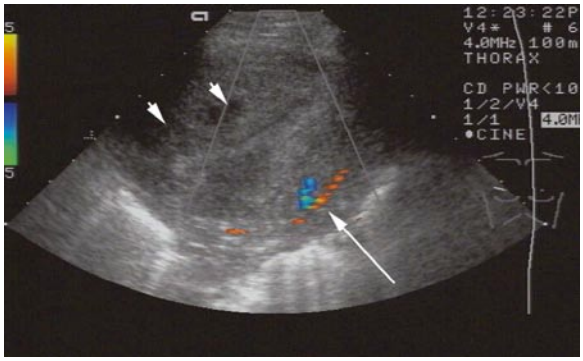

Fig. 4.32 Space-occupying lesion in the upper and middle lobe with several necrotic zones *(arrowheads)*. Initially there were marked signs of inflammation on clinical examination. Under antibiotic therapy the invasive pneumonic portion resolved (*arrow*). Sonographic biopsy from solid portions of the space-occupying lesion indicated squamous cell carcinoma

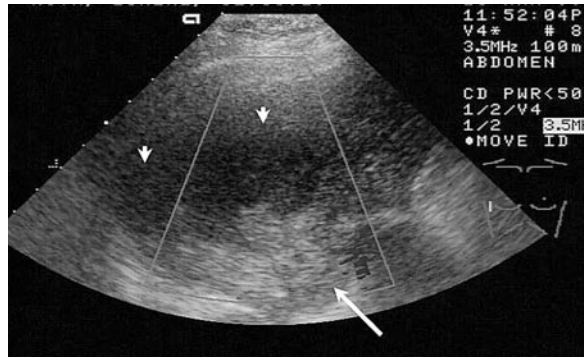

Fig. 4.33 Inhomogeneous and medially rather echodense (*arrow*) space-occupying lesion in the middle lobe. Sonographic biopsy from the more echodense portions showed, on histological examination, inflammatory lung parenchyma. Bacteriological investigation revealed *Aspergillus niger*. The sonographic biopsy from the more hypoechoic marginal areas (*arrowheads*) additionally showed a poorly differentiated, nonkeratinizing squamous cell carcinoma

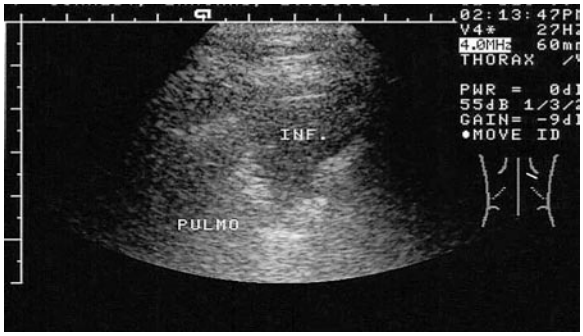

Fig. 4.34 In the right lower lobe, in the dorsal aspect, there is a nearly triangular invasive lesion with blurred margins. A bronchoalveolar carcinoma was confirmed by thoracoscopic biopsy. *INF.* invasion, *PULMO* lung

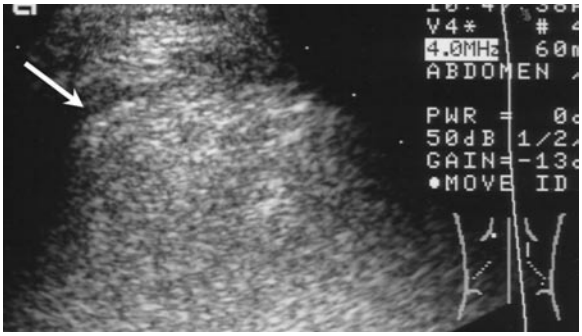

Fig. 4.35 This woman had a bronchoalveolar carcinoma confirmed on radiographic investigation and by bronchoscopic biopsy. The carcinoma fills the entire right lower lobe. Sonography only shows an irregular and finely grained surface of the lung (*arrow*)

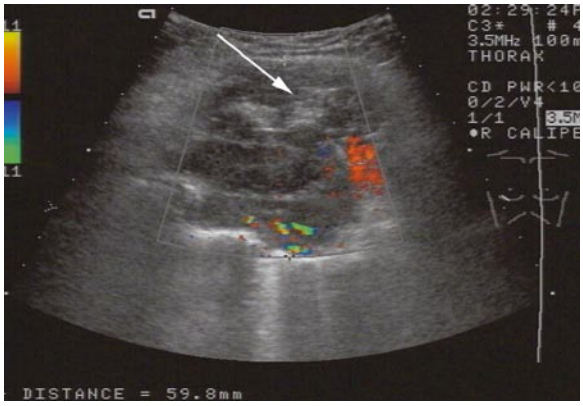

Fig. 4.36 This 77-year-old man complained of pain in the right chest. Sonography revealed a large tumor formation extending from the lung to the chest wall and leading to osteolytic destruction of a rib (*arrow*). Sonography-guided biopsy indicated metastasis of a urothelial carcinoma operated on 2 years ago

Table 4.3 Sonomorphology of pulmonary metastases

Morphology	Echotexture	Vessels
Round	Hypoechoic	Bizarre new vessel formation at the margin
Oval	No ventilated portions	–
Serrated	Necrosis possible	–
Sharp margins	–	–

giofibroma, might extend to the periphery of the lung as hypoechoic formations. Cyst walls may be of varying thickness. They usually have an anechoic content. Occasionally they contain fluid with internal echoes. In order to differentiate between a cyst and a pulmonary abscess or an encapsulated empyema, the diagnostic procedure must take clinical parameters and computed tomography investigations into account. In the final analysis, bacteriological, cytological and histological investigations are of decisive importance.

Acknowledgement We thank R. Loose, Head of the Institute of Diagnostic and Interventional Radiology at the Klinikum Nürnberg Nord, for providing radiology reports.

References

Beckh S, Bölcskei PL, Lessnau KD (2002) Real-time chest ultrasonography. A comprehensive review for the pulmonologist. Chest 122:1759–1773

Beckh S, Bölcskei PL (2003) Die Bedeutung der dynamischen Untersuchung in der Diagnostik thorakaler Herdbildungen. Praxis 92:1223–1226

Corrin B (1999) Actinomycosis. In: Corrin B (ed) Pathology of the lungs. Churchill Livingstone, London, pp 194–195

Detterbeck FC, Malcolm M, DeCamp Jr et al (2003) Invasive staging—the guidelines. Chest 123:167S–175

Fraser RS, Müller NL, Colman N, Paré PD (1999) Fraser and Paré's diagnosis of diseases of the chest. Saunders, Philadelphia, pp 299–338

Fultz PJ, Feins RH, Strang JG et al (2002) Detection and diagnosis of nonpalpable supraclavicular lymph nodes in lung cancer at CT and US. Radiology 222:245–251

Görg C, Bert T (2004) Transcutaneous colour Doppler sonography of lung consolidations. Ultraschall Med 25:221–226, 285–291
Görg C, Seifart U, Holzinger I et al (2002) Bronchioloalveolar carcinoma: sonographic pattern of "pneumonie". Eur J Ultrasound 15:109–117
Hsu WH, Ikezoe J, Chen CY et al (1996) Color Doppler ultrasound signals of thoracic lesions. Am J Respir Crit Care Med 153:1938–1951
Hsu WH, Chiang CD, Chen CY et al (1998) Color Doppler ultrasound pulsatile flow signals of thoracic lesions: comparison of lung cancers and benign lesions. Ultrasound Med Biol 24:1087–1095
Knopp MV, Hawighorst H, Flömer F (1998) Magnetresonanztomographie. In: Drings P, Vogt-Moykopf I (eds) Thoraxtumoren. Springer, Berlin, pp 180–190
Ko JC, Yang PC, Yuan A et al (1994) Superior vena cava syndrome. Am J Respir Crit Care Med 149:783–787
Landreneau RJ, Mack MJ, Dowling RD et al (1998) The role of thoracoscopy in lung cancer management. Chest 113:6S–12S
Mathis G (1997) Thoraxsonography—part II: peripheral pulmonary consolidation. Ultrasound Med Biol 23:1141–1153
Mathis G, Bitschnau R, Gehmacher O et al (1999) Ultraschallgeführte transthorakale Punktion. Ultraschall Med 20:226–235
Müller W (1997) Ultraschall-Diagnostik. In: Rühle KH (ed) Pleura-Erkrankungen. Kohlhammer, Stuttgart, pp 31–44
Pan JF, Yang PC, Chang DB et al. (1993) Needle aspiration biopsy of malignant lung masses with necrotic centers. Chest 103:1452–1456
Schönberg SO (2003) Magnetresonanztomographie. In: Drings P, Dienemann H, Wannenmacher M (eds) Management des Lungenkarzinoms. Springer, Berlin, pp 117–124
Suzuki N, Saitoh T, Kitamura S et al (1993) Tumor invasion of the chest wall in lung cancer: diagnosis with US. Radiology 187:3942
Thomas M, Baumann M, Deppermann M et al (2002) Empfehlungen zur Therapie des Bronchialkarzinoms. Pneumologie 56:113–131
Tuengerthal S (2003) Radiologische Diagnostik des Bronchialkarzinoms—Projektionsradiographie und Computertomographie. In: Drings P, Dienemann H, Wannenmacher M (eds) Management des Lungenkarzinoms. Springer, Berlin, pp 73–115
van Kaick G, Bahner ML (1998) Computertomographie. In: Drings P, Vogt-Moykopf I (eds) Thoraxtumoren. Springer, Berlin, pp 165–179
Yang PC (1996) Review paper: color Doppler ultrasound of pulmonary consolidation. Eur J Ultrasound 3:169–178
Yuan A, Chang DB, Yu CJ et al (1994) Color Doppler sonography of benign and malignant pulmonary masses. AJR Am J Roentgenol 163:545–549

4.3 Vascular Lung Consolidations: Pulmonary Embolism and Pulmonary Infarction

G. Mathis

Pulmonary embolism is the most frequent clinically nondiagnosed cause of death. Autopsy studies have demonstrated a frequency of 10–15%. In cases of chronic heart failure the rate is as high as 30%. Again, pulmonary embolism is the cause of death in 40% of these. Ten percent of deaths in clinics are due to pulmonary embolism. In a further 10%, pulmonary embolism is involved in a causal way (Table 4.4). As the clinical symptoms are nonspecific and the chest X-ray is not sensitive, the most important diagnostic step still is to consider the possibility of pulmonary embolism. The clinician is called upon to use every method that will improve the diagnosis of pulmonary embolism.

Table 4.4 Clinical diagnosis in cases of death due to pulmonary embolism established in the autopsy

Authors	Patients	Accuracy (%)
Morgentaler and Ryu (1995)	92	32
Morpurgo and Schmid (1995)	92	28

4.3.1 Pathophysiological Prerequisites for Sonographic Imaging of Pulmonary Embolism

A few minutes after a secondary pulmonary artery has been occluded, the surfactant collapses. Interstitial fluid and erythrocytes flow into the alveolar space. A hemorrhagic congestion offers the most ideal conditions for sonographic imaging. These consolidations are oriented towards the pleura. Practically along with their base they are open at the periphery, which creates good conditions for transthoracic sonography (Joyner et al. 1966; Mathis and Dirschmid 1993; Fig. 4.37).

The pulmonary embolism is a dynamic process. Small hemorrhages are rapidly absorbed by local fibrinolysis, as the intimal layer of pulmonary arteries has a substantial fibrinolytic capacity. A massive or fulminant pulmonary embolism is often preceded by small premonitory embolisms which, when detected in time, lead to the initiation of appropriate therapeutic measures.

The classic pulmonary infarction had two prerequisites:

1. Embolic closure of small branches of pulmonary arteries
2. A preexisting congestion of blood in the minor circulation

The latter prerequisite definitely is no longer valid, as pulmonary infarctions are often found in young patients with an entirely healthy cardiac system. When a larger pulmonary artery is occluded, compensatory blood supply is ensured via precapillary bronchopulmonary anastomoses so that an infarction rarely occurs.

The frequency of the *hemorrhagic pulmonary infarction* in cases of pulmonary embolism is reported to range

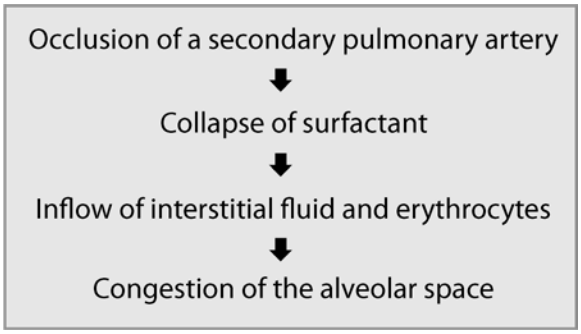

Fig. 4.37 Pathophysiological prerequisites for sonographic imaging in cases of pulmonary embolism. Peripheral engorgement of the alveolar lumen is a good prerequisite for pathological echo transmission

between 25 and 60% in the pathology literature. According to recent studies, however, the rate is much higher. This was proven by new imaging procedures that were previously not available. What pathologists described in the 1960s can be imaged today with sonography and computed tomography. The dynamics of change from the fresh early infarction that can be reperfused to the stage of marked tissue necrosis can be documented by sonography in a water bath and subsequently confirmed in terms of pathology, anatomy and even by histology (Könn and Scheijbal 1978; Hartung 1984; Heath and Smith 1988; Mathis and Dirschmid 1993).

4.3.2 Sonomorphology of Pulmonary Infarction

4.3.2.1 Early Pulmonary Infarctions

Recent *early pulmonary infarctions* that can be reperfused are visualized as homogeneous structures with a pleural base that is occasionally a little protruded. The lesion is relatively homogeneous and hypoechoic. The margin is a little indistinct in the first few hours but is otherwise marked by smooth margins; it is also protruded and rounded. The pleural base may protrude; the margin towards the ventilated lung may be slightly constricted (Fig. 4.38).

In early infarctions the central bronchial reflex is either weak or absent. On the one hand, this is an expression of the well-known bronchial constriction in cases of pulmonary embolism; on the other hand, it is caused by compression of the surrounding accumulation of edemas and hematomas. A clear bronchoaerogram is not seen in any early lung infarction (Mathis et al. 1993; Mathis and Dirschmid 1993).

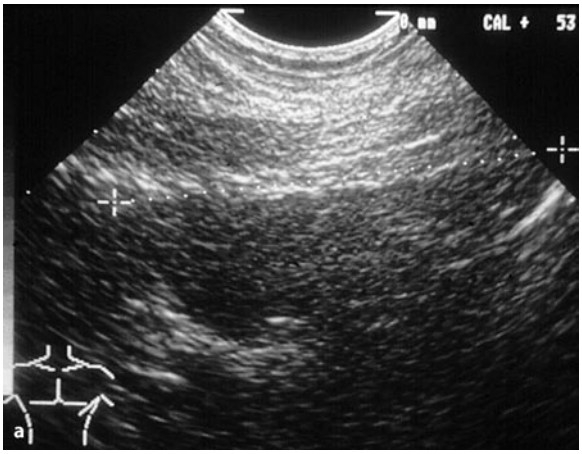

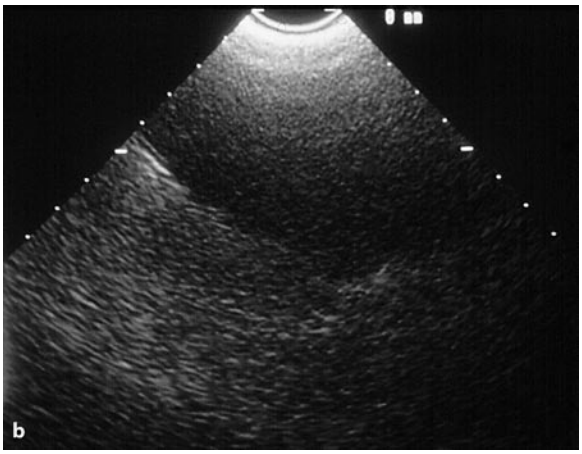

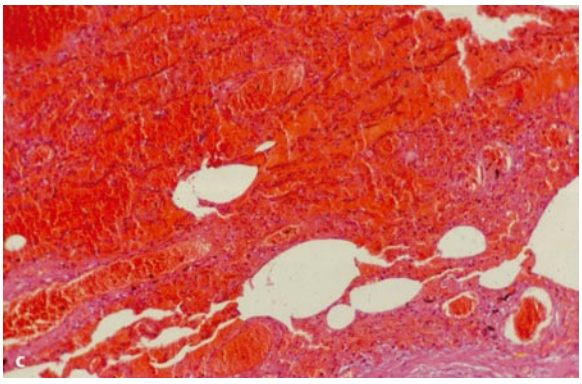

Fig. 4.38 **a** Recent pulmonary infarction (+ … +) 2 h after the embolism in the anterobasal lung. Hypoechoic texture with initial echoes, rounded towards the hilum. The position, form and early stage were confirmed by autopsy and histological investigation. **b** The same pulmonary infarction in a water bath: a largely homogeneous lesion with the structure of the lung preserved on histological investigation. **c** On histological investigation reveals the alveolar spaces to be congested with erythrocytes, but the structure of the lung is fully preserved

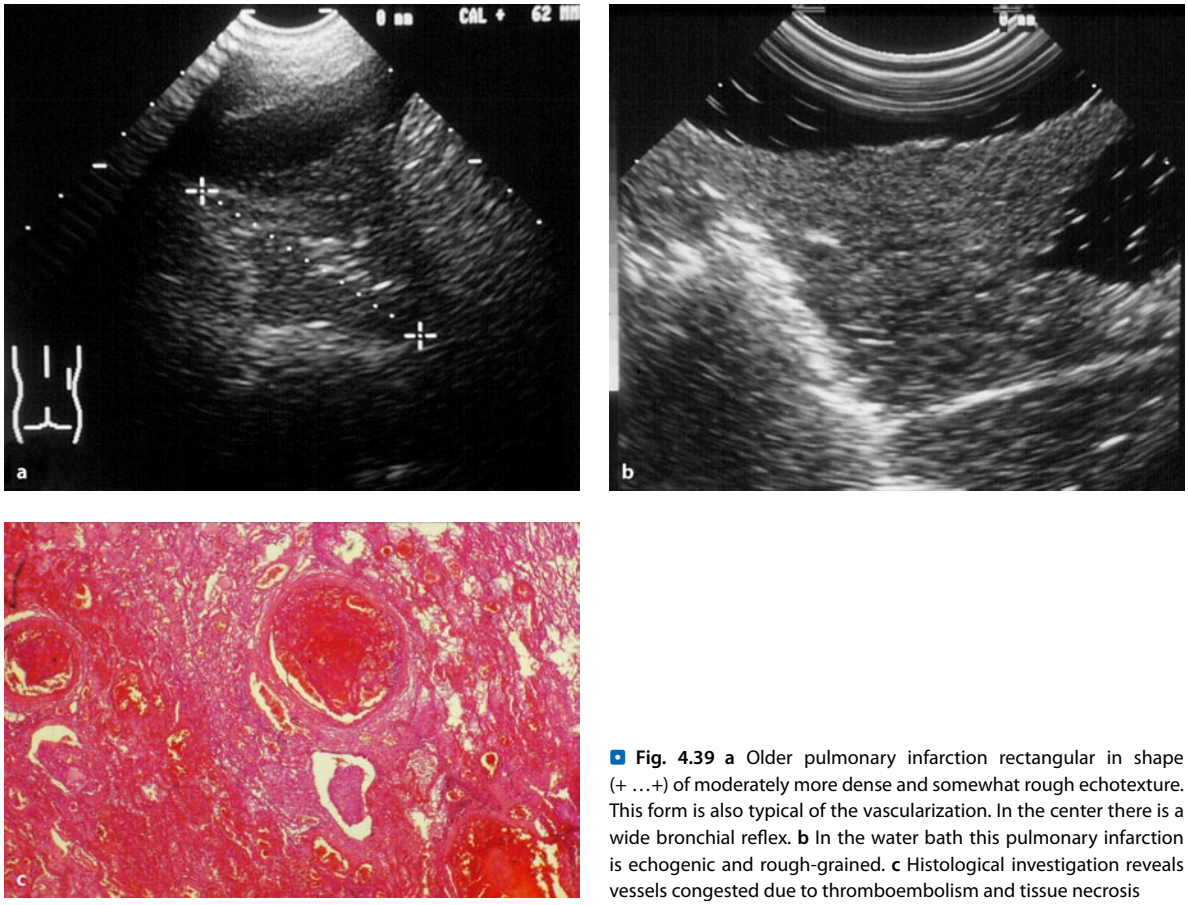

Fig. 4.39 a Older pulmonary infarction rectangular in shape (+ …+) of moderately more dense and somewhat rough echotexture. This form is also typical of the vascularization. In the center there is a wide bronchial reflex. **b** In the water bath this pulmonary infarction is echogenic and rough-grained. **c** Histological investigation reveals vessels congested due to thromboembolism and tissue necrosis

4.3.2.2 Late Pulmonary Infarction, Tissue Necrosis

The *late pulmonary infarction* is more coarse and grained in structure than the recent infarction. It has sharp and serrated margins, is frequently triangular or wedge-shaped, and is more rarely rounded or quadrangular. In most cases it is somewhat more echodense than the early infarction and has a pronounced central bronchial reflex which, on cross section, is found in the center of the triangle and is a sign of segmental infestation. Small lung infarctions up to 2 cm in size often have no bronchial reflex. They remain hypoechoic and homogeneous until their margins tend to become blurred (Figs. 4.39–4.43, 4.53).

Distinction between an early infarction that can be reperfused and a late infarction with tissue necrosis is rarely achieved; it is achieved only in larger lesions beyond a size of 2–3 cm. Nevertheless, these criteria (Table 4.5) are important to differentiate these from inflammatory infiltrates, which are usually larger.

Studies published in the last few years have provided a much more precise description of the sonomorphology of hemorrhage and infarctions in the presence of pulmonary embolism (Reißig and Kroegel 2003; Reißig et al. 2004; Mathis et al. 2005).

4.3.2.3 Localization

Two thirds of lung infarctions are located dorsally in the lower lobes of the lung, more often on the right side than on the left side. This is because of anatomical factors and because of hemodynamics: basal pulmonary arteries tend to run straight, while arteries of the upper lobe tend to branch off at a steeper angle. The dorsobasal region is particularly accessible to transcutaneous sonography (Fig. 4.44).

4.3.2.4 Number

The improved resolution available today allows the investigator to detect more lesions than he/she could several years ago. In cases of pulmonary embolism, on

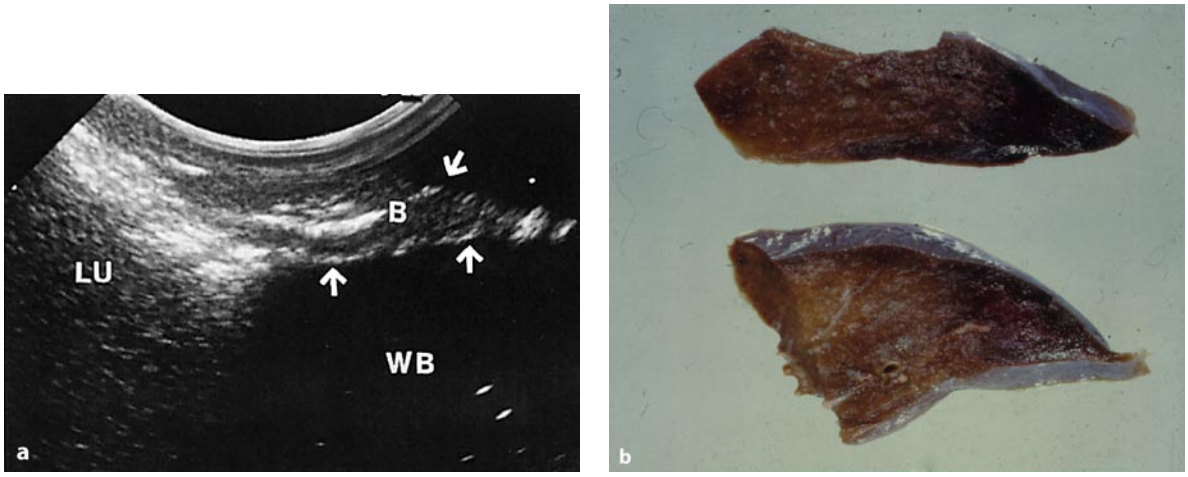

Fig. 4.40 **a** Older pulmonary infarction (*arrows*) in an autopsied lung in the water bath. *B* bronchial reflex, *LU* ventilated lung, *WB* water bath. **b** Gross pathological investigation of this lung infarction, which was also confirmed by histological investigation

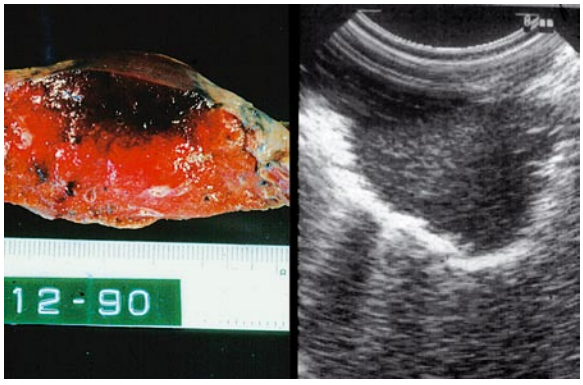

Fig. 4.41 Classic pulmonary infarction with tissue necrosis, in the autopsied lung (*left*) and on sonography in a water bath (*right*)

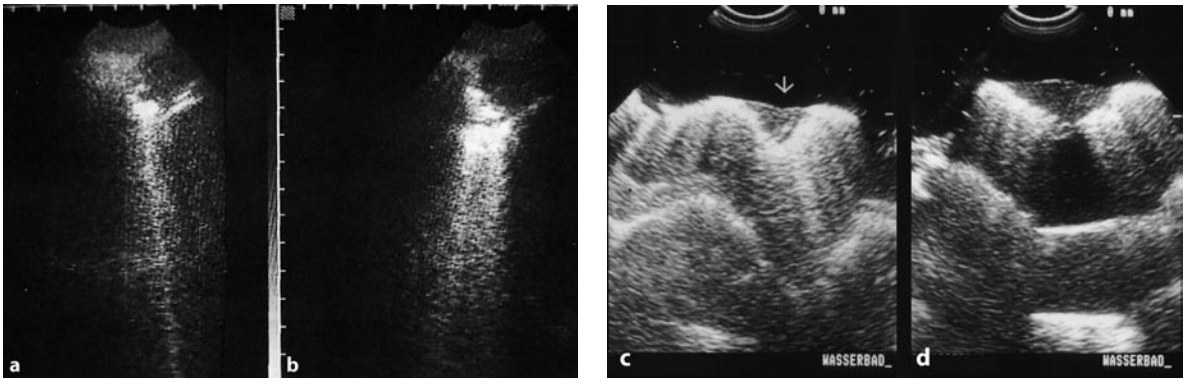

Fig. 4.42 This man underwent in-hospital treatment because of leg vein thrombosis at three levels. During mobilization he experienced a cardiovascular arrest. During reanimation, several signal emboli were registered on sonographic investigation using a "bedside device" (**a**,**b**); these were confirmed in terms of position, form and size by autopsy as well as in the water bath (**c**,**d**)

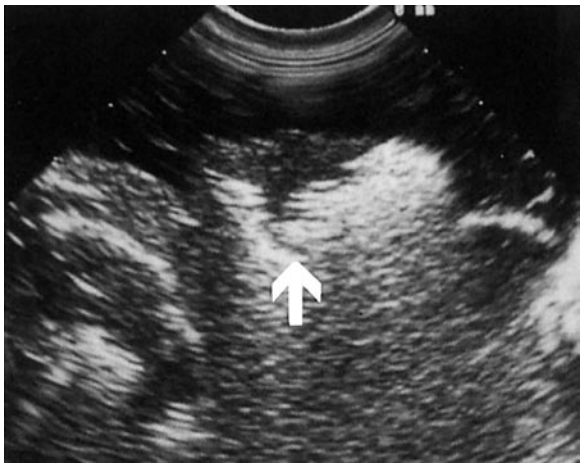

Fig. 4.43 Pulmonary infarction with "vascular signs" in the water bath. Histologically it was a recent pulmonary infarction; the supplying vessel was congested by thromboembolism

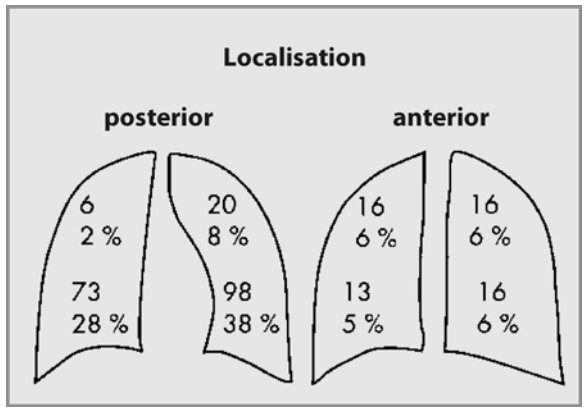

Fig. 4.44 Most pulmonary infarctions are found in dorsobasal location owing to anatomical and hemodynamic factors

Table 4.5 Sonomorphology of pulmonary infarctions beyond a size of about 2–3 cm

Early infarction	Late infarction
Homogeneous	Inhomogeneous/grained
Round, triangular	Triangular, round
Smooth margins	Serrated margins
Hardly any internal echoes	Segmental bronchial reflex
Circulation stop	Vascular signs

average 2.4 infarctions are seen on sonography. Given two or more lesions and the clinical likelihood of pulmonary embolism, the specificity of sonography is 99%. In slim patients it would be advisable to investigate the pleural reflex with a high-frequency transducer as well (Figs. 4.45–Fig. 4.53).

4.3.2.5 Size

The mean size of pulmonary infarctions is 12 mm×16 mm (range 5–70 mm). Lesions less than 5 mm in size should not be taken into account because they might be merely scars. If at all, their progress should be monitored. Pleuritis may be marked by a similar appearance. However, pleuritis will be found at the site of pain and is usually characterized by extensive fragmentation of the pleural reflex.

4.3.2.6 Morphology

Pulmonary infarctions are usually triangular in shape and have their base at the pleura. The pleural base may be slightly protruded. Quite often the lesions are rounded towards the hilum; occasionally they are also polygonal in shape (Reißig et al. 2003; Mathis et al. 2005; Fig. 4.45).

4.3.2.7 Vascular Signs

In some cases one finds an anechoic *band of vessels* on the B-mode image. The band of vessels is oriented from the tip of the lesion towards the hilum. It corresponds to the branch of the pulmonary artery congested by thromboembolism, as evidenced in computed tomography investigations as well (so-called vessel sign or vascular sign) (Ren et al. 1990; Figs. 4.43, 4.47f).

4.3.2.8 Pleural Effusion

In approximately half of cases the investigator finds small pleural effusions either focally above the lesion or in the pleural sinuses. The effusion is largely anechoic and smaller than an infarction, which is an important criterion to distinguish this entity from compression atelectasis. The pleural effusion may also lead to apparent

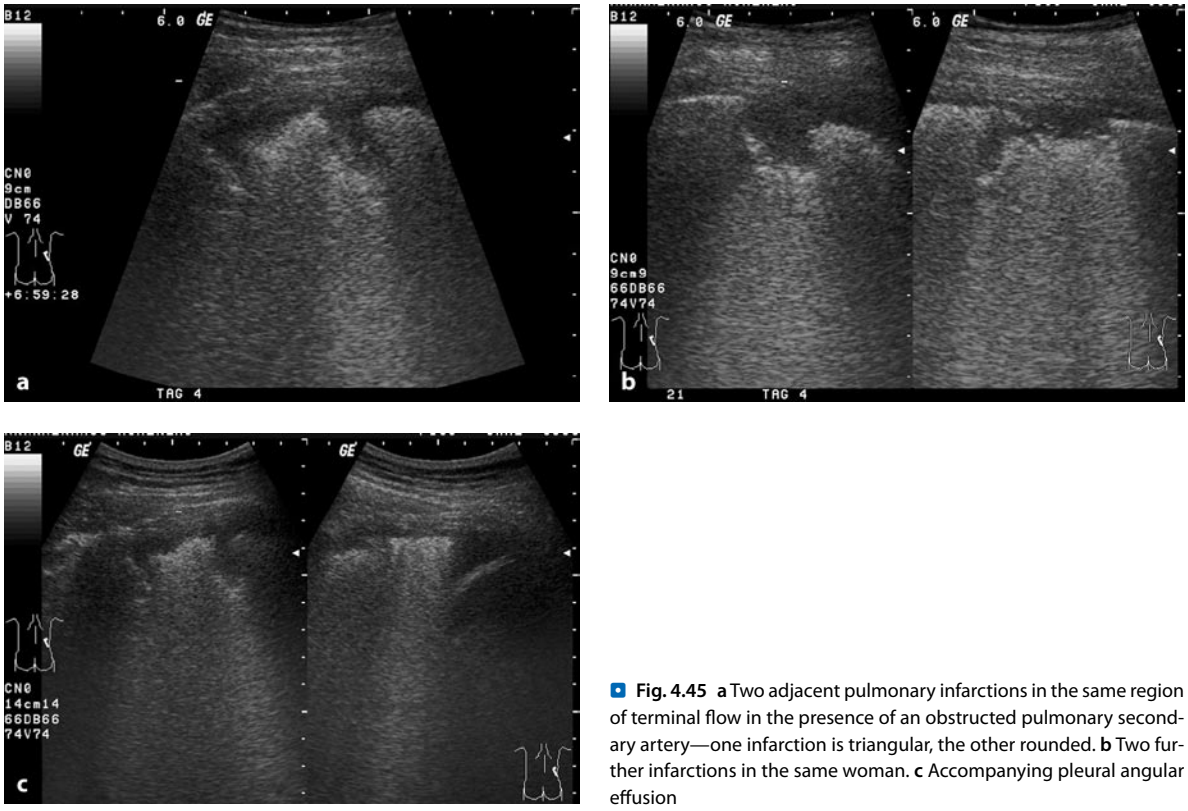

Fig. 4.45 **a** Two adjacent pulmonary infarctions in the same region of terminal flow in the presence of an obstructed pulmonary secondary artery—one infarction is triangular, the other rounded. **b** Two further infarctions in the same woman. **c** Accompanying pleural angular effusion

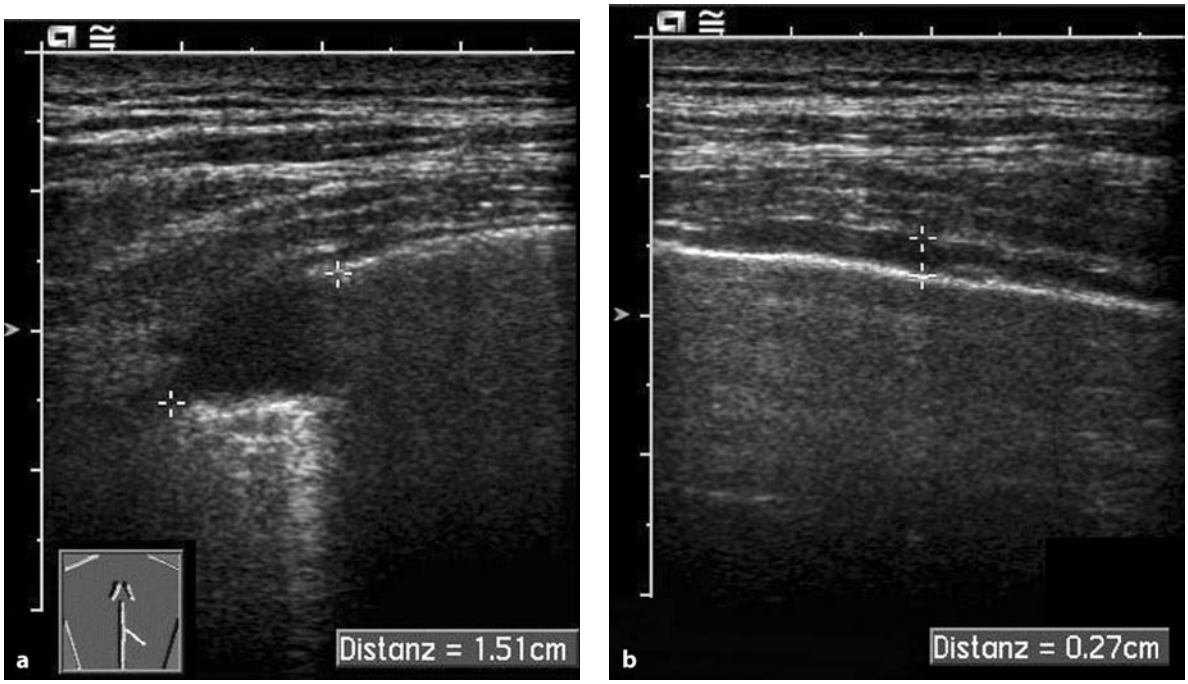

Fig. 4.46 **a** Triangular pulmonary infarction of typical form and size with protrusion of the pleura. **b** Narrow focal pleural effusion

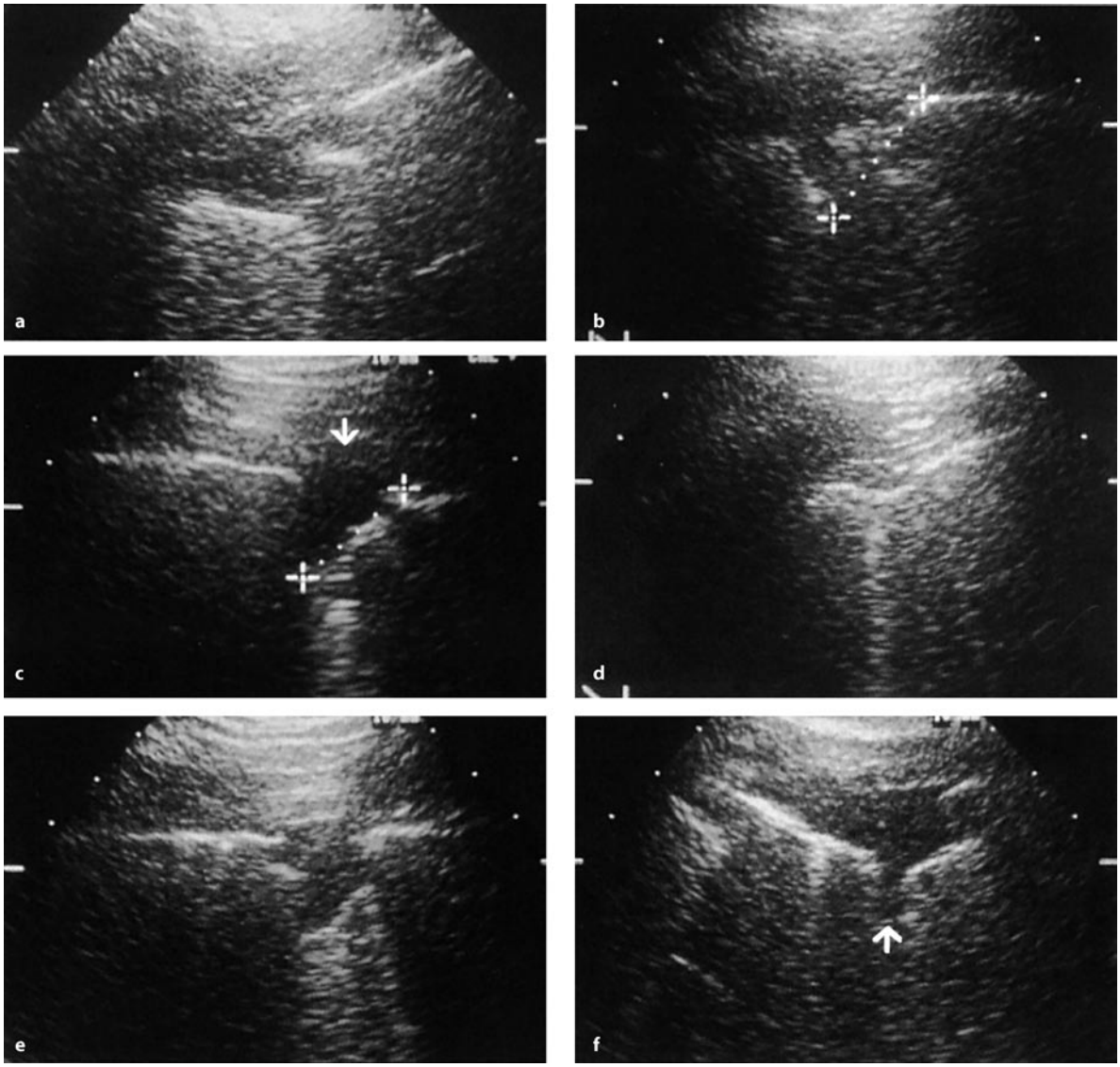

Fig. 4.47 This man had a leg vein thrombosis at three levels. Following an incident of dyspnea, pressure in the chest and cough, sonography revealed a total of six pulmonary infarctions measuring 1.5–3 cm in size (**a**–**f**); typical signal embolisms. The lesions are mainly wedge-shaped. In **c** (*arrow*) the pleural protrusion is clearly seen. Infarctions of this size escape detection by scintigraphy, particularly as shown in **d**. In this case only two perfusion defects were seen on the scintigram. The supplying vessel obstructed by thromboembolism is seen well in **f**

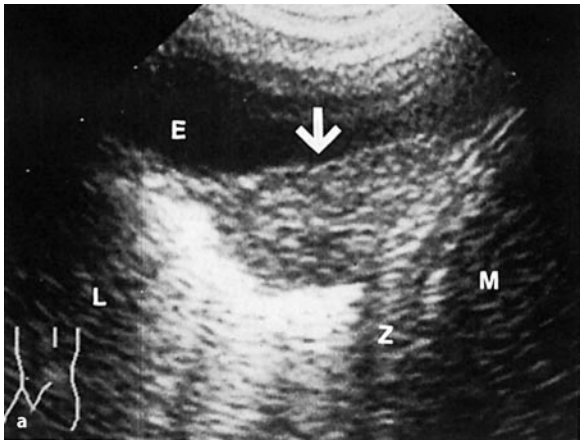

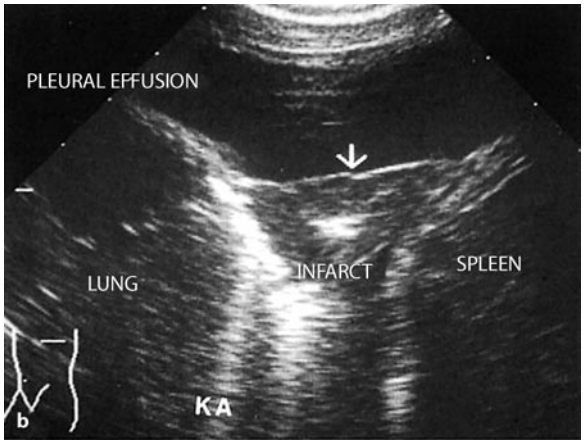

Fig. 4.48 **a** A 5-day-old pulmonary infarction: sharp margins, a little more echodense and roughly structured than that in the early stage, with a pronounced central bronchial reflex. *KA* comet-tail artifact. **b** The same lesion in longitudinal section; the echogenicity is somewhat intensified by the pleural effusion (*E*). *L* ventilated lung, *Z* diaphragm, *M* spleen

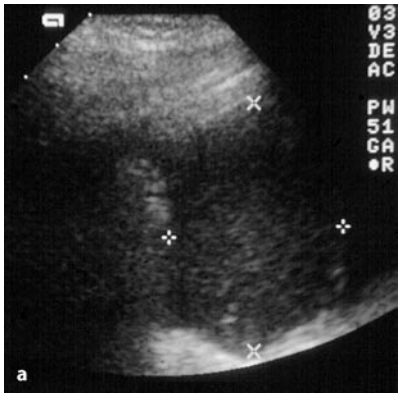

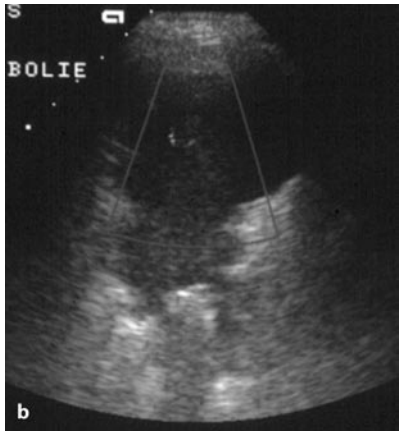

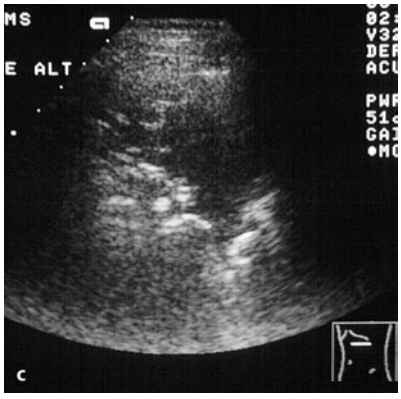

Fig. 4.49 **a** Five hours after the embolic event there is a rounded, homogeneous early infarction. **b** After 5 days the lesion is triangular in shape. **c** After 12 days the lesion has developed into a classic pulmonary infarction that is somewhat smaller than the original lesion, triangular in shape and marked by serrated margins

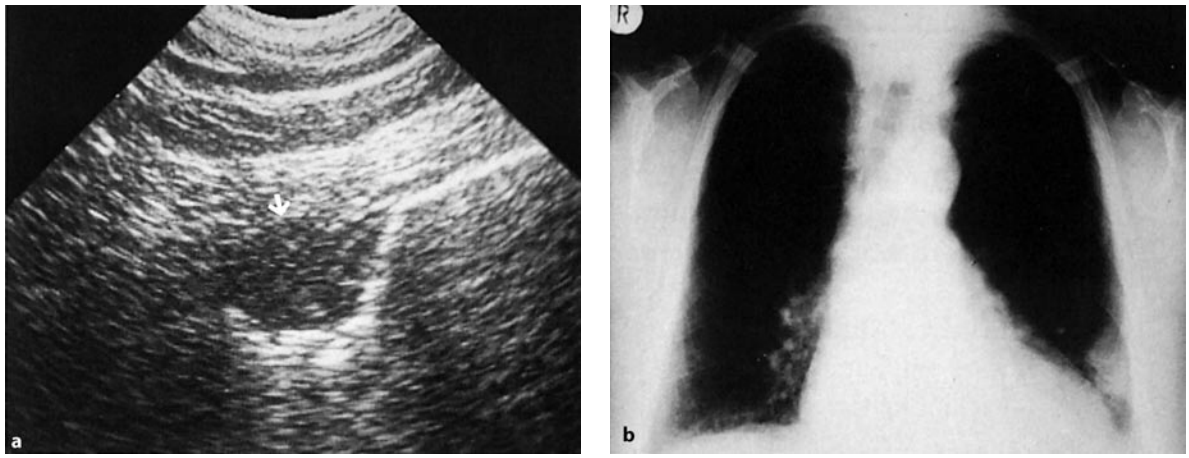

Fig. 4.50 **a** Older pulmonary infarction. Even in the absence of a pleural effusion the protruding surface of the pleural infarction is clearly seen (*arrow*). **b** This infarction was seen on sonography 4 days earlier than on the fluoroscopic chest X-ray

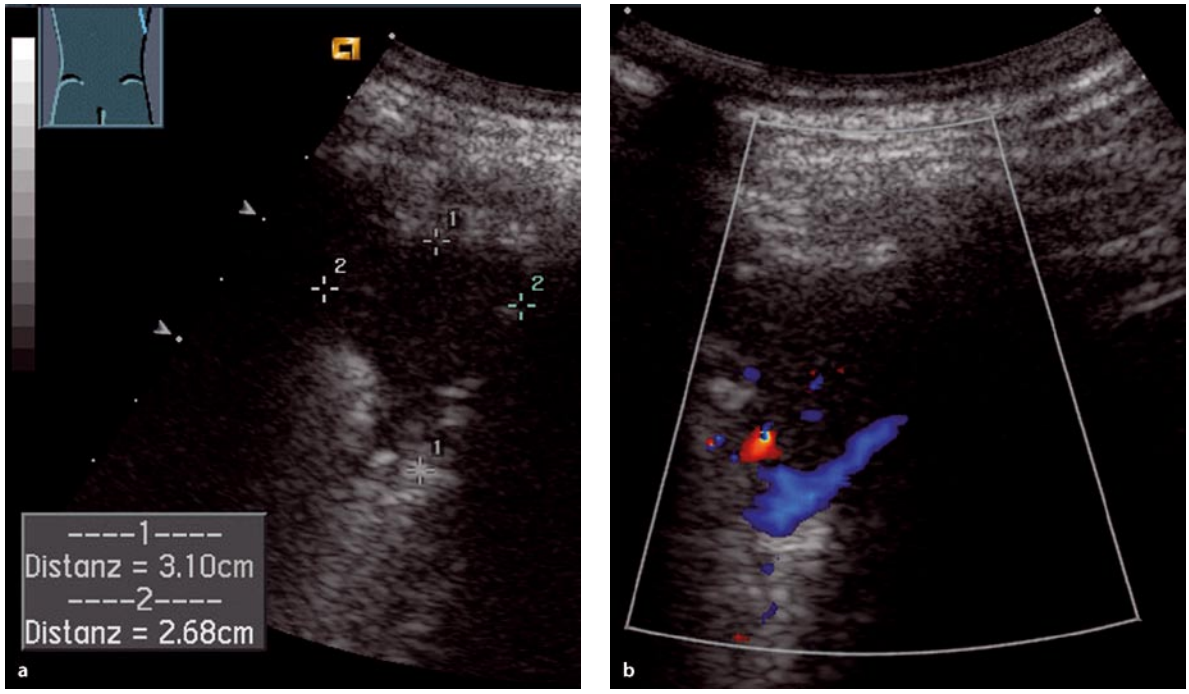

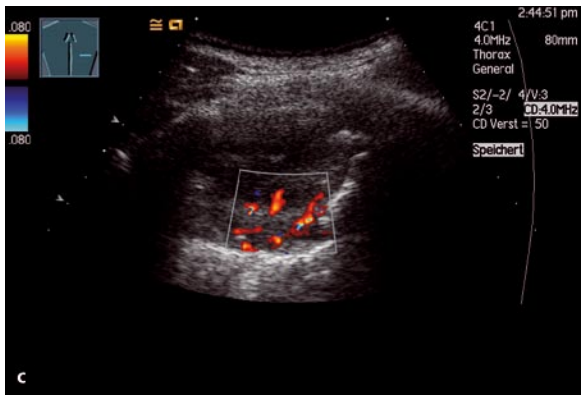

Fig. 4.51 **a** Early triangular pulmonary infarction. The D-dimer test was still negative at this time. **b** The infarction is vascularized only at the margin and not in the center. **c** Four days later the patient had an infarction pneumonia that was seen clinically as well. This is larger than the original lesion, partly ventilated and revascularized

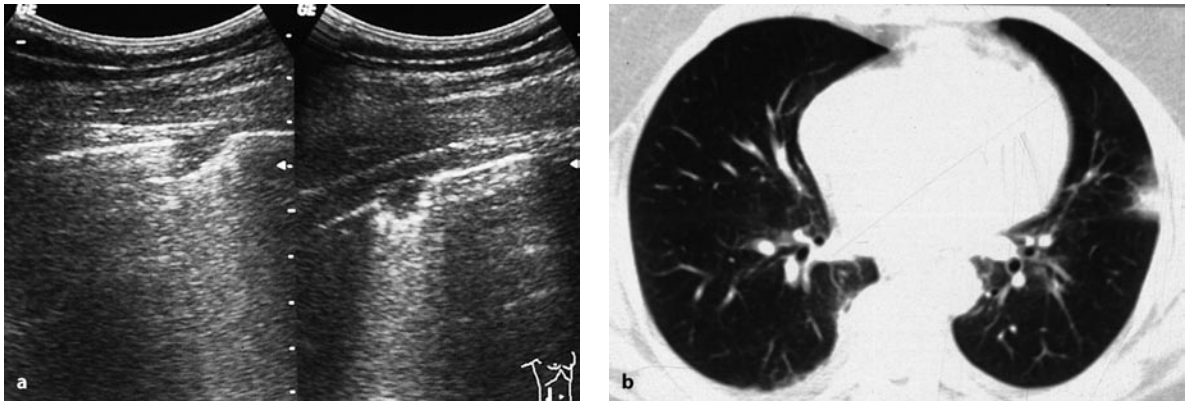

Fig. 4.52 A 25-year-old woman with sudden dyspnea and mild respiratory chest pain. **a** Sonography revealed two small pulmonary infarctions. **b** On spiral computed tomography the central pulmonary embolism was confirmed and only one lesion was seen in the periphery

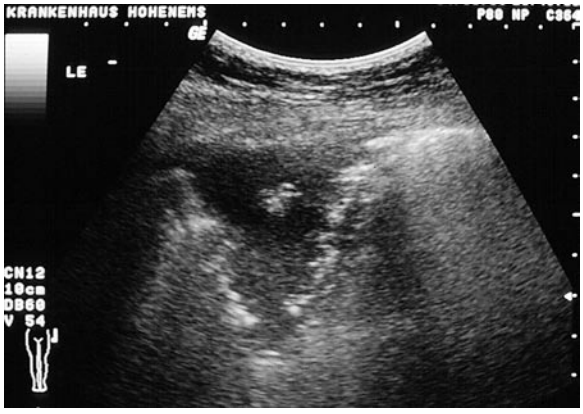

Fig. 4.53 Large, classic pulmonary infarction with highly serrated margins and a central bronchial reflex

echo enhancement in the pulmonary infarction. Internal echoes in the effusion and fibrin strands are indicative of infarction pneumonia (Mathis et al. 1993; Fig. 4.46).

4.3.2.9 Signal Embolism

A massive pulmonary embolism is frequently accompanied by smaller embolic events, which then appear as *signal embolisms*. They are visualized as individual triangular or rounded small lesions (Fig. 4.42). Several such small defects lying adjacent to each other create the image of a lacerated margin between the nonventilated portion of the lung lying close to the pleura and the normally ventilated portion of the lung. Such small lesions may be a precursor of an imminent pulmonary embolism or may even be present in conjunction with a massive central pulmonary embolism and thus confirm the diagnosis without the central embolus itself being demonstrated on chest sonography; it escapes detection because of air in the intervening space (Kroschel et al. 1991).

4.3.2.10 Color-Coded Duplex Sonography in Pulmonary Embolism

In very few cases is the investigator able to visualize, on color-coded duplex sonography, a circulation stop caused by embolism (Fig. 4.54). This limitation has several reasons:

- Patients with dyspnea cannot hold their breath long enough, which causes several artifacts on color-coded duplex sonography.
- It is difficult to locate the supplying vessel at the right level.
- When reperfusion occurs rapidly, the lesion is revascularized early. However, such perfusion is markedly less than that in pneumonic infiltrates.

Nevertheless, color-Doppler sonography is an important tool to differentiate subpleural pulmonary lesions (Yuan et al. 1993; Gehmacher and Mathis 1994).

4.3.2.11 Contrast-Assisted Sonography

Pulmonary infarctions and hemorrhage due to embolism are marked by the absence of circulation and the absence of contrast on contrast-assisted sonography as well as color-Doppler sonography. At the margin of the lesion there may be delayed or poor contrast enhancement be-

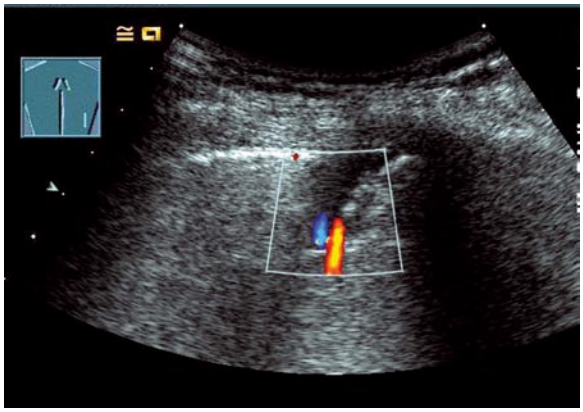

Fig. 4.54 Circulatory stop at the tip of the wedge-shaped pulmonary infarction

cause this area is supplied by a bronchial artery. Pleuritis and pneumonia, on the other hand, are contrasted early and strongly. Thus, contrast-assisted sonography is a very useful instrument for differential diagnosis (Görg and Bert 2006; Chap. 7).

4.3.2.12 Phase of Healing—Infarction Pneumonia

Several weeks after a pulmonary embolism, the sonomorphology of the pulmonary infarction is no longer characteristic. As reventilation progresses, the sonographic image resembles that of pneumonia (Fig. 4.51). Infarction pneumonias may develop in the region of infarction or even in the vicinity of the infarction and between multiple infarctions. Coughing up sequestrated infarctions creates infarction cavities, which may become subject to secondary infection and lead to a pulmonary abscess. Therefore, the processes of repair in late infarctions create diverse conditions for sonographic imaging. A sonomorphological distinction between this entity and other peripheral lung consolidations now becomes difficult. In patients who arrive for sonographic investigation in the stage of infarction pneumonia, 1 or 2 weeks after the event the lesion can be imaged by sonography but the sonomorphology offers very few criteria for differential diagnosis.

4.3.3 Sonomorphological Differential Diagnosis

Various criteria permit sonomorphological differential diagnosis between pneumonia and peripheral pulmonary lesions of other origin. *Pneumonias* are characterized by blurred margins on the sonogram, are inhomogenously structured, have numerous lenticular internal echoes, bronchoaerograms, and in cases of poststenotic pneumonias even fluid bronchograms. In the early stage pneumonia may be similar to the liver (Sect. 4.1).

Carcinomas and metastases tend to be rounded or polycyclic, grow in an invasive fashion, have crow's feet, tumor cones and, occasionally, central necrotic zones.

Compression atelectases are narrow, shaped like a pointed cap, concave at least on one side, and float in the effusion, which is much larger than the atelectasis (Mathis et al. 1993; Mathis 1997).

Color-coded duplex sonography is also suitable to differentiate between pneumonic and neoplastic lesions: pneumonias have a marked, regular central pattern of circulation, while carcinomas and metastases are nourished by atypical corkscrew-shaped vessels at their margins. Contrast-assisted sonography allows the investigator to distinguish between pulmonary infarctions and inflammatory infiltrates.

4.3.4 Accuracy of Chest Sonography in the Diagnosis of Pulmonary Embolism

Until recently we had seven prospective studies comprising 551 patients, which dealt with the accuracy of chest sonography to diagnose pulmonary embolism. The main problem in all investigations focusing on the diagnosis of pulmonary embolism is the virtual absence of a gold standard. Nevertheless, similar results have been achieved by the use of various comparable methods (Table 4.6).

A large multicenter study (TUSPE) comprising 352 patients in the ordinary clinical setting round the clock, which included less experienced investigators, showed that three fourths of patients with pulmonary embolism have typical peripheral lesions on sonography. A surprisingly high specificity of 95% was achieved in this study.

Caution. A normal chest sonogram does not exclude the presence of pulmonary embolism, as is true for a negative computed tomography or a negative D-dimer test as well.

4.3.5 Chest Sonography Compared with Other Imaging Procedures

4.3.5.1 Chest Radiograph

The chest radiograph, which is the basic imaging procedure for the diagnosis of lung disease, is known to be very unreliable in cases of pulmonary embolism. It serves the purpose of interpreting scintigraphic findings and may

Table 4.6 Chest sonography in the diagnosis of pulmonary embolism

Author	Patients (n)	Sensitivity (%)	Specificity (%)	PVW (%)	NVW (%)	Accuracy (%)	Reference method
Mathis et al. (1990b)	33	96	60	93	75	91	Scintigraphy, angiography
Kroschel et al. (1991)	100	90	81	100	81	93	Scintigraphy
Mathis et al. (1993)	58	98	66	91	89	90	Scintigraphy, angiography
Lechleitner et al. (1998)	119	86	67	55	91	73	Scintigraphy, dimer test
Mathis et al. (1999)	117	94	87	92	91	91	Spiral computed tomography
Reißig et al. (2001)	69	80	92	95	72	84	Spiral computed tomography
Lechleitner et al. (2002)	55	81	84	97	84	82	MRI
Mathis et al. (2005)	352	74	95	95	75	84	Spiral computed tomography

NVW negative predictive value, *PVW* positive predictive value

serve as a reason to perform chest sonography (Mathis et al. 1993).

4.3.5.2 Ventilation/Perfusion Scintigraphy

Since the largest study concerning the value of ventilation/perfusion scintigraphy (V/P scintigraphy) was performed, the value of this method for diagnosing pulmonary embolism is controversially discussed: only a minority of patients (11%) in whom a pulmonary embolism was eventually proven by angiography had a V/P scintigraphy with a high degree of diagnostic probability. Three fourths of patients needed further investigations to confirm or exclude a pulmonary embolism (PIOPED Investigators 1990).

Comparison of chest sonography and scintigraphy showed a high degree of concurrence between the two procedures in cases of "high-probability scans." However, in cases of "intermediate" and "low-probability" scans, typical embolisms were more frequently evidenced by sonography (Mathis et al. 1990a, b; Kroschel et al. 1991; Lechleiner et al. 1997).

In individual cases of discrepancy between spiral computed tomography and chest sonography, scintigraphy may well be helpful.

4.3.5.3 Angio Computed Tomography

Spiral angio computed tomography has revolutionized the diagnosis of pulmonary embolism (Remy-Jardin et al. 1992; Teigen et al. 1993). Currently it is the imaging method of choice in cases of suspected pulmonary embolism. Central pulmonary embolisms are directly visualized or excluded with a high degree of accuracy. Spiral angio computed tomography is contraindicated in patients with renal failure, those who are allergic to contrast media, and in pregnant women. Hemodynamically instable patients and those on ventilation cannot be easily transported and moved through the computed tomography device. Moreover, computed tomography is not immediately available at all sites.

For patients who cannot undergo angio computed tomography, chest sonography is an alternative—it can be used even at the bedside, thanks to the mobile systems available today.

Several years ago it was mentioned that a third of all pulmonary embolisms in segments or subsegments escape detection by single-slice computed tomography (Goodman et al. 1995; Oser et al. 1996; Ducker et al. 1998; Rathbun et al. 2000). With use of a small slice thickness in multislice computed tomography, movement artifacts can be reduced within seconds and the resolution is improved. The prob-

lem of small embolisms persists—their clinical relevance is still unclear and should not be underestimated. With use of current techniques, angio computed tomography is assigned a sensitivity of 85–90% (Goodman 2005).

In cases of small embolisms in the segmental and subsegmental region, chest sonography is a meaningful supplement to angio computed tomography. Even small hemorrhages that escape detection by computed tomography, including the multislice technique, are visualized by sonography. It would not be meaningful to indulge in discussions about slice thickness and millimeters. Rather, one should realize that sonography, which utilizes an entirely different physical imaging technique in the near field, simply provides better resolution.

This is clearly seen in lymph nodes—for instance, in the neck more lymph nodes are visualized by sonography. Even on the B-mode image one finds a better structure. In the TUSPE multicenter study 25% of all patients who eventually developed a pulmonary embolism could not be included in the study because computed tomography was not available in a timely manner even in very well equipped centers (Mathis et al. 2005).

4.3.6 The Sonographic Search for the Source of Embolism

In other anatomical locations, sonography has become the method of choice to diagnose thromboembolism. In a single investigation step the experienced investigator is able to inspect several actual clinically or potentially involved regions of the body using a single imaging procedure. He/she is able to study the *source*, *pathway* and *target* of the embolic event.

4.3.6.1 Duplex Sonography of Leg Veins

Much more than half of pulmonary embolisms originate from leg veins. In autopsies of 837 adults, the incidence of pelvic/leg vein thrombosis was 38.6%. Of these, 55.5% also had a pulmonary embolism (Feigl and Schwarz 1978). Among 105 patients with confirmed leg vein thrombosis, the prevalence of pulmonary embolism was 57%while it was only 4.7% in patients without leg vein thrombosis. A closer look at the source of embolism reveals the following prevalence of pulmonary embolism (Könn and Schejbal 1978):

- 46% in patients with calf thrombosis
- 67% in the thigh and
- 77% in pelvic vein thrombosis

Duplex sonography with compression is a safe procedure to confirm that an embolism is originating from a deep vein thrombosis. In cases of suspected leg vein thrombosis the median sensitivity is 95% (range, 38100%) and the median specificity is 97% (range, 81100%). Even in cases of the relatively frequent isolated lower leg thrombosis the median sensitivity is 89 % (range, 3696 %) and the median specificity is 92 % (range, 5098 %) (Jäger et al. 1993).

Visualization of the thrombus and the absence of flow are direct signs of leg vein thrombosis (Fig. 4.55). Detection of the thrombus in the B mode is indirectly improved by the application of color-Doppler sonography. The thrombosed vein is not compressible or is only partially compressible, which is indicative of an occluding coagulation. However, signs of compressibility are only reliable when they are found in the inguinal or popliteal region. The vena cava and pelvic veins are not sufficiently compressible. In cases of calf thrombosis the compression is painful on palpation. The respiratory phase of venous flow is lost at a location distal to any hindrance of flow. In cases of acute thrombosis the vein is markedly dilated and valvular movements are absent. A careful comparison of the veins of one leg with those of the other is absolutely essential (Eichlisberger 1995; Table 4.7).

4.3.6.2 Echocardiography

Since the introduction of transesophageal echocardiography the *heart* has also being investigated increasingly often as a *source of embolism*. In the right atrium, transthoracic echocardiography reveals sessile and floating thrombi (Fig. 4.56), occasionally even riding thrombi in the main central branches of pulmonary arteries (Kronik and the European Working Group 1989; Vuille et al. 1993).

An echocardiography for orientation, to assess the right heart load, can be performed rapidly on an emergency basis.

In cases of nearly massive and massive pulmonary embolism, the right side of the heart reveals characteristic changes on echocardiography:

- Dilatation of the right atrium
- Dilatation of the right ventricle
- Paradoxical movement of the septum, flattening of the septum
- Tricuspid insufficiency more than 2.5 m/s
- Increased pulmonary artery pressure of more than 39 mmHg.

A major advantage of sonographic investigation of embolism is its manifold applicability and its availability at the bedside, whether in the emergency department or in the intensive care unit. Echocardiography and leg vein compression sonography yield a sensitivity of more than 90% for pulmonary embolism (Mathis et al. 2005; Figs. 4.57, 4.58).

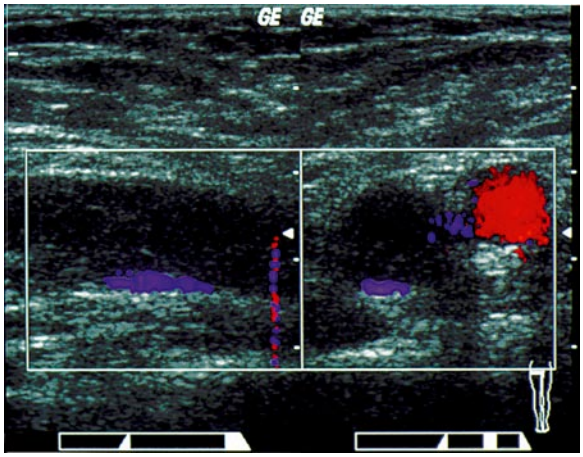

Fig. 4.55 Searching for the source of embolism: leg vein thrombosis in the femoral vein. The vein is larger than the artery, congested with echogenic material, and cannot be compressed. A small amount of flow is seen at the margin

Table 4.7 Duplex sonography of deep vein thrombosis (*DVT*) in the leg. (Based on Eichlisberger 1995)

Signs	Method of demonstration
Direct signs	
Visible thrombus	B-mode image
No flow	Pulsed-wave Doppler, color
Indirect signs	
Noncompressible vein	B-mode image
Non-breath-phase-dependent flow signals	Pulsed-wave Doppler, color
Flow signals are not present in the entire cross-section	Color
Larger diameter (acute DVT)	B-mode image
Collateral veins	B-mode, color
Absence of valve movement	B-mode image
Is not extensible during a Valsalva maneuver	B-mode image

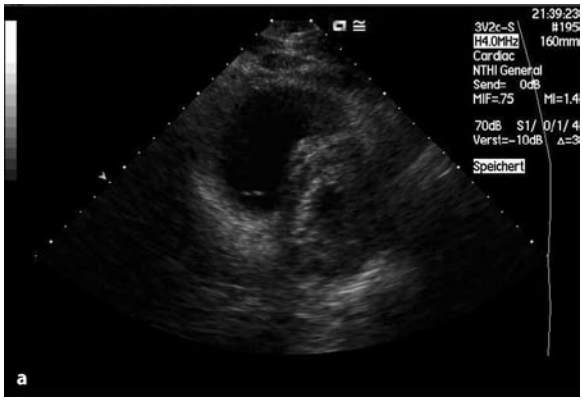

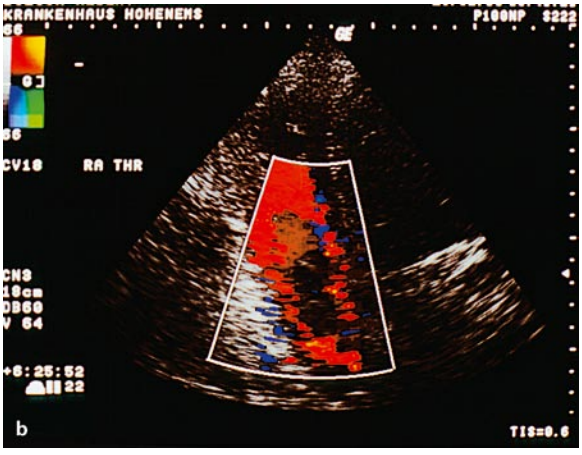

Fig. 4.56 **a** Acute load of the right side of the heart with massive dilatation of the right ventricle. **b** At the level of the valve there is a floating thrombus in the right side of the heart

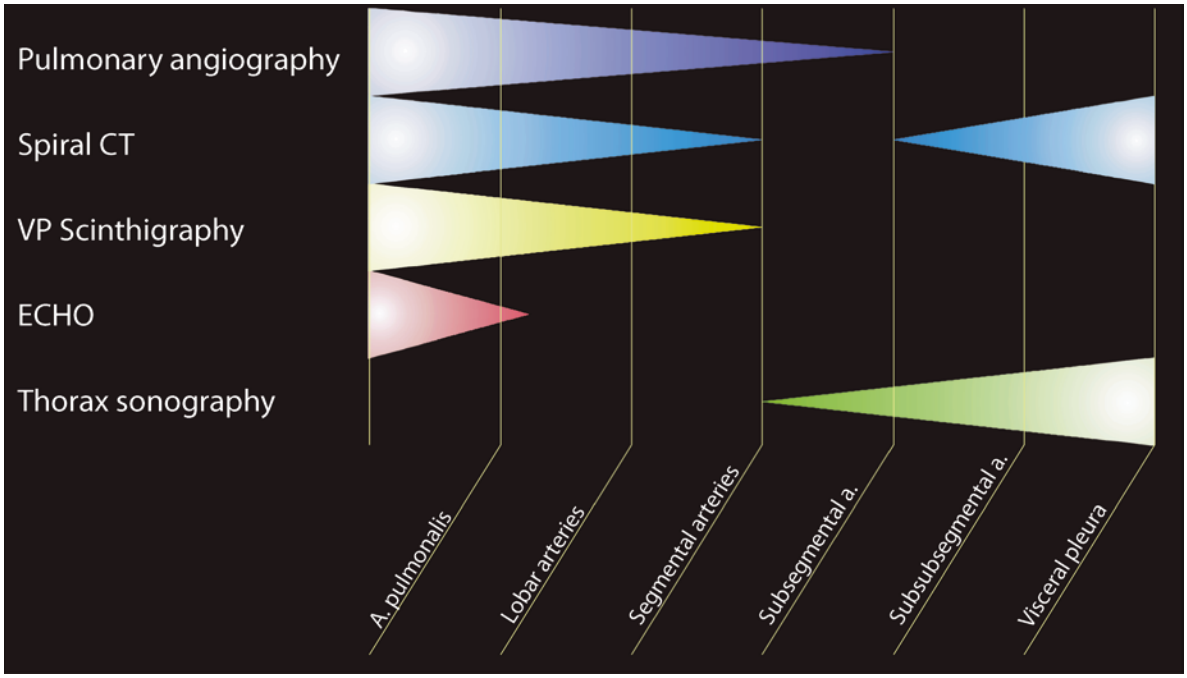

Fig. 4.57 Comparison of methods. (Adapted from Kroschel et al. 1991)

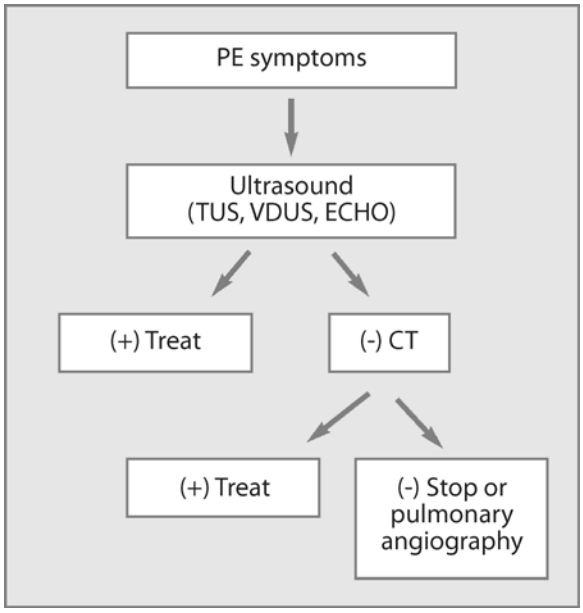

Fig. 4.58 Procedure in the case of a clinically suspected pulmonary embolism. In case of doubt, a scintigram may also be a useful adjunct. *CT* computed tomography, *TUS* transcutaneous sonography, *VDUS* vein duplex sonography. (Adapted from Goodman and Lipchik 1996)

Sonography in the presence of pulmonary embolism: "Kill three birds with one stone."

4.3.7 Summary

In the presence of a pulmonary embolism, lesions that transmit echoes can be visualized at subpleural location by chest sonography at least in three fourths of cases. This corresponds, on the one hand, to reperfusible alveolar edema and hemorrhage (early infarctions of the lung) due to embolism. On the other hand, they might be marked infarctions of the lung that have a typical sonomorphological appearance with small pleural-based triangular or slightly rounded lesions. In combination with echocardiography and leg vein compression sonography, the accuracy is more than 90%—a figure not achieved with any other method.

References

Ducker EA, Rivitz SM, Shepard JAO et al (1998) Acute pulmonary embolism: assessment of helical CT for diagnosis. Radiology 209:235–241

Eichlisberger R, Frauchinger B, Holtz D, Jäger KA (1995) Duplexsonographie bei Verdacht auf tiefe Venenthrombose und zur Abklärung der Varikose. In: Jäger KA, Eichlisberger R (eds) Sonokurs. Karger, Basel, pp 137–147

Feigl W, Schwarz N (1978) Häufigkeit von Beinvenenthrombosen und Lungenembolien im Obduktionsgut. In: Ehringer H (ed) Aktuelle Probleme in der Angiologie 33. Huber, Bern, pp 27–37
Gehmacher O, Mathis G (1994) Farkodierte Duplexsonographie peripherer Lungenherde—ein diagnostischer Fortschritt? Bildgebung 61(S2):11
Goodman LR (2005) Small pulmonary emboli: what do we know? Radiology 234:654–658
Goodman LR, Lipchik RJ (1996) Diagnosis of pulmonary embolism: time for a new approach. Radiology 199:25–27
Goodman LR, Curtin JJ, Mewissen MW et al (1995) Detection of pulmonary embolism in patients with unresolved clinical and scintigrafic diagnosis: helical CT versus angiography. AJR Am J Roentgenol 164:1369–1374
Görg C, Bert T (2006) Transcutaneous contrast enhanced sonography of peripheral lung lesions: review and pictorial essay. AJR Am J Roentgenol 187:420–429
Hartung W (1984) Embolie und Infarkt. In: Remmele W (ed) Pathologie 1. Springer, Berlin, pp 770–772
Heath D, Smith P (1988) Pulmonary embolic disease. In: Thurlbeck WM (ed) Pathology of the lung. Thieme, Stuttgart, pp 740–743
Jäger K, Eichlisberger R, Frauchinger B (1993) Stellenwert der bildgebenden Sonographie für die Diagnostik der Venenthrombose. Haemostaseologie 13:116–123
Joyner CR, Miller LD, Dudrick SJ, Eksin DJ (1966) Reflected ultrasound in the detection of pulmonary embolism. Trans Assoc Am Physicians 79: 262–277
Könn G, Schejbal E (1978) Morphologie und formale Genese der Lungenthromboembolie. Verh Dtsch Ges Inn Med 84:269–276
Kronik G, The European Working Group (1989) The European cooperative study on the clinical significance of right heart thrombi. Eur Heart J 10:1046–1059
Kroschel U, Seitz K, Reuß J, Rettenmaier (1991) Sonographische Darstellung von Lungenembolien. Ergebnisse einer prospektiven Studie. Ultraschall Med 12:263–268
Lechleitner P, Raneburger W, Gamper G, Riedl B, Benedikt E, Theurl A (1998) Lung sonographic findings in patients with suspected pulmonary embolism. Ultraschall Med 19:78–82
Lechleitner P, Riedl B, Raneburger W, Gamper G, Theurl A, Lederer A (2002). Chest sonography in the diagnosis of pulmonary embolism: a comparison with MRI angiography and ventilation perfusion scinitgraphy. Ultraschall Med 23:373–378
Mathis G (1997) Thoraxsonography—part II: peripheral pulmonary consolidation. Ultrasound Med Biol 23:1141–1153
Mathis G, Dirschmid K (1993) Pulmonary infarction: sonographic appearance with pathologic correlation. Eur J Radiol 17:170–174
Mathis G, Metzler J, Fußenegger D, Sutterlütti G (1990a) Zur Sonomorphologie des Lungeninfarktes. In: Gebhardt J, Hackelöer BJ, von Klingräff G, Seitz K (ed) Ultraschalldiagnostik '89. Springer, Berlin, pp 388–391
Mathis G, Metzler J, Feurstein M, Fußenegger D, Sutterlütti G (1990b) Lungeninfarkte sind sonographisch zu entdecken. Ultraschall Med 11:281–283
Mathis G, Metzler J, Fußenegger D, Sutterlütti G, Feurstein M, Fritzsche H (1993) Sonographic observation of pulmonary infarction and early infarctions by pulmonary embolism. Eur Heart J 14:804–808
Mathis G, Bitschnau R, Gehmacher O et al (1999) Chest ultrasound in diagnosis of pulmonary embolism in comparison to helical CT. Ultraschall Med 20:54–59
Mathis G, Blank W, Reißig A, Lechleitner P, Reuß J, Schuler A, Beckh S (2005) Thoracic ultrasound for diagnosing pulmonary embolism. A prospective multicenter study of 352 patients. Chest 128:1531–1538
Morgenthaler TI, Ryu JH (1995) Clinical characteristics of fatal pulmonary embolism in a referral hospital. Mayo Clin Proc 70:417–424
Morpurgo M, Schmid C (1995) The spectrum of pulmonary embolism. Clinicopathologic correlations. Chest 107(Suppl 1):18S–20S
Oser RF, Zuckermann DA, Guttierrez FR, Brink JA (1996) Anatomic distribution of pulmonary emboli at pulmonary angiography: implications for cross-sectional imaging. Radiology 199:31–35
PIOPED Investigators (1990) Value of the ventilation/perfusion scan in acute pulmonary embolism. JAMA 263:2753–2759
Rathbun SW, Raskob GE, Whitsett TL (2000) Sensitivity and specificity of helical computed tomography in the diagnosis of pulmonary embolism: a systematic review. Ann Intern Med 132:227–232
Reißig A, Kroegel C (2003) Transthoracic ultrasound of lung and pleura in the diagnosis of pulmonary embolism: a novel non-invasive bedside approach. Respiration 70:441–452
Reißig A, Heyne JP, Kroegel C (2001) Sonography of lung and pleura in pulmonary embolism: sonomorphologic characterization and comparison with spiral CT scanning. Chest 120:1977–1983
Reißig A, Heyne JP, Kroegel C (2004) Ancillary lung parenchymal findings at spiral CT scanning in pulmonary embolism. Relationship to chest sonography. Eur J Radiol 49:250--259
Remy-Jardin M, Remy J, Wattinne L, Giraud F (1992) Central pulmonary thromboembolism: Diagnosis with spiral volumetric CT with a single-breath-hold technique—comparison with pulmonary angiography. Radiology 185:381–387
Ren H, Kuhlman JE, Hruban RH, Fishman EK, Wheeler PS, Hutchins GM (1990) CT of infation-fixed lungs: wedge-shaped density and vasular sign in the diagnosis of infarction. J Comput Assist Tomogr 14:82–86
Teigen CL, Maus TP, Sheedy PF, Johnson CM, Stanson AW, Welch TJ (1993) Pulmonary embolism: diagnosis with electron-beam CT. Radiology 188:839–845
Vuille C, Urban P, Jolliet P, Louis M (1993) Thrombosis of the right auricle in pulmonary embolism: value of echocardiography and indications for thrombolysis. Schweiz Med Wochenschr 123:1945–1950
Yuan A, Yang PC, Chang CB (1993) Pulmonary infarction: use of color doppler sonography for diagnosis and assessment of reperfusion of the lung. AJR Am J Roentgenol 160:419—420

4.4 Mechanical Lung Consolidations: Atelectasis

C. Görg

4.4.1 Definition

Atelectasis is defined as the absence of ventilation in portions of the lung or the entire lung. Such lack of ventilation may be permanent or transient, complete or partial (dysatelectasis), congenital or acquired (Fig. 4.59).

4.4.2 Pathomorphology

Depending on the origin, a distinction is made between compression atelectasis and resorption atelectasis (obstructive atelectasis). Compression atelectasis may be anticipated when an accumulation of fluid causes intra-

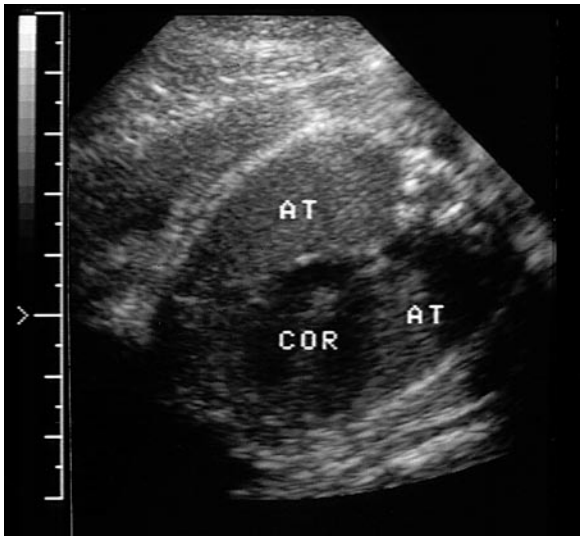

Fig. 4.59 Echo through the chest of a fetus in the 32nd gestational week. Both lungs are homogeneously hypoechoic, as in complete atelectasis (*AT*)

pleural pressure to increase to a level higher than that of external air. This may be expected when the effusion is more than 2 l (Grundmann 1986).

Resorption atelectasis occurs when a bronchus is displaced in terms of its region of vascular supply, as a result of external compression or endobronchial obliteration.

In cases of resorption or obstructive atelectasis, a distinction is made between the central and the peripheral form. Central obstruction is usually caused by endobronchial processes (e.g., bronchial carcinoma or foreign body) or extrabronchial alterations (e.g., enlarged lymph nodes), whereas peripheral bronchial obstructions are marked by inflammatory mucus plugs and displacement of small bronchial branches. Displacement of the lumen of the middle lobe by mucus or pus, scarred kinking of the bronchus, external lymph node compression or tumor leads to the middle lobe syndrome.

Atelectasis impairs circulation in parenchyma, causing undersaturation of arteries owing to reduced gas exchange in perfused but not ventilated atelectatic lung parenchyma.

In terms of pathological anatomy, the early phase of obstructive atelectasis is marked by high-protein fluid in intraalveolar spaces. The next stage is characterized by the migration of macrophages and lymphocytic infiltration. In cases of compression or even obstructive atelectasis of longer duration, the parenchyma shrinks and fibrous induration of lung tissue occurs.

Additional attendant phenomena or complications in cases of bronchial obstruction include retention of secretion; bronchiectasis is seen in approximately 40% of cases (Burke and Fraser 1988; Yang et al. 1990; Liaw et al. 1994). In rare cases the patient develops bacterial superinfection and microscopic or gross abscesses; necrotic or hemorrhagic lesions in atelectatic tissue may also be found.

4.4.3 Sonomorphology

Lung atelectases are characterized by partial or complete absence of ventilation; therefore, in principle, they can be imaged by sonography. Furthermore, the echotransparency of the lung allows the investigator to assess the parenchyma. Especially in the presence of obstructive atelectasis, atelectatic lung tissue serves as "an acoustic window" for the investigation of central structures that possibly underlie the atelectasis.

4.4.4 Compression Atelectasis

The most common form is accompanied by the formation of pleural effusion. Depending on the extent of intrapleural fluid, the patient may develop homogeneous hypoechoic transformations shaped like a wedge or a pointed cap (Fig. 4.60). The margin towards the adjacent aerated lung tissue is blurred. Usually the atelectatic lung is surrounded by fluid, but also may be partly adherent to the pleura. The following features help to confirm the diagnosis by sonography:

- Partial reventilation during inspiration (Fig. 4.61),
- Partial reventilation after aspiration of effusion (Fig. 4.62)

During inspiration sonography reveals an increasing quantity of air in atelectatic regions and the formation of a so-called air bronchogram. However, in the presence of exudative effusion, fibrin strands, septa and echogenic pleural effusion, one frequently observes poor reventilation during inspiration as a result of reduced elasticity of the lung. This condition has been described as a "trapped" lung (Lan et al. 1997).

Concomitant inflammatory invasion of parenchyma in atelectatic tissue is a further limitation. It leads to congestive pneumonia and restricts inspiratory ventilation. On the basis of sonomorphology alone this condition cannot be distinguished from pneumonia (Fig. 4.63).

Possible sonography findings in compression atelectasis:

1. B-mode sonography
   (a) Moderate to marked pleural effusion

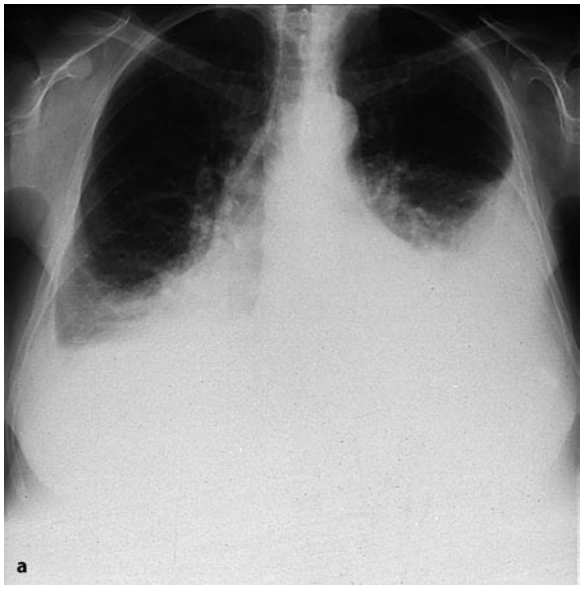

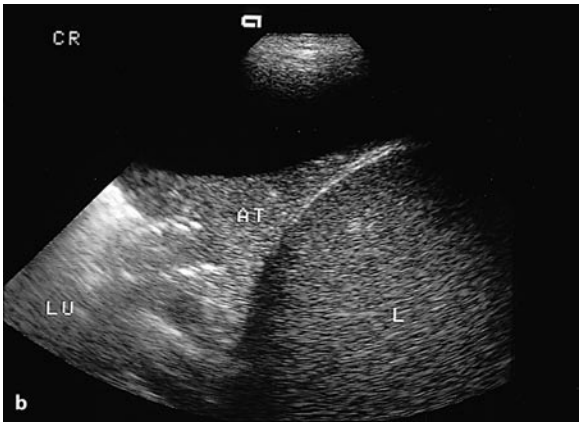

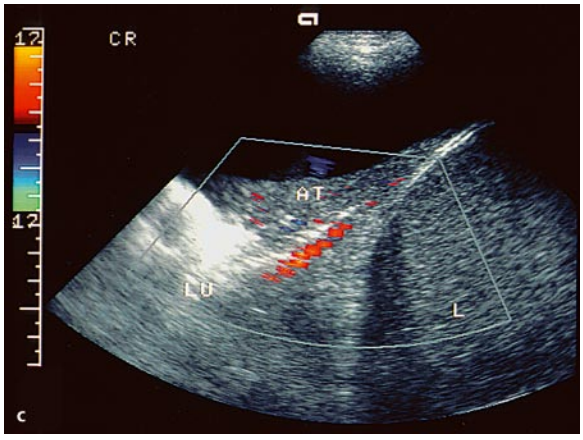

Fig. 4.60 **a** Chest X-ray: a 60-year-old man with global decompensated heart failure and bilateral pleural effusions. **b** Sonography: In right-lateral intercostal echo transmission one sees a pleural effusion with a wedge-shaped hypoechoic transformation of parts of the lower lobe of the lung as in the presence of atelectasis (*AT*). The demarcation to the ventilated lung (*LU*) is blurred. An extensive "air bronchogram" is seen. *L* liver. **c** Color-Doppler sonography reveals a flow signal along the bronchial branch filled with air

(b) Triangular pointed cap-like hypoechoic transformation of lung parenchyma
(c) Blurred margins towards the ventilated lung parenchyma
(d) Partial reventilation during inspiration ("air bronchogram")
(e) Partial reventilation after aspiration of the effusion

2. Color-Doppler sonography: on intraindividual comparison with the liver one finds enhanced flow phenomena

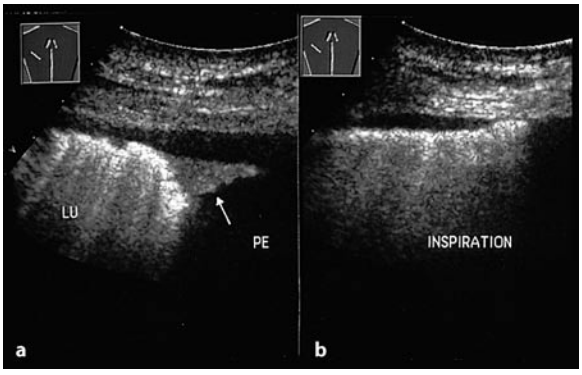

Fig. 4.61 **a** In left-lateral intercostal echo transmission one sees a pointed cap-like, smoothly margined hypoechoic transformation in the tip of the lower lobe of the left lung (*arrow*) in the presence of a pleural effusion. *Lu* lung, *PE* pleural effusion. **b** Reventilation of lung tissue is achieved after deep inspiration, as in the presence of compression atelectasis

In cases of compression atelectasis, lung tissue is partially reventilated after drainage of the effusion. This is also dependent on the elasticity of the lung. Of course, ventilation of the parenchyma after puncture of the effusion does not rule out the possibility of an additional central space-occupying lesion.

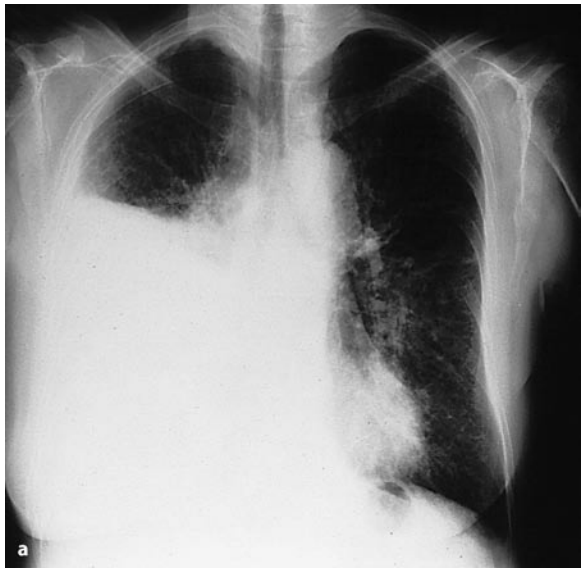

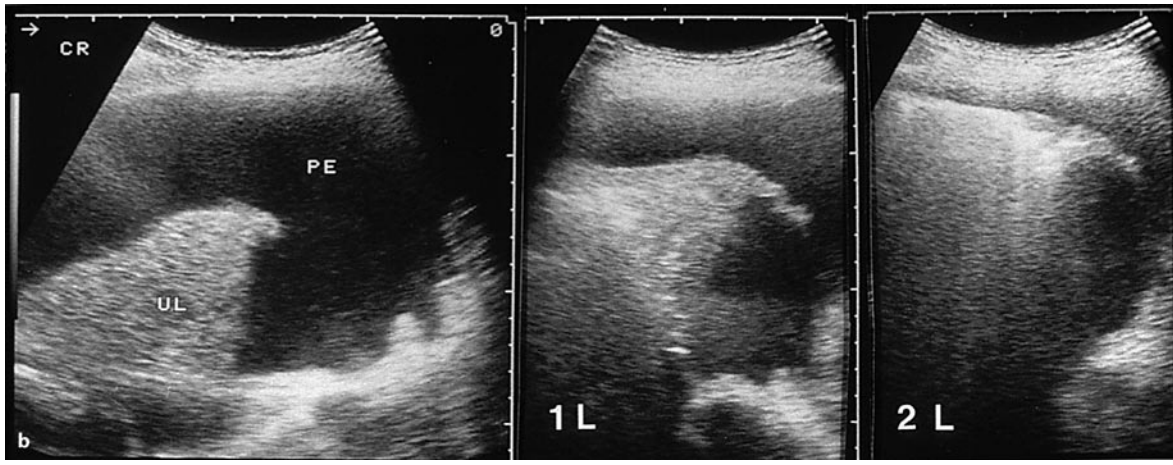

Fig. 4.62 A 66-year-old man with an alveolar carcinoma. **a** Chest X-ray: homogenous shadow of the caudal right-sided hemothorax. **b** Sonography: right-lateral intercostal echo transmission shows a marked pleural effusion (*PE*) with atelectasis in the lower lobe (*UL*). After aspiration of the effusion (1 l, *middle*, and (2 l, *right*) there is increasing reventilation

4.4.5 Obstructive Atelectasis

The sonographic image of obstructive atelectasis is marked by a largely homogeneous, hypoechoic presentation of lung tissue as in hepatization (Figs. 4.64, 4.65). Effusion is absent or is very mild. In cases of lobar atelectasis the margin towards ventilated lung tissue is rather distinct (Fig. 4.66). Depending on the duration of atelectasis, intraparenchymatous structures also may be seen:

- Hypoechoic vascular lines and echogenic reflexes (Figs. 4.67, 4.68)
- Anechoic, hypoechoic or echogenic focal lesions (Figs. 4.69, 4.70)

Atelectasis of long duration is accompanied by sonographic reflexes in the lung parenchyma. The reflexes are caused by dilated bronchi, as a result of secretory congestion (so-called fluid bronchogram; Fig. 4.71). Vessels along the bronchi are seen as branches of the pulmonary artery and the pulmonary vein on color-Doppler sonography (Fig. 4.66; Chap. 7).

Possible findings on sonography in cases of obstructive atelectasis:

1. B-mode sonography
   (a) Mild to no pleural effusion
   (b) Homogenous hypoechoic transformation of lung parenchyma
   (c) Hyperechoic reflexes may be seen (fluid bronchogram)
   (d) Focal intraparenchymatous lesions may be seen
      - Liquefaction of parenchyma

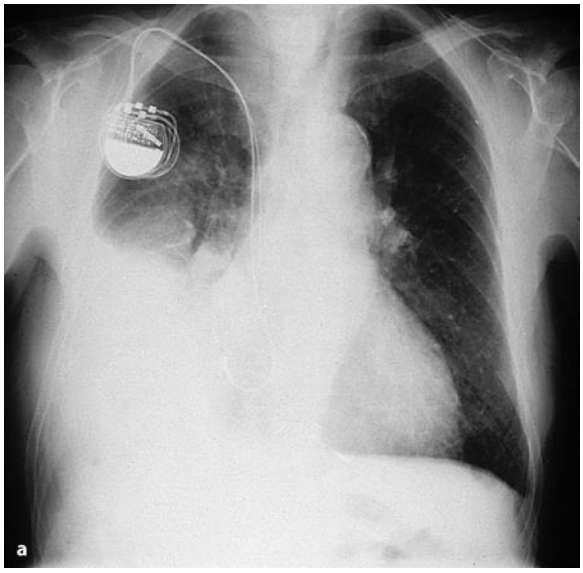

Fig. 4.63 A 75-year-old man with heart failure. **a** Chest X-ray: shadow in the region of the right caudal lung. **b** Sonography: right dorsal echo transmission shows a marked and partly septated pleural effusion (*PE*), and a circular hypoechoic consolidation of parts of the lung (*AT*). On color-Doppler sonography one finds pronounced flow signals. The marked pleural effusion and the absence of reventilation during inspiration are indicative of a fixed compression atelectasis. In principle, the image does not permit exclusion of concomitant congestive pneumonia. *LE* liver, *Lu* lung

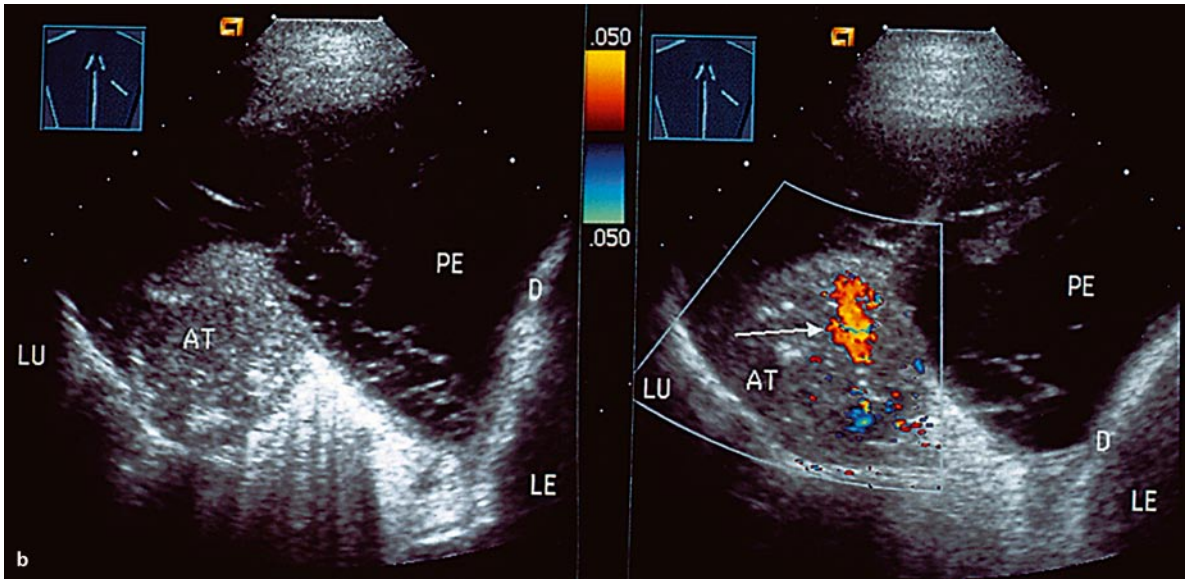

- Microabscesses, gross abscesses
- Metastases

(e) A central space-occupying lesion may be seen
(f) No reventilation during inspiration

2. Color-Doppler sonography
   (a) On intraindividual comparison with the liver, enhanced flow phenomena are visualized
   (b) Triphasic spectrum of the arterial flow curve of pulmonary arteries (type, arteries of the extremities)

Quite often the investigator finds *focal lesions* in the lung parenchyma. As a result of dilated bronchi (due to congestion of secretion), one occasionally finds small anechoic, hypoechoic or even echogenic lesions within the parenchyma. Given corresponding clinical features, the lesions are due to microabscesses. Occasionally the abscesses contain air echoes (Yang et al. 1992; Fig. 4.69). Atelectasis caused by tumor often leads to intraparenchymatous liquefaction, which is seen on sonography as large hypoechoic circular lesions with characteristic motion echoes on "real-time" investigation. This is primarily due to necrosis or tumor-related retention of secretion. Abscesses cannot be entirely excluded on the basis of sonomorphology alone. Here the clinical findings will be one of the main determinants of the diagnosis. However, sonography-guided aspiration will allow the investigator to confirm the diag-

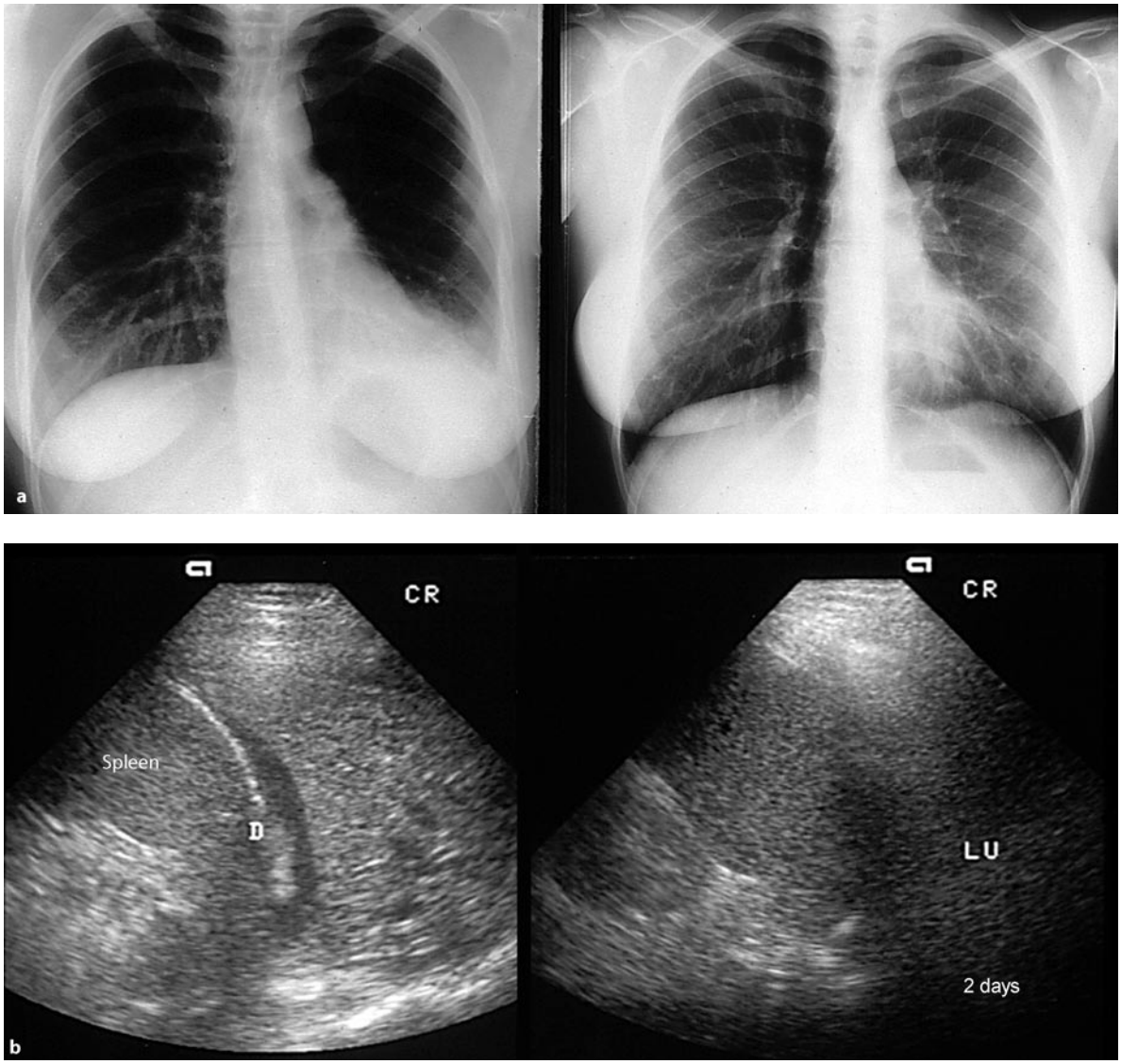

Fig. 4.64 A 20-year-old woman with fever and dyspnea. **a** Chest X-ray: signs of atelectasis in the lower lobe on the left side (*left*), which resolved spontaneously after 2 days (*right*). **b** Sonography: left lateral intercostal echo transmission shows a homogenous lung consolidation with a mild pleural effusion as in the presence of obstructive atelectasis (*left*). This image taken after 48 h shows that the lung has been reventilated. The most likely condition in this case is displacement of the bronchus by inflammatory mucus. *Lu* lung, *D* diaphragm

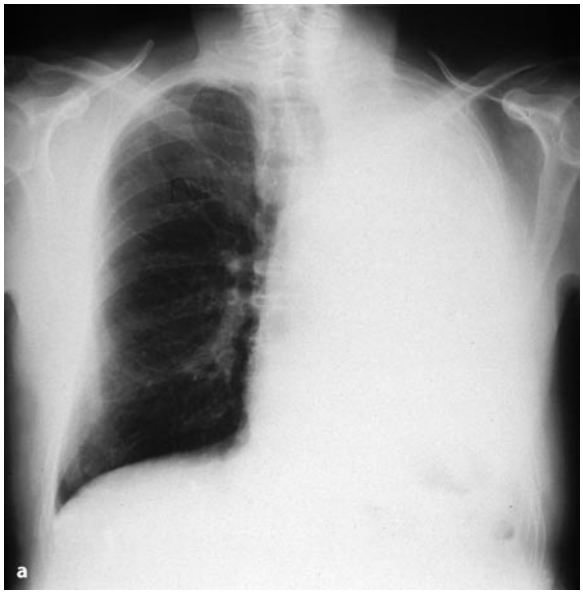

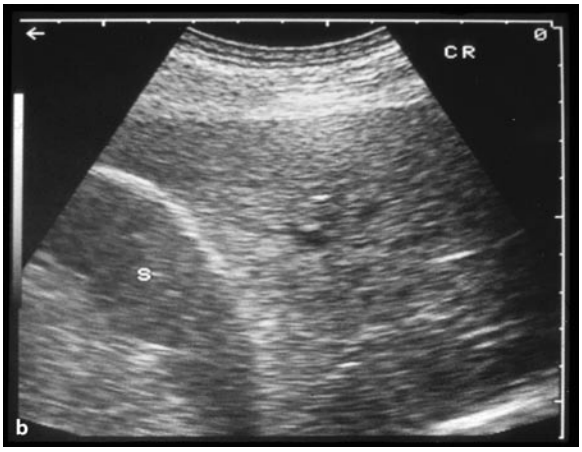

Fig. 4.65 A 68-year-old man with a bronchial carcinoma. **a** Chest X-ray: homogenous shadowing of the left hemothorax. **b** Sonography: left-lateral intercostal echo transmission shows a complete hypoechoic transformation of the left lung without effusion, similar to so-called hepatization in obstructive atelectasis. *S* spleen

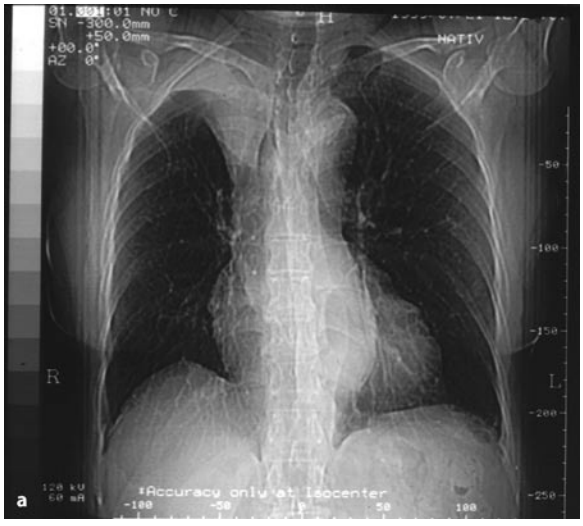

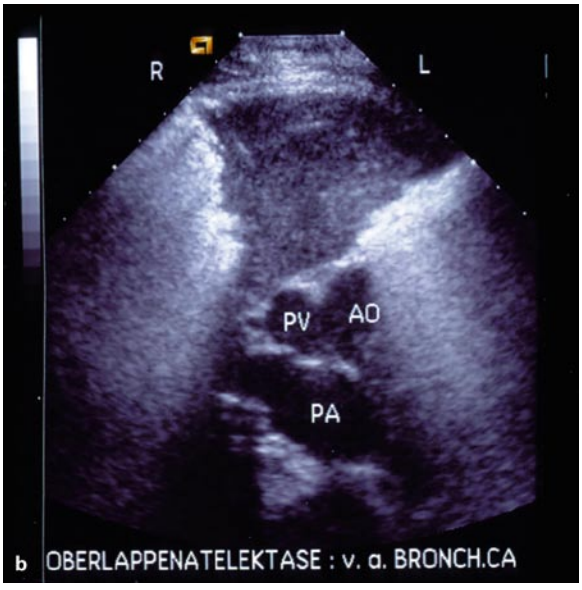

Fig. 4.66 A 74-year-old woman with dyspnea. **a** Chest X-ray: signs of right-sided upper-lobe atelectasis. **b** Sonography: right-ventral intercostal echo transmission shows a smoothly margined, wedge-shaped hypoechoic transformation of the lung as in atelectasis. The central vessels are seen; a shadow of the tumor core cannot be demarcated. *AO* aorta, *PV* pulmonary vein, *PA* pulmonary artery. **c** *see next page*

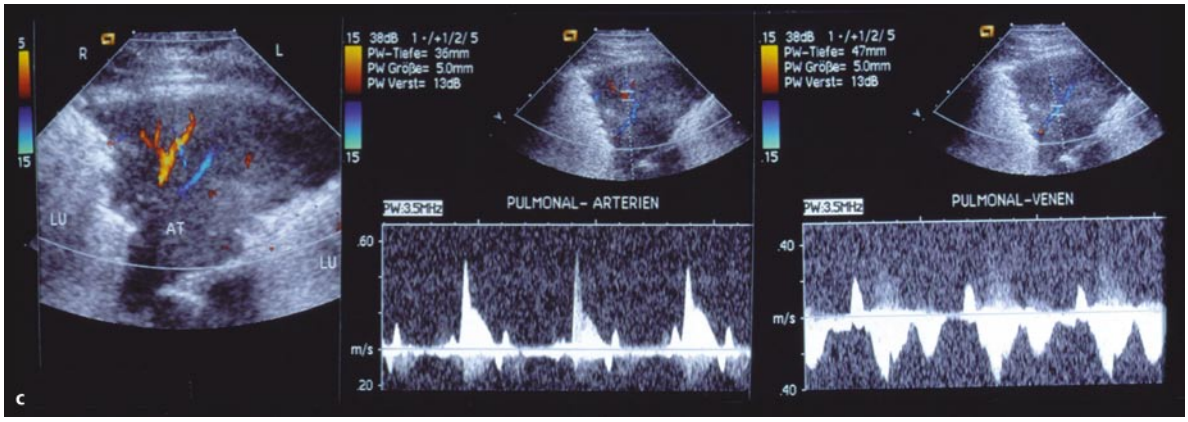

Fig. 4.66 *(continued)* **c** Color-Doppler sonography shows pronounced arterial and venous flow profiles. The characteristic flow profiles of the pulmonary artery and the pulmonary vein are seen

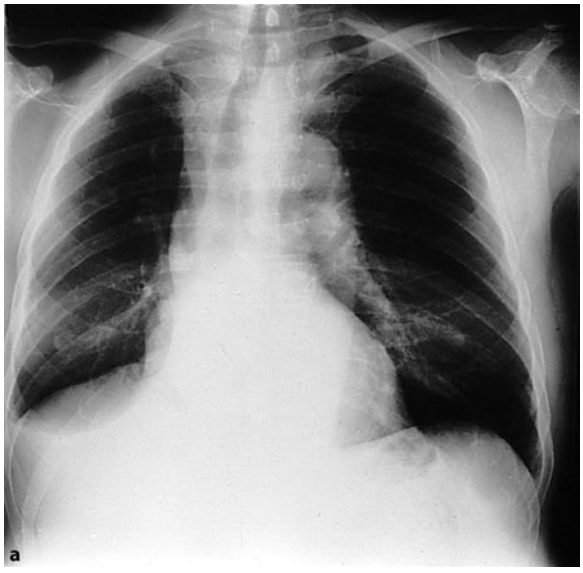

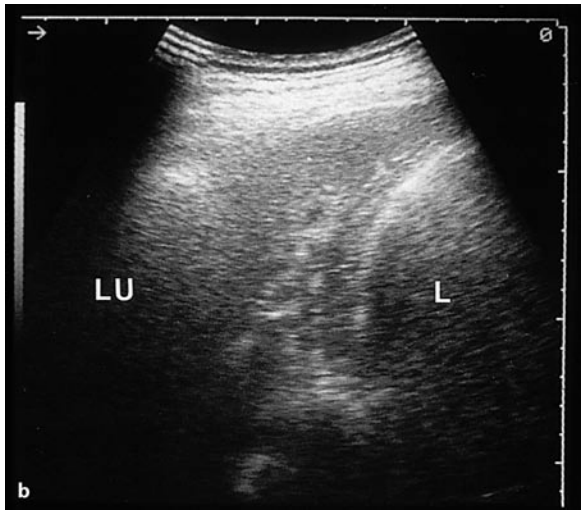

Fig. 4.67 An 84-year-old man with a bronchial carcinoma. **a** Chest X-ray: suspected lower-lobe atelectasis on the right side. **b** Sonography: right-lateral intercostal echo transmission shows a hypoechoic, poorly demarcated transformation with accentuated visualization of hyperechoic reflex bands in the atelectatic lung tissue

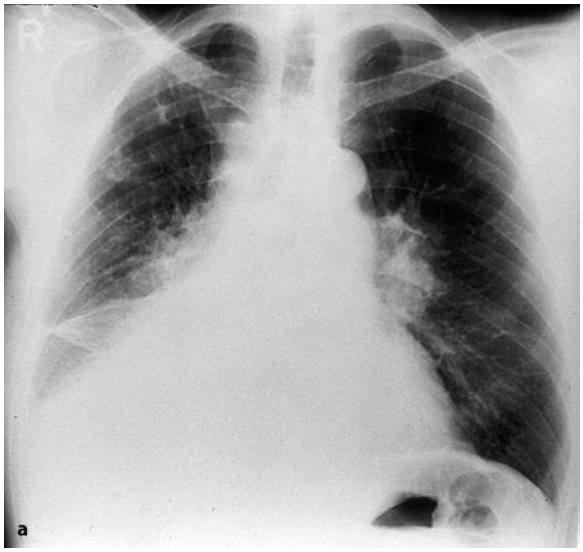

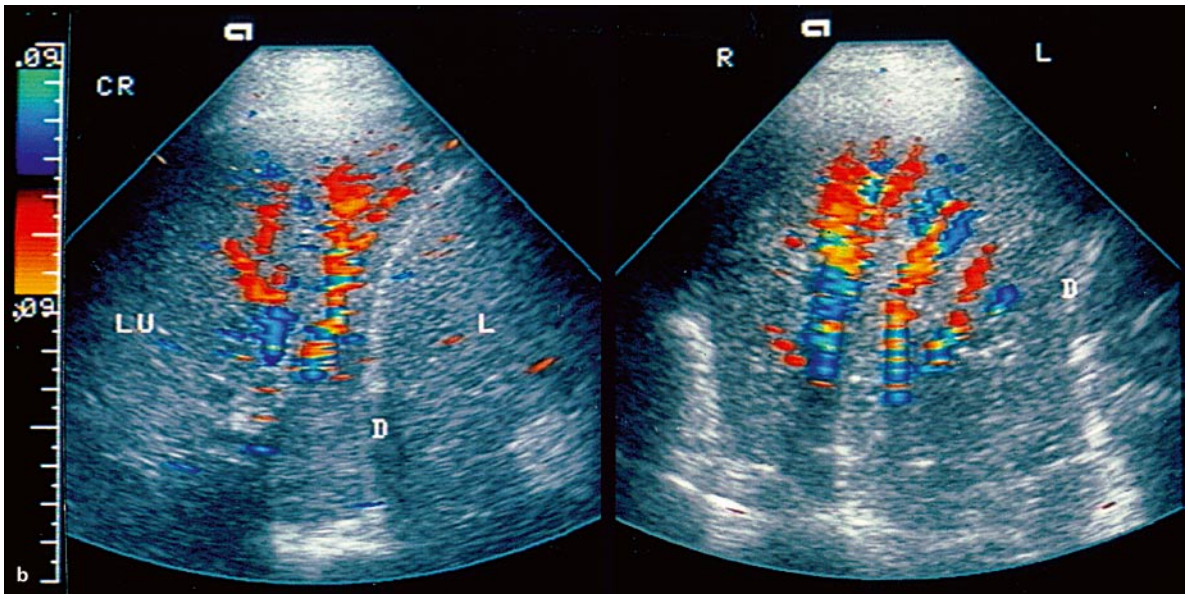

Fig. 4.68 A 58-year-old man with a bronchial carcinoma. **a** Chest X-ray:sSigns of right-sided lower-lobe atelectasis. **b** Sonography: right-sided intercostal echo transmission shows a hypoechoic transformation of the lower lobe of the lung. In contrast to the liver, color-Doppler sonography shows enhanced flow signals which are characteristic evidence of atelectasis. *D* diaphragm, *L* liver, *Lu* lung

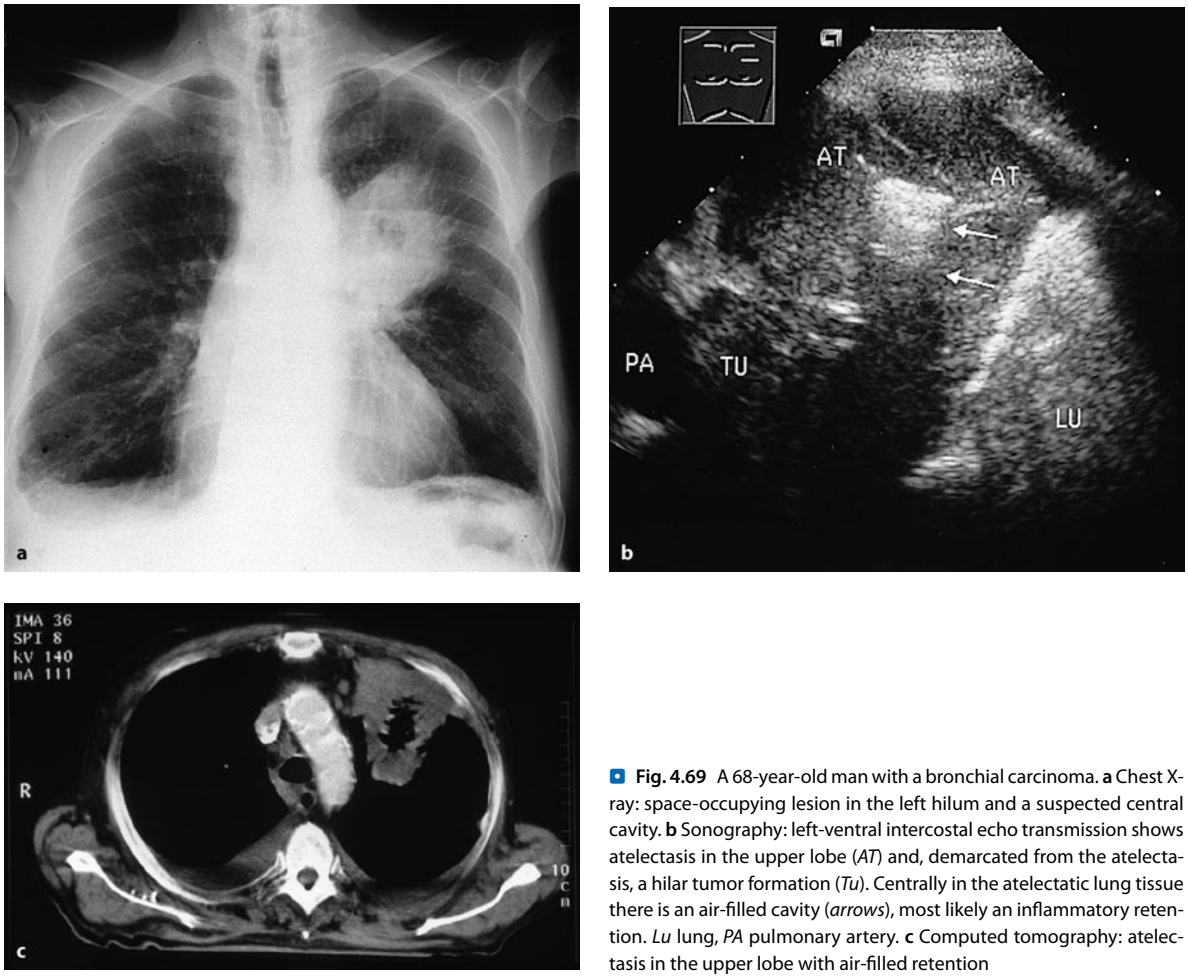

Fig. 4.69 A 68-year-old man with a bronchial carcinoma. **a** Chest X-ray: space-occupying lesion in the left hilum and a suspected central cavity. **b** Sonography: left-ventral intercostal echo transmission shows atelectasis in the upper lobe (*AT*) and, demarcated from the atelectasis, a hilar tumor formation (*Tu*). Centrally in the atelectatic lung tissue there is an air-filled cavity (*arrows*), most likely an inflammatory retention. *Lu* lung, *PA* pulmonary artery. **c** Computed tomography: atelectasis in the upper lobe with air-filled retention

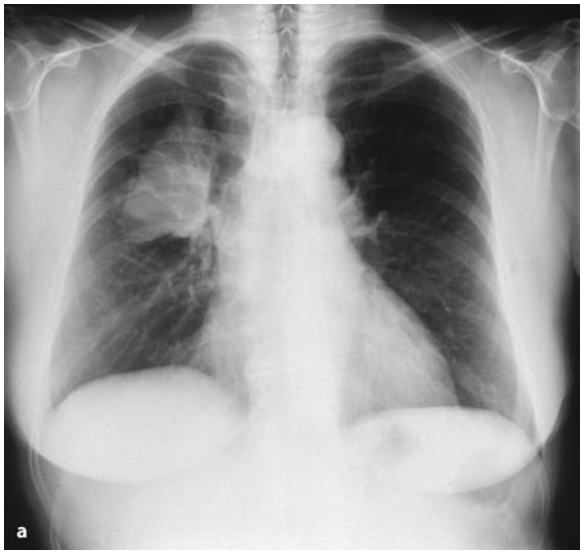

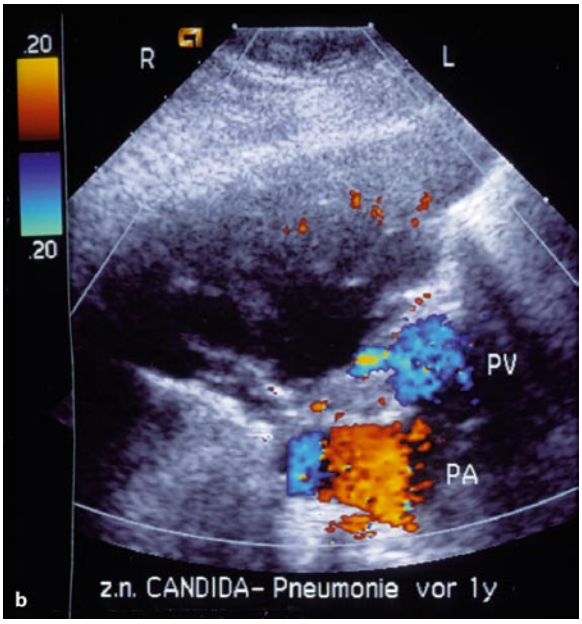

Fig. 4.70 A 63-year-old woman with a malignant lymphoma in the hilum after polychemotherapy and after *Candida* pneumonia. **a** Chest X-ray: central space-occupying lesion in the right hilum. **b** Sonography: right ventral intercostal echo transmission shows partial atelectasis in the region of the upper lobe. A hilar tumor formation is not seen. Centrally in the atelectatic lung tissue there is an anechoic pseudocyst formation which has been constant for more than 12 months at sonography controls. *PA* pulmonary artery, *PV* pulmonary vein

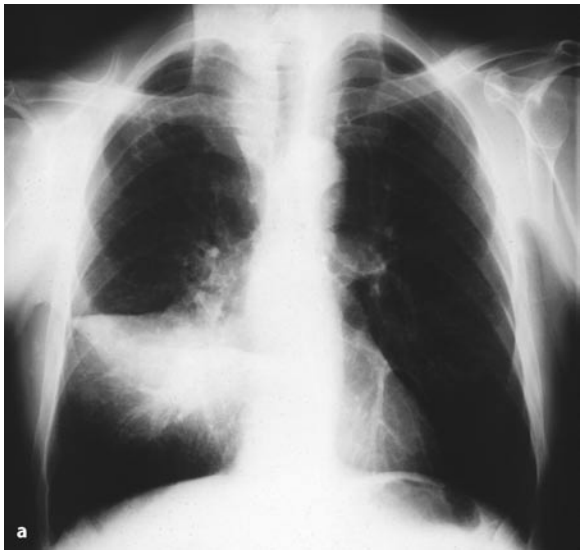

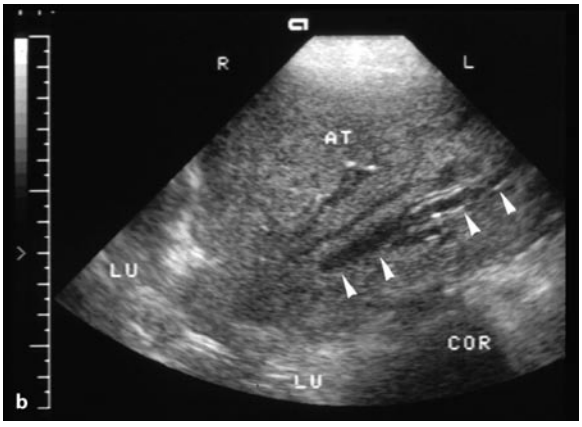

Fig. 4.71 A 68-year-old man with a bronchial carcinoma. **a** Chest X-ray: signs of middle-lobe atelectasis. **b** Sonography: right-ventral intercostal echo transmission shows atelectasis in the middle lobe (*AT*) with accentuated dilated bronchi, indicative of a fluid bronchogram ("sticks"). The central tumor formation cannot be clearly demarcated. **c** *see next page*

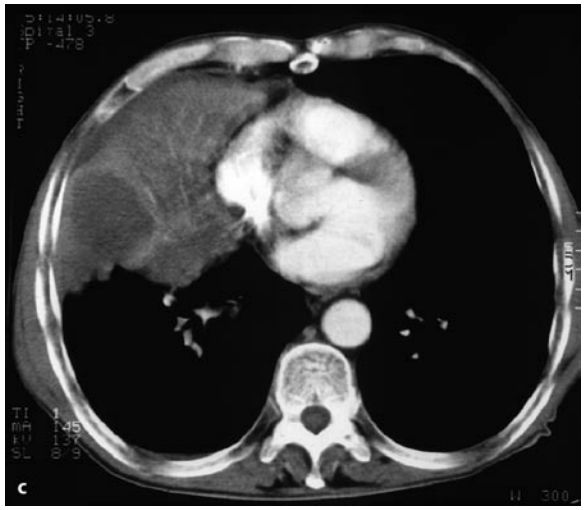

Fig. 4.71 *(continued)* **c** Computed tomography: visualization of atelectasis in the middle lobe

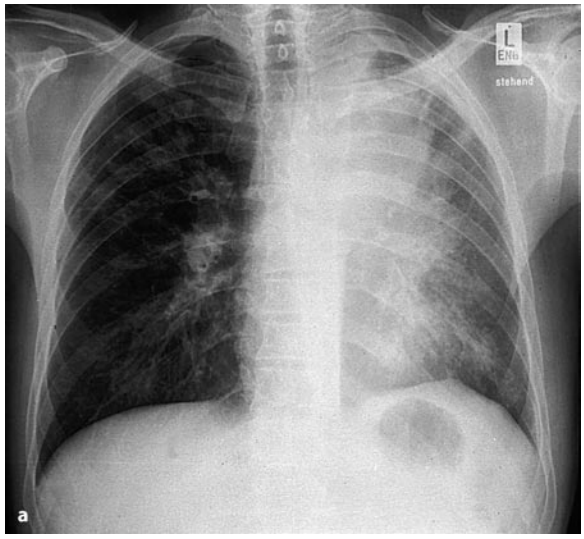

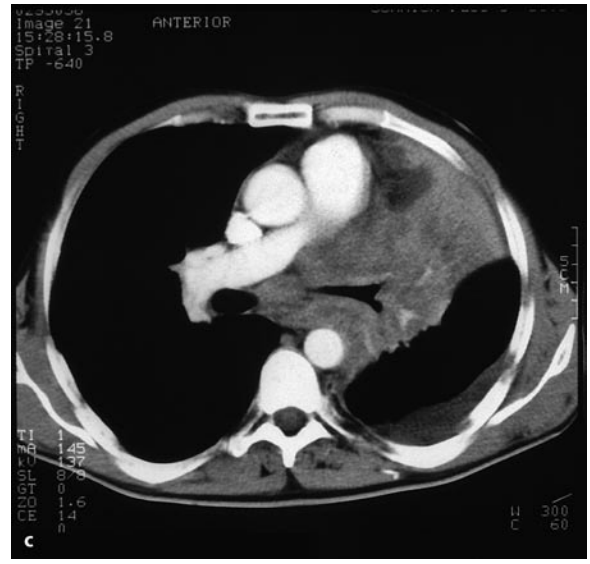

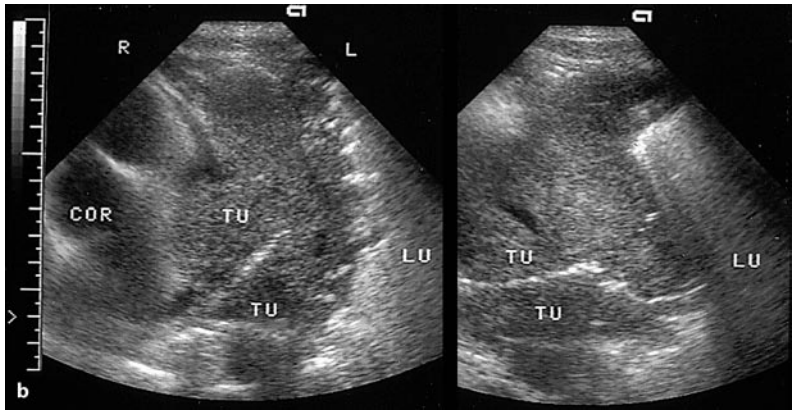

Fig. 4.72 A 44-year-old man with a bronchial carcinoma. **a** Chest X-ray: signs of left-sided upper-lobe atelectasis and dysatelectasis in the lower lobe. **b** Sonography: left-ventral intercostal echo transmission shows atelectasis in the upper lobe. The central tumor formation (*TU*) is rather poorly demarcated from the atelectasis. The highly constricted bronchus is seen as an air-filled band of several reflexes. *Lu* lung. **c** Computed tomography: visualization of the atelectasis in the upper lobe and the central tumor.

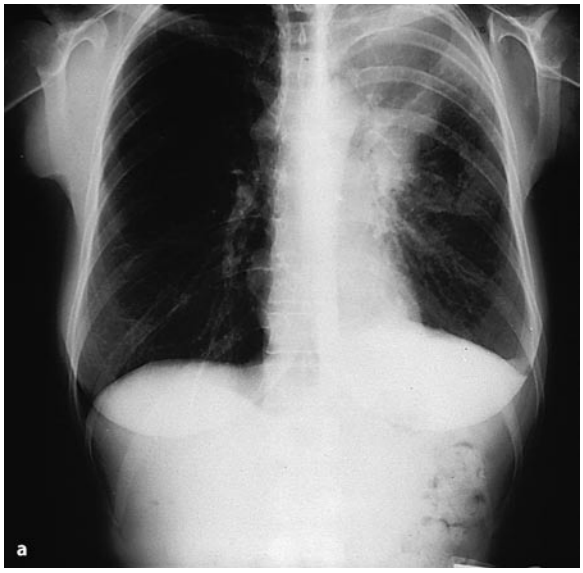

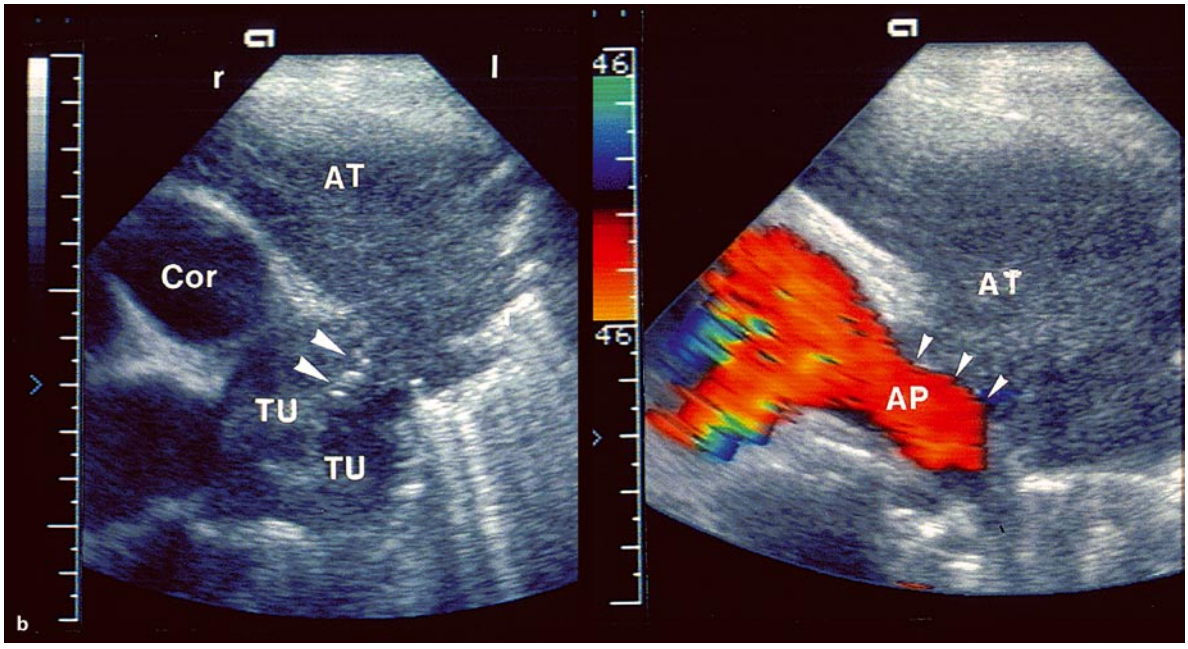

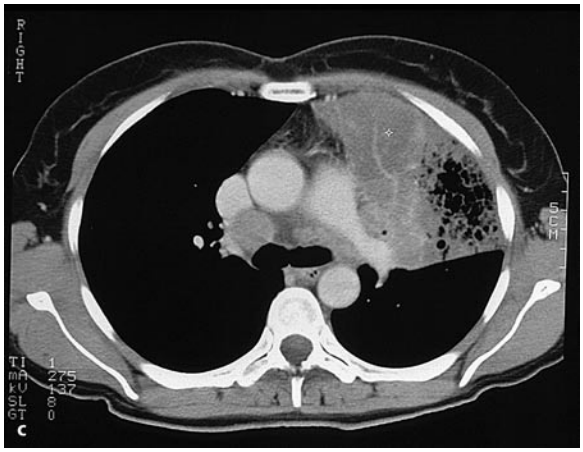

Fig. 4.73 A 48-year-old man with a bronchial carcinoma. **a** Chest X-ray: signs of upper-lobe atelectasis on the left side. **b** Sonography: left ventral intercostal echo transmission shows the atelectasis in the upper lobe (*AT*) and the central tumor (*TU*) demarcated from the atelectasis. On color-Doppler sonography the tumor is seen immediately next to the pulmonary artery (*AP*; "sticks"). **c** Computed tomography: visualization of the atelectasis in the upper lobe and the tumor surrounding the pulmonary artery

nosis and obtain material for bacteriological investigation (Görg 2003; Liaw et al 1994; Chap. 7).

Occasionally echogenic circular lesions or metastases may be found in atelectatic lung tissue. They show intralesional flow signals on color-Doppler sonography (Chap. 7).

Essentially, in the presence of lobar or pulmonary atelectasis, central portions can be imaged through atelectatic lung tissue by sonography. The main purpose here is to demonstrate the central tumor if there is one. On the basis of sonographic structural features, a definite distinction between atelectatic lung tissue and tumor tissue can be made in less than 50% of cases (Görg et al. 1996; Figs. 4.72, 4.73a, b).

4.4.6 Color-Doppler Sonography

Particularly in cases of compression atelectasis, the atelectatic lung tissue is characterized by accentuated flow phenomena compared with the liver (Görg et al. 1996; Fig. 4.68). Investigation by color-Doppler sonography is limited by motion artifacts due to respiration and a possibly paracardiac position. Analysis of the venous Doppler flow curve will reveal the characteristic triphasic course of pulmonary veins.

Visualization of the arterial flow curve will show a triphasic spectrum as in the presence of high peripheral resistance (type, arteries of the extremities) with a steep increase in the systolic rate, a rapid fall in late systole, short diastolic backflow and late diastolic forward flow. Measurement of resistance will show high resistance (more than 0.80) and pulsatility (more than 2.50; Yuan et al. 1994; Fig. 4.66) indices.

Additional color-Doppler sonography may be helpful to distinguish between central tumors and atelectatic lung tissue (Yuan et al. 1994), as tumor tissue is characterized by poor visualization of flow signals (Fig. 4.74) compared with atelectatic lung tissue. Measurement of resistance in arterial vessels located within the tumor reveals flow signals with a high diastolic flow and correspondingly low resistance (less than 0.80) and pulsatility (less than 2.50; Yuan et al 1994) indices. In obstructive atelectasis on the floor of a central bronchial carcinoma, during the progression of the tumor (independent of its structure), one finds increasing occlusion of the pulmonary arteries and, consequently, poor visualization of vessels in the atelectatic lung tissue on color-Doppler sonography (Chap. 7))

In a few cases one finds central tumor spread into large vessels such as the aorta, the pulmonary artery and the pulmonary vein (Fig. 4.75a, b).

The significance of being able to visualize the central tumor lies in the fact that the tumor can be punctured through atelectatic lung tissue under sonographic guidance, with practically no risk of complications (Yang et al. 1990; Figs. 4.76, 4.77).

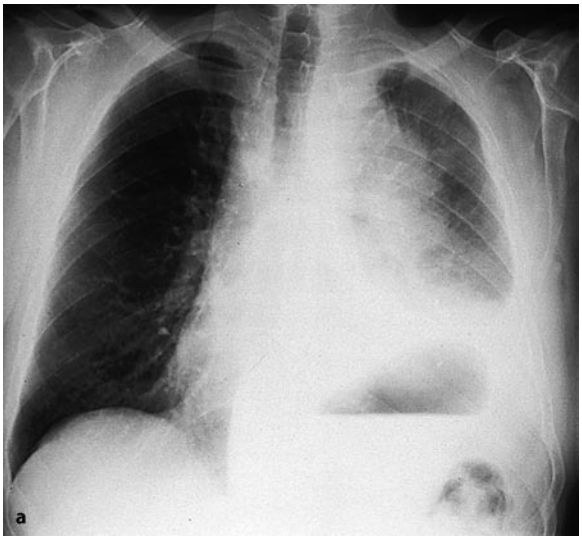

Fig. 4.74 A 70-year-old man with a bronchial carcinoma. **a** Chest X-ray: large tumor in the left upper field. **b**–**c** *see next page*

4.4.7 Lung Contusion

In cases of chest trauma, particularly serial rib fractures, pulmonary contusions are visualized better on sonography than on radiographs. Alveolar edema and alveolar hemorrhage caused by trauma are seen as moderately hypoechoic, blurred, pale lesions with indistinct margins (Figs. 2.17, 4.78). These are more pronounced in the presence of concomitant minimal pleural effusions, but are also imaged on sonography in the absence of pleural effusion. In the event of any clinically relevant chest trauma, radiographs as well as sonograms should be obtained (Chap. 2).

4.4.8 Summary

Depending on the extent of intrapleural fluid in case of compression atelectasis, one finds a pointed cap-like, wedge-shaped, homogenous, hypoechoic transformation with blurred margins towards the aerated adjacent lung tissue. The sonographic image of obstructive atelectasis is marked by largely homogenous hypoechoic lung tissue, similar to hepatization. An effusion is absent or is very

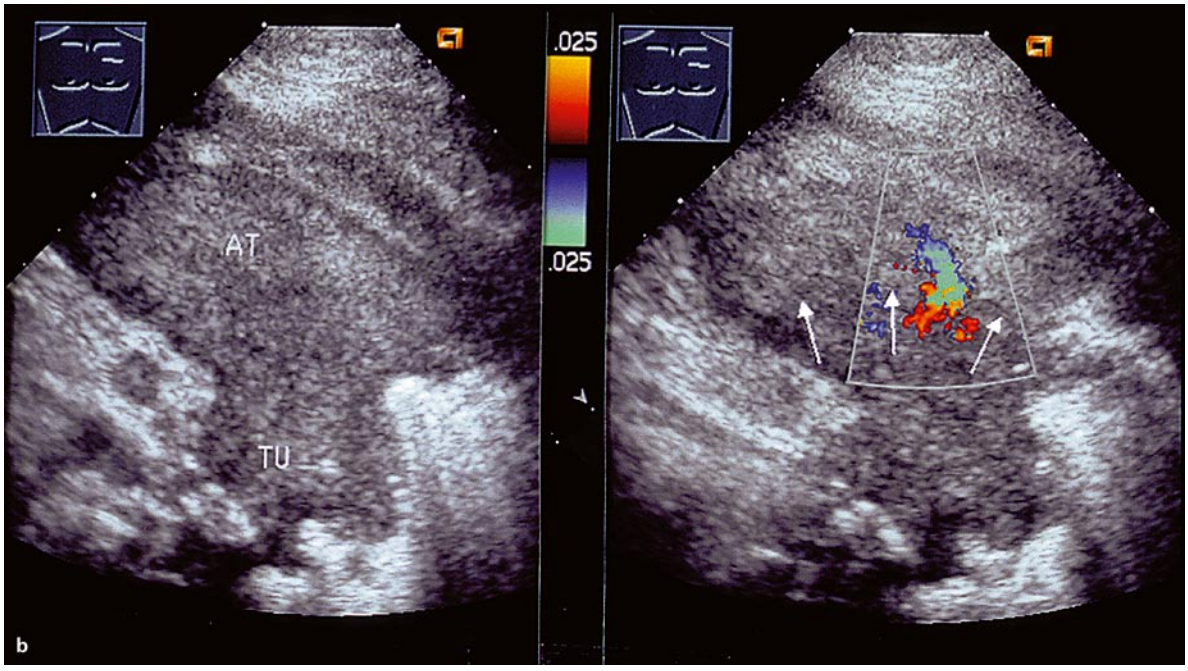

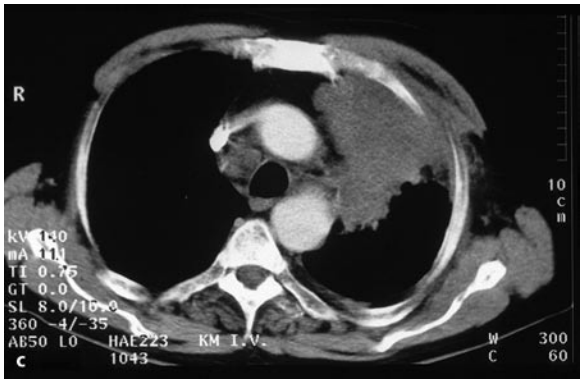

Fig. 4.74 *(continued)* **b** Sonography: hypoechoic tumor formation in the right upper lobe not clearly distinguishable from atelectatic lung tissue. On color-Doppler sonography one finds strong flow signals in the peripheral portions, possibly corresponding to atelectatic lung tissue. No flow signals are derived from the central part of the tumor. **c** Computed tomography: visualization of the tumor in the left hilum; suspicion of additional invasion of the chest wall

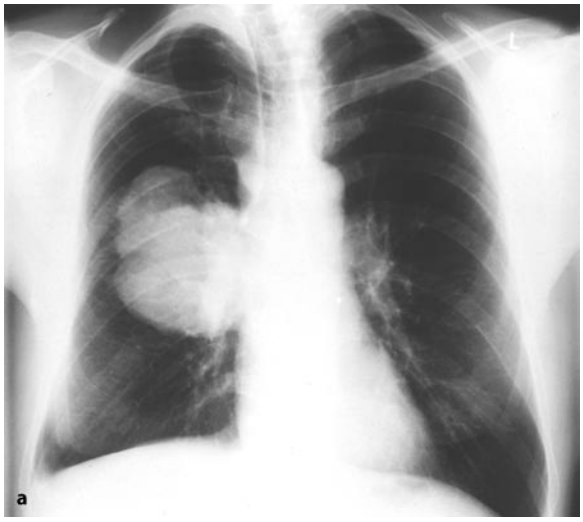

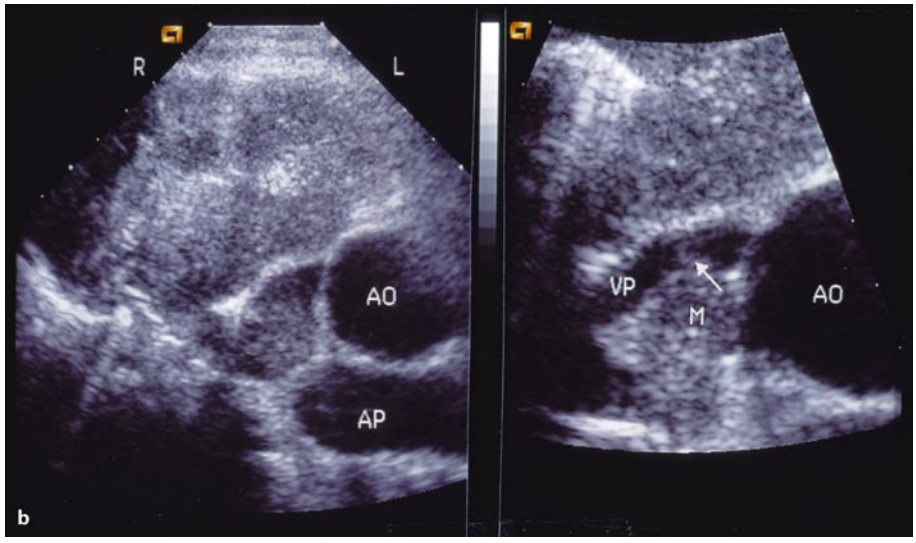

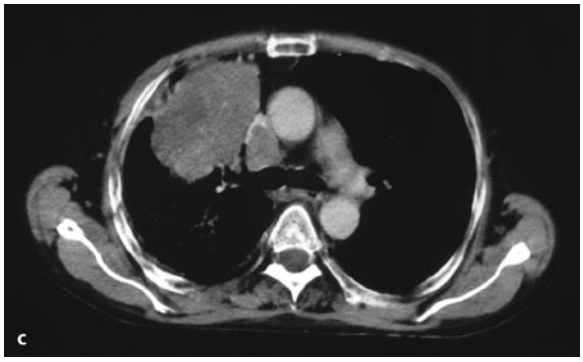

Fig. 4.75 A 49-year-old man with a bronchial carcinoma. **a** Chest X-ray: central space-occupying mass in the right hilum. **b** Sonography: right-ventral intercostal echo transmission shows a hypoechoic transformation. The atelectatic lung tissue cannot be demarcated from the central tumor in terms of its echomorphology. In the aortopulmonary window there are enlarged lymph nodes. Invasion of the aorta cannot be excluded. **c** Computed tomography: visualization of the tumor formation in contact with the aorta

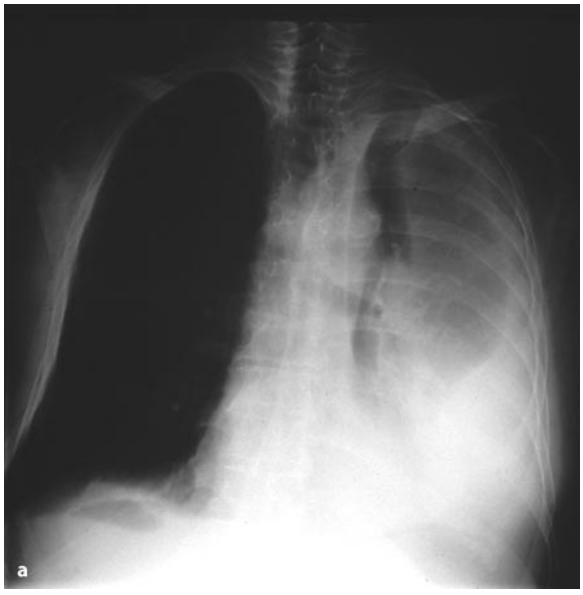

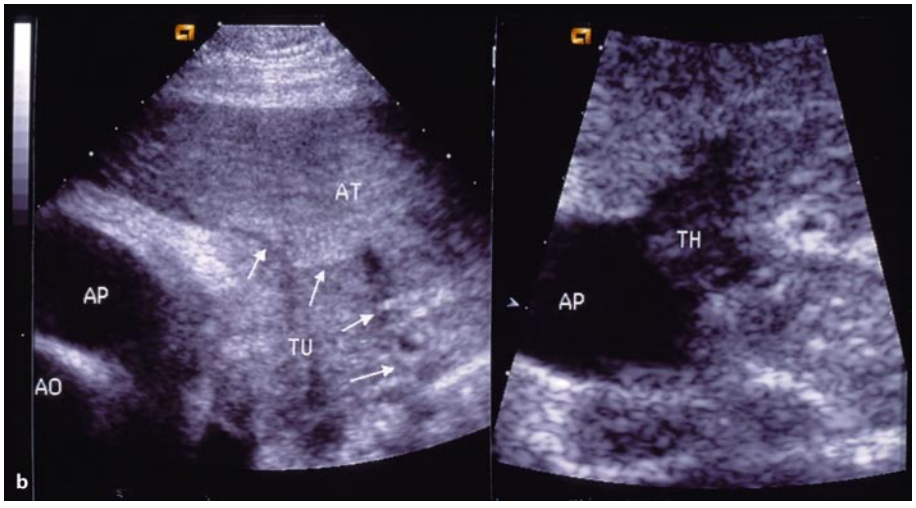

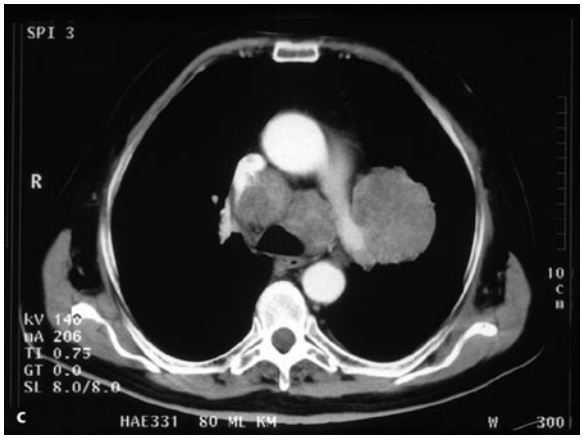

Fig. 4.76 A 77-year-old man with a bronchial carcinoma. **a** Chest X-ray: largely homogeneous shadowing of the left hemithorax. **b** Sonography: left-ventral intercostal echo transmission shows a central tumor (*TU*) and atelectasis (*AT*). The *arrows* point to the margin of the tumor where the atelectasis starts. Thrombotic material is seen in the pulmonary artery (suspected tumor thrombosis) **c**. Computed tomography: visualization of the tumor formation in contact with the pulmonary artery

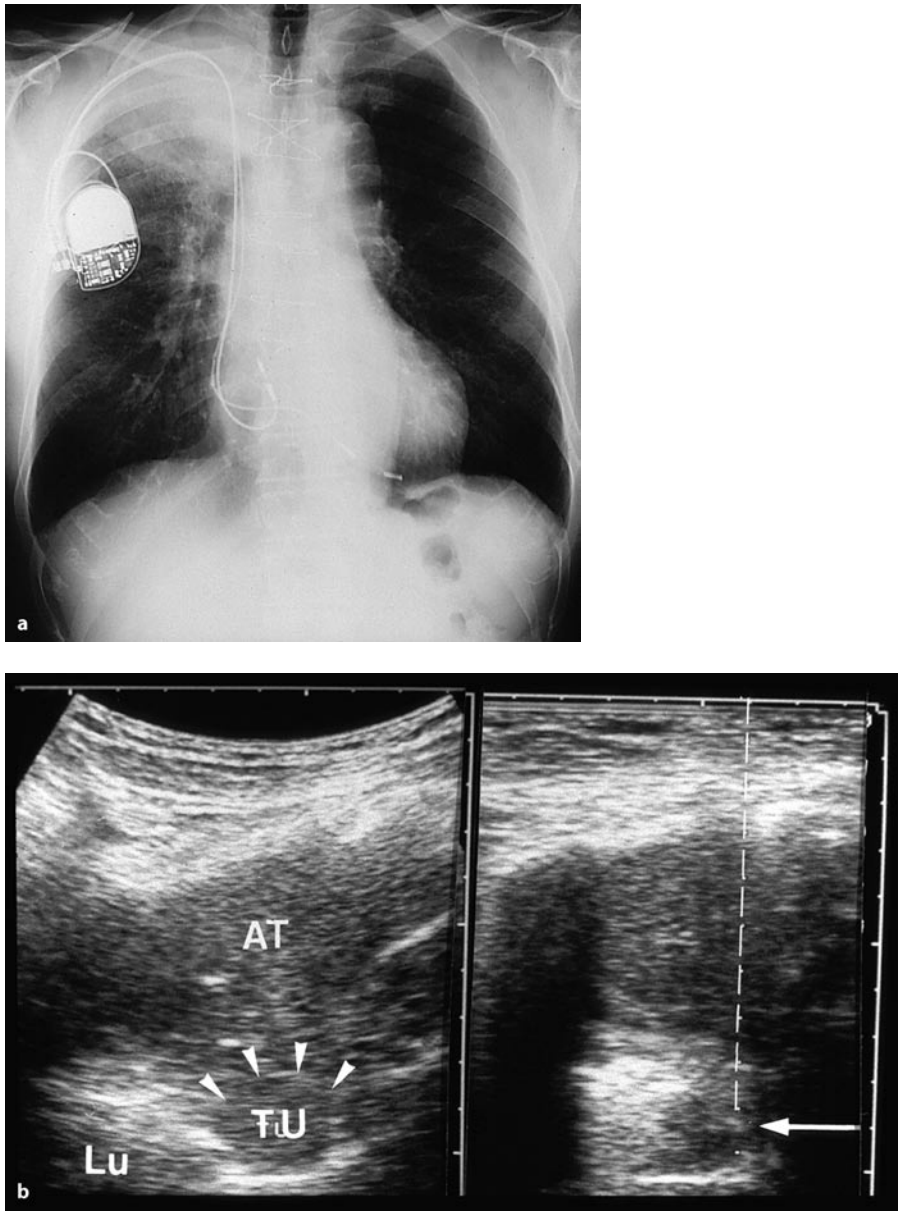

Fig. 4.77 A 67-year-old man with a bronchial carcinoma. **a** Chest X-ray: shadow in the region of the upper field on the right side. **b** Sonography: right-ventral echo transmission shows a small central tumor (*TU*) on the *left* with subsequent atelectasis (*AT*). The tumor could not be diagnosed by bronchoscopy. Under sonographic guidance the tumor was aspirated through the atelectatic lung tissue by means of a 16-gauge punch biopsy. The *arrow* on the *right* marks the needle tip reflex. An adenocarcinoma was diagnosed

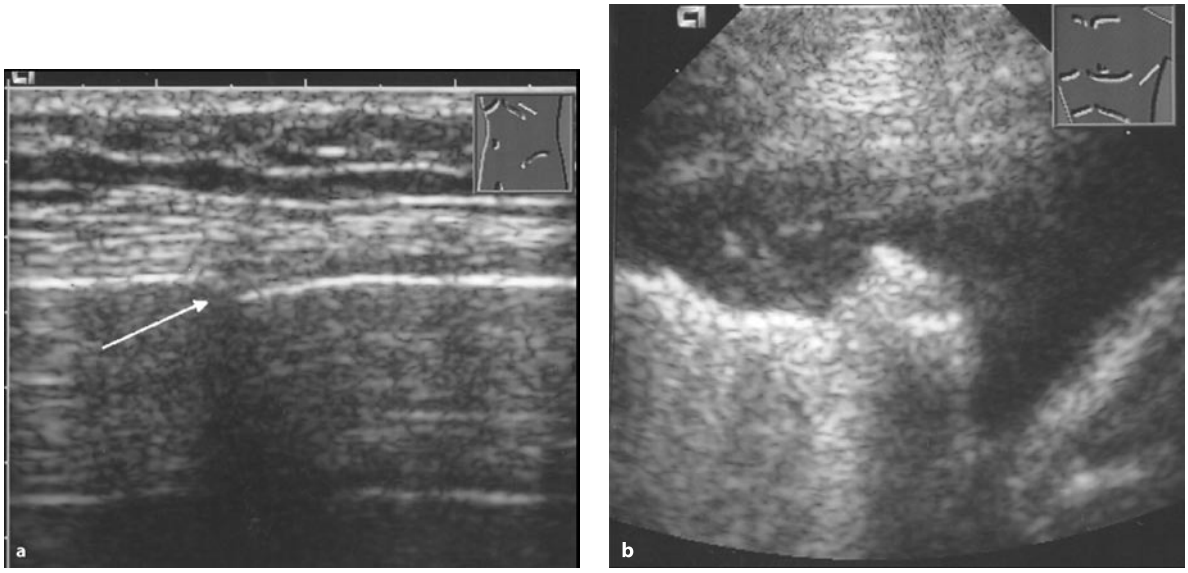

Fig. 4.78 Lung contusion and rib fracture. **a** On sonography one finds a step in the region of the rib—a sign of fracture. Additionally, free fluid is seen in the chest. Aspiration revealed a hemothorax. **b** The initial echo to the lung is irregular—a sign of contusion of the parenchyma

mild. In cases of lobar atelectasis the margin towards the ventilated lung tissue is rather blurred. Intraparenchymatous structures are seen as hypoechoic vascular lines, echogenic bronchial reflexes or focal lesions.

References

Burke M, Fraser R (1988) Obstructive pneumonitis: a pathologic and pathogenetic reappraisal. Radiology 166:699–704

Görg C, Weide R, Walters E, Schwerk WB (1996) Sonographische Befunde bei ausgedehnten Lungenatelektasen. Ultraschall Klin Prax 11:14–19

Görg C (2003) Focal lesions in the opacified lung: a sonographic pictorial essay. Ultraschall Med 24:123–128

Grundmann E (1986) Spezielle Pathologie, 7th edn. Urban & Schwarzenberg, Munich

Lan RS, Lo KS, Chuang ML, Yang CT, Tsao TC, Lee CM (1997) Elastance of the pleural space: a predictor for the outcome of pleurodesis in patients with malignant pleural effusion. Ann Intern Med 126:768–774

Liaw YS, Yang PC, Wu ZG et al (1994) The bacteriology of obstructive pneumonitis. Am J Respir Crit Care Med 149:1648–1653

Yang PC, Luh KT, Wu DH, Chang DB, Lee NL, Kuo SM, Yang SP (1990) Lung tumors associated with obstructive pneumonitis: US studies. Radiology 174:717–720

Yang PC, Luh KT, Chang DB, Yu CJ, Kuo SM, Wu HD (1992) Ultrasonographic evaluation of pulmonary consolidation. Am Rev Respir Dis 146:757–762

Yuan A, Chang DB, Yu CJ, Kuo SH, Luh KT, Yang PC (1994) Color Doppler sonography of benign and malignant pulmonary masses. AJR Am J Roentgenol 163: 545–549

4.5 Congenital Pulmonary Sequestration

G. Mathis

The very rare pulmonary sequestration underlines the value and importance of thorax sonography in neonatology and pediatrics. The neonate with this condition suffers from dyspnea and has a nonspecific systolic murmur. On chest radiograph, one may find a tumor-like shadow. On sonography, the echo texture of the pulmonary sequestration is similar to that of the liver, with wide arteries and veins (Gudinchet and Anderegg 1989). The supplying artery with the characteristic flow pattern can be identified on color-coded duplex sonography and the diagnosis is thus confirmed (Yuan et al. 1992). CT does not provide more information. If the lesion is imaged well on sonography, the infant can be spared the stress of angiography (Fig. 4.79).

References

Gudinchet F, Anderegg A (1989) Echography of pulmonary sequestration. Eur J Radiol 9:93–95

Yuan A, Yang PC, Chang DB, Yu CJ, Kuo SH, Luh KT (1992) Lung sequestration diagnosis with ultrasound and triplex doppler technique in an adult. Chest 102:1880–1882

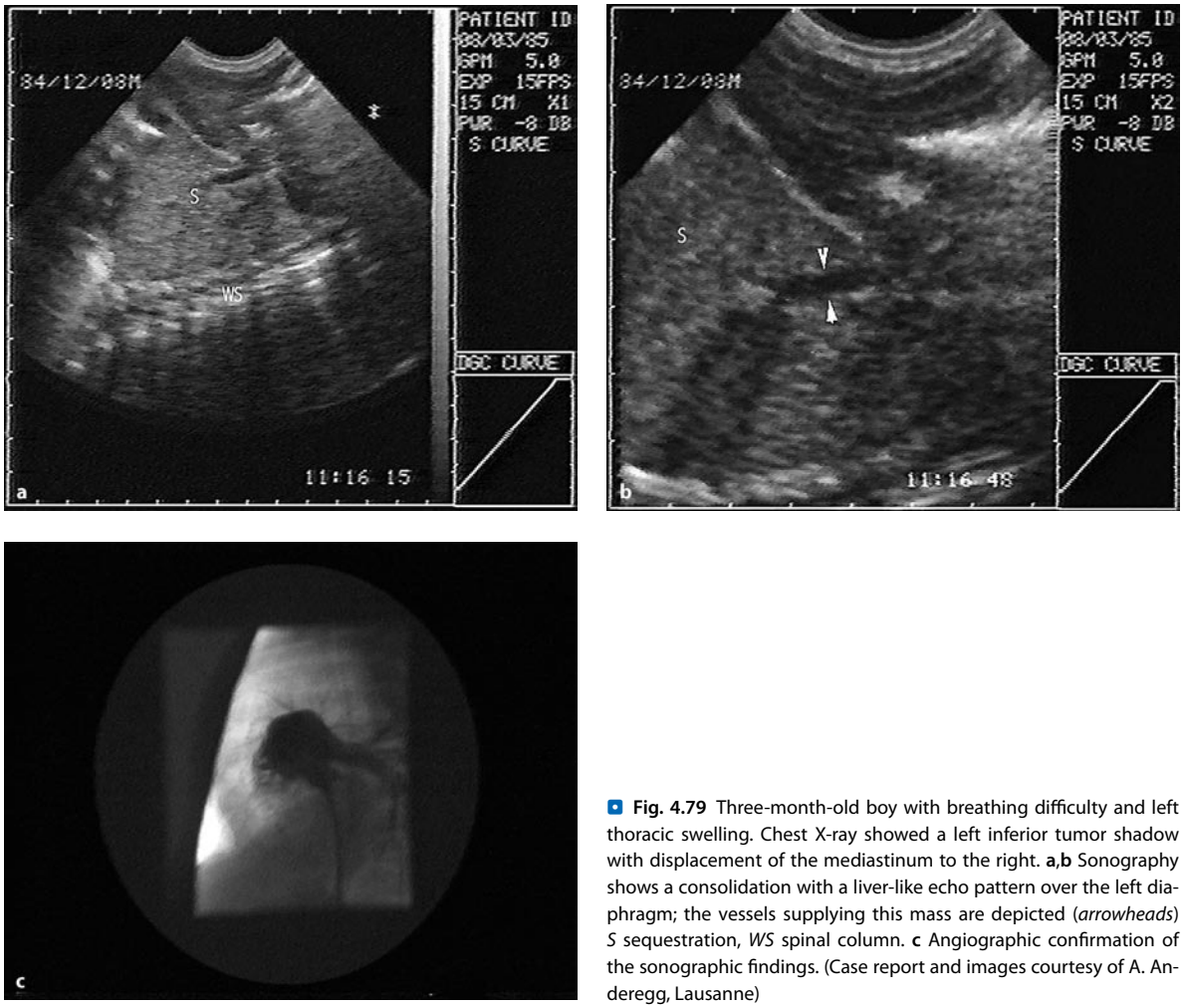

Fig. 4.79 Three-month-old boy with breathing difficulty and left thoracic swelling. Chest X-ray showed a left inferior tumor shadow with displacement of the mediastinum to the right. **a**,**b** Sonography shows a consolidation with a liver-like echo pattern over the left diaphragm; the vessels supplying this mass are depicted (*arrowheads*) *S* sequestration, *WS* spinal column. **c** Angiographic confirmation of the sonographic findings. (Case report and images courtesy of A. Anderegg, Lausanne)

5 Mediastinum

5.1 Transthoracic

W. Blank

Mediastinal structures can be visualized comprehensively by computed tomography as well as magnetic resonance tomography. Apart from echocardiography, transthoracic sonographic examination of the mediastinum has therefore not been widely applied until now.

However, its application in this location can be very worthwhile. As early as in 1971 Goldberg (1971) pointed out the suprasternal sonographic access to the mediastinum. In the 1970s the procedure was nearly forgotten outside of cardiology. In the mid-1980s sonography of the mediastinum was researched in pediatrics (von Lengerke and Schmidt 1988; Liu et al. 1988) as well as in adult medicine and its efficiency was proved (Braun 1983; Heckemann 1983; Blank et al. 1986; Wernecke et al. 1986; Brüggemann et al. 1991). In the following years the diagnostic potential of sonography was systematically researched (Heizel 1985; Wernicke et al. 1986; Wernicke 1991; Blank et al. 1996b). Further possibilities were disclosed by the application of color-Doppler sonography and, recently, through contrast-enhanced sonography (Betsch et al. 1992, 1994; Dietrich et al. 1997, 1999; Kunz et al. 2004).

5.1.1 Sonographic Investigation Technique and Reporting

Profound knowledge of anatomy is absolutely essential (Figs. 5.1, 5.2). The investigation procedure is based on Heinzmann's stratification of the mediastinum into eight compartments, which correspond to the various lymph node groups (Heinzmann 1988). Because of the small sonic window, only 3.5- and 5-MHz sector, convex and vector transducers with small apertures are suitable for sonographic diagnosis. In sonography the mediastinum is accessed from the suprasternal and the parasternal approach, occasionally also from the infrasternal approach (Blank et al. 1996a). The large vessels and their spatial relationship to the heart in the various planes serve as cardinal structures. The investigation from suprasternal is performed with the patient in the supine position. Viewing the upper mediastinum is facilitated by having the patient recline his/her head, ideally by cushioning the thoracic spine. Turning the head to the right and left is additionally helpful. In the right- and left-sided position described by Wernicke et al. in 1998 and by Brüggemann et al. in 1991 the mediastinum is shifted and the pulmonary cavity displaced, which permits better viewing of the mediastinum. It is easier to assess the mediastinum in expiration (Beckh et al. 2002; Koh et al. 2002; Braun and Blank 2005).

5.1.2 Sonoanatomy

In principle, from suprasternal the supraaortic and paratracheal region and the aorticopulmonary window can be imaged (Figs. 5.3–5.6a):

Suprasternal access (supine position): superior/anterior mediastinum

- Right side—tracheal region
- Truncus brachiocephalicus, a. carotis, a. subclavia
- Arcus aortae
- V. cava superior, vv. brachiocephalicus
- Truncus pulmonalis, aa. pulmonales
- Left atrium, vv. pulmonales
- Thymus
- Retrosternal space

For this purpose half-sagittal (from the right and left sides), coronary and transverse images are needed. Cervical portions of the esophagus (posterior mediastinum) can also be visualized (5–8 cm) (Blank et al. 1998; Zhu et al. 2005; Fig. 5.4d). From parasternal the combined use of right-sided and left-sided lateral decubitus position permits evaluation of the anterior and mid mediastinum (Figs. 5.7–5.9). For this purpose the transducer is placed adjacent to the sternum, cranially, and then moved caudad. Anatomical structures visualized through transverse and sagittal sections in angulated planes are summarized as follows (Figs. 5.4–5.6):

1. Parasternal access (lateral decubitus, right side): anterior/middle mediastinum
- V. cava superior
- Ascending aorta
- A. pulmonalis dextra
- Left atrium, vv. pulmonales
- Left ventricle, right ventricle

2. Parasternal access (lateral decubitus, left side): anterior/middle mediastinum
- Descending aorta
- Truncus pulmonalis
- Left atrium, vv. pulmonales
- Left ventricle, right ventricle, right atrium

The infrasternal access only provides a limited view of caudal portions of the posterior mediastinum. The esoph-

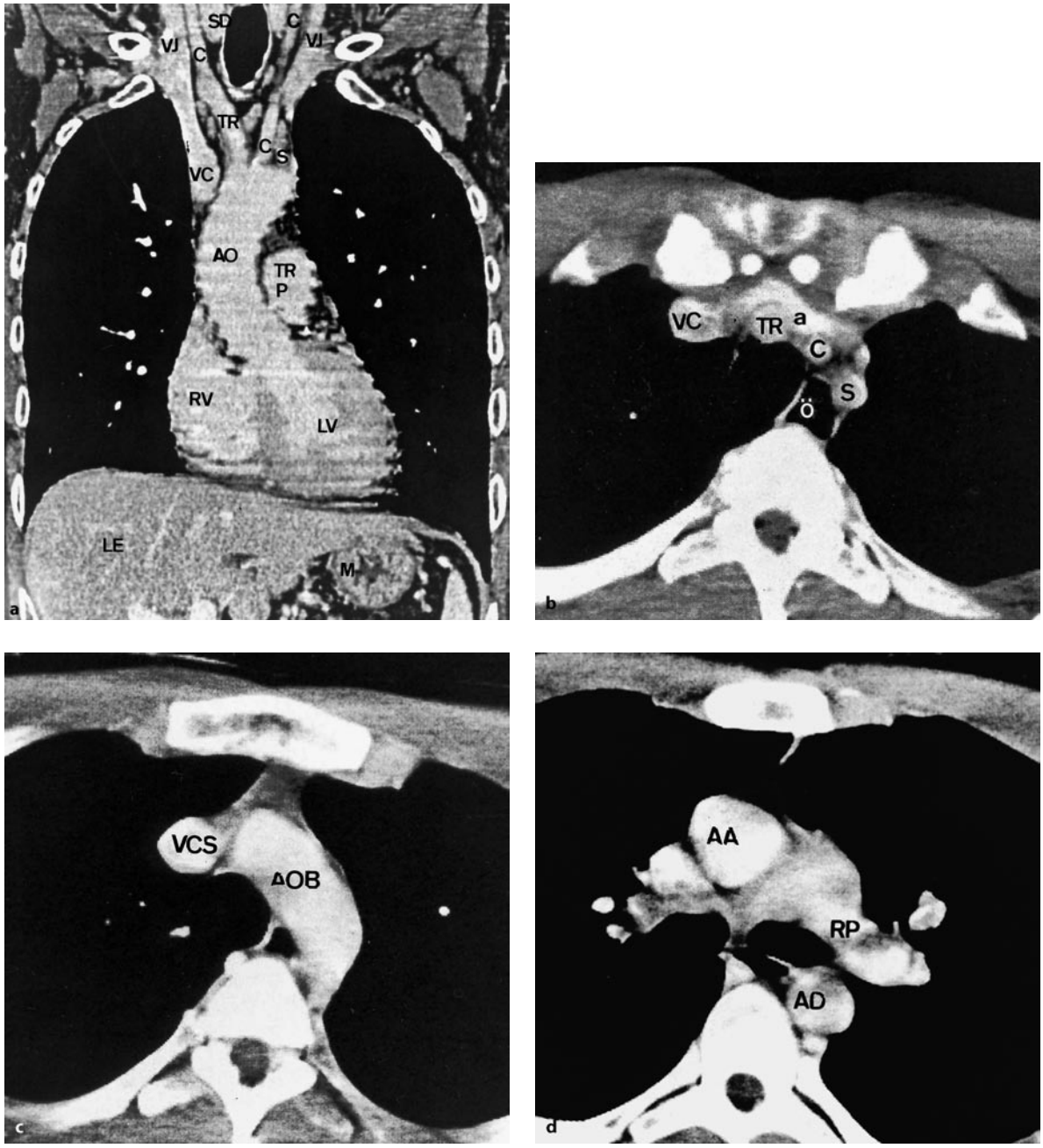

Fig. 5.1 Anatomy of the mediastinium on a computed tomogram. **a** Computed tomography reconstruction of the coronary section level. **b–d** Transverse sections of the mediastinum from caudal. a brachiocephalic veins, *AA* aorta ascendens, *AD* aorta descendens, *AO* aorta, *AOB* aortic arch, *C* carotid artery, *LP* left pulmonary artery, *LV* left ventricle, *Ö* esophagus, *RA* right atrium, *RP* right pulmonary artery, *RV* right ventricle, *S* subclavian artery, *SD,* thyroid, *TP* pulmonary trunk, *TR* brachiocephalic trunk, *VC*, *VCI* inferior vena cava; *VJ* jugular vein. **e–g** *see next page*

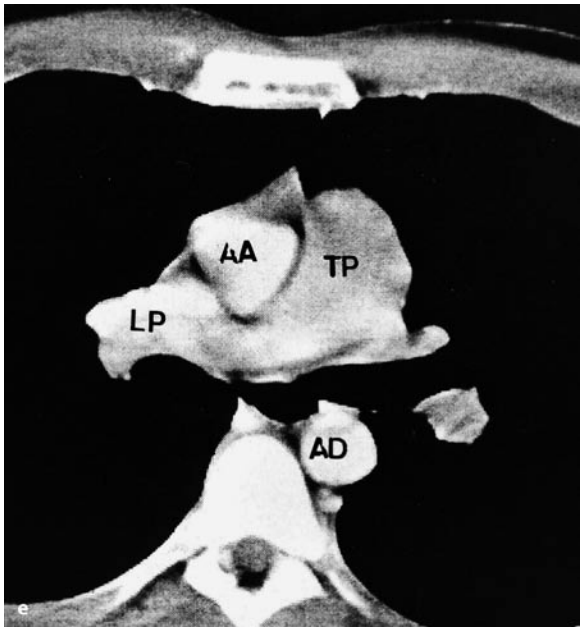

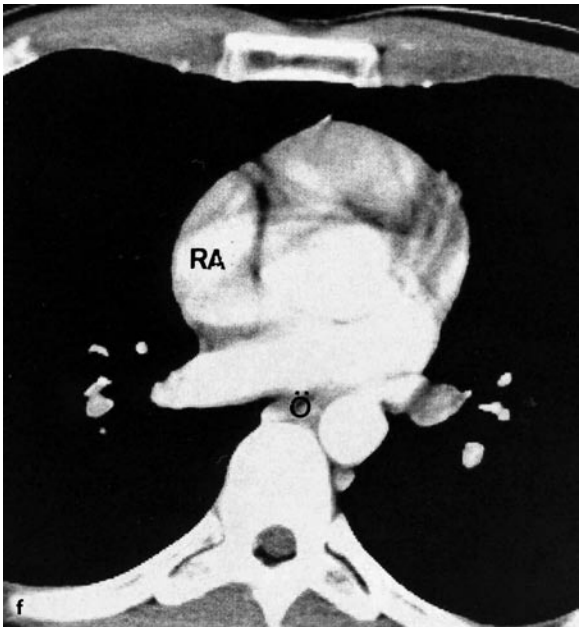

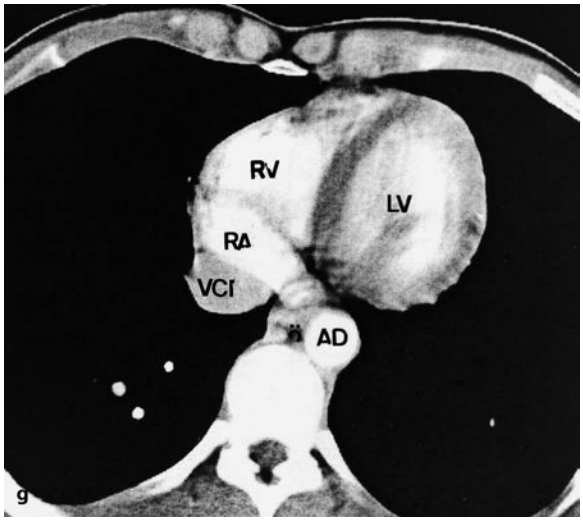

Fig. 5.1 *(continued)* **e–g** Transverse sections of the mediastinum from caudal. a brachiocephalic veins, *AA* aorta ascendens, *AD* aorta descendens, *AO* aorta, *AOB* aortic arch, *C* carotid artery, *LP* left pulmonary artery, *LV* left ventricle, *Ö* esophagus, *RA* right atrium, *RP* right pulmonary artery, *RV* right ventricle, *S* subclavian artery, *SD,* thyroid, *TP* pulmonary trunk, *TR* brachiocephalic trunk, *VC*, *VCI* inferior vena cava; *VJ* jugular vein

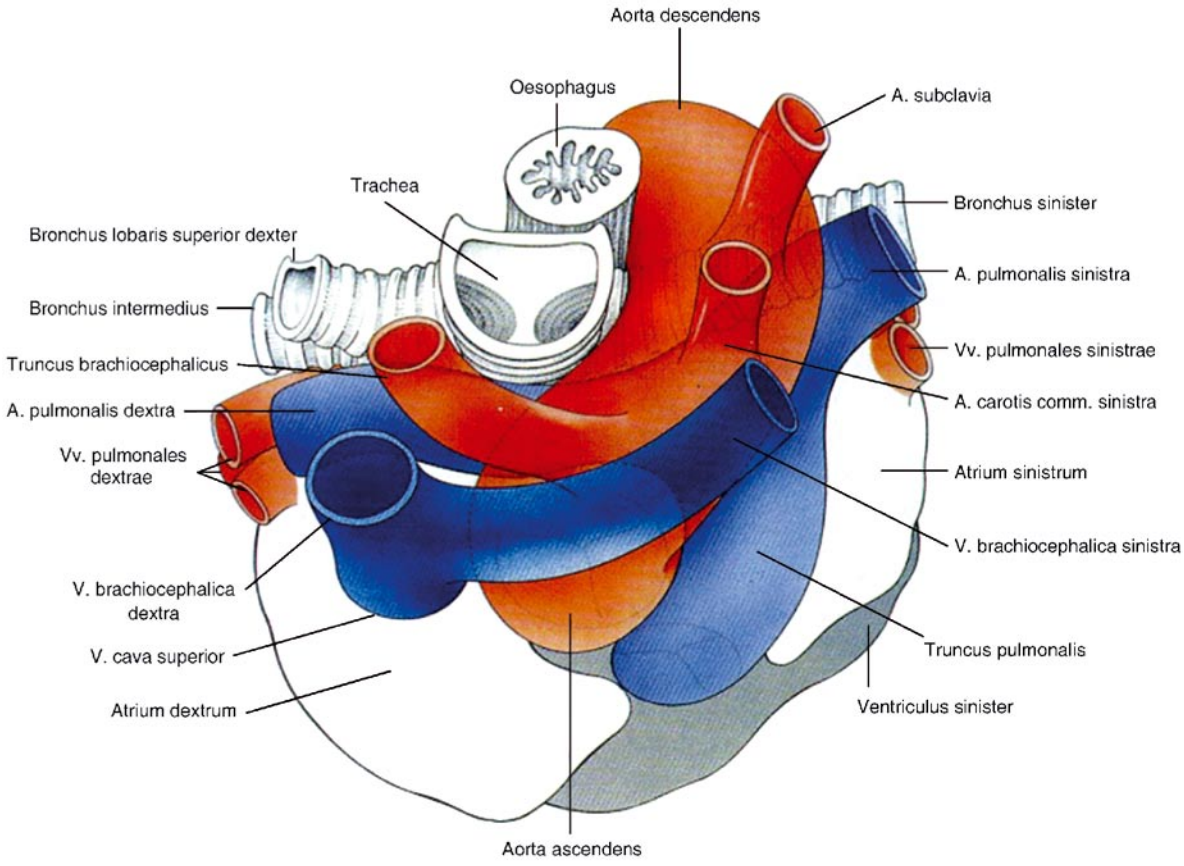

Fig. 5.2 Topographic anatomy of the mediastinal vessels—suprasternal view. (From Wernecke 1991)

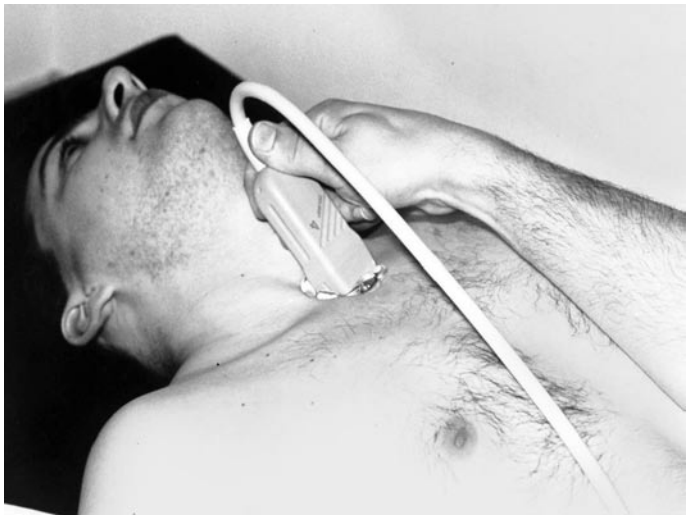

Fig. 5.3 Suprasternal examination. The ultrasound head is located in the jugular fossa, there is a cushion under the shoulders and the head is reclined at the maximum angle

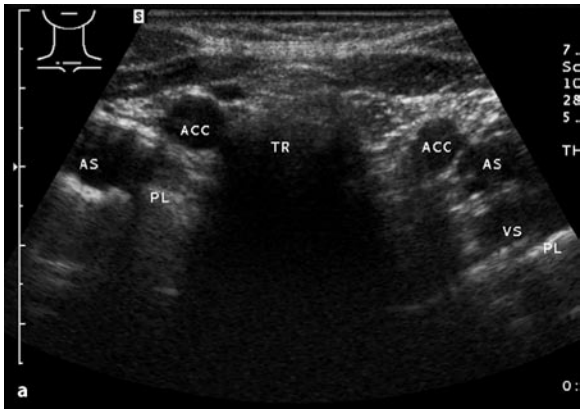

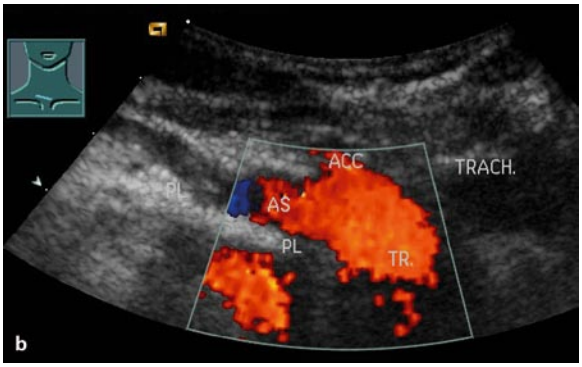

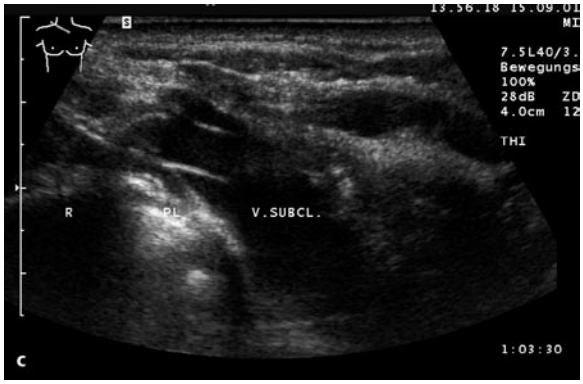

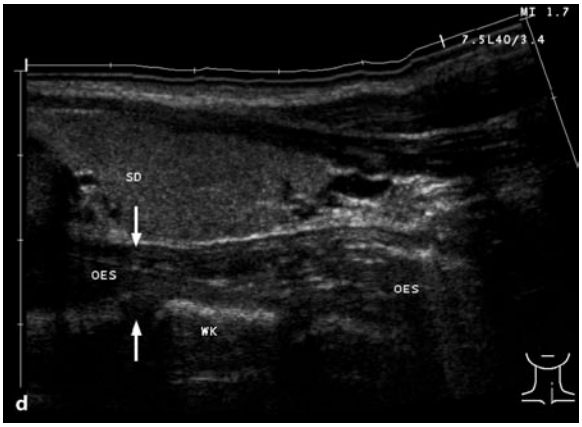

Fig. 5.4 Suprasternal examination. Supraaortal vessels. **a** The suprasternal transverse section demonstrates the cross section of the supraaortal vessels, right, distal to the branching of the brachiocephalic trunk. *ACC* common carotid artery, *AS* subclavian artery, *VS* subclavian vein, *TR* trachea, *PL* pleura/pulmonary reflex. **b** Half-sagittal right-hand section. The brachiocephalic trunk (*TR*) is shown by color-Doppler sonography, branching into the subclavian artery (*AS*) and the common carotid artery (*ACC*). The paratracheal region with its lymph nodes can be seen dorsal to the trunk in this section. Lateral to the reflex of the pleura/lung (*PL*) there is a mirror artifact of the artery. **c** A slight ventral tilting of the probe demonstrates the right subclavian vein. A venous valve can be distinguished. *PL* pleura/pulmonary reflex, *R* rib. **d** The cervical portions of the esophagus (*arrows*) show the left thyroid gland dorsomedial if the sonography probe is tilted slightly laterally. High-resolution sonography probes allow a five-layer separation to be made of the esophagus wall (*arrows*) When the patient swallows, the course of the peristalic wave and the passage of a high reflexogenic air–liquid portion can be observed. Average wall thickness is 2.5 mm. *OES* esophagus, *SD* thyroid, *WK* cervical vertebra

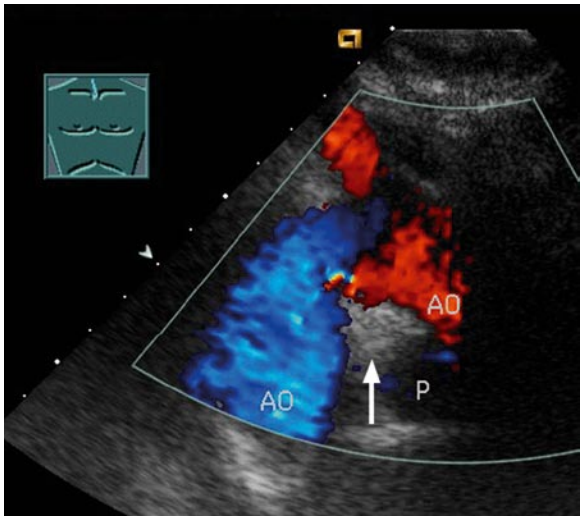

Fig. 5.5 Suprasternal examination. Suprasternal, sagittal section. The aorticopulmonary window (*arrow*) between the aortic arch and the pulmonary artery (*P*) shown in the cross section. If conditions for examination are difficult, the vessels can often be better differentiated from the surrounding soft-tissue structures by color-Doppler sonography and may be identified with more certainty (pulsed-Doppler sonography with characteristic frequency spectrum).

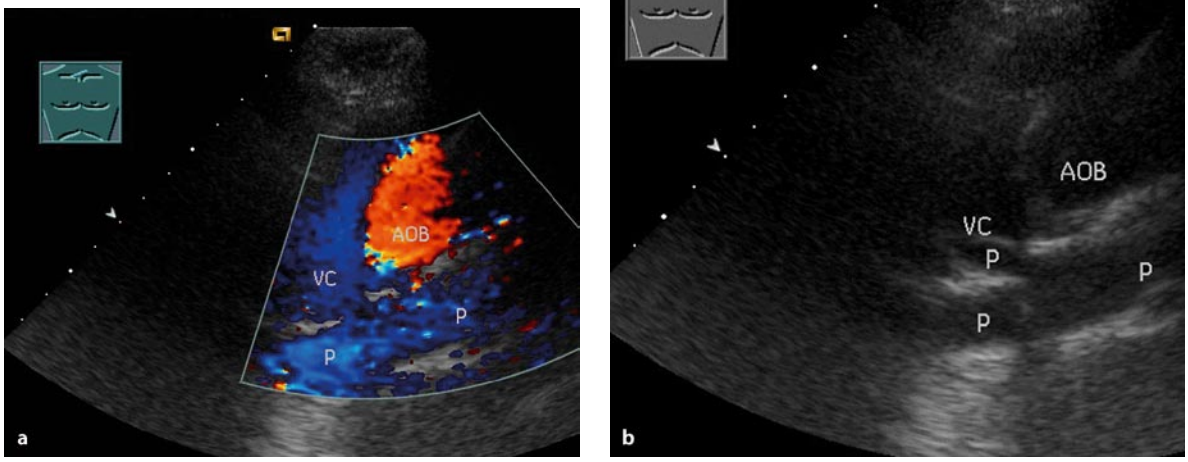

Fig. 5.6 Suprasternal examination. Suprasternal coronary section. **a** Lateral to the aortic arch (*AOB*), which is shown in an oblique section, the vena cava (*VC*) can be distinguished with certainty by color-Doppler sonography because of its reverse direction of flow (*coded blue*). **b** The branching of the pulmonary artery (*P*) and the aorticopulmonary window can be demonstrated better on B-mode after switching off the color Doppler

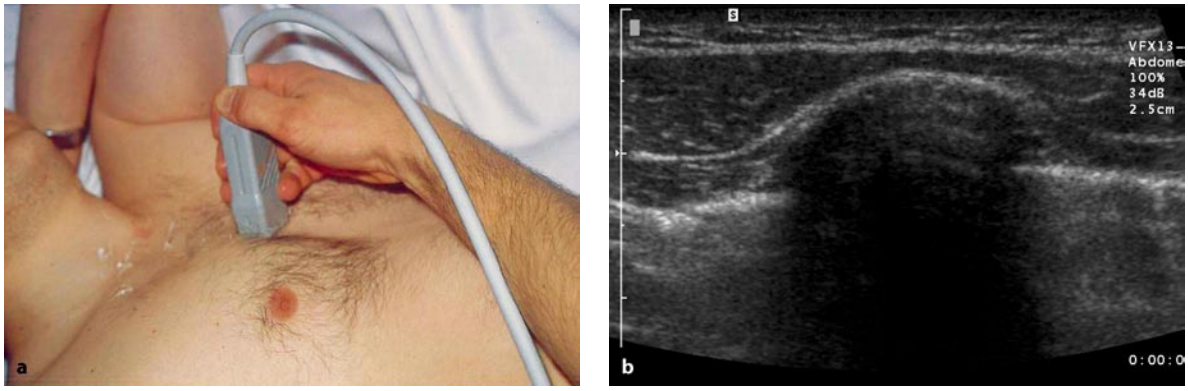

Fig. 5.7 **a** Parasternal section in the supine position. **b** Normal findings. The view into the mediastinum is blocked by the sternum (*S*) and the inflated lung

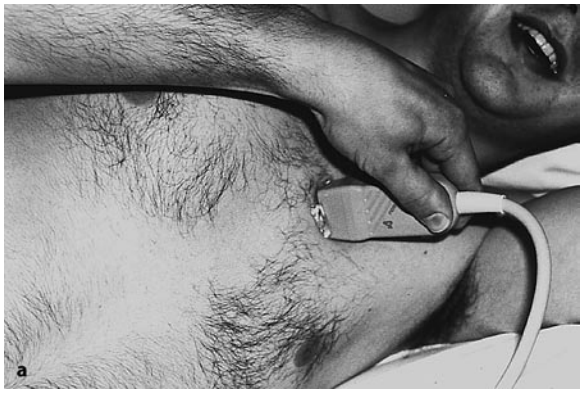

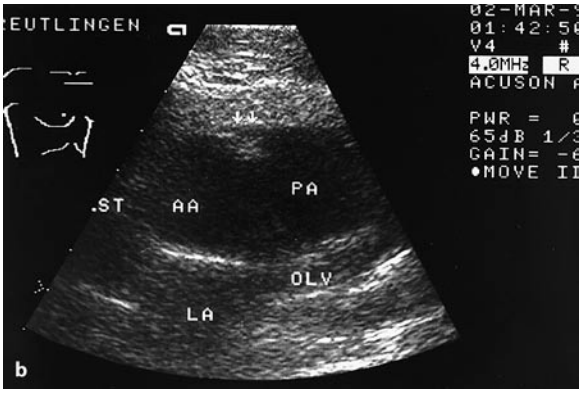

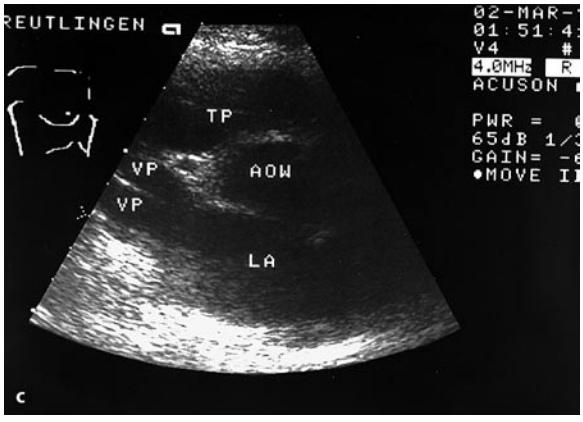

Fig. 5.8 a Parasternal examination in the left lateral position. **b** Left parasternal, transversal section. The pulmonary artery (*PA*) winds around the cross-sectional ascending aorta (*AA*). In-between is the upper pericardial recess (*double arrow*), sternum (*ST*), left atrium (*LA*, and upper lung veins (*OLV*). **c** Left parasternal, sagittal section. At the level of the aortic root (*AOW*) ventral crossing through the truncus pulmonalis (*TP*), dorsal left atrium (*LA*) joining pulmonary veins (*VP*)

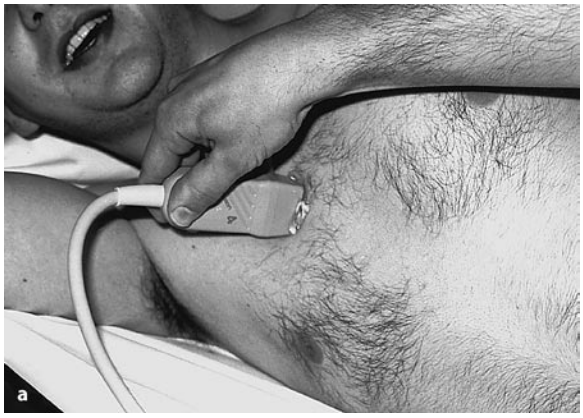

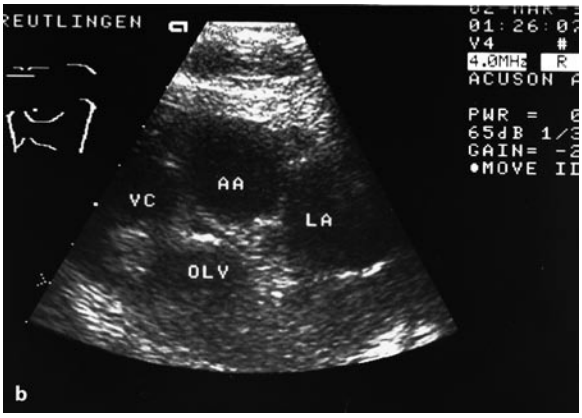

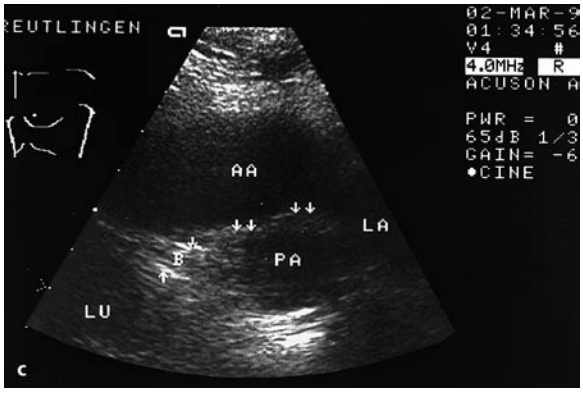

Fig. 5.9 a Parasternal examination in right lateral position. **b** Right parasternal transversal section. *AA* ascending artery, *VC* superior vena cava, *LA* left atrium *OLV,* upper lung vein. **c** Right parasternal sagittal section. A successful depiction of the ascending aorta (*AA*), the pulmonary artery (*PA*) in cross section with the aorticopulmonary window (*double arrow*) in-between, and of the subcarinal region. A bronchus (*B*) can be depicted as an echogenic reflection (*single arrow*). *LU* lung, *LA* left atrium

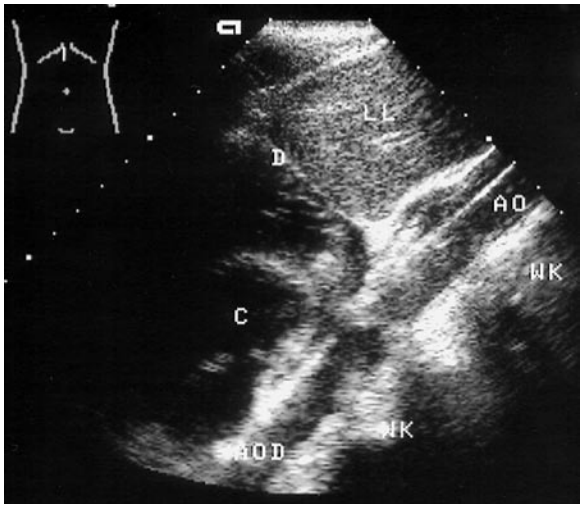

Fig. 5.10 Infrasternal sonography. Sagittal section. The esophagus can be observed at the passage through the diaphragm (*D*) ventrolaterally to the aorta (*AO*). The descending aorta (*AOD*) is partly covered by artifacts . *WK* vertebral body, *C* cor

agus, aorta and vena cava are seen at the point where they pass through the diaphragm. Transverse and sagittal images in angulated planes are obtained through the left lobe of the liver (Blank et al. 1996a; Janssen et al. 1997; Fig. 5.10).

5.1.3 Imaging Compartments of the Mediastinum

The upper and mid mediastinum can be imaged well on sonography. The suprasternal access permits adequate evaluation in 90–95% of cases. The posterior mediastinum, paravertebral region, the hilum of the lung and the immediate retrosternal space, however, can only be partly assessed from a transthoracic approach. Transthoracic sonography may be severely hampered by obesity, pulmonary emphysema, mediastinal distortion as well as spinal deformities.

Factors that limit visualization of mediastinal structures:

- Adiposity, large breasts
- Pulmonary emphysema
- Distortion of the mediastinum (surgery, inflammation, radiotherapy)
- Deformity of the vertebral column

5.1.4 Imaging Tumors in the Mediastinum

Approximately 75% of clinically relevant space-occupying masses in the adult mediastinum are located in the anterior and mid mediastinum and are therefore readily accessible for sonographic assessment (Rosenberg 1993). The topographic position of a mediastinal space-occupying mass, its size and mobility can be determined by sonography. High-resolution sonography permits good differentiation of tissue on the basis of echogenicity (cystic, solid to calcified). Surrounding vessels can usually also be imaged well in the B mode. More detailed information (differentiation of vessels, indicators of vessel infiltration, tumor vascularization) may be gathered by color-Doppler sonography (Betsch 1994; Blank and Braun 1995). Tumor vascularity can be demonstrated with much more sensitivity and without motion artifacts through contrast-enhanced sonography, if good-quality equipment is provided (Betsch 1994; Blank and Braun 1995). Various space-occupying masses in the mediastinum have a characteristic sonomorphology (Table 5.1). A definite diagnosis, however, is usually made after removal of tissue and its histological investigation (Chap. 9).

5.1.5 Diagnostic Value of Sonography, Chest Radiographs and Computed Tomography

Sonography is superior to survey radiographs of the chest in the assessment of nearly all portions of the mediastinum (with the exception of the paravertebral region). In the evaluation of supraaortic, pericardial, prevascular and paratracheal regions, sonography has a sensitivity 90–100% and is nearly as reliable as computed tomography. However, in the aorticopulmonary window and the subcavinal region, sonography achieves a sensitivity of only 82–70% (Wernicke et al. 1998; Wernicke 1991; Brüggemann et al. 1991; Betsch 1994; Dietrich et al. 1995). Thus, sonography occupies an intermediary position between chest radiographs and computed tomography (Castellino et al. 1986; Bollen et al. 1994; Table 5.2).

5.1.6 General Indications

Sonographic investigation of the mediastinum is performed after chest radiographs have been obtained, when the findings of the latter are not distinct or if a mediastinal space-occupying mass is suspected. Sonography is the first investigation procedure in cases of acute chest symptoms (Fig. 5.11). The general indications for transthoracic sonography of the mediastinum are:

Table 5.1 Sonomorphology of space-occupying masses in the mediastinum. (Modified according to Wernecke 1991)

Appearance	Type of space occupation
Anechoic	Cystic formations, vessels
Hypoechoic	Lyphomas, "active" lymph nodes, more rarely "silent" lymph nodes
Hypoechoic–inhomogeneous echoes:	Carcinoma, filiae, inflammation, aneurysm
Echodense	Physiological structures, thymus, scar (exception, rare liposarcoma and teratocarcinoma)

Table 5.2 Imaging of mediastinal compartments. Sonography and plain chest radiograph versus computed tomography. (Modified according to Wernecke 1991)

Region	Sonography (%)	Plain chest radiograph (%)
Supraaortal	98	67
Paratracheal	89	69
Aorticopulmonary window	81	62
Prevascular	92	46
Subcarinal	69	31
Pericardial	100	67
Posteriores mediastinum	6	6
Paravertebral	11	44

- Acute thoracic symptoms
- Chest radiograph: space-occupying mass in the mediastinum
- Chest radiograph: undefined space-occupying mass
- Tumor staging (vascular complications)
- Monitoring the course of disease/therapy (tumor therapy)
- Puncture and drainage

5.1.7 Specific Sonographic Findings in Selected Space-Occupying Masses in the Mediastinum

5.1.7.1 Lymph Node Disease

Lymphomas account for approximately one quarter of all primary mediastinal tumors, whereas lymph node metastases of bronchial carcinomas, for instance, are more common.

On the basis of their hypoechoic transformation, inflamed and enlarged lymph nodes (e.g., Boeck's disease) or lymph nodes invaded by tumor (Hodgkin's or non-Hodgkin's lymphoma, lymph node metastases) can be well differentiated from the surrounding hyperechoic tissue (Figs. 5.12–5.14).

Differentiation of the above mentioned diseases of lymph nodes by sonography alone is not possible without biopsy.

Under treatment lymph nodes again become increasingly echogenic (Wernicke 1990). Color-Doppler sonography and, as an even more sensitive method that has been recently employed, contrast-enhanced sonography will reveal reduced blood circulation (Betsch 1994; Braun and Blank 2005). With the use of high-resolution devices, normal mediastinal lymph nodes (hypoechoic) are also visualized very often (paratracheal, aorticopulmonary window). A reliable differentiation of pathological processes (Chap. 9), however, is not possible without obtaining bioptic material (Dietrich et al. 1995, 1999).

5.1.7.2 Tumors of the Thymus

The thymus is located in the anterior mediastinum, behind the sternum. In adults it cannot be distinguished from its hyperechoic surroundings. Approximately one quarter to one third of all primary mediastinal tumors originate from the thymus. There are various malignant tumors; thymomas and lymphomas are the most common ones (more rarely, germ cell carcinoma, carcinoids and carcinomas). These entities have characteristic sonographic features (Fig. 5.15, Table 5.3). The diagnosis is verified by performing a sonography-guided or com-

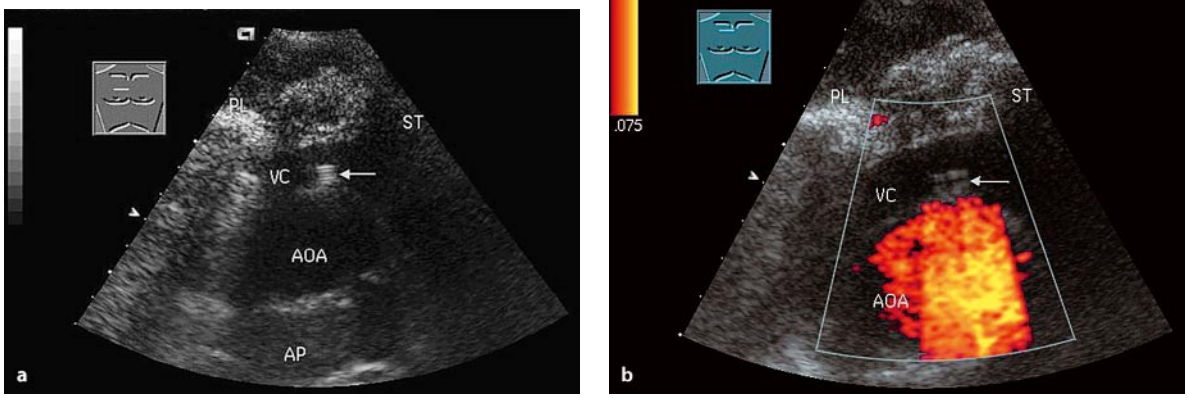

Fig. 5.11 Known non-Hodgkin`s lymphoma. **a** Acute upper inflow congestion. Condition after port implantation. B-image sonography of still parasternal tumor masses. The port catheter can be differentiated as an echogenic double structure (*arrow*) in the hypoechoic vena cava. *AOA* ascending aorta, *AP* right pulmonary artery, *ST* sternum, *PL* pleura. **b** Thrombosis of the vena cava superior (*VC*) can be substantiated

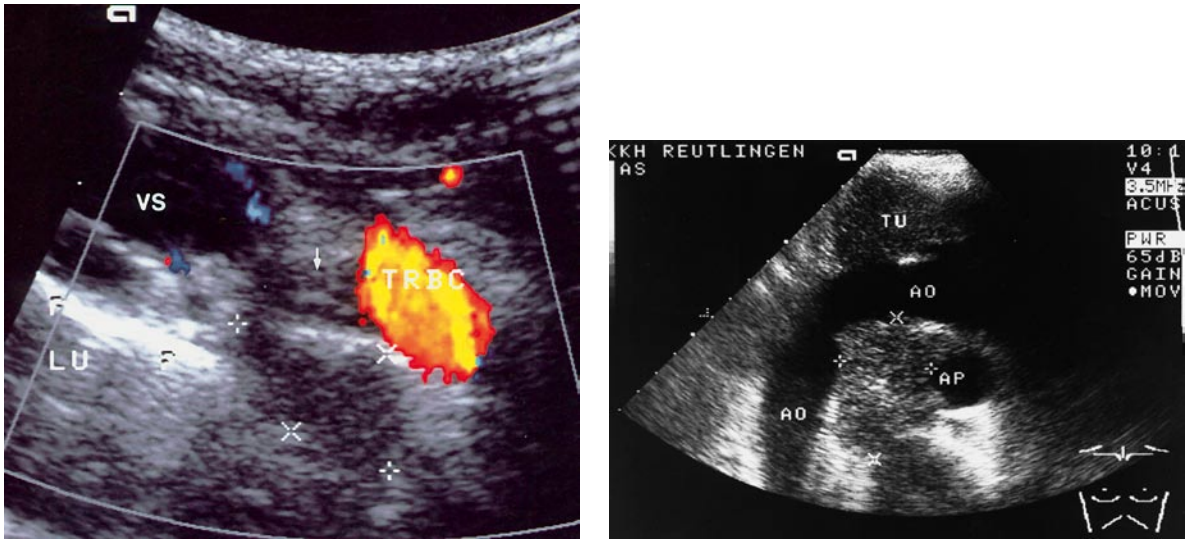

Fig. 5.12 Lymph node tuberculosis**.** Suprasternal semisagittal section, right. Dorsally to the color-Doppler sonography image of the brachiocephalic trunk (*TRBC*), one can see a hypoechoic, indistinctly delineated lymph node (*crosses*) in the paratracheal region, which normally has a homogeneous, hyperechoic structure. The diagnosis of lymph node tuberculosis was made possible by color-Doppler sonography of the fine-needle puncture. *LU* lung.

Fig. 5.13 Lymph node metastasis. Suprasternal sonography in a sagittal section. The aorta (*AO*) is surrounded by tumor masses (*TU*). A lymph node infiltration in the direction of the aortic arch and the pulmonary artery (*AP*) can be depicted in the aorticopulmonary window. Fine-needle puncture biopsy (0.9 mm). Histology indicated metastasis of a prostate carcinoma

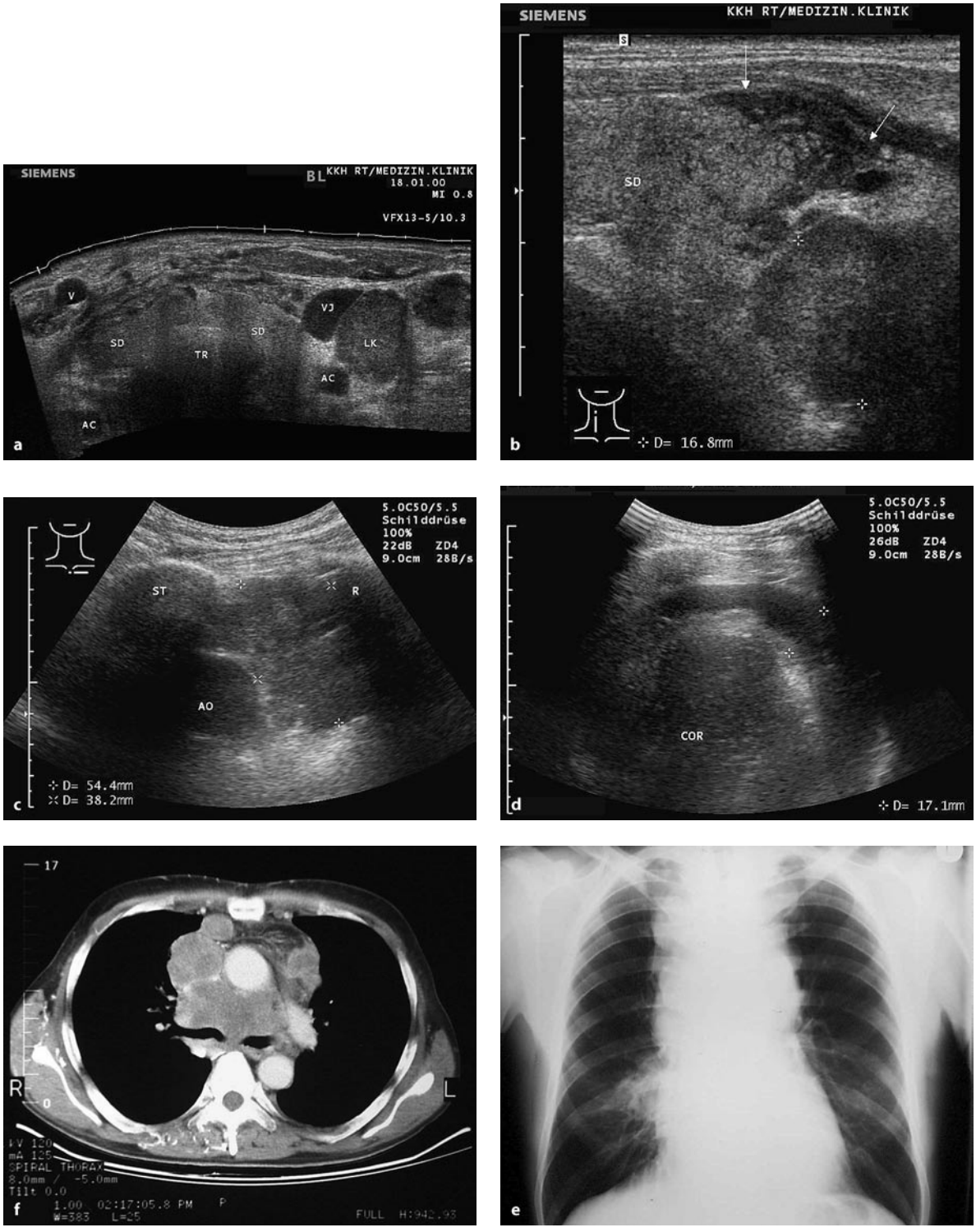

Fig. 5.14 Primary sonographic examination of an upper inflow congestion. **a** Multiple lymph nodes (*LK*) suspected of malignity in the neck region. The panorama presentation (SieScape, from Siemens) enables an impressive documentation of a relatively large region of the body. **b** Low-echo tumor infiltration into the thyroid gland. Tumor masses (*crosses)* reaching into the retrosternal region. **c** Left parasternal section, in the vicinity of the infiltrating low-echo mass (*crosses*). The wall of the aorta (*AO)* can no longer be sharply delineated. *ST* sternum, *R* rib. **d** Pericardial deposits and pericardial effusion (*crosses*). Suspected diagnosis of bronchial carcinoma (man, smoker) with substantiation of a mass suspected of being a metastasis in the region of the right adrenal gland (*crosses*). The diagnosis was confirmed by a sonographically controlled parasternal punch biopsy (Sonocan neddle, 1.2-mm diameter). Histology indicated small-cell bronchial carcinoma. **e** Chest X-ray overview. Mediastinal dissemination. **f** Computed tomogram. Tumor on the right lower lobar bronchus with extensive mediastinal metastases

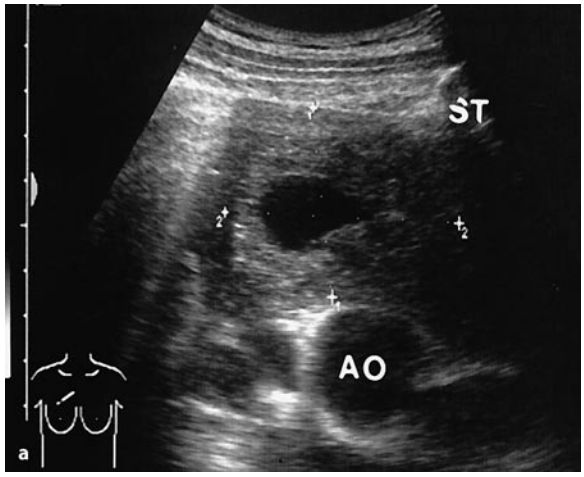

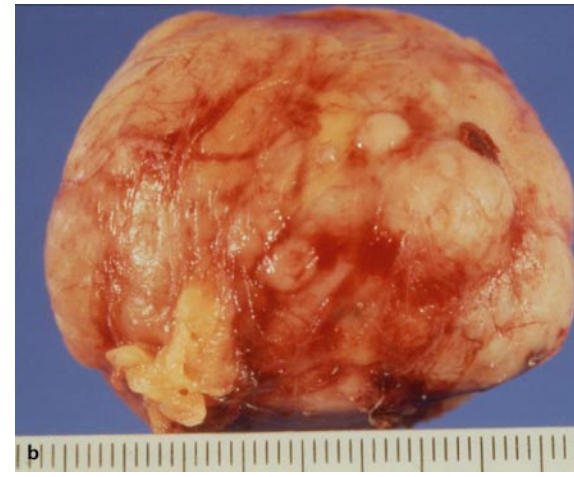

Fig. 5.15 Thymom. Parasternal, transversal section. Even with the patient in the supin position, it was possible to see a low-echo mass in a ventral position to the aorta and well delineated. Central liquid area. Sonographically controlled incision biopsy (diameter 1.2 mm). *AO* aorta, *ST* sternum. **b** Slide of pathology specimen. The tumor is clearly delineated

Table 5.3 Sonomorphology of thymomas

Benign	Malignant
Hypoechoic	Hypoechoic, inhomogeneous
Sharp margins	Blurred margins
Rounded, partly lobed	Tumor cones
No infiltration	Infiltration (pericardium, vessels)

puted tomography guided biopsy (Schuler et al. 1995; Chap. 9).

5.1.7.3 Germinal Cell Tumors

Teratomas and seminomas are mostly situated in the ventral and middle part of the mediastinum, accounting for approximately 10% of primary mediastinal tumors. Teratomas usually occur in the second and third decades, grow slowly and only produce symptoms if they have grown to a large size (encroaching upon surrounding structures). These tumors are clearly delineated, contain cystic as well as epithelial structures (skin and appendages) and also tissue of mesenchymal origin (cartilage, bone, smooth muscle). Twenty-five to 30% of tumors show malignant transformation (Fig. 5.16).

5.1.7.4 Neurogenic Tumors

Neurogenic tumors originate from the sympathetic trunk, intercostal nerves or the vagus nerve and therefore commonly grow in the posterior mediastinum. They can therefore only be demonstrated by transthoracic sonography if they have displaced pulmonary structures paravertebrally or extend cranially (retrosternal approach) or caudally (infrasternal approach). Transesophageal imaging and puncture, if necessary, are usually easy to perform.

5.1.7.5 Retrosternal Portions of the Thyroid and Parathyroid

These can be reliably assigned to the thyroid or the parathyroid on the basis of their topography and typical sonographic pattern. In problematic cases color-Doppler sonography may be used to prove the source organ of the lesion.

Parathyroid adenomas extending retrosternally usually appear as markedly hypoechoic well-vascularized space-occupying masses (typical laboratory constellation is increased parathyroid hormone and calcium). Puncture may be helpful to differentiate lymph node enlargement (Braun 1992).

5.1.7.6 Mediastinal Cysts

Pericardial and bronchial cysts usually can be clearly identified. If they contain highly viscous fluid, however,

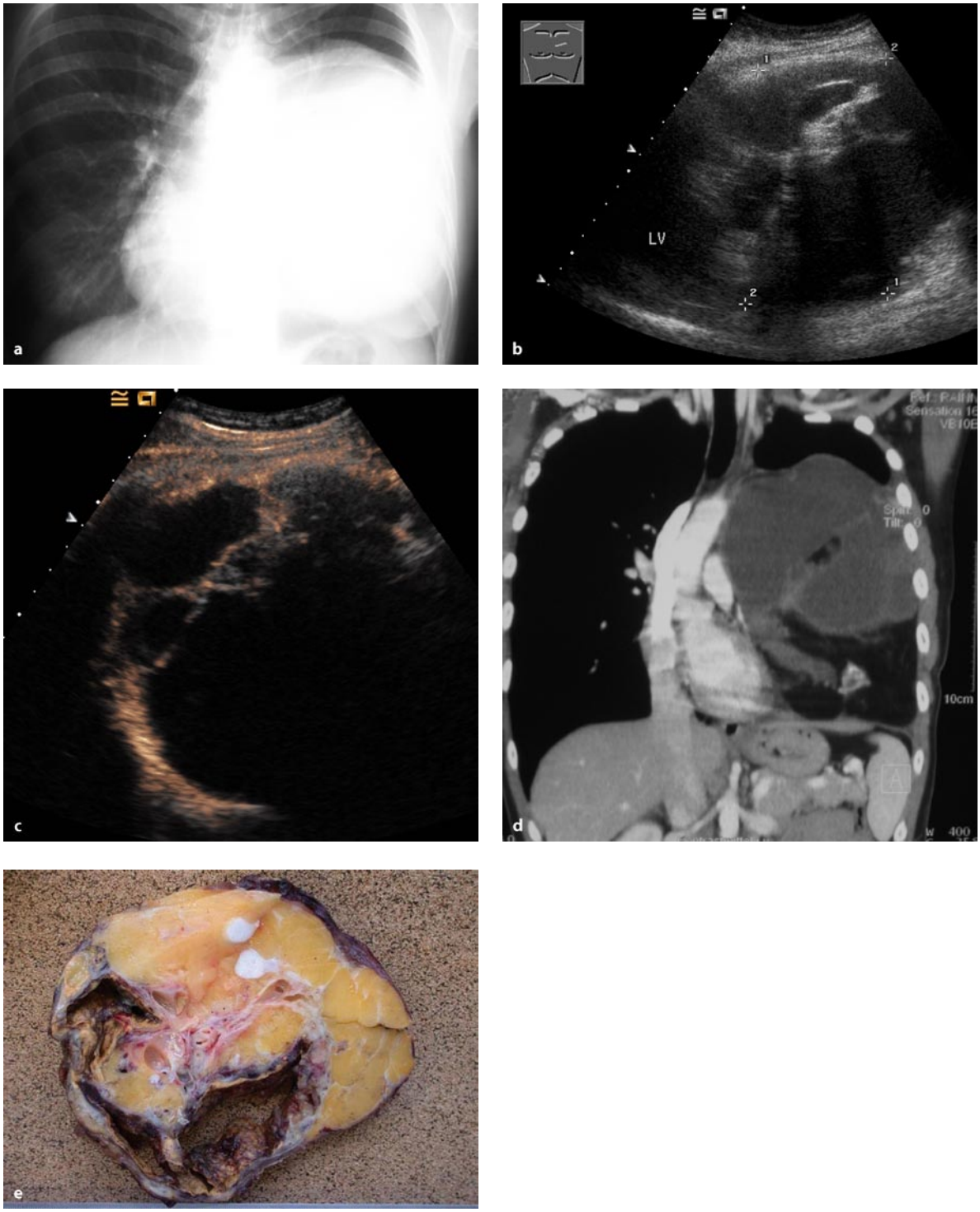

Fig. 5.16 Cystic teratoma. A 32-year-old patient, slight dyspnea when jogging. **a** Plain chest radiograph with tumor and mediastinal distortion to the right. **b** Left parasternal section in supine position. Clearly delineated mass with echogenic septum-like structures. In the *center*, high amplitude reflexes with dorsal shadowing. The space-occupying lesion displaces the pleura to the side towards the thoracic wall, which moves with breathing. The feeding vessels suggest a mediastinal origin of the lesion. **c** Contrast-enhanced sonography clearly demonstrates cystic parts of the tumor which otherwise only shows moderate vascularization and has a smooth border. A teratoma is suspected (central calcifications), and further preoperative diagnostics include computed tomography and transesophageal echocardiography. **d** Computed tomography reconstruction of the coronary section. **e** The gross pathological specimen demonstrates the smoothly demarcated tumor with septae, cystic areas, fatty tissue and cartilage/bone. Histology reveals a benign teratoma

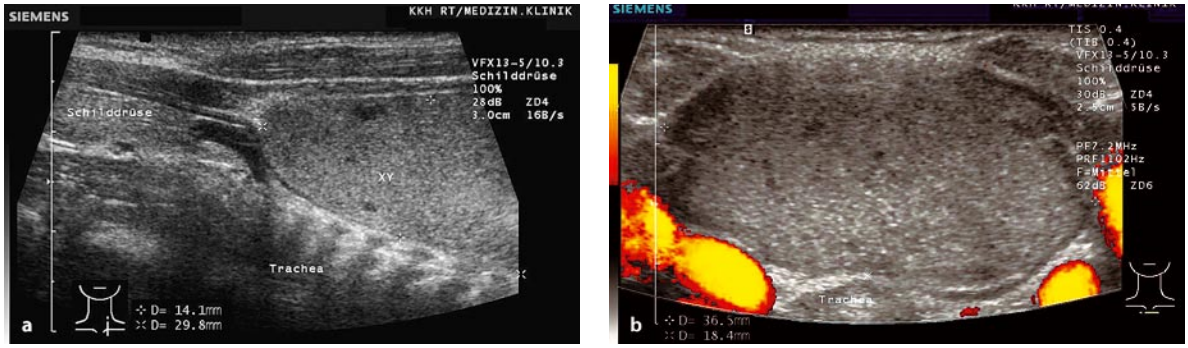

Fig. 5.17 Mediastianal cyst. **a** Suprasternal sagittal section. Smooth edged, homogeneously structured mass (*crosses*), ventral to the trachea. The proximal esophagus is recognizable dorsal to the thyroid gland on the *left*. **b** No blood circulation is detectable in the cross section even with highly sensitive technology. Movement of liquid is made recognizable in the B-image and in the color-Doppler sonography by a shaking movement. Diagnosic fine-needle puncture. Therapeutically operative resection due to compression syndrome

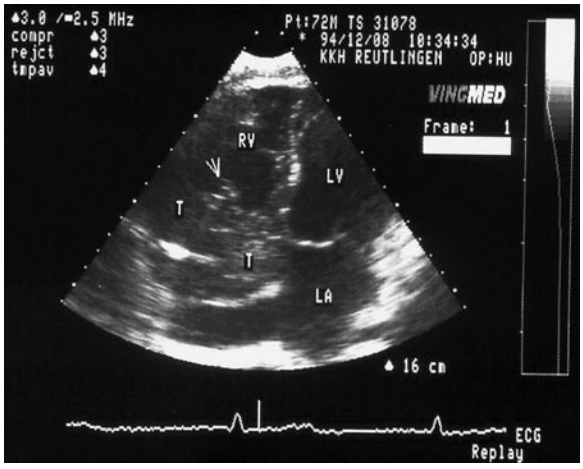

Fig. 5.18 Echocardiography. Chronic lymphatic leukemia affecting the right side of the heart (*T*). As a result, tricuspid stenosis and atrioventricular block, grade III. *LA* left atrium, *LV* left ventricle, *RV* right ventricle. (Image provided by Martin Hust, Cardiology, Reutlingen)

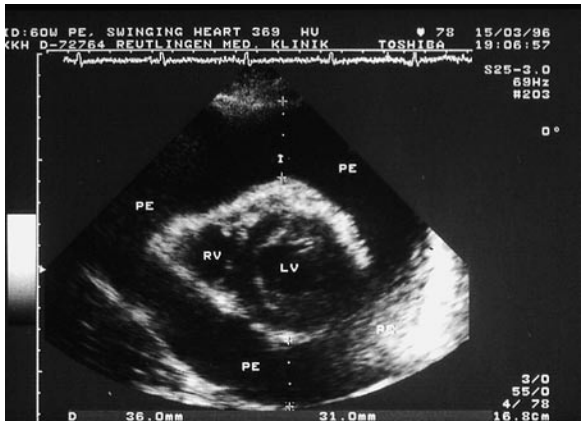

Fig. 5.19 Echocardiography. Large chronic pericardial effusion (*PE*). (Image provided by Martin Hust, Cardiology, Reutlingen)

differentiation may not always be possible even by dynamic B-mode imaging (change of patient positioning, etc.). Absence of vascularization (in color-Doppler or contrast-enhanced sonography) verifies the diagnosis (Fig. 5.17).

5.1.7.7 Pericardial Alterations

Pericardial alterations like pericardial effusion, hemopericardium and tumor infiltration are easily demonstrable (Figs. 5.18, 5.19).

5.1.7.8 Esophageal Disease

Proximal and distal portions of the esophagus can be clearly visualized by the suprasternal and infrasternal access. Esophageal tumors crossing the wall are seen as hypoechoic tumor formations with blurred margins (Fig. 5.20). In cases of surgical replacement of the esophagus, the upper anastomosis can be viewed. Recurrent tumors can also be detected (Blank et al. 1998; Fig. 5.21).

Sonography is a valuable aid in the detection of "dysphagia close to the cardia" (Blank et al. 1996a; Jannsen et al. 1997).

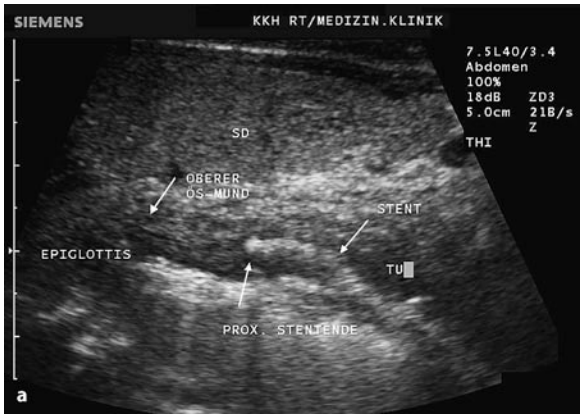

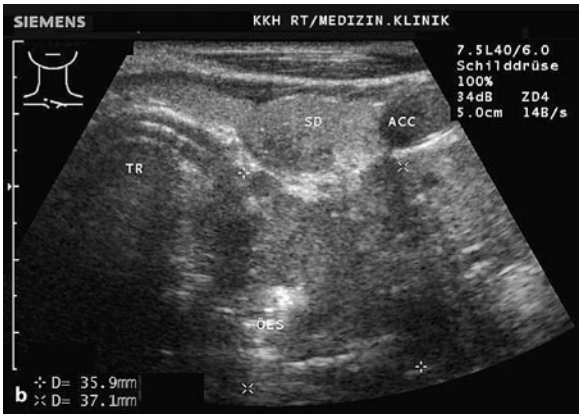

Fig. 5.20 **a** Proximal esophageal carcinoma spreading over the wall (*TU*) with infiltration into the epiglottis, upper esophageal sphincter (*OBERER ÖS-MUND*, *arrow*). The overgrown metal stent (*arrow*) is well delineated. An image with plenty of contrast and low in artifacts as a result of tissue-harmonic imaging. *THI* thyroid. **b** Tumor masses (*crosses*) with infiltration and stenosis of the esophagus (*OES*)

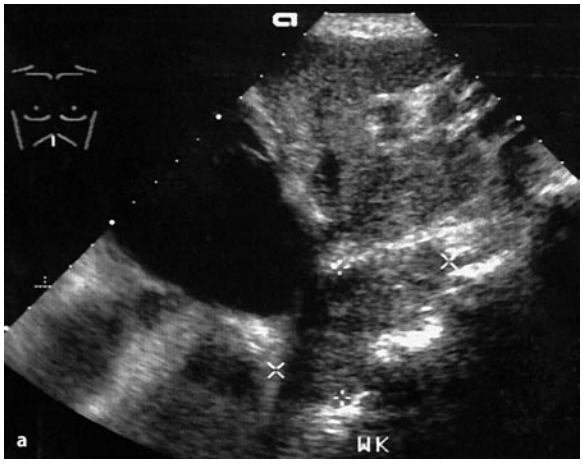

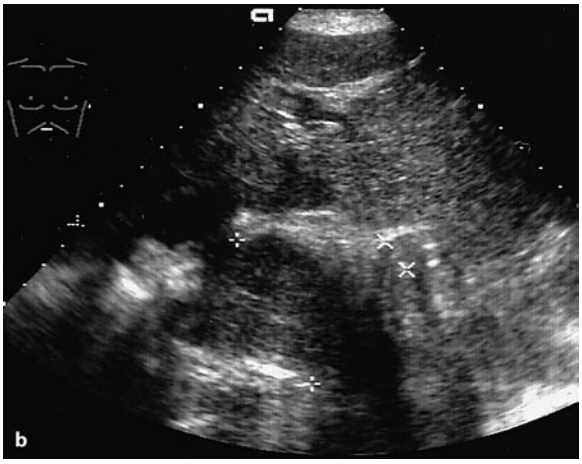

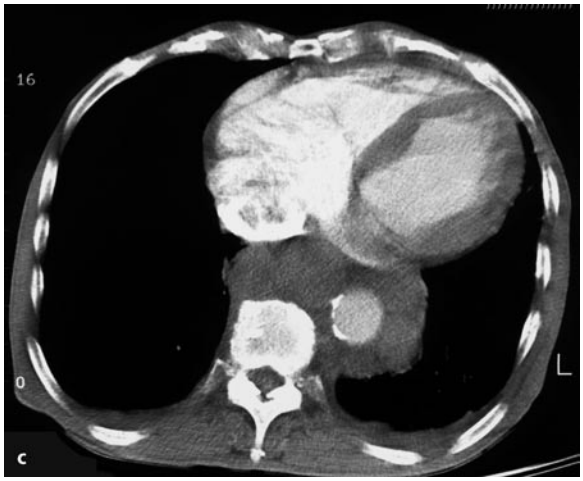

Fig. 5.21 Extensive esophageal carcinoma. **a** Clinical dysphagia. Endoscopic distal esophageal stenosis. No tumor could be established with certainty by biopsy. Sonography with infrasternal, sagittal section of the tumor formation lying ventrally to the spinal column (posterior mediastinum). *WK* vertebral body. **b** Tumor (*crosses*) located infrasternally in transverse section at the distal esophagus (*large crosses*) cannot be delineated. Percutaneously controlled transhepatic fine-needle cut biopsy (Sonocan, 0.9 mm). Histology indicated esophageal carcinoma. **c** Computed tomography. Mass in the posterior mediastinum surrounding the descending aorta

Table 5.4 Transthoracic sonography of the mediastinum

Advantages	Disadvantages
Dynamic imaging	Investigator-dependent
Free selection of sectional planes	Only parts of the mediastinum are accessible
Good imaging of the aorticopulmonary window	–
Punctures: low rate of complications	Only punctures in the anterior mediastinum are possible

5.1.8 Summary

Mediastinal space-occupying masses are most frequently found in the anterior upper mediastinum. They can be evaluated with transthoracic sonography nearly as reliably as with computed tomography, and histological material can usually be easily obtained by sonography-guided puncture (Herth and Becker 2003; Chap. 9).

The disadvantages of sonography, however, are significant. The procedure is strongly investigator-dependent and only reveals portions of the mediastinum compared with computed tomography. Moreover, the image quality is highly variable. Some of these disadvantages (Table 5.4) can be balanced by the application of endoluminal transesophageal and endobronchial sonography (Sect. 5.2, Chap. 6).

Acknowledgements I would like to express my thanks to Martin Lenz (chief consultant surgeon in the Radiology Department of the Steinenberg Clinic, Reutlingen) for preparing and providing the radiological findings, and my son Valentin for the technical photographic work.

References

Beckh S, Bolcskei PL, Lessnau KD (2002) Real-time chest ultrasonography. A comprehensive review for the pulmonologist. Chest 122:1759–1773

Betsch B (1994) Farbdopplersonographie des Mediastinums. Radiologe 34:599–604

Betsch B, Knopp MV, van Kaick G (1992) Malignant tumors and lymphomas of the mediastinum: diagnosis and follow-up with color assisted doppler sonography. Eur J Cancer Res Clin Oncol 118:107

Betsch B, Berndt R, Knopp MV, Schmähl A, Trost U, Delorme S (1994) Vergleich von Computertomographie und B-Bild-Sonographie in der bildgebenden Diagnostik des Mediastinums. Bildgebung 61:295–298

Blank W, Braun B (1995) Gewebsdiagnostik durch Dopplersonographie. Bildgebung 62:31–35

Blank W, Braun B, Gekeler E (1986) Ultraschalldiagnostik und Feinnadelpunktion pleuraler, pulmonaler und mediastinaler Prozesse. In: Hansmann M (ed) Ultraschalldiagnostik. Springer, Berlin, pp 562–565

Blank W, Braun B, Schuler A, Wild K (1996a) Die percutane Sonographie zur Differenzierung der Dysphagie. Ultraschall Med (Suppl 1) 32

Blank W, Schuler A, Wild K, Braun B (1996b) Transthoracic sonography of the mediastinum. Eur J Ultrasound 3:179–190

Blank W, Schwaiger U, Wild K, Braun B (1998) Die percutane Sonographie zur Darstellung des cervicalen Ösophagus. Ultraschall Med (Suppl 1) 4

Bollen EC, Goci R, van't Hof-Grootenboer BE, Versteege CWM, Engelshove HA, Lamers RJ (1994) Interobserver variability and accuracy of computed tomographic assessment of nodal status in lung cancer. Ann Thorax Surg 58:158–162

Braun B (1983) Abdominelle und thorakale Ultraschalldiagnostik. In: Bock HE (ed) Klinik der Gegenwart. Urban & Schwarzenberg, Munich, pp 1141–1145

Braun B (1992) Schilddrüse. In: Braun B, Günther R, Schwerk WB (eds) Ultraschalldiagnostik. Lehrbuch und Atlas, vol III-3.1. ecomed, Landsberg/Lech

Braun B, Blank W (2005) Sonographie von Hals und oberem Mediastinum. Internist 46(10):1133–1145

Brüggemann A, Greie A, Lepsien G (1991) Real-time-sonography of the mediastinum in adults: a study in 100 healthy volunteers. Surg Endosc 5:150–153

Castellino RA, Blank N, Hoppe RT et al (1986) Hodgkin disease: contributions of chest CT in the initial staging evaluation. Radiology 160:603–605

Dietrich CF, Liesen M, Wehrmann T, Caspary WF (1995) Mediastinalsonographie: Eine neue Bewertung der Befunde. Ultraschall Med 16:61

Dietrich CF, Liesen M, Buhl R, Herrmann G, Kirchner I, Caspary WF, Wehrmann T (1997) Detection of normal mediastinal lymphnodes by ultrasonography. Acta Radiol 38:965–969

Dietrich CF, Chickakli M, Burgon I, Wehrmann T, Wiewrodt R, Buhl R, Caspary WF (1999) Mediastinal lymphnodes demonstrated by mediastinal sonography: activity marker in patients with cystic fibrosis. J Clin Ultrasound 27:9–14

Goldberg GG (1971) Suprasternal ultrasonography. JAMA 15:245–250

Heckemann R (1983) Sonographische Tumordiagnostik im Mediastinum. Therapiewoche 33:123–137

Heinzmann EK (1988) The mediastinum. Springer, Berlin

Heizel M (1985) Sonographische Topographie des oberen vorderen Mediastinums. Ultraschall 6:101–109

Herth FJF, Becker HD (2003) Chest ultrasound; thoracic imaging; pleura mass; pleural effusion: ultrasound guidance. Respiration 70:84–94

Janssen J, Johanns W, Lehnhardt M, Jakobeit C, Greiner L (1997) Die transkutane Sonographie des gastroösophagealen Übergangs im prospektiven Vergleich mit der Endoskopie. Dtsch Med Wochenschr 122:1167–1171

Koh DM, Burke S, Davies N et al (2002) Transthoracic US of the chest: clinical uses and applications. Radiographics 22:E1. http://radiographics.rsnajnls.org/cgi/content/full/22/1/e1

Kunz A, Blank W, Gemacher O et al (2004) Echosignalverstärker am Thorax—work in progress. Ultraschall Med 25:37

Liu P, Daneman A, Stringer DA (1988) Real-time-sonography of mediastinal and juxtamediastinal masses in infants and children. J Can Assoc Radiol 39:198–203

Rosenberg JC (1993) Neoplasms of the mediastinum. In: De Vita VT, Hellman S, Rosenberg SA (eds) Cancer: principles & practice of oncology. Lippincott, Philadelphia, pp 759–775
Schuler A, Blank W, Braun B (1995) Sonographisch-interventionelle Diagnostik bei Thymomen. Ultraschall Med 16:62
von Lengerke HV, Schmid HC (1988) Mediastinalsonographie im Kindesalter. Radiologe 28:460–465
Wernecke K (1991) Mediastinale Sonographie, Untersuchungstechnik, diagnostische Effizienz und Stellenwert in der bildgebenden Diagnostik des Mediastinums. Springer, Berlin
Wernecke K, Peters PE, Galanski M (1986) Mediastinal tumors: evaluation of suprasternal sonographie. Radiology 159:405–409
Wernecke K, Pötter R, Peters PE (1988) Parasternal medisatinal sonography: sensitivity in the detection of anterior mediastinal and subcarinal tumors. AJR Am J Roentgenol 150:1021–1026
Zhu SY et al (2005) Sonographic demonstration of the normal thoraxic esophagus. J Clin Ultrasound 33(1):29–33

5.2 Transesophageal Sonography for Lung Cancer and Mediastinal Lesions

J.T. Annema, M. Veseliç, K.F. Rabe

Assessing a tissue diagnosis of mediastinal lesions, for example in patients with lung cancer and enlarged mediastinal lymph nodes, is often of major clinical importance. To date, surgical staging—such as mediastinoscopy and mediastinotomy—is still regarded as the standard of care for mediastinal assessment. However, these procedures are not only invasive and require clinical admission with associated high costs, they also have limitations in their diagnostic reach. The development of transesophageal sonography-guided fine-needle aspiration (FNA) provides a minimally invasive alternative for mediastinal analysis. Transesophageal sonography-guided FNA is currently used for the staging for various gastrointestinal malignancies. Since the first report in 1996 on transesophageal sonography-guided FNA for mediastinal staging (Pedersen et al. 1996), this method has evolved to an important diagnostic tool in chest medicine. In this part of the chapter, technical aspects as well as the use of transesophageal sonography-guided FNA in pulmonology will be discussed with an emphasis on the diagnosis and staging of lung cancer.

5.2.1 Technical Aspects

Transesophageal sonography is performed with technology which is also used by gasteroenterologists.

Both radial and linear sonography probes are available, which both enable visualization of paraesophageal lesions. Real-time sonography-controlled FNAs (Fig 5.22b), however, are only possible with linear or longitudinal probes. The fine needle aspirates obtained can be used for cytological as well as molecular analysis—for instance, PCR analysis in patients with suspected tuberculosis.

In chest medicine, only linear sonography probes are used as tissue sampling is indicated in the vast majority of cases. Patients are investigated in a left lateral position in an ambulatory setting under conscious sedation using a low dose of midazolam. After the pharynx has been anesthetized with a lidocaine spray, the echo-endoscope is introduced into the distal esophagus until the left liver lobe is visualized. From this point the echo-endoscope is slowly retracted—meanwhile making circular movements, which enables complete visualization of all paraesophageal lesions that are located in the mediastinum. Once lymph nodes have been identified, size, shape, echo texture and borders of lesions can be described. Mediastinal nodes with a short axis exceeding 1 cm, a hypoechoic texture, a round shape and sharp borders are suspected to be malignant. When indicated, images and short movies of mediastinal abnormalities can be recorded. In order to prove malignant nodal involvement it is necessary to obtain tissue (Toloza et al. 2003b). Suspected paraesophageal lesions can be aspirated under real-time sonographic guidance (Fig. 5.23). Nodes from which tissue is obtained should be classified according to the Naruke classification (Mountain and Dresler 1997; Fig. 5.24). In the case of suspected adrenal metastases, left-sided adrenal masses can by aspirated from the stomach (Eloubeidi et al. 2004). On-site cytological evaluation of aspirates has been proven be useful in order to ensure that representative samples are obtained. In experienced hands, a complete transesophageal sonographic examination for the diagnosis and staging of lung cancer takes about 25 min.

Although few absolute contraindications exist for transesophageal sonography procedures of the upper gastrointestinal tract, esophageal strictures and diverticula exhibit an increased perforation risk. Complications related to mediastinal lymph sampling have as yet not been reported. (Annema et al. 2005c, d; Eloubeidi et al. 2005b; Fritscher-Ravens et al. 2000a; Kramer et al. 2004; Larsen et al. 2002; Wallace et al. 2001; Williams et al. 1999). A cyst, however, poses an increased risk of infection and therefore should not be aspirated owing to an increased risk of mediastinitis (Annema et al. 2003a; Wildi et al. 2003).

The advantages of this novel diagnostic tool—as compared with radiological and surgical alternatives–are numerous (Table 5.5). Regarding mediastinal nodal staging, transesophageal sonography has a superior sensitivity compared with computed tomography (Hawes et al. 1994; Toloza et al. 2003a, b) and additionally provides the opportunity for tissue sampling. Compared with surgical alternatives, transesophageal sonography is less invasive,

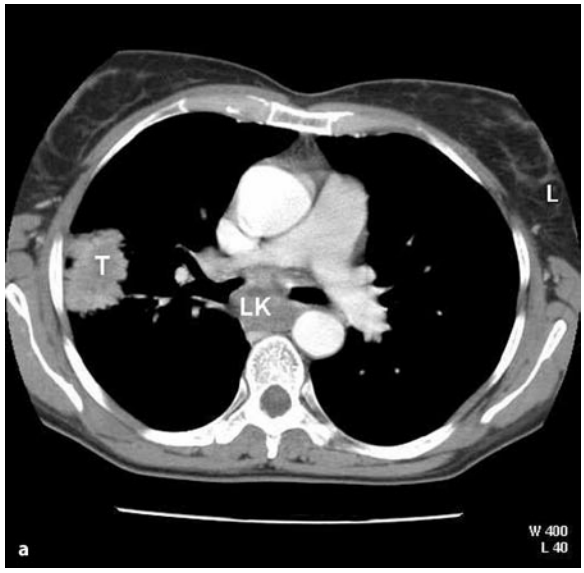

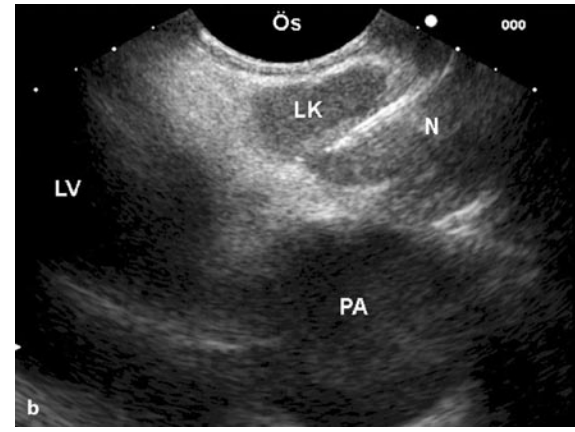

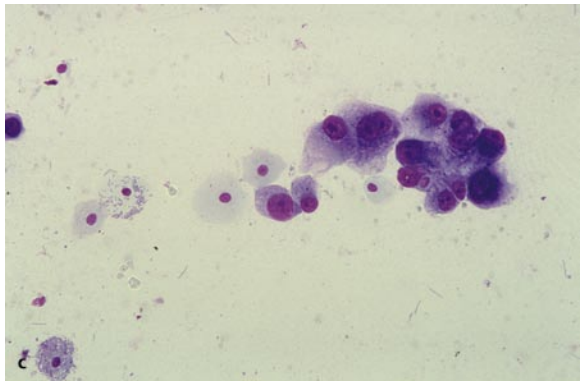

Fig. 5.22 **a** Computed tomography of the thorax. Right upper-lobe tumor (*T*) and enlarged subcarinal lymph node (*LK*). **b** Endosonography. Sonography-guided fine needle aspiration (*N* needle) of a hypoechoic lymph node with sharp borders located between the esophagus (*Ös*), pulmonary artery (*PA*) and left atrium (*LV*) (lymph node station 7). **c** Cytology. Fine-needle aspirate demonstrating adenocarcinoma with vacuoles and enlarged central nuclei. Squamous cells from the esophagus can be recognized on the *left*

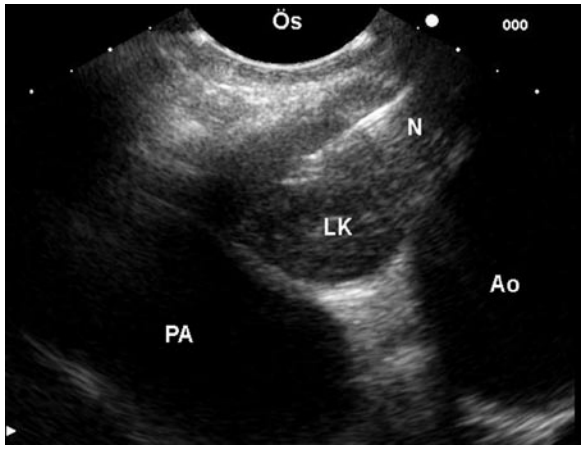

Fig. 5.23 Endosonography. Sonography-guided fine-needle aspiration (*N* needle) of a round hypoechoic lymph node with sharp borders, situated between the esophagus (*Ös*), aorta (*Ao*) and pulmonary artery (*PA*) (lymph node station 4L)

Table 5.5 Transesophageal sonography-guided fine-needle aspiration—advantages and limitations

Advantages	Limitations
Provides access to the lower mediastinum and aortico-pulmonary window	Pretracheal and paratracheal nodes
Real-time controlled tissue sampling	Operator dependency
Impressive safety record	
Minimally invasive	
Cost-effective	

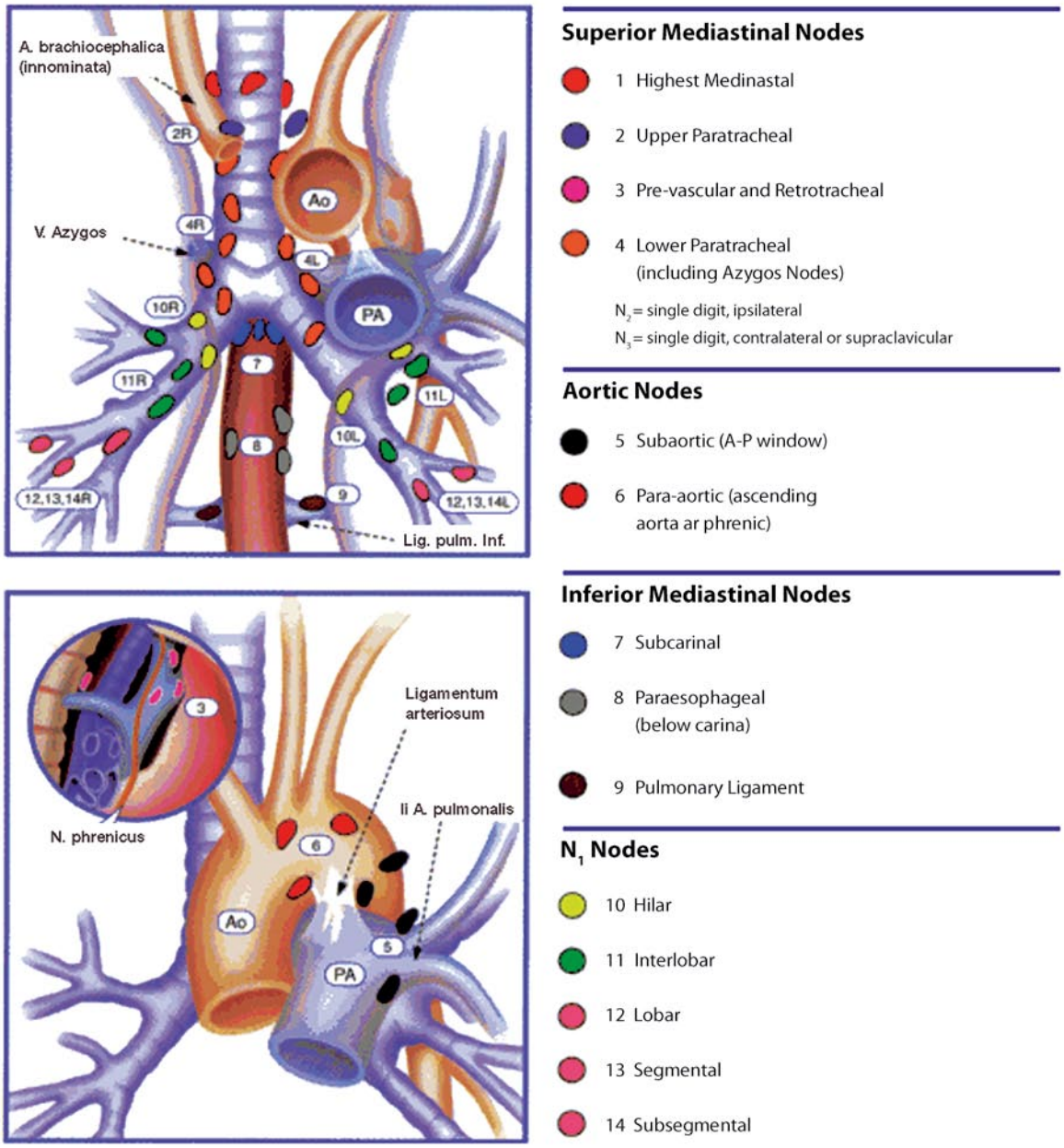

Fig. 5.24 Regional lymph node classification for lung cancer staging. (Adapted from Mountain and Dressler 1997)

is performed in an outpatient setting and is therefore more cost-effective (Kramer et al. 2004).

The lower mediastinum is the area which can be visualized completely by transesophageal sonography, especially regarding the subcarinal (station 7) and the lower paraesophageal (station 8) nodes as well as those nodes located in the pulmonary ligament (station 9) (Fig. 5.24). Although nodes located in the aortopulmonary window (station 5) and adjacent to the aorta (station 6) can be detected by transesophageal sonography, tissue sampling is not always possible owing to intervening vascular structures. Limitations of EUS are its inability to reach the upper (station 2) and lower (station 4) paratracheal nodes as air in the trachea and main bronchi regularly inhibits visualization of these areas of the mediastinum. EUS is complementary to both mediastinoscopy and endobronchial sonography regarding its diagnostic reach (Annema et al. 2005d; Eloubeidi et al. 2005a). Mediastinoscopy provides good access to both the upper and the lower paratracheal lymph nodes.

5.2.2 Transesophageal Sonography-Guided Fine-Needle Aspiration and Lung Cancer

5.2.2.1 Diagnosing Lung Cancer

Patients with suspected lung cancer and enlarged or PET-positive mediastinal nodes—for whom no diagnosis is obtained after bronchoscopy–are often good candidates for a transesophageal sonography-guided FNA investigation. If mediastinal metastases are assessed by transesophageal sonography-guided FNA, both a tissue diagnosis and locoregional staging are obtained with a single diagnostic test. In a prospective study of 142 patients with suspected lung cancer and enlarged mediastinal nodes, transesophageal sonography—after a nondiagnostic bronchoscopy—assessed a tissue diagnosis in 73% of patients (Annema et al. 2005d).

Transesophageal sonography-guided FNA is also indicated for diagnosing intrapulmonary tumors directly, provided they are located adjacent to the esophagus (Annema et al. 2005b; Varadarajulu et al. 2004a; Fig. 5.25). In a study of 32 patients with a centrally located lung tumor—in which bronchoscopy failed to achieve a tissue diagnosis—lung cancer was proven by transesophageal sonography-guided FNA in 97% of cases (Annema et al. 2005b).

5.2.2.2 Staging of Lung Cancer

Mediastinal staging of lung cancer is the most common indication for a transesophageal sonography-guided FNA investigation, and the accuracy is between 76 and 98% (Annema et al. 2005c, d; Eloubeidi et al. 2005b; Fritscher-Ravens et al. 2000a; Kramer et al. 2004; Larsen et al. 2002, 2005; Leblanc et al. 2005; Savides and Perricone 2004; Wallace et al. 2001, 2004; Williams et al. 1999; Table 5.6). So far, most studies have included selected patient with enlarged (short axis greater than 1 cm) or PET-positive (Annema et al. 2004; Eloubeidi et al. 2005b; Kramer et al. 2004) mediastinal nodes. For mediastinal restaging—an emerging indication for transesophageal sonography-guided FNA—an accuracy of 83% has been reported (Annema et al. 2003b).

Centrally located lung tumors can often be detected by transesophageal sonography, and in these cases it is often possible to assess whether mediastinal tumor invasion (T4) is present (Schroder et al. 2005; Varadarajulu et al. 2004b; Fig. 5.26). In a study with 97 patients with a lung tumor located immediately adjacent to the esophagus, transesophageal sonography had an accuracy of 92% regarding invasion in the aorta. (Schroder et al. 2005).

The left adrenal gland, a common site for distant metastases in patients with lung cancer, can be visualized from the stomach by transesophageal sonography. (Fig. 5.27). In a study of 31 patients with enlarged left adrenal glands on computed tomography, transesophageal sonography provided tissue proof of metastatic involvement in 42% of cases. (Eloubeidi et al. 2004). Whether the left adrenal gland should be investigated routinely during a transesophageal sonographic investigation for lung cancer staging is the subject of debate (Ringbaek et al. 2005).

5.2.2.3 Clinical Implications

Transesophageal sonographic investigations in patients with (suspected) lung cancer can prevent up to 70% of scheduled mediastinoscopies by providing tissue proof of mediastinal metastases (Annema et al. 2005c; Larsen et al. 2002). Patients prefer an ambulatory transesophageal sonographic investigation to surgical staging, which involves clinical admission and general anesthesia (Annema et al. 2005d). In the case of replacement of surgical staging by transesophageal sonography-guided FNA, cost reductions up to 40% can be achieved (Kramer et al. 2004).

5.2.2.4 Transesophageal Sonography in Lung Cancer Staging Algorithms

What are the indications for transesophageal sonography-guided FNA in the diagnosis and staging of lung cancer? On the basis of current evidence, transesophageal sonography-guided FNA is indicated early—after a nondiagnostic bronchoscopic evaluation that includes transbronchial needle aspiration—in the diagnostic workup or mediastinal staging of lung cancer.

When transesophageal sonography-guided FNA is added to mediastinoscopy, locoregional staging is improved owing to the complementary reach of both diagnostic methods in reaching different lymph nodes and the identification of mediastinal tumor invasion (T4) (Annema et al. 2005d; Eloubeidi et al. 2005a). Therefore, performing EUS as an additional staging test to routine mediastinoscopy leads to a significant reduction of futile thoracotomies (Larsen et al. 2005). Analyzing mediastinal lesions that are suspected for mediastinal metastases based on fluorodeoxyglucose PET by transesophageal sonography-guided FNA is regarded as an accurate, minimally invasive staging strategy for lung cancer (Annema et al. 2004; Eloubeidi et al. 2005b; Kramer et al. 2004).

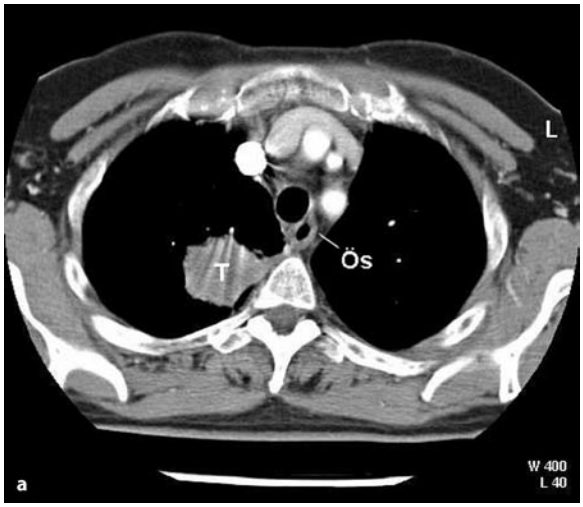

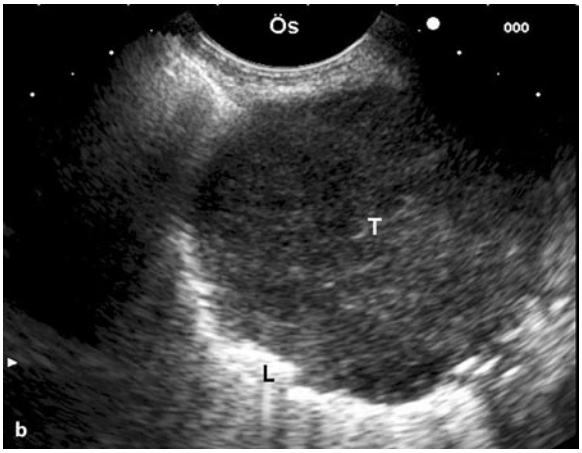

Fig. 5.25 a Computed tomography of the thorax. Relatively smooth shaped intrapulmonary lesion (*T*) located in the right upper lobe (3 cm × 3 cm × 6 cm) located adjacent to the esophagus (*Ös*). The esophagus is located behind the trachea. **b** Endosonography. Lesion with an inhomogeneous echo texture with irregular borders and bronchial carcinoma (*T*) which comprised lung tissue (*L*)

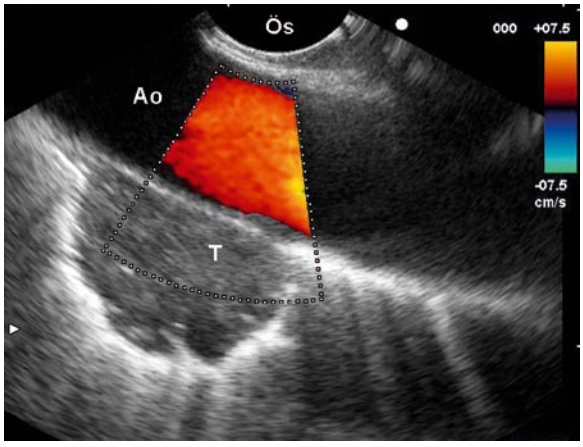

Fig. 5.26 Endosonography. Lung tumor (*T*) located in the left upper lobe with a close relation to the aorta (*Ao*). There are no signs of tumor invasion (T4) in the aorta. *Ös* esophagus

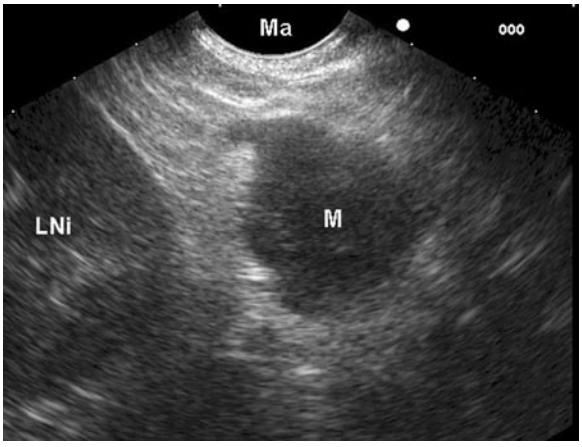

Fig. 5.27 Endosonography. Enlarged left adrenal gland with metastatic involvement (*M*) as assessed by transesophageal sonography-guided fine-needle aspiration. *Ma* stomach, *LNi* left kidney

Table 5.6 Transesophageal sonography-guided fine-needle aspiration—mediastinal lymph nodes

Authors	Number of patients	Accuracy (%)
Williams et al. (1999)	82	90
Fritscher-Ravens et al. (2000a)	153	97
Wallace et al. (2001)	107	97
Larsen et al. (2002)	79	94
Kramer et al. (2004)	81	77
Savides and Perricone (2004)	59	98
Wallace et al. (2004)	69	83[a]
Leblanc et al. (2005)	72	76
Annema et al. (2005d)	100	91
Eloubeidi et al. (2005b)	93	97[b]
Annema et al. (2005c)	215	93
	1.110	76–98

[a] Lymph nodes smaller than 1 cm

[b] PET-positive lesions

Transesophageal sonography-guided FNA indications in chest medicine:

- Suspected lung cancer, enlarged mediastinal nodes
- Suspected lung cancer, tumor located adjacent to the esophagus
- Mediastinal (re-)staging
- Analyzing PET-positive mediastinal lesions
- Staging of centrally located lung tumors suspected for tumor invasion (T4)
- Suspected left adrenal metastases (left-sided)
- Suspected sarcoidosis
- Suspected tuberculosis
- Suspected mediastinal cysts

5.2.3 Transesophageal Sonography-Guided Fine-Needle Aspiration and Sarcoidosis

Sarcoidosis is the most common interstitial lung disease in which mediastinal nodes are often involved. Frequently, a tissue diagnosis supporting the presumed diagnosis of sarcoidosis is needed, either before treatment with steroids or to rule out other diseases such as tuberculosis, lymphomas or malignant epithelial diseases. For the diagnosis of sarcoidosis, a state-of-the-art bronchoscopic evaluation—including several peripheral lung biopsies—has a diagnostic yield of 66% (Costabel and Hunninghake 1999). However, peripheral biopsies include the risk of a pneumothorax or hemoptysis. Transesophageal sonography has both a high yield (82%; Annema et al. 2005a) and a high sensitivity 89–94% (Fritscher-Ravens et al. 2000b; Wildi et al. 2004) in assessing noncaseating granulomas and so far no adverse events have been reported. Sonographic images of mediastinal nodes in patients with sarcoidosis often demonstrate a specific ultrasound pattern consisting of multiple, well-defined mediastinal nodes with an isoecpoic or hypoechoic texture and the absence of a centrally located hypoechoic area. Often vessels within these nodes can be detected by color-Doppler sonography (Fritscher-Ravens et al. 2000b). On cytological evaluation, mediastinal nodes in patients with sarcoidosis present as noncaseating granulomas without necrosis (Fig. 5.28).

5.2.4 Transesophageal Sonography and Cysts

Paraesophageal and parabronchial cysts account for a considerable portion of mediastinal lesions. Cysts located adjacent to the esophagus (Fig 5.29a) can be visualized by transesophageal sonography and often present with a round shape, well-defined borders and a echo-free or echo-poor content (Fig. 5.29b). Aspiration of cysts is not indicated owing to the risk of mediastinitis (Annema et al. 2003a; Wildi et al. 2003).

5.2.5 Summary

Ten years after the first reports of mediastinal evaluation by transesophageal sonography-guided FNA, there is strong evidence that transesophageal sonography-guided FNA qualifies as an accurate and safe method for diagnosing and staging of lung cancer. Additionally this test is helpful for the analysis of various other mediastinal lesions. When used in clinical practice, transesophageal sonography-guided FNA not only prevents surgical diagnostic procedures to a large extent, it also reduces the number of futile thoracotomies and is cost-effective. Recently, linear echo-bronchoscopes—derived from transesophageal sonography scopes—have become clinically available. Comparison studies between transesophageal sonography-guided FNA and endobronchial sonography-guided transbronchial needle aspiration are needed for definitive position of these echo-endoscopic methods in diagnostic and staging algorithms (Herth et al.

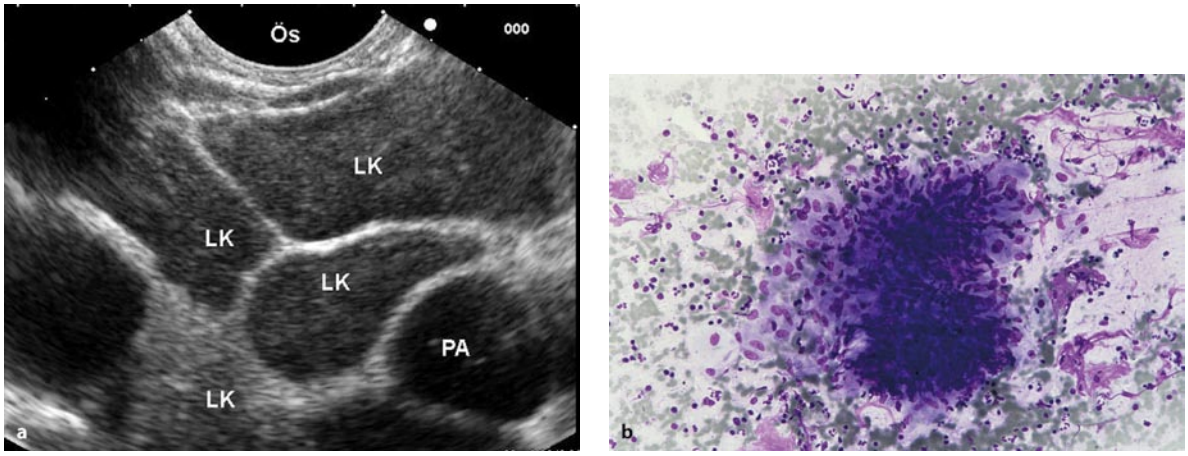

Fig. 5.28 **a** Endosonography. Multiple nodes (*LK*) with sharp borders and an isoechoic ultrasound pattern suggestive of sarcoidosis. *PA* pulmonary artery. **b** Cytology of this lymph node indicates a typical granuloma without central necrosis

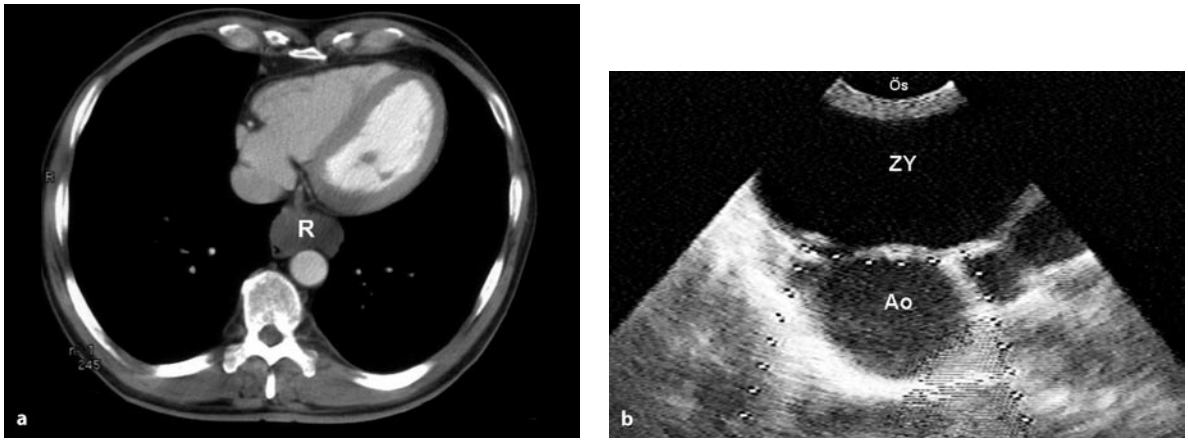

Fig. 5.29 **a** Computed tomography of the thorax. Sharp well-defined lesion (*R*) (2 cm × 1 cm × 1 cm) located in the lower mediastinum. The heart and descending aorta are easily identified. **b** Endosonography. Remarkably echo-poor, well-demarked, easily compressible lesion (cyst located immediately adjacent to the esophagus (*Ös*) without a signal on color-Doppler sonography—sonograpically compatible with a cyst.. *Ao* aorta

2005; Vilmann et al. 2005). The end point for such studies should include accuracy, safety, feasibility and patient preference. According to the authors, supported by the available peer-reviewed literature, transesophageal sonography-guided FNA can be regarded as an important diagnostic tool for the analysis of mediastinal lesions and the diagnosis and staging of lung cancer.

References

Annema JT, Veselic M, Versteegh MI, Rabe KF (2003a) Mediastinitis caused by EUS-FNA of a bronchogenic cyst. Endoscopy 35(9):791–793

Annema JT, Veselic M, Versteegh MI, Willems LN, Rabe KF (2003b) Mediastinal restaging: EUS-FNA offers a new perspective. Lung Cancer 42(3):311–318

Annema JT, Hoekstra OS, Smit EF, Veselic M, Versteegh MI, Rabe KF (2004) Towards a minimally invasive staging strategy in NSCLC: analysis of PET positive mediastinal lesions by EUS-FNA. Lung Cancer 44(1):53–60

Annema JT, Veselic M, Rabe KF (2005a) Endoscopic ultrasound-guided fine-needle aspiration for the diagnosis of sarcoidosis. Eur Respir J 25(3):405–409

Annema JT, Veselic M, Rabe KF (2005b) EUS-guided FNA of centrally located lung tumours following a non-diagnostic bronchoscopy. Lung Cancer 48(3):357–361

Annema JT, Versteegh MI, Veselic M, Voigt P, Rabe KF (2005c) Endoscopic ultrasound-guided fine-needle aspiration in the diagnosis and staging of lung cancer and its impact on surgical staging. J Clin Oncol 23(33):8357–8361

Annema JT, Versteegh MI, Veselic M, Welker L, Mauad T, Sont JK et al (2005d) Endoscopic ultrasound added to mediastinoscopy for preoperative staging of patients with lung cancer. JAMA 294(8):931–936

Costabel U, Hunninghake GW (1999) ATS/ERS/WASOG statement on sarcoidosis. Sarcoidosis Statement Committee. American Thoracic Society. European Respiratory Society. World Association for Sarcoidosis and Other Granulomatous Disorders. Eur Respir J 14(4):735–737

Eloubeidi MA, Seewald S, Tamhane A, Brand B, Chen VK, Yasuda I et al (2004) EUS-guided FNA of the left adrenal gland in patients with thoracic or GI malignancies. Gastrointest Endosc 59(6):627–633

Eloubeidi MA, Tamhane A, Chen VK, Cerfolio RJ (2005a) Endoscopic ultrasound-guided fine-needle aspiration in patients with non-small cell lung cancer and prior negative mediastinoscopy. Ann Thorac Surg 80(4):1231–1239

Eloubeidi MA, Cerfolio RJ, Chen VK, Desmond R, Syed S, Ojha B (2005b) Endoscopic ultrasound-guided fine needle aspiration of mediastinal lymph node in patients with suspected lung cancer after positron emission tomography and computed tomography scans. Ann Thorac Surg 79(1):263–268

Fritscher-Ravens A, Sriram PV, Bobrowski C, Pforte A, Topalidis T, Krause C et al (2000a) Mediastinal lymphadenopathy in patients with or without previous malignancy: EUS-FNA-based differential cytodiagnosis in 153 patients. Am J Gastroenterol 95(9):2278–2284

Fritscher-Ravens A, Sriram PV, Topalidis T, Hauber HP, Meyer A, Soehendra N et al. (2000b) Diagnosing sarcoidosis using endosonography-guided fine-needle aspiration. Chest 118(4):928–935

Hawes RH, Gress F, Kesler KA, Cummings OW, Conces DJ Jr (1994) Endoscopic ultrasound versus computed tomography in the evaluation of the mediastinum in patients with non-small-cell lung cancer. Endoscopy 26(9):784–787

Herth FJ, Lunn W, Eberhardt R, Becker HD, Ernst A (2005) Transbronchial vs. transesophageal ultrasound-guided aspiration of enlarged mediastinal lymph nodes. Am J Respir Crit Care Med 171(10):1164–1167

Kramer H, van Putten JW, Post WJ, van Dullemen HM, Bongaerts AH, Pruim J et al (2004) Oesophageal endoscopic ultrasound with fine needle aspiration improves and simplifies the staging of lung cancer. Thorax 59(7):596–601

Larsen SS, Krasnik M, Vilmann P, Jacobsen GK, Pedersen JH, Faurschou P et al (2002) Endoscopic ultrasound guided biopsy of mediastinal lesions has a major impact on patient management. Thorax 57(2):98–103

Larsen SS, Vilmann P, Krasnik M, Dirksen A, Clementsen P, Maltbaek N et al. (2005) Endoscopic ultrasound guided biopsy performed routinely in lung cancer staging spares futile thoracotomies: preliminary results from a randomised clinical trial. Lung Cancer 49(3):377–385

Leblanc JK, Devereaux BM, Imperiale TF, Kesler K, Dewitt JM, Cummings O et al (2005) Endoscopic ultrasound in non-small cell lung cancer and negative mediastinum on computed tomography. Am J Respir Crit Care Med 171:177–182

Mountain CF, Dresler CM (1997) Regional lymph node classification for lung cancer staging. Chest 111(6):1718–1723

Pedersen BH, Vilmann P, Folke K, Jacobsen GK, Krasnik M, Milman N et al (1996) Endoscopic ultrasonography and real-time guided fine-needle aspiration biopsy of solid lesions of the mediastinum suspected of malignancy. Chest 110(2):539–544

Ringbaek TJ, Krasnik M, Clementsen P, Skov BG, Rasmussen EN, Vilmann P (2005) Transesophageal endoscopic ultrasound/fine-needle aspiration diagnosis of a malignant adrenal gland in a patient with non-small cell lung cancer and a negative CT scan. Lung Cancer 48(2):247–249

Savides TJ, Perricone A (2004) Impact of EUS-guided FNA of enlarged mediastinal lymph nodes on subsequent thoracic surgery rates. Gastrointest Endosc 60(3):340–346

Schroder C, Schonhofer B, Vogel B (2005) Transesophageal echographic determination of aortic invasion by lung cancer. Chest 127(2):438–442

Toloza EM, Harpole L, McCrory DC (2003a) Noninvasive staging of non-small cell lung cancer: a review of the current evidence. Chest 123(1 Suppl):137S–146S

Toloza EM, Harpole L, Detterbeck F, McCrory DC (2003b) Invasive staging of non-small cell lung cancer: a review of the current evidence. Chest 123(1 Suppl):157S–166S

Varadarajulu S, Hoffman BJ, Hawes RH, Eloubeidi MA (2004a) EUS-guided FNA of lung masses adjacent to or abutting the esophagus after unrevealing CT-guided biopsy or bronchoscopy. Gastrointest Endosc 60(2):293–297

Varadarajulu S, Schmulewitz N, Wildi SF, Roberts S, Ravenel J, Reed CE et al (2004b) Accuracy of EUS in staging of T4 lung cancer. Gastrointest Endosc 59(3):345–348

Vilmann P, Krasnik M, Larsen SS, Jacobsen GK, Clementsen P (2005) Transesophageal endoscopic ultrasound-guided fine-needle aspiration (EUS-FNA) and endobronchial ultrasound-guided transbronchial needle aspiration (EBUS-TBNA) biopsy: a combined approach in the evaluation of mediastinal lesions. Endoscopy 37(9):833–839

Wallace MB, Silvestri GA, Sahai AV, Hawes RH, Hoffman BJ, Durkalski V et al (2001) Endoscopic ultrasound-guided fine needle aspiration for staging patients with carcinoma of the lung. Ann Thorac Surg 72(6):1861–1867

Wallace MB, Ravenel J, Block MI, Fraig M, Silvestri G, Wildi S et al (2004) Endoscopic ultrasound in lung cancer patients with a normal mediastinum on computed tomography. Ann Thorac Surg 77(5):1763–1768

Wildi SM, Hoda RS, Fickling W, Schmulewitz N, Varadarajulu S, Roberts SS et al (2003) Diagnosis of benign cysts of the mediastinum: the role and risks of EUS and FNA. Gastrointest Endosc 58(3):362–368

Wildi SM, Judson MA, Fraig M, Fickling WE, Schmulewitz N, Varadarajulu S et al (2004) Is endosonography guided fine needle aspiration (EUS-FNA) for sarcoidosis as good as we think? Thorax 59(9):794–799

Williams DB, Sahai AV, Aabakken L, Penman ID, Van Velse A, Webb J et al (1999) Endoscopic ultrasound guided fine needle aspiration biopsy: a large single centre experience. Gut 44:720–726

6 Endobronchial Sonography

F.J.F. Herth, R. Eberhardt

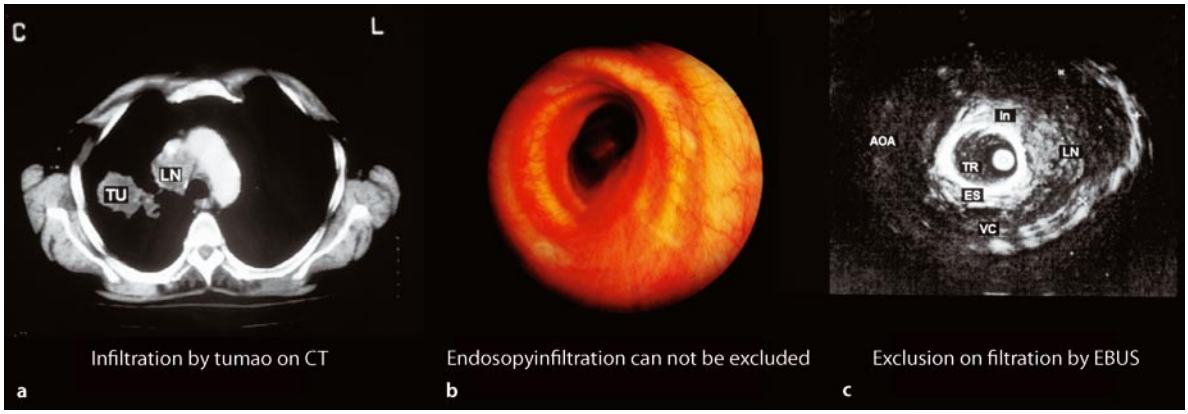

Fig. 6.1a–c Excision of the wall infiltration. *TU* tumor, *LN* lymph node, *AOA* ascending aorta, *TR* trachea, *ES* endoscopic probe, *In* small lymph node, *VC* vena cava

The endobronchial application of ultrasound was first described in 1992 (Hürther and Hanrath 1992). In the following years technical difficulties had to be solved and a clear view of the indication and diagnostic properties of endobronchial sonography had to be developed. Many abnormalities of the airways involve the bronchial wall and the parabronchial structures. Radiologic imaging has been proven to be unreliable in diagnosis of these structures (Sihoe and Yim 2004). The view of the endoscopist, however, is limited to the lumen and the internal surface of the airways. Processes within the airway wall and outside the airways can only be assessed by indirect signs. Especially in malignancies this can be of decisive importance for the fate of the patient. External mediastinal thoracic sonography is insufficient for imaging of the paratracheal and hilar structures. By endoesophageal sonography, the pretracheal region and the right hilar structures are inaccessible because of limited contact and interposition of the airways. Therefore, expanding the endoscopist's view beyond the airways is essential (Herth and Becker 2000).

Since 1999 endobronchial sonography has been commercially available and has gradually been introduced into bronchoscopic practice. This has broadened the view of the bronchoscopist and augmented the diagnostic possibilities for both bronchial and mediastinal pathology.

Some aspects have yet to be assessed when the technique is used more widely. Considering the fact that it takes at least 50 sessions to acquire basic experience even in regular diagnostic bronchoscopy, it takes considerably more effort to gain expertise in this new diagnostic method, showing structures like the tracheal wall that were not available for diagnosis up to now, and imaging mediastinal structures from uncommon angles and points of view.

Since 2004 another different endobronchial sonography technique has been available on the market, the so-called endobronchial sonography transbronchial needle aspiration (TBNA) scope.

6.1 Instruments and Technique

6.1.1 Endobronchial Sonography Miniprobes

The different impedance of soft tissues has made sonography an indispensable diagnostic tool in medicine. Instruments that are used for gastrointestinal application could not be applied inside the airways because of their diameter. For application inside the central airways, therefore, flexible catheters for the probes with a balloon at the tip were developed, which allows circular contact for the ultrasound, providing a complete 360° image of the parabronchial and paratracheal structures (Fig. 6.1a). Thus, under favorable conditions structures at a distance of up to 4 cm can be visualized (Herth and Becker 2000). The probes have been on the market since 1999 and can be applied with regular flexible endoscopes that have a biopsy channel of at least 2.6 mm.

6.1.2 Endobronchial Sonography Transbronchial Needle Aspiration

The latest developments are special bronchoscopes with an integrated curvilinear electronic transducer at the tip (Olympus BF-UC160F; Fig. 6.2). So a real-time needle puncture under endoscopic control is possible. The outer diameter of the insertion tube is 6.2 mm. The angulation range of the distal end of the endoscope is 160° upward

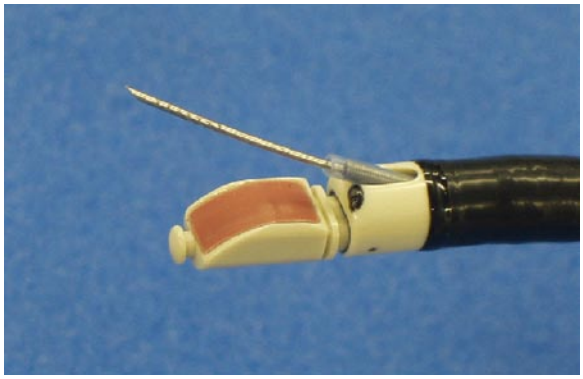

Fig. 6.2 Head of the sonography bronchoscope

and 90° downward. The instrument has a small curved linear-array electronic transducer, of length 10 mm, located at the distal end of the endoscope in front of a 30° oblique forward-viewing fiberoptic lens (angle of view 80). The endoscope has a biopsy channel of 2 mm. The ultrasonic frequency is 7.5 MHz with a penetration depth of 5 cm. The scanning direction is parallel to the longitudinal axis of the endoscope with a scanning angle of 50°, which enables full sonographic monitoring of a needle when it is inserted via the biopsy channel during scanning (Krasnik et al. 2003).

6.2 Sonographic Anatomy

The wall of the central airways show a seven-layer structure which can be demonstrated by high magnification only. The layers represent the mucosa and submucosa, the three layers of the cartilage and the adjacent external structures of loose and dense connective tissue, respectively (Kurimoto et al. 1999). Under low-power magnification and in the periphery only a three-layer structure is visible. Orientation by sonography within the mediastinum is difficult. Besides the complex mediastinal anatomy this is due to motion artifacts by pulsation and respiration as well as the unusual planes of the sonography images as with the probes we have to follow the course of the airways. For orientation, therefore, the analysis of characteristic anatomical structures is more reliable than observation of the position of the sonography probe inside the airway. Vessels can be diagnosed by their pulsation. But even after application of echo contrast media discrimination of venous and arterial vessels can be difficult owing to the great number of variations. However, as during the procedure pulse oxymetry is applied, arterial pulsations can be diagnosed according to their synchronism with the acoustic signal. Lymph nodes and solid structures can be differentiated down to a size of a few millimeters from the blood vessels by their higher echodensity.

6.3 Indications and Results for the Endobronchial Sonography Miniprobe

Since 1999 the probe has been on the market and endobronchial sonography is applied in several centers worldwide. For some indications the superiority of sonography over conventional imaging has been proven in prospective studies and in some centers endobronchial sonography is already established as a routine procedure According to the structures that can be analyzed, current indications comprise endoluminal, intramural and parabronchial structures; with respect to medical indications, early detection and tumor staging, inflammatory destruction of the airways, mediastinal lesions and malformations of mediastinal structures.

6.3.1 Early Cancer

In small radiologically invisible tumors the decision for local endoscopic therapeutic intervention is dependent on their intraluminal and intramural extent within the different layers of the wall. In contrast to radiological imaging by endobronchial sonography even very small tumors of a few millimeters can be analyzed and differentiated from benign lesions. As different authors demonstrated, endobronchial sonography is a very reliable tool in analyzing the extent of these small lesions. We could demonstrate that by endobronchial sonography in small autofluorescence-positive lesions that were negative in white light bronchoscopy we could improve specificity (predicting malignancy) from 50 to 90. Combination of endobronchial sonography with autofluorescence has been proven to be efficient in prospective studies and today has become the basis for curative endobronchial treatment of malignancies in some institutions (Herth and Becker 2003; Miyazu et al. 2002; Fig. 6.3). The most important paper in this respect was that of Miazyu et al.. They used the finding of endobronchial sonography for the therapy decision in patients with early cancer lesions. In 18 patients they found nine with a tumor limation to the bronchial wall; these patients were treated with photodynamic therapy. All other patients had extracartaligenous tumor growing and were treated nonendoscopically (surgery, radiation and chemotherapy). Using the finding as a decision maker they achieved a 100% complete remission rate in the endoluminal treated group. In a mean fol-

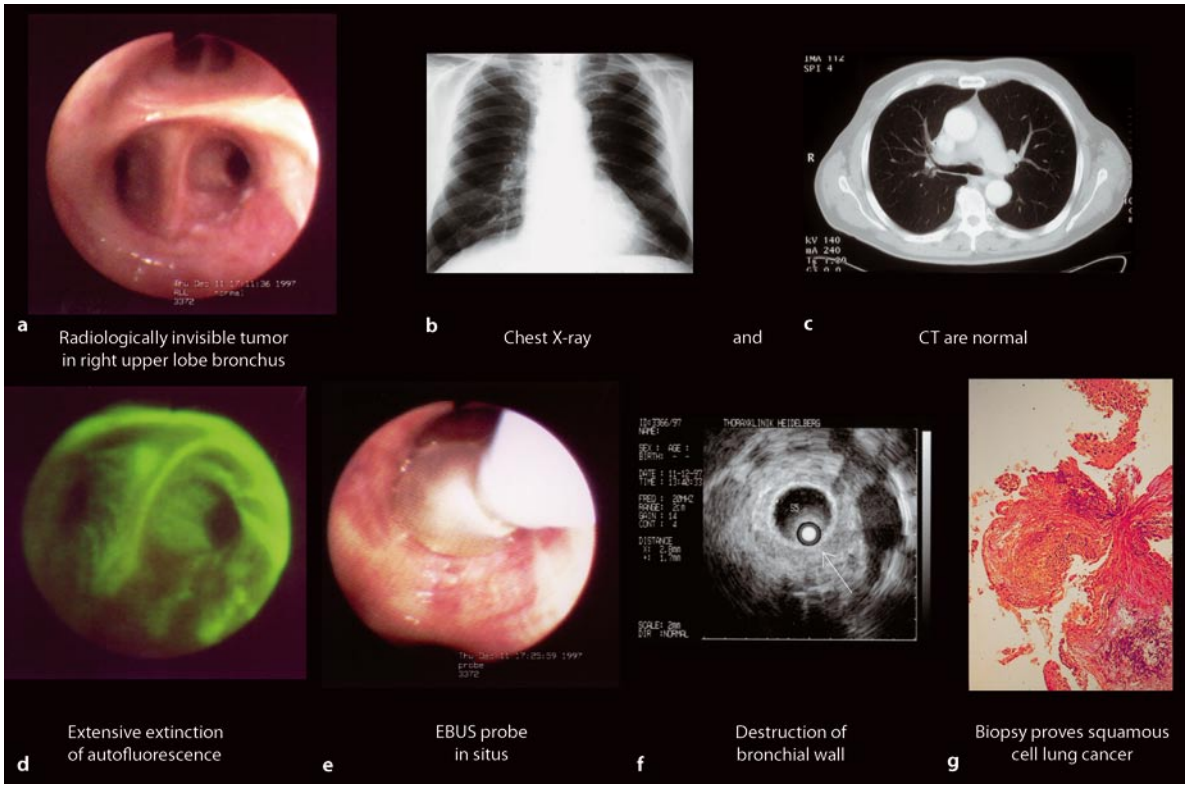

Fig. 6.3a–g Local staging of an early carcinoma. The *arrow* in **f** shows the destruction of the bronchial wall by the tumor

low-up time of 32 months none of the patients developed a recurrence. Compared with earlier published trials using endoluminal techniques in early cancer lesions, they could show that with the help of endobronchial sonography, endoluminal-treatable patients could be identified.

6.3.2 Advanced Cancer

In preoperative staging, endobronchial sonography allows detailed analysis of intraluminal, submucosal and intramural tumor spread, which can be essential for decisions regarding resection margins. Endobronchial sonography proved specially useful in diagnosis of mediastinal tumor involvement in the great vessels such as the aorta, the vena cava, the main pulmonary arteries and the esophageal wall which by conventional radiology frequently is impossible. In a trial it was shown that differentiation of external tumor invasion from impression of the tracheobronchial wall by endobronchial sonography is highly reliable (94%) in contrast to computed tomography imaging (51%). One hundred and four patients with a central tumor were examined with endobronchial sonography and computed tomography and the tumors were classified into invasion or impression types. All patients underwent surgery, and the findings were compared with the initial classification. The sensitivity (from 89 to 25%) and also the specifity (from 100 to 89%) shows the superiority of the sonography technique in the differantion between airway infiltration and compression by tumor. Thus, many patients considered to be nonresectable by the radiologist owing to supposed T4 tumors could be operated on in a curative approach after use of endobronchial sonography (Herth et al. 2003).

6.3.3 Peripheral Lesions

For histological diagnosis of peripheral intrapulmonary lesions by bronchoscopy an instrumental approach under fluoroscopic or computed tomography guidance is the standard procedure Fig. 6.6 a-c. This demands expensive X-ray equipment in the bronchoscopy suite or coordination with the radiology department and causes exposure to radiation for the patient and the staff. In a prospective study we were able to show that those lesions could be approached by endobronchial sonography guidance with the same success rate of approximately 75%. Recently these data were confirmed by a group of Japanese broncholo-gists. Shirakawa et al. also achieved a diagnostic yield of 75% using the miniprobe as a guidance tool for the forceps (Herth et al. 2002b, 2006a; Shirakawa et al. 2004).

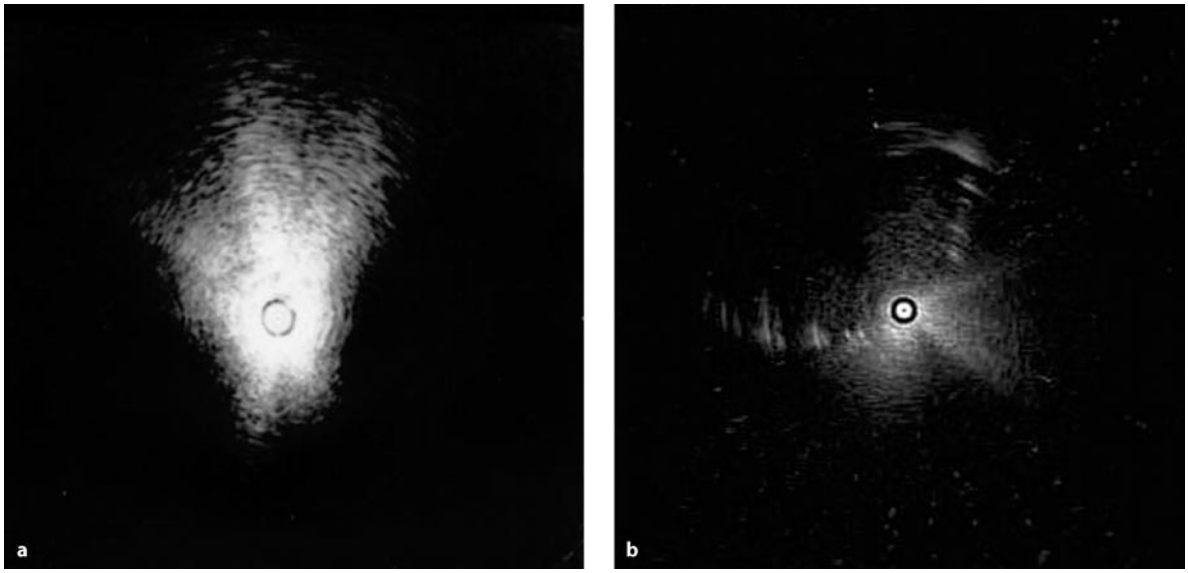

Fig. 6.4 **a** Complete reflection of sound waves in lung parenchyma. **b** A peripheral intrapulmonary lesion can be distinguished from the lung parenchyma with the probe head

6.3.4 Lymph Node Staging

Under favorable conditions lymph nodes can be detected by endobronchial sonography down to a size of 2–3 mm and the internal structure (sinuses and folliculi) as well as small lymph vessels can be analyzed. By endosonographic localization of lymph nodes the results of TBNA can be significantly improved up to 85%. This is especially true for those positions in which reliable landmarks on the computed tomogram are missing, e.g., high and low paratracheal localization. Herth et al. (2004) investigated the results of an endobronchial sonography-guided TBNA compared with those of conventional TBNA. In this randomized study, they confirmed that the yield of an endobronchial sonography-guided TBNA is higher than that of the conventional TBNA (85 vs. 66%). In an additional analysis of the lymph node station they showed that especially in locations without endoscopic landmarks (lymph node stations 2, 3, 4, Mountain scheme) the detection technique is helpful to increase the yield. On the other hand, they showed that in the case of enlarged subcarinal nodes a conventional TBNA has the same yield as the TBNA after endobronchial sonography detection.

6.3.5 Endobronchial Sonography in Therapeutic Interventions

Especially for making decisions in potentially curative endobronchial therapy of malignancies such as photodynamic therapy or endoluminal high-dose radiation by brachytherapy, diagnosis of limitation of the lesion to the bronchial wall or to the close vicinity is essential. Here endobronchial sonography is superior to all other imaging procedures owing to the detailed analysis of the layers of the bronchial wall.

In decision-making for endobronchial therapy of advanced lung cancer, endobronchial sonography provides important data (Herth et al. 2002a). In complete bronchial obstruction, the base and the surface of the tumor can be assessed as can whether the different layers of the bronchial wall are involved, how far the tumor is penetrating into the mediastinal structures and whether the airways beyond the stenosis are patent. Also patency of the adjacent pulmonary artery can be diagnosed, which is important to predict postinterventional perfusion of the dependent lung and prevent increase of dead-space ventilation (Fig. 6.4). Endobronchial sonography is also useful for exploration of benign central airway stenosis to assess the extent and the cause of the disease, the relationship to vessels and other surrounding structures and to make the correct decision for therapy, such as mechanical dilatation, laser ablation or stent implantation and endoscopic control of the results Fig. 6.7a–c.

6.4 Indications and Results for the Endobronchial Sonography Transbronchial Needle Aspiration Scope

The lymph node staging is also the main indication for the new endobronchial sonography TBNA scope.

The sonography bronchoscope is introduced via an endotracheal tube under visual control or under local

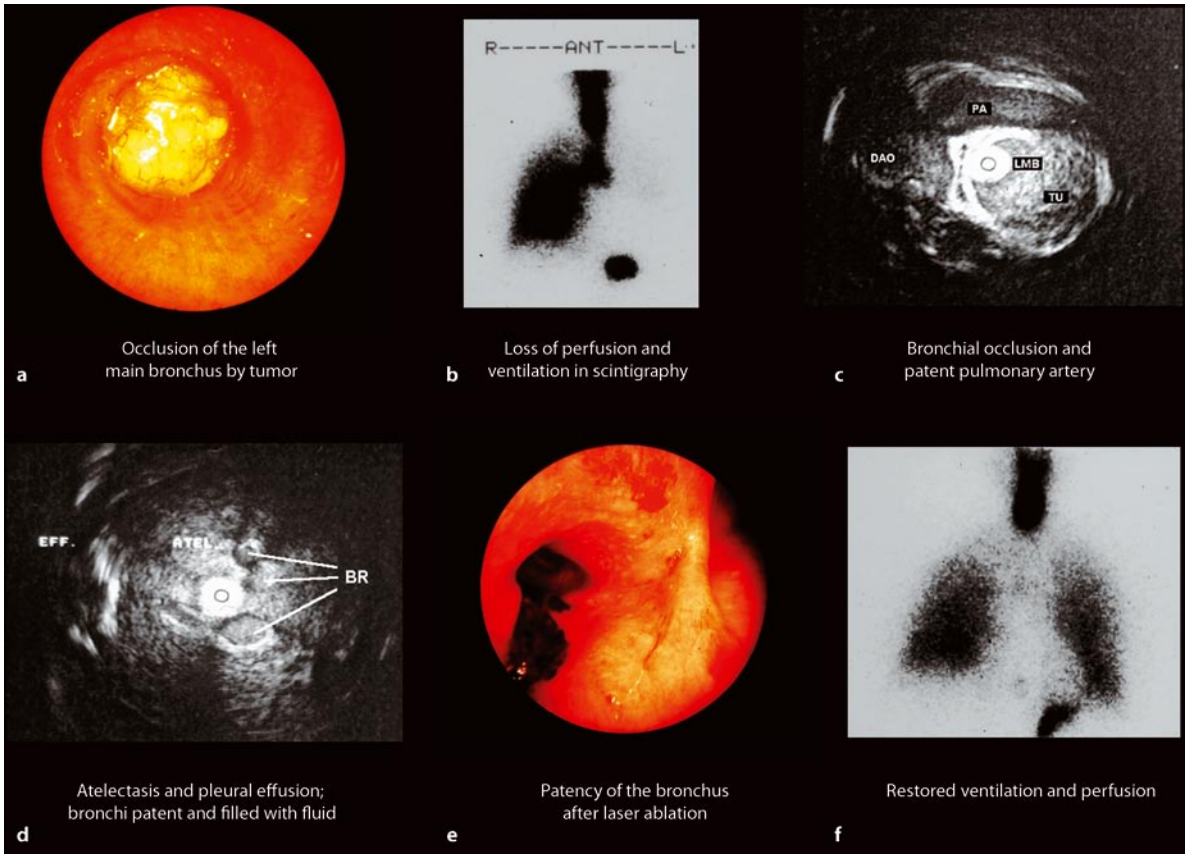

Fig. 6.5a–f Local staging of an advanced tumor. *DAO* descending aorta, *PA* pulmonary artery, *TU* tumor, *LMB* left main bronchus

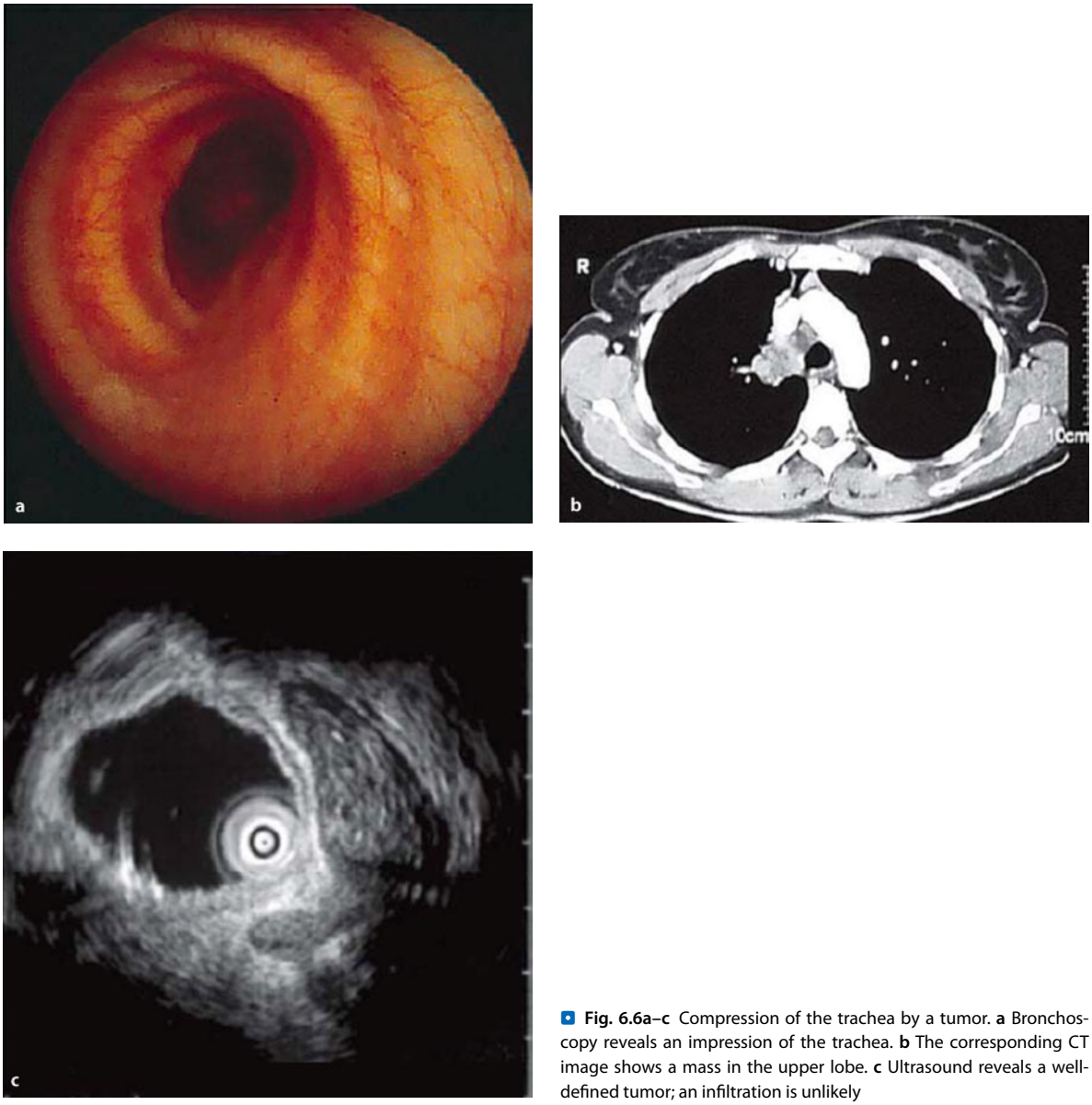

Fig. 6.6a–c Compression of the trachea by a tumor. **a** Bronchoscopy reveals an impression of the trachea. **b** The corresponding CT image shows a mass in the upper lobe. **c** Ultrasound reveals a well-defined tumor; an infiltration is unlikely

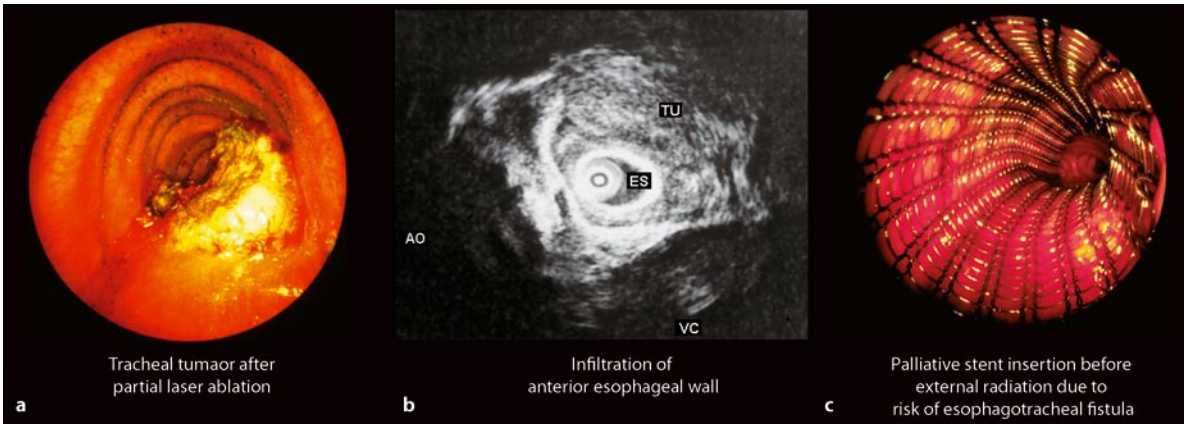

Fig. 6.7a–c Tumor in the trachea, after partial laser resection an infiltration in the esophageal wall is detected by EBUS and a stent was placed before the additional treatment

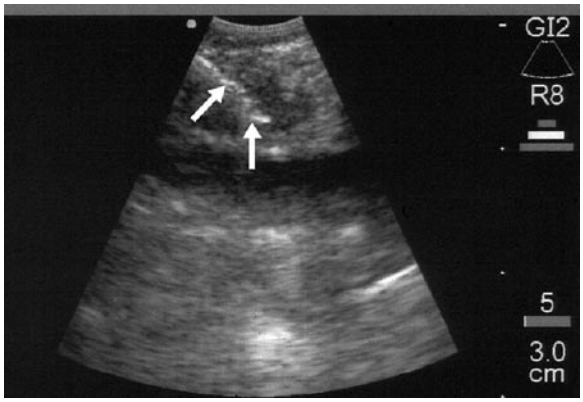

Fig. 6.8 Ultrasound-controlled lymph node puncture. The needle is clearly deliniated in the lymph node

anaesthesia to the area of interest. Endobronchial sonography TBNA is performed by direct transducer contact with the wall of the trachea or bronchus. When a lesion is outlined, a prototype 22-gauge full-length steel needle is introduced via the biopsy channel of the endoscope. Power-Doppler examination was used immediately before the biopsy in order to avoid unintended puncture of vessels between the wall of the bronchi and the lesion. Under real-time sonographic guidance the needle was placed in the lesion Fig. 6.8. Suction was applied with a syringe and the needle was moved back and forth inside the lesion.

To date, several papers have been published on this procedure.

The largest trial (Herth et al. 2006b) reports the results of the technique in 502 patients. A total of 572 lymph nodes were punctured, and 535 (94%) resulted in a diagnosis. Biopsies were taken from all reachable lymph node stations (2l, 2r, 3, 4r, 4l, 7, 10r, 10l, 11r and 11l). The mean diameter of the nodes was 1.6 cm (0.36 cm) and the range was 0.8–3.2 cm. The sensitivity was 92%, the specificity was 100% and the positive predictive value was 93%. Like in all other trials no complications occurred.

Herth et al (2006c) also examined the accuracy of endobronchial sonography TBNA in sampling nodes less than 1 cm in diameter. Among 100 patients, 119 lymph nodes with a size between 4 and 10 mm were detected and sampled. Malignancy was detected in 19 patients but missed in two others; all diagnoses were confirmed by surgical findings. The mean diameter of the punctured lymph nodes was 8.1 mm. The sensitivity of endobronchial sonography TBNA for detecting malignancy was 92.3%, the specificity was 100% and the negative predictive value was 96.3%. Again no complications occurred. They summarized that endobronchial sonography TBNA can sample even small mediastinal nodes, therefore avoiding unnecessary surgical exploration in one fifth of patients who have no computed tomography evidence of mediastinal disease. Potentially operable patients with clinically nonmetastatic non-small-cell lung cancer may benefit from presurgical endobronchial sonography TBNA biopsies and staging.

6.5 Summary

Endobronchial sonography has been widely available for more than 5 years. A growing body of good-quality literature supports its significant role in airway assessment and procedure guidance. Its usefulness is especially well documented in lymph node staging via guided TBNA and in lending support for therapeutic decision-making with regard to endoluminal or alternative treatment strategies for malignant airway abnormalities.

Endobronchial sonography is a routine adjunct to endoscopy in many centers, and we expect its role to grow in the near future.

References

Herth F, Becker HD (2000) Endobronchial ultrasound of the airways and the mediastinum. Monaldi Arch Chest Dis 55(1):36–45

Herth F, Becker HD (2003) EBUS for early cancer detection. J Bronchol 10:249–253

Herth F, Ernst A, Becker HD (2002a) Endobronchial ultrasound in therapeutic bronchoscopy. Eur Respir J 20:118–121

Herth F, Ernst A, Becker HD (2002b) Endobronchial ultrasound (EBUS) guided transbronchial lung biopsy (TBBX) in solitary pulmonary nodules and peripheral lesions. Eur Respir J 20:972–975

Herth FJ, Ernst A, Schulz M, Becker HD (2003) Endobronchial ultrasound reliably differentiates between airway infiltration and compression by tumor. Chest 123:458–462

Herth F, Becker HD, Ernst A (2004) Conventional vs endobronchial ultrasound-guided transbronchial needle aspiration: a randomized trial. Chest 125:322–325

Herth FJ, Eberhardt R, Becker HD, Ernst A (2006a) Endobronchial ultrasound-guided transbronchial lung biopsy in fluoroscopically invisible solitary pulmonary nodules: a prospective trial. Chest 129:147–150

Herth FJF, Eberhardt R, Vilman P, Krasnik M (2006b) EBUS-TBNA—a new device for endoscopic transbronchial real time ultrasound guided biopsy for diagnosis and staging of mediastinal lymph nodes. Thorax 61:795–798

Herth FJF, Krasnik M, Eberhardt R, Ernst A, Vilman P, Dienemann H (2006c) EBUS guided biopsy for the staging of mediastinal lymph nodes in a radiologically normal mediastinum. Eur Respir J 28:910--914

Hürther T, Hanrath P (1992) Endobronchial sonography: feasibility and preliminary results. Thorax 47:565–567

Krasnik M, Vilmann P, Larsen SS, Jacobsen GK (2003) Preliminary experience with a new method of endoscopic transbronchial real time ultrasound guided biopsy for diagnosis of mediastinal and hilar lesions. Thorax 58:1083–1086

Kurimoto N, Murayama M, Yoshioka S (1999) Assessment of usefulness of endobronchial ultrasonography in tracheobronchial tumor invasion. Chest 115:1500–1506

Miyazu Y, Miyazawa T, Kurimoto N, Iwamoto Y, Kanoh K, Kohno N (2002) Endobronchial ultrasonography in the assessment of centrally located early-stage lung cancer before photodynamic therapy. Am J Respir Crit Care Med 165:832–837

Shirakawa T, Imamura F, Hamamoto J, Honda I, Fukushima K, Sugimoto M, Shirkakusa T (2004) Usefulness of endobronchial ultrasonography for transbronchial lung biopsies of peripheral lung lesions. Respiration 71:260–268

Sihoe AD, Yim AP (2004) Lung cancer staging. J Surg Res 117:92–106

7 Vascularization

C. Görg

7.1 Introduction

In addition to the sonographic characteristics of the B-mode image, the type of vascularization is of major importance for assessment of a lesion in terms of differential diagnosis. In sonographic examinations, the established procedures of color-Doppler sonography and, since recently, contrast-assisted sonography are used for this purpose.

However, the definitive value of color-Doppler sonography and contrast-assisted sonography for the diagnosis of solid peripheral consolidations in the lung, compared with other sectional imaging procedures for the chest, is yet to be fully established. In the last few years the color-Doppler sonography characteristics of bacterial pneumonia, obstructive atelectasis, lung infiltrates and bronchial carcinoma have been described (reviewed in Görg and Bert 2004a, b). Preliminary studies show that contrast-assisted sonography can be performed on the chest. Various diseases of the lung are characterized by specific contrast-assisted sonography findings (reviewed in Görg and Bert 2006a).

The purpose of the present chapter is to describe color-Doppler sonography and contrast-assisted sonography findings in the presence of peripheral lung consolidations.

7.2 Pathophysiological Principles

The lung is characterized by dual vascularization. Perfusion is achieved on the one hand by lung circulation, which is responsible for pulmonary gas exchange. Lung circulation is accomplished by the pulmonary arteries and their ramifications as well as venules and lung veins. The lung itself is nourished by the bronchial arteries.

In contrast to systemic circulation, circulation by the pulmonary arteries is marked by specific characteristics. Pulmonary arteries and their initial branches are elastic. The subsequent arteries have muscular walls. From the level of the arterioles onward, these arteries turn into partly muscular and nonmuscular precapillaries. In contrast to systemic circulation in which arterioles are the main vessels of resistance, in lung circulation the resistance is more or less equally distributed between arteries, capillaries and veins. Thus, flow in the pulmonary arteries and capillaries is pulsatile and not continuous. In contrast to hypoxic vasodilatation in systemic circulation, hypoxic vasoconstriction occurs in lung circulation. The purpose of such vasoconstriction is to reduce the intrapulmonary shunt volume (Euler–Liljestrand mechanism). When lung tissue is affected by a malignant tumor, the carcinoma has been reported to invade the pulmonary arteries of the affected lung segment in 56–87% of cases (Kolin and Koutllakis 1988; Fissler-Eickhoff and Müller 1994). Particularly in the center of the tumor the regular vascular pattern is completely altered. Vascularization is reduced by stenosis and occlusion of the pulmonary arteries.

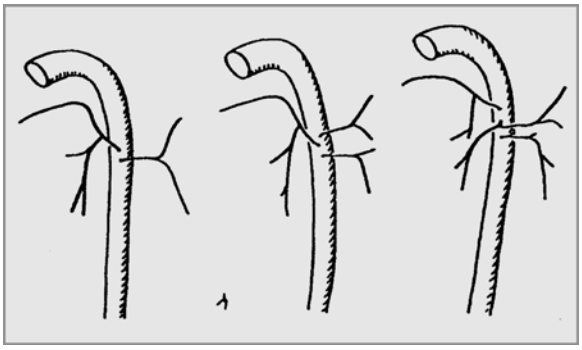

Fig. 7.1 The anatomy of the bronchial arteries. (After Uflacker et al. 1985)

As a rule the bronchial arteries originate on the left side from the aortic arch and on the right side from the intercostal artery. They form a vascular ring at the hilum of the lung. From this vascular ring the branches run parallel to the bronchial branches and the pulmonary vessels (Fig. 7.1). The bronchial branches (rami bronchiales) supply the bronchi, pulmonary vessels, alveoles and supporting tissue. Interstitial branches run into the interlobar and interlobular septa and supply the visceral pleura. Anastomoses (blocked arteries) between the two systems are normally closed. In cases of occluded pulmonary vessels, the anastomoses become open owing to hypoxia and blood supply is provided by bronchial arteries. Angiographic studies have shown that particularly peripheral lung processes at the pleural wall, such as benign cavitary lesions, lung cysts, lung abscesses and liquefying pneumonia, are nourished by bronchial arteries (Görg and Bert 2004a). However, malignant primary lung tumors and lung metastases are vascularized by bronchial arteries to a differing extent (Müller and Meyer-Schwickerath 1978; Fig. 7.2).

The intercostal arteries originate from the thoracic aorta and run a strictly intercostal course in the chest wall along the ribs. They are the only vessels that can be visualized on sonography, even in healthy volunteers. Particularly in cases of lesions in the chest wall these vessels play an important role in tumor vascularization.

Tumor neoangiogenesis of primary bronchial carcinomas mainly originates in the bronchial arteries. The neoangiogenesis potential of pulmonary vessels appears to be low (Müller and Meyer-Schwickerath 1978; Hsu et al. 1996).

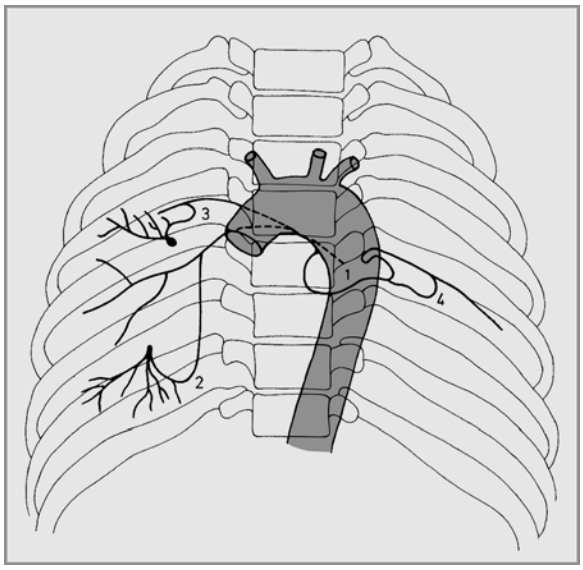

Fig. 7.2 The pathophysiology of the supply of the bronchial arteries. *1* Bronchobronchial anastomoses, *2* bronchopulmonary anastomoses, *3* intercostopulmonary anastomoses, *4* intercostobronchial anastomoses. (After von Babo et al. 1979)

7.3 Principles of Color-Doppler Sonography

The hemodynamic parameters used in transcutaneous color-Doppler sonography at the chest to evaluate vessels can be divided into qualitative and semiquantitative parameters:

1. Qualitative findings of parenchymal vascularization
   (a) Absence of flow signals
   (b) Individual flow signals
   (c) Pronounced flow signals
   (d) Arterial turbulence phenomena
2. Spectral curve analysis: patterns of different arterial flow signals
   (a) Pulmonary artery
   (b) Bronchial artery
   (c) Intercostal artery
   (d) Tumorneoangiogenesis
3. Contrast-enhanced sonography
   (a) Time to enhancement
      • Pulmonary arterial phase
      • Bronchial arterial phase
   (b) Extent of enhancement

Qualitative findings include assessment of the presence, the direction and the characteristics of blood flow. In this regard a distinction is made between the absence of flow signals (Fig. 7.3), evidence of individual flow signals (Fig. 7.4), evidence of markedly disorganized vascularization (Fig. 7.5) or pronounced tree-shaped vascularization (Fig. 7.6), and evidence of arterial turbulence phenomena in consolidated areas (Fig. 7.7). Semiquantitative parameters such as the resistance index and the pulsatility index are used for spectral curve analysis of arterial blood flow. Spectral curves of pulmonary arteries, bronchial arteries, intercostal arteries and arteries of tumor angiogenesis can be differentiated within pathological processes, and can be used to differentiate ambiguous peripheral lung lesions. In principle, evidence and documentation of flow signals at the chest is device-dependent and is additionally influenced and limited by the location and the size of the lesion, its cause, and breath-dependent or pulsation-dependent movements. For instance, 20% of peripheral lung lesions emit no flow signals (Yuan et al. 1994). Local fluid, lung cysts and lung infarctions show no flow signals on color-Doppler sonography. The color-Doppler sonography pattern of poorly visualized vessels is primarily seen in malignant pleural lesions. Markedly ramified vessels are characteristic for pneumonia and atelectasis (Yuan et al. 1994; Civardi et al. 1993). Turbulence phenomena within a lesion have been reported in pleural arteriovenous fistulae and vascular abnormalities in connection with Osler's disease.

Quantitative parameters such as the resistance index and the pulsatility index are used to analyze arterial spectral curves. Civardi et al. (1993) were the first to perform quantitative and qualitative spectral curve analyses for peripheral lung lesions. They found a triphasic flow signal more commonly in benign lesions and a monophasic flow signal in malignant lesions. Yuan et al. (1994) registered a sensitivity and specificity of more than 95% for differentiation of benign lesions from malignant ones by the use of arterial spectral curve analysis. The authors interpreted the monophasic low-impedance flow primarily seen in tumors as flow signals of tumor neoangiogenesis, while they correlated the high-impedance flow of pneumonias and atelectases with vessels of the pulmonary arteries (Yuan et al. 1994). In a subsequent study the authors registered different resistance indices for atelectasis and pneumonia, indicative of differing vasoconstriction due to hypoxia (Yuan et al. 2000). In a controlled histological study, Hsu et al. (1996) were the first to show that the vessels from which low-impedance monophasic flow signals originated were not tumor vessels but were bronchial arteries. "True" tumor vessels are characterized by nearly constant flow without variations between the systolic and the diastolic phase (Hsu et al. 1996). Owing to the technical limitations of commercially available ultrasound devices for slow blood flow (less than 2 cm/s), tumor vessels are usually not seen on sonography (Harvey

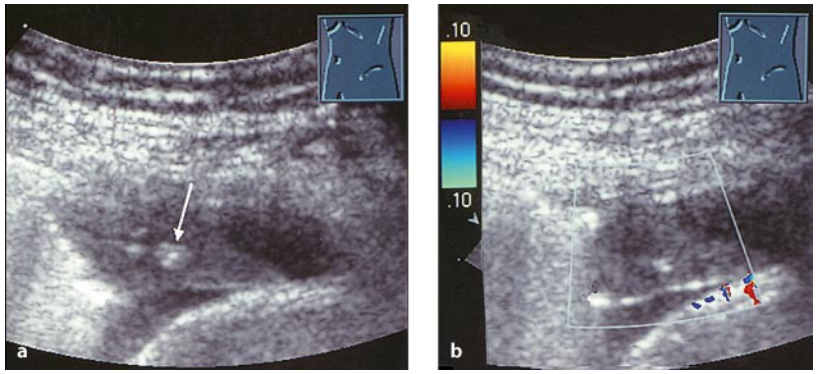

Fig. 7.3 A 43-year-old man with a lung infarction. **a** On the B-mode image one finds a hypoechoic wedge-shaped lesion with a central bronchial reflex (*arrow*). **b** Color-Doppler sonography shows the absence of vascularization

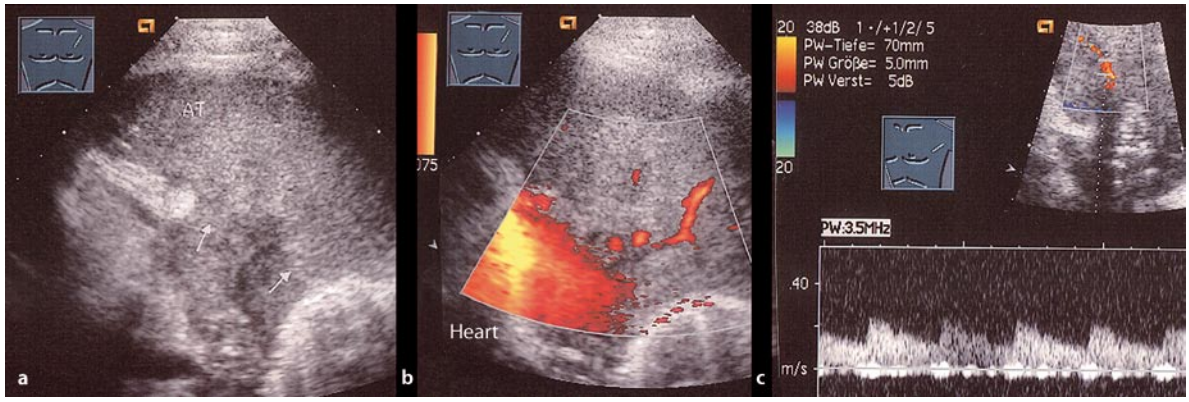

Fig. 7.4 A 36-year-old man with Hodgkin's disease in the mediastinum. **a** On the B-mode image one finds a hypoechoic central tumor formation with atelectasis (*AT*; *arrows*). **b** Color-Doppler sonography shows limited vascularization within the atelectasis, which is a sign of constriction of the pulmonary artery. **c** Spectral curve analysis shows a monophasic flow signal with reduced arterial flow resistance, indicative of a bronchial artery

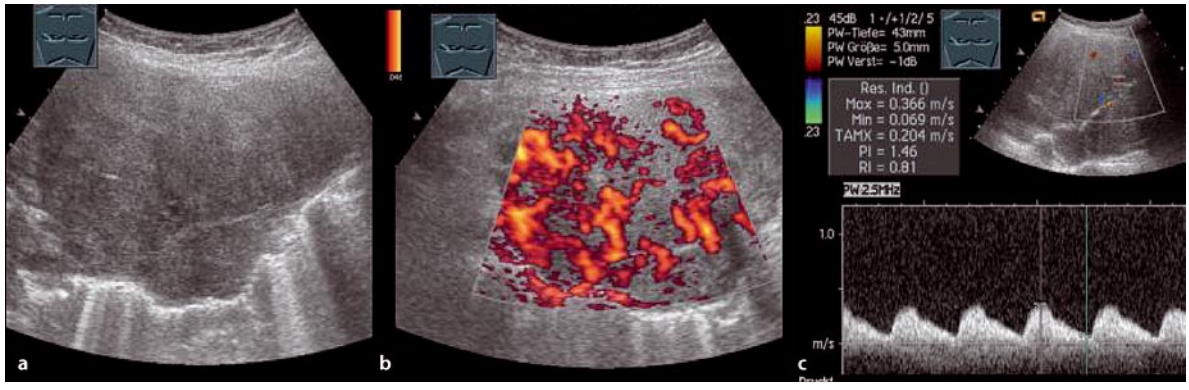

Fig. 7.5 A 62-year-old man with lung metastases in the presence of renal cell carcinoma **a** The B-mode image reveals a large hypoechoic round lesion. **b** Color-Doppler sonography shows strong and disorganized vessels. **c** Spectral curve analysis shows a monophasic flow signal indicative of a bronchial artery

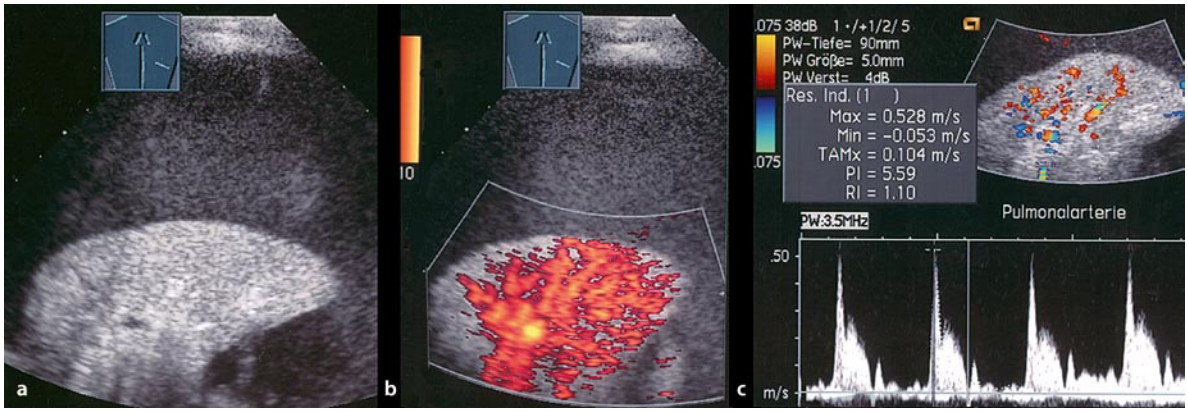

Fig. 7.6 A 37-year-old man with a pleural effusion and compressive atelectasis. **a** The B-mode image reveals a pleural effusion with atelectasis in the lung. **b** Color-Doppler sonography shows ramified vascularization. **c** Spectral curve analysis shows a high-impedance flow pattern, indicative of a pulmonary artery

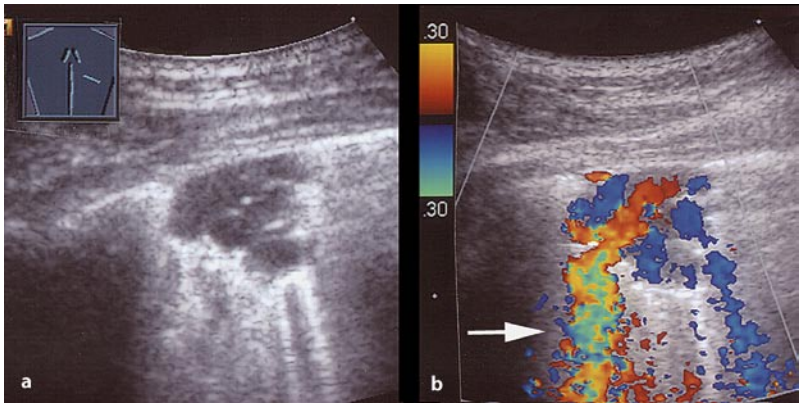

Fig. 7.7 A 14-year-old male patient with Osler–Weber–Rendu syndrome. **a** The B-mode image shows an anechoic space-occupying lesion close to the pleura. **b** Color-Doppler sonography reveals a large vessel that supplies the ectatic vessels close to the pleura. On spectral curve analysis this vessel was identified as a pulmonary artery

and Albrecht 2001). In a subsequent study, Hsu et al. (1998) registered a much lower sensitivity and specificity of 53 and 72% for differentiation of benign lesions from malignant ones by the use of arterial spectral curve analysis. A common feature of all of these studies is that the authors only used one arterial spectral curve pattern to analyze a lesion. By sonographic "mapping," the authors of a more recent study were able to demonstrate several different flow signals within a lesion in nearly half of the patients with pleural lesions examined (Görg et al. 2003; Fig. 7.8). This may be interpreted as an indication of the fact that arterial blood supply to peripheral lung lesions is a complex phenomenon. In a subsequent study, chest wall lesions were examined with the aid of arterial spectral curve analysis and were found to be vascularized by intercostal arteries among other sources (Görg et al. 2005a). However, intercostal arteries have a monophasic high-impedance flow signal.

Thus, the following flow signals may be distinguished with the aid of arterial spectral curve analysis (Fig. 7.9):

1. *Pulmonary arteries* may be present in various locations, run a centrifugal course from the hilum to the surface of the lung and have a high-impedance, usually triphasic flow signal.
2. *Bronchial arteries* are present in various locations, vary in terms of their direction of flow and have a low-impedance monophasic flow signal.
3. *Intercostal arteries* are characterized by their strictly intercostal location, run a nearly horizontal course and have a high-impedance, usually monophasic flow signal.
4. Arterial vessels of *tumor neoangiogenesis* are present in various locations, vary in terms of their direction of flow and are marked by a nearly constant flow with no variation between the systolic and the diastolic phase (Fig. 7.10).

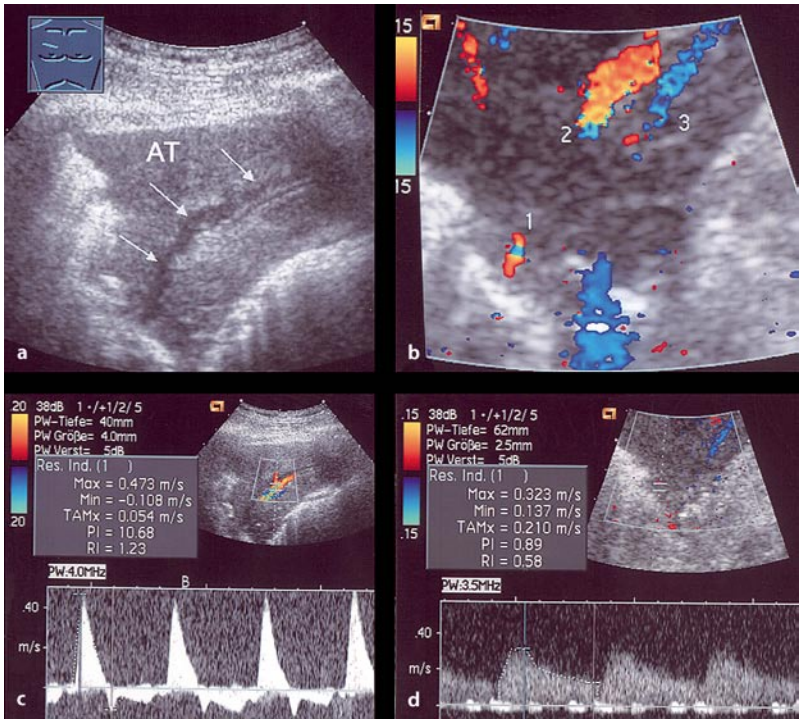

Fig. 7.8 A 65-year-old man with a centrally located bronchial carcinoid tumor and obstructive atelectasis. **a** The B-mode image shows a triangular hypoechoic consolidation with a fluid bronchogram (*arrows*). *AT* atelectasis. **b** Color-Doppler sonography reveals different vessels in the central region of the atelectasis (*1* bronchial artery, *2* pulmonary artery, *3* pulmonary vein). **c** Spectral curve analysis shows a high-impedance triphasic flow signal as a sign of a pulmonary artery (designated *2* in **b**). **d** Spectral curve analysis reveals a low-impedance arterial flow signal oriented towards the periphery, indicative of a bronchial artery (designated *2* in **b**)

7.4 Basic Principles of Contrast-Assisted Sonography

In the last few years contrast-assisted sonography has become a widely used procedure to investigate the liver, particularly to describe focal liver lesions. The second generation of contrast media now available for clinical use cause microscopic blisters in the vessel lumen which lead to enhanced redispersion of the ultrasound wave, thus increasing the signal amplitude and eventually yielding better contrast of vessels than that achieved with color-Doppler sonography. The use of contrast-assisted sonography allows infinitesimally small vessels whose width is just a little larger than that of capillaries to be visualized. In the experimental setting, vessels with a diameter of 74–134 µm were demonstrated by contrast-assisted sonography. Vessels smaller than 38 µm in diameter have not been visualized thus far even with the use of contrast medium. In principle, contrast-assisted sonography should be applied according to the guidelines of the EFSUMB (Albrecht et al. 2004).

With regard to the application of contrast-assisted sonography in the lung it should be noted that, as with all transcutaneous sonographic modalities, investigation of the healthy lung is not possible. However, like the liver, the lung is marked by dual arterial supply and is therefore predestined for the use of contrast-assisted sonography. Consolidated lung tissue can be examined with contrast-assisted sonography. Pathological lung lesions are first characterized by starting contrast enhancement. In cases of vascularization by the pulmonary arteries alone, this time point is marked by early arterial contrast enhancement about 1–6 s after application of contrast medium. The contrast medium can be demonstrated by sonography in the right side of the heart just a few seconds later. In cases of vascularization of a lesion by the bronchial arteries alone, contrast enhancement may be expected only after the contrast medium has passed through the lung. Thus, contrast enhancement of the left ventricle is seen at the earliest 7–10 s after application of contrast medium in the peripheral vein (Fig. 7.11). The extent of contrast enhancement is basically dependent on the presence or absence of vascularization, the type of vascularization—whether through the pulmonary arteries or through the bronchial arteries—and also by the presence of collaterals or vessels of tumor neoangiogenesis. Depending on

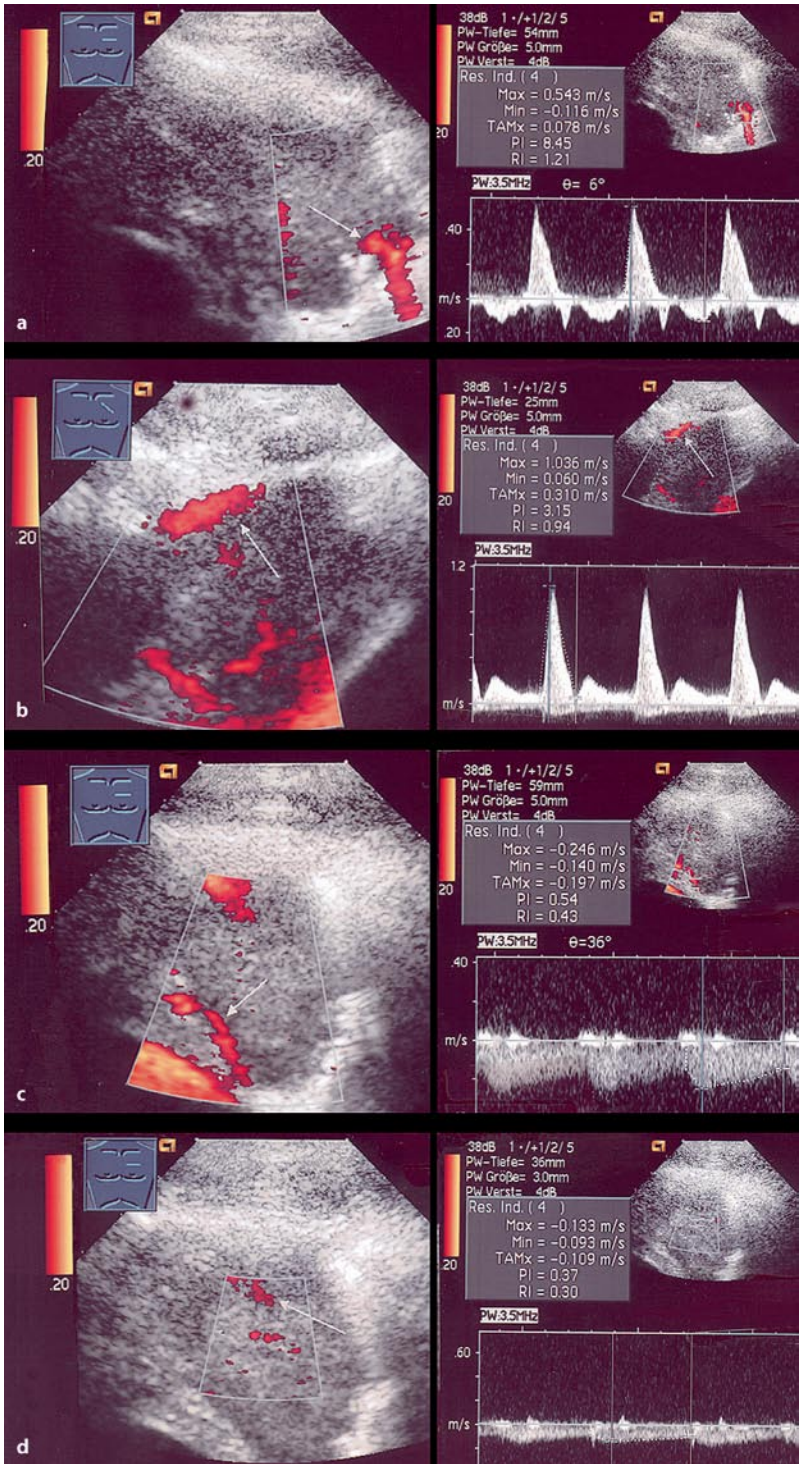

Fig. 7.9 A 31-year-old man with a malignant lymphoma affecting the lung. **a** Color-Doppler sonography shows a biphasic high-impedance flow pattern in the central portion of the consolidated lung—a sign of a pulmonary artery (*arrow*). **b** In the periphery of the tumor there is a monophasic high-impedance arterial flow pattern, typical of an intercostal artery (*arrow*). **c** In the central portion of the consolidated lung there is a monophasic low-impedance arterial flow signal—a sign of a bronchial artery (*arrow*). **d** Within the tumor one finds a nearly uniform flow signal without fluctuations in the diastolic and the systolic phase. Here one is inclined to suspect a vessel of tumor neoangiogenesis (*arrow*)

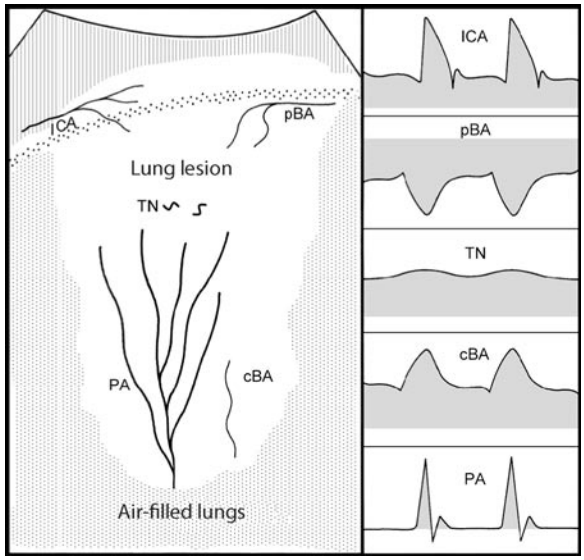

Fig. 7.10 Possible arterial supply of pulmonary lesions with corresponding spectral curves. *ICA* intercostal artery, *pBA* peripheral bronchial artery, *TN* tumorneoangiogenesis, *cBA* central bronchial artery, *PA* pulmonary artery

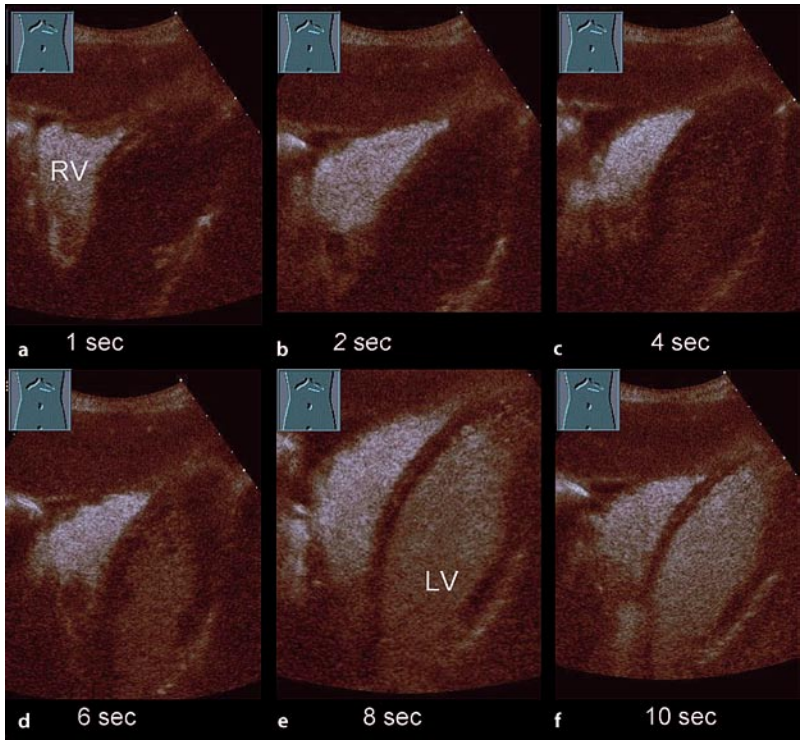

Fig. 7.11 Visualization of the time until contrast enhancement: four-chamber view in a healthy proband. After injection of contrast medium one sees contrast enhancement in the right ventricle as early as 1 s later (**a**–**d**). After 8 s there is contrast enhancement in the left ventricle (**e**,**f**)

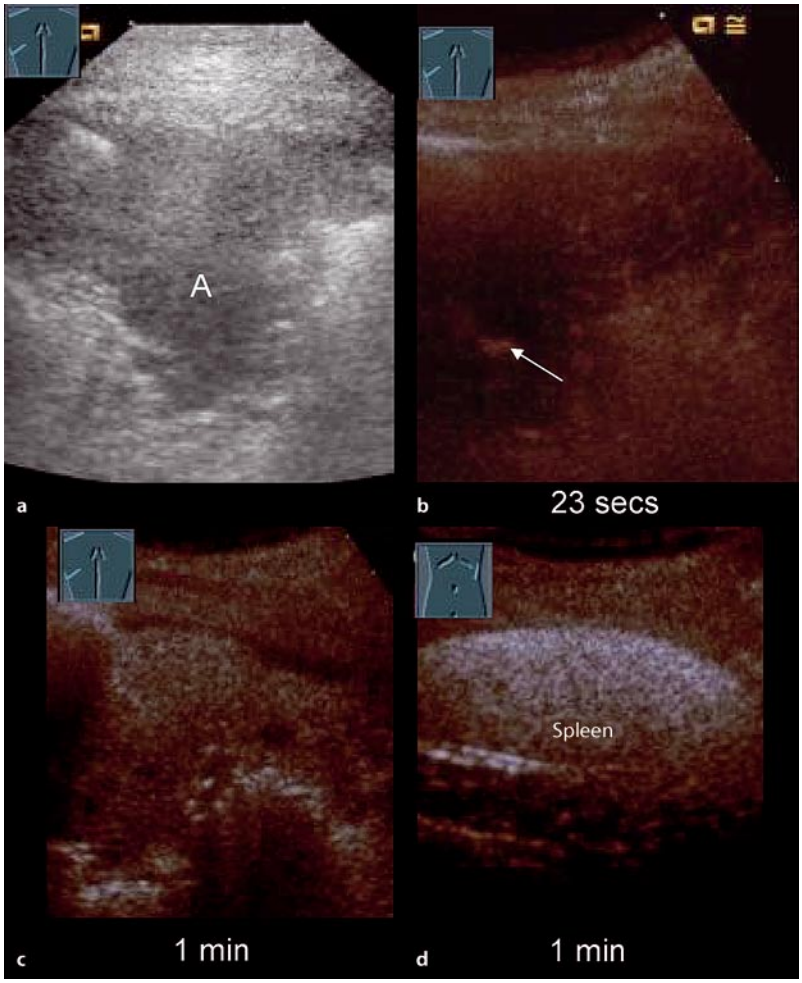

Fig. 7.12 A 24-year-old man with a pleural effusion and compressive atelectasis in the presence of amyloidosis. **a** On the B-mode image one finds a pleural effusion (*P*), an atelectasis (*AT*) and in subcostal location the spleen. **b–e** Contrast-assisted sonography shows early arterial contrast enhancement after 2 ss (**b**). The *arrow* marks the vessel with starting contrast enhancement. After 20 s there is marked contrast enhancement in the atelectatic tissue, which is hyperechoic compared with the parenchyma of the spleen (**c**). In the parenchymatous phase, after 3 min one finds continued strong contrast enhancement in the atelectasis (**d**), which is also seen after 7 min (**e**). This contrast behavior is indicative of vascularization purely through the pulmonary arteries

the phase, a distinction may be made between the arterial phase (1–30 s) and the parenchymatous phase (1–5 min). The extent of contrast enhancement has been quantified so far only in comparison with an intra-individual reference; a distinction is made between reduced and increased contrast enhancement. A parenchymatous organ such as the spleen is a suitable in vivo reference (Forsberg et al. 1999; Görg and Bert 2006b). The healthy spleen is known to be characterized by organ-specific contrast tropism and homogenous contrast enhancement. Pathological changes in the spleen are rare compared with those in the liver.

Thus, with the use of contrast-assisted sonography the following vascularization patterns can be distinguished:

1. Vascularization solely through pulmonary arteries is marked by a short period of time until the start of contrast enhancement and strong contrast enhancement compared with the situation for the spleen (Fig. 7.12).
2. Vascularization achieved purely through bronchial arteries is marked by a delay until the start of contrast enhancement and reduced contrast enhancement compared with the situation for the spleen (Fig. 7.13).

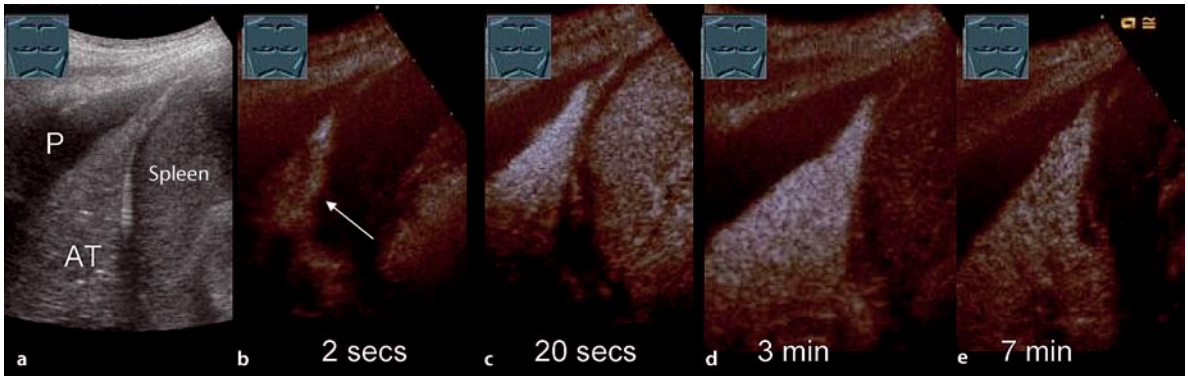

Fig. 7.13 An 80-year-old woman with a non-small-cell bronchial carcinoma (adenocarcinoma) of the left lung and evidence of atelectasis. **a** The B-mode image shows a wedge-shaped lesion with irregular margins, corresponding to atelectatic lung tissue. **b** After application of contrast medium, 23 s later one finds mild contrast enhancement in one vessel (*arrow*). **c** After 1 min one finds homogeneous contrast enhancement in the atelectatic lung tissue. **d** As a reference: very pronounced contrast enhancement in the spleen. This contrast behavior is indicative of vascularization exclusively by the pulmonary arteries

7.5 Predominantly Anechoic Peripheral Lung Consolidation

7.5.1 Color-Doppler Sonography

These lesions are rare and constitute an important differential diagnosis for localized effusion. Primary lung cysts at the pleural wall are seen on B-mode images as anechoic, usually polycystic tumors. Color-Doppler sonography shows qualitative flow signals in the septa and the region of the visceral pleura. On semiquantitative spectral analysis they show a monophasic pattern and thus correspond to bronchial and intercostal arteries (Fig. 7.14). Vascular tumors at the pleural wall, such as those associated with Osler's disease, have a characteristic appearance on color-Doppler sonography. The supplying pulmonary artery can be visualized (Fig. 7.6). The malignant cystic lung tumor shows centrally liquefied areas usually on a floor of liquefactions and is seen on the sonographic B-mode image as a semiliquid structure with septa in some cases. The tumor receives its blood supply from bronchial arteries, and more rarely from pulmonary arteries. Therefore, the spectral curve reveals a monophasic high-impedance arterial flow in keeping with bronchial arteries and occasionally a biphasic high-impedance arterial flow that corresponds to pulmonary arteries (Fig. 7.15). The aortic aneurysm at the dorsal wall of the pleura is a notable pitfall (Fig. 7.16); the same is true for the right lateral part of the heart at the chest wall in cases of cardiomegaly (Fig. 7.17).

7.5.2 Contrast-Assisted Sonography

Specific studies focusing on contrast-assisted sonography for the assessment of anechoic lung consolidations have not yet been published. Lung abscesses, pleural effusions, pleural empyema and liquefied lung tissue, however, are marked by the absence of contrast enhancement (Fig. 7.18).

7.6 Predominantly Echogenic Lung Consolidation

7.6.1 Lung Infarction

7.6.1.1 Color-Doppler Sonography

The lung infarction could be a correlate of pulmonary embolism. In the case of peripheral obstruction of branches of the pulmonary arteries and insufficient nourishment from the bronchial arteries the patient may develop intra-alveolar hemorrhage which is visualized morphologically on the B-mode image as displaced air (Mathis and Dirschmid 1993). On qualitative color-Doppler sonography the lesion characteristically shows the absence of flow signals (Fig. 7.1). On semiquantitative spectral analysis one occasionally finds a monophasic pattern close to the pleura; this pattern can be attributed to bronchial arteries. In some cases the disconnected supplying branch of the pulmonary artery is visualized.

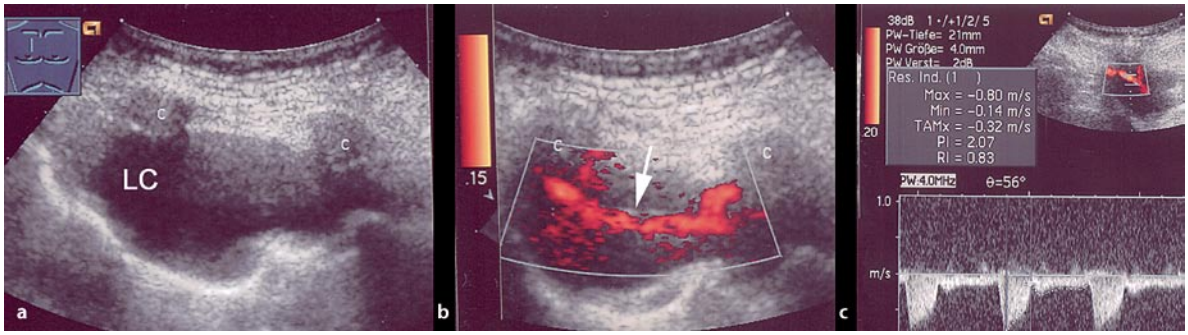

Fig. 7.14 A 70-year-old man with a primary lung cyst. **a** On the B-mode image one finds an anechoic lesion close to the pleura. *C* ribs, *LC* lung cyst. **b** Color-Doppler sonography in the power mode shows a strong vessel surrounding the lesion (*arrows*). **c** Spectral curve analysis demonstrates a monophasic high-impedance flow signal indicative of an intercostal artery

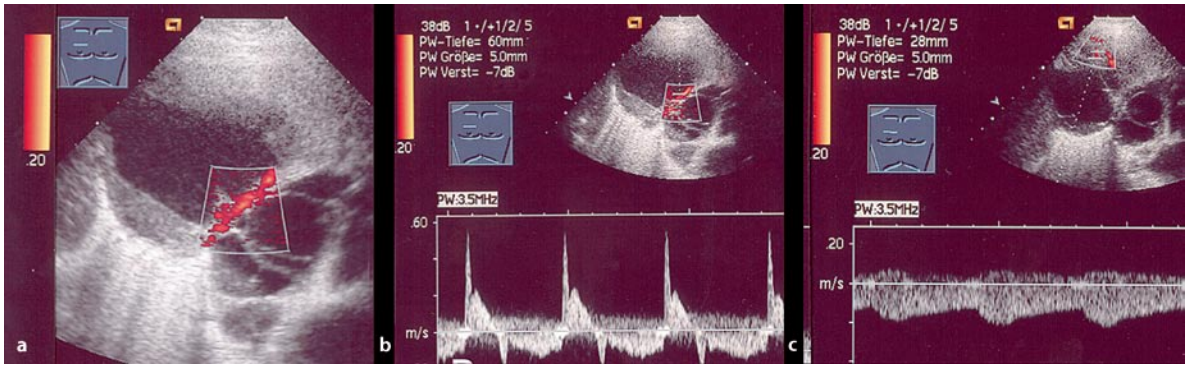

Fig. 7.15 A 44-year-old man with sarcoma of the lung. **a** Color-Doppler sonography shows a tumor with solid and cystic portions and vessels in the seventh course. **b** Spectral curve analysis reveals an arterial high-resistance flow signal. This is indicative of a pulmonary artery. **c** Visualization of a low-impedance flow signal in the margin of the lesion, indicative of a bronchial carcinoma

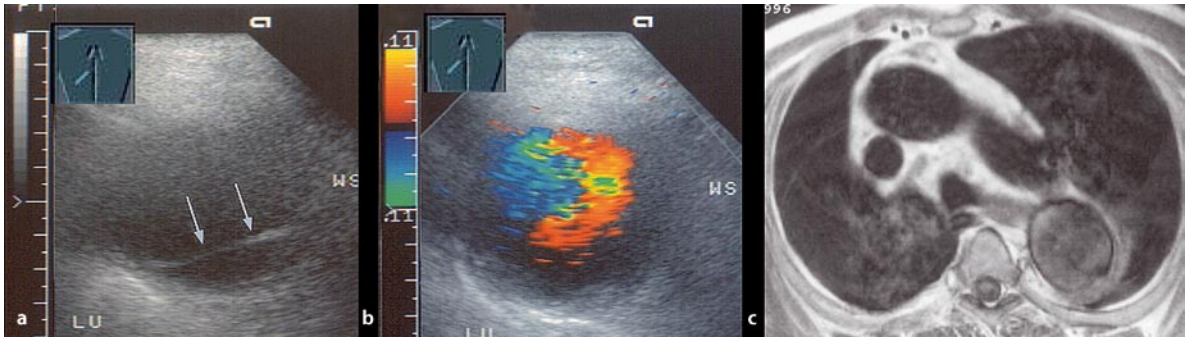

Fig. 7.16 A 49-year-old man with dissection of the aorta in the chest. **a** The B-mode image shows an anechoic septated round lesion close to the pleura (*arrow*). *LU* lung, *WS* spine. **b** Color-Doppler sonography reveals a turbulent flow pattern in the lesion, indicative of an aneurysm in the aorta. **c** The aneurysm in the aorta—on magnetic resonance tomography

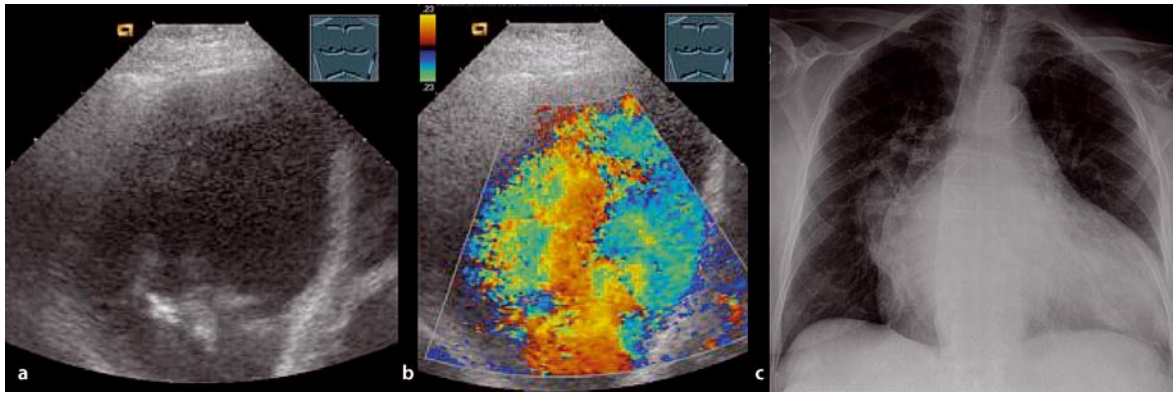

Fig. 7.17 A 78-year-old woman with dyspnea who came for puncture of a pleural effusion. **a** The B-mode image shows an anechoic space-occupying mass in the chest on the left side. **b** Color-Doppler sonography reveals a turbulent flow pattern within this lesion, indicative of the left ventricle being located at the chest wall. **c** The X-ray shows a large heart; the left ventricle is in contact with the lateral chest wall

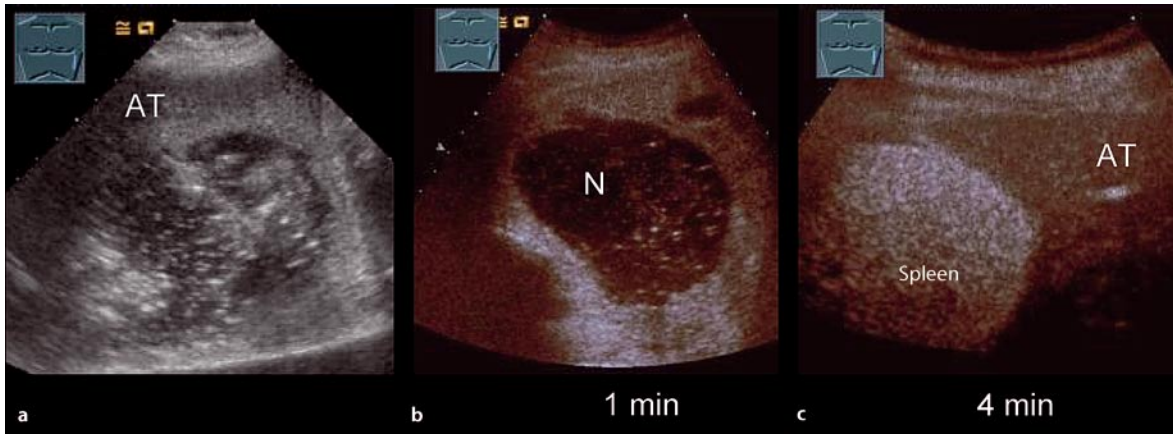

Fig. 7.18 A 54-year-old woman with a non-small-cell bronchial carcinoma **a** A consolidated lung on the left side, with a central anechoic content with air reflexes. **b** After 1 min the contrast investigation shows no contrast enhancement in the central portion of the consolidated lung, indicative of liquefaction. **c** On the left-sided intercostal section one finds regular contrast enhancement of the spleen. The atelectatic lung tissue of the left lower lobe shows reduced contrast enhancement compared with the spleen

7.6.1.2 Contrast-Assisted Sonography

In keeping with findings on color-Doppler sonography, lung infarctions/lung hemorrhages are marked by the absence of contrast enhancement on contrast-assisted sonography (Fig. 7.19). Occasionally one finds delayed and reduced contrast enhancement in the margins, which is indicative of vascular nourishment being provided by bronchial arteries (Fig. 7.20). It should be noted that contrast-assisted sonography allows the investigator to make a reliable distinction between vascularized and nonvascularized peripheral lung tissue and therefore possesses a potential for differential diagnosis in respect of delineating pleurisy or compressive atelectasis due to pleural effusion (Görg et al. 2006a; Fig. 7.21).

7.6.2 Pleurisy

7.6.2.1 Color-Doppler Sonography

The appearance of pleurisy on the B-mode image is similar to that of a lung infarction (Gehmacher et al. 1997). Depending on the size of the invasion, which is transformed into pleural pneumonia, the qualitative color-Doppler sonography characteristically shows pronounced vessels

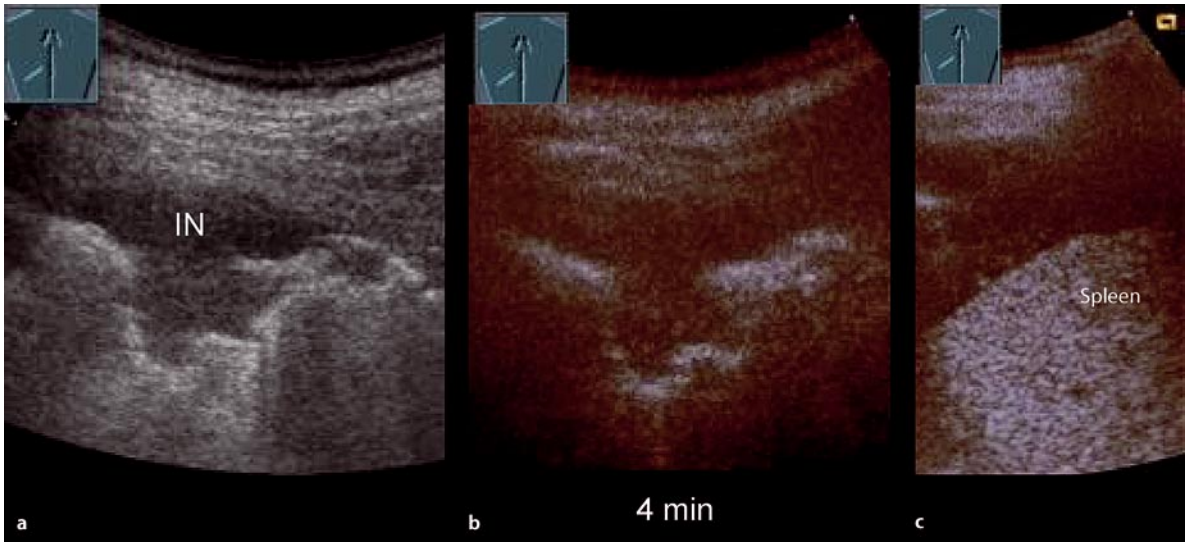

Fig. 7.19 A 32-year-old woman with a pulmonary embolism confirmed on computed tomography. **a** B-mode sonography shows a wedge-shaped homogeneous hypoechoic lung consolidation with irregular margins. **b** The contrast investigation reveals no contrast enhancement of the lesion. **c** The spleen as an in vivo reference shows regular contrast enhancement

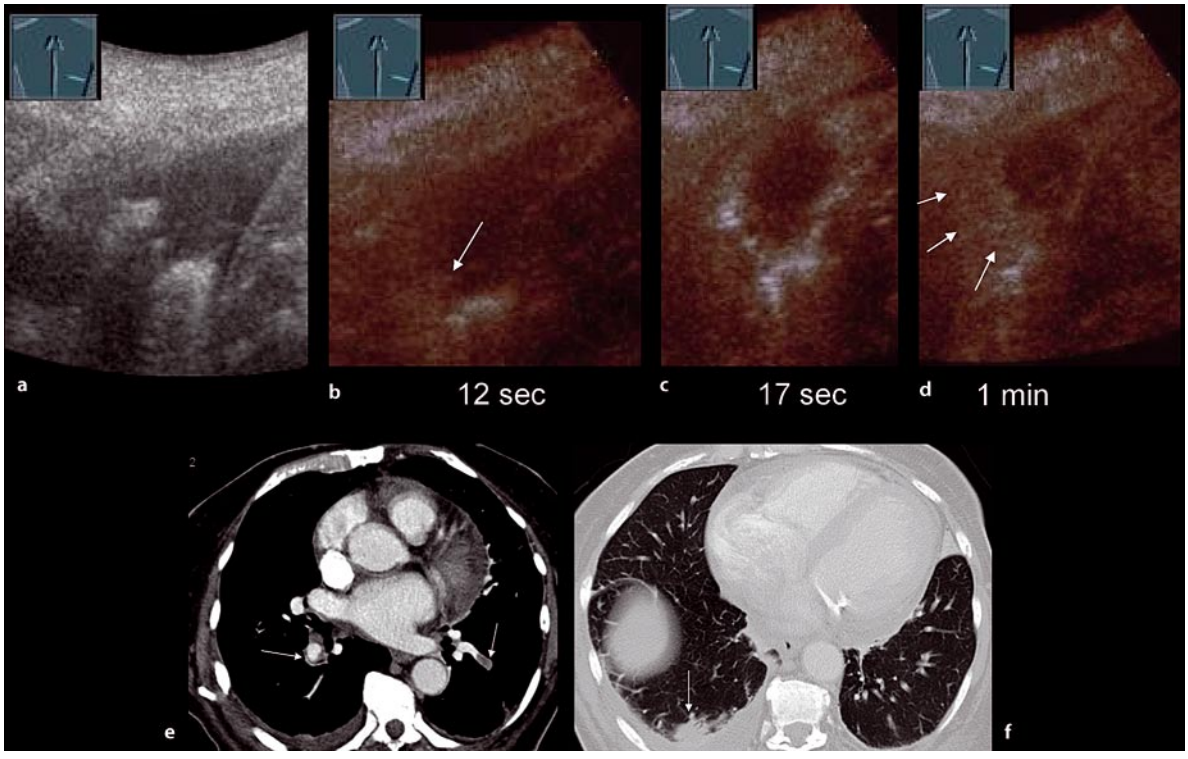

Fig. 7.20 A 71-year-old woman with a pulmonary embolism confirmed on computed tomography. **a** B-mode sonography reveals a wedge-shaped homogeneous hypoechoic consolidation with irregular margins in the right lower lobe. **b** In the early arterial phase, after 12 s there is starting contrast enhancement of peripheral vessels. The lesion shows no contrast enhancement. **c** After 17 s one finds contrast enhancement in the margins. The lesion itself shows no contrast enhancement. **d** After 1 min the lesion reveals contrast enhancement in the margins; only a small wedge of consolidated tissue reveals no contrast enhancement. **e** Computed tomography shows recesses in the branches of the pulmonary arteries on both sides (*arrows*). **f** The lung window reveals the defect in lung parenchyma in dorsal location on the right side

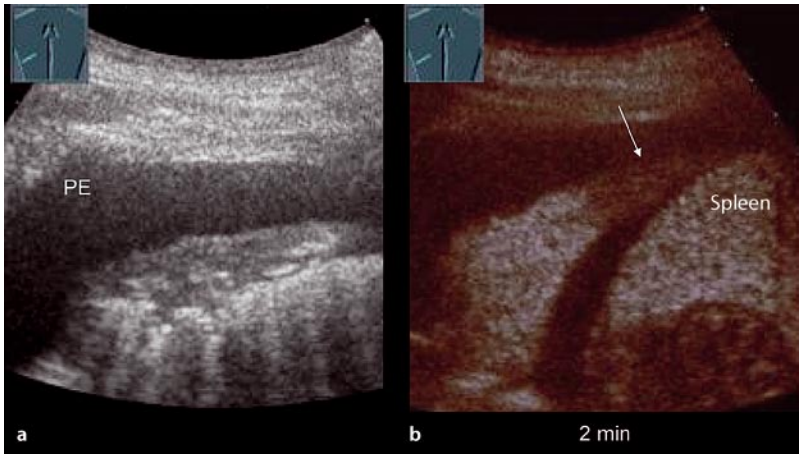

Fig. 7.21 A 45-year-old woman with pulmonary embolism confirmed by scintigraphy. **a** B-mode sonography shows a pleural effusion (*PE*) and a partial consolidation in the region of the dorsal lower lobe. **b** Contrast-assisted sonography shows isoechogenic contrast enhancement compared with the spleen. At the tip of the atelectasis one finds no contrast enhancement (*arrow*). This area is the actual peripheral lung embolism

with predominant evidence of an arterial high-impedance flow profile on spectral analysis such as that seen in branches of the pulmonary artery (Fig. 7.22).

7.6.2.2 Contrast-Assisted Sonography

In keeping with color-Doppler sonography findings, pleurisy takes very little time for contrast enhancement to start and is marked by strong contrast enhancement on contrast-assisted sonography. This is indicative of primary vascularization through pulmonary arteries (Fig. 7.23). The value of contrast-assisted sonography lies in its potential for differential diagnosis of nonvascularized peripheral lung lesions such as lung infarction, malignant lesions or scar tissue when the patient has respiration-related pain as the cardinal clinical symptom (Görg et al. 2005b).

7.6.3 The Peripheral Round Lesion

7.6.3.1 Color-Doppler Sonography

A peripheral round lesion of the lung at the wall of the pleura occurring as the cardinal symptom may be due to a benign or malignant lesion. Of decisive importance is the fact that, independent of the cause, the evidence of flow signals is dependent on the size of the lesion. On careful investigation one frequently finds arterial high-impedance flow signals from pulmonary arteries and low-impedance flow signals from bronchial arteries in benign as well as malignant peripheral lung lesions (Figs. 7.24, 7.25). In the published literature, poor visualization of vessels on qualitative color-Doppler sonography and evidence of arterial monophasic flow signals with low resistance indices are reported to be characteristic features of malignant peripheral lung tumors or metastases (Yuan et al. 1994; Hsu et al. 1996, 1998; Civardi et al. 1993). In some cases the vessels seen on sonography may be identified as those resulting from tumor neoangiogenesis (originating from bronchial arteries) on pathological investigation (Hsu et al. 1998; Fig. 7.9d). However, studies that have used a single impedance measurement to assess the benign or malignant nature of a lesion must be viewed with caution. In principle color-Doppler sonography is not suitable for distinguishing between benign and malignant peripheral round lesions.

7.6.3.2 Contrast-Assisted Sonography

In keeping with the variable findings on color-Doppler sonography, contrast-assisted sonography also shows a heterogeneous pattern of vascularization. Malignant lesions—whether lung metastases or peripheral bronchial carcinomas—are marked by delayed start of contrast enhancement and reduced extent of contrast enhancement. This is indicative of predominant vascularization through bronchial arteries (Fig. 7.26, Table 7.1). Depending on the underlying structure, however, lung metastases of renal cell carcinomas and frequently also metastases of malignant lymphoma show pronounced contrast enhancement (Fig. 7.27). Contrast-assisted sonography, like color-Doppler sonography, is not suitable for distinguishing between benign and malignant peripheral round lesions.

7.6.4 Large Lung Consolidation: Pneumonia

7.6.4.1 Color-Doppler Sonography

Pneumonia is seen on X-rays and sonography in conjunction with the principal finding of a peripheral lung consolidation at the pleural wall. On B-mode image sonogra-

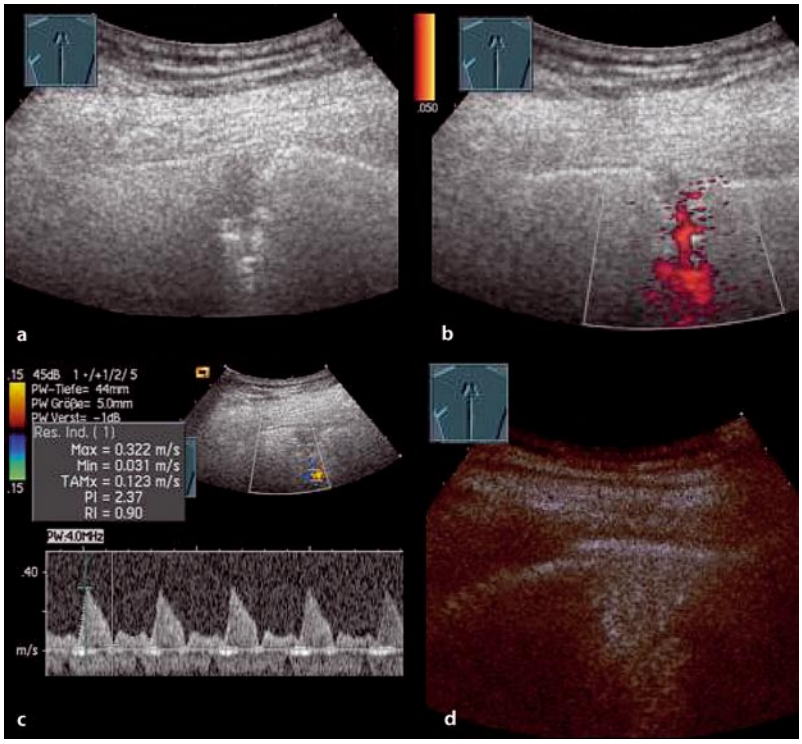

Fig. 7.22 A 55-year-old woman with respiration-related pain; suspected pleurisy **a** B-mode sonography shows a small wedge-shaped pleural defect. **b** Color-Doppler sonography shows vessels within the defect. **c** Spectral curve analysis reveals a high-impedance flow signal such as that seen in pulmonary arteries. **d** Contrast-assisted sonography shows contrast enhancement of the lesion such as that seen in the presence of pleurisy

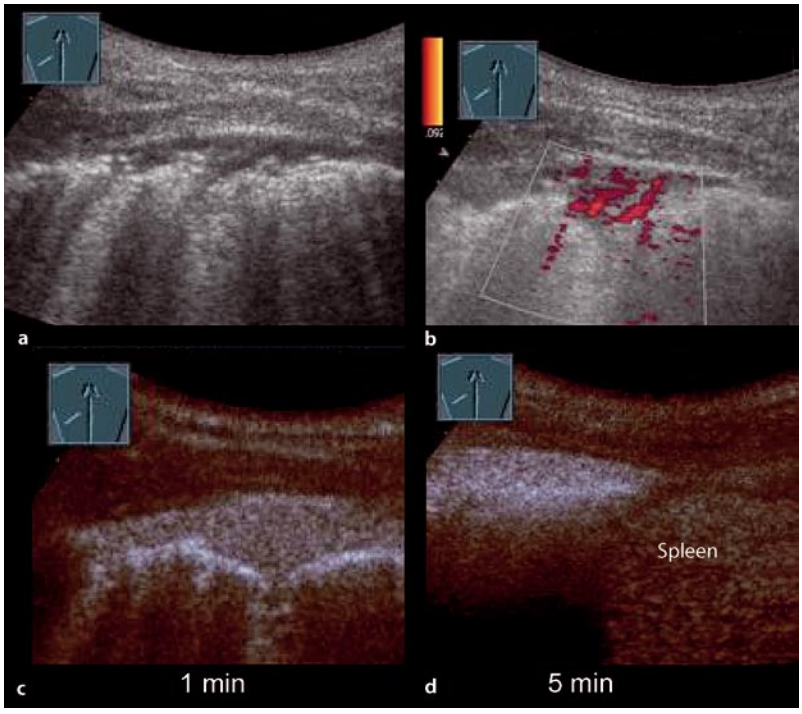

Fig. 7.23 A 15-year-old male patient with pain on breathing. **a** The B-mode image shows a long irregular initial echo in the region of the lower lobe of the left lung. **b** Color-Doppler sonography shows flow signals in the lesion. **c** Contrast-assisted sonography reveals marked contrast enhancement of the lesion. **d** In the late parenchymatous phase the lesion shows marked contrast enhancement compared with the spleen

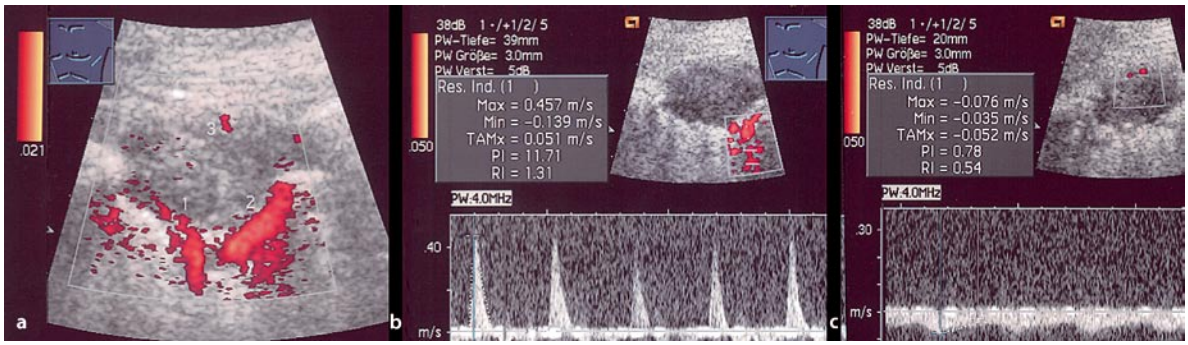

Fig. 7.24 A 56-year-old man with a plasmocytoma and histologically confirmed amyloidosis in the lung. **a** On color-Doppler sonography one finds several vessels. *1* pulmonary artery, *2* pulmonary vein, *3* bronchial artery. **b** Spectral curve analysis shows a high-impedance flow signal indicating a pulmonary artery (marked *1* in **a**). **c** Spectral curve analysis shows a low-impedance monophasic flow pattern oriented towards the hilum of the lung, as a sign of a bronchial artery close to the pleura (marked *3* in **a**)

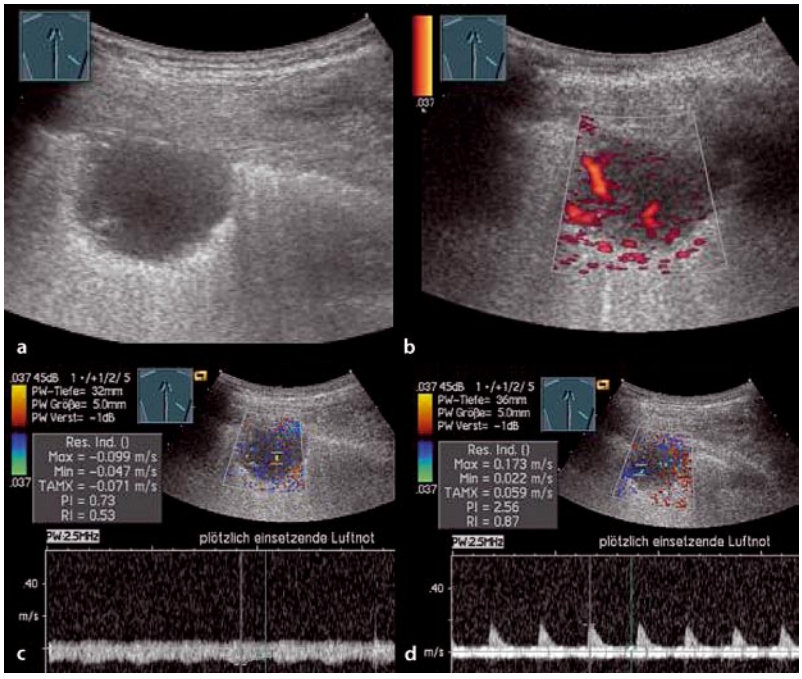

Fig. 7.25 A 30-year-old woman with sudden onset of dyspnea and fever. **a** B-mode sonography shows a peripheral hypoechoic round lesion of the lung. **b** On color-Doppler sonography one finds evident flow signals in the lesion. **c** Spectral curve analysis of a central vessel shows a low-impedance flow signal such as that seen in a bronchial artery. **d** Spectral curve analysis of a vessel from the margin shows a high-impedance flow signal such as that seen in pulmonary arteries. Under antibiotic therapy the lesion resolved completely

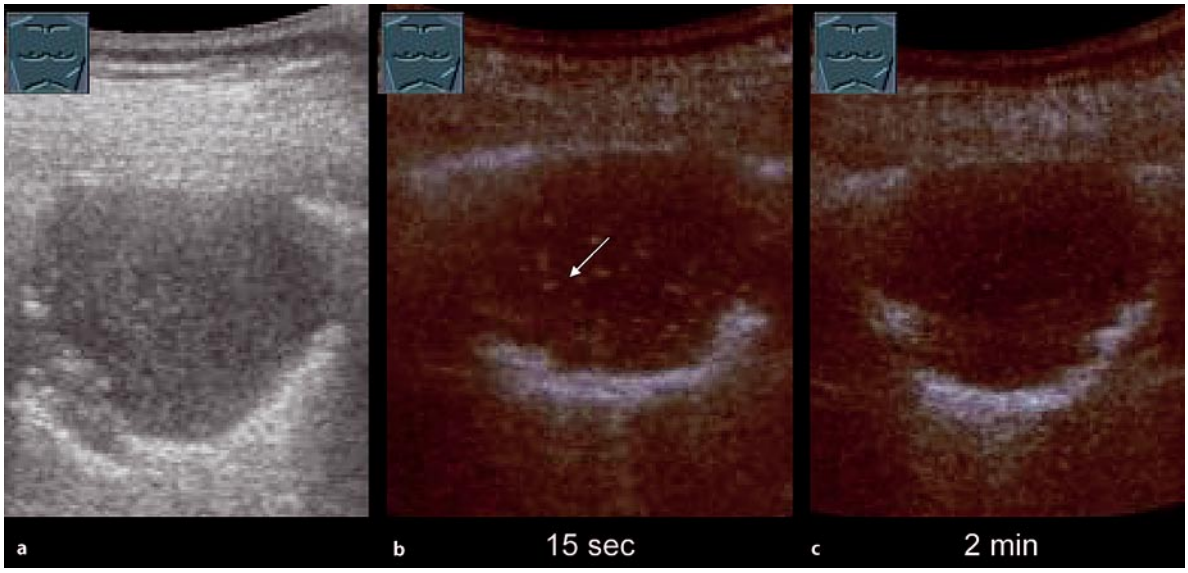

Fig. 7.26 A 55-year-old woman with small-cell bronchial carcinoma and lung metastases. **a** B-mode sonography shows a homogeneous hypoechoic lung lesion at the margin of the pleura. **b** On contrast-assisted sonography there is contrast enhancement in tumor vessels after 15 s, indicative of vascularization by the bronchial artery. **c** In the parenchymatous phase there is practically no contrast enhancement in the lesion

Table 7.1 Time to enhancement (short vs. delayed) and extent of enhancement (reduced vs. marked) in 137 patients with pleural-based pulmonary lesions subdivided into patients with pneumonia, compression atelectasis, pulmonary embolism, benign pleural-based lesions, central lung cancer and peripheral malignant lesions

	Pneumonia (*n*=32)		Compression atelectasis (*n*=17)		Pulmonary embolism (*n*=20)		Benign nodules (*n*=8)		Central lung cancer (*n*=31)		Peripheral malignant lesion (*n*=29)	
	Reduced EE	Marked EE	Reduced EE	Marked EE	Reduced EE	Marked EE	Reduced EE	Marked EE	Reduced EE	Marked EE	Reduced EE	Marked EE
Delayed TE	2	4	0	0	20	0	4	2	8	5	18	4
Short TE	6	20	0	17	0	0	1	1	6	12	5	2

After Görg et al. (2006b)

TE time to enhancement, *EE* extent of enhancement

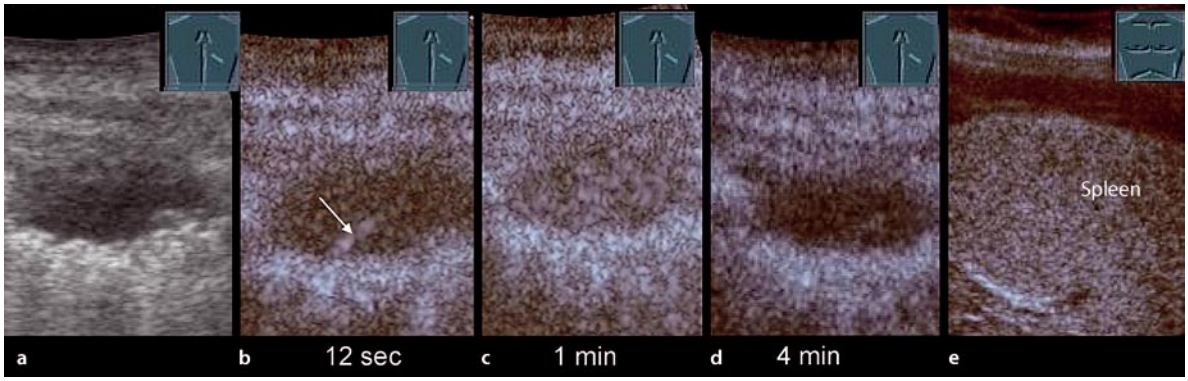

7

Fig. 7.27 A 53-year-old man with known Hodgkin's disease and multiple round lesions in the lung. **a** B-mode sonography shows an oval homogeneous hypoechoic lesion at the margin of the pleura. **b** On contrast-assisted sonography there is contrast enhancement in a vessel at the margin after 12 s—a sign of vascularization through the bronchial artery. **c** After 1 min there is homogeneous contrast enhancement of the lesion. **d** After 4 min the lesion shows no contrast enhancement. **e** On individual comparison the spleen shows homogeneous contrast enhancement

phy, pneumonia is seen as a more or less pronounced air bronchogram (Gehmacher et al. 1995), while a complete consolidation is seen as so-called lung hepatization. On color-Doppler sonography, pneumonia is marked by significantly ramified vessels that correspond to segmental branches of the pulmonary artery (Fig. 7.28). Here also, owing to hypoxia one frequently finds an arterial monophasic flow signal of central bronchial arteries in the invaded lung tissue (Fig. 7.29). In principle it should be noted that certain subtypes of adenocarcinoma may appear similar to pneumonia on the B-mode image and on color-Doppler sonography as well (Görg et al. 2002). Depending on the extent of hypoxic vasoconstriction in the pulmonary artery, the peripheral vascular tree of pulmonary arteries may not be visualized on qualitative color-Doppler sonography in the presence of advanced pneumonia. Bronchial arteries react to hypoxia by developing vasodilatation, as do all other arteries in the body. This explains the different resistance indices of pneumonia and atelectasis (Yuan et al. 2000). Thus, in the presence of lobar pneumonia parallel to the pulmonary arteries one occasionally finds an arterial monophasic flow pattern with low resistance indices, indicative of central bronchial arteries. The tuberculous infiltrate is a special phenomenon. It is characterized by marked vessels on color-Doppler sonography in terms of qualitative findings. On spectral analysis, however, it is seen as a monophasic curve, corresponding to bronchial arteries (von Babo et al. 1997; Fig. 7.30). Cavitary lesions such as tuberculosis, liquefactions, necrosis, abscesses and pseudocysts are characterized by the presence of predominant vascularization through the bronchial artery in the marginal areas around the lesion.

7.6.4.2 Contrast-Assisted Sonography

In keeping with the findings on color-Doppler sonography, classic pneumonia is characterized by a short period until the start of contrast enhancement and strong contrast enhancement on contrast-assisted sonography. This is indicative of predominant vascularization though pulmonary arteries (Fig. 7.31). Reduced contrast enhancement is observed in cases of lobar pneumonia and can be explained by hypoxic vasoconstriction of the pulmonary artery (Fig. 7.28; Table 7.1). Delayed contrast enhancement indicates vascularization by the bronchial artery and is observed in cases of liquefaction and chronic pneumonia (Fig. 7.32). Such avascular areas in the region of pneumonia can be clearly demarcated on contrast-assisted sonography.

7.6.5 Large Lung Consolidation: Compressive Atelectasis

7.6.5.1 Color-Doppler Sonography

Compressive atelectasis is seen on radiographs and sonography in conjunction with the cardinal finding of a peripheral basal lung consolidation at the pleural wall.

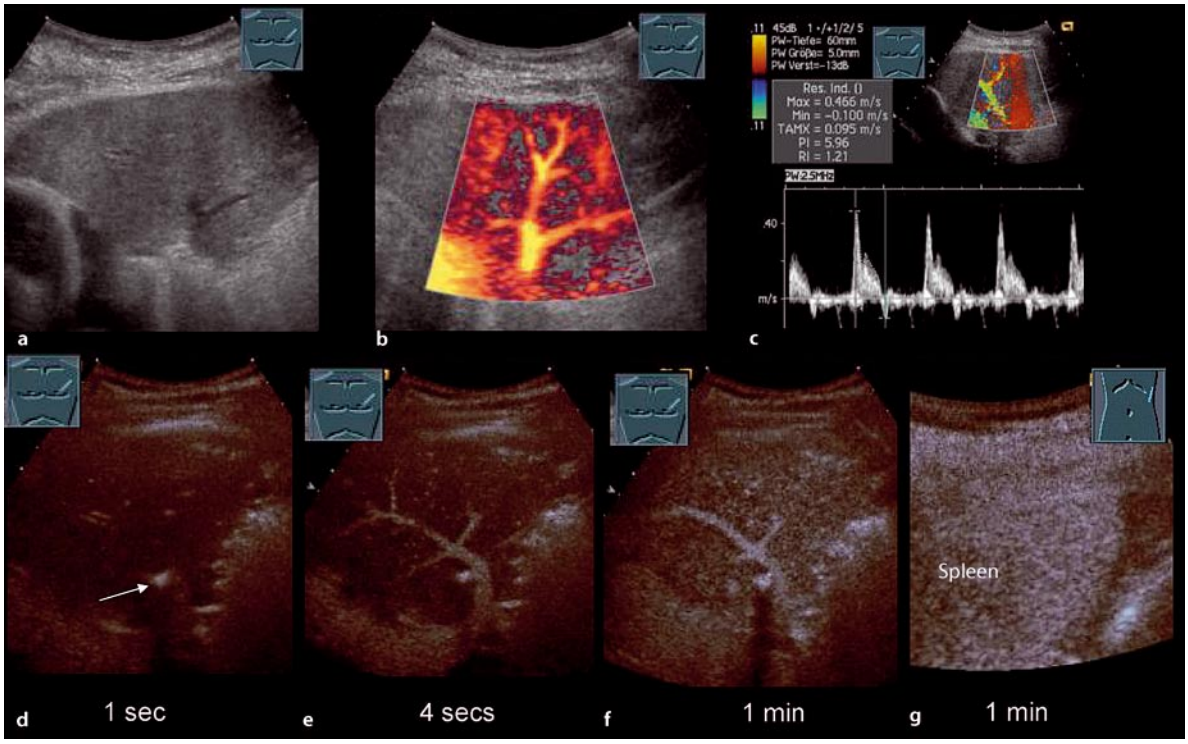

Fig. 7.28 A 45-year-old woman with dyspnea at rest in the presence of lobar pneumonia. **a** On B-mode sonography one finds a nearly homogeneously consolidated lung indicating hepatization. **b** Color-Doppler sonography shows ramified and strong vascularization. **c** Spectral curve analysis shows a high-impedance biphasic flow signal such as that seen in a pulmonary artery. **d** On contrast-assisted sonography one finds starting contrast enhancement in a central vessel already after 1 s. **e** After 4 s the central pulmonary artery is visualized with a few branches. The remaining parenchyma of the lung shows no significant contrast enhancement. **f** After 1 min in the parenchymatous phase there still is good contrast enhancement in the central pulmonary artery and its larger branches. The lung parenchyma itself shows reduced contrast enhancement compared to the spleen. **g** The spleen is marked by strong and regular contrast enhancement. This finding is indicative of hypoxic vasoconstriction of the pulmonary arteries (Euler–Liljestrand mechanism)

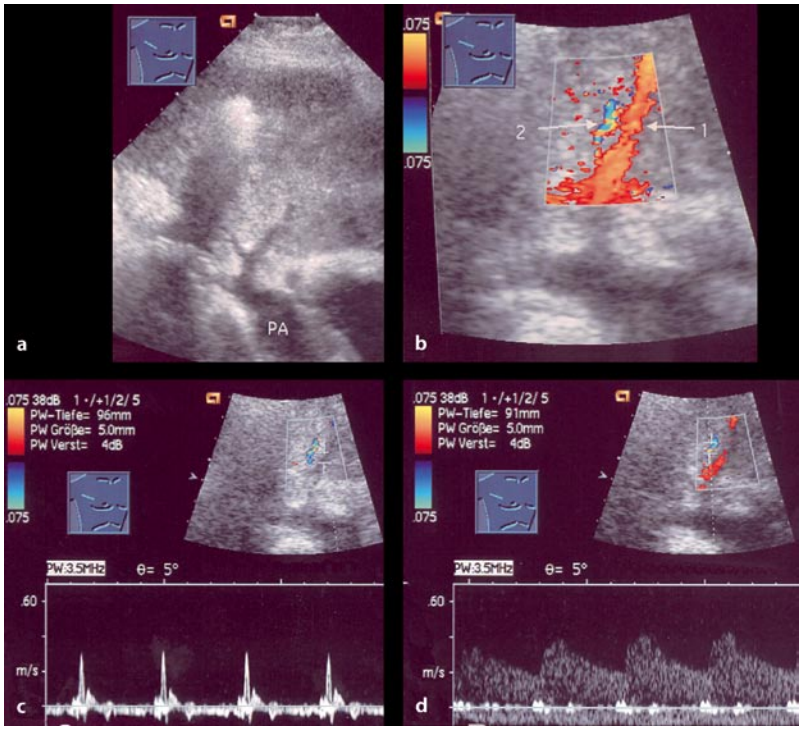

Fig. 7.29 A 59-year-old man with pneumonia. **a** On B-mode sonography one finds a nearly complete hypoechoic transformation ("hepatization") of the lung. *PA* pulmonary artery. **b** Color-Doppler sonography shows two vessels (*1* pulmonary artery, *2* bronchial artery). **c** Spectral curve analysis reveals an arterial biphasic high-impedance flow signal indicative of a pulmonary artery (marked *1* in **b**). **d** Spectral curve analysis shows a monophasic low-impedance flow signal oriented to the periphery, as a sign of a bronchial artery (marked *2* in **b**)

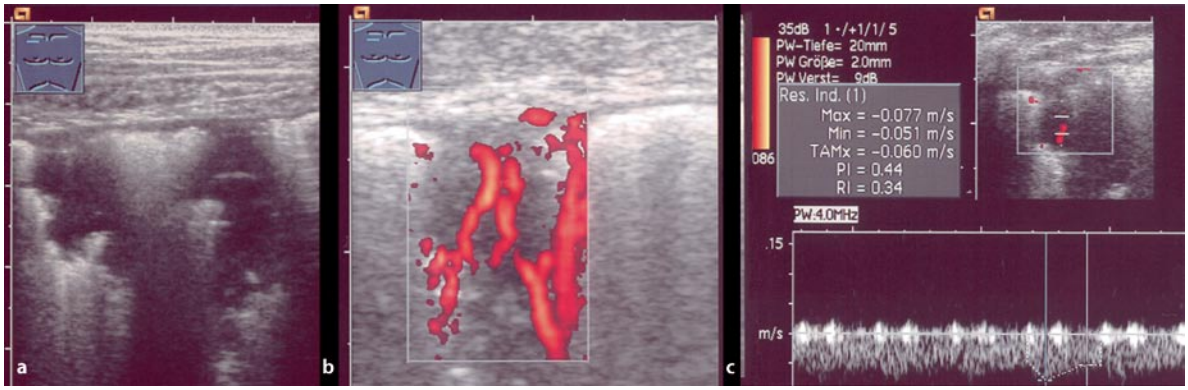

Fig. 7.30 A 37-year-old man with primary lung tuberculosis. **a** On the B-mode image one finds a hypoechoic consolidation with a central air-filled cavity. **b** On color-Doppler sonography one finds strong vascularization. **c** Spectral curve analysis shows a monophasic low-impedance arterial flow pattern oriented towards the lung hilum, most likely a bronchial artery close to the pleura

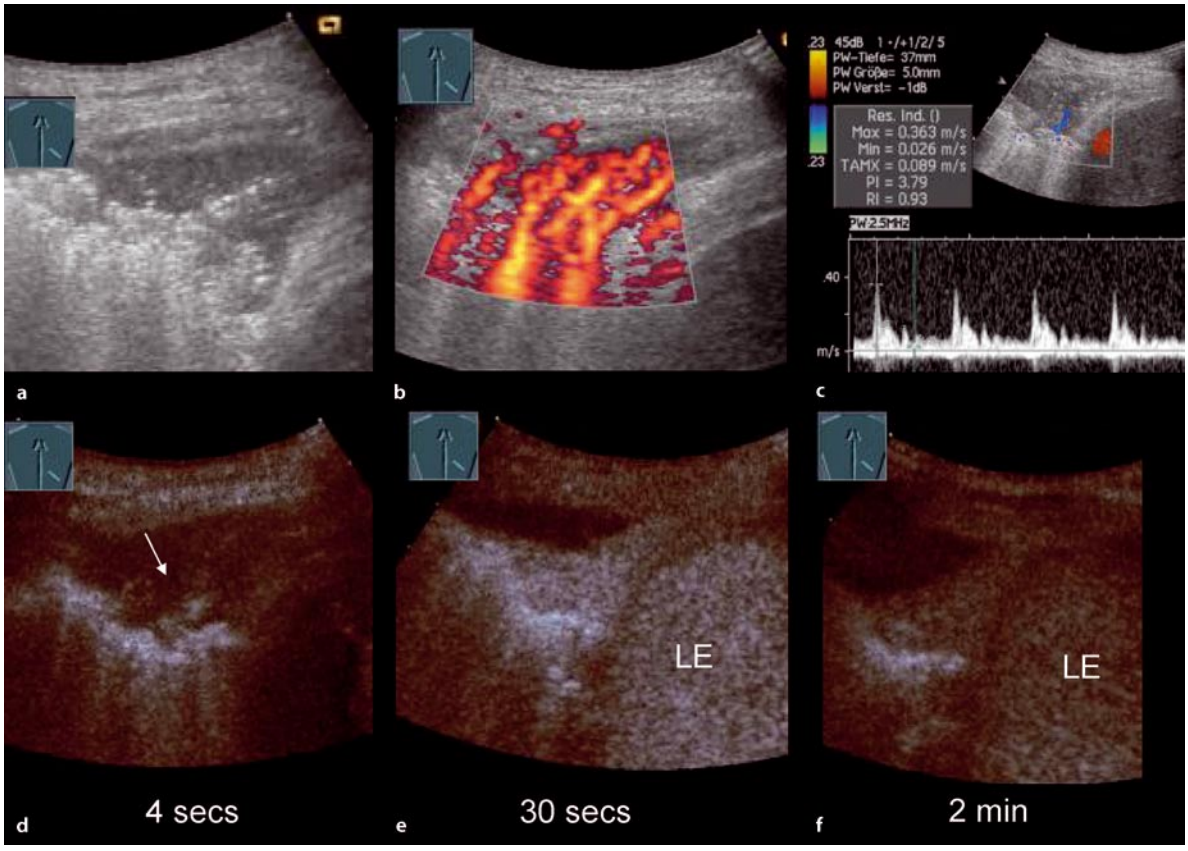

Fig. 7.31 A 71-year-old woman with pneumonia. **a** On B-mode sonography one finds a wedge-shaped hypoechoic transformation with a central air bronchogram. **b** Color Doppler sonography shows ramified and strong vascularization. **c** Spectral curve analysis reveals a high-impedance flow signal such as that seen in pulmonary arteries. **d** On contrast-assisted sonography, after 4 s one finds starting contrast enhancement in a central vessel, as a sign of vascularization from pulmonary arteries. **e** After 30 s there is homogeneous contrast enhancement of the consolidated lung tissue compared with the liver (*LE*) shown here. **f** In the parenchymatous phase, after 2 min both lung tissue and liver tissue show reducing contrast enhancement

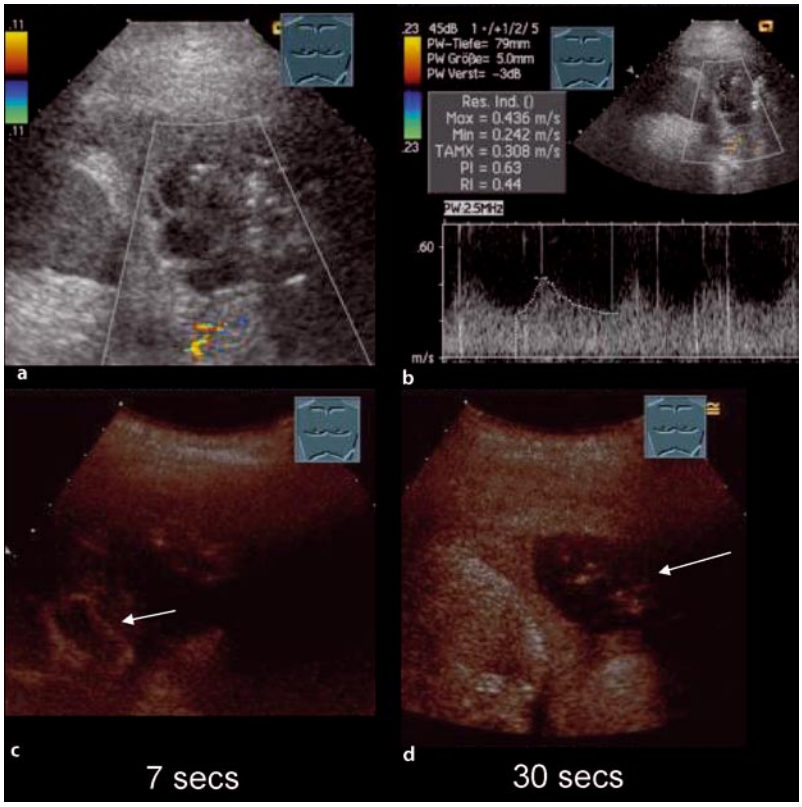

Fig. 7.32 A 66-year-old man with abscessing pneumonia. **a** On color-Doppler sonography one finds a complete consolidation of the lower lobe of the left lung. In the central portions there are liquid areas. Flow signals are visualized only in the central portion. **b** Spectral curve analysis reveals a monophasic high-impedance flow signal in the central vessels, such as that seen in bronchial arteries. **c** On contrast-assisted sonography, after 7 s there is starting contrast enhancement in a central vessel, an indication of vascularization from bronchial arteries. **d** After 30 s the infiltrated lung tissue shows contrast enhancement. In the central portion there is an area with no contrast enhancement. This indicates the presence of a lung abscess or sequestration

The main finding is a pleural effusion, followed by the visualization of compressed lung tissue. On qualitative color-Doppler sonography atelectasis is seen as a strongly ramified vessel. On arterial spectral analysis one usually finds a high-impedance flow signal indicative of pulmonary arteries (Fig. 7.33).

7.6.5.2 Contrast-Assisted Sonography

In concurrence with color-Doppler sonography findings, compressive atelectasis is characterized by a brief period until the start of contrast enhancement and strong contrast enhancement on contrast-assisted sonography (Figs. 7.14, Fig. 7.33). This is indicative of vascularization exclusively through the pulmonary arteries. The contrast-assisted sonography pattern of compressive atelectasis is very specific (Table 7.1). Round lesions in atelectatic lung tissue are marked by poor contrast enhancement (Fig. 7.34).

7.6.6 Large Lung Consolidation: Obstructive Atelectasis

7.6.6.1 Color-Doppler Sonography

The obstructive lung atelectasis is seen as a largely homogeneous hypoechoic transformation on the B-mode image. Depending on the duration of the obstruction, evidence of a "fluid bronchogram" is a characteristic feature in this setting. On qualitative color-Doppler sonography one finds pronounced vessels with evidence of an arterial high-impedance flow signal due to the branches of the pulmonary artery. Here also one finds an arterial monophasic flow profile of central bronchial arteries in atelectatic tissue as a result of hypoxia (Fig. 7.35). A frequent finding is the central tumor underlying the atelectasis, in which the consolidated atelectatic lung tissue serves more or less as an "acoustic window" to explore central lung structures (Fig. 7.36). According to Fissler-Eickhoff and Müller (1994), invasion and infiltration of the pul-

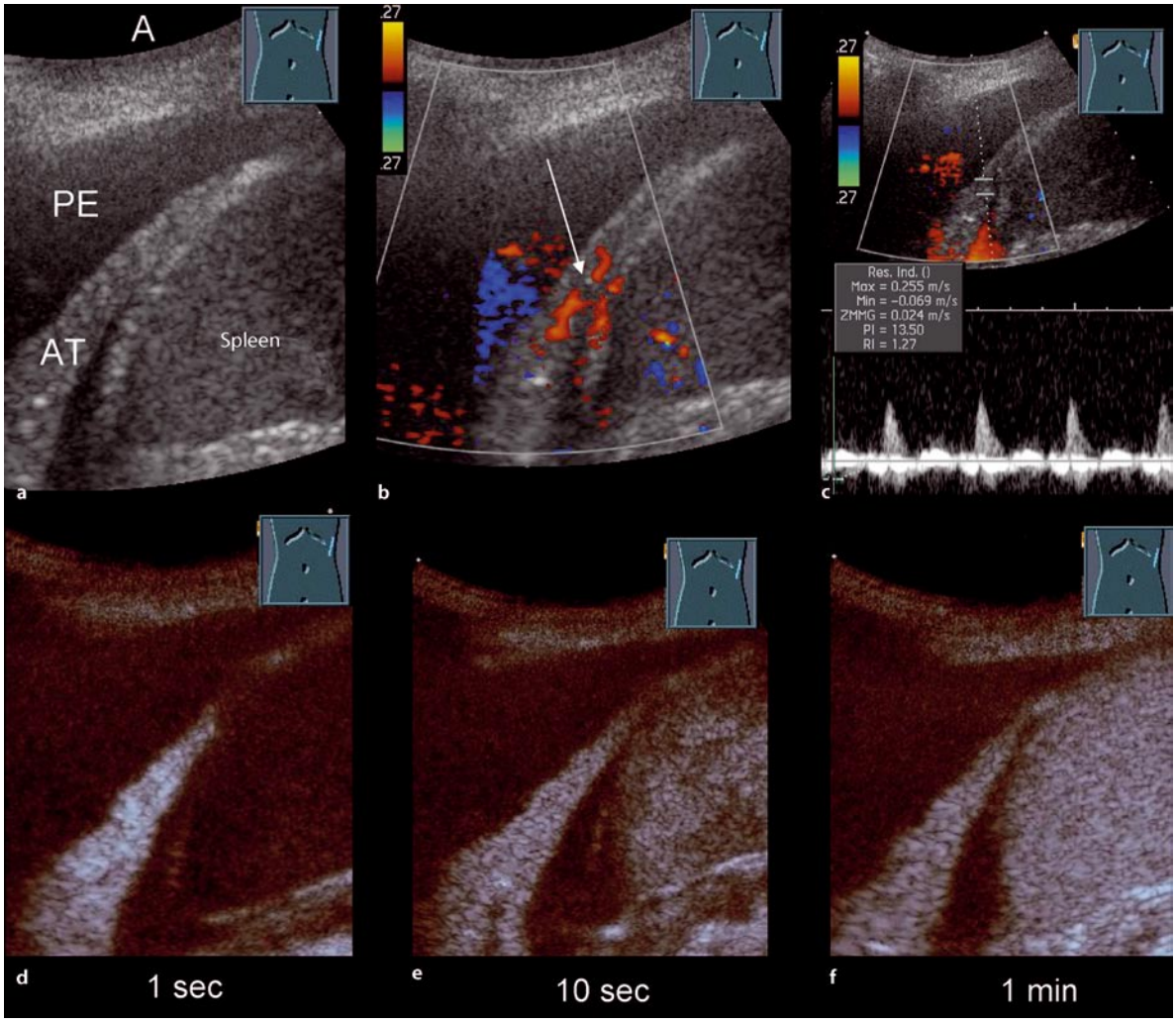

Fig. 7.33 A 42-year-old woman with a pleural effusion. **a** On B-mode sonography there is a pleural effusion and atelectasis in the lower lobe of the left lung. **b** Color-Doppler sonography shows marked vascularization of the atelectatic lung tissue (*arrow*). **c** Spectral curve analysis reveals a high-impedance flow signal such as that seen in pulmonary arteries. **d** On contrast-assisted sonography, as early as 1 s later one finds strong contrast enhancement in the atelectatic tissue. The adjacent tissue of the spleen shows no contrast enhancement at this time. **e** After 10 s the lung tissue shows unaltered and marked contrast enhancement. In the spleen one finds a speckled inhomogeneity as an indication of starting contrast enhancement. **f** In the parenchymatous phase, after 1 min there is homogeneous contrast enhancement of the lung atelectasis and the spleen. This finding is indicative of vascularization exclusively through pulmonary arteries

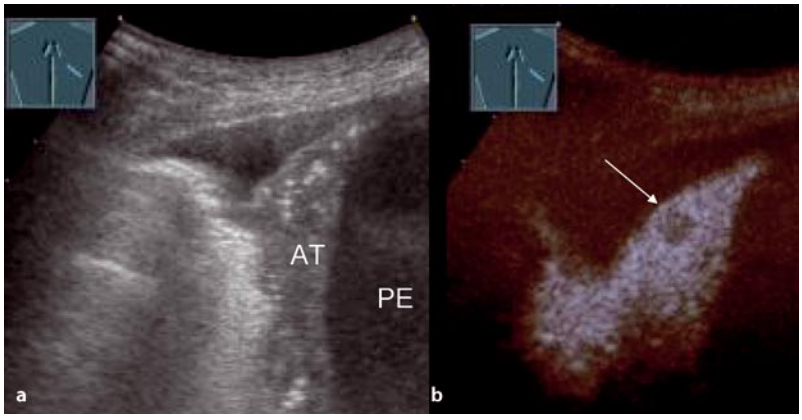

Fig. 7.34 A 74-year-old man with a known thyroid carcinoma and a right-sided pleural effusion. **a** On B-mode sonography one finds a pleural effusion (*PE*) and a lung atelectasis (*AT*), most likely a compressive atelectasis. Centrally one finds an air bronchogram. **b** Contrast-assisted sonography reveals homogeneous contrast enhancement of the atelectatic lung tissue. Demarcation of a small round lesion of the lung with reduced uptake of contrast medium. This finding is indicative of the presence of metastatic lung disease (*arrow*)

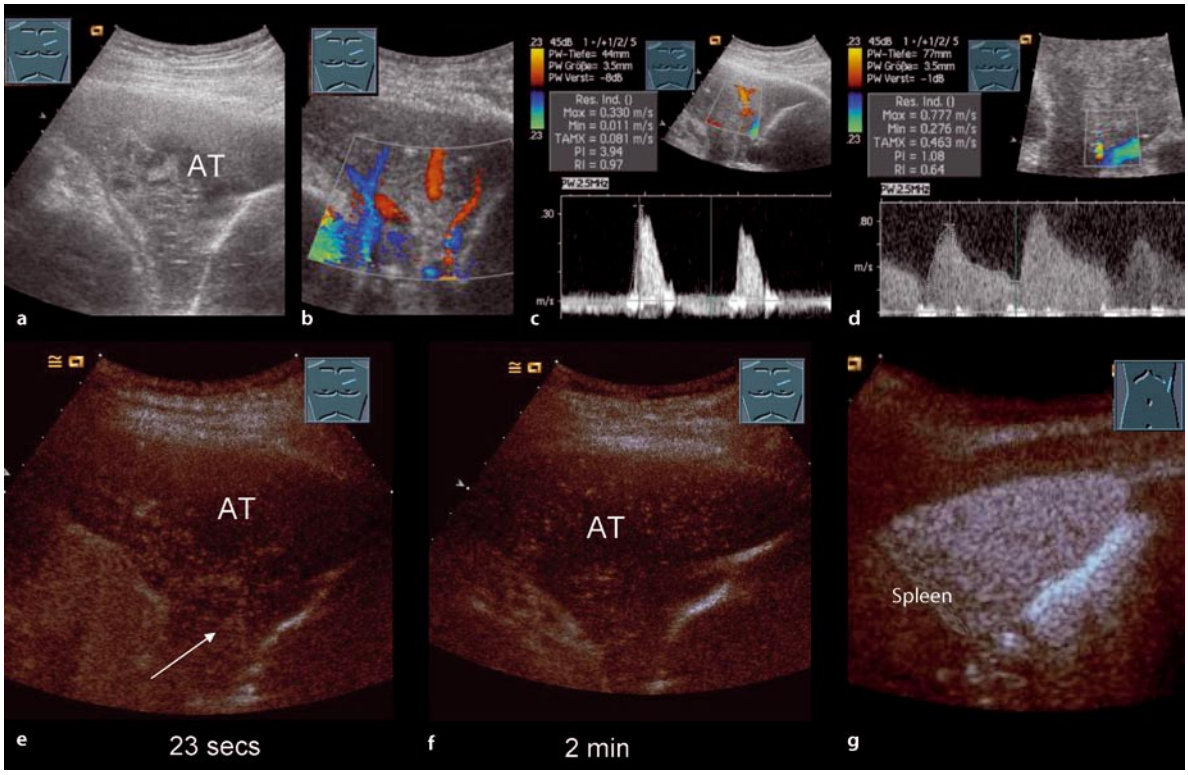

Fig. 7.35 A 75-year-old man with a non-small-cell bronchial carcinoma. **a** On the B-mode image one finds a large wedge-shaped lung consolidation in the upper lobe of the left lung such as that seen in the presence of atelectasis (*AT*). **b** Color-Doppler sonography demonstrates the vessels. **c** Spectral curve analysis shows the presence of a high-impedance flow signal within the atelectatic lung tissue as a sign of vascularization through pulmonary arteries. **d** Spectral curve analysis of a central vessel shows a low-impedance monophasic flow signal such as that seen in bronchial arteries. **e** Contrast-assisted sonography reveals starting contrast enhancement of vessels in the atelectasis only after 23 s. This is indicative of vascularization by bronchial arteries. **f** After 2 min there is markedly reduced, and in fact no, contrast enhancement of atelectatic lung tissue. **g** Visualization of normal contrast enhancement in the spleen as an in vivo reference

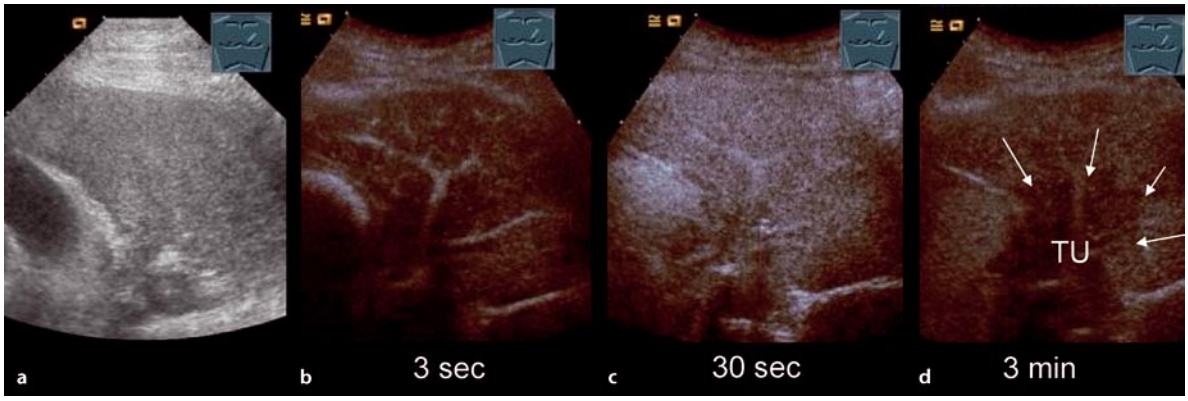

Fig. 7.36 A 71-year-old woman with known non-small-cell bronchial carcinoma and atelectasis of the upper lobe of the left lung. **a** On B-mode sonography one finds a homogeneous consolidation of the upper lobe of the lung. A tumor formation cannot be clearly demarcated. **b** On contrast-assisted sonography, 3 s after contrast application one finds central, branch-like enhancement of contrast medium in the large pulmonary arteries. **c** After 30 s there is homogeneous contrast enhancement of the lung atelectasis. **d** After 3 min, in the parenchymatous phase there is no or reduced contrast enhancement in the central tumor formation (*TU*); it can be demarcated from the surrounding atelectatic lung tissue (*arrows*)

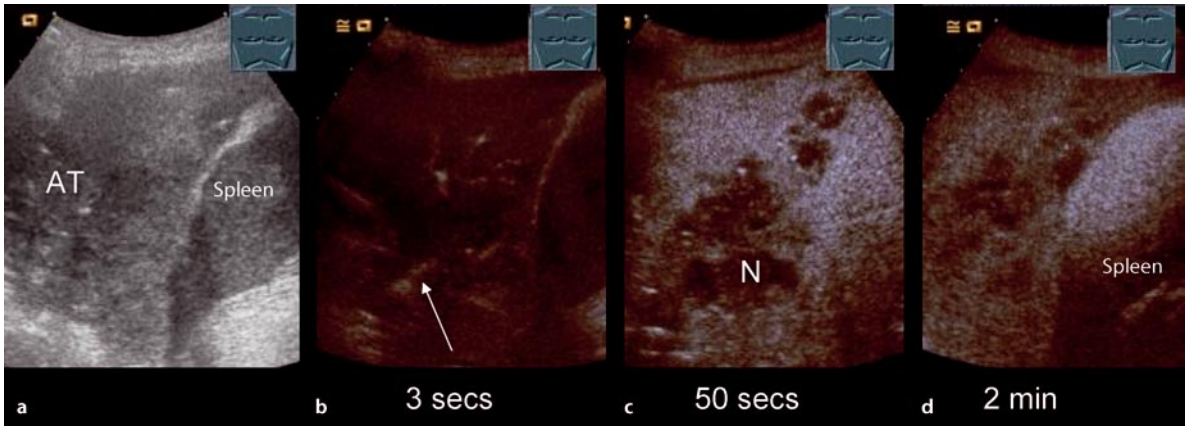

Fig. 7.37 A 47-year-old woman with a non-small-cell bronchial carcinoma. **a** On B-mode sonography there is an inhomogeneous atelectasis (*AT*) in the lower field of the left lung. **b** On contrast-assisted sonography, after 3 s there is starting contrast enhancement in the atelectatic tissue (*arrow*). This indicates the presence of vascularization through pulmonary arteries. **c** After just 1 min there is marked contrast enhancement in the atelectatic lung tissue. In central portions one finds lesions with no contrast enhancement, most likely necrotic areas (*N*). **d** After 2 min the atelectatic lung tissue shows reduced contrast enhancement compared with the spleen

monary arteries located in the region of the tumor occurs in 96% of the cases of bronchial carcinoma investigated. This disturbed vascular architecture of the pulmonary artery is seen on sonography as reduced or no visualization of vessels in atelectatic lung tissue.

7.6.6.2 Contrast-Assisted Sonography

In keeping with the color-Doppler sonography findings, a recent obstructive atelectasis is marked by the same features as compressive atelectasis—a short period of time until contrast enhancement and strong contrast enhancement on contrast-assisted sonography. This is indicative of atelectatic lung tissue being entirely vascularized by the pulmonary arteries (Fig. 7.37). In this phase, in patients with a central tumor formation, the tumor may be demarcated from atelectatic lung tissue more clearly by contrast-assisted sonography than by B-mode sonography (Fig. 7.36). In cases of obstruction of longer duration, within the atelectasis one may find liquefactions and abscesses (Fig. 7.37). These potential lesions as well as metastases in atelectatic lung tissue can be reliably diagnosed by contrast-assisted sonography (Fig. 7.38). In the course of a tumor-related obstructive atelectasis, depending on the structure of the tumor there may be infiltration and occlusion of pulmonary arteries. In this situation contrast-assisted sonography shows delayed start of contrast enhancement and reduced contrast enhancement (Fig. 7.35). This is indicative of a switch to vascularization of atelectatic lung tissue by bronchial arteries (Görg et al. 2006a). In general the contrast-assisted sonography pattern in cases of obstructive atelectasis is heterogeneous (Table 7.1).

7.6.7 Space-Occupying Lesion of the Chest Wall

7.6.7.1 Color-Doppler Sonography

Sonography is the method of choice to explore the chest wall. The intercostal arteries supplying the chest wall are usually seen even in healthy individuals by the use of color-Doppler sonography (Fig. 7.39). Tumors in the chest wall or pleural metastases are characterized by predominantly intercostal vascularization with a monophasic flow profile when the lesions are adherent to the chest wall (Fig. 7.40). When the tumor has invaded the lung, color-Doppler sonography may show different flow signals as a sign of complex arterial tumor vascularization (Görg et al. 2005a; Fig. 7.41).

7.6.7.2 Contrast-Assisted Sonography

Specific studies to assess the value of contrast-assisted sonography in cases of space-occupying lesions of the chest wall are not available. Intercostal arteries are strong vessels. On contrast-assisted sonography, intercostal arteries are marked by delayed start of contrast enhancement. The extent of contrast enhancement of the arterial phase may vary. As specific contrast enhancement of the chest wall does not appear to occur, usually there is rapid flow

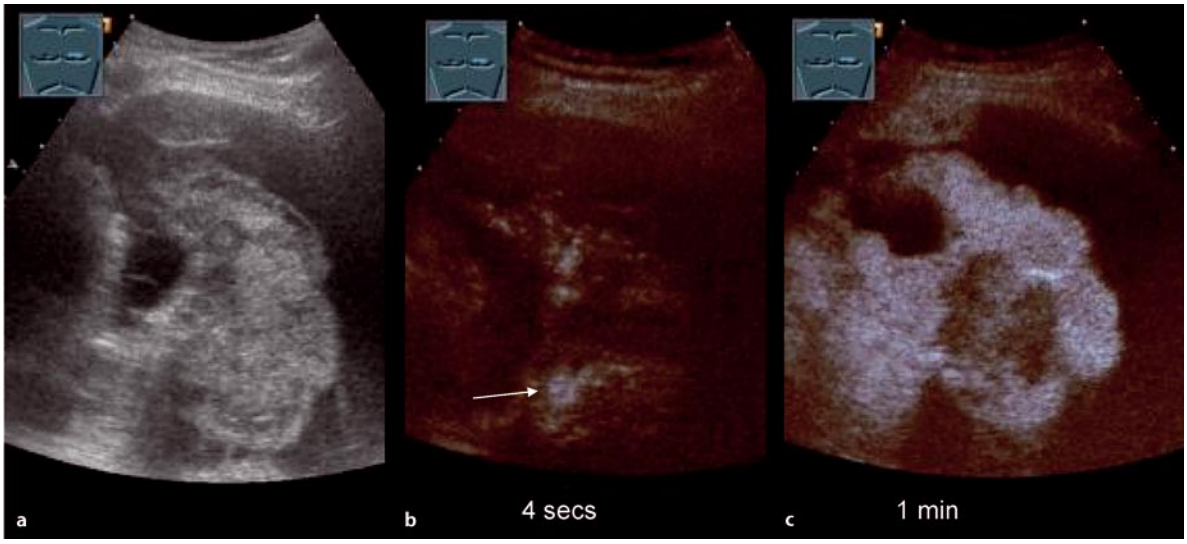

Fig. 7.38 A 64-year-old man with a known malignant melanoma. **a** On B-mode sonography one finds a complete consolidation of the left lung. It is hypoechoic. Adjacent to it there is a marked pleural effusion. **b** On contrast-assisted sonography, already after 4 s contrast enhancement starts to occur in the central vessels. This is indicative of vascularization through pulmonary arteries. **c** Strong contrast enhancement is seen in the atelectatic lung tissue after 1 min. In the central portion of the lung atelectasis one finds a larger confluent hypoechoic space-occupying lesion. This finding is urgently indicative of lung metastases

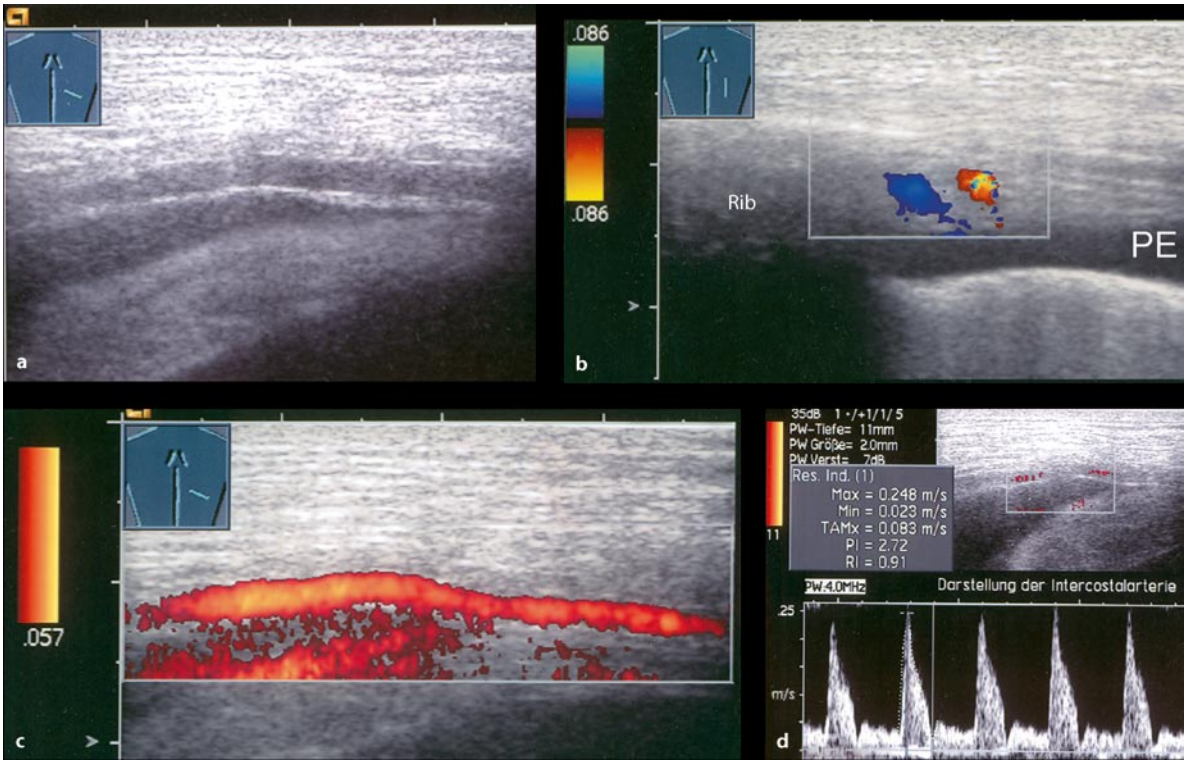

Fig. 7.39 Visualization of a normal intercostal artery in a healthy proband. **a** On B-mode sonography, intercostal transducer guidance demonstrates the intercostal artery. **b** On color-Doppler sonography, the craniocaudal section shows vascular reflexes beneath the ribs. *PE* pleural effusion. **c** Color-Doppler sonography demonstrates the intercostal artery in the longitudinal section. **d** Spectral curve analysis shows a monophasic high-impedance flow signal. This flow signal is characteristic of an intercostal artery

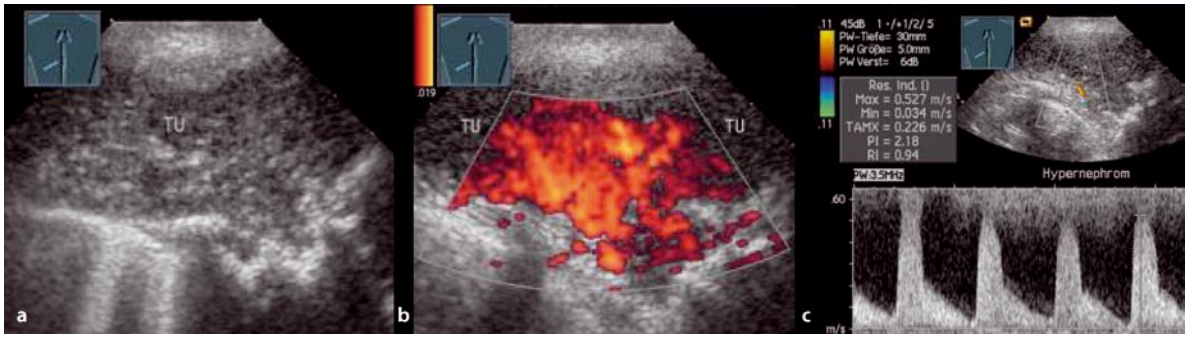

Fig. 7.40 A 45-year-old man with a chest wall metastasis and known hypernephroma. **a** B-mode sonography reveals a large hypoechoic transformation of the chest wall (*TU*) on the left side. **b** Color-Doppler sonography shows strong vascularization of the tumor lesion. **c** Spectral curve analysis shows a monophasic high-impedance flow signal such as that seen in intercostal arteries

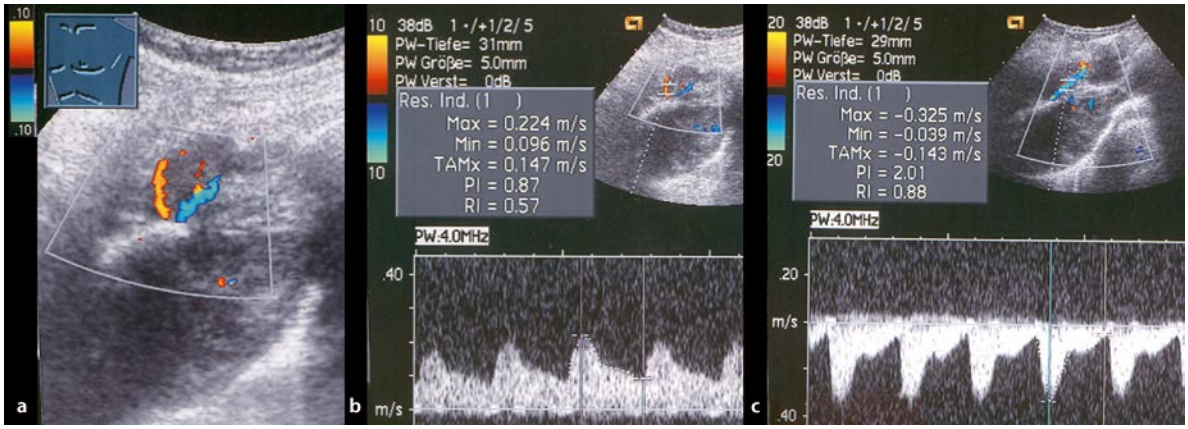

Fig. 7.41 A 34-year-old man with testicular carcinoma and metastatic disease in the chest wall. **a** Color-Doppler sonography reveals a tumor formation growing into the lung. Vessels are seen within the tumor tissue. **b** Spectral curve analysis shows a monophasic low-impedance flow signal such as that seen in bronchial arteries. **c** Spectral curve analysis shows a monophasic high-impedance flow signal such as that seen in intercostal arteries. This finding is indicative of complex tumor vascularization

of contrast medium during the parenchymatous phase (Figs. 7.42, 7.43).

7.7 Summary

Qualitative color-Doppler sonography shows varied and partly characteristic findings in the presence of various types of lung consolidations and is therefore a valuable adjunct to B-mode sonography with regard to the etiological classification of peripheral lung lesions. In keeping with the physiological dual vascularization of the lung by the pulmonary arteries and the bronchial arteries, on color-Doppler sonography one can distinguish between arterial high-impedance spectral curves and arterial low-impedance spectral curves in consolidated lung tissue. The former are assigned to pulmonary arteries and the latter to bronchial arteries. Within peripheral lung consolidations, different entities show characteristic distribution patterns of pulmonary-artery and bronchial-artery flow signals in respect of frequency and location. Arterial spectral curve analysis is time-consuming. Reliable demarcation of vessels of tumor neoangiogenesis is currently not possible with color-Doppler sonography.

Experience concerning contrast-assisted sonography in cases of peripheral lung lesions is limited. Contrast-assisted sonography at the chest can be performed easily and rapidly, and is therefore basically suitable for routine clinical use. Lung lesions can be distinguished by the time they require until the start of contrast enhancement and the extent of contrast enhancement. Initial studies show that contrast-assisted sonography at the chest can be helpful to differentiate ambiguous lung lesions (Görg et al. 2006b; Table 7.1).

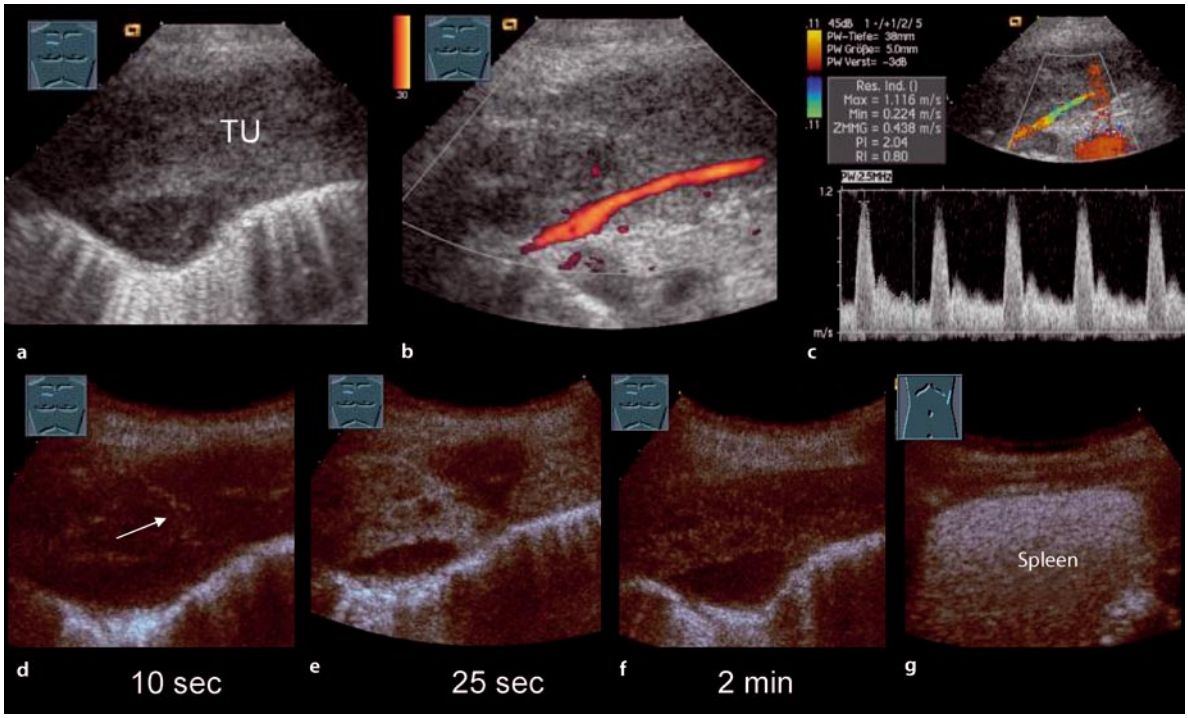

Fig 7.42 A 69-year-old man with histologically confirmed pleural mesothelioma. **a** B-mode sonography shows a large hypoechoic transformation of the chest wall (*TU*) **b** On color-Doppler sonography one finds a strong intratumoral vessel. **c** Spectral curve analysis shows a monophasic flow signal such as that seen in intercostal arteries. **d** Starting contrast enhancement of vessels (*arrow*) is seen after 10 s on contrast-assisted sonography. This is indicative of arterial vascularization from the systemic circulation, such as that seen in intercostal arteries. **e** After 25 s there is marked contrast enhancement of the tumor lesion and areas with less contrast enhancement. **f** After 2 min the lesion shows reduced contrast enhancement. **g** In vivo reference: regular contrast enhancement in the spleen

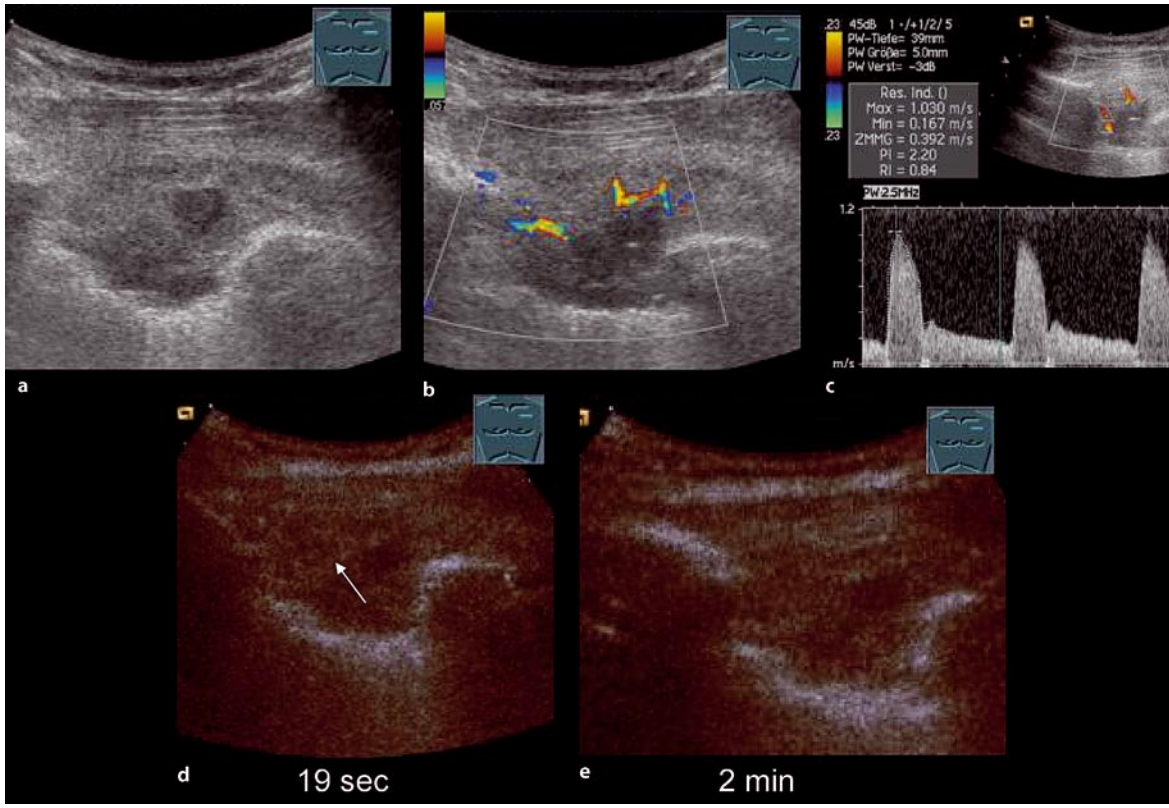

Fig. 7.43 A 54-year-old man with histologically confirmed pleural carcinosis in the presence of colon cancer **a** B-mode sonography shows a hypoechoic nodular inhomogeneous tumor formation along the parietal pleura, which cannot be clearly demarcated from the lung. **b** Color-Doppler sonography shows small vessels extending from the chest wall into the lesion. **c** Spectral curve analysis shows a monophasic flow signal such as that seen in intercostal arteries. **d** After 19 s, starting contrast enhancement of vessels at the margin of the lesion (*arrow*) is seen on contrast-assisted sonography. This is indicative of vascularization from the systemic circulation, such as that seen in intercostal arteries. **e** After 2 min the lesion shows reduced contrast enhancement

References

Albrecht T, Blomley M, Bolondi L et al (2004) Guidelines for the use of contrast agents in ultrasound. Ultraschall Med 25:249–256

Civardi G, Fornari F, Cavanna L, Di Stasi M, Sbolli G et al (1993) Vascular signals from pleural-based lung lesions studied with pulsed doppler ultrasonography. J Clin Ultrasound 21:617–622

Fissler-Eickhoff A, Müller KM (1994) Pathologie der Pulmonalarterien bei Lungentumoren. Dtsch Med Wochenschr 119:1415–1420

Forsberg F, Goldberg BB, Liu BB et al (1999) Tissue specific US contrast agent for evaluation of hepatic and splenic parenchyma. Radiology 210:125–132

Gehmacher O, Mathis G, Kopf A, Schreier M (1995) Ultrasound imaging of pneumonia Ultrasound Med Biol 21:1119–1122

Gehmacher O, Kopf A, Scheier M et al (1997) Can pleurisy be detected with ultrasound? Ultraschall Med 18:214–219

Görg C, Bert T (2004a) Trancutaneous colour Doppler sonography of lung consolidations: review and pictorial essay. Part 1: pathophysiologic and CDS basics of pulmonary vascularity. Ultraschall Med 25:221–226

Görg C, Bert T (2004b) Trancutaneous colour Doppler sonography of lung consolidations: review and pictorial essay. Part 2: CDS patterns of pulmonary consolidations. Ultraschall Med 25:285–291

Görg C, Bert T (2006a) Transcutaneous contrast enhanced sonography of peripheral lung lesions: review and pictorial essay. AJR Am J Roentgenol 187:420–429

Görg C, Bert T (2006b) Contrast enhanced sonography for differential diagnosis of perisplenic lesions with a second-generation contrast agent AJR Am J Roentgenol 186:621–626

Görg C, Seifart U, Holzinger I, Wolf M, Zugmaier G (2002) Bronchioloalveolar carcinoma: sonographic pattern of "pneumonia". Eur J Ultrasound 15:109–117

Görg C, Seifart U, Görg K et al (2003) Color Doppler sonographic mapping of pulmonary lesions: evidence of dual arterial supply by spectral analysis. J Ultrasound Med 22:1033–1039

Görg C, Bert T, Görg K, Heinzel-Gutenbrunner M (2005a) Color Doppler sonographic mapping of chest wall lesions Br J Radiol 78:303–307

Görg C, Bert T, Görg K (2005b) Contrast enhanced sonography for differential diagnosis of pleurisy and focal pleural lesions of unknown cause. Chest 128:3894–3899

Görg C, Bert T, Kring R (2006a) Contrast enhanced sonography of the lung for differential diagnosis of atelectasis J Ultrasound Med 25:35–39

Görg C, Bert T, Kring R, Dempfle A (2006b) Transcutaneous contrast enhanced sonography of the chest for evaluation of pleural based pulmonary lesions Ultraschall Med 27:437–444

Harvey CJ, Albrecht T (2001) Ultrasound of focal liver lesions. Eur Radiol 11:1578–1593

Hsu WH, Ikezoe J, Chen CY, Kwan PC, Hsu CP et al (1996) Color doppler ultrasound signals of thoracic lesions: correlation with resected histologic specimens. Am J Respir Crit Care Med 153:1938–1951

Hsu WH, Chiang CD, Chen CY, Kwan PC, Hsu JY et al (1998) Color doppler ultrasound pulsatile flow signals of thoracic lesions: comparison of lung cancer and benign lesions. Ultrasound Med Biol 24:1087–1095

Kolin A, Koutllakis T (1998) Role of arterial occlusion in pulmonary scar cancers. Hum Pathol 19:1161–1170

Mathis G, Dirschmid K (1993) Pulmonary infarction: sonographic appearance with pathologic correlation. Eur J Radiol 17:170–174

Müller KM, Meyer-Schwickerath M (1978) Bronchial arteries in various stages of bronchogenic carcinoma Pathol Res Pract 163:34–46

Uflacker R, Kaemmerer A, Picon PD, Rizzon CF, Neves CM, Oliveira ES, Oliveira ME, Azevedo SN, Ossanai R (1985) Bronchial artery embolization in the management of hemoptysis: technical aspects and long-term results. Radiology 157:637–644

von Babo H, Müller KMG, Huzky A, Bosnjakovic-Buscher S (1979) Die Bronchialarteriographie bei Erkrankungen der Lunge. Radiologe 19:506–513

Yuan A, Chang DB, Yu CJ, Kuo SM, Luh KT, Yang PC (1994) Color doppler sonography of benign and malignant pulmonoray masses. AJR Am J Roentgenol 163:545–549

Yuan A, Yang PC, Lee L, Wu DH, Kuo SH et al (2000) Reactive pulmonary artery vasoconstriction in pulmonary consolidation by color doppler ultrasonography. Ultrasound Med Biol 26:49–56

8 Image Artifacts and Pitfalls

A. Schuler

The diagnostic outcome of chest ultrasonography is greatly influenced by the investigator's knowledge and careful handling of artifacts in the B-mode image (and color Doppler).

8.1 Artifacts

Artifacts are a system-immanent aspect of ultrasonography. They arise due to physical phenomena when ultrasound waves pass through the human body (Table 8.1). Artifacts are disruptive artificial products that make it very difficult to image and evaluate the thorax, especially due to the anatomical features of this region. Artifacts can distort existing structures in terms of their size, position, form, and echogenicity; cause incorrect or incomplete imaging of their topography; or suggest the presence of structures that, in fact, do not exist. On the other hand, artifacts are indispensable and very important determinants of the diagnosis of specific diseases. The absence of certain typical artifacts (air: reverberation; bone: acoustic shadow) at the surface of the lung or in the bony thorax enables the investigator to diagnose certain diseases (lung lesion, rib lesion), as it is then possible to evaluate parenchyma, bone, and/or soft tissue. Artifacts also serve as a diagnostic criterion when they are seen at an unusual site, e.g., air with reverberation echoes in the pleural space in cases of pneumothorax.

Table 8.1 Physical phenomena of ultrasound waves

• Reflection	• Refraction
• Absorption	• Dispersion
• Diffraction	• Attenuation

8.2 Pitfalls

These are sources of error in ultrasonographic diagnosis, caused by anatomical, topographic, pathophysiological, or physical ultrasound-based misinterpretation on the part of the investigator, leading to incorrect diagnosis. Incomplete history taking, missing clinical information or examination, or insufficient knowledge of sonographic (and clinical) differential diagnosis may also be the reason for such "pitfalls." Last, but not least, every conscientious ultrasonographer must be aware of the limitations of the method so that additional diagnostic procedures can be applied efficiently, economically, and in a manner that is conducive to the patient's well-being. By so doing, several pitfalls can be avoided or resolved.

8.3 Ultrasound Physics in the Chest

Ultrasound images are created by the transmission and passage of ultrasound waves in the human body and the registration and processing of the backscattered/received echo of the emitted ultrasound beam. In an entirely homogeneous medium, a sound wave is carried forward in a uniform fashion. It is altered at the margin between two media. The phenomena/changes that are liable to occur in this process are summarized in Table 8.1. They include the geometry of the ultrasound wave, the angle at which it strikes the reflector, the physical properties of the reflector, and its surface consistency. The magnitude of the impedance difference between two different media is represented by various factors, one of them being the intensity of the backscattered echo. Thus, on the B-mode image, it is represented by the brightness of a pixel. Human tissue contains a number of marginal surfaces whose anatomical origin can be determined characteristic ultrasound phenomena.

In contrast to the abdomen, ultrasonography of the chest is more frequently confronted with disturbing artifacts because of the surrounding "echo-opposing" structures (aerated lung, bony chest). Therefore, the specific ultrasound phenomena in air and bony structures will be briefly discussed in the following.

Air. This is a strong ultrasound beam reflector. Depending on the structure of the surface, the impedance difference and the gas volume at the marginal surface, ultrasound waves differ in terms of their reflex behavior:

- Large extent of absorption
- Total reflection with acoustic shadow
- Partial reflections with change of transmission and a narrow acoustic shadow

The most common phenomenon is that up to 99% of the ultrasound wave is reflected at the first marginal surface between tissue and air, i.e., the "initial lung echo." Therefore, it is not possible to visualize the deeper lung parenchyma by ultrasonography. Only when the structure of the surface is altered and in the presence of specific physical features (e.g., the absence of air in inflammatory or tumor-related processes, atelectasis, etc.) is it possible to image lung parenchyma. However, in such cases, the lung itself has several marginal surfaces (air in the bronchoalveolar space, bronchial wall, interstitial space, vascular wall, blood). The above-mentioned alterations in the ultrasound wave also occur at these marginal surfaces.

Bone. In bone, there is nearly complete absorption of ultrasound energy. As a result, the "dorsal" ultrasound wave is obliterated (no further echoes in axial direction of the

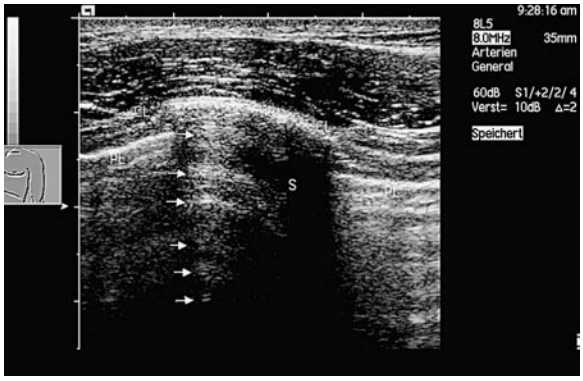

Fig. 8.1 Reflective shadowing at the clavicle (*CL*). Dorsal acoustic shadow (*S*) due to absorption of ultrasound waves at the surface of the clavicle. Additional reverberations (repetitive echoes, *arrows*) at the surface of the clavicle when the ultrasound waves hit perpendicularly. *PL*, pleural reflex

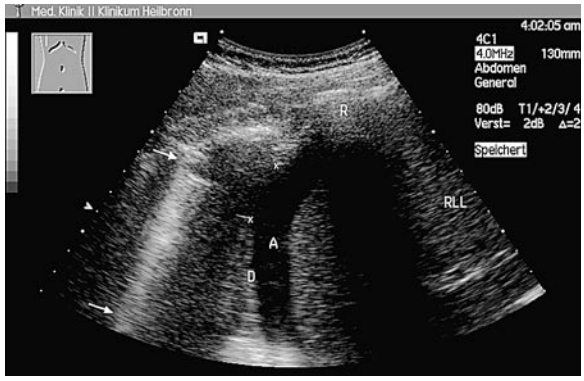

Fig. 8.2 "Diaphragmatic gap". A female patient with a primary peritoneal mesothelioma, ascites (*A*) and basal pleural pneumonia. The central portion of the diaphragm (*D*) is found to be markedly thickened. In areas dose to the transducer, there seems to be a gap (*x–x*). Furthermore, a lateral marginal shadow phenomenon is seen in the diaphragm and also a comet-tail artifact in air in the cranially located lung (*arrows*). *RLL*, right lobe of liver; *R*, rib with dorsal acoustic shadow

beam). When ultrasound waves hit bone at right angles, they may cause strong reflection and repetitive echoes of the bone surface in deeper portions (Fig. 8.1).

8.4 Imaging of Marginal Surfaces of the Pleura and the Diaphragm

The image varies, depending on the angle of incidence of ultrasound waves and the consistency (roughness) of the surfaces. Furthermore, the improved resolution of ultrasound probes and continuous advancement of technology permit differentiated imaging. At an angle of incidence of 0 to about 25°, total reflection may be expected to occur at the marginal surface between the Pleura and the lung. Only when the surface of the pleura/lung is thickened due to inflammation or scars and the surface is irregular and "roughened, " is it imaged even in the presence of a steeper angle of incidence (Mathis 1996).

Most of the diaphragm can be imaged by the transabdominal approach (as a rule through the liver from the right side and through the spleen from the right side). Due to the high impedance difference as well as scatter phenomena, the diaphragm is visualized as much thicker than it actually is (Fig. 8.2). Central portions of the diaphragm are not imaged well by the intercostal approach because of the unfavorable angle of incidence of the ultrasound wave. Apparent gaps might irritate the investigator. Moreover, lateral marginal shadow phenomena limit the assessment. Indistinct processes must be imaged in the complementary second plane.

8.5 B-Mode Artifacts

Based on their mechanism of origin and physical ultrasound features, artifacts may be divided into four categories (Table 8.2; Kremkau and Taylor 1986; Schuler 1998).

8.5.1 Ultrasound Beam Artifacts in Chest Sonography

8.5.1.1 Reverberations (Repetitive Echoes): Margin Between Tissue and Air, Bone Fracture Fissures

They arise due to nearly complete reflection of the emitted ultrasound wave at the marginal surface between tissue and air (initial lung echo). This marginal surface acts as a strong reflector. It reflects the striking ultrasound wave back to the transducer membrane, where the wave is re-reflected and re-emitted, hits the marginal surface again, etc.

Depending on the duration, the marginal surface reflex is imaged dorsally, in axial direction of the ultrasound wave. Deeper reflectors are weaker and are imaged darker (Figs. 8.2, 8.3). The artifact caused by insufficient probe-to-specimen contact (Fig. 8.10), e.g., when a linear ultrasound probe is used on the surface of the thorax, actually is a reverberation artifact (at the transducer membrane).

A narrow fissure in a rib fracture might become noticeable because of a reverberation artifact (so-called

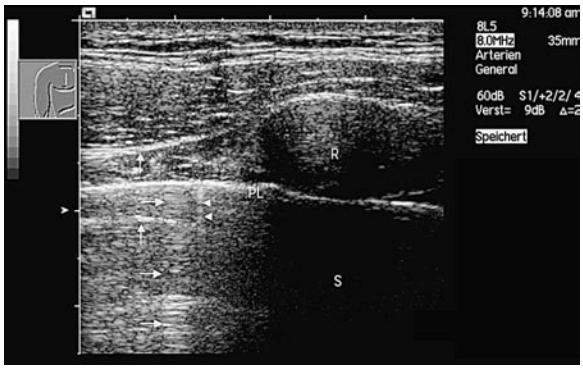

Fig. 8.3 Reverberations and comet-tail, parasternal longitudinal section from the right side. One finds reverberation artifacts (*horizontal arrows*) dorsally in the aerated lung, and a short comet-tail artifact (*arrowheads*). Furthermore, a muscle fascia of the thorax musculature is mirrored dorsally (*vertical arrows*) at the pleural reflex (*PL*). Rib (*R*) with an incomplete acoustic shadow (*S*); the pleural reflex acts as a strong reflector and is imaged here through partly cartilaginous rib with partial echo transmission

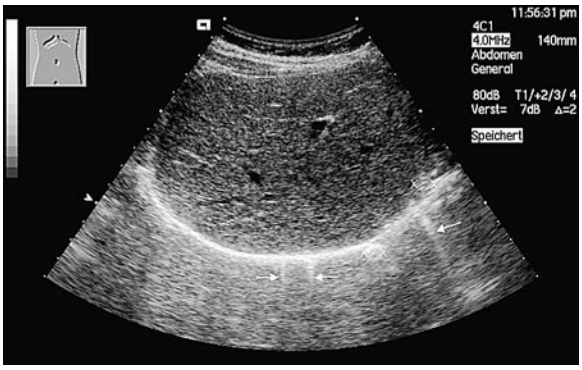

Fig. 8.4 Mirror artifact. Subcostal oblique section from the right side. "Classical" mirror artifact of the liver at the diaphragm. Portions lying at a distance from the transducer and the diaphragm, i. e., cranially by the subcostal approach, are not "lung parenchyma" but liver parenchyma reflected at the strong reflector, namely the diaphragm. A hemangioma (*x–x*) lying immediately subdiaphragmal in the original image is more clearly seen in the mirror image (*x–x*) and is displaced centrally to the mid portion of the image. In some cases, the mirror image might reveal structures outside the main beam that cannot be imaged (multiple beam artifacts) and cause considerable confusion. Additional comet-tail artifacts (*arrows*) in air

Table 8.2 Classification of artifacts

- Ultrasound beam artifacts
- Ultrasound enhancement artifacts
- Ultrasound resolution artifacts
- Other artifacts

chimney phenomenon) (Dubs-Kunz 1992). The fracture end of the rib serves as a strong reflector in this setting (Figs. 2.13, 2.14).

8.5.1.2 Mirror Artifacts: Liver Parenchyma in the Diaphragm, Vessels at the "Pleura"

These are caused by incidence-angle-dependent reflection of the ultrasound wave at a strong reflector (e.g., the diaphragm), oblique deflection in issue, repeated reflection on a reflector, back-scatter to the first reflector, and back-reflection to the ultrasound probe. This is imaged as a structure tot primarily in the axial direction of the ultrasound beam, within a region axial-distal to the actual reflector.

This causes the classical mirror artifact phenomena of the liver at the diaphragm (Fig. 8.4), but also of the subclavian artery at the initial lung reflex. This artifact phenomenon exists not only in B-mode sonography, but also in color Doppler and the Doppler frequency spectrum (Fig. 8.5). As a rule, the multiple backscattered echoes of mirror images are more hypoechoic and somewhat more blurred or distorted as a result of previous weakening of the ultrasound beam when it passes through tissue.

8.5.1.3 Arcuate Artifacts: Rib Reflex in Pleural Effusion

Arcuate artifacts may arise due to displacement of a reflex at a strong reflector in the lateral ultrasound beam or side lobe into the center of the main beam. Characteristically, in sector transducers and upwardly oriented curved arrays, one finds upwardly open circular arches. In linear probes, one finds a hyperbola. Thus, a reflection in a bony portion of the thorax could mimic a septation in a pleural effusion (Fig. 8.6). This problem can be resolved by altering the echo angle or the echo plane.

8.5.1.4 Scatter Lens Artifact/Shortening Phenomenon: Distortion of the Lung Surface Dorsal to Rib Cartilage

This artifact phenomenon is a result of the different transmission rates of ultrasound waves in rib cartilage (faster) than in the adjacent soft tissue of the chest wall. This may mimic a pseudolesion at the marginal surface of air/lung, because there is an apparent protrusion of contours in the direction of the ultrasound probe (Fig. 8.7). This artifact

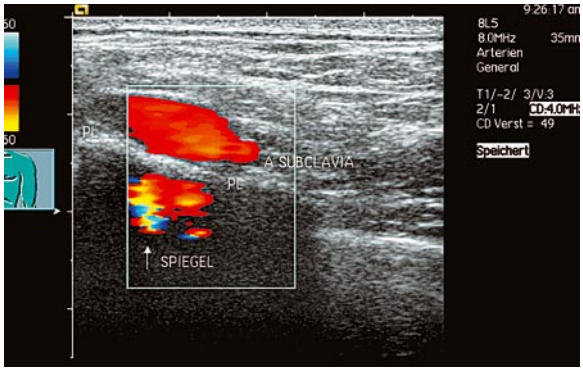

Fig. 8.5 Mirror artifact on color Doppler. The subclavian artery (*A. SUBCLAVIA*) is reflected at the pleura (*PL*). A vessel (*arrow*) lying dorsal to the pleura is seen on the mirror image; the vessel, however, does not really exist

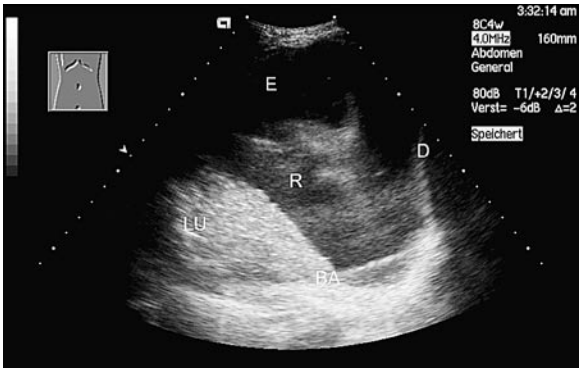

Fig. 8.6 Arcuate artifact in the pleural effusion. A female patient with pulmonary and pleural metastatic breast carcinoma. A strong reflector (bony thorax) lying outside the main beam is visualized as a circular arch (*AA*, arcuate artifact), discretely opening upward. Distally, it may mimic septation of the pleural effusion (*E*). The internal echoes (*R*) are not corpuscular portions of the effusion but noise artifacts ("speckles"). *D*, diaphragm; *LU*, lung atelectasis in the presence of pleural effusion

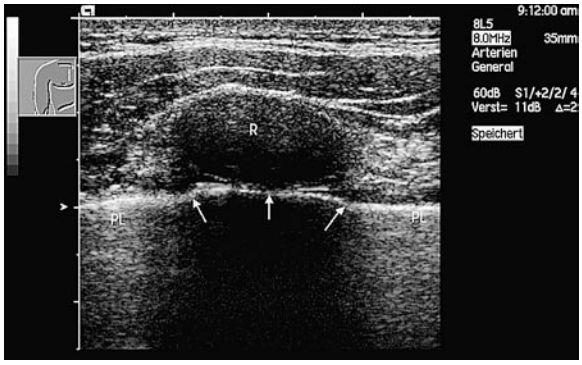

Fig. 8.7 Scatter lens artifact. The pleura (*PL*) dorsal to the rib cartilage (*R*) is shifted ventrally towards the transducer (*arrows*) as a result of various ultrasound beam rates in cartilage and soft tissue of the chest wall

is simple to detect and plays a rather important role in abdominal diagnosis of the liver (apparent space-occupying mass on the surface of the liver) dorsal to rib cartilage (Bönhof and Linhart 1985).

8.5.1.5 Marginal Shadows: Diffraction/Refraction at Strong Reflectors ("Diaphragmatic Gap")

This artifact occurs when the ultrasound beam hits a surface obliquely. It is the result of diffraction and refraction phenomena at strong reflectors (e.g., the diaphragm; Fig. 8.2). The artifact is detected by the fact that it disappears when the echo plane or the echo angle is changed.

8.5.2 Artifacts Caused by Alterations in Echo Enhancement

8.5.2.1 Acoustic Shadow/Echo Obliteration: Formation of Plaque on All Bony Structures of the Chest

This certainly is one of the most common artifact phenomena in the thorax and greatly hinders the assessment of structures lying dorsal to such strong reflectors. Due to strong absorption, dorsal bone structures (ribs, scapula, clavicle, sternum, vertebral column) are nearly completely obliterated and practically all information is lost (Fig. 8.1). However, interruptions of the otherwise regular acoustic shadow in the bony thorax (bone contour, bone surface, joints) may be very helpful for diagnosis, as pathological changes will be present in such cases (fracture, bone tumor, joint effusion, joint empyema). Acoustic shadows in the pleura are also signs of pathological alterations, e.g., of plaque in the presence of asbestosis or calcification during the healing of pleural lung lesions or lung lesions dose to the pleura (pneumonia, tuberculosis) or in lymph nodes.

8.5.2.2 Echo Enhancement: Distal to Hypoechoic Structures (Pleural Effusion, Cyst, Vessel, Hypoechoic Space-Occupying Mass)

This phenomenon of "brighter," more hyperechoic areas distal to the above-mentioned structures is not due to echo enhancement but due to lesser weakening of ul-

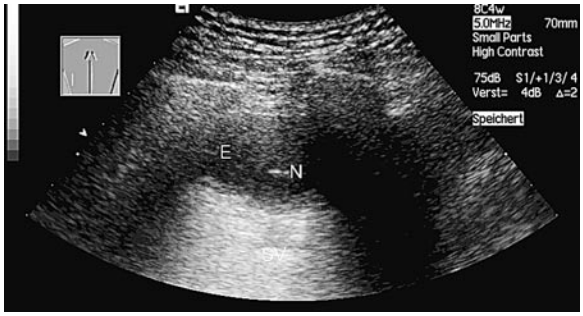

Fig. 8.8 Echo enhancement. Dorsal to a small, not entirely anechoic pleural effusion (*E*) there is marked "echo enhancement" (*EE*). This actually is reduced weakening of the echo, as the spread of the ultrasound beam in the pleural effusion is altered in comparison with adjacent tissue. Also note the nonanechoic effusion dose to the chest wall. The reflexes are noise artifacts. Furthermore, an echodense small bright linear reflex (*N*) is seen, the tip of the puncture needle introduced under sonographic guidance

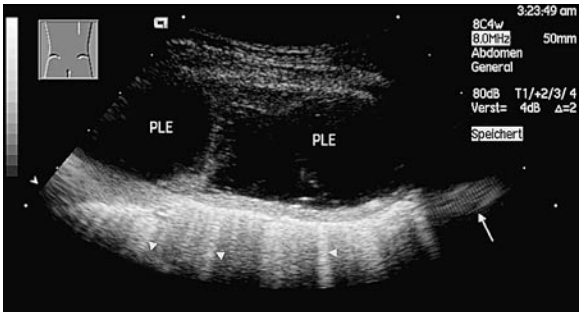

Fig. 8.9 Comet-tail and probe-to-specimen artifact. Dorsal to a septate pleural effusion in the presence of breast carcinoma one finds numerous comet-tail artifacts (*arrowheads*) arising in the air at the margin between the visceral pleura and the lung. Furthermore, given insufficient contact between the ultrasound probe and the chest wall, a shadow with an artifact reflex (*arrow*), although not like a classical ring-down artifact. Dorsal to the pleural effusion, there is marked echo enhancement. *PLE*, pleural effusion

trasound waves in the more hypoechoic portions closer to the probe. This causes distal parts to appear brighter (more hyperechoic and stronger echoes) than the surrounding areas, which have uniformly weakened echoes. In the thorax, this is found in the presence of large quantities of fluid in the pleural space or hypoechoic peripheral pulmonary processes (Figs. 8.8, 8.9).

8.5.2.3 Echo Resolution Artifacts

Noise: In Fluid-Filled Structures

At the surface of anechoic areas, one finds diffuse "noise" caused by interference from returning echoes at different marginal surfaces, such as those caused by "background noise," depending on general enhancement (this is also true for Doppler sonography). Here caution is advised, as apparently internal structures that in fact do not exist might be mimicked (e.g., in the pleural effusion; Figs. 8.6, 8.8). Marginal surfaces are frequently blurred.

Slice Thickness Artifact: at Reflectors with a Strong Impedance Difference (Pleura, Diaphragm)

This common and irritating artifact also belongs to the category of resolution artifacts. When the ultrasound beam hits strong reflectors obliquely and in the presence of a high impedance difference, the marginal layer is much thicker, (partly) blurred, and distorted. This phenomenon might mimic pleural and diaphragmatic lesions or thickening (Fig. 8.2), but also thrombosis or sediments in vessels.

8.5.3 Other Artifacts

8.5.3.1 Comet-Tail (Resonance Artifact): in Aerated Structures

At the margin, of the lung surface and air one frequently finds small comet-tail artifacts (Figs. 8.2-8.4, 8.9). They are seen as bright, narrow strips of strong dorsal reflectors and their origin is controversially discussed. One explanation is reverberations (repetitive echoes) between two very closely located reflectors and resonance phenomena (vibrations) with a strong echo response. In addition to air or other gas bubbles, a common site of origin is metal foreign bodies.

8.5.3.2 Artifacts Caused by Foreign Bodies: Needle Tip, Drainage

Iatrogenic or accidental foreign bodies introduced into the body cause artifact phenomena. As a result, projectiles, fragments of glass or wood, other substances might be imaged in the chest wall and in soft tissue. This is significant when such artifacts are visualized during sonography-guided diagnostic or therapeutic measures. Small pulmonary consolidations dose to the pleura, pleural effusions a few millimeters in size, or pleural empyema can be punctured or drained under real-time sonographic guidance. Space-occupying masses in the soft tissue of the thorax or rib cage should also be punctured under sonographic guidance. Detection of the needle reflex in aerated structures might be difficult. Here, real-time

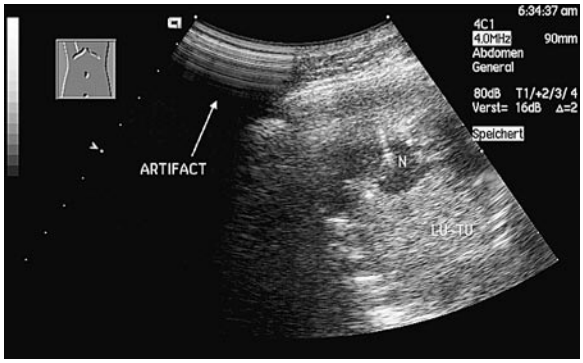

Fig. 8.10 Ring-down (probe-to-specimen artifact). Patient with a peripheral bronchial carcinoma in a ventral location on the right side. A probe-to-specimen artifact (*arrow*) is caused by insufficient contact between the transducer and the chest wall. A simultaneous fine-needle puncture performed for histological verification of the diagnosis shows the needle artifact (*N*) in the tumor (*LU-TU*)

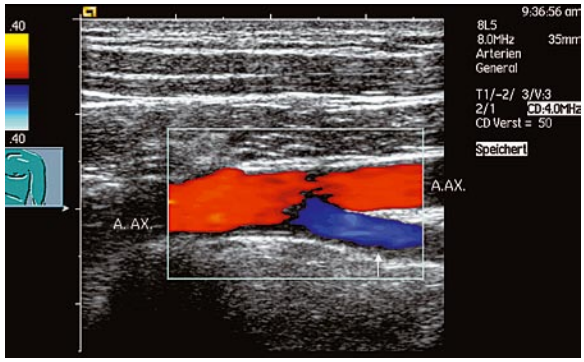

Fig. 8.11 Directional artifact (color Doppler). The axillary artery (infraclavicular) (*A.AX.*) with a branch for the musculature/chest wall. Blood flowing towards the ultrasound probe is coded red; blood flowing away from the probe is coded blue (see color scale). The branching artery (*arrow*) is blue, the change of color from red to blue occurs via black. Thus, here (at a 90° Doppler angle to the ultrasound probe), there is no blood flow relative to the ultrasound probe

8

control through subtle movement of the needle tip under simultaneous sonographic imaging is useful Blank 1994; Fig. 8.8).

8.5.3.3 Ring-Down Artifact: Insufficient Probe-to-Specimen Contact

If the geometric configuration of the probe is unfavorable in relation to the investigated region (for instance a linear probe in a curved chest wall), this artifact can easily be detected by characteristic repetitive echoes (arising between the ultrasound crystal and the transducer membrane) (Fig. 8.10).

8.6 Color Doppler Artifacts and Pitfalls in the Chest

The basic principles and settings of the various Doppler modalities will not be presented in this chapter. They have been discussed in detail elsewhere (Wild 1996).

8.6.1 Pulse Repetition Frequency, Overall Enhancement, Filter, Background Noise

Insufficient or incorrect setting of the overall enhancement of color Doppler either leads to incorrect imaging of actual blood flow (excessively low gain) or "over-radiation" due to numerous color pixels that do not represent blood flow but only background noise (poor signal-to-noise ratio).

A low pulse repetition frequency (PRF) should be selected for small vessels with low flow rates so that flow signals are not "overlooked." When large arteries are visualized (mediastinum, suprasternal, parasternal), it may be necessary to increase the PRF or reduce overall enhancement. The same is true for spectral Doppler. Selection of the wall filter should also be controlled, so that slow flow signals or signals of low intensity are not "filtered away."

8.6.2 Directional Artifact

The directional artifact is not actually an artifact phenomenon but evidence of directionally encoded visualization of blood flow on color Doppler (Fig. 8.11). Thus, in a vessel with blood flow in the opposite direction of the ultrasound probe (for instance, when the vessel has a curved flow), the colors red and blue will be present in one and the same vessel. The actual change in the direction of blood flow is seen at the margin of the two colors; this area will be black (corresponding to null flow; see color scale).

8.6.3 Aliasing

In contrast to directional artifacts, aliasing is marked by a change of color through the bright color zones. This phenomenon is expressed as a colorful mosaic in the transition zone between two colors and will be seen at higher flow rates than the selected PRF (Fig. 8.12a). In spectral Doppler, portions of higher frequency appear as being "cut off" at the lower or upper margin of the Doppler fre-

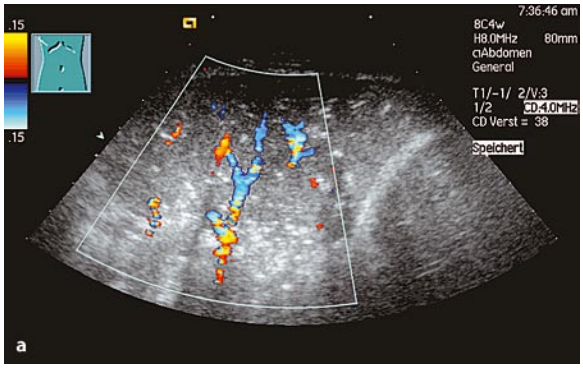

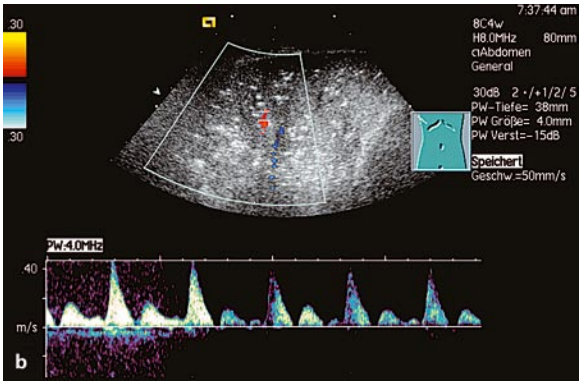

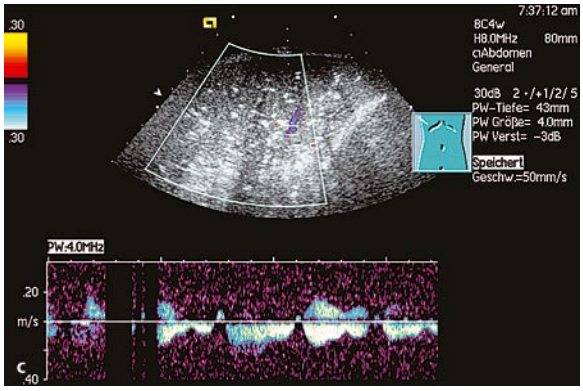

Fig. 8.12 **a** Aliasing on color Doppler in a pulmonary vessel in the presence of pneumonia. Given a low pulse repetition frequency in color Doppler (color scale, here 15 cm/s), color alone does not permit the investigator to conclusively establish the direction of flow. The change of color in the vessel is achieved via brighter colors. Thus, the mean flow rate in this vessel is more than 15 cm/s. **b** Pulmonary artery. Only when pulse repetition frequency is increased to 3o cm/s is it possible to clearly distinguish pulmonary vessels. On red color coding, color Doppler shows an afferent artery. On spectral Doppler, the corresponding Doppler frequency spectrum, suggesting four-phase flow. **c** Pulmonary vein. Blue color coding shows centrally aligned blood flow. Spectral Doppler shows the venous flow signal

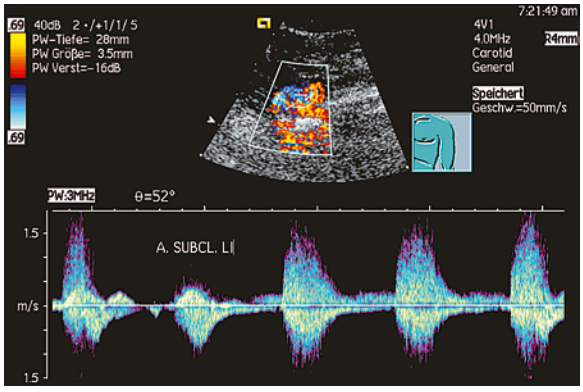

Fig. 8.13 Stenosis of the subclavian artery. In spite of high pulse repetition frequency (maximum 69 cm/s), there is markedly faster flow within the vessel, which is imaged by the bright color pixels in the vessel. Furthermore, the vessel itself is poorly delineated; color pixels are also seen outside of it. This is also known as a vibration artifact and is caused by tissue vibration secondary to stenosis and due to concomitant pulsations that cannot be reliably distinguished from the vessel in terms of space. Spectral Doppler shows flow maxima of about 1.5 m/s and retrograde flow (below the null line), as well as pathological, non-triphasic flow in this extremity artery

quency spectrum. Aliasing shows, for instance, higher-grade stenosis and disturbance of flow within vessels (Fig. 8.13). Increasing the PRF of color and spectral Doppler (up to the Nyquist limit) will help at least to reduce aliasing. It might also be possible to clearly determine the direction of flow (Fig. 8.12b, c).

8.6.4 Motion Artifacts

Mechanical movement of tissue against the ultrasound probe (breathing, musculature, cardiac and vascular pulsation, etc.) causes an apparent "frequency shift," which creates a signal in color Doppler as well. This disturbs, in particular, the assessment of structures dose to the heart and vessels due to persistent superimposition, and is a limitation of the method, e.g., in the detection of low blood flow in such areas. Various "artifact suppression" modalities proposed by manufacturers of ultrasound devices have achieved some improvement in this regard. Even in the presence of stenosis, movement of tissue due to concomitant motion (vibrations) on color Doppler might represent apparent flow signals outside the vessel (Fig. 8.13).

8.6.5 Unfavorable Angles

An angle of more than 60–90° may lead to incorrect Doppler measurements or incorrect imaging of blood flow (color Doppler and spectral Doppler). In such cases, the modality of power Doppler would at least help to image vessels in the thorax/lung (Yang 1996). In this setting, a largely angle-independent, directionally non-encoded, more sensitive documentation of blood flow is achieved by the visualization of amplitude (not frequency shift) of the backscattering echo.

8.7 Summary

On the one hand, artifacts are disturbing synthetic products which render visualization and assessment especially difficult in the chest because of the special anatomical features of this region. On the other hand, the absence of typical artifacts at the surface of the lung or the bony thorax makes it possible to diagnose certain diseases in the first place (subpleural lung lesion, rib fracture), as it allows assessment of parenchyma or bone. Finally, artifacts also nerve as a diagnostic criterion, e.g., air with reverberation echoes in the pleural space in the presence of pneumothorax.

References

Blank W (1994) Sonographisch gesteuerte Punktionen und Drainagen. In: Braun B, Günther RW, Schwerk WB (Hrsg) Ultraschalldiagnostik Lehrbuch und Atlas. ecomed, Landsberg. Bd III/11.1 S 20 f

Bönhof JA, Linhart P (1985) A pseudolesion of the liver caused by rib cartilage in B-mode ultrasonography. J Ultrasound Med 4:135–137

Bönhof JA, Bönhof B, Linhart P (1984) Acoustic dispersing lenses cause artifactual discontinuities in B-mode ultrasonograms. J Ultrasound Med 3:5–7

Dubs-Kunz B (1992) Sonographische Diagnostik von Rippenfrakturen. In: Anderegg A, Despland P, Henner H (Hrsg) Ultraschalldiagnostik 91. Springer, Berlin Heidelberg New York Tokyo, S 286–273

Kremkau FW, Taylor KJW (1986) Artifacts in Ultrasound Imaging. J Ultrasound Med 5:227–237

Mathis, G (1996) Lungen- und Pleurasonographie. 2. Aufl., Springer, Berlin Heidelberg New York Tokyo, S 110

Reading CC, Charboneau JW, Allison JW, Cooperberg PL (1990) Color and spectral doppler mirror-image artifact of the subclavian artery. Radiology 174:41–42

Schuler A (1998) Untersuchungstechnik und Artefakte. In: Braun B, Günter RW, Schwerk WB (Hrsg) Ultraschalldiagnostik Lehrbuch und Atlas, Bd I. ecomed, Landsberg, S 1–42

Wild K (1996) Periphere Gefäße. In: Braun B (Hrsg.) Ultraschalldiagnostik Lehrbuch und Atlas, ecomed Landsberg, S 10–13

Yang PC (1996) Color doppler ultrasound of pulmonary consolidation. European J Ultrasound 3:169–178

9 Interventional Chest Sonography

W. Blank

The cause of many diseases in chest organs can be determined by a combined evaluation of the patient's history, clinical findings and diagnostic imaging procedures. An elaborate diagnostic "cascade" which strings together any available methods is neither justifiable economically nor sensible from a medical viewpoint.

A definitive evaluation often requires additional biochemical, microbiological, cytological or histological expert assessment. The material needed for such investigations can be obtained by targeted puncture. Given the appropriate indication, the puncture may be followed by interventional therapeutic measures.

One should always employ the interventional method which provides a definite diagnosis in the fastest and least stressful manner for the patient.

Interventional measures in the thorax—various procedures:

1. Percutaneous access
   (a) Sonography
   (b) Radiographs (fluoroscopy, computed tomography, CT)
2. Endoluminal access
   (a) Bronchoscopy
   (b) Endoluminal sonography
3. Surgical (mediastinoscopy, thoracoscopy, surgical exposure)

9.1 General Indications

In addition to the frequent use of puncture for pleural effusion, space-occupying masses accessible to sonographic investigation, located in the chest wall, pleura, lung or anterior mediastinum, are important indications (Braun 1983; Börner 1986; Weiss and Weiss 1994; Pedersen et al. 1986)

Depending on their topographical position and the diagnostic availability and expertise, pathological changes not detectable by a transthoracic approach may be identified diagnostically by one of the interventional procedures displayed in the list in the previous section.

Interventions in the thorax—indications:

1. Space-occupying mass in the thoracic wall (tumors, abscesses, hematomas, changes in the skeletal parts)
2. Space-occupying masses in the pleura
3. Pleural effusion and pleural empyema (very small quantities, loculated effusions)
4. Peripheral lung consolidations (lung tumor, pneumonia, lung abscess)
5. Mediastinal processes (anterior mediastinum)

Because of the potential risk of complications, the indication for the procedure should be established with care.

Even if any sonographically demonstrable space-occupying lesion can be punctured in principle, one should only perform punctures if therapeutic consequences (e.g., radiation, chemotherapy) or important prognostic information is to be expected. In a patient who is operable, a suspected malignant tumor located in the periphery will normally not be punctured but will be resected as a first-line measure. It is not reasonable to merely seek confirmation of already established or plausible diagnoses. If the same information may be gathered in a less invasive way, puncture should not be performed. (Blank 1994, 2007; Beckh and Bölcskei 1997; Schwerk and Görg 2007).

9.2 Contraindications

Severe blood coagulation disorders (international normalized ratio more than 1.8, partial thromboplastin time more than 50 s and platelet count below 50,000) are an absolute contraindication. Bullous pulmonary emphysema and pulmonary hypertension are relative contraindications. When respiratory function is severely restricted or blood gas values are poor, a puncture should only be performed when the patient's condition is expected to be improved by the therapeutic intervention. High-risk puncture sites should be avoided (Yang et al. 1992; Mathis et al. 1999).

9.3 Sonography-Guided or CT-Guided Puncture

In several diseases of the lung and mediastinum, CT provides the best overview. It should, however, only be used as an interventional measure when the target and pathway of puncture cannot be reliably assessed with sonography (Blank 1994, 2007; Mathis 1997a).

The advantages of sonography-guided puncture are manifold: fast availability and bedside application (intensive care unit, emergency room), low rate of complications, absence of radiation exposure and low cost. In contrast to CT-guided puncture, the sonographic puncture can be carefully observed during the process. The investigator is free to use the pathway he/she desires in terms of direction; the ventilated lung is protected (low rate of pneumothorax). The nerve cords of the plexus in the region of the upper thoracic aperture may be demonstrated

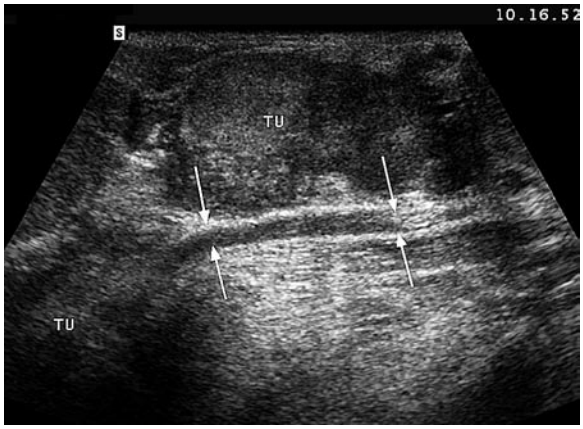

Fig. 9.1 Brachial plexus (*arrows*). Tumor masses (*TU*) in the region of the upper thoracic aperture

with high-resolution ultrasound probes, thus avoiding injury through puncture (Fig. 9.1).

Vessels are detected with color-Doppler sonography (upper thoracic aperture, parasternal). Active (vascularized) sections of a tumor may be identified by color-Doppler sonography and, recently, by the even more sensitive method of contrast-enhanced sonography. Diagnostic puncture may be performed with a high success rate or the tumor may be ablated therapeutically, if advisable. Atelectic or pneumonia-affected parts of peripheral lung consolidations may be differentiated from tumors by color-Doppler sonography or contrast-enhanced sonography (fewer motion artifacts)(Wang et al. 1995; Yang 1996; Zimmermann et al. 2003; Fig. 9.2).

Sonography-guided percutaneous puncture also has its limitations, however. If the space-occupying mass is hardly or not at all visible percutaneously on sonography, or if the puncture channel is not safe, other endoluminal procedures (bronchoscopy, endoluminal sonography) may be used or a computer-assisted puncture may

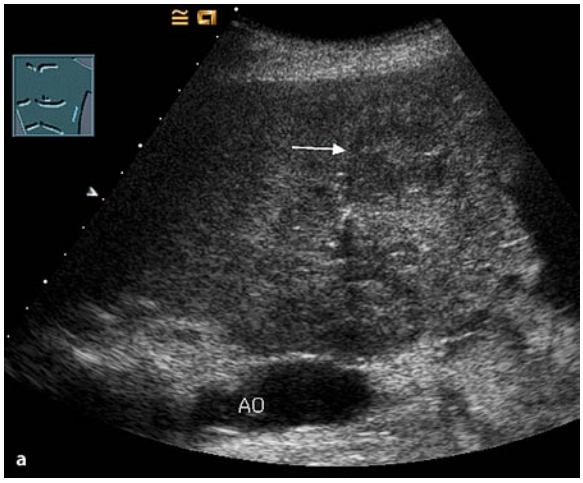

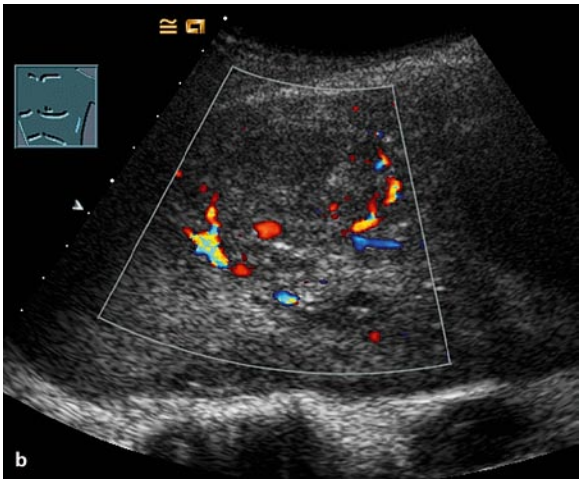

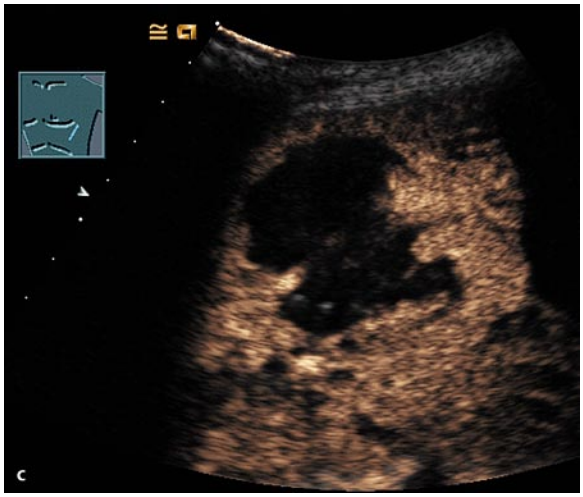

Fig. 9.2 Tumor inside an atelectasis. Computed tomography: obstruction atelectasis, cause not discernable. Bronchoscopy: no tumor found. **a** On B-mode sonography extensive atelectasis with a slightly conspicuous focal structural change(*arrow*). **b** In the area of structural irregularity there is no recognizable "normal" vessel architecture. **c** Space-occupying mass with little contrast on signal-enhanced sonography

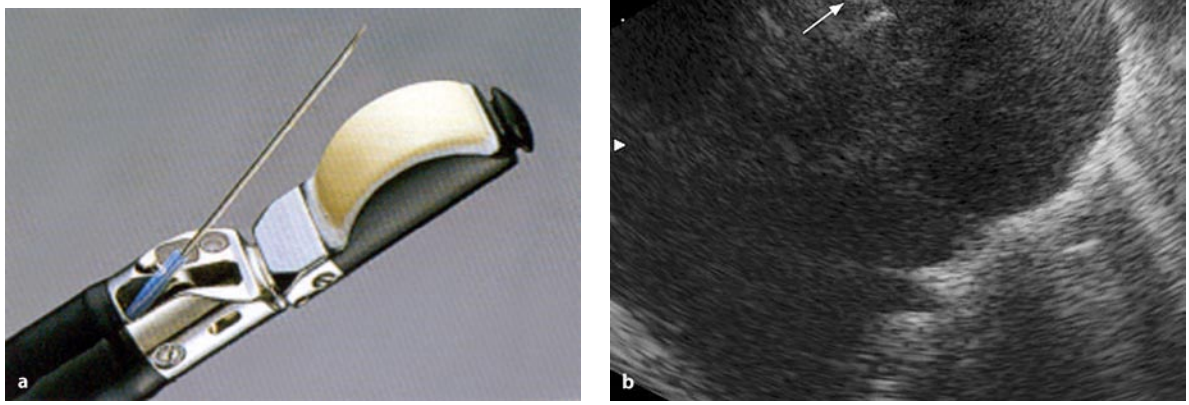

Fig. 9.3 Transesophageal puncture. **a** Longitudinal probe with puncture unit (Hitachi) **b** Paraesophageal hypoechoic tumor mass in the dorsal mediastinum. The puncture needle is easily recognizable (*arrows*). Cytology indicated small-cell bronchial carcinoma

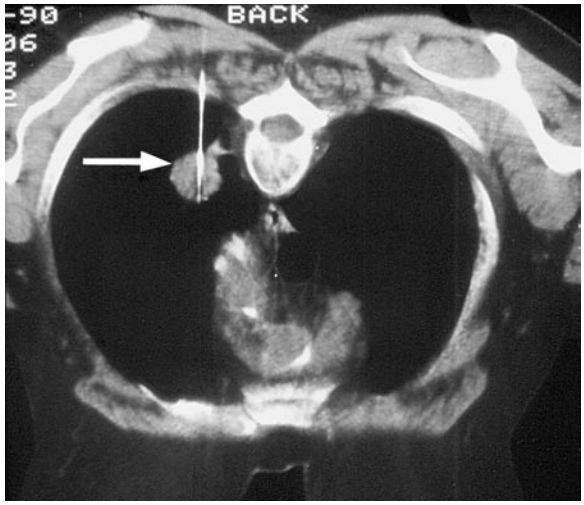

Fig. 9.4 Computed tomography assisted puncture of a round pulmonary mass which cannot be depicted by sonography, with a cutting biopsy needle (Tru-Cut 0.9 mm). The needle can be seen in longitudinal section. Histology indicated small-cell bronchial carcinoma

The advantages of sonography-guided punctures are as follows:

1. The method can be carried out quickly and at the bedside.
2. There is no exposure of radiation to patients, assisting personnel or physicians.
3. The direction of puncture may be chosen freely, and the needle monitored continuously.
4. Nerves (plexus in the upper thoracic aperture), vessels (color-Doppler sonography), and the ventilated lung are spared (lower rate of pneumothorax).
5. Active tumor parts (color-Doppler sonography, contrast-enhanced sonography) may be punctured with a higher success rate.
6. Lung tumors may be differentiated from areas of pneumonia or atelectasis by color-Doppler sonography and contrast-enhanced sonography (fewer motion artifacts)
7. It is a low-cost procedure, and it may often be performed on an outpatient basis.

be performed (Klose and Günther 1996; Mikloweit et al. 1991; Figs. 9.3, 9.4).

In principle, the interventional procedure constituting the fastest means of arriving at the diagnosis and placing the least stress on the patient should be used.

In US you see what you do, in CT you see what you have done" (Heilo 1996)

9.4 Apparatus, Instruments and Puncture Technique

For lesions of the chest wall, the investigator should use high-frequency linear probes. Lesions in the pleural space and lung should be investigated with sector-like probes equipped with a narrow covering. For endosonography-guided puncture, special intraluminal probes with biopsy canals are available (Kelbel et al. 1996).

The puncture needle can be guided in many ways (Fig. 9.5). A simple and economical method is so-called free puncture. Ninety percent of interventions are performed by the free-hand technique under sonographic visual control.

9.4.1 Puncture Needles

A distinction is made between fine (diameter less than 1 mm) and gross (diameter more than 1 mm) needles (Fig. 9.6). The rate of complications increases with the thickness of the needle and the duration of the procedure. The ideal puncture needle should fulfill the following criteria: it should be as thin as possible, sufficiently stiff to maintain the direction of puncture, cut sharply, be such that it can be advanced forward fast and be able to obtain sufficient material for investigation (Weiss and Düntsch 1996; Westcott 1980). Table 9.1 compares different classifications of needle diameters.

Table 9.1 Conversion table—needle diameter

Millimeters (mm)	Gauge (G)	French (Fr), Charriere (Charr)
0.7	22	
0.8	21	
0.9	20	
1.0	19	3
1.2	18	
1.35		4
1.4	17	
2.0	14	6
3.0	11	9
4.0	8	12
5.0	6	15

9.4.1.1 Fine Needles

For aspiration cytology, fine needles with a diameter of 0.7–0.9 mm are sufficient. They are available with and without a mandrin and have no cutting tip (economical injection needles, spinal puncture needles and Chiba needles).

Mandrins are usually not necessary, but their use is advisable if the pathway for puncture is long (through pulmonary tissue, for instance), because the needle bends less and there is no danger of abrading tissue outside the region to be punctured. A needle diameter of 0.7–0.9 mm is sufficient for cytological or bacteriological examination. If the liquid which needs to be aspirated is highly viscous (pus, blood), needles of a larger diameter must be chosen (1–2 mm maximum).

The puncture technique is as follows. Once the target of puncture has been reached, the puncture is performed, if possible, in a fan-like fashion under suction, in order to collect tissue from different areas (Fig. 9.7). With smaller tumors (less than 2 cm), it is often only possible to aim in one direction. In this case, turning the needle shaft may be helpful in collecting a tissue sample.

During forward and backward movement, cells are peeled off and aspirated into the tube. No suction should be applied during backward movement, so that material is not sucked into the syringe and dissemination of tumor tissue into the puncture canal is avoided.

A cytological slide is prepared by injecting the material collected onto the middle of the slide with high pressure. With use of a second slide, the material is spread with slight pressure and then, according to the agreement with the "house pathologist," fixated with alcohol (fixating spray, Merckofix, for instance) or air-dried. It is necessary to immediately scan the material under a microscope in order to make sure that there are enough cells for evaluation, so that a repeat puncture may be performed in the same session, which is necessary in one third of patients with suspected tumors. Bacteriological slides are made with Gram stain and bacteriological cultures started. If tuberculosis is suspected, special examinations are instigated (cultures, PCR, etc.)

The material obtained by this procedure usually only allows a cytological investigation which distinguishes between malignant and benign disease; it does not permit the investigator to determine the type of malignant lesion (e.g., lymphomas). If a quick diagnosis is needed and the proof of malignancy is sufficient, cytology is preferable at least as a first step. Recent immunocytological techniques with specially coated slides have improved results, but determining the type of many malignant changes (lymphomas, for instance) is usually not possible, so examinations of histological material become necessary. Immunohistological techniques have also distinctly improved the results of cut biopsies.

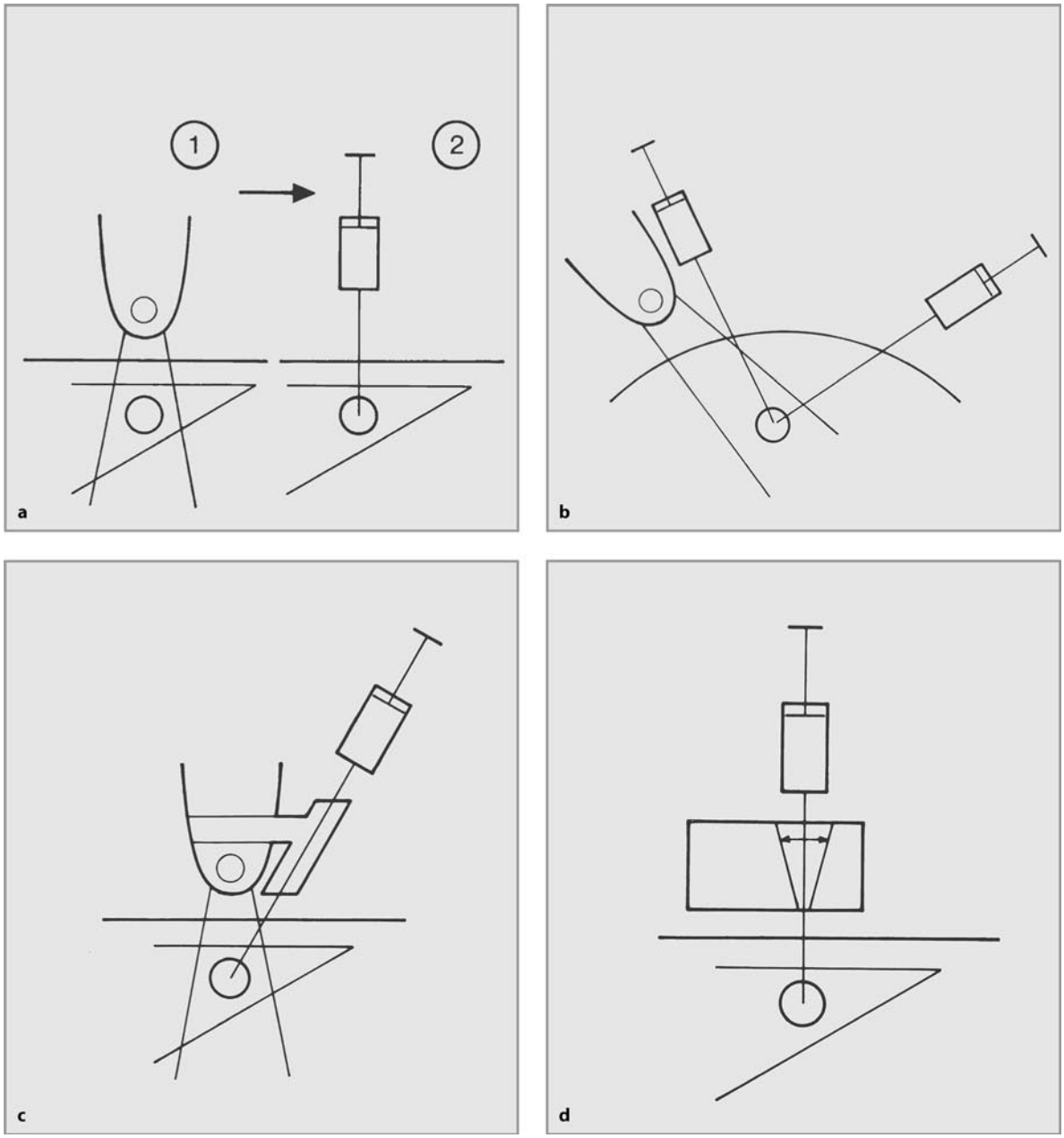

Fig. 9.5 Various puncture methods. **a**, **b** Free puncture. **a** Free-hand puncture after sonographic location. Inexpensive two-step method (no visual surveillance of the target area during the puncture). Very suitable for small processes located on the surface. **b** Puncture under sonographic observation. Low cost, puncture route variable, so punctures are possible from various areas, needle well visible, difficult with small processes located on the surface. Sterile gloves should be used for therapeutic procedures. **c**, **d** Guided puncture. **c** Ultrasound puncture probe. Expensive, puncture route not very variable, limited imaging through the perforation region, needle not easily visible, good view at close range. Seldom necessary for punctures of the thorax. **d** Sector/curved array scanner with attachment. Relatively cheap, needle is easily visible, but poor view at close range, puncture route prescribed but can be superimposed electronically, disinfection of the attachment necessary. Not sensible on the thorax

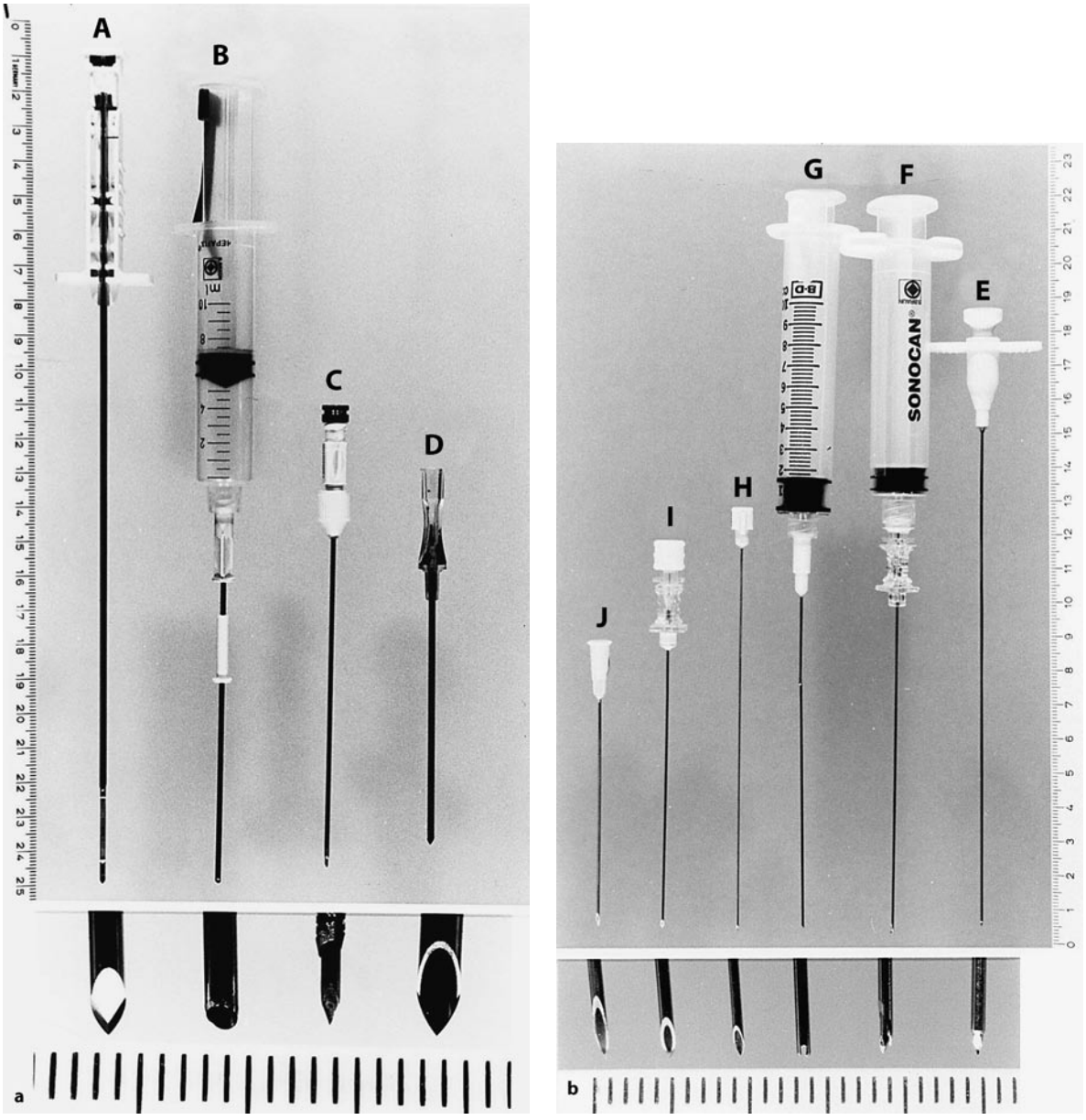

Fig. 9.6 Puncture needles. **a** Coarse needles. *A* Tru-Cut needle, diameter 1.4–2 mm. *B* Menghini needle, diameter 1.6 mm. *C* Bone punch needle (Angiomed). *D* Aspiration needle for viscous liquids, diameter 2.0 mm. **b** Fine needles. *E* Vaku-Cut needle based on Köhler (Angiomed). When the puncture destination has been reached, the stiletto is withdrawn three quarters of its length to create a partial vacuum. Diameter 0.8–1.2 mm. *F* Sonocan biopsy needle (Braun, Melsungen, Germany), diameter 0.8–1.4 mm, length 100–160 mm. Puncture technique as for the Otto needle, but without any rotating movement. *G* Cutting biopsy needle based on the Otto needle with a mandrin (Angiomed), diameter 0.8–1.2 mm, length 100–200 mm. *H* Chiba needle with a mandrin, diameter 0.6–0.9 mm. *I* Lumbal puncture cannula with a mandrin, diameter 0.9 mm. *J* Puncture cannula with no mandrin, diameter 0.7 mm

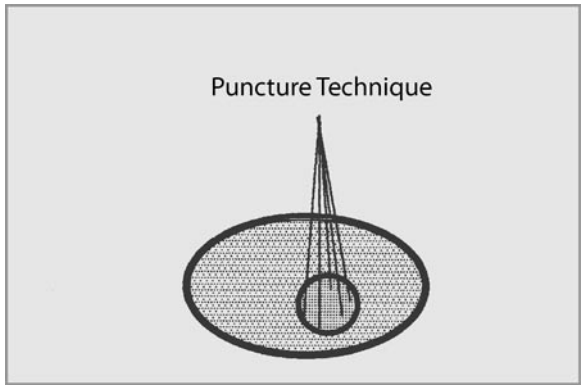

Fig. 9.7 Fine-needle aspiration puncture. Fan-shaped puncture technique

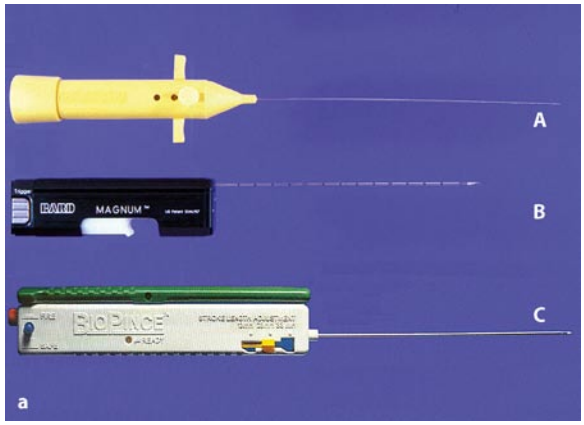

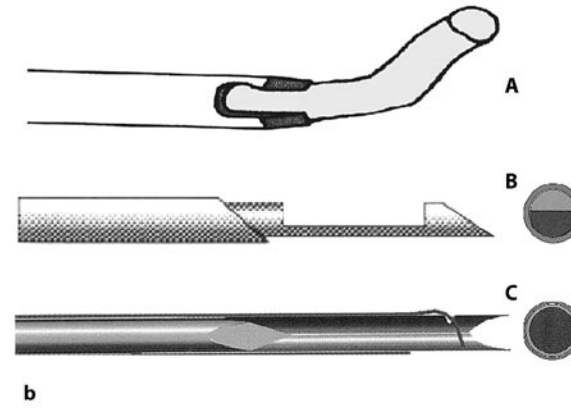

Fig. 9.8 **a** Automatic single-hand needle. The required depth of injection (measured sonographically) can be preset. *Top*: Auto-Vac puncture, disposable set (Bard). *Middle*: Reusable pistol from Barth with insertable Tru-Cut needles. The Tru-Cut needle contains a biopsy chamber. An advantage is that the cut cylinder of tissue cannot be lost when the needle is withdrawn. A disadvantage is the short tissue cylinder. *Bottom*: BioPince – biopsy pistol (Pflugbeil-Amedic). The full tissue cylinder is secured inside the needle by a special holding wire. **b** Surecut needle (*top*), Tru-Cut needle (*middle*) and BioPince needle (*bottom*)

Possible mistakes in punture cytology are:

1. Insufficient puncture technique
2. Little or useless material (possibly repuncture)
3. Aspiration of blood
4. False technique of slide prepration or fixation procedure
5. Little experience in cytology

9.4.1.2 Cutting Biopsy Needles

Tissue cylinders for histological assessment can be obtained with these needles. One-hand needles are useful, as *one* investigator performs the sonographic investigation and the puncture. Automatic one-hand needles (so-called puncture guns) are especially suitable in the thorax, as the procedure of puncture is fast, does not require the investigator to avoid the lung, and very representative puncture cylinders can be punched out from soft tissue (Fig. 9.8). The results of puncture are better and the complication rate is lower—especially the rate of pneumothorax. In the case of hard tumors or tumors of the bony skeleton, the spring pressure of the automatic needle is often not sufficient to penetrate the tumor.

Disadvantages are the cumbersome procedure and the absence of the sensation of performing a puncture (Mathis 1997b).

In the meantime, there are a variety of equivalent needles available on the market. It is sensible to familiarize oneself with *one or two* needle types. Three needle techniques can be differentiated:

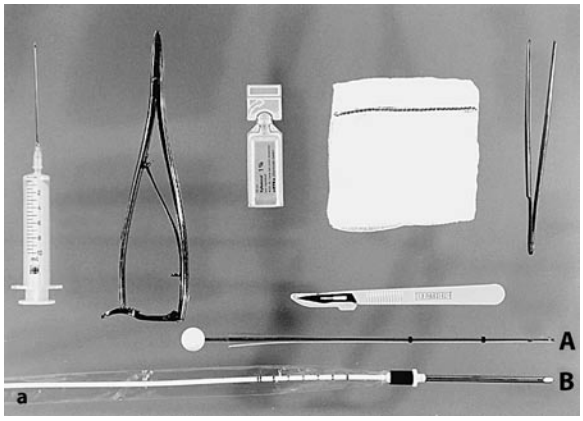

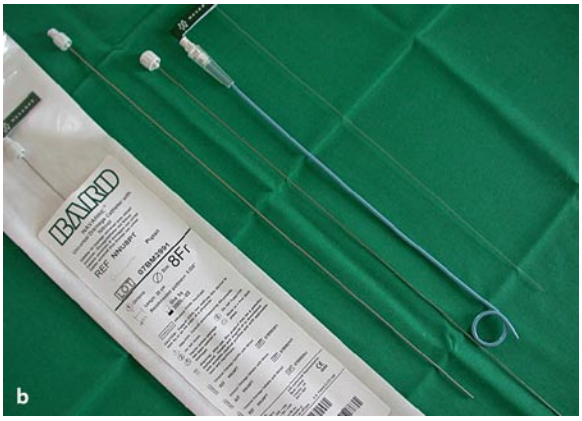

Fig. 9.9 **a** Pleural drainage set (trocar technique). *A* Thin (12-Fr) pneumo-catheter (Intra). *B* Trocar catheter (Argyle). **b** Navarre universal draining catheter (Bard—Angiomed 8–12 Fr) This catheter has many advantages: direct puncture only requires a small incision, introduction is possible without preceding dilatation, it does not kink, the lumen rarely occludes and the pig-tail prevents dislocation

1. *Tru-Cut principle*: The True-Cut needle contains a biopsy chamber, securing the cylinder which has been cut. A disadvantage is that the volume of the tissue particle is thinner in comparison with the needle diameter and also is only half-cylindrical.
2. *Surecut principle*: The cutting process happens through a quick forward movement of the needle. On retraction, the tissue cylinder is held within the cylinder by suction. If the negative pressure fails, the tissue cylinder may be lost (Fig. 9.8)
3. *BioPince principle*: Similar to the Surecut principle, complete cylinders are cut, thus yielding large tissue volumes (needle diameter 1.2 mm), producing better histological results. The needle combines the advantages of both principles mentioned above. A special "fixation wire" which gets propelled within the needle after the puncture procedure secures the tissue cylinder. Tumor seeding is very unlikely with this method (Fig. 9.8)

9.4.1.3 Gross Needles

Gross needles (1.2–2 mm) are usually only needed for aspiration of highly viscous fluid. For histological differentiation of benign lesions of the thoracic wall, pleural afflictions or interstitial pulmonary disease, True-Cut needles of a large size might be necessary (Gleeson et al. 1990; Ikezoe et al. 1990; Fig. 9.8).

9.4.2 Drainage Catheter

The diameter of the selected catheter depends on the viscosity of the liquid formation. In principle, drainage may be performed using the trocar or Seldinger's technique. *The trocar technique* is commonly used in the thorax (Fig. 9.9). Both drainage techniques are preceded by diagnostic puncture (Fig. 9.10).

9.4.3 Checking the Position of the Needle and the Catheter

Correct placement of the needle is not demonstrated by sonography alone. Moreover, the "sensation of puncture" usually changes when the target of puncture is reached. Depending on the situation, resistance is noticeable. The feeling of hitting something hard suggests a malignant tumor. The absence of any palpable sensation when cutting a cylinder is one of the few disadvantages of using a "puncture pistol." Optical visualization of the needle depends on the angle of the needle and the ultrasound beam. Ideally, when a needle is introduced at the level of the transducer, the needle shaft is seen as an echogenic double reflex. However, in deeper lesions, only the tip of the needle is seen as a bright double reflex (Fig. 9.11b). A compromise must be found between demonstrability of the needle (better with a larger angle) and targeting precision (better with a smaller angle). The choice of the points of approach is often limited in the thorax by the anatomy.

In tissue with high echodensity it may be difficult to localize the needle. Here, it is useful to move the needle or the mandrin backwards and forwards and even to em-

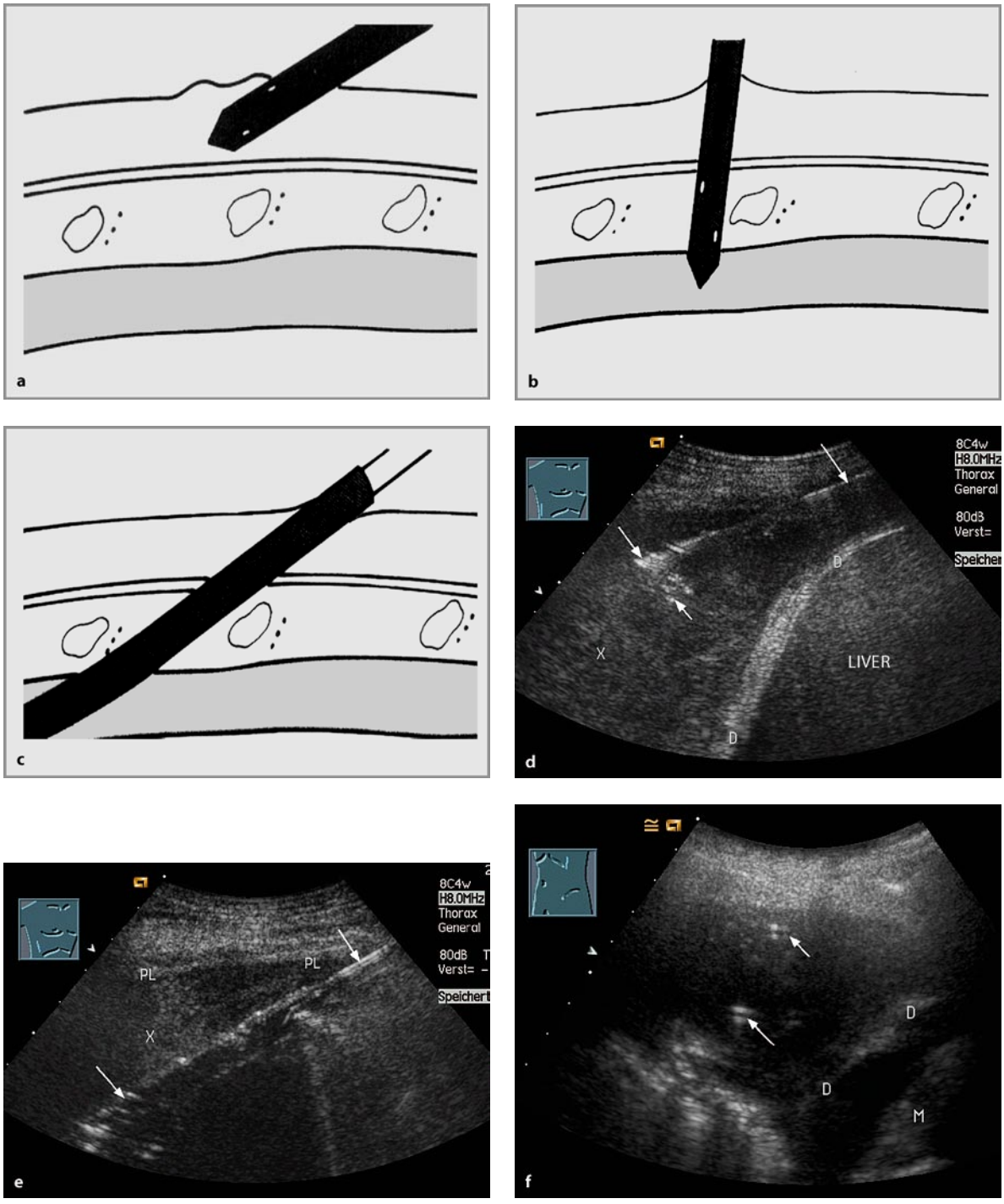

Fig. 9.10 Empyema of the pleura. **a**-**c** Pleural drainage. Outline of the technique. **d** On diagnostic puncture, the puncture needle (*large arrows*) is inserted in an upward direction at the upper edge of the rib. After instillation of liquid, an echogenic cloud shows up at the tip of the needle. *X* empyema.. **e** On insertion, the trocar is visible as a straight echogenic reflex, partly producing acoustic shadowing (*arrows*). *X* empyema, *PL* parietal pleura. **f** After removal of the trocar, the soft draining tube (double reflex) is more difficult to recognize because of its winding course

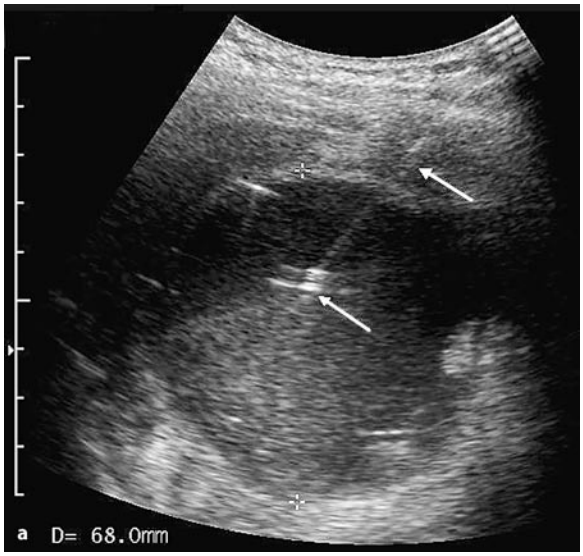

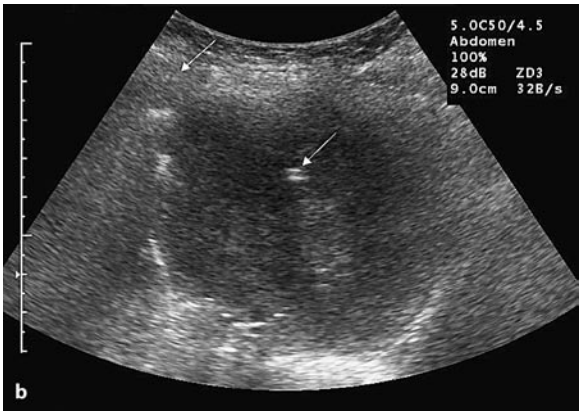

Fig. 9.11 **a** The needle shaft can be depicted at a great angle (45–90°) as an echogenous, straight-line reflex (*arrows*). The needle tip appears as an echogenic double reflex (*arrow far from the sound head*), but only if the needle is being guided correctly at the sound level. *Crosses* encapsulated pleural empyema. **b** Echogenic double reflex of the needle tip: double reflex is indicated by the *arrow far from the sound head*. As is so often the case, the puncture was not possible exactly at the insonation level. The needle shaft could only be indicated by wobbling movements (*arrow close to the sound head*). Hypoechic tumor on the thoracic wall. Peripheral bronchial carcinoma (squamous cell)

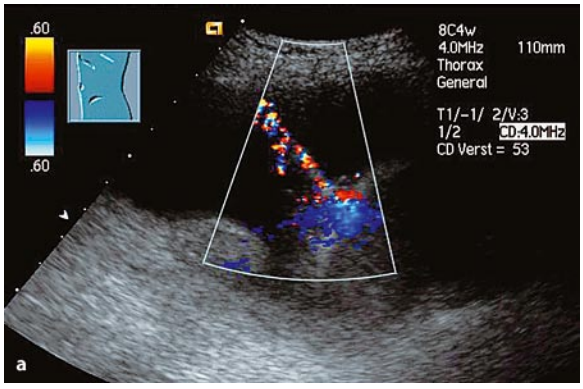

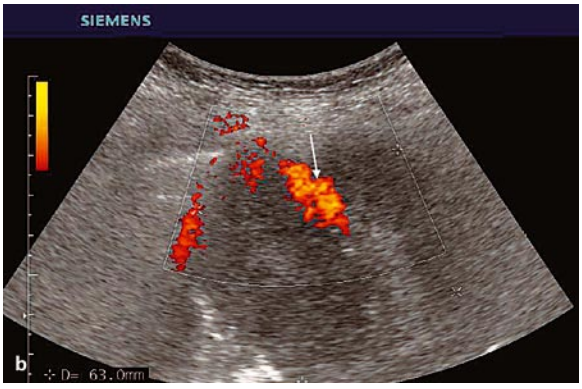

Fig. 9.12 **a** Color-Doppler sonography allows liquid movements in the needle to be detected. The exit of the liquid at the tip of the needle can be seen as a cloud of color. **b** Tissue shifts in the region of the needle tip (slight movement of the needle, or caused by suction) can also be detected by color-Doppler sonography (power Doppler). *Crosses* peripheral bronchial carcinoma

ploy brief suction. Color-Doppler sonography will show the needle as a colored line (Fig. 9.12). When a gun is used, the incision canal (air) is visible even several seconds after the puncture.

A drainage catheter is typically visualized as a bright double contour, which might not show up the whole way, however. On color-Doppler sonography, the course of the catheter during instillation of fluid is clearly depicted by color-coding (Wang 1995).

The coordination between the ultrasound probe and the needle tip works best if carried out as "one person–one hand puncture." Visualization of the spatial relations is better and necessary corrections in the position of the needle tip can be performed more quickly.

The inexperienced investigator should practice on models, e.g., on a steak interlarded with olives, or in a water bath (Mathis et al. 1999).

9.4.4 Preparation and Execution of Puncture

Most diagnostic puncture and draining procedures (of pleural effusions, for instance) may be performed on an outpatient basis. In principle, interventional procedures may be carried out in any room (emergency rooms, normal wards, intensive care wards), provided daily disinfection measures are guaranteed. (Sonnenberg et al. 1998). Transportable ultrasound machines may be advantageous.

Special puncturing equipment should be available: syringes, cannulas, puncture needles, drainage sets, gloves, disinfection spray, local anesthetics, sterile draping material and containers for further diagnostic processing (microbiological, chemical, cytological and histological examination) of the material obtained.

Coagulation status should be known (except in the case of lesions of the thoracic wall). Platelet aggregation inhibitors should be stopped 4–5 days before an elective procedure, if possible (in cases of coronary stent, the cardiologists should be consulted). In an emergency case, the risk must be calculated individually.

As with any invasive procedure, the patient must be informed of the course and risk of the procedure. The sonographical status of the thorax is evaluated. Utilizing other imaging methods (plain chest radiograph, CT), the puncture goal, the site of puncture needle placement, puncture direction and puncture pathway are determined (the four P's).

The nonsterile ultrasound gel is removed. In cases of diagnostic puncture the investigator should use sterile gloves, local disinfectant spray and sterile catheter gel if necessary. The patient is positioned such that the focus is optimally accessible in a sitting, dorsal, lateral or ventral decubitus position. Local anesthesia is only required in cases of multiple puncture or needles with a thick lumen though many patients opt for it.

During the puncture the patient must be asked to briefly hold his/her breath.

Interventional procedures of the thorax—preparation and performance:

1. Preparation
   (a) Acknowledging preexisting findings (bronchoscopy, chest radiograph, CT).
   (b) Sonographic thorax status.
   (c) Verifying the indication for puncture.
   (d) Is a sonography-guided intervention technically feasible?
   (e) Are there contraindications for an intervention?
   (f) Has the patient received prophylactic antibiotic treatment (especially in the case of an abscess)?
   (g) Have information about the procedure and written consent by the patient obtained?
   (h) Cytology or histology?
   (i) Selection of puncture equipment (needle, drainage).
2. Performance of intervention
   (a) Positioning the patient (sitting, dorsal, lateral or ventral decubitus position).
   (b) Visualization of the goal of puncture, the pathway and direction.
   (c) Disinfection and local anesthesia, if wanted.
3. Follow-up
   (a) For outpatients
   - Three hours of surveillance after intervention.
   - Sonographical check before discharge of patient (pneumothorax? bleeding?).
   - Preliminary report for referring doctor.
   - Final evaluation of the procedure.
   - Immediate return to the hospital in case of symptoms.
   - Decision on who informs about the result and when.

   (b) For inpatients
   - Preliminary report for doctor in charge.
   - Instructions for nursing personnel (checkup examinations, suction for drainage, etc.).
   - Sonographic reevaluation after 3 h (pneumothorax?, bleeding?).
   - Checkup examinations after therapeutic punctures and drainage.
   - Possibly repuncture in cases of inconclusive result.

Sonographically guided interventions—conditions for achieving good results:

1. Careful formulation of indication (clinical experience)
2. Experience in sonography and puncturing
3. Knowledge of possible complications and limitations of the method
4. Quality of and preparation of material obtained
5. Experience of the pathologist (immunohistology) and microbiologist
6. Interdisciplinary cooperation

9.5 Indications

9.5.1 Processes of the Chest Wall

Soft-tissue tumors should be punctured parallel to the surface of the lung as far as possible. The needle can

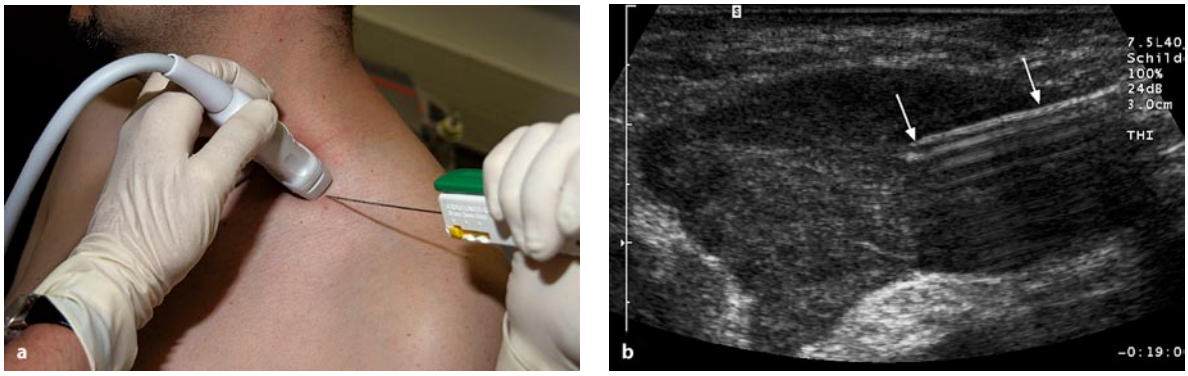

Fig. 9.13 **a** Classic puncture technique, upper thoracic aperture. **b** Classic puncture technique. Metastasis of the thoracic wall. The needle shaft (*arrows*) can be delineated very well at this favorable angle

then be (at a suitable angle) nearly completely imaged in its length and the risk of pneumothorax is minimized (Fig. 9.13).

Needles with a large caliber may be used for this technique (1.4–2 mm). By doing so, even benign lesions are better differentiated (Gleeson et al. 1990; Bradley and Metreweli 1991; Sistrom 1997).

Postoperative accumulation of fluid is treated by multiple puncture or, if necessary, with drainage.

Pathological processes of the bony skeleton are a domain of computer-assisted puncture, if the cortical bone is still intact. Frequently, diseases lead to defects in the cortical bone and may consequently be visualized well by sonography and also punctured (Fig. 9.14). Fine-needle aspiration puncture is usually sufficient for differentiation of inflammation/malignoma and carries a success rate of 88–100%. If plasmocytoma is suspected, puncture is always preferable to cut biopsy, because diagnosis is easier from a slide preparation. For typification of a malignoma, a cut biopsy might be preferred in some cases.

Before puncturing tumors of the upper thoracic aperture, the nerve cords (brachial plexus) and vessels (color-Doppler sonography) should be identified in order to avoid injury to these structures (Vogel 1993; Civardi et al. 1994; Blank 1995, 2007).

9.5.2 Pleural Cavity

9.5.2.1 Thoracocentesis

In cases of large quantities of effusion, sonography helps to establish the extent of the effusion and mark the site of puncture in the optimal intercostal space. The puncture is then performed on the ward (Reuß 1996). In cases of complex effusions (small, loculated, encapsulated, inconvenient location), the puncture is safer when performed under continuous sonographic visual control (Fig. 9.15). By doing so, the rate of pneumothorax is markedly reduced (less than 1%). The success rate is 97% (O'Moore et al. 1987). Unsuccessful punctures can be avoided when "the fluid color sign" is demonstrated (Wu et al. 1995; Fig. 9.16). Synthetic indwelling catheters should be given preference over metal ones because of the risk of injury to the lung from metal.

After application of local anesthesia, the synthetic tube is pushed forward at the upper margin of the rib (in order to avoid injury of the nerve-vessel bundles running along the lower edge of the ribs) upwards to the pleura with a mandrin (Abbocath; Abbott, Abbott Park III). Entry into the pleura is marked by a mild increase in resistance. The mandrin is then removed. In a closed system, special pleural drainage sets can be used to perform manual aspiration.

Uncomplicated pleural effusions in the presence of cardiac failure, pneumonia and even small pneumothorax after puncture can be treated with thoracocentesis.

Malignant pleural effusions, accumulation of pus or blood should be treated with a drain because of the risk of septation (Blank 1994).

The success rate of cytology in malignant effusions is no more than 50–75% (Gartmann 1988). In tuberculous effusions, pathogens are demonstrated in only 20–40% of cases (Vladutiu 1986).

9.5.2.2 Pleura Biopsy

Since even the classic pleural blind biopsy according to Abrams or Ramell has an accuracy of no more than 50% in malignant effusions, video-assisted thoracoscopy is being used more and more. Sonography-guided pleural biopsy is one alternative. The procedure has only been used in a very small number of cases so far, however (Mueller

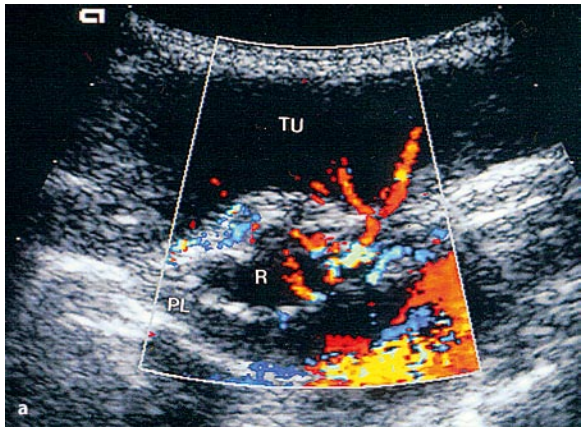

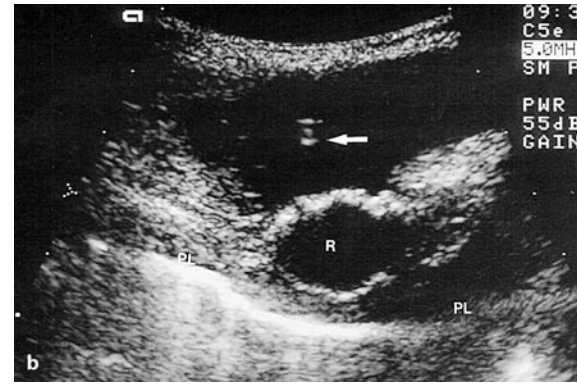

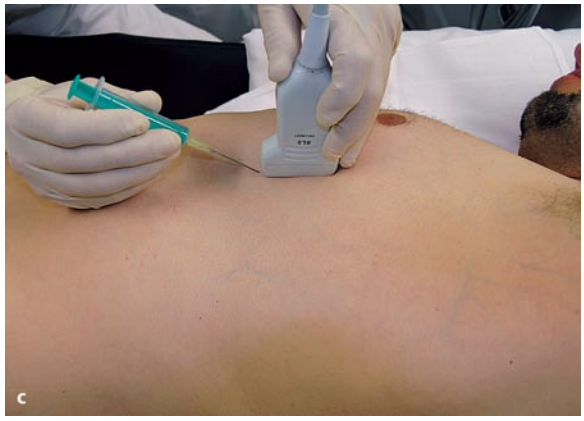

Fig. 9.14 **a** Destructed rib (*R*). Echo-free "soft tissue tumor" (*TU*). Color-Doppler sonography allows vessels to be depicted in the destructed rib and in the surrounding soft tissue tumor. *PL* pleura. **b** Fine-needle puncture of the soft-tissue tumor. The tip of the needle can be seen as an echogenous double reflex (*arrow*). Cytology indicated plasmocytoma. **c** Classic puncture technique

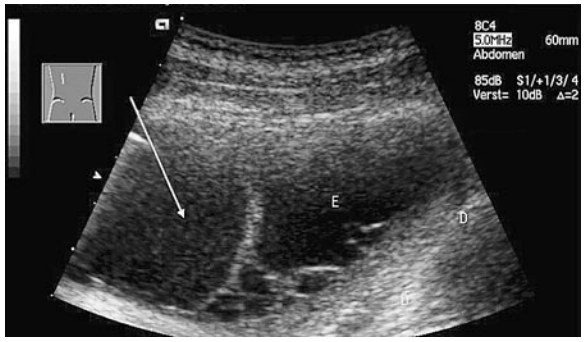

Fig. 9.15 Septated pleural effusion. Primary diagnostic puncture disclosing an encapsulated empyema (*arrow*). The secondary step involved pleura drainage. *D* diaphragm

1988). As an alternative, automatic single-hand needles (BioPince needle, for instance) may be used successfully (sensitivity 70–80%, specificity 100%) (Chu 1994; Heilo 1996). The recently introduced forceps biopsy needles might be helpful (Seitz et al. 1999; Fig. 9.17). Fine-needle aspiration biopsy of tissue taken from a pleural thickening is of no value and is even hazardous (danger of bleeding). It may only be employed in the presence of focal lesions (Mathis et al. 1999).

9.5.2.3 Percutaneous Pleural Drainage

Given the appropriate indication, malignant, hemorrhagic and inflammatory pleural effusions may normally be treated with a sonography-guided pleural drain quickly, safely and successfully (Klein et al. 1995). Only rarely CT-guided puncture is necessary if the approach is difficult. Thin catheters (8–14 Fr, Pleurocat, for instance) are sufficient. These thin catheters are tolerated better by

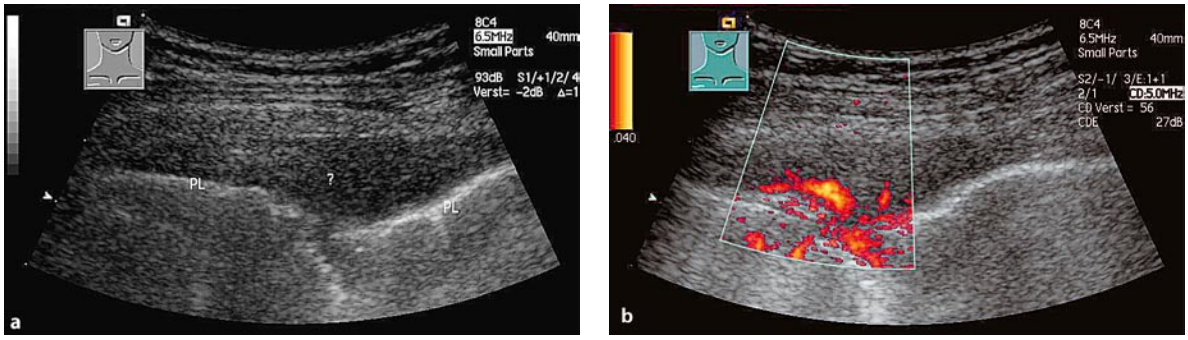

Fig. 9.16 **a** B-mode sonography for a differential diagnosis of an encapsulated effusion or fresh rind. *PL* visceral pleura. **b** Power Doppler demonstrates advanced vascularization with high-caliber vessels. Fresh pleural rind

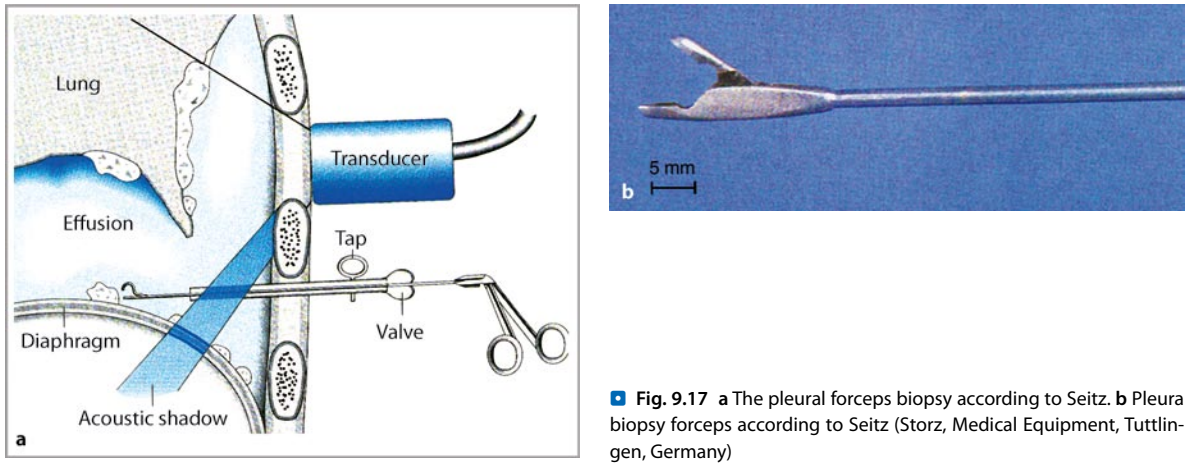

Fig. 9.17 **a** The pleural forceps biopsy according to Seitz. **b** Pleura biopsy forceps according to Seitz (Storz, Medical Equipment, Tuttlingen, Germany)

most patients than thick catheters traditionally used in many hospitals. Their success rate is equivalent, and they carry a much lower complication rate. Puncture is usually performed with the trocar technique. The catheter should be placed in the lowest possible part of the pleural cavity.

Parapneumonic fluid collections should be drained soon in cases of septum formation and a pH level below 7.2. A drain should be left in place for 5–10 days, depending on the extent of inflammation.

In cases of malignant effusions, catheters with a narrow lumen (7–12 Fr, e.g., Pleurocat, Plastimed), will suffice. The puncture is usually performed using the trocar technique. The catheter is placed in the lowest part of the pleural cavity.

Early diagnostic verification of a pleural empyema is important, as percutaneous therapy is only successful (success rate, 72–88%) in the acute phase (weeks 1–4) (Klose and Günther 1996; Blank 1994; Figs 9.10, 9.15, 9.18). The success of drainage in the presence of septation can be markedly improved by the instillation of urokinase (50–100,000 IU per treatment) (Sistrom 1997).

9.5.2.4 Lung Consolidations

Peripheral pulmonary lesions may be visualized sonographically if they are situated in a favorable topographical position. They may be punctured if they reach the visceral pleura or if a poststenotic atelectasis or pneumonia provides an acoustic window.

At the time of diagnosis, two thirds of lung carcinomas are no longer curable by surgery. The histological type must be determined before palliative therapeutic measures are employed. In the diagnosis of the peripheral lung tumor, sonography-guided puncture is markedly superior to bronchoscopy, much easier and faster to perform than radiography or even computer-assisted percutaneous biopsy, and devoid of radiation (Chan-

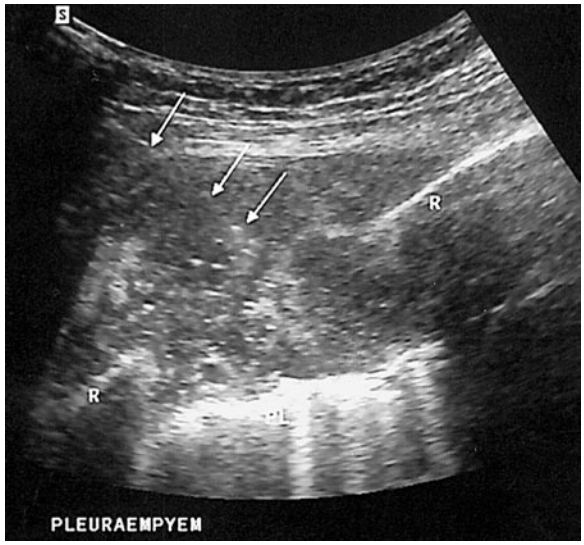

Fig. 9.18 An 80-year-old patient, whose temperature rose rapidly a few days after a fall which injured the left side of the thorax. X-ray image reveals a shadow located on the thoracic wall, suggestive of a fractured rib. Sonographic mass with infiltration into the thoracic wall. Minor liquid movements were perceptible during the dynamic examination. The diagnostic puncture was not successful until a coarse needle (with a diameter of 2 mm) was used. It proved possible to extract highly viscous pus. A pleural drainage was then inserted. *Arrows* needle shaft

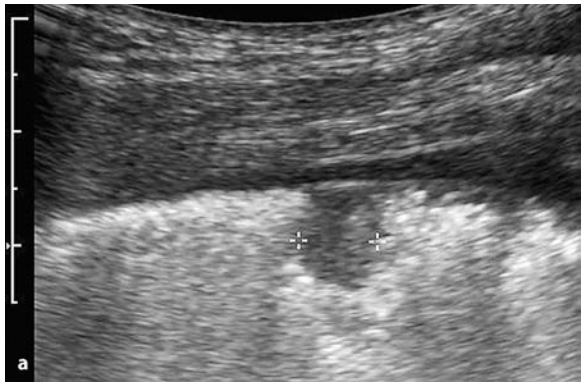

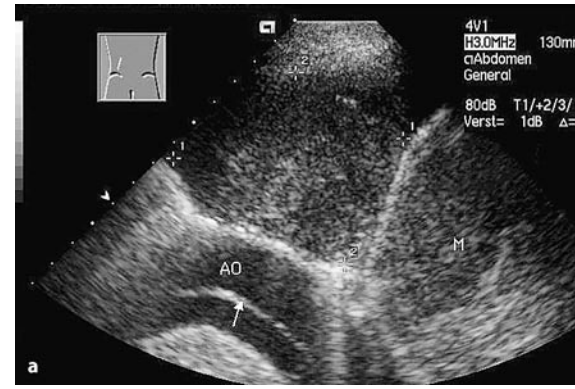

Fig. 9.19 **a** Several small peripheral lung tumors (maximum diameter 18 mm) located on the thoracic wall. Delicate pleural effusion. Fine-needle aspiration cytology indicated small-cell bronchial carcinoma. **b** Large mass, left dorsobasal location (*crosses*), alongside the diagraphragm and also the descending aorta (*AO*). A dissecting aortic aneurysm had been identified in this patient 4 years earlier. *Arrow* dissection membrane. Fine-needle incision biopsy (Sonocan needle, 0.9 mm in diameter). Histology indicated squamous cell carcinoma

drasekhar et al. 1976; Börner 1986; O'Moore et al. 1987; Hsu et al. 1996; Fig. 9.19).

Peripheral tumors larger than 3 cm in size should be diagnosed by fine needle cut-biopsy (histology) (Mathis and Gemacher 1999; Schubert et al. 2005). Peripheral tumors smaller than 3 cm in size can be better diagnosed by fine-needle aspiration cytology (Sistrom 1997). Biopsy is not always sufficient (accuracy 70%) to distinguish benign tumors. Wedge resections obtained by thoracoscopy are given preference in many cases (Beckh and Bölcskei 1997).

9.5.2.5 Special Puncture Technique

A safe pathway for puncture circumventing the ventilated lung is an important prerequisite of avoiding pneumothorax. Larger tumors may be punctured in the classical way. The needle is inserted at the level of the ultrasound probe. The needle tip is pushed towards the parietal pleura under continuous sonographic observation. While the patient holds his/her breath, the lesion is punctured in such a way that the needle does not reach the ventilated lung. To achieve this, the puncture depth is measured before-

hand and marked on the needle in the case of using an automatic one-hand needle.

Small (less than 1-cm) tumors located in the periphery may also be punctured if expertise is sufficient. Puncture technique must be adjusted to the individual type of lesion. Similar to puncture of the thyroid, atypical puncture is often necessary (Blank 2007). The tip of the needle must be inserted through the skin almost vertically, near the middle of and parallel to the probe, which has as little contact with the skin as possible. By tilting the probe in a plane vertical to the plane of the probe, one can identify the needle tip inside the thoracic wall, push it towards the pleura and insert it into the lesion under observation. Visualization of the needle tip is facilitated by moving it back and forth abruptly.

Alternatively, small lesions may be punctured "from memory" after marking the intended site of puncture with a ballpoint pen, for instance (small ring pressed into the skin). The results are no worse in the hands of experienced examiners.

If a small perforated ultrasound probe is available, this may also be used for a successful puncture.

9.5.2.6 Pneumonia and Pulmonary Abscesses

The cause of consolidation of sections of the lung may be difficult to classify in immunosuppressed patients, especially. Aspiration puncture or cut biopsies of the areas with consecutive microbiological, cytological and histological examination of the material obtained allow a diagnosis in up to 93% of cases (Yang et al. 1985).

Even small pulmonary abscess that escape detection on the radiograph can be imaged by sonography (6–7 mm). If antibiotic therapy does not yield the desired result, fluid may be aspirated from the region of the abscess under sonographic guidance. By this means, the pathogen can be isolated in about 65–93% of cases (Gehmacher et al. 1986; Yang et al. 1992). If therapy continues to fail, a lung abscess drainage may be performed under sonographic guidance but this is rarely necessary (Sonnenberg et al. 1991; Klein et al. 1995; Fig. 9.20). The risk of bronchopleural fistula formation is minimized when the investigator uses the shortest access and traverses solid, homogeneous, infiltrated or atelectatic tissue (Mathis et al. 1999).

9.5.3 Mediastinum

Few space-occupying masses in the mediastinum (retrosternal goiter, cyst, aneurysm, thrombosis) can be reliably classified on the basis of characteristic sonographic features. An investigation of fine tissue is needed in order to determine the cause of the lesion. Gentle removal of tissue without causing a large defect is very important in the diagnosis of space-occupying masses that can be removed by surgery (Rosenberg 1993). Therefore, puncture under image guidance should be the first procedure. When this is done, space-occupying masses in the mediastinum can be easily punctured from a suprasternal or parasternal approach under sonographic guidance (Nordenstrom 1967; Rubens et al. 1997). The accuracy is 54–100%, and the rate of complications is 0–4%. Vessels should be avoided (color-Doppler sonography) (Blank et al. 1996; Figs. 9.21, 9.22). In cases of superficial lesions (thymomas, lymphomas), gross needles are given preference. With use of a needle with a thick lumen, correct histological classification is achieved in up to 93% of cases and the rate of complications is only slightly higher, at less than 1% (Fig. 9.23). In our experience, a needle diameter of 1.2 mm (BioPince needle) is normally sufficient.

In contrast to radiographic or CT-guided puncture (10–44%), pneumothorax is rarely encountered (Yang et al. 1992; Heilo 1993, 1996; Schuler et al. 1995; Gupta et al. 1998).

In recent years, endosonographic transesophageal guided puncture has also been used successfully. It is a good complement to percutaneous puncture, as lesions in the anterior mediastinum are not easily accessed, in contrast to those in the posterior and lower mediastinum (Schlotterbeck et al. 1997; Pedersen et al. 1996; Hüner et al. 1998; Jannsen et al. 1998).

9.6 Risks

Sonography-guided puncture has a low rate of complications. The rate of pneumothorax is 2.8%; 1% require drainage (Table 9.2). Hemorrhage or hemoptysis is observed in 0–2 %. Data concerning air embolism or even death are not available so far. Tumor dissemination through the procedure of puncture (vaccine metastases) is of little clinical significance and very rare, in less than 0.003% of cases. In cases of malignant pleural mesothelioma, it is slightly more common. When surgery is performed, the site of puncture is also resected (Weiss and Düntsch 1996; Mathis et al. 1999).

9.7 Pneumothorax After Puncture

If the focus is no longer visible after the puncture, the likelihood of a pneumothorax is high. This can be reliably detected by sonography, through the absence of respiration-dependent gliding movement of the pleura (Blank 1994; Herth et al. 2004; Reissig and Kroegel 2005; Fig. 9.24).

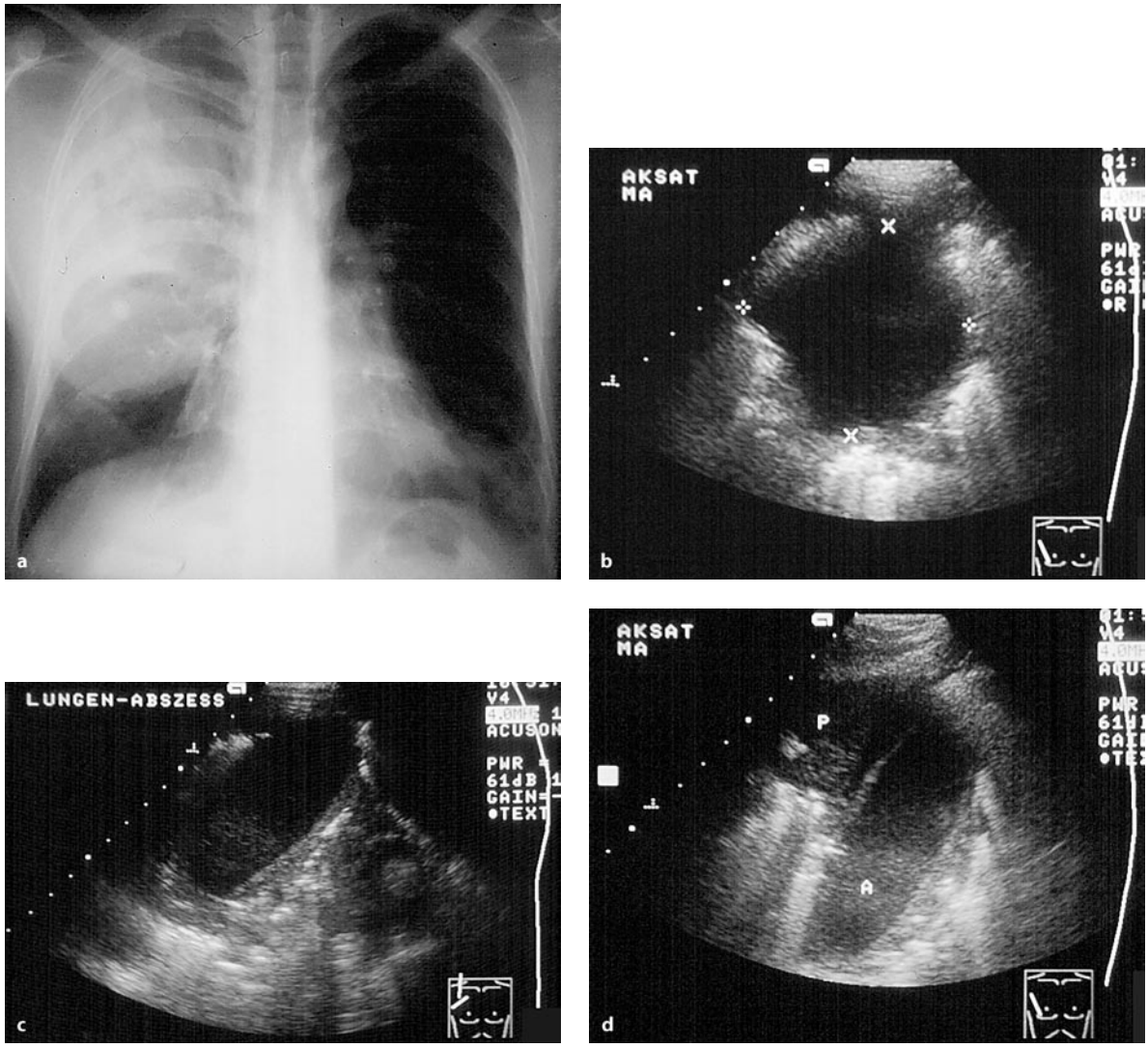

Fig. 9.20 Lung abscess with drainage. Young man with community-acquired pneumonia not responding to standard antibiotic therapy. Continuing high temperatures and respiratory deterioration. **a** On chest X-ray, extensive infiltration of the right upper lobe of the lung. **b** Sonography clearly demonstrates abscess formation. **c** Next to the abscess *(A)*, pneumonic consolidation *(P)* is visible. If this does not contain air, puncture passing through this section would be feasible. The abscess is encapsulated by a membrane. **d** The shortest pathway for transthoracic puncture is chosen, and pus can be aspirated through the needle. **e–f** *see next page*

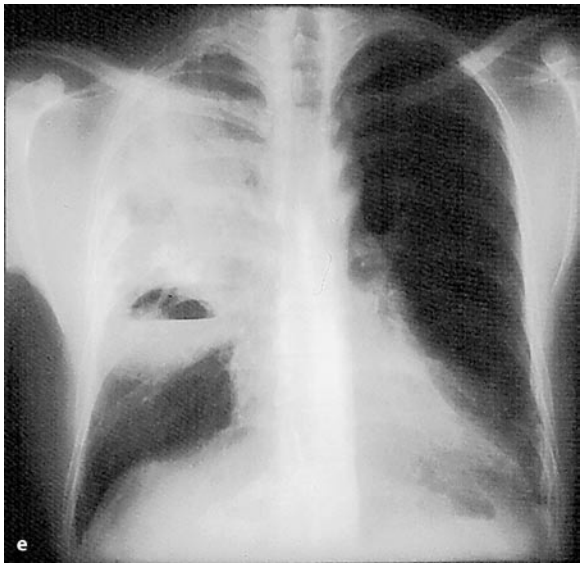

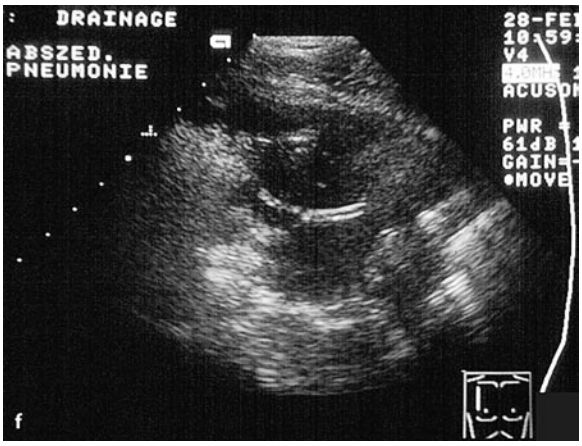

Fig. 9.20 *(continued)* **e** Abscess formation on chest X-ray. **f** The abscess is drained by a suction-rinse-drainage (echogenic double lumen) over 4 days. Quick recovery ensues

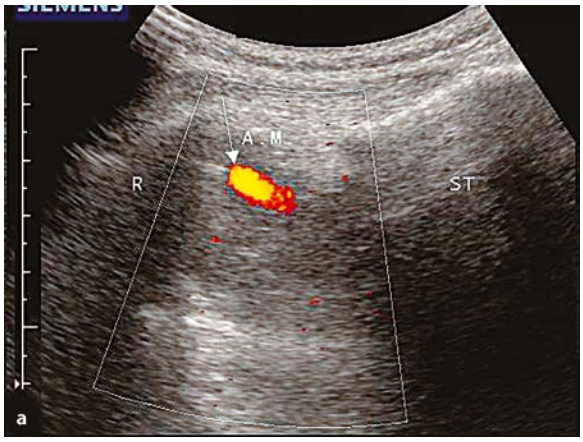

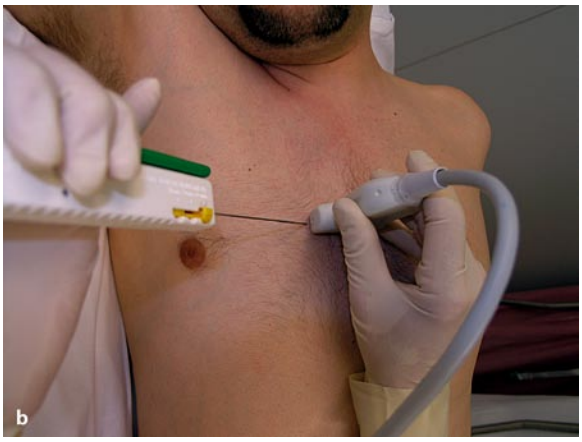

Fig. 9.21 **a** Mediastinal tumor. Parasternal plumb line in the right lateral position. Hypoechoic, indistinctly delineated mass (located in the color window). Color-Doppler sonography in "power" mode shows the mammary vessels located parasternally, **b** which have to be avoided during a punch biopsy

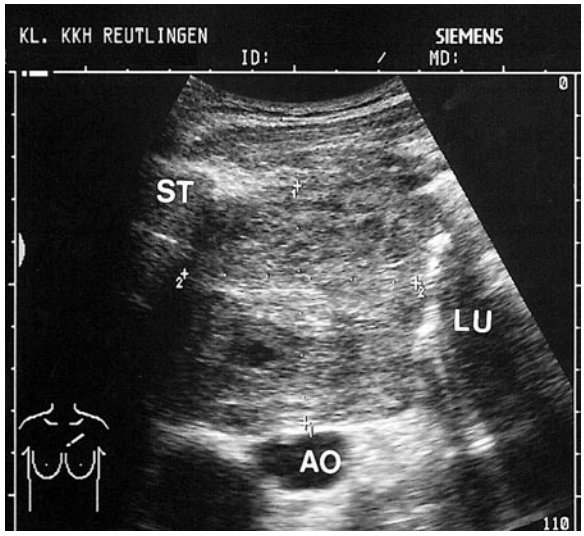

Fig. 9.22 A large mediastinal mass was discovered primarily by sonography, located parasternally on the left, in a 19-year-old patient during emergency treatment connected with a superior vena cava syndrome. A punch biopsy was performed immediately (Sonocan needle, 1.2-mm diameter). Histologically, a highly malignant non-Hodgkin lymphoma was diagnosed. *ST* sternum, *LU* lung, *AO* descending aorta

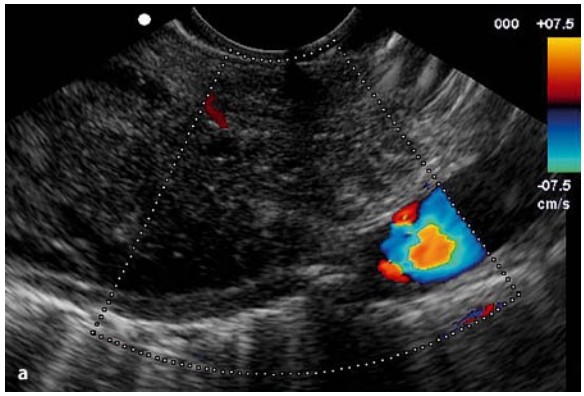

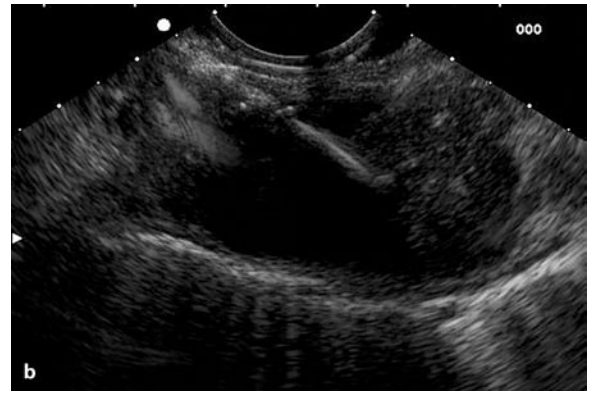

Fig. 9.23 Paravertebral abscess in a case of spondylodiscitis. At first, open surgical drainage of the spondylodiscitis was performed, followed by endosonographically-guided nasal/transesophageal drainage used for rinsing with isotonic saline. **a** Space-occupying mass located next to the spine and the aorta. **b** Insertion of drain

The quantity of free air can only be measured by obtaining a chest radiograph. A pneumothorax usually reaches its maximum dimensions after 3 h, so the decision regarding a therapeutic procedure is made thereafter, when the pneumothorax is small. If the patient is symptomatic or if a larger volume is present, the patient is initially given protracted thoracocentesis. The success rate within the first 10 h is 90% (Klose and Günther 1996). In the event of renewed collapse, the clinician should use a percutaneous drain and a catheter with a small lumen.

A routine chest radiograph is not required after sonography-guided puncture.

9.8 Summary

Provided the indication is established with care, interventional measures in the thorax are very successful. The rate of complications is low when the procedure is performed by trained therapists.

The basic principle to be applied is: "Try ultrasound first" (Sistrom 1997).

Table 9.2 Sonography- guided chest puncture: accuracy and rate of pneumothorax

Authors	Year	Patients (*n*)	Accuracy (%)	Pneumo-thorax (%)
Izumi et al.	1982	20	80	0
Schwerk et al.	1982	15	93	0,5
Cinti and Hawkins	1984	12	83	0
Ikezoe et al.	1984	38	79	0
Yang et al.	1985	25	84	8
Pedersen et al.	1986	45	84	2
Pang et al.	1987	54	85	4
Heckemann et al.	1988	42	98	6
Yin	1989	85	98	2.4
Ikezoe et al.	1990	124	90/67	4
Bradley and Metreweli	1991	30	90	0
Mikloweit et al.	1991	45	85	4.4
Targhetta et al.	1992	64	86	3
Schulz	1992	75	91	2.5
Yang et al.	1992	218	95	1.3
Yuan et al.	1992	30	92/83[a]	3
Metz et al.	1993	41	84.6	5
Tikkakoski et al.	1993	200	93	2.5
Chu et al.	1994	116	92/53	?
Czwerwenka and Otto	1994	82	83	0
Vogel	1995	110	70	3.6
Hsu et al.	1996	188	94	1.6
Knudsen et al.	1996	128	93	4
Beckh and Bölcskei	1997	50	92	2
Dallari et al.	1999	45	92/33	?
Mathis et al.	1999	155	92/87[a]	1.9
Diacon et al.	2004	91	85	4
Total		1.967		2.6

[a] Malignant/benign lesions

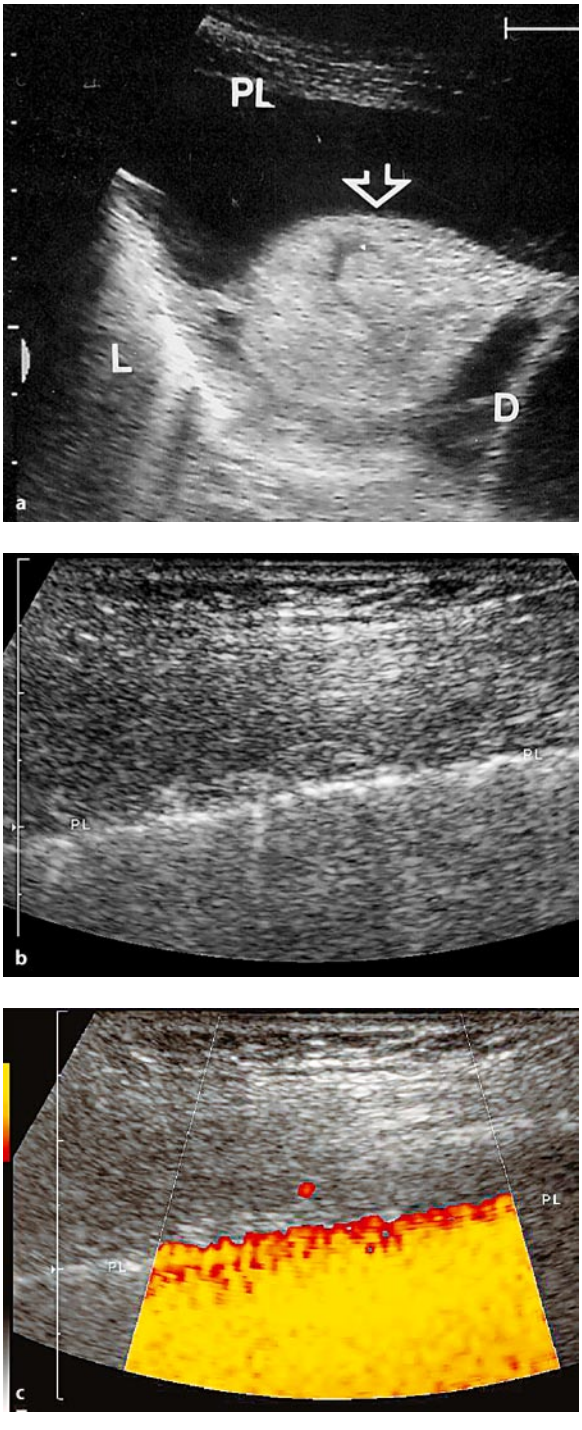

Fig. 9.24 **a** A blood clot (*arrow*) as a complication following a diagnostic puncture of a pleural effusion. *PL* parietal pleura, *L* compressed lung, *D* diaphragm. **b** Pneumothorax was excluded by showing the sliding sign of the pleura. **c** Color-Doppler sonography in "power" mode allowed the respiration-dependent sliding sign to be documented in an impressive way even in the static image. The repeat echoes that could be demonstrated with B-mode sonography (artifact) dorsal to the pulmonary surface show up accordingly as a color artifact. This cannot be demonstrated in cases of pneumothorax

9.9 List of Materials

Sterican. Disposable injection cannula, size 1 (G 20/0.9×40/80 mm). B. Braun Melsungen AG, 34209 Melsungen, Germany

BioPince. Disposable full-cylinder biopsy pistol (G 18/1.2×100/150 mm). Inter.V, Gainesville, FL 32608 USA. Distributor Peter Pflugbeil GmbH, Georg-Wimmer-Ring 21, 85604 Zorneding, Germany, Fax: +44-8106-241333, email: info@pflugbeil.com, Internet: http://www.pflugbeil.com

Sonocan. Disposable set for sonography-guided full-cylinder biopsy by B. Braun Melsungen AG (G 20/0.9×100 mm/150 mm). Distibutor Nicolai GmbH & Co. KG, Ostpassage 7, 30853 Langenhagen, Germany, Fax: +44-511-733235

Max Core Disposable biopsy pistol (G 20-16/0. 9–1,2 × 100/160 mm). Bard

Magnum Core. Reusable biopsy pistol. Bard GmbH, Wachhausstrasse 6, 76227 Karlsruhe, Germany

Magnum disposable needles. (G 20-16/0.9–1,2 × 100/160 mm). Bard

Navarre universal drainage catheter with Nitinol (6–12 Fr × 30cm). Bard

Universal adapter with Luer-Lock. Bard

Argyl trocar catheter (Charr 12–17/4–6 mm). Sherwood-Medical Company, Tullamore, Ireland

Argyl Sentinel Seal Thoracic drainage unit. Tyco Healthcare Company, Tullamore, Ireland

Acknowledgements I would like to express my thanks to Martin Lenz (chief consultant surgeon in the Radiology Department of the Steinenberg Clinic, Reutlingen) for preparing and providing the radiological findings, and my son Valentin for the technical photographic work.

References

Beckh S, Bölcskei PL (1997) Biopsie thorakaler Raumforderungen—von der computertomographischen zur ultraschallgezielten Punktion. Ultraschall Med 18:220–225

Blank W (1994) Sonographisch gesteuerte Punktionen und Drainagen. In: Braun B, Günther R, Schwerk WB (eds) Ultraschalldiagnostik. Lehrbuch und Atlas, vol III-11.1. ecomed, Landsberg/Lech, pp 1–79

Blank W (1995) Weichteil- und Knochentumoren. In: Braun B, Günther R, Schwerk WB (eds) Ultraschalldiagnostik. Lehrbuch und Atlas, vol III-9.9. ecomed, Landsberg/Lech, pp1–27

Blank W, Schuler A, Wild K, Braun B (1996) Transthoracic sonography of the mediastinum. Eur J Ultrasound 3:179–190

Blank W (2007) Sonographisch gezielte Punktionen und Drainagen. In: Seitz K, Schuler A, Rettenmaier G (eds) Sonographische Diagnose und Differenzialdiagnose. Thieme, Stuttgart

Börner N (1986) Sonographische Diagnostik pleuropulmonaler Erkrankungen. Med Klin 81:496–500

Bradley MJ, Metreweli C (1991) Ultrasound in the diagnosis of the juxta-pleural lesion. Br J Radiol 64:330–333

Braun B (1983) Abdominelle und thorakale Ultraschalldiagnostik. In: Bock HE, Gerok W, Hartmann F et al (eds) Klinik der Gegenwart. Urban & Schwarzenberg, Munich, pp 1141–1145

Chandresakar AJ, Reynes CJ, Churchill RJ (1976) Ultrasonically guided transthoracic percutaneous biopsy of peripheral pulmonary masses. Chest 70:627–630

Chu CY, Hsu WH, Hsu JY, Huang CM, Shih CM, Chiang DC (1994) Ultrasound-guided biopsy of thoracic masses. Chung Hua I Hsueh Tsa Chih 54:336–342

Cinti D, Hawkins HB (1984) Aspiration biopsy of peripheral pulmonary masses using real-time sonographic guidance. AJR Am J Roentgenol 142:1115–1116

Civardi G, Livraghi T, Colombo MD (1994) Lytic bone lesions suspected for metastasis: ultrasonically guided fine-needle aspiration biopsy. J Clin Ultrasound 22:307–311

Ckzerwenka W, Otto RC (1994) Die ultraschallgezielte Lungenpunktion. Bildgebung 61(S2):12

Dallari R, Gollini C, Barozzi G, Gilioli F (1999) Ultrasound-guided percutaneous needle aspiration biopsy of peripheral pumonary lesions. Monaldi Arch Chest Dis 54:7–10

Diacon AH, Schurmanns MM, Theron J, Schubert PT, Wright CA, Bolliger CT (2004) Safety and yield of ultrasound-assited transthoracic biopsy performed by pulmonologists. Respiration 71(5):519–522

Gartmann JC (1988) Der unklare Pleuraerguß: Praktisch-diagnostisches Vorgehen. Ther Umsch 45:308–313

Gehmacher O, Mathis G, Kopf A, Scheier M (1986) Ultrasound imaging of pneumonia. Ultrasound Med Biol 21:1119–1122

Gleeson F, Lomas DJ, Flower CDR, Stewart S (1990) Powered cutting needle biopsy of the pleura and chest wall. Clin Radiol 41:199–200

Gupta S, Gulati M, Rajwanski A, Gupta P, Suri S (1998) Sonographically guided fine-needle aspiration biopsy of superior mediastinal lesions by the suprasternal route. AJR Am J Roentgenol 171:1303–1306

Heckemann R, Hohner S, Heutz J, Nakhosten J (1988) Ultraschallgeführte Feinnadelpunktion solider pulmonaler und pleuraler Tumoren. Ultraschall Klin Prax S1:83

Heilo A (1993) Tumors in the mediastinum: US-guided histologic core-needle biopsy. Radiology 189:143–146

Heilo A (1996) US-guided transthoracic biopsy. Eur J Ultrasound 3:141–153

Herth FJ. Eberhardt R, Becker HD, Ernst A (2004). Diagnosis of pneumothorax (PTX) by means of transthoracic ultrasound—a prospective trial. Chest 126(49):892

Hsu WH, Chiang DC, Hsu JY, Kwan PC, Chen CL, Chen DY (1996) Ultrasound guided fine-needle aspiration biopsy of lung cancers. J Clin Ultrasound 24:225–233

Hüner M, Ghadim BM, Haensch W, Schlag DM (1998) Transesophageal biopsy of mediastinal and pulmonary tumors by means of endoscopic ultrasound guidance. J Thorac Cardiovasc Surg 116:554–559

Ikezoe J, Sone S, Higashihara T, Morimoto S, Arisawa J, Kuriiyama K (1984) Sonographically guided needle biopsy for diagnosis of thoracic lesions. AJR Am J Roentgenol 143:229–243

Ikezoe J, Morimoto S, Arisawa J, Takasgima S, Kozuka T, Nakahara K (1990) Percutaneous biopsy of thoracic lesions: value of sonography for needle guidance. AJR Am J Roentgenol 154:1181–1185

Izumi S, Tamaki S, Natori H, Kira S (1982) Ultrasonically guided aspiration needle biopsy in diseases of the chest. Am Rev Respir Dis 125:460–464

Janssen J, Johann W, Luis W, Greiner L (1998) Zum klinischen Stellenwert der endosonographisch gesteuerten transoesophagealen Feinnadelpunktion von Mediastinalprozessen. Dtsch Med Wochenschr 123:1402–1409

Kelbel C, Stephany P, Lorenz J (1996) Endoluminal chest sonography. Eur J Ultrasound 3:191–195

Klein JS, Schultz S, Heffner JE (1995) Interventional radiology of the chest: image-guided percutaneous drainage of pleural effusions, lung abscess, and pneumothorax. AJR Am J Roentgenol 164:581–588

Klose KC, Günther RW (1996) CT-gesteuerte Punktionen. In: Günther RW, Thelen M (eds) Interventionelle Radiologie. Thieme, Stuttgart, pp 750–775

Knudsen DU, Nielsen SM, Hariri J, Christersen J, Kristersen S (1996) Ultrasonographically guided fine-needle aspiration biopsy of intrathoracic tumors. Acta Radiol 37:327–331

Mathis G (1997a) Thoraxsonography—part I: chest wall and pleura. Ultrasound Med Biol 23(8):1131–1139

Mathis G (1997b) Thoraxsonography—part II: peripheral pulmonary consolidation. Ultrasound Med Biol 23(8):1141–1153

Mathis G, Gehmacher O (1999) Ultrasound-guided diagnostic and therapeutic interventions in peripheral pulmonary masses. Wien Klin Wochenschr 111:230–235

Mathis G, Bitschnau R, Gehmacher O, Dirschmid K (1999) Ultraschallgeführte transthorakale Punktion. Ultraschall Med 20:226–235

Metz V, Dock W, Zyhlarz R, Eibenberger K, Farres MT, Grabenwöger F (1993) Ultraschallgezielte Nadelbiopsien thorakaler Raumforderungen. RoFo 159:60–63

Mikloweit P, Zachgo W, Lörcher U, Meier-Sydow J (1991) Pleuranahe Lungenprozesse: Diagnostische Wertigkeit Sonographie versus Computertomographie (CT). Bildgebung 58:127–131

Mueller PR, Sanjay S, Simeone JF et al (1988) Image-guided pleural biopsies: Indications, technique and results in 23 patients. Radiology 169:1–4

Nordenstrom B (1967) Paraxiphoid approach to mediastinum for mediastinography and mediastinal needle biopsy: a preliminary report. Invest Radiol 2:141–146

O'Moore PV, Mueller PR, Simeone JF, Saini S, Butch RJ, Hahn PF (1987) Sonographic guidance in diagnostic and therapeutic interventions in the pleural space. AJR Am J Roentgenol 149:1–5

Pang JA, Tsang MB, Hom L, Metreweli C (1987) Ultrasound guided tissue-core biopsy of thoracic lesions with trucut and surecut needles. Chest 91:823–828

Pedersen BH, Vilmann P, Folke K, Jacobsen GK, Krasnik M, Milman N, Hancke S (1996) Endoscopic ultrasonogarhy and real-time guided fine-needle aspiration biopsy of solid lesions of the mediastinum suspected of malignancy. Chest 110:539–544

Pedersen OM, Aasen TB, Gulsvik A (1986) Fine needle aspiration biopsy of mediastinal and peripheral pulmonary masses guided by real time sonography. Chest 89:504–508

Reissig A, Kroegel C (2005) Accuracy of transthoracic sonography in excluding post-interventional pneumothorax and hydropneumothorax. Comparison to chest radiography. Eur J Radiol 53(3):463–470

Reuß J (1996) Sonographic imaging of the pleura: nearly 30 years experience. Eur J Ultrasound 3:125–139

Rosenberg JC (1993) Neoplasms of the mediastinum. In: De Vita VT, Hellman S, Rosenberg SA (eds) Cancer: principles & practice of oncology. Lippincott, Philadelphia, pp 759–775

Rubens DJ, Strang JG, Fultz PJ, Gottleib RH (1997) Sonographic guidance of mediastinal biopsy: an effective alternative to CT guidance. AJR Am J Roentgenol 169:1605–1610

Schlotterbeck K, Schmid J, Klein F, Alber G (1997) Transesophageal sonography in the staging of lung cancer. Ultraschall Med 18:153–158

Schubert P, Wright CA, Louw M, Brundyn K, Theron J, Bolliger CT, Diacon AH (2005) Ultrasound assisted transthoracic biopsy: cells or sections? Diagnostic Cytopathol. 33(49): 233–237

Schuler A, Blank W, Braun B (1995) Sonographisch-interventionelle Diagnostik bei Thymomen. Ultraschall Med 16:62

Schulz G (1992) Interventionelle Thoraxsonographie bei brustwandnahen soliden Raumforderungen. Ultraschall Klin Prax 7:202

Schwerk WB, Görg C (2007) Pleura und Lunge. In: Braun B, Günther R, Schwerk WB (eds) Ultraschalldiagnostik. Lehrbuch und Atlas, vol III-2.2. ecomed, Landsberg/Lech, pp 1–44

Schwerk WB, Dombrowski H, Kalbfleisch H (1982) Ultraschalltomographie und gezielte Feinnadelbiopsie intrathorakaler Raumforderungen. Ultraschall Med 3:212–218

Seitz K, Pfeffer A, Littmann M, Seitz G (1999) Sonographisch gesteuerte Zangenbiopsie der Pleura. Ultraschall Med 20:60–65

Sistrom CI (1997) Thoracic sonography for diagnosis and intervention. Curr Probl Diagn Radiol 1 6–46

Sonnenberg E, Agostino H, Casola G, Wittich GR, Varney RR, Harker C (1991) Lung abscess: CT-guided drainage. Radiology 178:347–351

Sonnenberg E, Wittich GR, Goodacre BW, Zwischenberger JB (1998) Percutaneous drainage of thoracic collections. J Thorac Imaging 13:74–82

Targhetta R, Bourgeois JM, Chavagneux R, Balmes P (1992) Diagnosis of pneumothorax by ultrasound immediately after ultrasonically guided aspiration biopsy. Chest 101:855–856

Tikkakoski T, Lohela P, Taavitsainen M et al. (1993) Transthoracic lesions: diagnosis by ultrasound-guided biopsy. RoFo 159:444–449

Vladutiu AO (1986) Pleural effusion. Futura, Mount Kisco

Vogel B (1993) Ultrasonographic detection and guided biopsy of thoracic osteolysis. Chest 104:1003–1005

Vogel B (1995) Ultraschallgezielte perthorakale Punktion. Prax Klein Pneumol 39:632–635

Wang HC, Yu DJ, Yang PC (1995) Transthoracic needle biopsy of thoracic tumor by color Doppler ultrasound puncture guided device. Thorax 50:1258–1263

Weiss H, Düntsch U (1996) Komplikationen der Feinnadelbiopsie—DEGUM-Umfrage II. Ultraschall Med 17:118–130

Weiss H, Weiss A (1994) Therapeutische interventionelle Sonographie. Ultraschall Med 15:152–158

Westcott JL (1980) Direct percutaneous needle aspiration of localized pulmonary lesions: result in 422 patients. Radiology 137:31–35

Wu RG, Yang PC, Kuo SH, Luh KT (1995) "Fluid color" sign: a useful indicator for discrimination between pleural thickening and pleural effusion. J Ultrasound Med 14:767–769

Yang PC (1996) Color Doppler ultrasound of pulmonary consolidation. Eur J Ultrasound 3:169–178

Yang PC, Luh KT, Sheu JC, Kuo SH, Sang SP (1985) Peripheral pulmonary lesions: ultrasonography and ultrasonically guided aspiration biopsy. Radiology 155:451–456

Yang PC, Chang DB, Yu CJ, Lee YC, Kuo SH, Luh KT (1992) Ultrasound-guided core biopsy of thoracic tumors. Am Rev Respir Dis 146:763–767

Yin XJ (1989) Ultrasound-guided percutaneous needle biopsy in diseases of the chest. Chung Hua Wai Ko Tsa Chih 27:107–108

Yuan A, Yang PC, Chang DB, Yu CJ, Lee YC, Kuo SH, Luh KT (1992) Ultrasound-guided aspiration biopsy of small peripheral pulmonary nodules. Chest 101:926–930

Zimmermann C, Werle A, Schuler A, Reuss J, Gemacher O, Blank W (2003) Echosignalverstärker in der sonographischen Diagnostik des Thorax. Ultraschall Med 24:31

10 The White Hemithorax

C. Görg

The „white hemithorax“ is primarily a radiographic finding caused by reduced radiotransparency. Although radiographic findings are of primary importance for evaluating the extent of lung opacity, occasionally the findings cannot be interpreted in such a way that the cause of the condition can be established.

Large spreading lung consolidations are homogeneous on radiographs. They may be caused by pneumonic infiltration, atelectasis, tumor growth, pleural effusion, or combinations of these. In the majority of cases, unilateral lung opacity is caused by at least reduced quantity of air in the lung, either due to compression or infiltration.

Thus, the finding of a „white hemothorax“ is a sonographic challenge. In order to assess it properly, the investigator must have knowledge of the entire spectrum of thorax sonography.

Potential causes of unilateral lung opacity are listed in Table 10.1.

Table 10.1 Potential causes of unilateral lung opacity

Predominantly liquid space-occupying mass
• Pleural effusion
• Pyothoray
• Chylothorax
• Hemothorax
Predominantly solid space-occupying mass
• Obstructive atelectasis
• Lobular pneumonia
• Tumor
• Fibrothorax

10.1 Predominantly Liquid Space-Occupying Mass

The cause is nearly always a fluid exudate. Sonographic evaluation is performed bearing the following features in mind:

1. Echogenicity of the effusion
   (a) Anechoic (e.g., transudate) (Fig. 10.1)
   (b) Echogenic (e.g., exudate, hemothorax, pyothorax chylothorax) (Figs. 10.2–10..5)
2. Evidence of fibrin strands and septa (e.g., exudate) (Fig. 10.6)
3. Evidence of widespread nodular thickening of the pleura (e.g., pleural carcinomatosis, mesothelioma) (Figs. 10.1, 10.7, 10.8)
4. Sonographic characterization of lung parenchyma

10.2 Predominantly Solid Space-Occupying Mass

A solid space-occupying mass is assessed bearing the following features in mind:

1. Homogeneity of the space-occupying mass (e.g., atelectasis, tumor, fibrothorax) (Figs. 10.9–10.12)
   (a) „Air bronchogram“ (e.g., pneumonia, atelectasis) (Figs. 10.13–10.16)
   (b) „Fluid bronchogram“ (e.g., atelectasis) (Fig. 10.17)
   (c) Focal intraparenchymatous foci (e.g., metastasis, necrosis, abscess) (Figs. 10.18–10.20)
2. Possible imaging of a central space-occupying mass (e.g., carcinoma, lymphoma)
3. Qualitative and quantitative color-Doppler sonography of the solid space-occupying mass (Figs. 10.3, 10.9, 10.18)

With regard to the differential diagnosis of sonographic findings, the reader is referred to the preceding chapters.

In the following, the spectrum of sonographic manifestations of the white hemithorax are presented in the form of a pictorial essay.

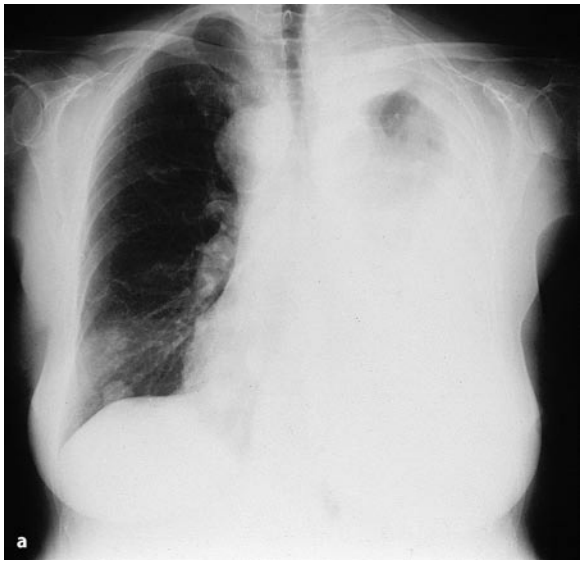

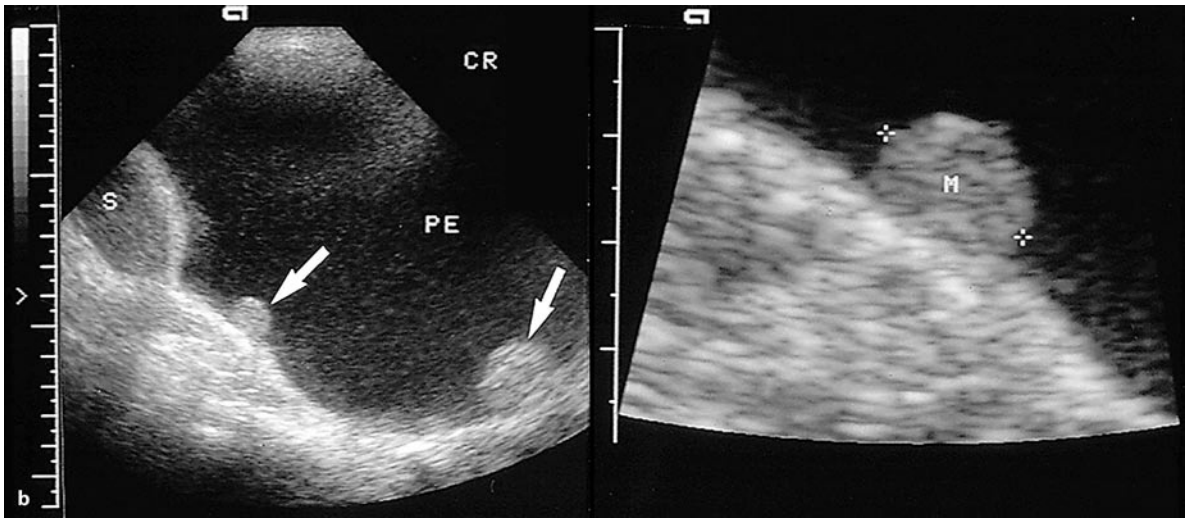

Fig. 10.1 A 46-year-old woman with breast carcinoma. **a** Chest radiograph. Nearly complete opacity of the lung on the left side. **b** Sonography. The lateral intercostal transmission of the ultrasound beam on the left side shows a marked pleural effusion (*PE*) with small foci about 1 cm in size lying on the diaphragm and the mediastinal pleura (*arrows*). Pleural carcinomatosis was confirmed on cytology. *S*, spleen; *CR*, cranial; *M*, metastasis

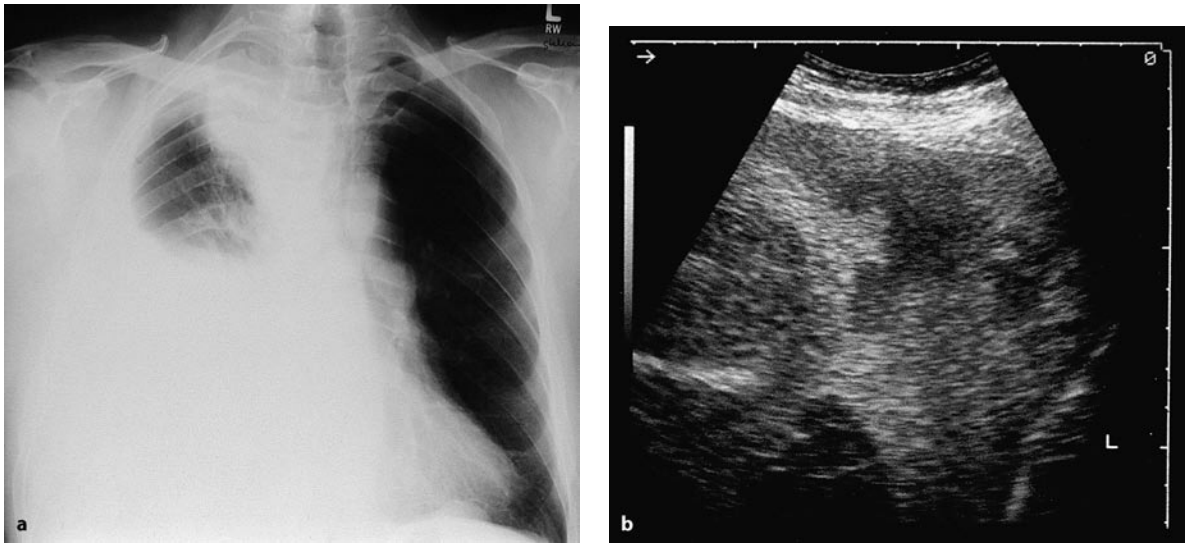

Fig. 10.2 A 60-year-old man with bronchial carcinoma. **a** Chest radiograph. Nearly complete lung opacity on the right side. **b** Ultrasonography. The lateral intercostal ultrasound beam transmission on the right side shows an inhomogeneous hyperechoic structure that corresponds to respiration-dependent mobile echoes. Thoracentesis of the effusion confirmed a hemothorax

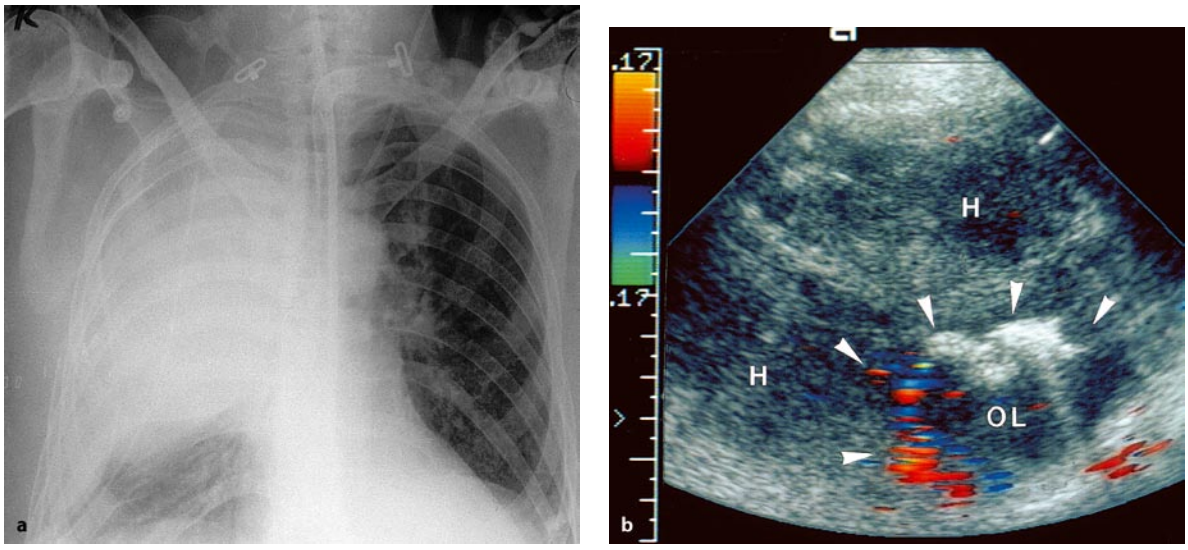

Fig. 10.3 A 45-year-old man with sepsis and consumption coagulopathy, on long-term artificial respiration. **a** Chest radiograph. Almost complete opacity of the lung on the right side. **b** Ultrasonography. The lateral intercostal ultrasound beam transmission on the right side shows a complex intrathoracic consolidation with no evidence of flow phenomena on color-Doppler sonography. Aerated lung tissue is seen in the central portion. The patient underwent surgery and a large hematoma (*H*) in the thorax was removed. *Arrows* indicate the upper lobes (*UL*)

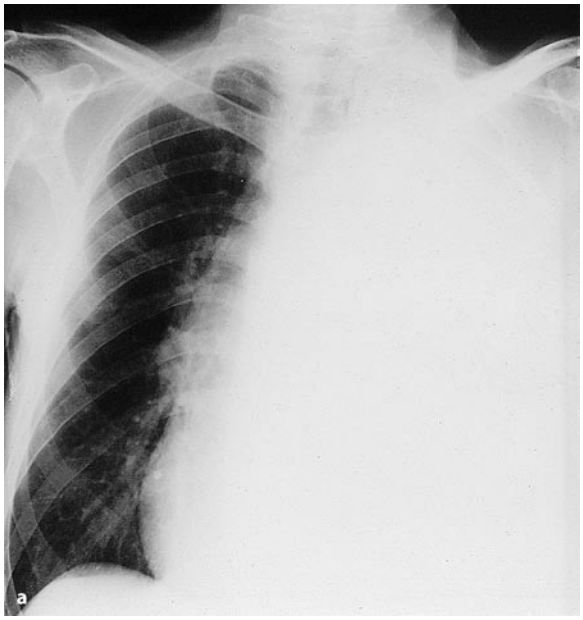

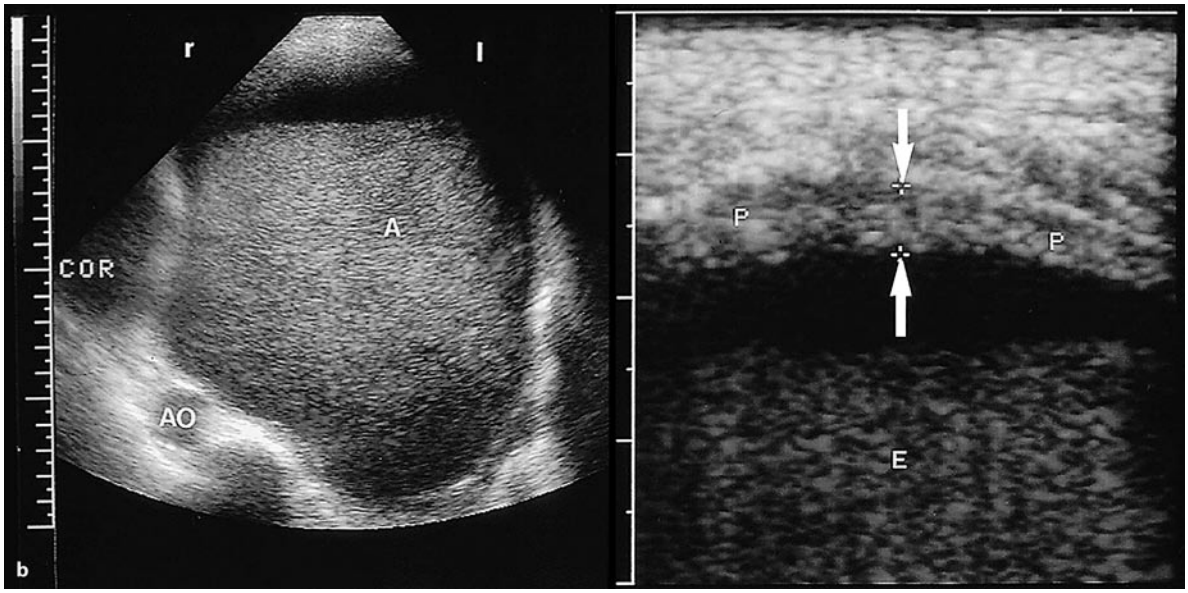

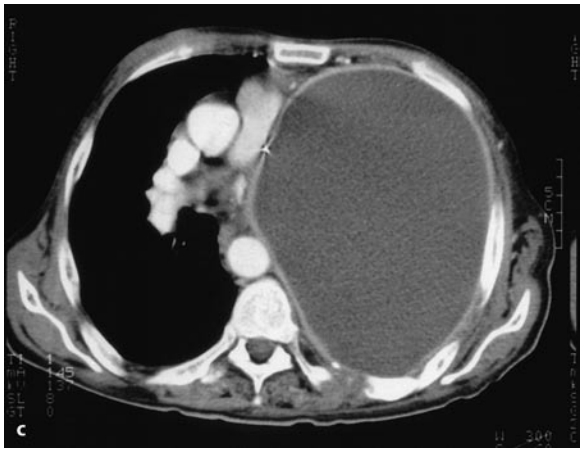

Fig. 10.4 A 60-year-old man with high fever; bronchial carcinoma after left-sided pneumonectomy. **a** Chest radiograph. Complete opacity of the hemithorax on the left side. **b** Ultrasonography. The lateral intercostal ultrasound beam transmission on the left side shows an echogenic effusion (*A*) with sedimentation phenomena. In the vicinity of this entity, the pleura is thickened (*P*) to 5 mm (*arrows*). Diagnostic puncture produced purulent fluid, indicative of a pyothorax. *AO*, aorta; *E*, empyema; *COR*, heart. **c** Computed tomography. Homogeneous space-occupying mass with prominent walls, filling the hemithorax

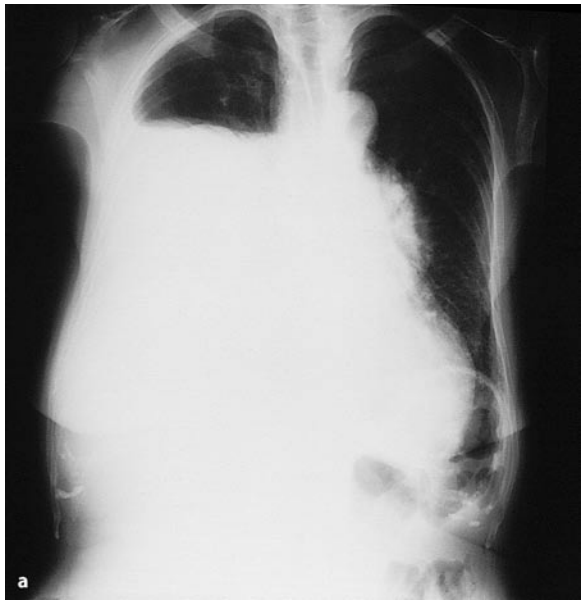

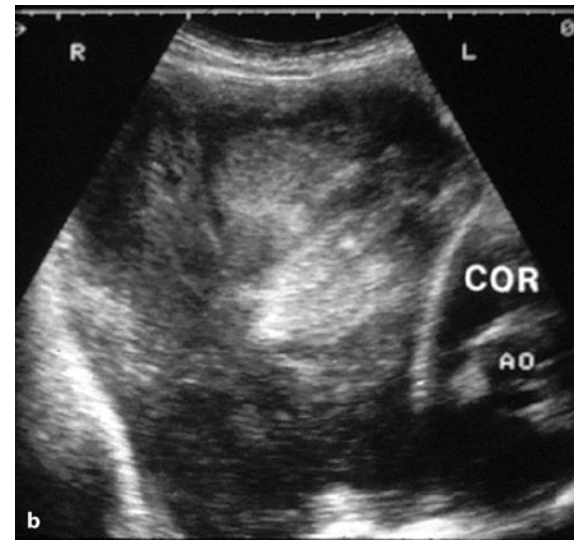

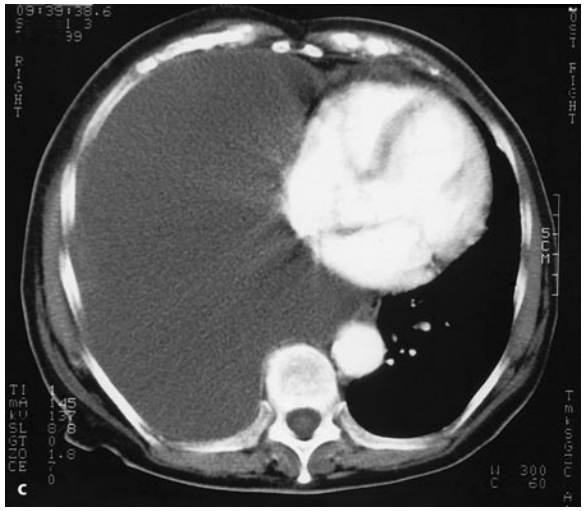

Fig. 10.5 A 74-year-old woman with metastatic mucusproducing ovarian carcinoma. **a** Chest radiograph. Nearly complete opacity of the lung on the right side. **b** Ultrasonography. The ventral intercostal ultrasound beam transmission on the right side shows an inhomogeneous echogenic space-occupying mass with discrete respiration-dependent, mobile echoes. Puncture produced mucinous material from a displacing, mucus-forming metastasis in the presence of ovarian carcinoma. *COR*, heart; *R*, right; *L*, left; *AO*, aorta. **c** Computed tomography. Homogeneous space-occupying mass filling the hemithorax

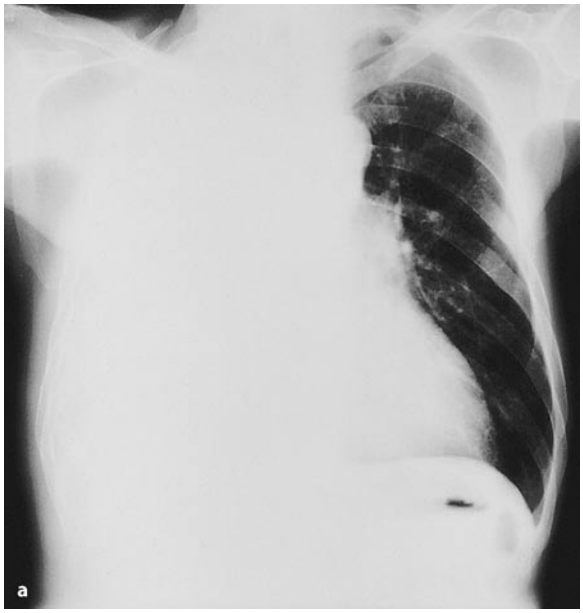

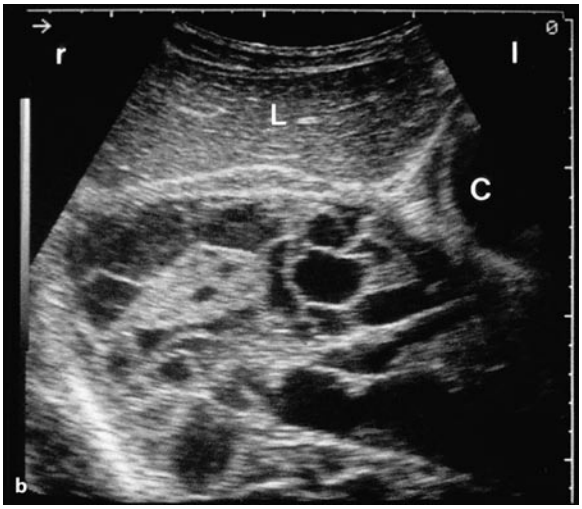

Fig. 10.6 A 58-year-old man with bronchial carcinoma. **a** Chest radiograph. Complete opacity of the lung on the right side. **b** Ultrasonography. The subcostal transhepatic ultrasound beam transmission shows a marked, honey-comb-shaped, loculated pleural effusion. No clear tumor formations could be imaged. *L*, liver; *C*, heart; *r*, right; *1*, left

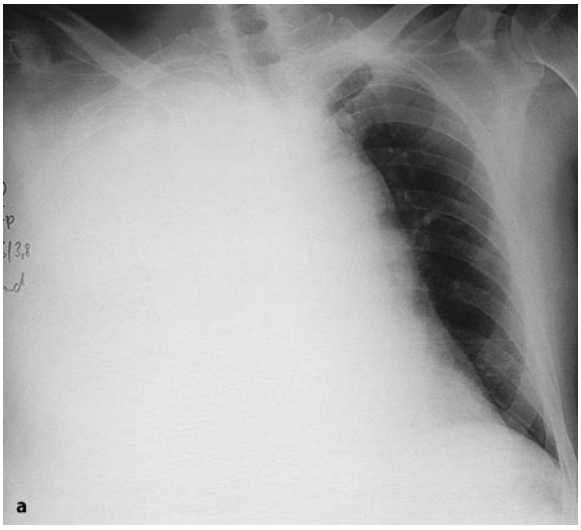

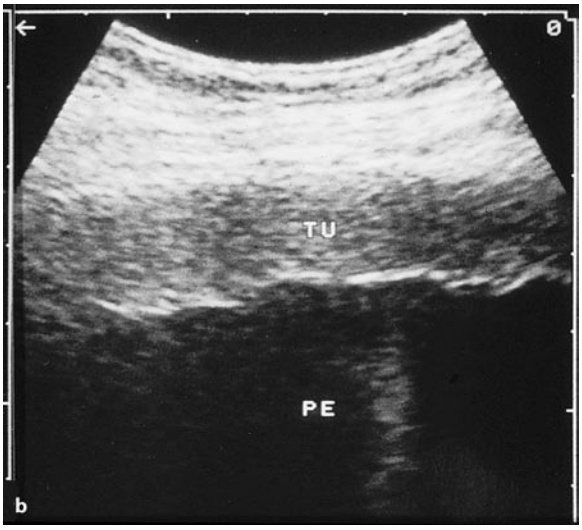

Fig. 10.7 A 64-year-old man with bronchial carcinoma. **a** Chest radiograph. Complete opacity of the lung on the right side. **b** Ultrasonography. The lateral intercostal ultrasound beam transmission on the right side shows a pleural effusion (*PE*) with widespread, 1.3-cm-thick hypoechoic infiltration of the parietal pleura (*TU*). Pleural carcinomatosis was confirmed by histology

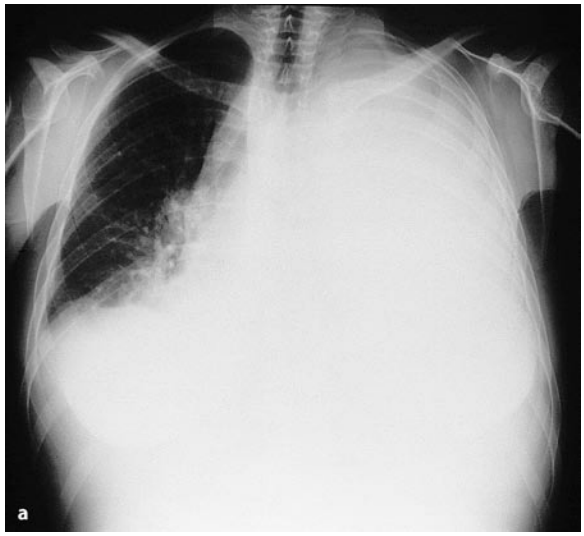

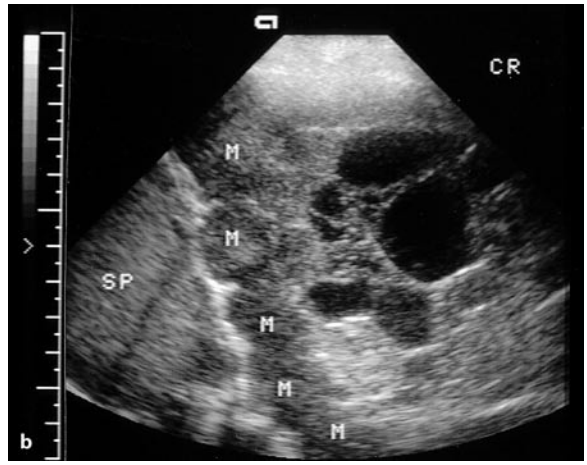

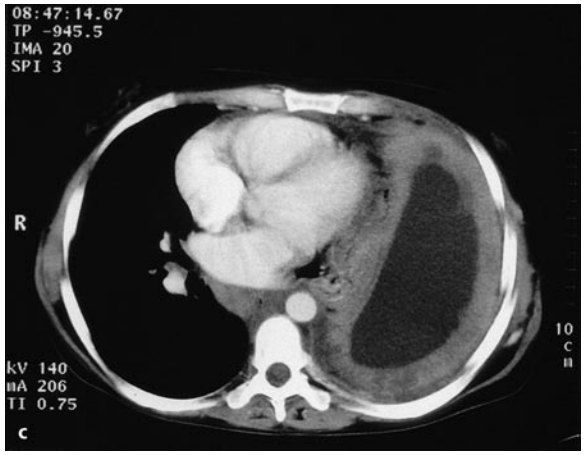

Fig. 10.8 A 21-year-old woman with non-Hodgkin's lymphoma of low malignancy. **a** Chest radiograph. Complete lung opacity on the left side. **b** Ultrasonography. The lateral intercostal ultrasound beam transmission on the left side shows a markedly loculated pleural effusion. Along the diaphragmatic pleura there are moniliform nodular tumor formations (*M*). Lymphoma of the pleura was confirmed by cytology. *CR*, cranial; *SP*, spleen. **c** Computed tomography. Widespread tumor infiltration of the pleura

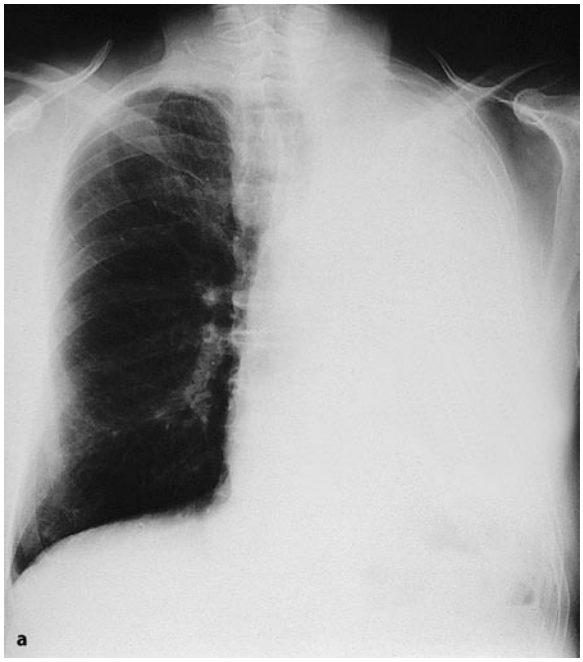

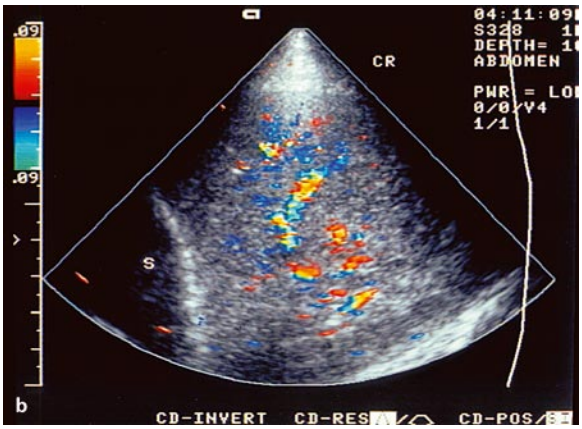

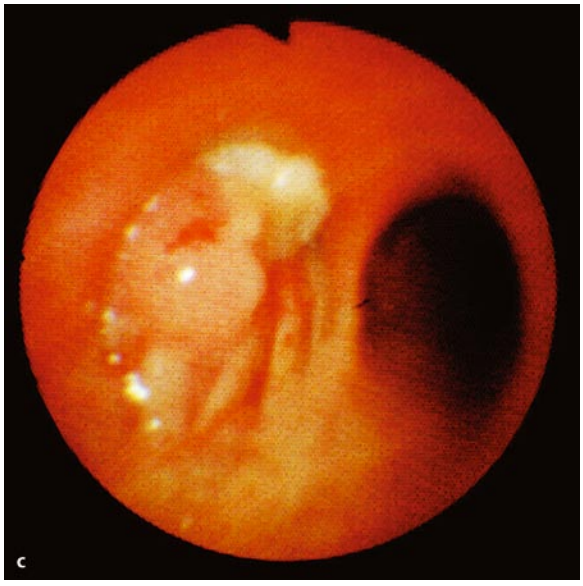

Fig. 10.9 A 68-year-old man with bronchial carcinoma. **a** Chest radiograph. Complete opacity of the lung on the left side. **b** Ultrasonography. The lateral intercostal ultrasound beam transmission on the left side shows a homogeneously hyperechoic supradiaphragmatic space-occupying mass with marked flow signals on color-Doppler sonography, corresponding to right-sided pulmonary atelectasis. *CR*, cranial; *S*, spleen. **c** Bronchoscopy. Complete tumor-related obstruction of the main bronchus on the left side

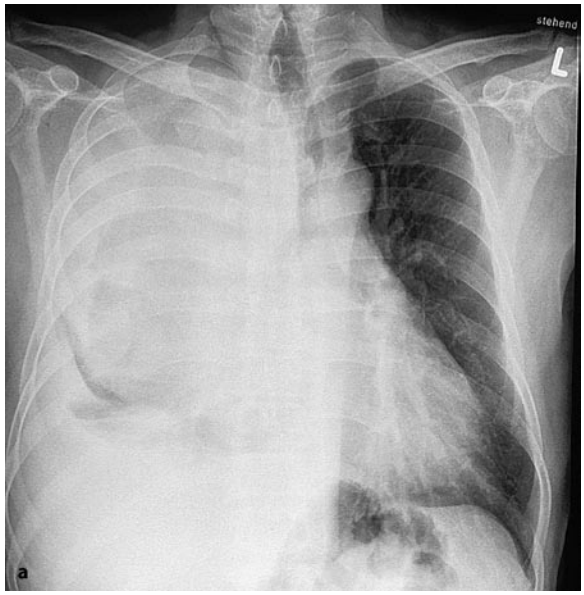

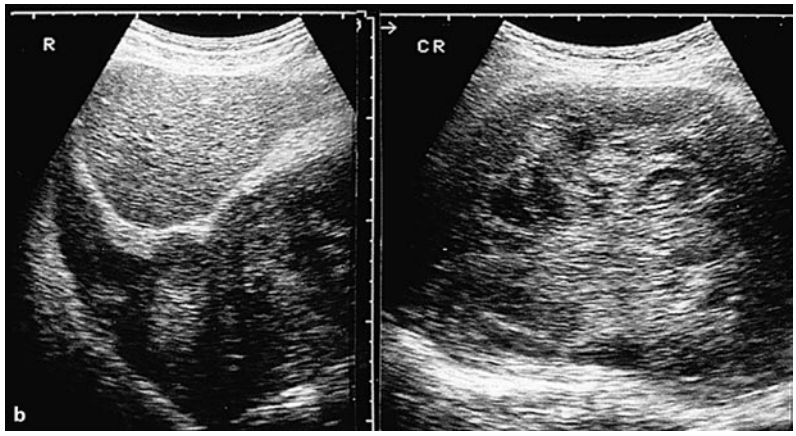

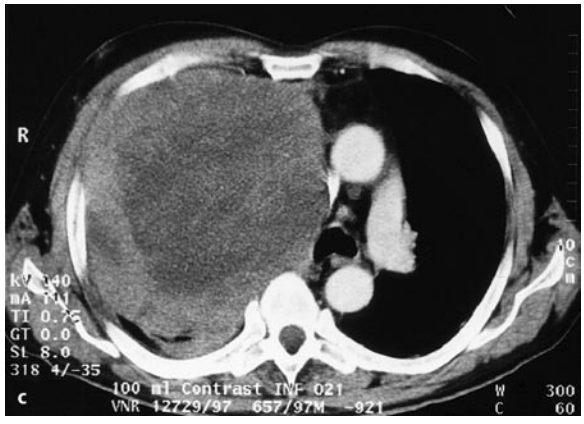

Fig. 10.10 A 60-year-old man with a peripheral neuroendocrine tumor. **a** Chest radiograph. Nearly complete opacity of lung parenchyma on the side. **b** Ultrasonography. The subcostal transhepatic ultrasound beam transmission (*left image*) shows a small pleural effusion and a large solid tumor in a subdiaphragmatic location. The lateral intercostal ultrasound beam transmission on the right side (*right image*) reveals the complex tumor that nearly fills the hemithorax. *CR*, cranial. **c** Computed tomography. Large tumor filling the right hemithorax

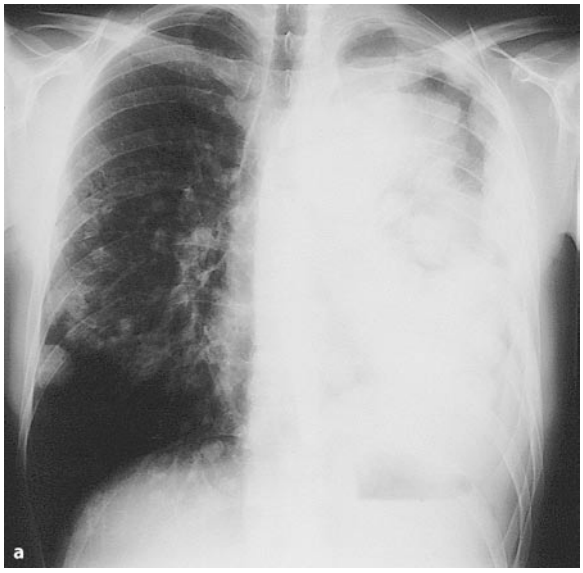

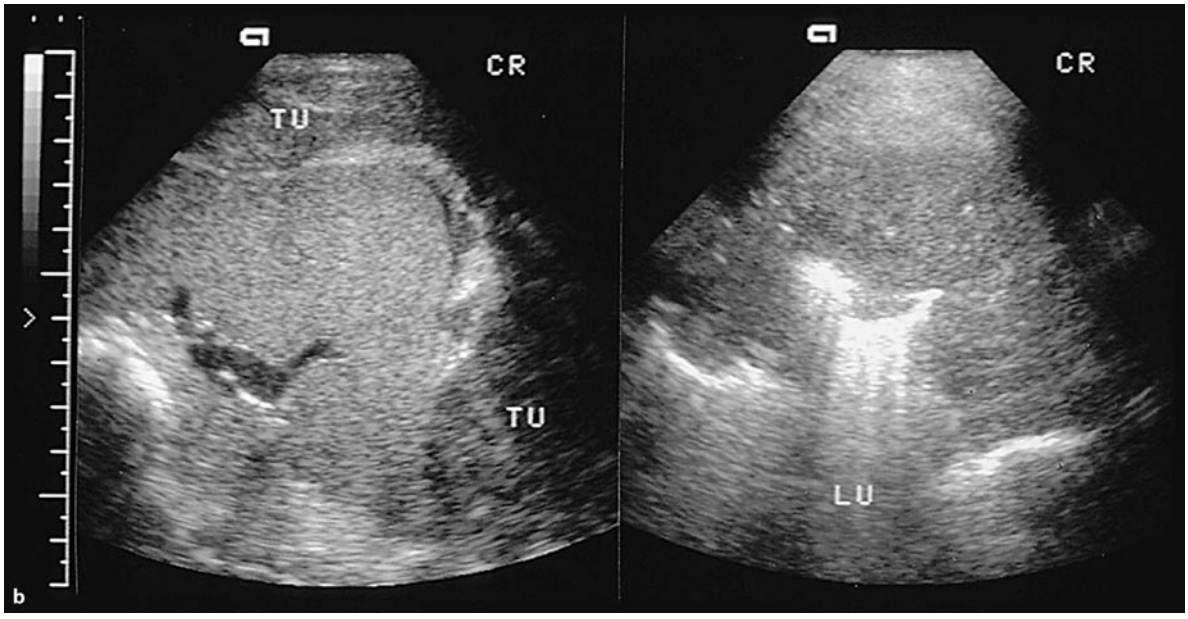

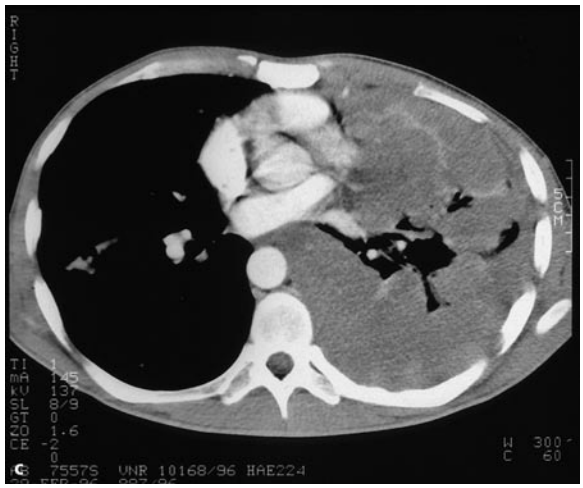

Fig. 10.11 A 34-year-old man with pulmonary blastoma. **a** Chest radiograph. Nearly complete opacity of lung parenchyma on the left side. **b** Ultrasonography. The lateral intercostal ultrasound beam transmission on the left side shows, in the caudal section (*left image*), a tumor (*TU*) that is completely infiltrating the basal diaphragmatic portions of the lung. The tumor appears to perforate the diaphragm and surrounds the spleen like a hood. In the apical portion (*right image*) the tumor walls in and invades the lung (*LU*), growing from the periphery towards the center. *CR*, cranial. **c** Computed tomography. Nearly complete tumor infiltration of the left lung

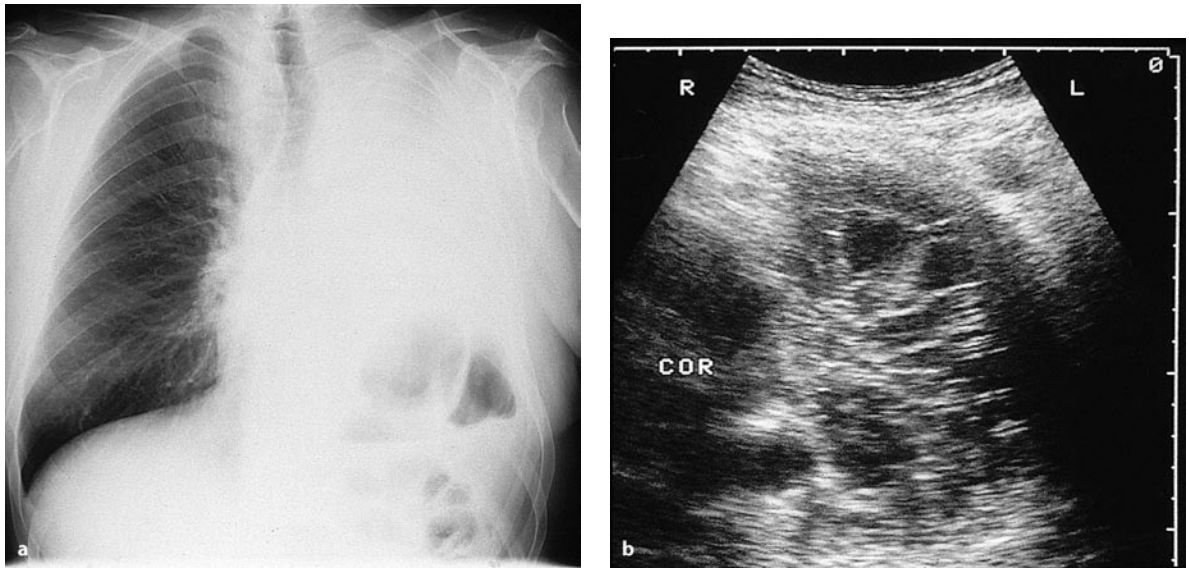

10

Fig. 10.12 A 65-year-old man with bronchial carcinoma, after pneumectomy. **a** Chest radiograph. Complete opacity of the lung on the left side. **b** Ultrasonography. The left-ventral intercostal ultrasound beam transmission shows an inhomogeneous, partly solid and partly cystic space-occupying mass, indicative of a fibrothorax. *R*, right; *L*, left; *COR*, heart

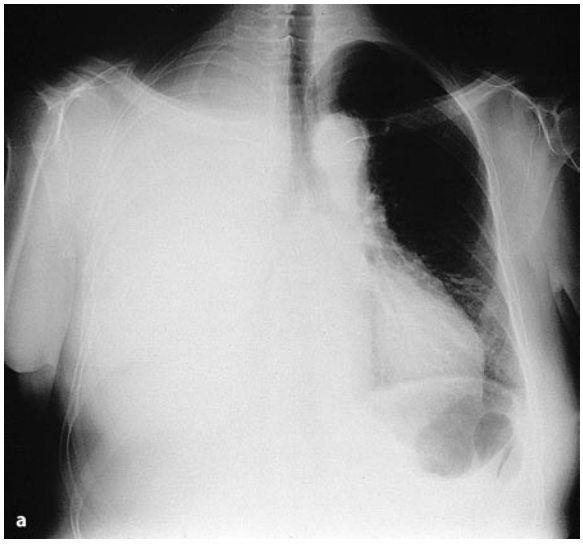

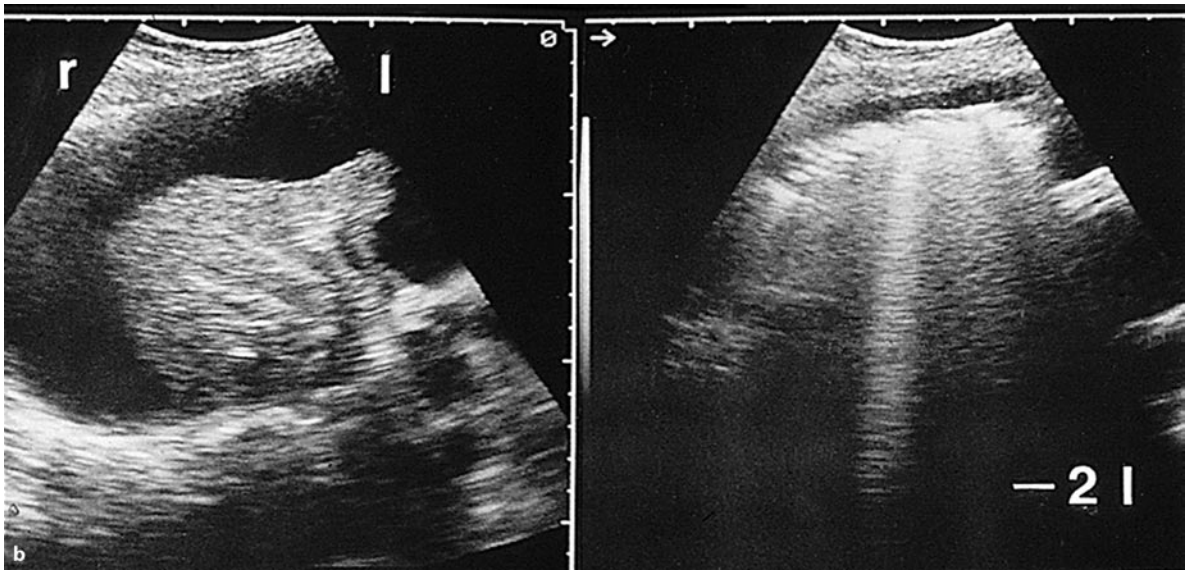

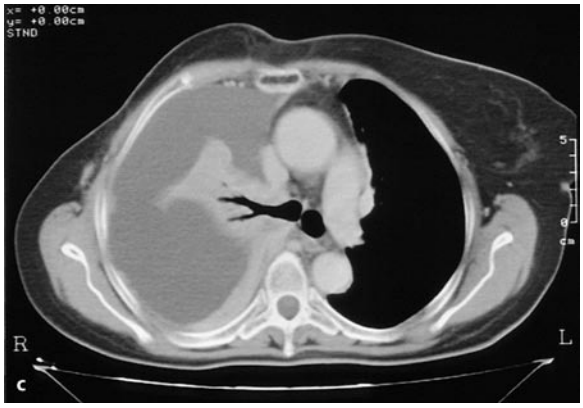

Fig. 10.13 A 66-year-old alcoholic, cachectic male patient with lobar pneumonia. **a** Chest radiograph. Complete opacity of the lung on the left side. **b** Ultrasonography. The left ventral intercostal ultrasound beam transmission (*upper image*) shows a nearly completely hypoechoic upper lobe with a discrete central air bronchogram. *AO*, aorta; *PA*, pulmonary artery; *UL*, upper lobe. The left-lateral intercostal ultrasound beam transmission (*lower image*) shows an invasive process with an "air bronchogram" as in pneumonia of the lower lobe (*LL*). **c** corrosponding CT

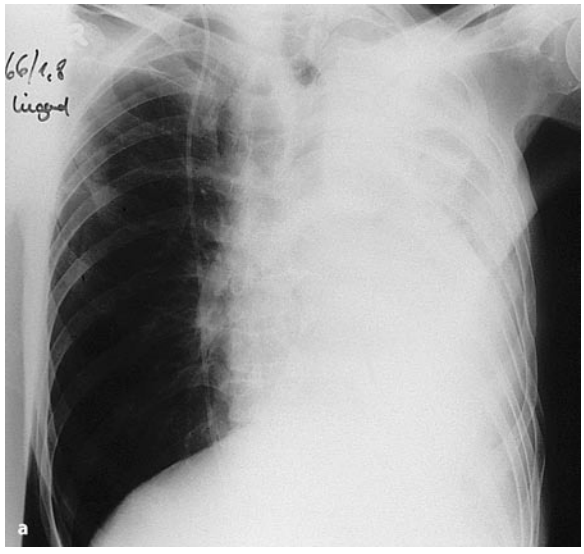

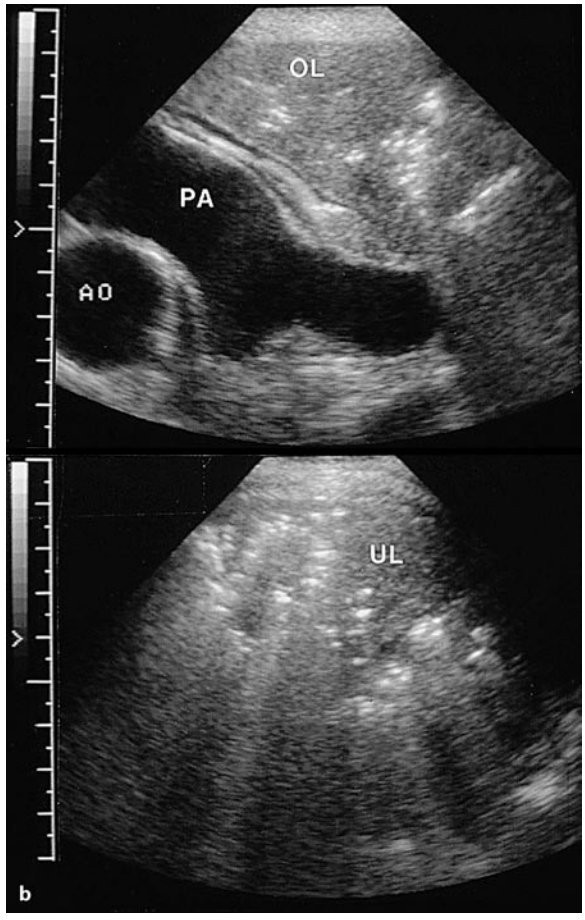

Fig. 10.14 A 61-year-old woman with breast carcinoma. **a** Chest radiograph. Complete opacity of the lung on the right side. **b** Ultrasonography. The infraclavicular right-ventral intercostal ultrasound beam transmission reveals nearly complete atelectasis of the upper lobe and a positive air bronchogram. After puncture of the effusion, the upper lobe is reventilated, as in the presence of compression atelectasis; *r*, right, *l*, left. **c** Computed tomography. Effusion with compression atelectasis of the right upper lobe

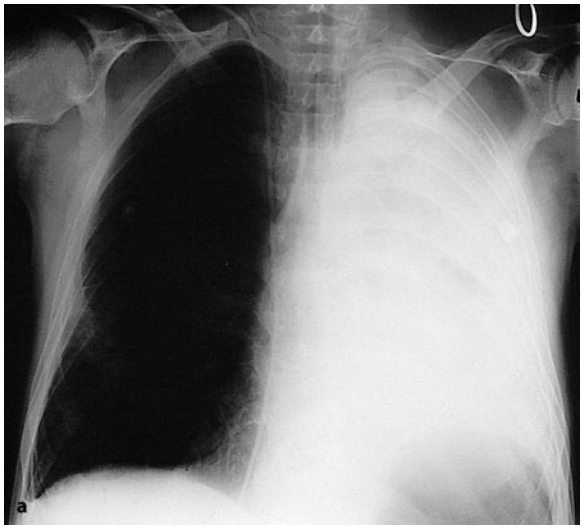

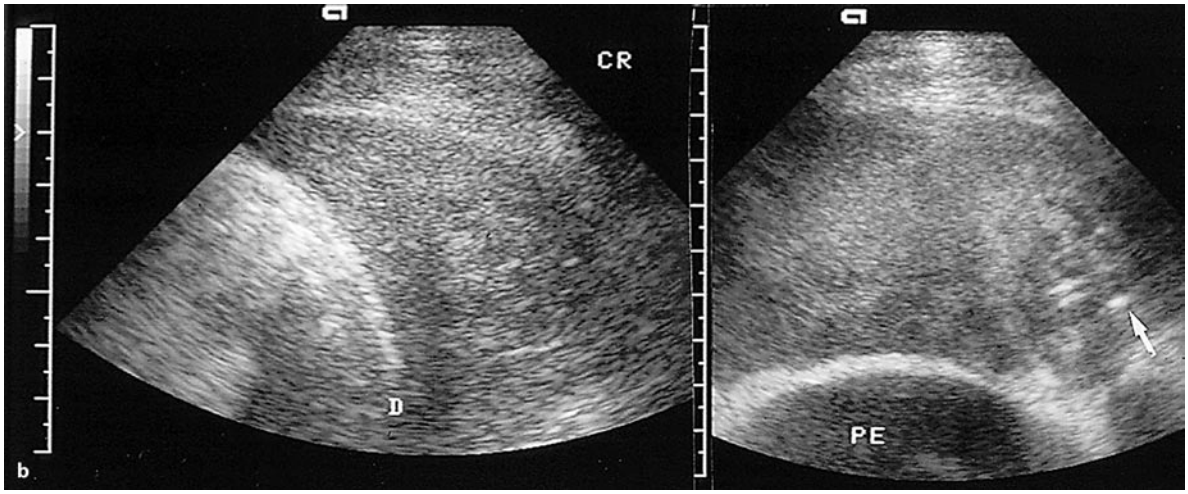

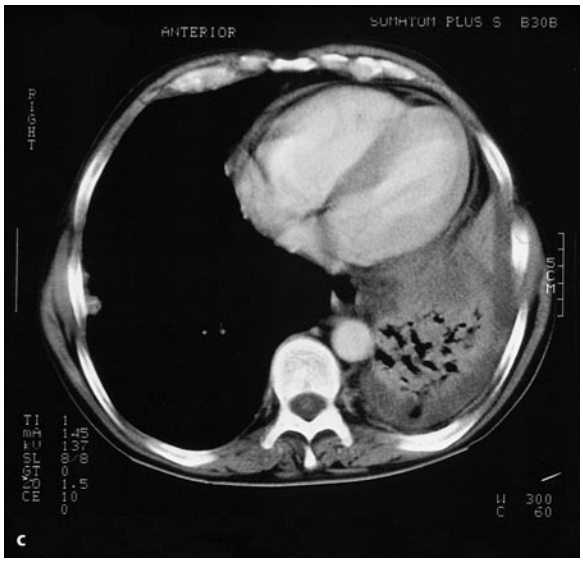

Fig. 10.15 A 48-year-old alcoholic male patient with lobar pneumonia. **a** Chest radiograph. Complete opacity of the lung on the left side. **b** Ultrasonography. The left lateral intercostal ultrasound beam transmission (*left image*) and the sectional plane at right angles to it (*right image*) reveal so-called hepatization of the lung. Small air reflexes are indicative of a potential inflammatory process (*arrow*), but the appearance is nearly identical to that of atelectasis. *CR*, cranial; *D*, diaphragm; *PE*, pleural effusion formation. **c** Computed tomography. Invasive process in the left lung. Central air bronchogram

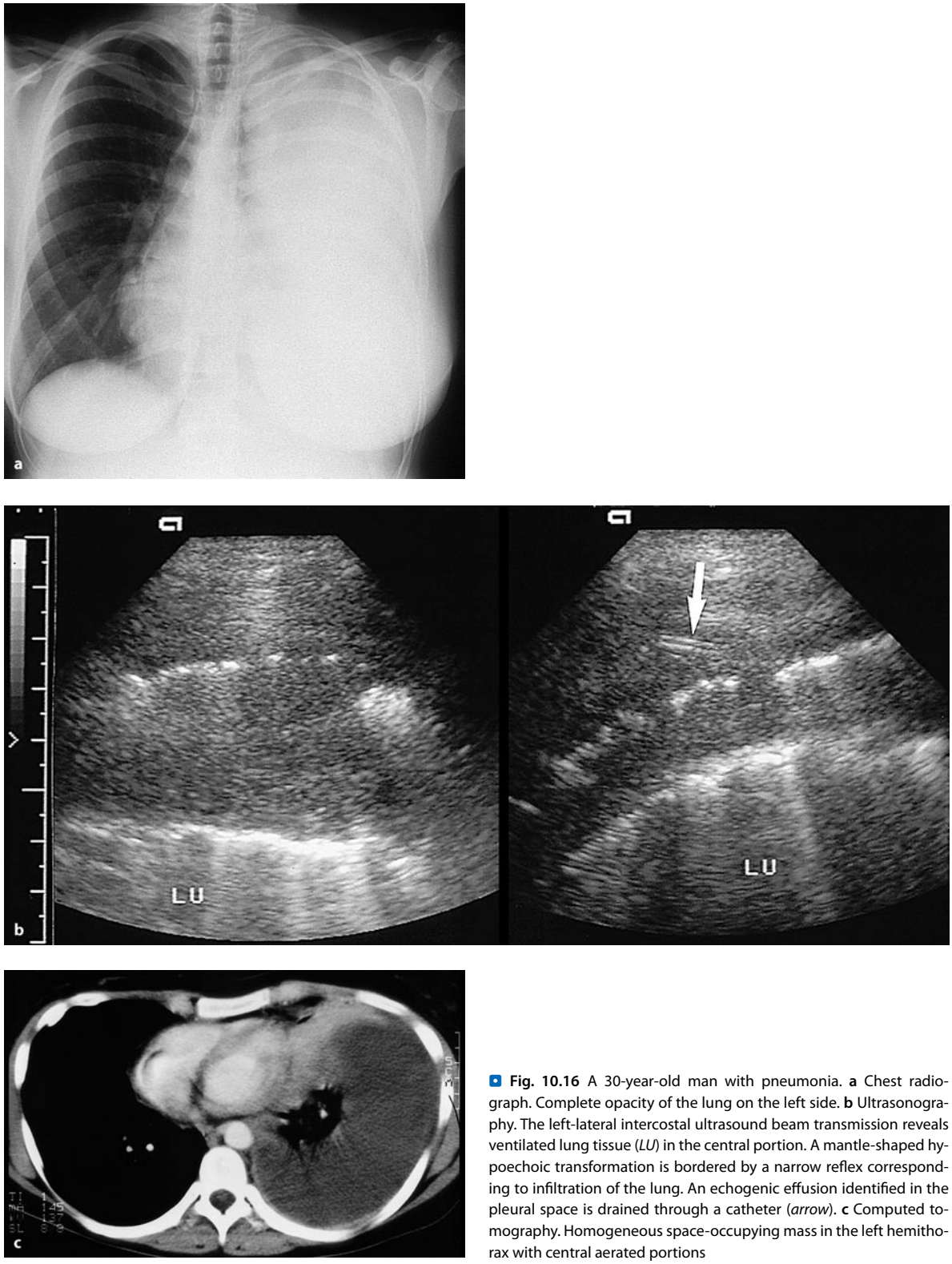

Fig. 10.16 A 30-year-old man with pneumonia. **a** Chest radiograph. Complete opacity of the lung on the left side. **b** Ultrasonography. The left-lateral intercostal ultrasound beam transmission reveals ventilated lung tissue (*LU*) in the central portion. A mantle-shaped hypoechoic transformation is bordered by a narrow reflex corresponding to infiltration of the lung. An echogenic effusion identified in the pleural space is drained through a catheter (*arrow*). **c** Computed tomography. Homogeneous space-occupying mass in the left hemithorax with central aerated portions

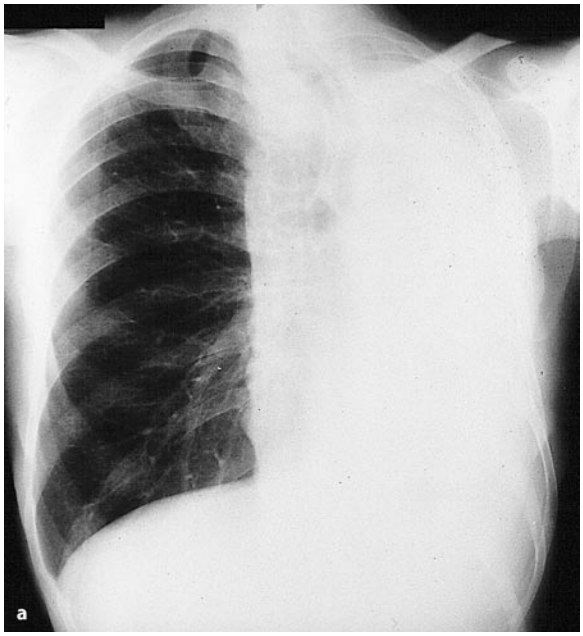

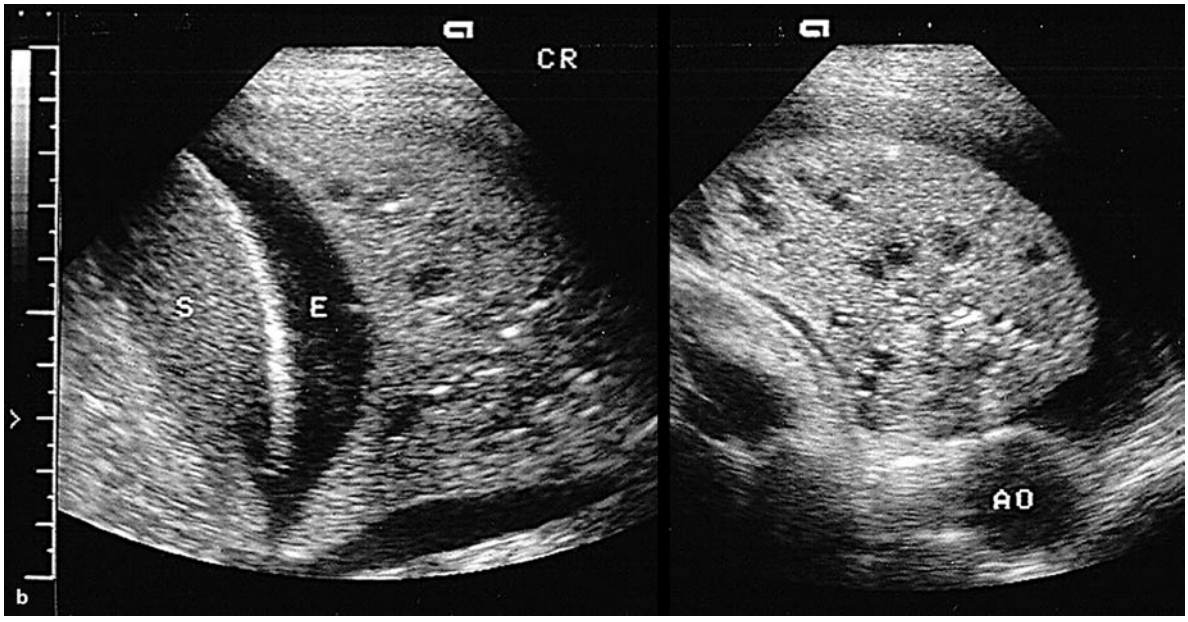

Fig. 10.17 A 65-year-old man with bronchial carcinoma. **a** Chest radiograph. Complete opacity of the lung on the left side. **b** Ultrasonography. The left-lateral intercostal ultrasound beam transmission (*left image*) and the sectional plane at right angles to it (*right image*) show a discrete pleural effusion and complete atelectasis of the lower lobe with multiple, dilated bronchi corresponding to a "fluid bronchogram". *S*, spleen; *E*, effusion; *AO*, aorta; *CR*, cranial

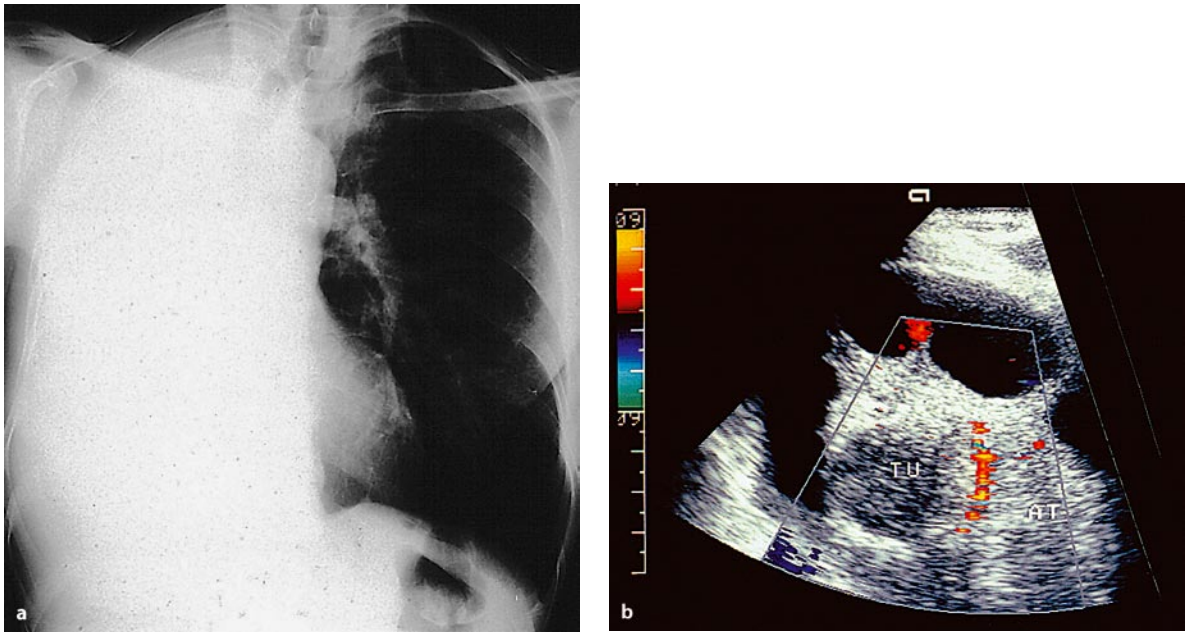

Fig. 10.18 A 64-year-old man with bronchial carcinoma. **a** Chest radiograph. Complete opacity of the lung on the right side. **b** Ultrasonography. The right-ventral intercostal ultrasound beam transmission through the upper lobe reveals a loculated pleural effusion, atelectasis of the upper lobe (*AT*) with flow signals on color-Doppler sonography, and a hypoechoic circular focus in the lung parenchyma as in metastasis (*TU*)

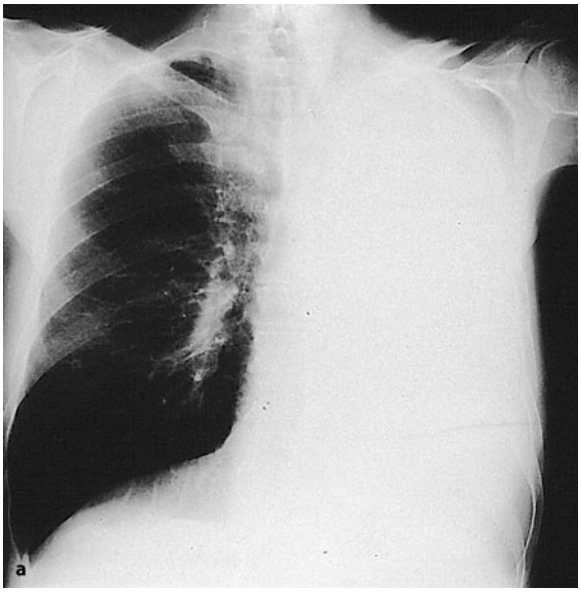

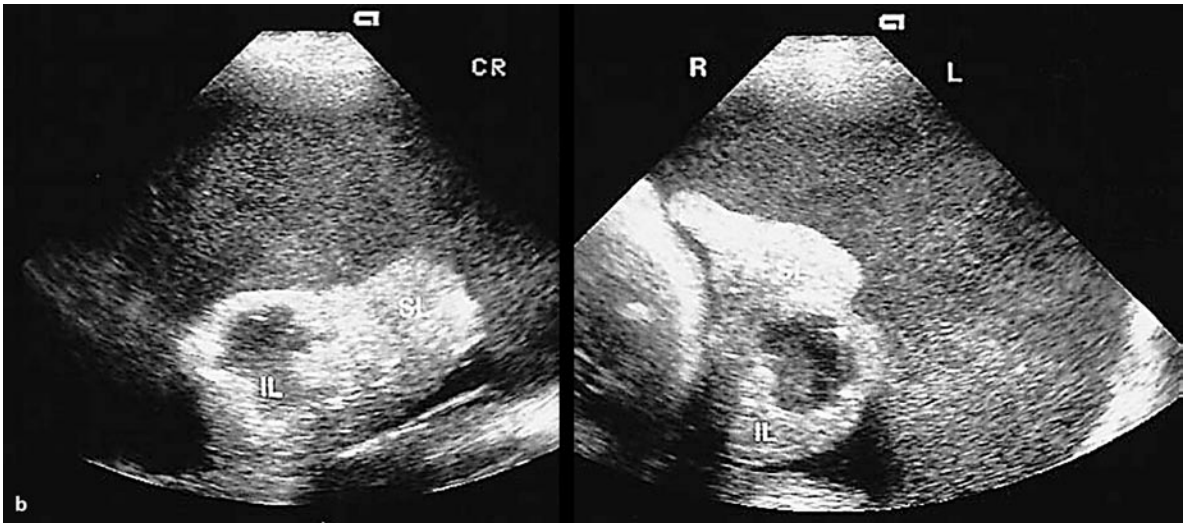

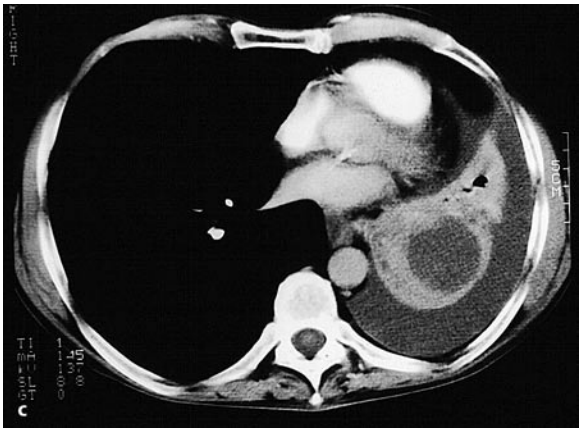

Fig. 10.19 A 63-year-old man with bronchial carcinoma. **a** Chest radiograph. Complete opacity of the lung on the left side. **b** Ultrasonography. The left-lateral intercostal ultrasound beam transmission (*left image*) and the sectional plane at right angles to it (*right image*) show a hyperechoic effusion with total atelectasis of the upper lobe (*UL*) and lower lobe (*LL*). In the central portion of the lower lobe there is a liquid space-occupying mass corresponding to colliquation (necrosis). *CR*, cranial. **c** Computed tomography. Effusion, formation of atelectasis, and central liquefaction

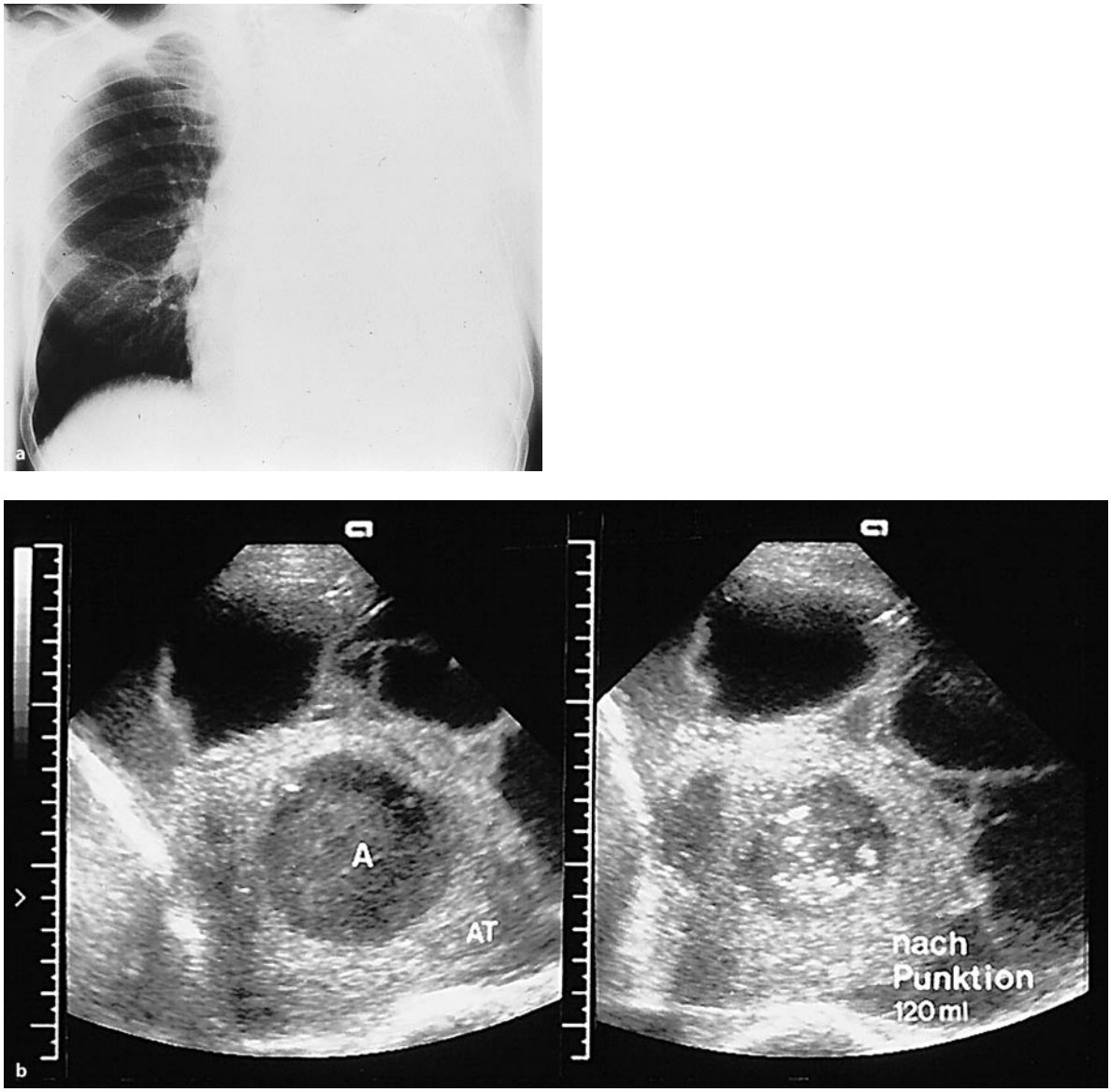

Fig. 10.20 A 52-year-old highly febrile (temperature above 39°C) man with bronchial carcinoma. **a** Chest radiograph. Complete opacity of the lung on the left side. **b** Ultrasonography. The left-lateral intercostal ultrasound beam transmission reveals a loculated effusion with complete atelectasis (*AT*) of the lower lobe and central liquefaction (*A*) (*left image*). The central abscess-like space-occupying mass was punctured and 120 ml of pus removed (*right image*). **c** Computed tomography. Effusion, atelectasis, and a parenchymatous space-occupying mass

11 From the Symptom to the Diagnosis

S. Beckh

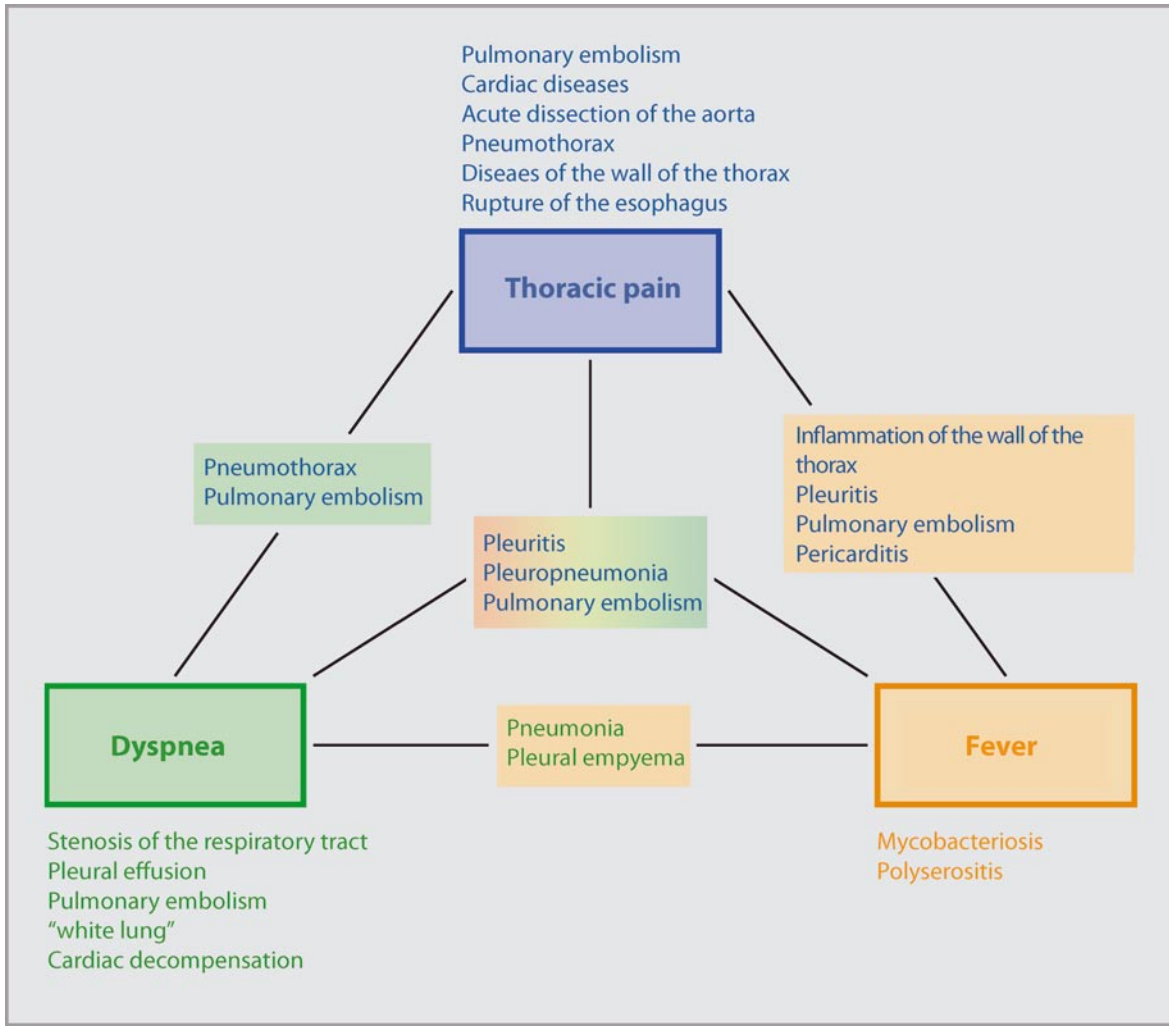

Fig. 11.1 Symptoms in diseases of the chest

Technical advancements in sonography devices, which have led to the production of mobile and even portable units, have allowed rapid use of sonography at the bedside for a large number of indications. The transducer virtually serves as a technical extension of the palpating hand or the stethoscope. In the presence of chest diseases the cardinal symptoms are chest pain, fever and dyspnea. These symptoms may occur either separately or in combination, and thus allow the diagnostician to orient himself/herself to the situation (Fig. 11.1). The extent and the intensity of the individual symptoms are mainly determined by the severity of the respective disease.

The great diversity of symptoms in pulmonary embolism (Goldhaber 1998) may render the diagnosis of this condition extremely difficult (Sect. 4.3).

11.1 Chest Pain

Chest pain is a common symptom in the emergency setting as well as the out-patient setting. It is always necessary to identify the cause, and particularly the five life-threatening diseases, namely, myocardial infarction, acute dissection of the aorta, pulmonary embolism, tension pneumothorax and rupture of the esophagus (Kurz et al. 2005).

The character of pain and the findings of clinical and sonographic investigation provide information about differential diagnosis in the presence of various diseases (Table 11.1):

The fibers responsible for the perception of pain are located in the parietal pleura, the soft tissues and the bony structures of the chest wall. The lung and the visceral pleura, on the other hand, are insensitive to stimuli

Table 11.1 Findings in the presence of diseases accompanied by chest pain

Diagnosis	Characteristic of pain	Findings obtained from investigation	Sonographic findings
Tension pneumothorax	Sudden onset, sharp	Vesiculotympanitic resonance, no respiratory sounds, dyspnea, possibly symptoms of shock	The pleural reflex does not glide, repetitive echoes
Pulmonary embolism	Increased during inspiration	Pleural rales, dyspnea or fever may be present	Usually hypoechoic lesions in subpleural location; a small pleural effusion may be present
Acute dissection of the aorta	Strong pain, either in sub-sternal location or between the shoulder blades, may radiate into the neck	Breath sounds are normal, diastolic murmur above the aortic valve may be present, symptoms of shock	Dissection of the aortic wall, dilated aorta
Myocardial infarction	Retrosternal, persistent, independent of breathing	Symptoms of shock may be present	Chest sonography is normal, diagnosis by ECG, laboratory findings, possibly echocardio-graphy
Rupture of the esophagus	Retrosternal	Mediastinal emphysema	Not informative, diagnosis by X-ray
Chest wall processes	Local	Pain is increased on palpation or movement, fever in case of inflammation	Fracture: step formation and hematoma Abscess: hypoechoic, internal echoes Malignancy: destruction and infiltration
Pleuritis	Increased during inspiration	Pleural rales, fever; dyspnea may be present	Fragmentation of the pleural line, subpleural infiltrates, possibly pleural effusion
Pleuropneumonia	Increased during inspiration	Pleural rales, bronchial respiration, rales, fever, cough, dyspnea	„Hepatization" of lung tissue, aerobronchogram, hypervascu-larization, pleural effusion may be present
Pericarditis	Increased during inspiration and in relation to position	Pericardial rales, fever	A small pericardial effusion may be present; diagnosed by ECG

that trigger pain. Pain that accompanies an inflammation in the medial portion of the diaphragm is projected into the ipsilateral shoulder and neck region (Murray and Gebhart 2005).

The ultrasound transducer is specifically targeted to the site of maximum pain, the site indicated by palpation or the physical investigation. In a physician's office, in the emergency setting or at the bedside, sonography contributes to the establishment of the diagnosis, may even provide an unequivocal diagnosis or may lead to further meaningful imaging procedures. Sonography is particularly useful to diagnose diseases of the chest in children (Kim et al. 2000).

11.1.1 Chest Pain as a Symptom of Life-Threatening Diseases

11.1.1.1 Tension Pneumothorax

Sudden onset of pain is the main characteristic of a tension pneumothorax. Depending on the magnitude of the pneumothorax, it may be accompanied by mild or excessive dyspnea. Within a very short period of time the patient develops symptoms of shock owing to the pressure of mediastinal organs and vessels.

Sonography reveals repetitive echoes on the affected side and the absence of a gliding echogenic pleural reflex

(Chap. 3). An overview radiograph (Fig. 11.20) is needed to determine the depth of the pneumothorax space. High-resolution computed tomography reveals the extent and size of the emphysematous bulla (Fig. 11.2).

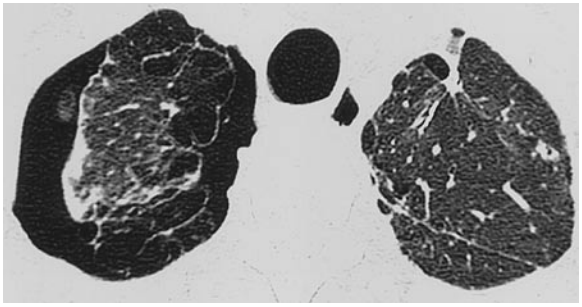

Fig. 11.2 Patient with a spontaneous pneumothorax. On high-resolution computed tomography one finds an extensive emphysematous bulla in the right upper lobe

11.1.1.2 Pulmonary Embolism

A pulmonary embolism (Sect. 4.3) is accompanied by pain on breathing when the parietal pleura is also inflamed. The larger the number of typical subpleural lesions one finds on sonography (Fig. 11.3a, b), the greater is the certainty of the diagnosis. When the Doppler sonography investigation is extended to the leg veins in order to look for the site of thrombosis (Fig. 11.3c) and when echocardiography is additionally performed in the case of circulatory symptoms to evaluate the right heart load, the diagnosis can be made efficiently within a short period of time.

11.1.1.3 Acute Dissection of the Aorta

This condition is typically accompanied by severe pain, frequently in dorsal location; maximum pain occurs between the shoulder blades. The pain may resolve for a short period of time but may also extend in the direction of dissection of vessels, for instance, in the neck when the carotid arteries are involved. Insonation from suprasternal or parasternal (Chap. 5) permits immediate viewing of the ascending aorta, the aortic arch with the vessels connected to it, and the upper part of the descending aorta, even in the emergency setting.

11.1.2 Pain Due to Diseases of the Chest Wall

The cardinal symptom is local pain, which is usually stronger during palpation or movement. In the case of irritated intercostal nerves or nerve roots the pain radiates into the area supplied by these nerves. The various structures of the chest wall are very well accessible to sonographic investigation (Chap. 2).

11.1.2.1 Rib Fracture

Rib fractures are usually triggered by trauma of appropriate magnitude. In patients with osteoporosis, however, fractures may even by caused by severe coughing. Sonography reveals the formation of a step at the site of maximum pain (Wüstner et al. 2005), frequently a smaller hematoma and occasionally the so-called chimney phenomenon (Figs. 2.13, 2.14). Even in the presence of older fractures the patient experiences pain, which is seen on sonography as a starting callus formation (Fig. 11.4).

11.1.2.2 Tumor Invasion of the Chest Wall

A peripheral lung tumor that reaches the visceral pleura causes no pain. Only when it has invaded the parietal pleura and the muscular and bony structures of the chest does irritation of nerve fibers (which lead to pain receptors) occur. The term "Pancoast's tumor" (Chap. 2, Sect. 4.2) refers to a tumor that passes through the apex of the lung. The high resolution of sonography visualizes branches of the brachial plexus (Chap. 1), their erosion and their position in relation to the subclavian vessels in the event of penetration of the superior sulcus (Fig. 11.5).

Tumor formations of the chest wall that extend across various structures can be identified well on B-mode sonography because of their different echogenicity and destruction of local tissue. Pathological formation of new vessels is a further sonomorphological criterion of malignancy. Tumor manifestations in the joints are extremely painful (Figs. 11.6, 11.7).

11.2 Fever

The occurrence of fever is always an expression of inflammatory disease activity. The reasons may be numerous. On the one hand it may be a reaction of the organism to pathogens; on the other hand it may be a manifestation of pathological processes in the body, triggered without external influences. Depending on the structures of the chest affected by inflammation, the condition may be accompanied by pain. Respiratory pain is indicative of

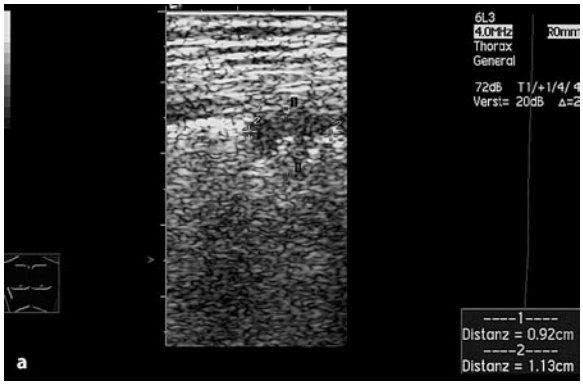

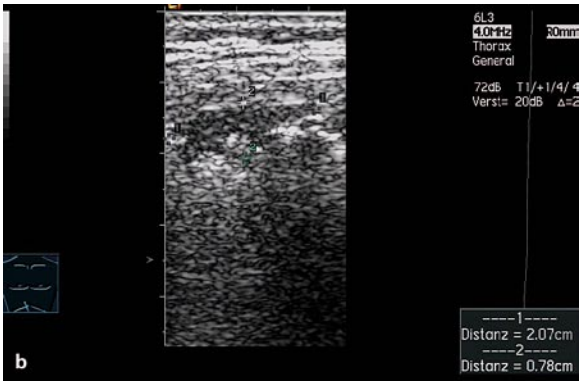

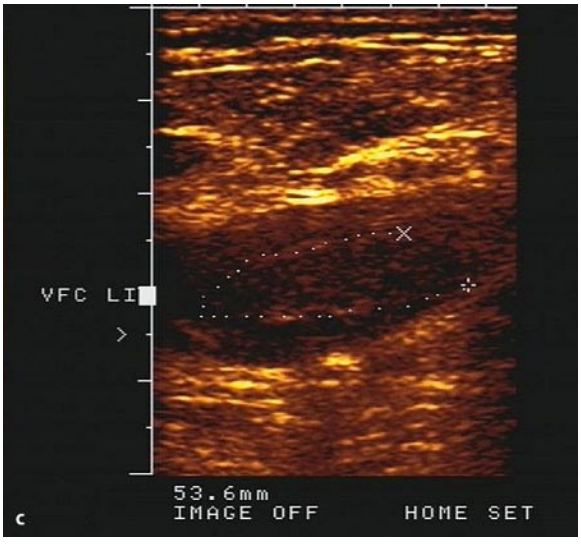

Fig. 11.3 a–c A 39-year-old woman with sudden onset of pain in the right side of the chest after removal of an adnexal tumor. Sonography reveals small subpleural lesions characteristic of embolism in the right lower lobe in lateral (**a**) and ventral (**b**) location. On leg vein sonography (**c**) a fresh thrombus (*dotted line*) is found in the left common femoral vein

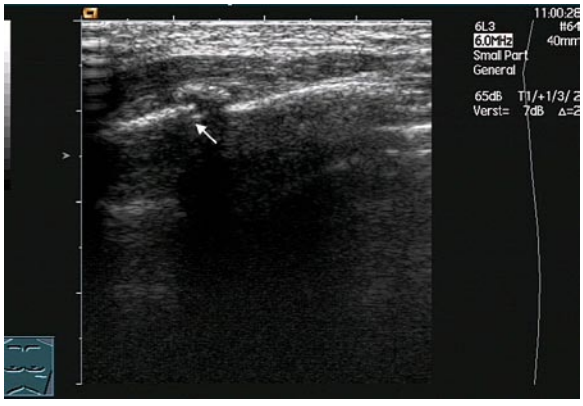

Fig. 11.4 Callus formation (the *arrow* is pointing to the fracture site) 2 weeks after a traumatic rib fracture

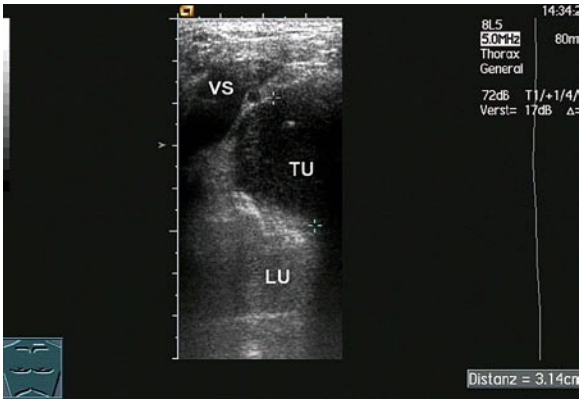

Fig. 11.5 A 46-year-old woman (40 pack years) with an adenocarcinoma (*TU*) in the left upper lobe which has perforated the superior sulcus and nearly reached the subclavian vessels. *VS* vena subclavia, *LU* lung

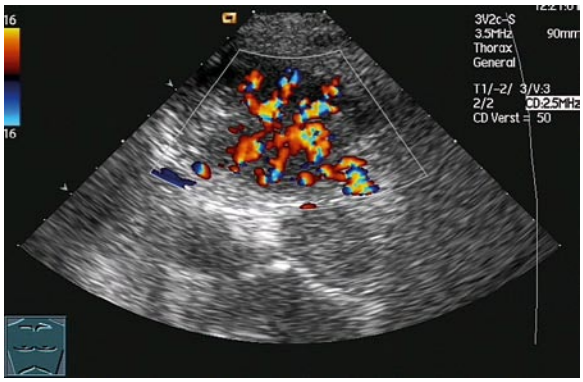

Fig. 11.6 An 83-year-old man with a swelling that is tender to pressure in the left sternoclavicular joint. On sonography there is a hypervascularized tumor formation accompanied by elimination of the joint space and the cortical reflex. The primary tumor was an adenocarcinoma in the left upper lobe

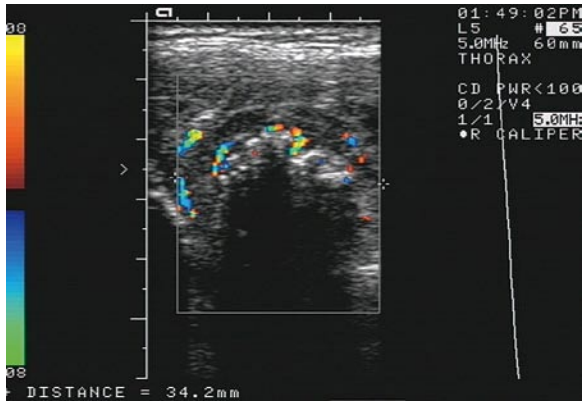

Fig. 11.7 A 51-year-old man with a painful swelling in the left sternoclavicular joint. Sonography reveals fragmentation of the cortical bone, which is surrounded by hypoechoic and strongly vascularized tissue. The surgical biopsy specimen yielded the diagnosis of a plasmocytoma. Clinically the patient had a solitary manifestation of a plasmocytoma which, however, was not secretory on laboratory investigation

11

pleural involvement. The intensity of fever—for instance, it may be low in the presence of pulmonary embolism or very high in the presence of pneumonia—as well as laboratory findings and bacteriological investigations serve as additional aids to establish the diagnosis.

11.2.1 Fever with Chest Pain

11.2.1.1 Abscesses in the Chest Wall

Inflammation in the soft tissues of the chest wall, for instance, in the presence of an abscess (Fig. 2.3), causes local pain occasionally accompanied by swelling. Abscesses in the chest wall may be quite extensive in the case of actinomycosis (Fig. 11.8).

Actinomyces infection is usually accompanied by fever (Sect 4.2, Fig. 4.27c). Spread of the infection into the chest organs (Müller et al. 2003a) and the development of further symptoms finally depend on the duration of the disease at the time of diagnosis.

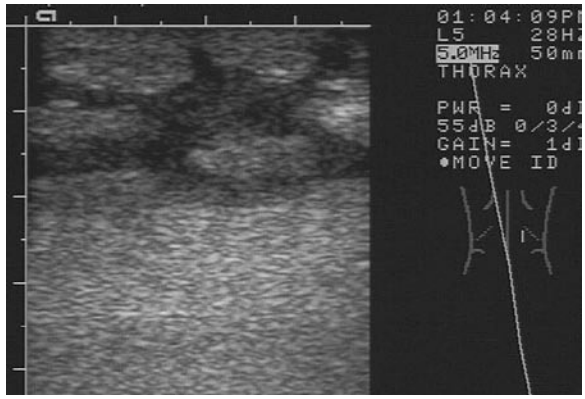

Fig. 11.8 A 44-year-old man with fever and pain in the right side of the chest in basal location. Sonography reveals fox-earth-like spread of abscesses in the soft tissue of the chest wall. The aspirated substance shows evidence of actinomyces

11.2.1.2 Pleuritis

Inflammatory diseases of the pleura (Chap. 3) cause pain which is enhanced during inspiration. Auscultation frequently discloses marked pleural rales. High-resolution transducers reveal changes that cannot be detected on conventional overview radiographs. Most of all, sonography is a useful imaging procedure when one has to avoid irradiation (Fig. 11.9).

11.2.1.3 Pulmonary Embolism

In some cases of recurrent pulmonary embolism (Sect. 4.3) the only symptoms may be intermittent chest pain and fever for a long period of time; however, fever rarely exceeds 38.3°C (Fedullo and Morrus 2005). In one investigation of geriatric patients, fever was frequently

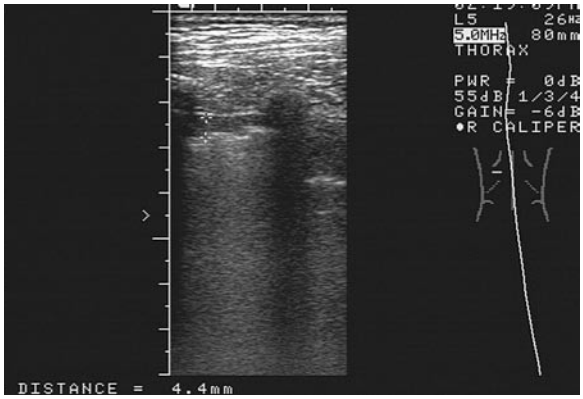

Fig. 11.9 A 35-year-old pregnant woman (ninth week of gestation) with pain in the right side of the chest, increased during inspiration, fever (38.5°C), and 4 mg/dl C-reactive protein. Sonographic fragmentation of the visceral pleura in the region of pain is indicative of pleuritis. The changes as well as signs of inflammation resolved under antibiotic treatment with penicillin

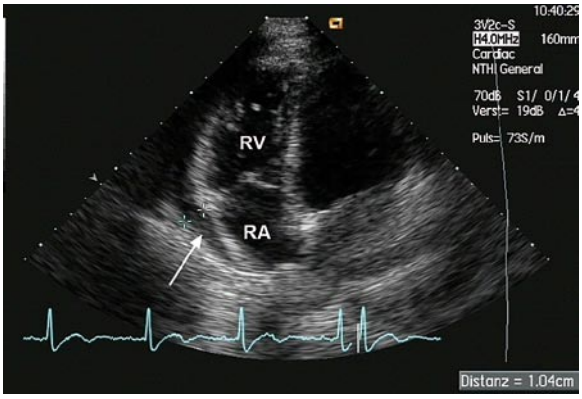

Fig. 11.10 A 25-year-old woman with a narrow pericardial effusion (*arrow*) in the presence of Churg–Strauss disease. *RA* right atrium, *RV* right ventricle

observed in connection with pulmonary embolism (Ceccarelli et al. 2003).

11.2.1.4 Pericarditis

Pericarditis is associated with moderately high fever, breath-related and position-related precordial pain. The main diagnostic tool is ECG, assisted by laboratory investigations. On sonography, at the onset of the disease one usually finds a fluid margin of lesser or greater magnitude in the pericardial space (Fig. 11.10). In every case sonography is the method of choice for further assessment of the progress of the disease.

11.2.2 Fever with Dyspnea

When a patient with fever develops dyspnea it is always a clinical sign of impairment of respiratory or ventilatory function.

11.2.2.1 Pneumonia

Pneumonia is usually associated with very high fever. In cases of pneumococcal pneumonia the patient typically experiences sudden fever without prolonged onset of the disease. Inflammatory exudation of fluid in the alveoles eliminates air from the parenchyma and permits sonographic imaging even if the invasion extends up to the visceral pleura (Sect. 4.1). Secretory retention due to obstruction secondary to a tumor leads to atelectasis and frequently also poststenotic pneumonia. The sonographic image shows the distribution of vessels as well as necrosis in the parenchyma. A bronchoscopy must be performed to assess the central bronchial system (Fig. 11.11).

11.2.2.2 Pleural Empyema

Pleural empyema, or collection of pus in the pleural space, is associated with fever, dyspnea and a severely impaired general condition. The disease is usually a threatening toxic condition which, if not identified on time or if treated too late, exposes the patient to the risk of sepsis and high lethality (Kolditz et al. 2004). Pleural empyema may occur as an inflammation of the pleura, for instance, in the presence of a tuberculotic infection, or may be a complication of a parapneumonic effusion in case of bacterial pneumonia. The emergence of a pleural empyema always heralds a more severe course of disease, whether due to the impaired resistance of the individual or a particularly virulent pathogen. Pain usually occurs in the initial stage of the disease and disappears as the exudation in the pleural space increases. On sonography the fluid is frequently seen in conjunction with dense internal echoes which correlate with the high cell content of the fluid. The longer an empyema exists, the more pronounced are the septations and chambers (Fig. 11.12).

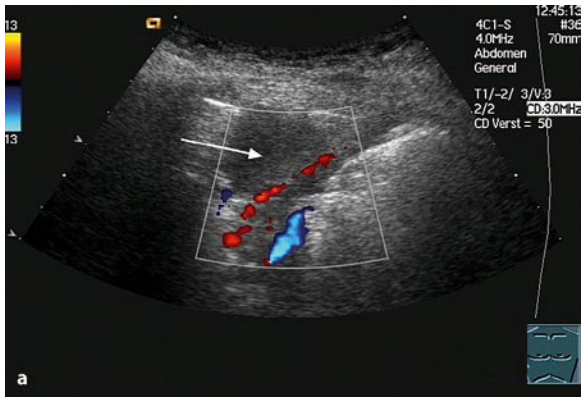

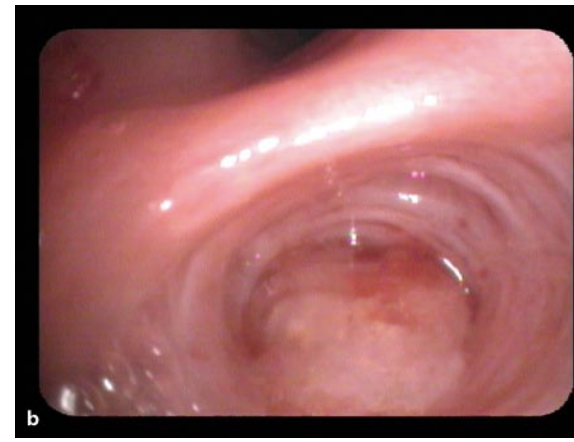

Fig. 11.11a,b A 91-year-old woman with middle-lobe pneumonia, a large peripheral colliquation (*arrow*) and regular central vessels (**a**). Bronchoscopy (**b**) reveals obstruction of the middle lobe secondary to the tumor, which proved to be an adenocarcinoma on histological investigation. Partial resolution of the middle-lobe invasion under antibiotic therapy

11

Sonography also permits localization of the optimum site of aspiration, even at the bedside (Levin and Klein 1999), to obtain material for investigation and place a drain. On the basis of the sonography report, the extent of empyema can be assessed in children (Carey et al. 1998; Ramnath et al. 1998) and the investigator will be able to decide whether conservative or surgical treatment should be used. In adults—as far as possible–computed tomography should be performed to plan the treatment and determine the exact extent and size of the chambers (Fig. 11.13).

When a suppurative effusion fills more than half a hemithorax, the patient has a pH below 7.2 and positive evidence of bacteria, a drain needs to be placed immediately (Colice et al. 2000). In cases of chambered empyema, immediate intrapleural fibrinolysis therapy may be successful (Hamm 2005). The largest study conducted thus far on local fibrinolysis of empyema (Maskell et al. 2005) revealed no advantages in terms of the duration of disease or mortality in patients treated with streptokinase. However, the significant difference between chambered and nonchambered empyema was not taken into account. Video-assisted thoracoscopy and thoracotomy are surgical treatment procedures which, however, must be viewed under consideration of other factors present in the individual patient (Hamm 2005).

11.2.3 Fever with Dyspnea and Chest Pain

The more extensively the pleura is affected in case of pleuritis, or the more extensively the lung parenchyma and pleura are affected in the case of pleuropneumonia, the more likely one will find a combination of all three symptoms. Fluid in the pleural space as well as invasion of peripheral portions of the lung can be viewed rapidly by sonography, independent of the patient's condition or mobility. Further investigations such as diagnostic aspiration of the pleura or additional radiological investigations serve to conclude the diagnostic procedures and make the diagnosis.

11.2.4 Fever as the Sole Symptom in Chest Diseases

In the case of ambiguous fever the investigator is confronted with a large number of possibilities in terms of differential diagnosis (Roth and Basello 2003). As a rule the first diagnostic step is laboratory investigations, which serve as the basis for further diagnostic procedures. The sonography investigation is not the first step for diseases of the chest because it does not provide a general overview of the chest organs. Sonography of the chest is usually requested in connection with a specific question in the case of an appropriate suspected diagnosis.

11.2.4.1 Polyserositis

Sonography, the most sensitive procedure to provide evidence of fluid, is used to investigate small pleural effusions (Chap. 3) that frequently occur on both sides and usually cause no symptoms for the patient. Even small

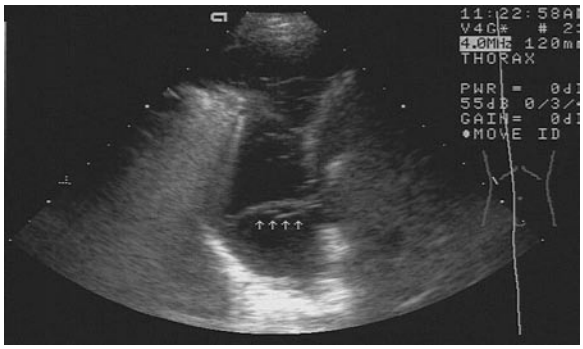

Fig. 11.12 A 36-year-old man with a septated (*arrows*) effusion and numerous internal echoes in the fluid. The aspirated material showed evidence of *Mycobacterium tuberculosis*

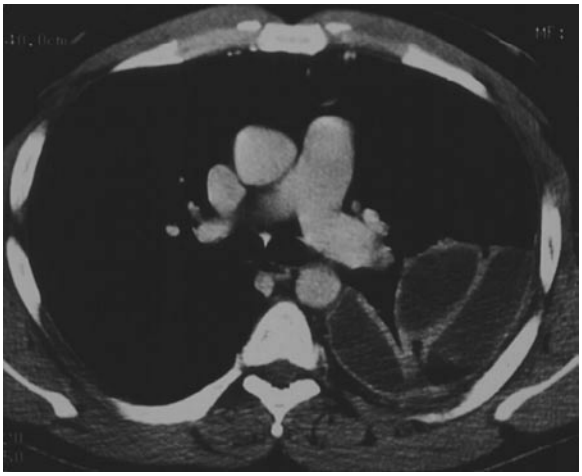

Fig. 11.13 Computed tomography section of an empyema with several chambers, which developed in the complex course of bacterial pleuropneumonia

pericardial effusions (Fig. 11.10) in the course of autoimmune diseases or vasculitis can be very well demonstrated by sonography.

11.2.4.2 Mycobacteriosis

The disease starts slowly and insidiously, and is associated with a gradual reduction of physical performance, nocturnal sweating and intermittent fever. Months may pass before an overview radiograph showing the pulmonary manifestation is performed. Pulmonary symptoms might be entirely absent. Some patients have a persistent dry cough which initially misleads the clinician in terms of diagnostic procedures and treatment. Depending on the individual's immune defense and additional organs that may be affected, the symptoms of disease may be very diverse (Hopewell 2005).

In the case of active disease the conventional chest X-ray shows soft, pale infiltrates, occasionally in conjunction with colliquations. Peripheral inflammatory lesions are accessible to sonography (Figs. 11.14, 11.15). Sonomorphological or radiological criteria that permit a reliable distinction between atypical mycobacteriosis and infection with *Mycobacterium tuberculosis* do not exist (Müller et al. 2003b). A differentiation can be made only by the use of microbiological methods such as PCR.

In cases of mycobacteriosis, sonography may be used in addition to radiological investigations, in order to evaluate the progress of peripheral lesions under treatment or when a sonography-guided biopsy is indicated for diagnostic purposes. However, conventional overview radiographs, possibly complemented by computed tomography, are always needed to assess the entire lung.

11.2.4.3 Endocarditis

Fever, physical weakness and loss of physical performance may be the only signs of endocarditis. In the presence of good transthoracic insonation, vegetation in the heart valves is visualized. Blood cultures should be performed to obtain evidence of bacteria. In the case of Löffler's endocarditis, transient thrombi may be observed at the endocardium. A sonography investigation of the heart for the purpose of orientation can be performed even by the less experienced investigator. For a more detailed examination the investigator must possess the knowledge and skills required to perform echocardiography.

11.3 Dyspnea

The symptom of dyspnea is strongly dependent on the patient's subjective experience. Specific receptors that may be responsible for triggering dyspnea have not been identified thus far (Fitzgerald and Murray 2005). A multifactorial mechanism via medullary and peripheral chemoreceptors, pulmonary vagal afferences, and mechanoreceptors in the locomotor apparatus are presumed to exist (ATS 1999; Pfeifer 2005; Stulbarg and Adams 2005). In the meantime, clinically a distinction is made between acute, chronic, resting and stress dyspnea. Even the investigator finds it difficult to quantify dyspnea; therefore,

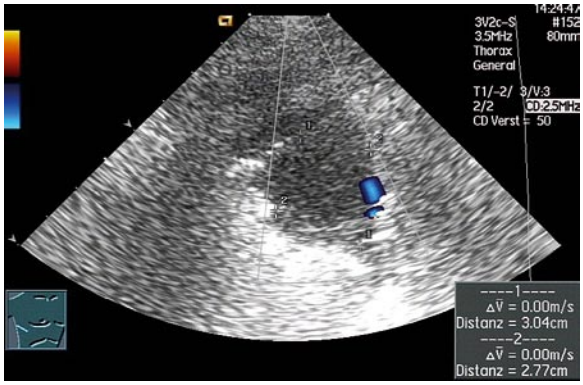

Fig. 11.14 A 68-year-old man with loss of strength and bouts of fever for several months. In the right upper lobe, in lateral location, there is a relatively homogeneous area with blurred margins and vessels at the margin. The sonographic biopsy (in NaCl!) showed bacteria on microscopic investigation; the bacteria were subsequently differentiated as atypical mycobacteria using PCR

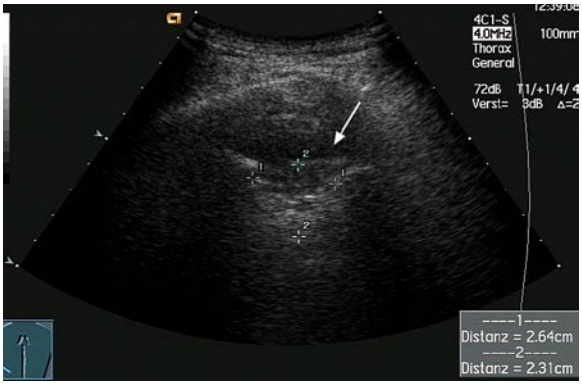

Fig. 11.15 A 73-year-old man with a chronic cough, who was known to suffer from chronic obstructive pulmonary disease. Sonography showed an area with blurred margins in dorsal and basal location, with residual air. A small pleural effusion (*arrow*). *Mycobacterium tuberculosis* was cultured in the bronchial and pleural secretion

11

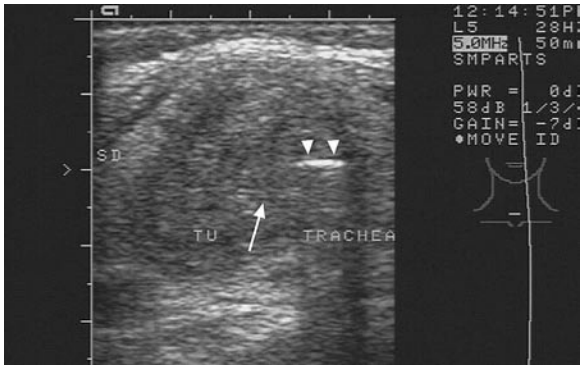

Fig. 11.16 A 55-year-old woman with advancing stress dyspnea for several weeks; inspiratory stridor. Sonography shows a space-occupying lesion arising from the right lobe of the thyroid, entering the trachea (*arrow*) and destroying the right lateral tracheal wall. A narrow air reflex (*arrowheads)* remains in the constricted trachea

particularly acute dyspnea should be rapidly investigated on the basis of clinical parameters (breath and pulse rate, auscultation, blood pressure), by laboratory investigation (blood gas analysis, determination of the acid–base balance of the body, blood count, typical enzymes associated with infarction) and imaging procedures. A strong respiratory drive is triggered by hypoxia and hypercapnia through afferent stimuli acting on the respiratory center. Reduction of the gas-exchange surface, mechanical hindrance of dilatation of the lung, muscular and neurogenic deficits lead to greater respiratory effort. Cerebral disorders cause varying degrees of respiratory impairment. The possibilities of sonographic imaging in the presence of dyspnea, for the various compartments involved in respiration, are presented in the following.

11.3.1 Respiratory Tract

The upper and deeper respiratory tracts are the domain of endoscopy in terms of diagnosis. In the case of dyspnea with inspiratory stridor, sonography of the thyroid should always be considered as part of the routine investigation (Fig. 11.16).

Large intrathoracic tumors may lead to compression of the central respiratory tract. If no ventilated lung tissue lies in the field of insonation, the sonographer is able to view the bronchi (Fig. 11.17).

11.3.2 Pleura

Fluid in the pleural space, depending on its quantity, leads to compression of lung tissue and reduces the respiratory surface. In patients with concomitant cardiopulmonary disease, even a few hundred milliliters of effusion can lead to dyspnea. Patients with a healthy contralateral lung may tolerate several liters of effusion and experience only mild dyspnea. Sonography allows rapid estimation of the quantity of effusion (Fig. 11.18) and the possibility of septation (Fig. 11.19).

As in a pleural effusion, the extent of a pneumothorax and the presence of concomitant diseases are of decisive importance for the emergence of dyspnea. A conventional X-ray is always needed to determine the size of the pneumothorax (Fig. 11.20).

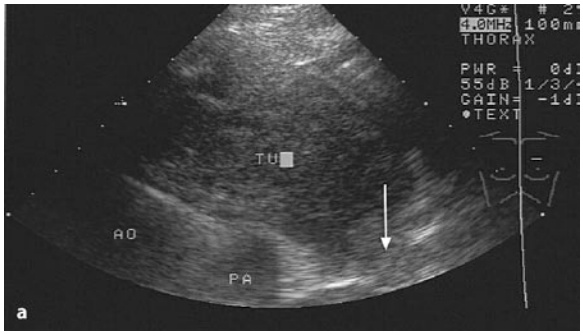

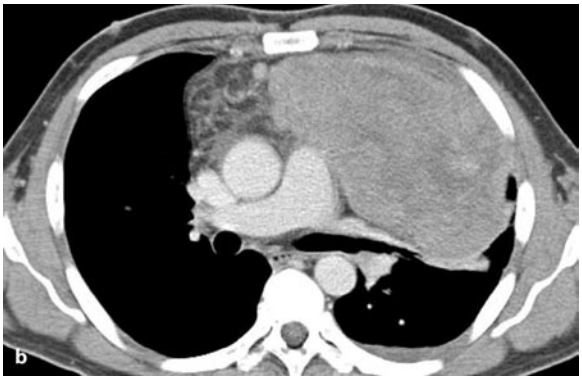

Fig. 11.17 A 44-year-old man with progressive dyspnea and persistent dry cough. **a** Sonography reveals a large tumor compressing the left main bronchus (*arrow*). **b** The corresponding computed tomography image. A sonographic biopsy could not be performed because of the extremely hard tissue. On surgical biopsy, Hodgkin's disease of the nodular sclerosis type was diagnosed

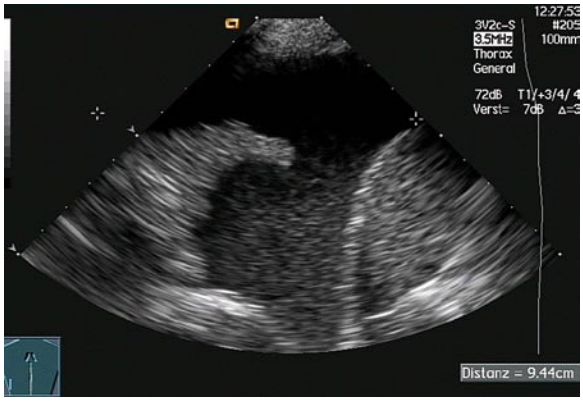

Fig. 11.18 A 68-year-old woman with known pleural carcinosis of a breast carcinoma. Repeat investigation due to dyspnea at rest. Sonography reveals a large pleural effusion which has led to compression atelectasis of the lower lobe

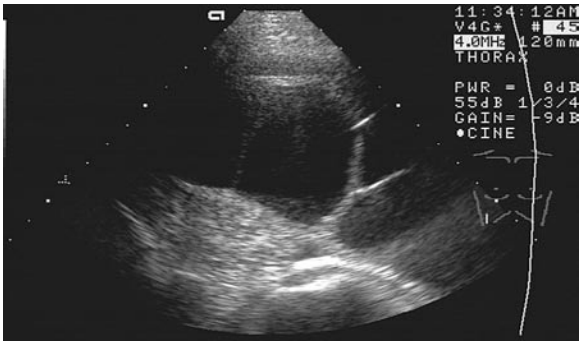

Fig. 11.19 A 36-year-old woman with a chylous effusion and genetic dysplasia in the lymphatic pathways

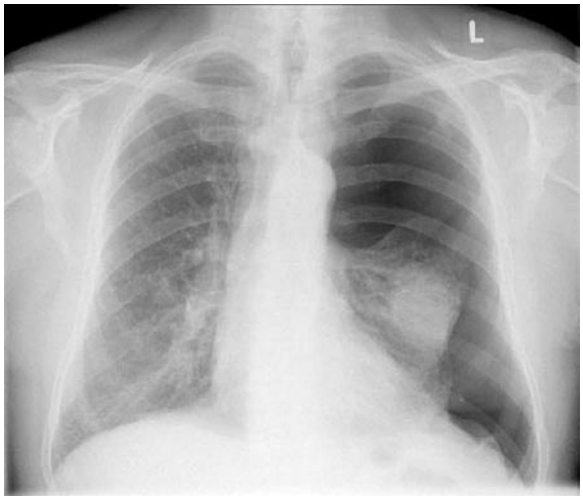

Fig. 11.20 A 63-year-old man with a tumor in the left upper lobe. Four hours after a biopsy had been obtained by transaxillary sonography, the patient developed dyspnea accompanied by elimination of gliding of the lung surface on sonography. The tumor previously seen on sonography was no longer visible. X-ray investigation showed a pneumothorax that needed drainage

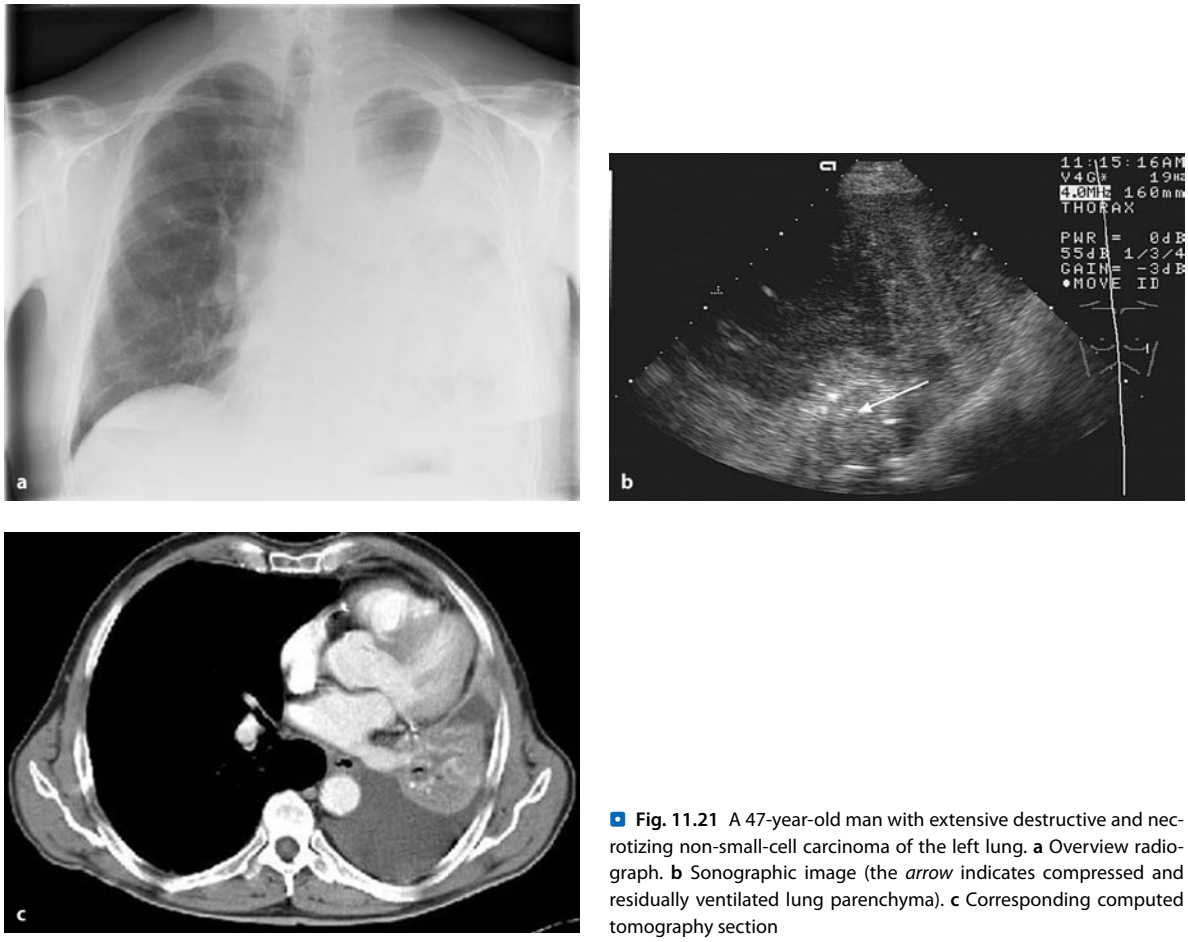

Fig. 11.21 A 47-year-old man with extensive destructive and necrotizing non-small-cell carcinoma of the left lung. **a** Overview radiograph. **b** Sonographic image (the *arrow* indicates compressed and residually ventilated lung parenchyma). **c** Corresponding computed tomography section

11.3.3 Lung

Diseases of the lung parenchyma reduce the gas-exchange surfaces. Acute dyspnea may be caused by inflammatory, vascular or tumor diseases of the lung (Chap. 4). Lung diseases accompanied by interstitial and chronic progressive loss of substance are more often accompanied by chronic and stress dyspnea. Pneumonia (Sect. 4.1), tumors (Sect. 4.2) and vascular consolidations (Sect. 4.3) are accessible to sonographic diagnosis when ventilated tissue does not superimpose the path of insonation. Sonography serves as a valuable diagnostic adjunct when the investigator is confronted with the radiological report of a so-called white lung (Sect. 4.2). Liquid, solid and necrotic portions can be well differentiated (Fig. 11.21).

11.3.4 Heart

In cases of acute dyspnea the investigator must include cardiac diseases in the differential diagnosis. A physician trained in general internal medicine, as well as sonography, should be familiar with typical sonographic findings. In case of failure of the left side of the heart (Ware and Matthay 2005) owing to left-ventricular cardiomyopathy, one finds a massively dilated and ballooned left ventricle (Fig. 11.22).

In the case of cor pulmonale, diseases of the right side of the heart are manifested in terms of dilatation of the right side of the heart and hypertrophy of the right ventricle (Fig. 11.23).

Determination of the size of the right side of the heart helps to assess the severity of disease in cases of a suspected pulmonary embolism (Goldhaber 1998; Sect. 4.3).

An indirect criterion of cardiac decompensation, easy to identify by sonography, is investigation of the vena cava in longitudinal section in the upper abdomen, through the left lobe of the liver. The diameter of the vena cava is more than 20 mm, and its diameter is inadequately reduced during inspiration.

A hemodynamically significant pericardial effusion leads to impairment of the systolic and diastolic function

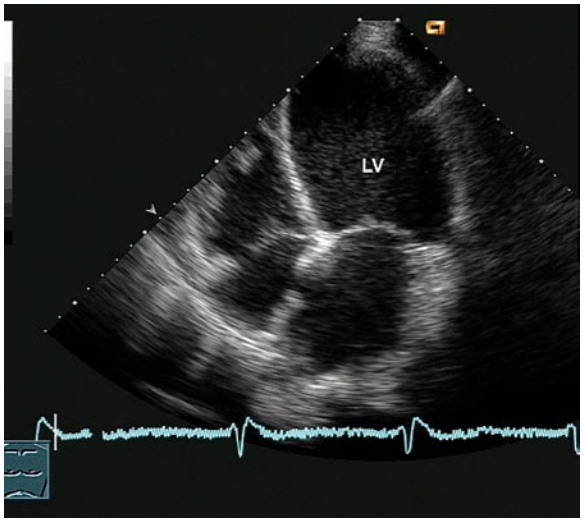

Fig. 11.22 A 55-year-old man with a pulmonary edema as a result of left-ventricular cardiomyopathy due to alcohol toxicity. The apical four-chamber view shows a dilated and ballooned left ventricle (*LV*)

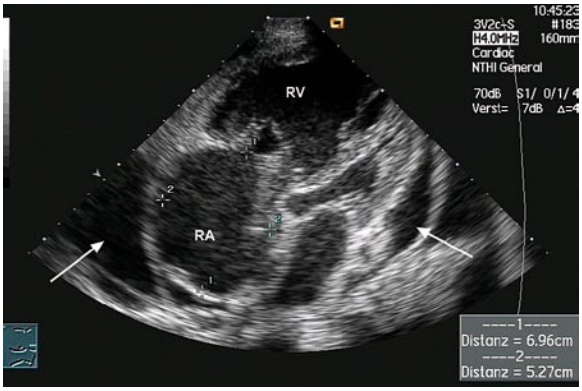

Fig. 11.23 A 64-year-old man with decompensated cor pulmonale as a result of pulmonary hypertension in the presence of the CREST syndrome. The apical four-chamber view reveals an enlarged right atrium (*RA*) and a massively dilated and hypertrophic right ventricle (*RV*). A pericardial effusion (*arrows*) lateral to the right atrium, the right ventricle and the left ventricle

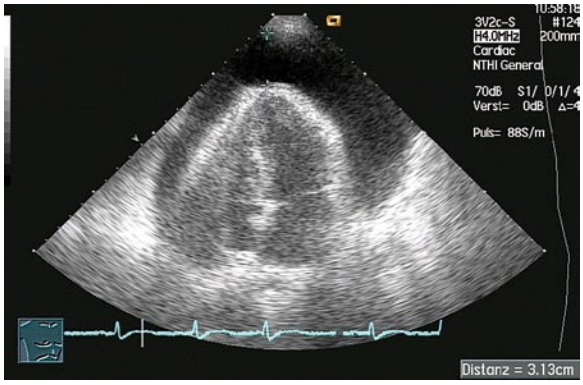

Fig. 11.24 A 91-year-old woman with global cardiac decompensation and a large circular pericardial effusion. Under diuretic therapy that reduced the cardiac load, the effusion resolved partially and dyspnea improved; therefore, in consideration of the patient's age a diagnostic aspiration was not performed

of the left ventricle, as well as congestion of venous blood flow. Large pericardial effusions can also be seen well in subcostal insonation from the epigastrium (Fig. 11.24).

11.3.5 Respiratory Muscles

The most important respiratory muscle is the diaphragm (Chap. 3). In the rare event of bilateral paresis of the diaphragm the patient may be unable to lie supine because of dyspnea, which starts immediately (Fitzgerald and Murray 2005). Reduced mobility of the diaphragm due to fixation of the lung at the diaphragmatic pleura and unilateral partial or complete paresis of the diaphragm are seen well in the dynamic sonography investigation, particularly on comparison of the right and the left side.

11.4 Summary

Chest pain, fever and dyspnea are frequent symptoms in cases of chest disease. The combination and varying intensity of symptoms allows conclusions to be drawn about the structures involved and the severity of the disease. Sonography, a readily available method that is very suitable for investigation at the bedside, makes a significant contribution to the diagnosis when investigating regions that can be viewed by the procedure. Sonography provides very significant information about the cause of sudden chest pain in the presence of a tension pneumothorax, in cases of pulmonary embolism, and in acute aortic dissection. Pathological changes in the chest wall can be visualized in an excellent manner because of the high quality of near-field resolution on the sonography

image. Fever is a symptom in cases of inflammation of the chest wall, the pleura and the lung. Sonography not only shows which structures are affected, but is also a reliable method for targeted diagnostic isolation of fluid and tissue. Sonography control investigations are particularly valuable in the course of pleural and pericardial effusions. In the case of dyspnea, sonography permits a distinction between a cardiac and a pulmonary cause of the condition. The dynamic investigation allows assessment of functional disorders of the diaphragm.

Acknowledgement We thank R. Loose, Head of the Institute of Diagnostic and Interventional Radiology at the Klinikum Nürnberg Nord, for providing radiology reports.

References

ATS (1999) Dyspnea—mechanisms, assessment, and management: a consensus statement. Am J Respir Crit Care Med 159:321–340

Carey JA, Hamilton JR, Spencer DA, Gould K, Hasan A (1998) Empyema thoracis: a role for open thoracotomy and decortication. Arch Dis child 79:510–513

Ceccarelli E, Masotti L, Barabesi L, Forconi S, Capelli R (2003) Pulmonary embolism in very old patients. Aging Clin Exp Res 15:117–122

Colice GI, Curtis A, Deslauriers J et al. (2000) ACCP consensus statement: medical and surgical treatment of parapneumonic effusions—an evidence-based guideline. Chest 118:1158–1171

Fedullo PF, Morrus TA (2005) Pulmonary thromboembolism. In: Mason RJ, Murray JF, Broaddus VC, Nadel JA (eds) Textbook of respiratory medicine. Elsevier Saunders, Philadelphia, pp 1425–1458

Fitzgerald FT, Murray JF (2005) History and physical examinations. In: Mason RJ, Murray JF, Broaddus VC, Nadel JA (eds) Textbook of respiratory medicine. Elsevier Saunders, Philadelphia, pp 493–510

Goldhaber SZ (1998) Medical progress: pulmonary embolism. N Engl J Med 339:93–104

Hamm H (2005) Die Behandlung des parapneumonischen Ergusses and des Pleuraempyems. Pneumologie 59:696–703

Hopewell PC (2005) Tuberculosis and other mycobacterial diseases. In: Mason RJ, Murray JF, Broaddus VC, Nadel JA (eds) Textbook of respiratory medicine. Elsevier Saunders, Philadelphia, pp 979–1043

Kim OH, Kim WS, Kim MJ, Jung JY, Suh JH (2000) US in the diagnosis of pediatric chest diseases. Radiographics 20:653–671

Kolditz M, Halank M, Höffken G (2004) Parapneumonischer Erguss and Pleuraempyem—aktuelle Aspekte zu Einteilung, Diagnose and Therapie. Pneumologie 58:83–91

Kurz K, Giannitsis E, Meyer FJ (2005) Thoraxschmerz. Pneumologe 2:188–197

Levin DL, Klein JS (1999) Imaging techniques for pleural space infections. Semin Respir Infect 14:31–38

Maskell NA, Davies CWH, Nunn AJ et al (2005) U.K. trial of intrapleural streptokinase for pleural infection. N Engl J Med 352:865–874

Müller NL, Fraser RS, Lee KS, Johkoh T (2003a) Diseases of the lung. Lippincott, Philadelphia, pp 34–36

Müller NL, Fraser RS, Lee KS, Johkoh T (2003b) Diseases of the lung. Lippincott, Philadelphia pp 45–46

Murray JF, Gebhart GF (2005) Chest pain. In: Mason RJ, Murray JF, Broaddus VC, Nadel JA (eds) Textbook of respiratory medicine. Elsevier Saunders, Philadelphia, pp 848–865

Pfeifer M (2005) Dyspnoe. Pneumologe 2:177–187

Ramnath RR, Heller RM, Ben-Ami T et al (1998) Implications of early sonographic evaluation of parapneumonic effusions in children with pneumonia. Pediatrics 101:68–71

Roth AR, Basello GM (2003) Approach to the adult patient with fever of unknown origin. Am Fam Physician 68:2223–2228

Stulbarg MS, Adams L (2005) Dyspnea. In: Mason RJ, Murray JF, Broaddus VC, Nadel JA (eds) Textbook of respiratory medicine. Elsevier Saunders, Philadelphia, pp 815–830

Ware LB, Matthay MA (2005) Acute pulmonary edema. N Engl J Med 353:2788–2796

Wüstner A, Gehmacher O, Hämmerle S et al (2005) Ultraschalldiagnostik beim stumpfen Thoraxtrauma. Ultraschall Med 26:285–290

Subject Index